ADA073438

LEVEL III

2

FINAL REPORT

9433 DESPIN POINTING ANOMALY

REPORT NO. 28600-AR-010-01

30 JANUARY 1976

VOLUME II

APPENDICES

APPROVED FOR PULBIC RELEASE; DISTRIBUTION UNLIMITED.

UNDER CONTRACT NO. F04701-75-C-0257
CDRL ITEM SEQUENCE NO. A009

DDC FILE COPY

TRW
SYSTEMS GROUP
ONE SPACE PARK • REDONDO BEACH, CALIFORNIA 90278

79 08 29 006

SAMSO-TR-79-13

2

AO 73437

FINAL REPORT
9433 DESPIN POINTING ANOMALY

REPORT NO. 28600-AR-010-01

30 JANUARY 1976

DDC
AUG 30
C

VOLUME II
APPENDICES

Approved for public release; distribution unlimited.

UNDER CONTRACT NO. F04701-75-C-0257
CDRL ITEM SEQUENCE NO. A009

TRW
SYSTEMS GROUP

ONE SPACE PARK • REDONDO BEACH, CALIFORNIA 90278

This final report was submitted by TRW Defense and Space Systems Group, One Space Park, Redondo Beach, CA 90278, under Contract F04701-75-C-0257, with the Space and Missile Systems Organization, Deputy for Space Communications Systems, P.O. Box 92960, Worldway Postal Center, Los Angeles, CA 90009.

Captain G. D. Nordley, SAMSO/SKD, was the Project Officer for Space Communications Systems.

This report has been reviewed by the Information Office (OI) and is releasable to the National Technical Information Service (NTIS). At NTIS, it will be available to the general public, including foreign nations.

This technical report has been reviewed and is approved for publication. Publication of this report does not constitute Air Force approval of the report's findings or conclusions. It is published only for the exchange and stimulation of ideas.

GERALD D. NORDLEY, Capt, USAF
Project Officer,
Deputy for Space Comm Systems

LAWRENCE A. BARLOCK, Lt Col, USAF
Director of Engineering, DSCS II
Deputy for Space Comm Systems

FOR THE COMMANDER

JAMES E. FREYTAG, Col, USAF
System Program Director, DSCS
Deputy for Space Comm Systems

Accession For
NTIS GRA&I
DDC TAB
Unannounced
Justification
By
Dist

UNCLASSIFIED

SECURITY CLASSIFICATION OF THIS PAGE (When Data Entered)

(18) (19) REPORT DOCUMENTATION PAGE		READ INSTRUCTIONS BEFORE COMPLETING FORM
1. REPORT NUMBER: SAMSO-TR-79-13 -VOL-2	2. GOVT ACCESSION NO.	3. RECIPIENT'S CATALOG NUMBER
4. TITLE (and Subtitle): 9433 DESPIN POINTING ANOMALY, VOL I, AND APPENDICES, VOL II (10)		5. TYPE OF REPORT & PERIOD COVERED: (9) Final Report,
		6. PERFORMING ORG. REPORT NUMBER: TRW TR-28600-AR-010-01
7. AUTHOR(s): P.C. Wheeler		8. CONTRACT OR GRANT NUMBER(s): (15) F04701-75-C-0257
9. PERFORMING ORGANIZATION NAME AND ADDRESS: TRW Defense and Space Systems Group, One Space Park, Redondo Beach, CA 90278		10. PROGRAM ELEMENT, PROJECT, TASK AREA & WORK UNIT NUMBERS
11. CONTROLLING OFFICE NAME AND ADDRESS: Space and Missile Systems Organization, Air Force Systems Command, Los Angeles, CA 90009 (11)		12. REPORT DATE: 30 January 1976
		13. NUMBER OF PAGES: Vol I - 263 & Vol II 354
14. MONITORING AGENCY NAME & ADDRESS (if different from Controlling Office): (12) 431 p.		15. SECURITY CLASS. (of this report): Unclassified
		15a. DECLASSIFICATION/DOWNGRADING SCHEDULE

16. DISTRIBUTION STATEMENT (of this Report)

Approved for public release; distribution unlimited.

17. DISTRIBUTION STATEMENT (of the abstract entered in Block 20, if different from Report)

(6) 9433 Despin Pointing Anomaly. Volume II. Appendices.

18. SUPPLEMENTARY NOTES

19. KEY WORDS (Continue on reverse side if necessary and identify by block number)

Satellite
Despin Mechanical Assembly

(14) TRW-28600-AR-010-01-VOL-2

20. ABSTRACT (Continue on reverse side if necessary and identify by block number)

This report presents the 9433 Despin Control anomaly investigations, resulting conclusions and recommendations. General recommendations are identified in two categories; design changes and process changes. First category includes a retainer design, increase of DEA current limit to increase motor capability of DMA. Secondary design considerations are positive lubrication system, a flexure payload mechanism for the bearing race and a controller rate loop redesign to make the system insensitive to torque perturbations. Second category relates to the processing of metal parts, non-metal parts, bearing screening, lubricants, assembly and test procedures, and DMA handling and storage.

DD FORM 1473 (FACSIMILE)

409637

UNCLASSIFIED

SECURITY CLASSIFICATION OF THIS PAGE (When Data Entered)

CONTENTS

APPENDIX A

THERMAL ANALYSES

1.0 INTRODUCTION

Anomalous behavior of S/C 9433 has been accompanied by changes in the DMA temperature telemetry data. The temperature data was available only for a limited number of locations, not sufficient for detailed inspection. One object of the analyses outlined in Appendix A was thus to simulate the detailed temperature profile behavior using telemetry data for boundary conditions and check points. In addition, various abnormal mechanical conditions were postulated and added to the thermal model to obtain signatures of possible failure mechanisms.

The basic thermal model was originally generated by the Ball Brothers Research Corporation as reported in

> IOC B5502.70.004, "TRW DMA Thermal Analysis Updated Report", A. Melikian to R. C. Culver, Ball Brothers Research Corporation, dated 27 March 1970.

The 38 node model was reformatted at TRW for use in our SINDA simulation system for both transient and steady state analyses. An expanded model having 81 nodes was generated at TRW for the motor shaft circumferential gradient analysis.

We begin this section by summarizing the findings and then present system torque and power dissipation equations, data tables, and a description of the thermal model.

2.0 SUMMARY

- DMA beryllium rotor shaft temperature, between the S/C cross beam interface and titanium motor shaft interface, closely follows the crossbeam temperature. In addition, the DMA housing temperature depends strongly upon the despun platform temperature. This thermal coupling is demonstrated by the DMA temperature sensitivity ratio of 0.95 (i.e. change in DMA temperature due to change in S/C temperature near DMA attachment points).

- The titanium motor/resolver mounting shaft is thermally isolated from the beryllium rotor shaft which connects to it. Thus the top bearing thermistor mounted on the rotor shaft is not particularly sensitive to changes in the titanium shaft temperature.
- The DMA temperature telemetry for the 1974 year is comparable to that of 1975 prior to September 1. After this date telemetry showed an increased temperature gradient (from a previous 4°F level to 7°F) between the upper and lower main bearing inner race locations which would indicate an increase in energy dissipation in the upper portion of the DMA. It should be noted that this temperature gradient increase occurred before the heater test of September 8-9. During the heater-on activity, the gradient between the upper and lower bearings increased further to a level of 10°F. After the heaters were turned off the gradient returned to the 7°F level.

A transient simulation of the heater test reproduced the 10°F gradient by applying a 96 oz-in. friction drag equally divided between the races of the top main bearing, concurrent with a motor power dissipation based on telemetered error voltage.

A steady state analysis using 13 November telemetry data was run, and the 7°F temperature gradient between the top and bottom bearing thermistors was reproduced when the 71 in-oz friction increase was placed in the top bearing.

An additional steady state analysis is based on a set of higher temperature boundary conditions (13 September). The temperature gradients across critical components in the DMA revealed no apparent source of failure mechanism.

- Analysis has shown that the temperatures at the beryllium rotor shaft near the upper main bearing are uniform (no circumferential gradient). This establishes the upper bearing telemetry temperature as representative of the shaft near the upper bearing.
- Results of a detailed analysis of the titanium motor shaft show substantial gradients (axial and circumferential) at the active motor winding attachment which decreases significantly near the interface with the beryllium shaft.

3.0 DISCUSSION

3.1 Spacecraft Temperature Telemetry

Figures 1 and 2 illustrate the 4 thermistor locations on the platform and DMA. The top bearing thermistor is located on the beryllium rotor shaft and is fairly well isolated from the motor/resolver section by the titanium shaft nodes 25 and 31. This thermistor combined with the one on the housing were used as check points in the simulations. The platform and bottom bearing thermistors were used to provide temperature boundary conditions. Telemetry readouts for these 4 sensors were available at two minute intervals. One count on the telemetry was equivalent to 0.5 - 0.8 °F depending on the calibration range, so this indicates the temperature resolution limit for the available spacecraft data.

3.2 DMA Power Dissipation and Torque

The major sources of drag torque in the nominal DMA are the main bearings and slipring assembly. From test data on several units we adopted the following baseline torque distribution.

Item	Friction Torque (Oz-in)	Viscous Torque (Oz-in)		Total Torque (Oz-in)
Top Main Bearing (Sum of 2 races)	2.0	7.0		9.0
Bottom Main Bearing (Sum of 2 races)	2.2	10.0		12.0
Slip Ring Assembly	8.0	-		8.0
			Sum	29.0 oz-in

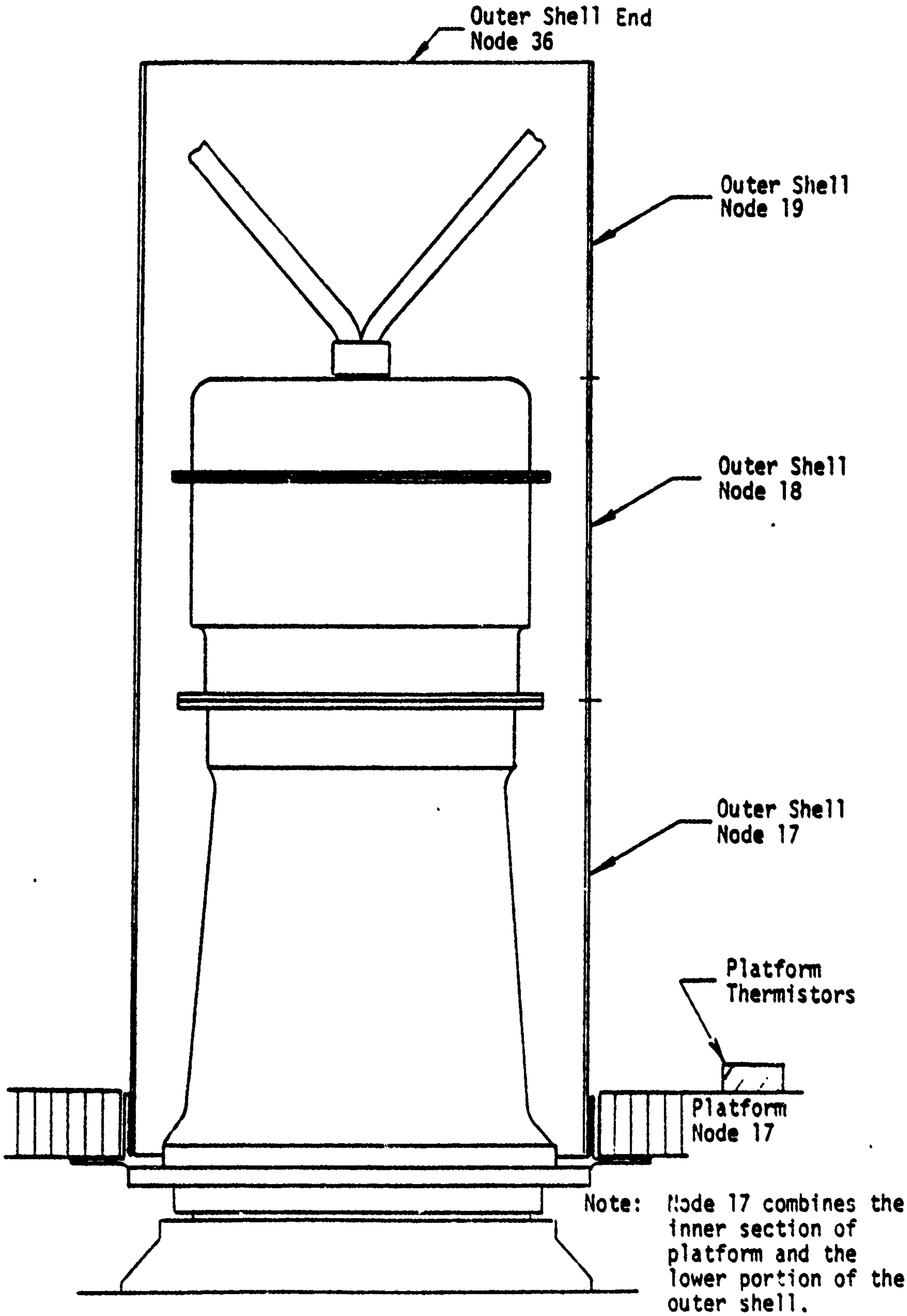

Figure 1. 38 Node Thermal Model, DMA Cover

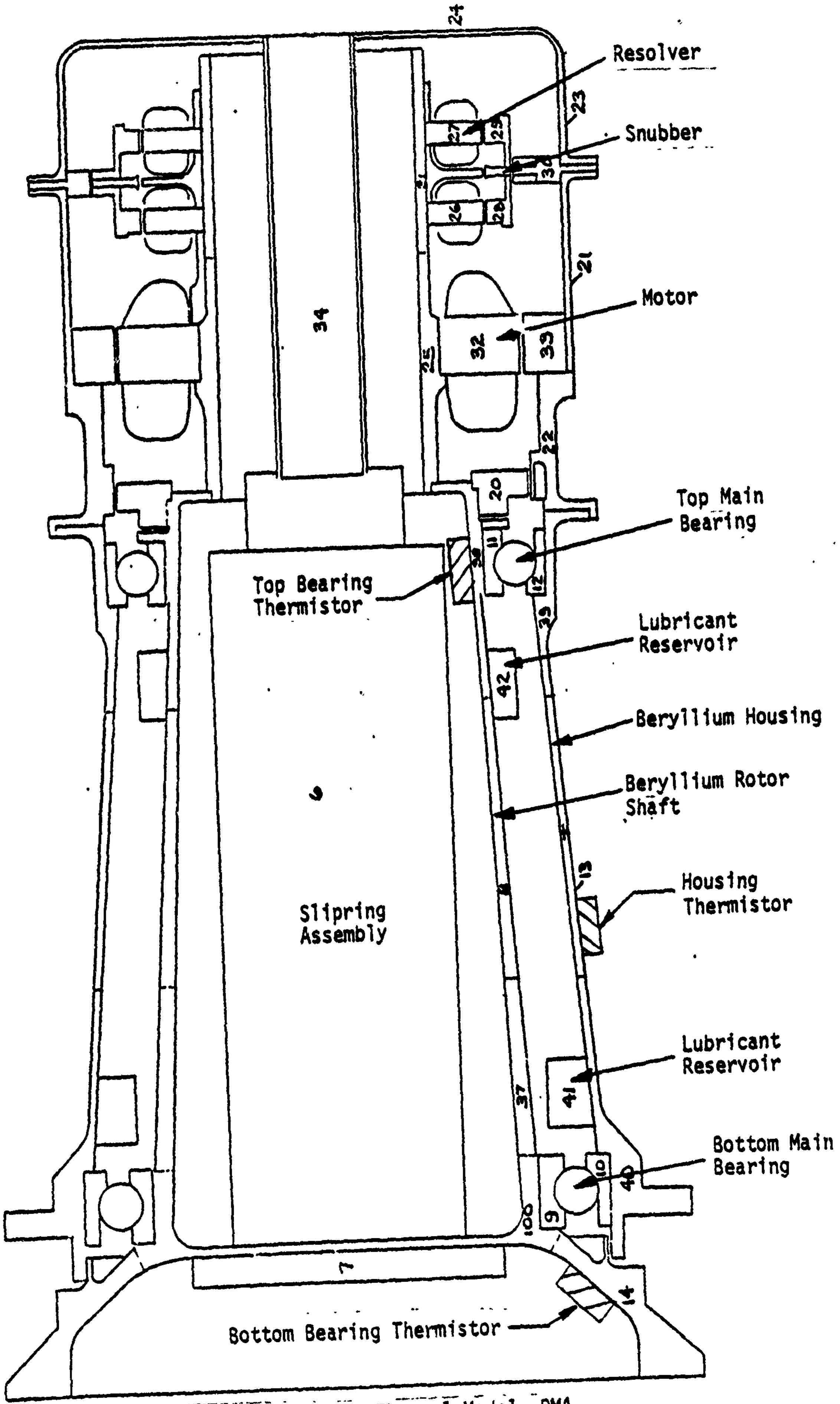

Figure 2. 38 Node Thermal Model, DMA

To simplify things we assumed that drag torque was not a function of RPM. Thus drag torque power dissipation was given by the general expression:

(1) Q_{TOT} (BTU/hr) = 0.00252 x T(oz-in) x RPM

In all of the analyses we divided the total torque of each bearing evenly between the inner and outer races, ignoring both retainer heating and the difference between inner and outer race-to-ball speed differences.

The DMA motor is a two-phase copper wound device having a resistance per phase of 10.5 ohms at 77°F. The temperature dependence of the winding resistance is given by

(2) $R(\text{ohms}) = 10.5\ (1 + .00237\ (T_{winding} - 77°F)$

For equal sinusoidal current in each phase (non-saturated operation) the total power dissipation is given by the peak current in one phase as

(3) $P(\text{watts}) = I^2{}_{o-p}\ R$

Motor torque can be obtained from the peak phase current.

(4) $T(\text{oz-in}) = I_{o-p}\ K_T$

where K_T = motor torque constant = 110. oz-in/amp

Motor current can be obtained from loop error voltage for non-saturated operation:

(5) $$I_{o-p} = \left(V_i K_A - \frac{K_{Tw}}{142.}\right) \frac{1}{R}$$

where

I_{o-p} = peak phase current (amps)

V_i = error voltage (volts)

K_T = motor torque constant

w = shaft speed (rad/sec)

R = winding resistance (ohms)

For V_i = 1.9 volts at 60 RPM:

$$(6) \quad I_{op} = \frac{0.9568}{1 + .00237(T32 - 77.)} \quad \text{(amps)}$$

$$(7) \quad \text{Torque} = \frac{105.25}{1 + .00237(T32 - 77.)} \quad \text{(oz-in)}$$

$$(8) \quad I^2R = \frac{9.596}{1 + .00237(T32 - 77.)} \quad \text{(watts)}$$

Where T32 = motor winding temp (°F)

3.3 Steady-State Temperature Predictions for Abnormal Operation

Three abnormal mechanical conditions were postulated which, if they were to occur in the DMA, would modify the temperature distribution. The first was a loss of oil in the slip fit gap between the rotor and inner race of either the top or bottom main bearing. This condition would deprive the inner race of a conductive path to the rotor heat sink, possibly causing premature race wear. The second condition was an increase in drag torque in the top main bearing. A torque increase of 96 oz-in. was chosen as being near the upper limit of motor torque capability. A third situation involving a bottomed out preload mechanism was explored to determine the temperature effect of an increased heat path for the inner race of the top main bearing. These three conditions were combined into seven cases and each case was analyzed twice using different motor dissipation assumptions.

The first analysis was based on the telemetry data obtained on 13 November. The torque distribution and motor power levels are summarized in Table 1, for each of the nine postulated cases. The resultant temperature profile of the DMA components are tabulated in Table 2. Case #6 correlated well to the telemetry data, and the temperature gradient between top and bottom main bearing thermistors agreed with the 7°F telemetered data.

TABLE 1. SIMULATION INPUTS

BOUNDARY CONDITIONS (NOV 13, 1975 TELEMETRY DATA):

SPEED	- 40.7 RPM
TOTAL TORQUE	- 100 IN-OZ
PLATFORM TEMPERATURE	- 61°F (NODE 17)
BOTTOM BEARING THERMISTOR	- 69°F (NODE 14)

CHECK POINTS (NOV 13, 1975 TELEMETRY DATA):

TOP BEARING THERMISTOR	- 76°F (NODE 38)
HOUSING THERMISTOR	- 66°F (NODE 13)

POSTULATED CASES:

Case No.	Torque (in-oz)				Motor Current
	Slip Ring	Bottom Bearing (Each Race)	Top Bearing (Each Race)	Snubber (Each Ring)	(Amp. o-p)
1	8.0	6.0	4.5	0	.269
2	8.0	6.0	4.5	0	.269
3	8.0	41.5	4.5	0	.926
4	8.0	41.5	4.5	0	.926
5	8.0	6.0	4.5	0	.269
6	8.0	6.0	40.0	0	.926
7	8.0	6.0	40.0	0	.926
8	8.0	6.0	40.0	0	.926
9	8.0	6.0	40.0	0	.926

Table 2

Effect of Bottom Main Bearing on DMA
Steady State Temperature Prediction

Motor Current Based on Error Voltage and Motor Temperature. Speed = 40.7 rpm

DMA Item	Thermal Model Node Number	Predicted Temperature (°F)			
		Case 1 Nominal Operation. Total Drag 29.2 oz-in	Case 2 Oil Loss at Inner Race/Bore Interface Total Drag 29.2 oz-in	Case 3 Increase Drag to 83 oz-in in Bottom Bearing	Case 83 oz-in Drag + Preload Washer Contact
Top Main Bearing					
Inner Race	11	67.8	67.9	74.7	74.[illegible]
Outer Race	12	65.2	65.0	73.7	73.7
Oil Reservoir	42	67.2	67.1	73.5	73.5
Thermistor	38	68.2	68.2	74.7	74.7
Bottom Main Bearing					
Inner Race	9	68.5	62.9	69.8	69.8
Outer Race	10	62.6	62.0	64.6	64.6
Oil Reservoir	41	68.1	68.1	70.3	70.3
Thermistor *	14	69.0	69.0	69.0	69.0
Housing					
Upper	39	65.0	64.8	73.6	73.6
Middle (corrected)	13	63.3	63.0	67.5	67.5
Lower	40	62.3	61.9	64.2	64.2
Rotor Shaft					
Upper	38	68.0	68.2	74.7	74.7
Middle	8	68.2	68.4	72.2	72.2
Lower	37	68.4	66.7	70.5	70.5
Motor					
Winding	32	76.1	76.0	184.7	184.6
Rotor	33	66.0	65.8	80.3	80.[illegible]
Snubber					
Inner Ring	31	72.3	72.2	130.0	130.1
Outer Ring	30	66.3	66.1	81.0	81.0
Platform *	17	61.0	61.0	61.0	61.0

*Fixed boundary condition from 13 November 1975 0840 Zulu telemetry data.

Table 2 (continued)

Effect of Top Main Bearing on DMA
Steady State Temperature Prediction

Motor Current Based on Error Voltage and Motor Temperature. Speed = 40.7 rpm

DMA Item	Thermal Model Node Number	Predicted Temperature (°F)			
		Case 1 Nominal Operation	Case 5 Oil Loss at Inner Race/Bore Interface. Total Drag 29.2 oz-in	Case 6 Increase Drag to 80 oz-in in Top Bearing	Case 7 80 oz-in Drag + Preload Washer Contact
Top Main Bearing					
Inner Race	11	67.8	65.3	76.4	76.5
Outer Race	12	65.2	64.5	75.3	75.3
Oil Reservoir	42	67.0	67.3	74.7	74.7
Thermistor	38	68.0	68.6	76.0	76.0
Bottom Main Bearing					
Inner Race	9	68.5	68.5	69.7	69.7
Outer Race	10	62.6	62.5	64.4	64.4
Oil Reservoir	41	68.1	68.2	70.5	70.5
Thermistor *	14	69.0	69.0	69.0	69.0
Housing					
Upper	39	65.0	64.4	74.9	75.0
Middle (corrected)	13	63.3	63.1	67.9	67.9
Lower	40	62.3	62.2	64.2	64.2
Rotor Shaft					
Upper	38	68.0	68.6	76.0	76.0
Middle	8	68.2	68.5	72.8	72.8
Lower	37	68.4	68.6	70.7	70.7
Motor					
Winding	32	76.1	76.0	185.7	185.6
Rotor	33	66.0	65.5	81.6	81.6
Snubber					
Inner Ring	31	72.3	72.1	131.2	131.1
Outer Ring	30	66.3	65.8	82.2	82.3
Platform *	17	61.0	61.0	61.0	61.0

* Fixed boundary condition from 13 November 1975 0840 Zulu telemetry data.

Table 2 (continued)

Effect of Top Main Bearing on DMA
Steady State Temperature Prediction

Motor Current Based on Error Voltage and Motor Temperature. Speed 40.7 rpm

DMA Item	Thermal Model Node Number	Predicted Temperatured (°F)			
		Case 1 Nominal Operation 29.2oz-in	Case 8 80 oz-in Drag in Top Bearing. Oil Loss Race/Bore	Case 9 71 oz-in Drag at Snubber	
Top Main Bearing					
Inner Race	11	67.8	81.0	75.5	
Outer Race	12	65.2	76.5	75.5	
Oil Reservoir	42	67.0	74.3	74.4	
Thermistor	38	68.0	75.0	75.4	
Bottom Main Bearing					
Inner Race	9	68.5	69.6	69.7	
Outer Race	10	62.6	64.6	64.5	
Oil Reservoir	41	68.1	70.3	70.4	
Thermistor *	14	69.0	69.0	69.0	
Housing					
Upper	39	65.0	75.9	75.5	
Middle (corrected)	13	63.3	68.4	68.2	
Lower	40	62.3	64.3	64.3	
Rotor Shaft					
Upper	38	68.0	75.0	75.4	
Middle	8	68.2	72.2	72.5	
Lower	37	68.4	70.5	70.6	
Motor					
Winding	32	76.1	185.9	191.1	
Rotor	33	66.0	82.5	83.8	
Snubber					
Inner Ring	31	72.3	131.6	146.2	
Outer Ring	30	66.3	83.1	85.2	
Platform *	17	61.0	61.0	61.0	

* [illegible] ..ed boundary condition from 13 November 1975 0840 Zulu telemetry data.

Because the housing thermistor was located below the housing mid-point, the average housing temperature (Node 13) was corrected, using the expression developed below:

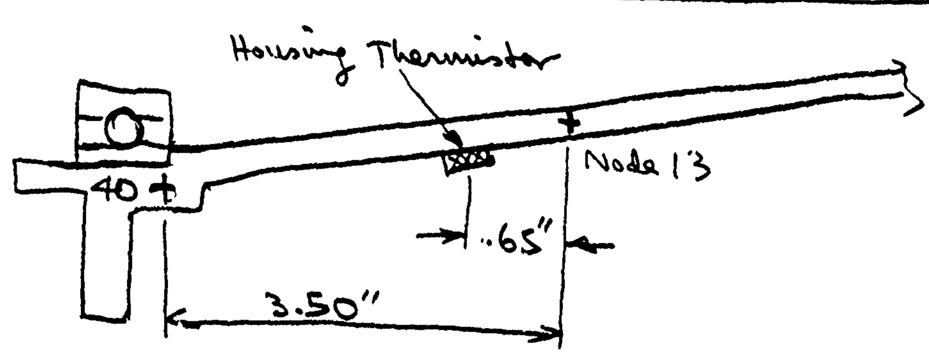

$$T_{Housing} = T_{13} - \frac{.65}{3.5}(T_{13} - T_{40})$$

$$\therefore T_{Housing} = T_{13} - .186\,(T_{13} - T_{40})$$

The second analysis was based on a set of higher temperature boundary conditions of 13 September 1975 for the purpose of detecting any significant temperature gradients leading to a potential failure mechanism. Results of this simulation are tabulated in Table 3.

Table 3

Effect of Bottom Main Bearing on DMA
Steady State Temperature Prediction

Motor Current Based on Required Torque, Speed = 60 rpm

DMA Item	Thermal Model Node Number	Predicted Temperature (°F)			
		Case 1 Nominal Operation. Total Drag 29.2 oz-in.	Case 2 Oil Loss at Inner Race/Bore Interface. Total Drag 29.2 oz-in	Case 3 Increase Drag to 96 oz-in in Bottom Bearing	Case 4 96 oz-in Drag + Preload Washer Contact
Top Main Bearing					
Inner Race	11	82.4	82.3	91.6	92.5
Outer Race	12	84.3	84.5	95.9	96.8
Oil Reservoir	42	82.7	82.7	91.5	92.1
Thermistor	38	82.1	82.0	91.1	91.7
Bottom Main Bearing					
Inner Race	9	80.8	85.8	82.7	82.8
Outer Race	10	84.5	85.1	87.4	87.6
Oil Reservoir	41	81.2	81.2	84.3	84.5
Thermistor *	14	80.0	80.0	80.0	80.0
Housing					
Upper	39	84.4	84.6	96.1	97.0
Middle (corrected)	13	84.5	84.7	91.2	91.7
Lower	40	84.6	84.9	87.3	87.5
Rotor Shaft					
Upper	38	82.1	82.0	91.1	91.7
Middle (corrected)	8	81.4	81.3	90.5	90.9
Lower	37	80.9	80.7	83.8	83.9
Motor					
Winding	32	92.3	92.4	226.1	234.5
Rotor	33	84.6	84.8	104.0	105.6
Snubber					
Inner Ring	31	89.1	89.2	159.1	163.5
Outer Ring	30	84.5	84.7	104.4	106.0
Platform *	17	85.0	85.0	85.0	85.0

*Fixed boundary condition from 13 September 1975 telemetry data.

Table 3 (continued)

Effect of Top Main Bearing on DMA
Steady State Temperature Prediction
Motor Current Based on Required Torque, Speed = 60 rpm

DMA Item	Thermal Model Node Number	Predicted Temperature (°F)			
		Case 1 Nominal Operation	Case 5 Oil Loss at Inner Race/Bore Interface. Total Drag 29.2 oz-in.	Case 6 Increase Drag to 96 oz-in in Top Bearing	Case 7 96 oz-in Drag + Preload Washer Contact
Top Main Bearing					
Inner Race	11	82.4	85.7	94.7	95.5
Outer Race	12	84.3	85.2	98.7	99.7
Oil Reservoir	42	82.7	82.5	93.5	94.2
Thermistor	38	82.1	81.4	93.4	93.9
Bottom Main Bearing					
Inner Race	9	80.8	80.7	82.6	82.7
Outer Race	10	84.5	84.6	87.2	87.3
Oil Reservoir	41	81.2	81.1	84.6	84.8
Thermistor *	14	80.0	80.0	80.0	80.0
Housing					
Upper	39	84.4	85.1	98.5	99.4
Middle (corrected)	13	84.5	84.8	91.3	91.8
Lower	40	84.6	84.8	87.3	87.5
Rotor Shaft					
Upper	38	82.1	81.4	93.4	93.9
Middle	8	81.4	81.1	87.9	88.3
Lower	37	80.9	80.7	84.1	84.3
Motor					
Winding	32	92.3	92.4	227.9	236.3
Rotor	33	84.6	85.2	106.3	107.9
Snubber					
Inner Ring	31	89.1	89.4	160.9	165.3
Outer Ring	30	84.5	85.2	106.7	108.3
Platform *	17	85.0	85.0	85.0	85.0

*Fixed boundary condition from 13 September 1975 telemetry data.

Table 3 (continued)

Effect of Top Main Bearing on DMA
Steady State Temperature Prediction
Motor Current Based on Required Torque, Speed = 60 rpm

DMA Item	Thermal Model Node Number	Predicted Temperatured (°F)			
		Case 1 Nominal Opera-tion 29.2oz-in	Case 8 96 oz-in Drag in Top Bearing. Oil Loss Race/Bore		
Top Main Bearing					
Inner Race	11	82.4	110.8		
Outer Race	12	84.3	103.7		
Oil Reservoir	42	82.7	92.9		
Thermistor	38	82.1	90.7		
Bottom Main Bearing					
Inner Race	9	80.8	82.2		
Outer Race	10	84.5	87.8		
Oil Reservoir	41	81.2	84.2		
Thermistor *	14	80.0	80.0		
Housing					
Upper	39	84.4	102.7		
Middle (corrected)	13	84.5	93.3		
Lower	40	84.6	88.0		
Rotor Shaft					
Upper	38	82.1	90.7		
Middle	8	81.4	86.5		
Lower	37	80.9	83.5		
Motor					
Winding	32	92.3	236.9		
Rotor	33	84.6	110.9		
Snubber					
Inner Ring	31	89.1	166.7		
Outer Ring	30	84.5	111.2		
Platform *	17	85.0	85.0		

*Fixed boundary condition from 13 September 1975 telemetry data.

3.4 Steady-State Temperature Effects Due to Motor Power Dissipation

Motor power dissipation ranging from 6 to 40 watts was applied to the DMA thermal model and the results listed in Table 4 for two torque distributions. Each case used the same platform and shaft temperature boundary conditions, 85°F and 80°F respectively. The first 6 cases assume the nominal system torque distribution described in Section 3.2. Cases 6-12 applied 96 oz-in. evenly distributed between both races of the top main bearing.

The gradient across the snubber was plotted in Figure 3 for exploring the possiblity of thermally induced mechanical interference. The gradient was found to rise from 27°F to 99°F in the range 6 to 40 watts.

3.5 DMA Motor/Resolver Shaft Gradient Steady-State Analysis

An 81 node thermal model, Figure 4, was assembled to determine the circumferential gradients in the DMA due to the non-symmetric motor power distribution. The baseline 38 node model assumed a symmetric 360° power dissipation; however the actual dual motors are "D" shaped with a limited 180° active perimeter. The heat must flow to the idle half in order to use the full cooling capability assumed in the less detailed model.

The results are illustrated in Figure 4. Note that the beryllium shaft conductivity, nodes 70-77, effectively reduces the circumferential gradient in the titanium motor mount, 50-57.

3.6 Transient Simulation of Orbital Data

Three orbital sequences were modeled in order to obtain detailed temperature profiles for further mechanical analyses.

A DMA on-orbit heater test, Figure 5, was performed on September 8, 1975. This provided telemetry for a temperature transient which could be simulated using the 38 node thermal model, Figures 1 and 2. Telemetry provided the boundary condition temperatures for the platform node 17 and rotor base node 14. Error voltage telemetry data was used with equations (3) and (5) to provide motor power dissipation. The simulation predicted the proper top bearing and housing gradients with respect to the boundary conditions when 96 oz-in. drag was applied to the top main bearing. Attempts to simulate the gradient without the increased heat source left a temperature deficit of approximately 3°F in the top bearing.

Table 4

Effect of Motor Power Dissipation on DMA
Steady State Temperature Prediction

Nominal Operating Torque

29.2 oz-in, 60 rpm

DMA Item	Thermal Model Node Number	Predicted Temperature (°F)					
		Case 1 6 Watts Motor Dissipation	Case 2 10 Watts Motor Dissipation	Case 3 15 Watts Motor Dissipation	Case 4 20 Watts Motor Dissipation	Case 5 30 Watts Motor Dissipation	Case 6 40 Watts Motor Dissipation
Top Main Bearing							
Inner Race	11	85.7	88.2	91.2	94.2	99.9	105.7
Outer Race	12	88.3	91.5	95.4	99.4	107.4	115.4
Oil Reservoir	42	85.8	88.2	91.0	93.9	99.5	105.0
Thermistor	38	85.4	87.8	90.7	93.5	99.1	104.5
Bottom Main Bearing							
Inner Race	9	81.3	81.7	82.1	82.6	83.5	84.4
Outer Race	10	85.3	85.9	86.6	87.4	88.9	90.4
Oil Reservoir	41	82.2	82.9	83.8	84.7	86.5	88.2
Thermistor *	14	80.0	80.0	80.0	80.0	80.0	80.0
Housing							
Upper	39	88.5	91.6	95.6	99.7	107.8	115.9
Middle (corrected)	13	86.5	88.0	90.7	91.9	85.9	99.8
Lower	40	85.4	86.0	86.8	87.5	89.1	90.6
Rotor Shaft							
Upper	38	85.4	87.8	90.7	93.5	99.1	104.5
Middle	8	83.3	84.7	86.4	88.0	91.2	94.4
Lower	37	81.8	82.5	83.4	84.2	85.8	87.4
Motor							
Winding	32	148.2	185.1	225.9	262.1	324.5	377.3
Rotor	33	91.4	96.8	103.6	110.4	124.3	138.3
Snubber							
Inner Ring	31	118.4	137.6	158.9	177.8	210.6	238.7
Outer Ring	30	91.6	97.1	104.0	110.9	125.0	139.1
Platform *	17	85.0	85.0	85.0	85.0	85.0	85.0

*Fixed boundary condition from 13 September 1975 telemetry data.

Table 4 (continued)

Effect of Motor Power Dissipation on DMA
Steady State Temperature Prediction

96 oz-in Drag in Upper Main Bearing

116 oz-in Total DMA Torque, 60 rpm

DMA Item	Thermal Model Node Number	Predicted Temperature (°F)					
		Case 7 6 Watts Motor Dissipation	Case 8 10 Watts Motor Dissipation	Case 9 15 Watts Motor Dissipation	Case 10 20 Watts Motor Dissipation	Case 11 30 Watts Motor Dissipation	Case 12 40 Watts Motor Dissipation
Top Main Bearing							
Inner Race	11	89.2	91.7	94.7	97.6	103.4	109.1
Outer Race	12	91.7	94.8	98.7	102.7	110.7	118.6
Oil Reservoir	42	88.3	90.7	93.5	96.4	101.9	107.4
Thermistor	38	88.1	90.4	93.3	96.2	101.7	107.2
Bottom Main Bearing							
Inner Race	9	81.7	82.1	82.6	83.0	83.9	84.8
Outer Race	10	85.8	86.4	87.2	87.9	89.4	90.9
Oil Reservoir	41	83.0	83.7	84.6	85.5	87.3	89.0
Thermistor *	14	80.0	80.0	80.0	80.0	80.0	80.0
Housing							
Upper	39	91.3	94.4	98.4	102.5	110.6	118.7
Middle (corrected)	13	87.9	89.4	91.3	93.3	97.3	101.1
Lower	40	86.0	86.6	87.3	88.1	89.6	91.2
Rotor Shaft							
Upper	38	88.1	90.4	93.3	96.2	101.7	107.2
Middle	8	84.8	86.2	87.9	89.5	92.7	95.9
Lower	37	82.6	83.3	84.1	85.0	86.6	88.1
Motor							
Winding	32	150.4	187.0	227.6	263.7	325.9	378.5
Rotor	33	94.1	99.5	106.3	113.1	127.0	141.0
Snubber							
Inner Ring	31	120.7	139.8	160.8	179.6	212.3	240.3
Outer Ring	30	94.2	99.7	106.6	113.6	127.6	141.6
Platform *	17	85.0	85.0	85.0	85.0	85.0	85.0

*Fixed boundary condition from 13 September 1975 telemetry data.

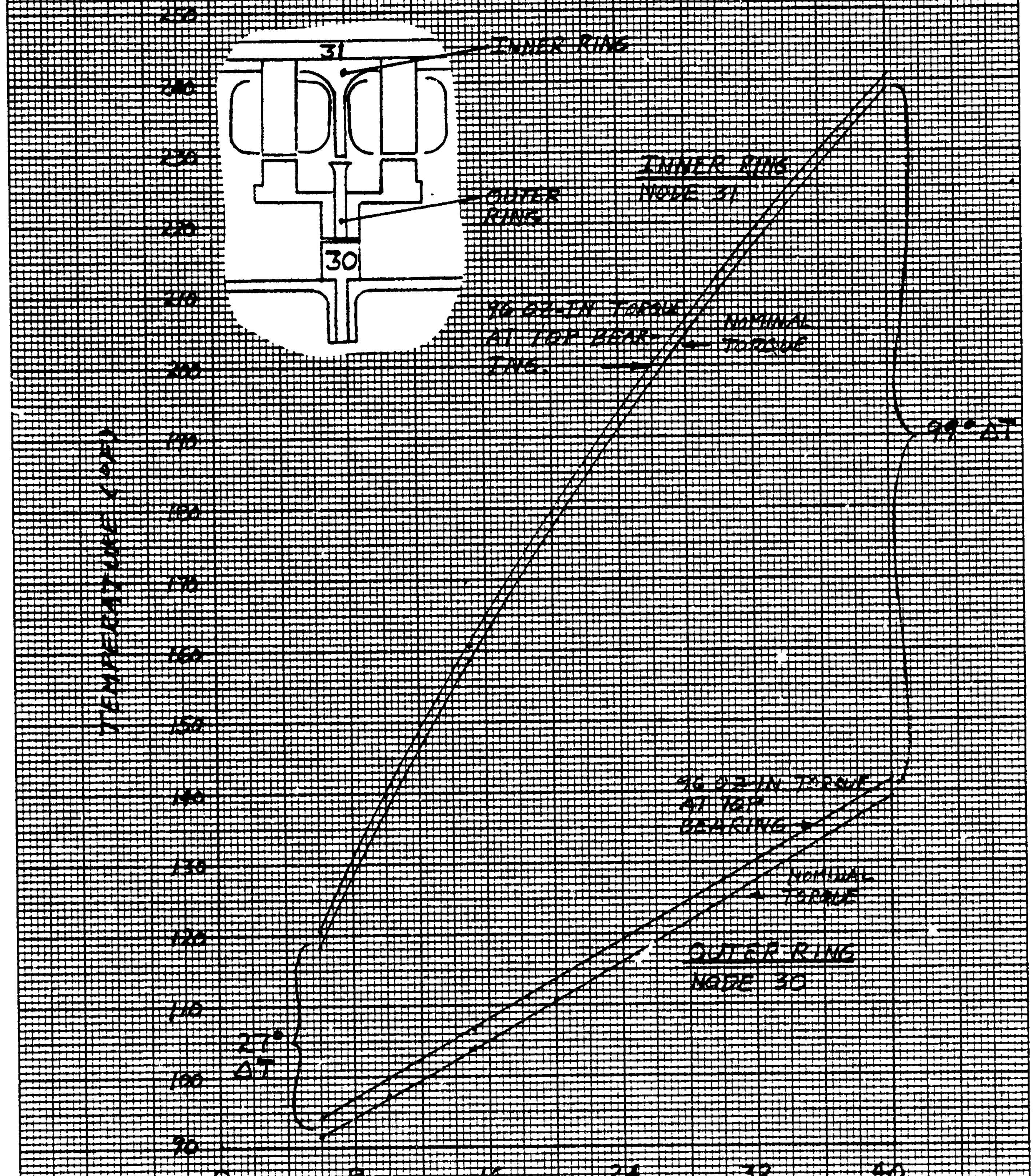

DMA SNUBBER TEMPERATURE
AS A FUNCTION OF MOTOR POWER DISSIPATION.

Figure 3

46 1473
K+E 10 X 10 TO ½ INCH • 7½ X 10 INCHES KEUFFEL & ESSER CO. MADE IN U.S.A.

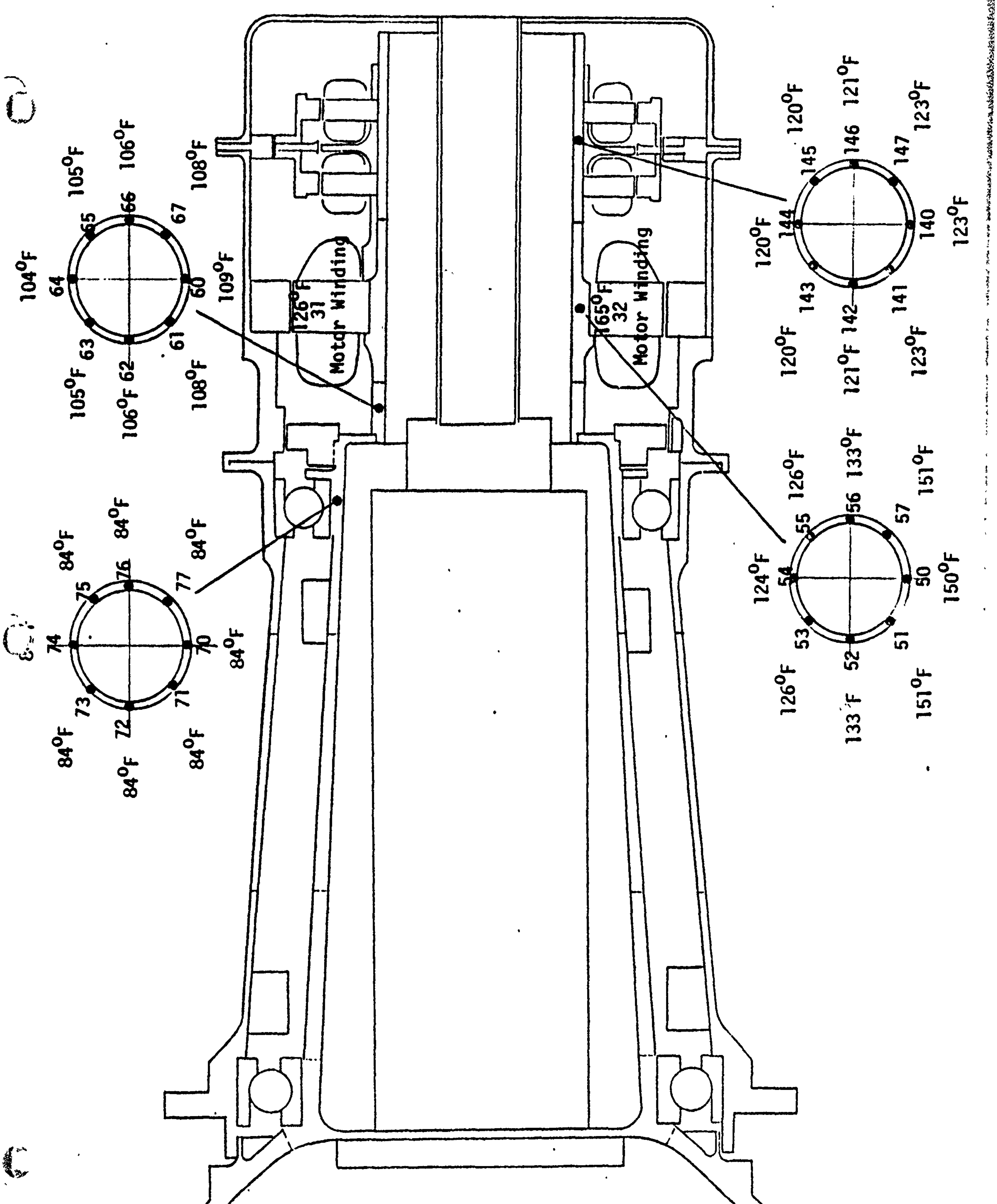

Figure 4. 81 Node DMA Motor Shaft Thermal Model

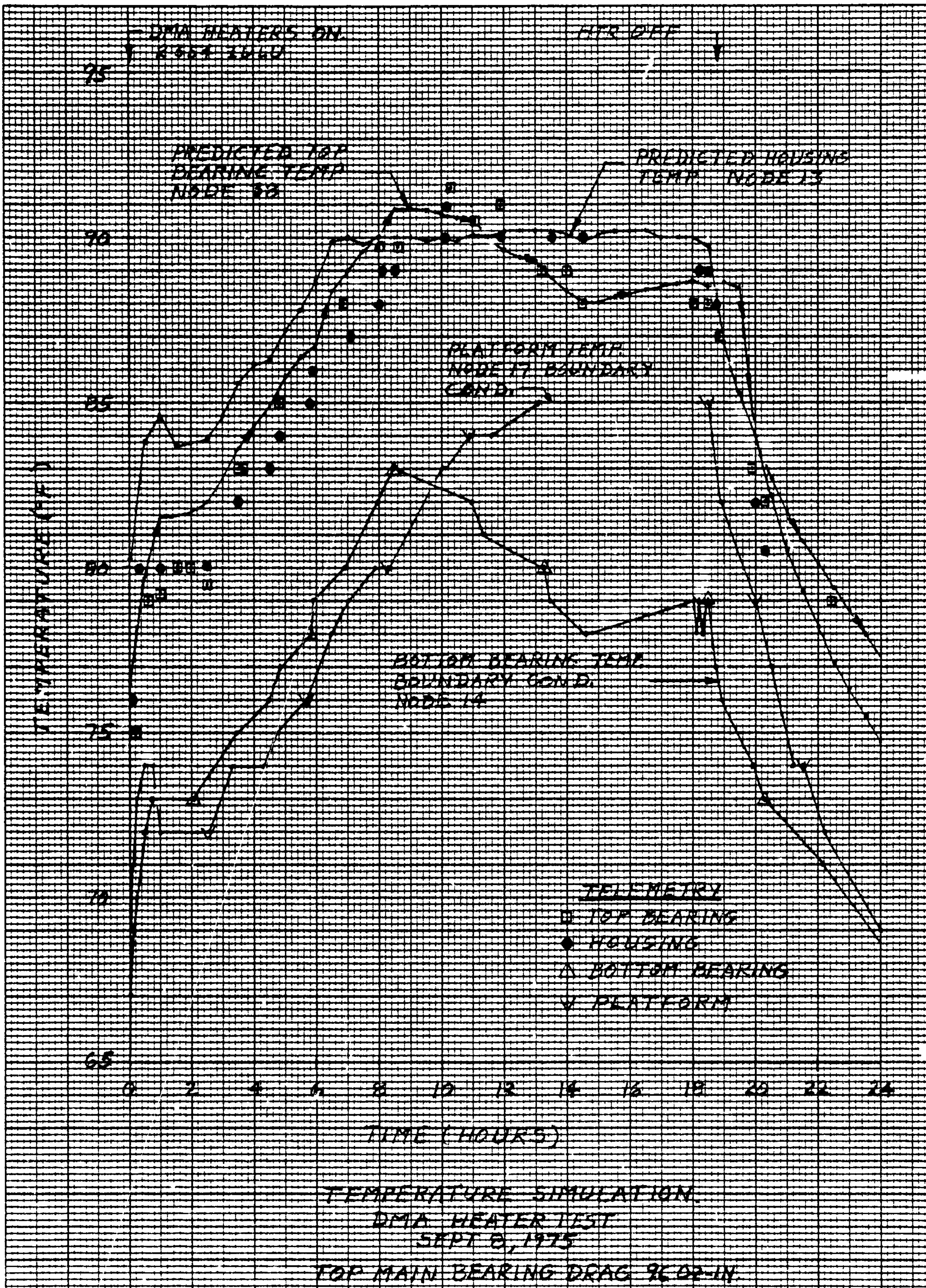

Figure 5

46 1473
K·E 10 X 10 TO ½ INCH • 7½ X 10 INCHES KEUFFEL & ESSER CO. MADE IN U.S.A.

On September 30, 1975 an on-orbit friction test provided the telemetry shown in Figure 6. For this simulation the motor power dissipation was based on an assumed motor current shown on the top of Figure 6. Again it was necessary to apply 96 oz-in. friction torque to the top bearing to provide sufficient heat to simulate the orbital data. Note that the top bearing temperature was not very sensitive to a change in motor current from .45 to 1.0 amps in the central portion of the plot. The housing temperature, node 13, ran approximately 3°F too warm. Some of the difference could be corrected since the housing thermistor is not precisely located at node 13 on the thermal model. In addition, there may be a temperature gradient between the platform thermistor and the platform DMA housing interface.

A major friction transient occurred on October 13, 1975. The calculated friction torque rose to 575 oz-in. The occurrence was modeled as shown in Figure 7. For the simulation increase torque was applied to the top bearing as shown at the top of the graph, and the motor current was maintained at 2.1 amps using equation (3) for the motor power dissipation. Again the housing ran too warm, and the temptation at this point was to transfer a greater percentage of the top bearing dissipation to the inner race. Two bearing torques were tried for the last portion of the run as shown. Note that the top bearing thermistor temperature is not particularly sensitive to bearing drag.

4.0 DESCRIPTION OF THE THERMAL MODEL

The nodal locations for the basic 38 node model are shown in Figures 1 and 2. The model is rotationally symmetric. At the dual motor, node 32, the model symmetry implies a uniform distribution of heat around the winding circumference. The degree of approximation introduced by motor assymetry was checked using the 81 node model shown in Figure 4.

Material thermal properties are listed in Table 5. Tables 6 - 8 document the conduction and radiation coefficients.

K+E 10 X 10 TO ½ INCH • 7½ X 10 INCHES KEUFFEL & ESSER CO. MADE IN U.S.A.
46 1473

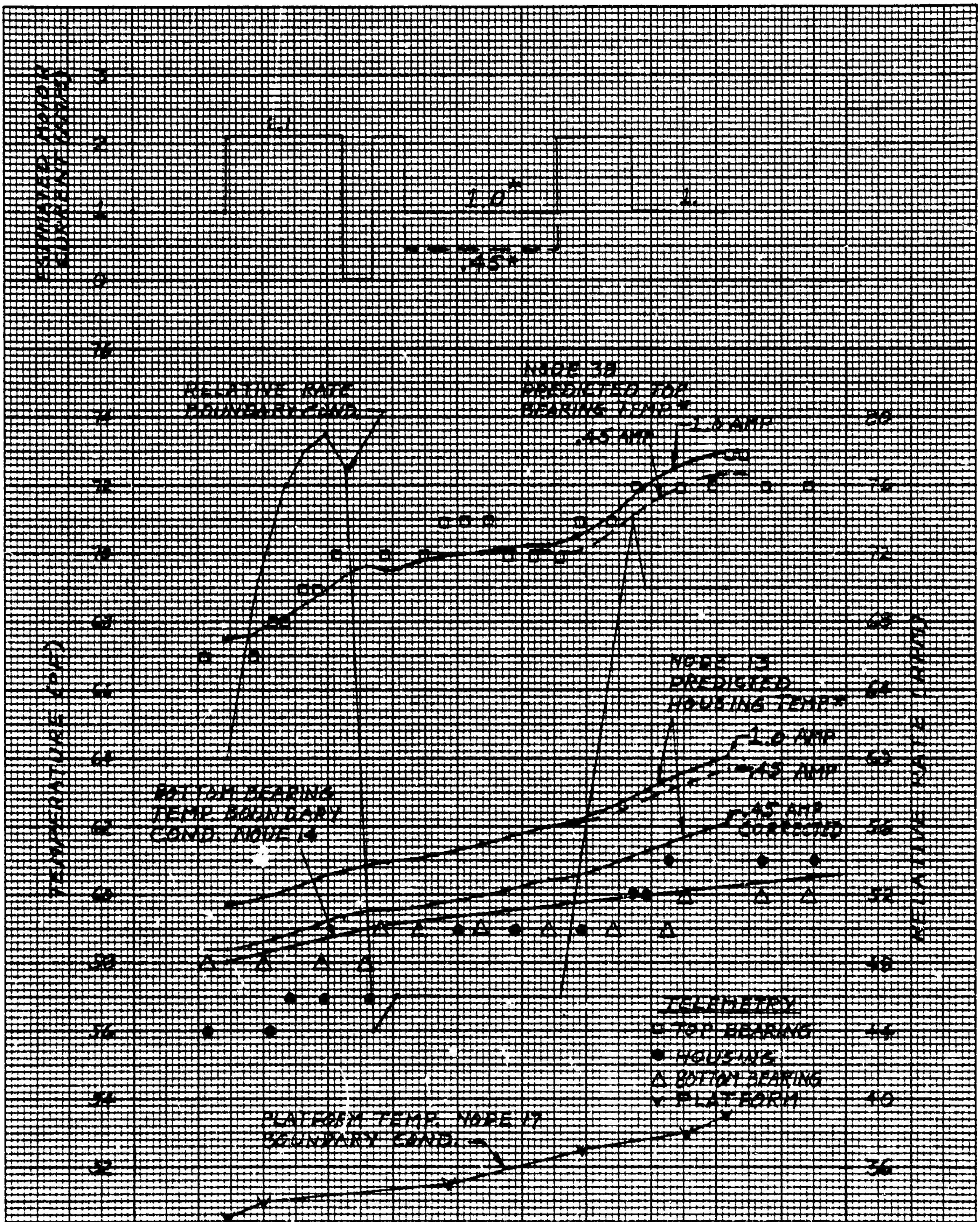

Figure 6 TEMPERATURE SIMULATION
SEPTEMBER 30 FRICTION TEST
TOP MAIN BEARING DRAG = 96 oz-in.

K+E 10 X 10 TO 1/2 INCH • 7 1/2 X 10 INCHES
KEUFFEL & ESSER CO MADE IN U.S.A.
46 1473

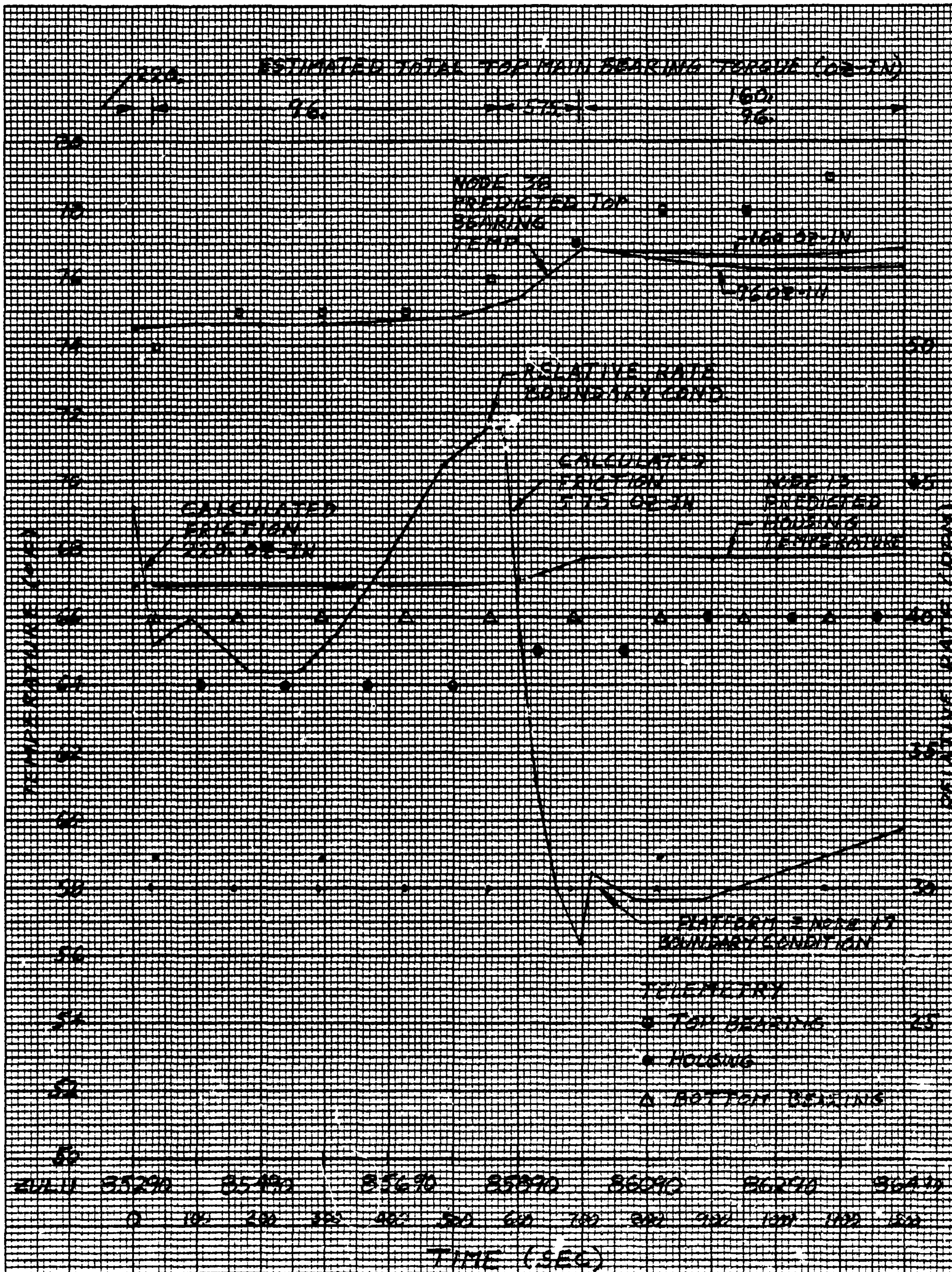

Figure 7 TEMPERATURE SIMULATION
MAJOR DROPOUT, 13 OCT 1975

Table 5

THERMAL PROPERTIES OF MATERIALS

Material	Conductivity Btu/hr-ft-°F	Specific Heat Btu/lb-°F	Density lb/in³
Al 2024-T3	67.5	0.23	0.100
Al 2024-T351	67.5	0.23	0.100
Al 2024-T4	67.5	0.23	0.100
Al 6061-T6	96.0	0.23	0.098
Titanium 6AL-4V	4.2	0.135	0.16
CRES 302	9.4	0.12	0.29
CRES 303	9.4	0.12	0.29
CRES 347	9.35	0.12	0.29
CRES 440C	14.0	0.11	0.28
Beryllium	93.4	0.45	0.066
Iron	38.0	.11	0.287
Copper	225.	.10	0.323

Table 6

NODE LISTING AND THERMAL PROPERTIES

Node No.	Node Identification	Material	Surface Finish	Surface Emissivity
1	Slip-ring shaft	Al 2024	Black Anodize	0.8
3	Ball bearing race inner top	Cres	None	0.3
6	Slip-ring outer shell	Al 2024	Black Anodize	0.8
7	Flange	Al	Black Anodize	0.8
8	Shaft (Mid portion)	Beryllium	Black	0.8
9	Ball bearing race-inner,lower	Cres	None	0.3
10	Ball bearing race-outer,lower	Cres	None	0.3
11	Ball bearing race-inner,upper	Cres	None	0.3
12	Ball bearing race-outer,upper	Cres	None	0.3
13	Housing (mid portion)	Beryllium	Black	0.8
14	Mounting flange	Beryllium	Black	0.8
17	Outer shell	Al	Black Anodize	0.8
18	Outer shell	Al	Black Anodize	0.8
19	Outer Shell	Al	Black Anodize	0.8
20	Spring and Retainer	Al & Cres	Black	0.8
21	Motor Housing (lower half)	Al 2024	Black Anodize	0.8
22	Motor Housing (upper half)	Al 2024	Black Anodize	0.8
23	Resolver Housing	Al 2024	Black Anodize	0.8
24	End Plate Cap	Al 5052	Black Anodize	0.8
25	Shaft (lower half)	Titanium	None	0.04
26	Resolver	Cu, Fe	Black Paint	0.8
27	Resolver	Cu, Fe	Black Paint	0.8
28	Resolver	Cu, Fe	Black Paint	0.8
29	Resolver	Cu, Fe	Black Paint	0.8
30	Resolver	Cu, Fe	Black Paint	0.8
31	Shaft (upper half)	Titanium	None	0.04
32	Motor Armature	Cu, Fe	Black Paint	0.8
33	Motor Magnets	Iron	Black Paint	0.8
34	Shaft Wire	Al & Cres	Black Anodize	0.8
35	Wire Bundle	Plastics	None	0.8

Table 6 (continued)

NODE LISTING AND THERMAL PROPERTIES

38 Node Model

Node No.	Node Identification	Material	Surface Finish	Surface Emissivity
36	Outer Shell End	Al	Black Anodize	0.8
37	Shaft (lower portion)	Beryllium	Black	0.8
38	Shaft (upper portion)	Beryllium	Black	0.8
39	Housing (upper portion)	Beryllium	Black	0.8
40	Housing Flange End	Beryllium	Black	0.8
41	Lubricant Reservoir	---	None	0.8
42	Lubricant Reservoir	---	None	0.8
100	Shaft (lower portion)	Beryllium	Black	0.8

Table 7 Node - Capacitance Data In SINDA Format (Btu/°F)

38 Node Model

```
       Initial
       Temp
Node   |
No.    |        M*Cp
 |     |         |
   1.  70.0.  0.200.    2,  70.0.  0.230
   6.  70.0.  0.120.    7.  70.0.  0.200
   8.  70.0.  0.110.    9,  70.0,  0.058,   10,  70.0,  0.058
  11,  70.0,  0.064,   12,  70.0,  0.064,   13,  70.0,  0.149
  20,  70.0,  0.019,   21,  70.0,  0.126,   22,  70.0,  0.126
  23,  70.0,  0.025,   24,  70.0,  0.025,   25,  70.0,  0.050
  26,  70.0,  0.200,   27,  70.0,  0.200,   28,  70.0,  0.020
  29,  70.0,  0.020,   31,  70.0,  0.080,   32,  70.0,  1.000
  33,  70.0,  0.250,   34,  70.0,  0.108,   35,  70.0,  0.500
  37,  70.0,  0.200,   38,  70.0,  0.200,   39,  70.0,  0.131
  40,  70.0,  0.629,   41,  70.0,  0.074,   42,  70.0,  0.033
 100,  70.0,  0.200,   30,  70.0,-1.000
 -14,  80.0,  1.000,  -17,  85.0,  1.000,  -18,  85.0,  1.000
 -19,  75.0,  1.000,  -36,  75.0,  1.000
END
```

Neg denotes boundary condition node

Table 8 Conduction and Radiation Couplings in SINDA Format 38 Node Model

Conduction $\frac{KA}{L}\left(\frac{BTU}{hr^{\circ}F}\right)$

```
Node
 No.   i    j    CF
  1.  20.  38.  3.400,  2.  11.  20.  1.226,   3,  22,  39,  4.126
  4.  24.  34.  0.063,  5.  25.  32.  0.816,   6,  31,  26,  0.316
  7.  31.  27.  0.316,  8.  22.  33.  0.861,   9,  21,  33,  2.009
 10.  28.  30.  0.746, 11.  29.  30.  0.746,  12,  21,  30,  5.573
 13.  23.  30.  8.170, 14.  23.  24.  3.863,  15,  21,  23,  0.215
 16.  21.  22.36.930,  17.  14,100,14.490,  18,  37,100,17.650
 19.   8.  37.  7.810, 20.   8,  38,  5.320,  21,   7,100,  3.000
 22.   7.  14.  1.100, 23.   1.   2,  1.400,  24,   1,   7,  0.700
 25.   2.   7.  0.466, 26.   6.   7,  0.410,  27,   9,100,45.450
 28.   9.  10.  0.920, 29.  11.  12,  0.840,  30,  40,  13,  5.620
 31.  13.  39.  4.660, 32.  40.  10.20.400,  33,  40,  17,11.000
 34.  39.  12.13.900,  35.  41.  37,  0.296,  36,  42,  38,  0.235
 37.  38.  11.  8.000, 38.  38,  25,  0.054,  39,  35,   1,  0.007
 40.  35.  36.  0.007, 41.  25.  31,  0.156.  42,  20,  25,  0.0456
-49.   9,  100, 3.9930E-11
-50.  38,   11, 3.1770E-11
```

Radiation $\overline{AF}$ (ft^2)

```
CAL  -51.  24,  25.  1.714E-9,  9.421E-3,  1.0,  1.0
CAL  -52.  24,  23.  1.714E-9,  4.000E-2,  1.0,  1.0
CAL  -53.  24,  30,  1.714E-9,  1.178E-2,  1.0,  1.0
CAL  -54.  24,  29,  1.714E-9,  1.232E-2,  1.0,  1.0
CAL  -55.  24,  27.  1.714E-9,  2.064E-2,  1.0,  1.0
CAL  -56.  31,  23.  1.714E-9,  1.147E-2,  1.0,  1.0
CAL  -57.  31,  27.  1.714E-9,  6.727E-3,  1.0,  1.0
CAL  -58.  23.  30,  1.714E-9,  2.199E-2,  1.0,  1.0
CAL  -59.  23,  29.  1.714E-9,  2.616E-2,  1.0,  1.0
CAL  -60.  23,  27.  1.714E-9,  1.205E-2,  1.0,  1.0
CAL  -61.  30,  29.  1.714E-9,  9.311E-3,  1.0,  1.0
CAL  -62.  29,  27.  1.714E-9,  4.285E-3,  1.0,  1.0
CAL  -63.  30,  28.  1.714E-9,  9.067E-3,  1.0,  1.0
CAL  -64.  30,  32.  1.714E-9,  4.877E-3,  1.0,  1.0
CAL  -65.  30.  33.  1.714E-9,  7.498E-3,  1.0,  1.0
CAL  -66.  30,  21.  1.714E-9,  2.188E-2,  1.0,  1.0
CAL  -67.  28,  26.  1.714E-9,  4.631E-3,  1.0,  1.0
CAL  -68.  28,  32,  1.714E-9,  7.045E-3,  1.0,  1.0
CAL  -69.  28,  33.  1.714E-9,  4.779E-3,  1.0,  1.0
CAL  -70.  28,  21.  1.714E-9,  2.549E-2,  1.0,  1.0
CAL  -71.  26,  31.  1.714E-9,  7.829F-2,  1.0,  1.0
CAL  -72.  26,  32,  1.714E-9,  1.816E-2,  1.0,  1.0
CAL  -73.  26,  33,  1.714E-9,  1.204E-2,  1.0,  1.0
CAL  -74,  26,  21.  1.714E-9,  1.176E-2,  1.0,  1.0
CAL  -75.  25,  32,  1.714E-9,  2.194E-2,  1.0,  1.0
CAL  -76.  25,  21.  1.714E-9,  5.924E-3,  1.0,  1.0
CAL  -77.  32,  33.  1.714E-9,  9.849E-3,  1.0,  1.0
CAL  -78.  32,  21.  1.714E-9,  3.002E-2,  1.0,  1.0
CAL  -79.  32,  20,  1.714E-9,  2.058E-2,  1.0,  1.0
CAL  -80.  32,  22,  1.714E-9,  4.309E-2,  1.0,  1.0
CAL  -81.  32,  38,  1.714E-9,  7.273E-3,  1.0,  1.0
CAL  -83.  33,  22.  1.714E-9,  1.181E-2,  1.0,  1.0
CAL  -84.  20,  38,  1.714E-9,  2.170E-2,  1.0,  1.0
CAL  -85.  20.  25.  1.714E-9,  7.877E-3,  1.0,  1.0
CAL  -86.  22,  20,  1.714E-9,  1.049E-2,  1.0,  1.0
CAL  -87.  22,  25.  1.714E-9,  9.589E-3,  1.0,  1.0
CAL  -88.  38,  25.  1.714E-9,  6.059E-3,  1.0,  1.0
```

σ(BTU/ft^2 hr or 4)

Table 8 (continued)

CAL	-89.	11,	38.	1.714E-9,	3.851E-3,	1.0,	1.0
CAL	-90.	11.	39.	1.714E-9,	5.092E-3,	1.0,	1.0
CAL	-91.	11.	42.	1.714E-9,	6.688F-3,	1.0,	1.0
CAL	-92.	12.	38,	1.714E-9,	2.088E-3,	1.0,	1.0
CAL	-93.	12,	39,	1.714E-9,	4.361E-3,	1.0,	1.0
CAL	-94,	12,	40.	1.714E-9,	3.661E-3,	1.0,	1.0
CAL	-95.	38,	39,	1.714E-9.	1.727E-2,	1.0,	1.0
CAL	-96.	38,	42,	1.714E-9,	7.611E-3,	1.0,	1.0
CAL	-97,	42,	39,	1.714E-9,	3.479E-2,	1.0,	1.0
CAL	-100,	42,	8,	1.714E-9,	1.332E-2,	1.0,	1.0
CAL	-101.	8,	39,	1.714E-9,	7.102E-3,	1.0,	1.0
CAL	-102.	8,	40.	1.714E-9,	1.364E-2,	1.0,	1.0
CAL	-103.	8,	41,	1.714E-9,	4.852E-3.	1.0,	1.0
CAL	-104.	37,	40.	1.714E-9,	4.625E-2,	1.0,	1.0
CAL	-105.	37,	41.	1.714E-9,	2.566E-2,	1.0,	1.0
CAL	-106.	37,	9,	1.714E-9,	7.900E-3,	1.0,	1.0
CAL	-107,	37,	10.	1.714E-9,	7.569E-3,	1.0,	1.0
CAL	-108.	9,	41.	1.714E-9,	1.041E-2,	1.0,	1.0
CAL	-109,	10.	41.	1.714E-9,	9.642E-3.	1.0,	1.0
CAL	-110,	9,	40,	1.714E-9,	2.307E-3,	1.0,	1.0
CAL	-111,	13,	8,	1.714E-9,	1.279E-1,	1.0,	1.0
CAL	-112,	13.	37,	1.714E-9,	4.177E-2,	1.0,	1.0
CAL	-113.	13,	41,	1.714E-9,	1.633E-2,	1.0,	1.0
CAL	-114.	13,	42,	1.714E-9,	5.421E-2,	1.0,	1.0
CAL	-115.	10,	40.	1.714E-9,	4.703E-3,	1.0,	1.0
CAL	-116.	26,	28,	1.714E-9,	1.288E-2.	1.0,	1.0
CAL	-117.	28,	29,	1.714E-9,	3.798E-3,	1.0,	1.0
CAL	-118.	27,	29,	1.714E-9,	1.312E-2,	1.0,	1.0
CAL	-119.	26,	28,	1.714E-9.	1.312E-2,	1.0,	1.0
CAL	-120.	28,	29,	1.714E-9,	3.798E-3,	1.0,	1.0
CAL	-121.	27,	29,	1.714E-9,	1.312E-2,	1.0,	1.0
CAL	-122.	35,	19,	1.714E-9,	4.044E-2,	1.0,	1.0
CAL	-123,	35,	36,	1.714E-9,	1.270E-2,	1.0,	1.0
CAL	-124,	35,	24,	1.714E-9,	2.188E-2,	1.0,	1.0
CAL	-125.	35,	18,	1.714E-9,	4.749E-3,	1.0,	1.0
CAL	-126.	6,	8.	1.714E-9,	1.211E-1,	1.0,	1.0
CAL	-127,	6.	37,	1.714E-9,	7.979E-2,	1.0,	1.0
CAL	-128.	6,	38.	1.714E-9,	9.220E-2.	1.0,	1.0
CAL	-129.	6,	100,	1.714E-9,	4.465E-2,	1.0,	1.0
CAL	-130.	1.	2.	1.714E-9,	2.292E-2,	1.0,	1.0
CAL	-131.	1.	6.	1.714E-9,	3.244F-3,	1.0,	1.0
CAL	-132.	1,	7.	1.714E-9,	4.056E-3,	1.0,	1.0

Table 8 (continued)

```
CAL -133.  1, 34, 1.714E-9, 4.056E-3, 1.0, 1.0
CAL -134,  2,  6, 1.714E-9, 2.531E-1, 1.0, 1.0
CAL -135,  2,  7, 1.714E-9, 3.244E-3, 1.0, 1.0
CAL -136,  2, 34, 1.714E-9, 3.244E-3, 1.0, 1.0
CAL -137, 24, 35, 1.714E-9, 2.487E-2, 1.0, 1.0
CAL -138, 26, 24, 1.714E-9, 9.945E-3, 1.0, 1.0
CAL -139, 36, 21, 1.714E-9, 2.151E-3, 1.0, 1.0
CAL -140, 36, 23, 1.714E-9, 3.055E-3, 1.0, 1.0
CAL -141, 24, 19, 1.714E-9, 3.890E-2, 1.0, 1.0
CAL -142, 24, 22, 1.714E-9, 5.551E-3, 1.0, 1.0
CAL -143, 24, 21, 1.714E-9, 1.217E-2, 1.0, 1.0
CAL -144, 24, 23, 1.714E-9, 1.984E-2, 1.0, 1.0
CAL -145, 19, 21, 1.714E-9, 8.070E-3, 1.0, 1.0
CAL -146, 19, 23, 1.714E-9, 1.363E-2, 1.0, 1.0
CAL -147, 18, 39, 1.714E-9, 3.955E-3, 1.0, 1.0
CAL -148, 18, 22, 1.714E-9, 1.248E-2, 1.0, 1.0
CAL -149, 18, 21, 1.714E-9, 2.530E-2, 1.0, 1.0
CAL -150, 18, 23, 1.714E-9, 1.591E-2, 1.0, 1.0
CAL -151, 17, 40, 1.714E-9, 3.223E-2, 1.0, 1.0
CAL -152, 17, 13, 1.714E-9, 3.449E-2, 1.0, 1.0
CAL -153, 17, 39, 1.714E-9, 1.679E-2, 1.0, 1.0
CAL -154, 17, 22, 1.714E-9, 3.294E-3, 1.0, 1.0
CAL -155, 40, 13, 1.714E-9, 9.894E-2, 1.0, 1.0
CAL -156, 40, 39, 1.714E-9, 5.112E-2, 1.0, 1.0
CAL -157, 40, 22, 1.714E-9, 1.073E-2, 1.0, 1.0
CAL -158, 13, 39, 1.714E-9, 5.275E-2, 1.0, 1.0
CAL -159, 13, 22, 1.714E-9, 1.175E-2, 1.0, 1.0
CAL -160, 39, 22, 1.714E-9, 1.180E-2, 1.0, 1.0
CAL -161, 39, 21, 1.714E-9, 1.422E-2, 1.0, 1.0
CAL -162, 22, 21, 1.714E-9, 4.041E-2, 1.0, 1.0
CAL -163,  7, 14, 1.714E-9, 4.600E-2, 1.0, 1.0
END
```

APPENDIX B

DIMENSIONAL ANALYSES

CONTENT

1. 777 DMA Anomaly - Structural Bearing Subassembly Analysis
IOC 75-7345.4-038, Revised 01/20/76, by J. G. Zaremba

   Abstract: Analysis considers the DMA's dimensional design sufficiency in terms of the orbital temperature environment and the DMA's temperature gradients necessary to equate the anomaly's Δ friction torques.

2. 777 DMA - Dimensional Analysis of Bearing Balls Separators
IOC 76-7345.4-043, 1/20/76, by J. G. Zaremba

   Abstract: Critical edge distance between the ball equator and the extreme thickness dimension of the separator is considered together with the suitability of the separator's width dimension.

3. 777 DMA Anomaly - Miscellaneous Dimensional Analyses
IOC 76-7345.4-044, 01/23/76, by W. B. Palmer/J.G. Zaremba

   Abstract: Worst case bearing fits, DMA's main shaft and motor shaft interface, main shaft and spacecraft structural interface, resolver gapclosure at platform's spin down condition and top bearing misalignment are considered.

4. 777 DMA Analyses -
IOC 75.7340.3-24, 12/02/75 by R. L. Farrenkopf

   Abstract: Likelihood of relative motion between the inner race and shaft diameters associated with the top bearing is analyzed.

5. Analyses of DMA's Dimensional Changes - As a Function of Platform Spin-up
IOC 75.7345.4-041, revised 01/20/76, by J. G. Zaremba

   Abstract: The criticality of relative dimensional changes between the housing mounted and the shaft mounted elements is analyzed.

6. Angular Velocities of 777 DMA Bearing Suspension Elements
IOC 75-7345.4-040, 10/31/75, by J. Z. Zaremba

   Abstract: Calculations of pertinent bearings element angular velocities for the case ~~as~~ inner race riding retainer are given.
   OF

TRW
SYSTEMS GROUP

INTEROFFICE CORRESPONDENCE

75-7345.4-038

TO: P. C. Wheeler

CC: A. H. Rosenberg
File

DATE: 21 October 1975
Revised: 1/20/76

SUBJECT: 777 DMA Anomaly - Structural Bearing Subassembly Analysis

FROM: J. G. Zaremba

BLDG	MAIL STA.	EXT.
82	1367	50993

1.0 INTRODUCTION AND SCOPE

The documented analysis represents an attempt to develop a malfunction mechanism, explaining the steady-state friction torque increase, associated with the No. 9433, 777 Spinning Communication Satellite. The anomaly is characterized by a steady-state torque demand from the DMA (Despun Mechanical Assembly) motor of approximately 95 in-oz and the random increases of that torque demand lasting for time periods of 60 ms or greater. The noted steady-state torque is a 60 in-oz demand increase with respect to the nominal level of 35 in-oz. This Δ torque is the principal factor to which the malfunction mechanism will equate if indeed it is a true model of the observed anomaly.

The analysis itself was keyed to the re-establishment of the design sufficiency of the DMA's structural bearing's subassembly. (The latter (Figure A) consists of two large 440C bearings, Beryllium housing and shaft and the preload mechanism exhibiting a 170 lb/in stiffness.) The basic approach characterizing the analysis was: (1) to develop the necessary analytical tooling; (2) hypothesize a likely mechanism of malfunction; (3) test the hypothesis by analytical approach, existing orbital data; and, (4) reject or accept the hypothesis.

The details of this work are given in paragraph 3.0 and the summary and conclusions are presented in paragraph 2.0.

The basic analytically developed torque expressions were substantiated by experimental 1"g" environment characterization of the DMA's bearing subassembly in terms of friction torque versus thrust load and the friction torque versus misalignment angle of the 90 MM bearing. This data was obtained through the courtesy of the Aerospace Corporation.

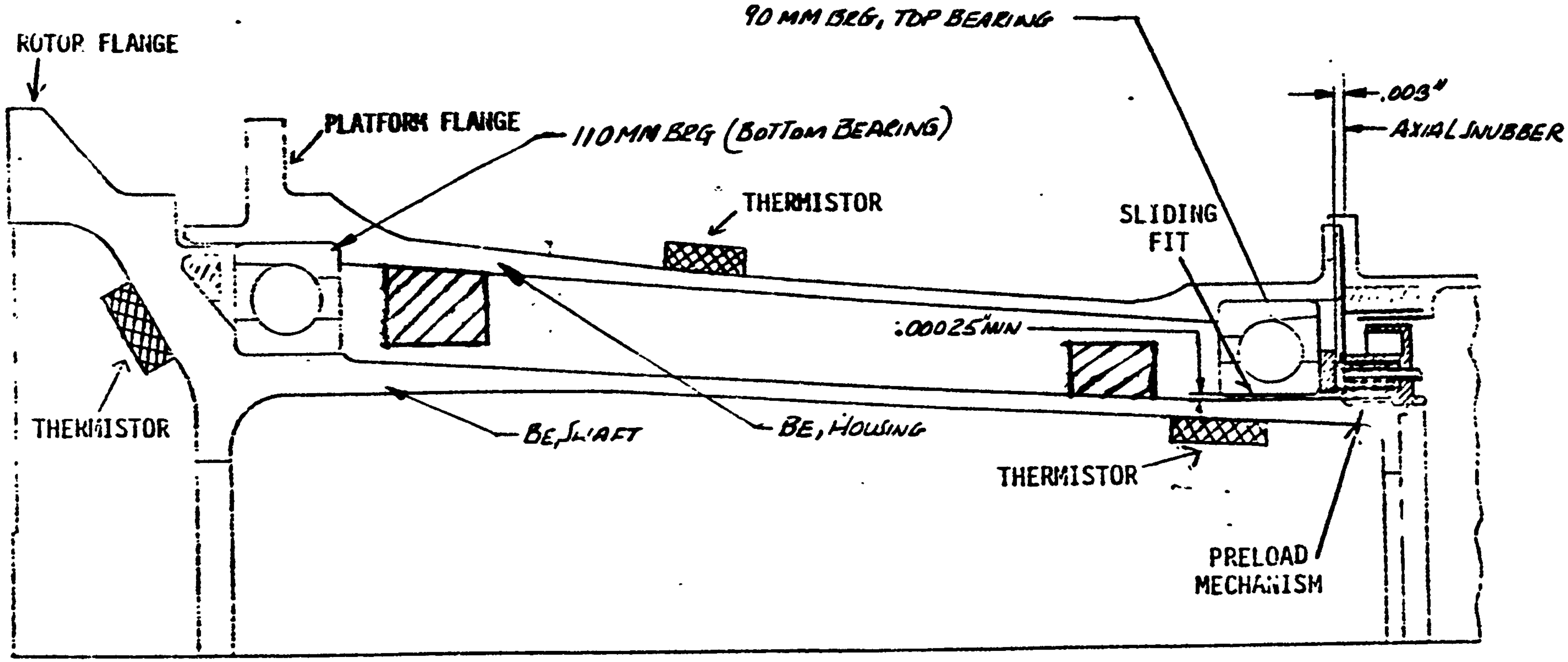

FIGURE A. BEARING SUBASSEMBLY

2.0 CONCLUSIONS AND SUMMARY

The analyses performed lead to the conclusion that the DMA's bearing assembly design and its dimensional configuration is sufficient and will not cause the observed anomaly. This statement excludes the effects of the lubricant deterioration, the slip-ring assembly and the motor performance, and the resolvers snubber geometry. At best, a 17.5 in-oz friction torque increase from nominal appears to be analytically feasible. This torque is the consequence of hypothesized top bearing misalignment causing a locked preload mechanism condition.

Of interest is to note that for the given bearing's geometries, a higher preload value (100 lbs or greater) would tend to nullify the effects of the larger than expected temperature gradients across the inner races by slowing down the saturation event of the preload mechanism (closure of the .003 in gap, Figure A). The increase of friction for the examplified 100 lb preload is small, approximately 1.5 in-oz.

Table A summarizes the results of the analytical effort that led to the concluding statement.

TABLE A. Summary of Analysis

Subject Item		Bearings 110 MM	Bearings 90 MM	Remarks
(1) Bearing Geometry (nominal)				
Outside diameter, inch	OD_B	5.905300	4.921100	
Inside diameter, inch	ID_B	4.330575	3.543175	
Pitch diameter, inch	d_m	5.1400	4.2400	
Ball diameter, inch	D	0.5000	0.4687	
Percent, curvature, inch				
Inner race	f_i	0.5175	0.5175	
Outer race	f_o	0.5275	0.5275	
Diametral clearance, inch	C_D	1.4×10^{-3}	1.4×10^{-3}	
Interference fit, diametral, inch				
Housing to OD_B, tight	$\Delta_{i,H}$	-8×10^{-4}	-8×10^{-4}	i denotes interference
Shaft to ID_B, loose	$\Delta_{i,s}$	$+5 \times 10^{-5}$	$+5 \times 10^{-4}$	h denotes housing
Decrease of clearance	$K_j \Delta_{ij}$			s denotes shaft
housing.		$0.682\Delta_{i,H}$	$0.667\Delta_{i,H}$	Applicable only for thermal considerations or for $\Delta_{is} < 0$
shaft.		$0.759\Delta_{i,s}$	$0.734\Delta_{i,s}$	
Free angle of contact	α_o	14.6	15.1	Nominal values @ 72°F
Installation angle of contact	α_o'	11.1	11.6	
Load angle of contact	α	12.7	13.3	
(2) Loads, Nominal Operation				
Axial, lbs	F_A	64		Preload
Radial, lbs	F_R	8		Due to dynamics

TABLE A (Continued)

Subject Item		Bearings		Remarks
		110 MM	90 MM	
(3) Hertzian Ellipse				
Major axis, inch	a	0.02661	.03750	At 64 lbs
Minor axis, inch	b	0.00279	.00352	
(4) Hertzian Stress lb/in^2	σ	60×10^3	62×10^3	
(5) Axial Stiffness of Bearings, lb/in		200,000	198,000	For 72°F
Note: Axial stiffness of housing and shaft approach $12\times10^{+6}$ and 10×10^6 lb/in, respectively and was not considered in the analyses				
(6) Friction Torque (Coulomb) in-oz				
Nominal	T_{fC}	5.42		As installed @ 72°F
Operational	T_{fC}	5.56		Orbital Environment (see Figure 8)
Viscous Drag.	T_v	17.00		Nominal operation at 60 RPM @ 72°F

TABLE A (Continued)

Subject Item	Bearings		Remarks
	110 MM	90 MM	
(7) Events of Interest*			*For constraints, refer to paragraphs 3.5.2.1, 3.5.2.2, 3.5.2.3, 3.5.2.4
• Temperature at which loose fit will occur between housing and bearing .	+241°F(1)	+275°F(1)	
• Housing temperature at which the bearing diametral clearance will no longer exist	-162°F(1)	-220°F(1)	
• Inner race temperature at which tight fit will occur between the shaft and ID_B	+70°F(2)	+49°F(2)	(1) Not a plausible temperature in view of orbital and thermal model data.
• Shaft temperature at which tight fit will occur between shaft and ID_B	+86°F(4)	+240°F(1)	(2) Plausible
• Shaft temperature at which diametral clearance no longer exists	118°F(1)	130°F(1)	(3) Not possible in view of orbital and thermal model data.
• Housing temperature at which the bearings' diametral clearance approaches zero	+34°F(3)	+26°F(3)	(4) Effect insignificant.
• Shaft outer race temperature at which bearing's diametral clearance no longer exists	340°F(1)	260°F(1)	(5) Inner race temperature less shaft temperature
• Inner race temperature gradient(5) which the bearings' diametral clearance approaches zero	+122°F(1)	+134°F(1)	(6) Average housing temperature less average shaft temperature
• Preload mechanism saturation gradient(6)	<67°F(1)		

TABLE A (Continued)

Subject Item	Temperature Gradients	Remarks
(7) Continued		
• Inner race temperature gradient[7] of the 90 MM bearing at which the diametral clearance no longer exists for orbital environment indicated on Figure 8.	37°F[1]	(7) Temperature of inner race less shaft temperature
• Friction torque increase from nominal of 0.5* in-oz is caused by gradient[7]. The gradient is. . .	37°F	*The small value is due to relative large load angle maintained by preload
• Inner race bearing (90 MM) temperature gradient[7] necessary to cause 60 in-oz torque increase is. . .	270°F[1]	Refer to Figure 9
• Preload mechanism is saturated at 40°F gradient between the inner race (90 MM bearing) and shaft. The gradient[8] necessary to cause 60 in-oz Δ torque is. . .	147°F[1]	(8) Average housing less average shaft temperature superimposed over orbital temperature of Figure 8
• Gradient[8] necessary to saturate the preload mechanism and produce 60 in-oz Δ torque is . . .	216°F[1]	
• Top bearing is misaligned. Gradient[8] necessary to cause total Δ torque of 60 in-oz is. . .	128°F[1]	
• Preload mechanism's axial clearance of 0.003 inch exits; top bearing is jammed by debries; gradient[8] producing Δ torque of 60 in-oz is . .	149°F[1]	

3.0 TECHNICAL DISCUSSION

3.1 Bearing Geometry

3.1.1 Coordinate Sets Definition (Refer to Figure 1)

Figure 1 is a geometric planar representation of the basic bearing elements, a ball, the outer and the inner races. The shown system is in a free state, that is, no forces act on it. The various geometric parameters indicated are defined in Table 1.

TABLE 1. Definitions of Parameters
(For the bearing in free state, refer to Figure 1 and Figure 2)

Inner race radius of curviture	ρ_i
Outer race radius of curviture	ρ_o
Reference ball radius	ρ_B
Distance from center of rotation to ball center	ρm
Distance from ball center to the inner race center	A_i'
Distance from ball center to the outer race center	A_o'
Clearance between the ball and the outer race	C_o
Clearance between the ball and the inner race	C_i
Coordinate set of the ball	X_B, Y_B, Z_B
Coordinate set of the inner race	X_i, Y_i, Z_i
Coordinate set of the outer race	X_o, Y_o, Z_o
Reference coordinate set defining axis of rotation	X_R, Y_R, Z_R
Rotational angles of vectors $\overline{\rho}_i, \overline{\rho}_o, \overline{\rho}_B$ about x_j axes	ϕ_i, ϕ_o, ϕ_B
Index, associated with inner race	i
Index, associated with outer race	o

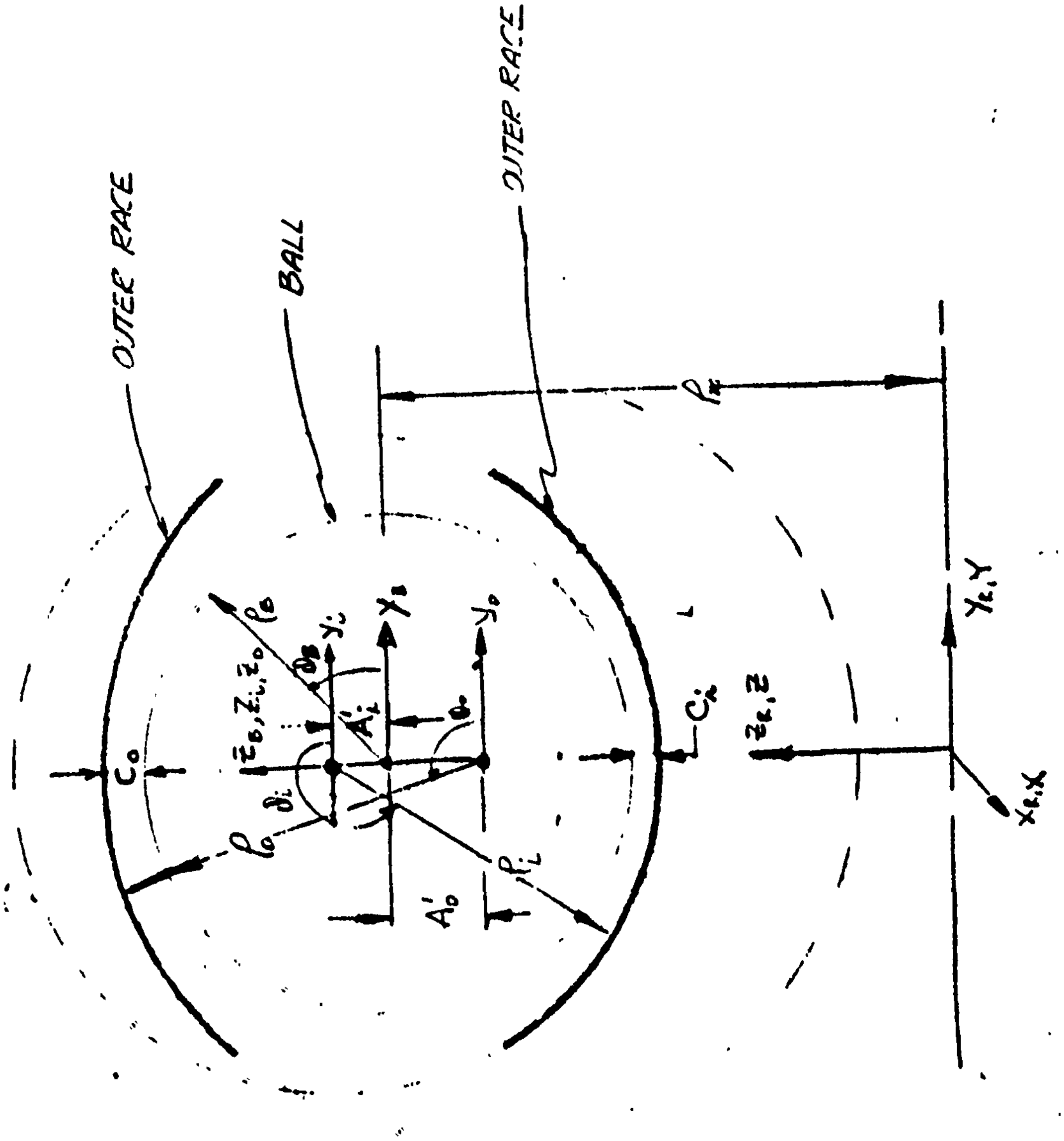

FIG 1 BALL BEARING GEOMETRY

3.1.2 Linear Transformation Equations

With respect to the reference coordinate set X_R, Y_R, Z_R (Figure 1), the coordinates of interest are linearily transformed as shown:

- **Reference Ball**

$$\left.\begin{aligned} X_B &= X_R \\ Y_B &= Y_R \\ Z_B &= Z_R - \rho_m \end{aligned}\right\} \quad \text{EQ 1}$$

also,

$$\left.\begin{aligned} X_R &= X_B \\ Y_R &= Y_B \quad = \rho_B \cos \phi_B \\ Z_R &= Z_{B+} \quad = \rho_m + \rho_B \sin \phi_B \end{aligned}\right\} \quad \text{EQ 2}$$

- **Outer Race**

$$\left.\begin{aligned} X_R &= X_o \\ Y_R &= Y_o \quad = \rho_o \cos\phi \\ Z_R &= Z_o + (\rho_m - A_o') = \rho_o \sin \phi_o + (\rho_m - A_o') \end{aligned}\right\} \quad \text{EQ 3}$$

- **Inner Race**

$$\left.\begin{aligned} X_R &= X_i \quad = X_i \\ Y_R &= Y_i \quad = \rho_i \cos \phi_i \\ Z_R &= Z_i \quad = \rho_i \sin \phi_i + (\rho_m + A_i) \end{aligned}\right\} \quad \text{EQ 4}$$

3.2 Free Angle of Contact (Figure 2)

The free angle of contact is defined as the angle made by a line segment with Z_B axis. The line segment is established by the contact points p_o and p_i, where p_o and p_i are point contacts of the ball surface with the outer and the inner races.

To derive the free contact angle α_o, let the reference ball coordinate set with respect to X_R, Y_R, Z_R remain fixed (Figure 1) and translate to inner and outer races' coordinate sets to the right and left of "Z_R axis, respectively, by the quantities $Y_R = a_i$, $Y_R = a_o$. The amplitudes of $|a_o|$

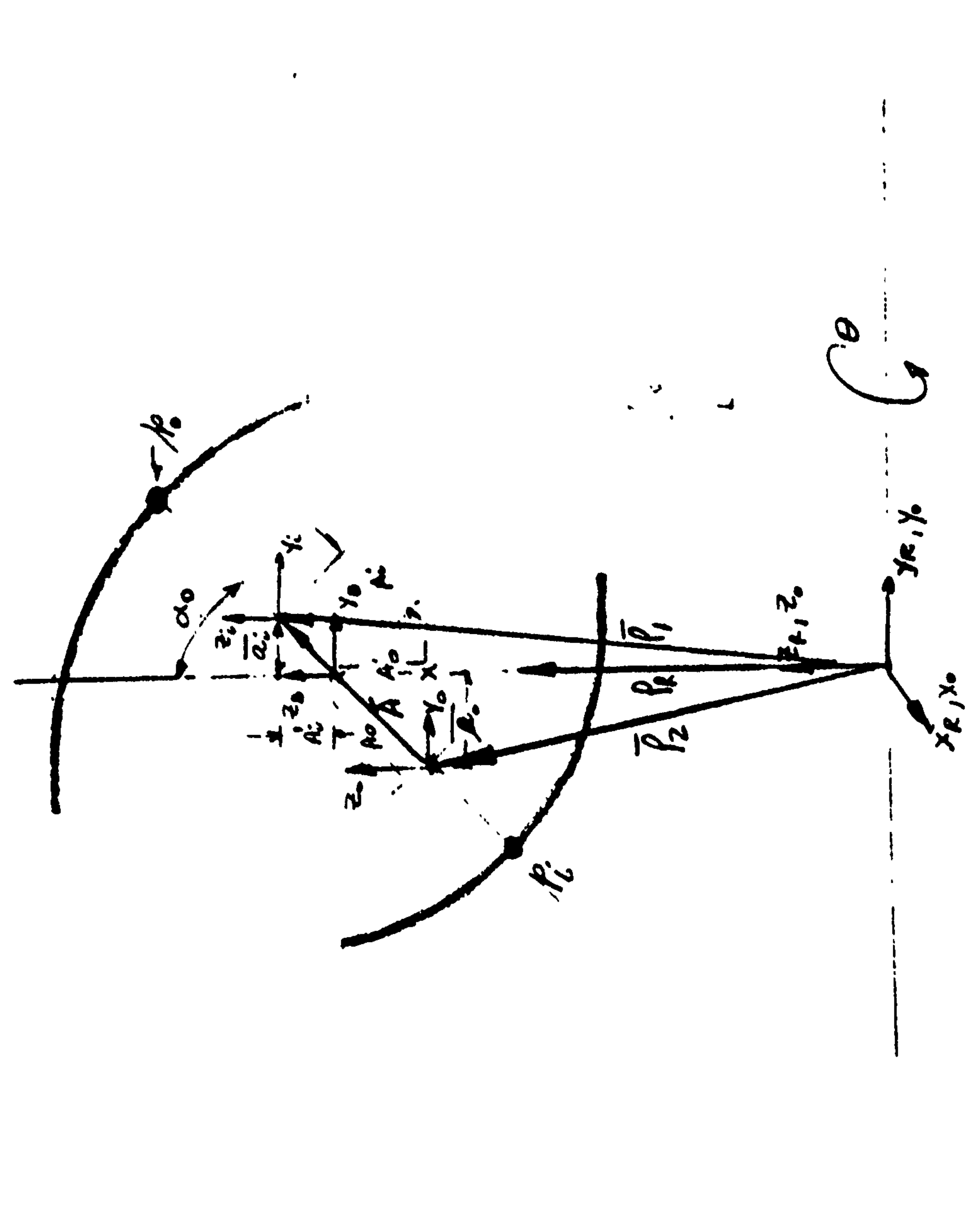

FIG 2 FREE CONTACT ANGLE

and $|a_i|$ must be such that the origins of the translated coordinate set (inner and outer races) will belong to the line segment connecting the points of contact "ρ_o" and "p_i". Analytically, this definition yields the following:

- Translation of the inner race's coordinate set

$$\left.\begin{aligned} X_{R,i} &= X_R = X_i = 0 \\ Y_{R,i} &= Y_R = Y_i + a_i = \rho_i(\cos\phi_i) + a_i \\ Z_{R,i} &= Z_R = Z_i + \rho_m + A_i = \rho_i \sin\phi_i + (\rho_m + A_i) \end{aligned}\right\} \quad \text{EQ 5}$$

- Translation of the outer race's coordinate set

$$\left.\begin{aligned} X_{R,o} &= X_R = X_o = 0 \\ Y_{R,o} &= Y_R = Y_o - a_o = \rho_o(\cos\phi_o) - a_o \\ Z_{R,o} &= Z_R = Z_o + (\rho_m - A'_o) = \rho_o \sin\phi_o + (\rho_m - A'_o) \end{aligned}\right\} \quad \text{EQ 6}$$

Since the origins of the translated coordinate sets belong to the line segment p_i, p_o, it follows that:

- $$\left.\begin{aligned} Y_{R,i} &= Y_{R,B} \\ \rho_i \cos\phi_i + a_i &= \rho_B \cos\phi_{B,i} \end{aligned}\right\} \quad \text{EQ 7}$$

- $$\left.\begin{aligned} Z_{R,i} &= Z_{R,B} \\ \rho_i \sin\phi_i + (\rho_m + A_i) &= \rho_B (\sin\phi_{Bi}) + \rho_m \end{aligned}\right\} \quad \text{EQ 8}$$

- $$\phi_i = \phi_{B,i} = 270° - \alpha_o \quad \text{EQ 9}$$

- $$\left.\begin{aligned} Y_{R,o} &= Y_{R,B} \\ \rho_o \cos\phi_o - a_o &= \rho_B \cos\phi_{B,o} \end{aligned}\right\} \quad \text{EQ 10}$$

$$Z_{R,o} = Z_{RB}$$

$$\left.\begin{array}{l} Z_{R,o} = Z_{RB} \\ \rho_o \sin \phi_o + (\rho_m - A_o') = \rho_B \sin \phi_{B,o} + \rho_m \end{array}\right\} \quad \text{EQ 11}$$

- $\phi_o = \phi_{B,o} = \alpha_o + 180°$ EQ 12

Substitution of EQ 9 into EQ 7 and 8 and EQ 12 into EQ 10 and 11 yields,

$$a_i = (\rho_i - \rho_B) \sin \alpha_o \qquad \text{EQ 13}$$

$$A_i' = (\rho_i - \rho_B) \cos \alpha_o \qquad \text{EQ 14}$$

$$a_o = (\rho_o - \rho_B) \sin \alpha_o \qquad \text{EQ 15}$$

$$A_o' = (\rho_o - \rho_B) \cos \alpha_o \qquad \text{EQ 16}$$

From the condition of contact it is also known that:

$$A_i = (\rho_i - \rho_B) \qquad \text{EQ 17}$$

$$A_o = (\rho_o - \rho_B) \qquad \text{EQ 18}$$

$$(A_i + A_o) = \rho_o + \rho_i - 2\rho_B \qquad \text{EQ 19}$$

From the condition of free state (Figure 1) the following relationship can be observed:

$$\rho_i = C_i + A_i' + \rho_B \qquad \text{EQ 20}$$

$$\rho_o = C_o + A_o' + \rho_B \qquad \text{EQ 21}$$

Taking the sum of EQ 21 and EQ 22 results in:

$$\rho_i + \rho_o = (C_i + C_o) + (A_i' + A_o') + 2\rho_B \qquad \text{EQ 22}$$

Noting that:

$$(C_i + C_o) = \frac{C_D}{2}, \quad C_D = \text{total diametral clearance}$$
(refer to Figure 1)

$(A_i'+A_o') = (A_i+A_o) \cos \alpha_o$ (from EQ's 14, 16, 17, 19)

$(A_i'+A_o') = A \cos \alpha_o$

where: A = distance between centers of curvatures

$$A = (\rho_o+\rho_i)-2\rho_B = [(\rho_o+\rho_i)-D] = D[f_i+f_o-1]$$

$D = 2\rho_B$ = diameter of the ball

$[\rho_i+\rho_o] = (f_o+f_i)D \quad ; \quad f_i = \rho_i D^{-1}$

Equation 22 takes on the following forms:

$$D(f_o+f_i) = \frac{C_D}{2}+(A \cos \alpha_o)+D$$

$$A = \frac{C_D}{2}+A \cos \alpha_o$$

from which

$$\text{Cos } \alpha_o = [1-\frac{C_D}{2A}] \qquad \text{EQ 23}$$

- Summary of parametric relationships

$$a_i = (\rho_i-\rho_B) \sin \alpha_o = D[f_i-\tfrac{1}{2}] \sin \alpha_o = D[f_i-.5][\frac{C_D}{A}(1-\frac{C_D}{2A})]^{1/2}$$

$$a_o = (\rho_o-\rho_B) \sin \alpha_o = D[f_o-.5] \sin \alpha_o$$

$$A_i = D(f_i-.5) \cos \alpha_o = A_i \cos \alpha_o$$

$$A_o' = D[f_o-.5] \cos \alpha_o = A_o \cos \alpha_o$$

$$A = (A_i+A_o) = (f_o+f_i-1)D = (\rho_o+\rho_i-D)$$

$$\alpha_o = \cos^{-1}[1-\frac{C_D}{2A}]$$

$$C_i = (\rho_i-\rho_B)[1-\cos \alpha_o]$$

$$C_o = (\rho_o-\rho_B)[1-\cos \alpha_o]$$

$$C_i+C_o = \frac{C_D}{2}$$

- Contact angles

The specific values of the free contact angle (α_0) are calculated as shown in Table II.

TABLE II. Free Contact Angle Calculation for 777 DMA Bearings

Parameters		Bearings 110 mm	Bearings 90 mm
Diametral clearance (inch),	$C_{D(min)}$	0.0013	.0013
Focus inner race (inch),	$f_{i(min)}$	0.515	.515
Focus outer race (inch),	$f_{o(min)}$	0.525	.525
Ball Diameter (inch),	D	0.500	.4687
Length, between centers of radii of curvature (inch),	$A = (f_i+f_o-1)D$	0.02000	.018748
Contact angle (degrees),	$\alpha_o = \cos^{-1}[1-\frac{C_D}{2A}]$	14.647	15.1314

NOTE: The given angles are contact angles arising from the smallest possible diametral clearances and the smallest focii.

3.3 Contact Angle Due to Axial, Radial and Moment Loads

Refering to Figure 2 note that the vector $\bar{A}$ representing the distance between the centers of curvatures in X_R, Y_R, Z_R coordinate is given by

$$A = \bar{\rho}_1-\bar{\rho}_2 \qquad \text{EQ 24}$$

Let the bearing be subjected to axial, radial and moment loading and assume that the outer race is fixed with respect to coordinate set X_o, Y_o, Z_o (Figure 2). Also assume that the elastic displacements due to the applied loads act only on the inner race.

For the stated conditions, the radius of curvature of the outer race ($\bar{\rho}_o'$) is allowed perfect motion about the bearing rotation axis Y_1. The components of this rotating vector, with respect to the reference coordinate set, is given by

$$\begin{bmatrix} q_{XR} \\ q_{YR} \\ q_{ZR} \end{bmatrix} = \begin{bmatrix} \cos\theta & 0 & \sin\theta \\ 0 & 1 & 0 \\ -\sin\theta & 0 & \cos\theta \end{bmatrix} \begin{bmatrix} 0 \\ 0 \\ \rho_0' \end{bmatrix} \qquad \text{EQ 25}$$

where:

θ = rotational angle about Y_1

q_{jR} = components of vector ρ_0'

ρ_0' = absolute value of vector ρ_0'

Notice that for any rolling element the radius of curvature (any ball) is given in the Y_R, Z_R place by

$$\overline{\rho_0'} = \hat{i}_R(o)+\hat{j}_R(o)+\hat{K}_R\rho_0' \cos\theta \qquad \text{EQ 26}$$

or

$$\overline{\rho_0'} = \hat{i}_R(o)+\hat{j}_R(o)+\hat{k}_R(\rho_i' \cos\theta - A\cos\alpha_o)$$

where:

$$\rho_0' = [\rho_m+[f_i-.5]D\cos\alpha_o](\cos\theta)-A\cos\alpha_o$$

$$\rho_0' = [\rho_i'(\cos\theta)-A\cos\alpha_o]$$

$$\rho_i' = [\rho_m+(f_i-.5)D\cos\alpha_o]$$

$$f_i = \rho_i/D$$

From which the vector $\overline{\rho_2}$ in the Y_R, Z_R plane becomes

$$\overline{\rho_2} = \hat{i}_R(o)-\hat{j}_R A_o(\sin\alpha_o)+\hat{k}_R[\rho_i'(\cos\theta)-A\cos\alpha_o] \qquad \text{EQ 27}$$

<u>NOTE</u>: Refer to Figure 2.

The inner race's radius $\overline{\rho_i'}$ undergoes both transtation and rotation. Its position is defined as shown on Figure 3.

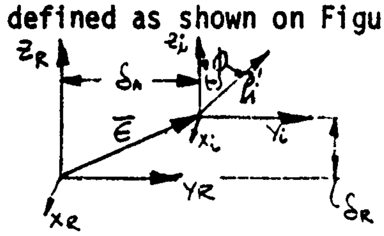

δ_A = axial displacement
δ_R = radial displacement
ϕ = misalignment angle

<u>FIGURE 3. Rotation and Translations of Vector $\overline{\rho_i'}$</u>

The components of the translation vector $\bar{\varepsilon}$ in the X_R, Y_R, Z_R coordinate set is

$$\begin{bmatrix} \varepsilon_{XR} \\ \varepsilon_{YR} \\ \varepsilon_{XR} \end{bmatrix} = \begin{bmatrix} \cos\Theta & 0 & \sin\Theta \\ 0 & 1 & 0 \\ -\sin\Theta & 0 & \cos\Theta \end{bmatrix} \begin{bmatrix} 0 \\ \delta_A \\ \delta_R \end{bmatrix} \qquad \text{EQ 28}$$

and for any ball the effect of the translation $\bar{\varepsilon}$ are given in the Y_R, Z_R plane as

$$\bar{\varepsilon} = \hat{i}_R(o)+\hat{j}_R(\delta_R)+\hat{k}_R\delta_R \cos\Theta \qquad \text{EQ 29}$$

With respect to the X_i, Y_i, Z_i, the components of the vector $\bar{\rho}_i'$ are defined by

$$\begin{bmatrix} q_{Xi} \\ q_{Yi} \\ q_{Zi} \end{bmatrix} = \begin{bmatrix} \cos\Theta & 0 & \sin\Theta \\ -\sin\Theta\sin\phi & \cos\phi & \cos\Theta\sin\phi \\ -\sin\Theta\cos\phi & -\sin\phi & \cos\Theta\cos\phi \end{bmatrix} \begin{bmatrix} 0 \\ 0 \\ \rho_i' \end{bmatrix} \qquad \text{EQ 30}$$

where: ϕ = misalignment angle

For small ϕ the vector $\bar{\rho}_i'$ in the X_i, Y_i, Z_i coordinate set is defined by

$$\bar{\rho}_i' = \hat{i}_i(\rho_i' \sin\Theta)+\hat{j}_i(\rho_i'\phi\cos\Theta)+\hat{k}_i\rho_i' \cos\Theta \qquad \text{EQ 31}$$

Linear translation into the X_R, Y_R, Z_R set via EQ 29 yields

$$\bar{\rho}_i = \hat{i}_R(\delta_R+\rho_i')(\sin\Theta)+\hat{j}_R(\delta_A+\rho_i\phi\cos\Theta)+\hat{k}_R(\delta_R\cos\theta+\rho_i'\cos\theta) \qquad \text{EQ 32}$$

From which the vector $\bar{\rho}_1$ is derived by setting $\hat{i}_R = 0$ and adding the vector $\bar{a}_i$. Hence

$$\bar{\rho}_1 = \hat{i}_R(o)+\hat{j}_R[\delta_A+\rho_i'\phi(\cos\Theta)+A_i \sin\alpha_o]+\hat{K}_R(\delta_R\cos\theta+\rho_i'\cos\theta) \qquad \text{EQ 33}$$

From EQ 24

$$\bar{A} = \bar{\rho}_1 - \bar{\rho}_2 = A\{\hat{i}_R(o) + \hat{j}_R(\bar{\delta}_A + \rho_i\phi \cos\Theta + \sin\alpha_o) + \hat{k}_R(\delta_R\cos\theta + A\cos\alpha_o)\}$$

where

$$\bar{\delta}_A = \delta_A/A; \quad \bar{\delta}_R = \delta_R/A; \quad \bar{\phi} = \phi/A \qquad \text{EQ 34}$$

Defining the load contact angle in terms of the vector cross product yields

$$\sin\alpha = \frac{\bar{\rho}_R \times \bar{A}}{|\rho_R||A|}$$

$$\sin\alpha = \frac{[\bar{\delta}_A + \rho_i'\bar{\Theta}\cos\Theta + \sin\alpha_o]}{\{[\bar{\delta}_A + \rho_i'\phi\cos\Theta + \sin\alpha_o]^2 + [\bar{\delta}_R\cos\theta + \cos\delta_p]^2\}^{1/2}} \qquad \text{EQ 35}$$

and in terms of the vector dot product yields

$$\cos\alpha = \frac{\bar{\rho}_R \cdot \bar{A}}{|\rho_R|\cdot|A|}$$

$$\cos\alpha = \frac{[\delta_R\cos\theta + \cos\alpha_o]}{\{[\bar{\delta}_A + \rho_i'\phi\cos\Theta + \sin\alpha_o]^2 + [\delta_R\cos\theta + \cos\alpha_o]^2\}^{1/2}} \qquad \text{EQ 36}$$

The change of contact angle has an effect on the bearing's stiffness and its normal loads, as well as the bearing friction. Particular utilization of the derived load contact angle equations will be made in conjunction with the bearing ball forces and friction torque evaluations.

3.4 Installation Fit Up

3.4.1 Introduction

The bearing installation with interference fits has an effect on the diametral clearance of the bearings. The amount of decrease of the diametral clearance is solved by using the elastic thick ring theory. The same expressions can be used for computing the clearance due to uniform heating or cooling of the bearings, the shaft and the housing.

3.4.2 Applicable Equations

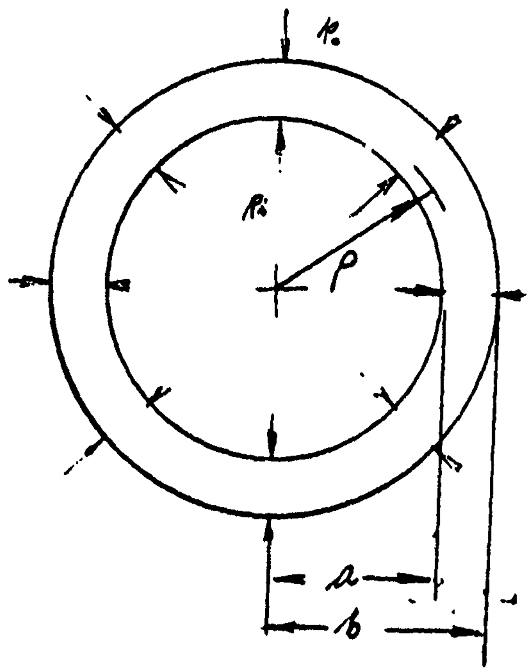

FIGURE 4. Thick Ring Under External and Internal Pressure

From reference (3), page 241, and Figure 4, the deformation of a cylinder due to external p_o and internal pressures p_i is given by

$$\Delta = [\frac{(1-\xi)}{E}] \frac{a^2p_i-b^2p_o}{(b^2-a^2)}\rho + \frac{(1-\xi)}{E}\frac{a^2b^2(p_i-p_o)}{(b^2-a^2)\rho} \qquad \text{EQ 37}$$

where:

Δ = total radial displacement inch

ξ = Poisson's ratio

E = Young's modulus

a = internal radius

b = external radius

ρ = radius to any desired point

For the condition of $p_o = 0$, $\rho = a$ the radial increase of the radius "a" is

$$\Delta_a = a\frac{p_i}{E}\left(\frac{a^2+b^2}{(b^2-a^2)} + \xi\right) \qquad \text{EQ 38}$$

When the cylinder is subject to external pressure only (pi = 0), the radial decrease of the external radius b for ρ = b becomes

$$\Delta_b = -\frac{pb_o}{E}\left(\frac{a^2+b^2}{b^2-a^2} - \xi\right) \qquad \text{EQ 39}$$

For the condition of the bearing inner race mounted on a shaft larger than the bore diameter of the inner race,

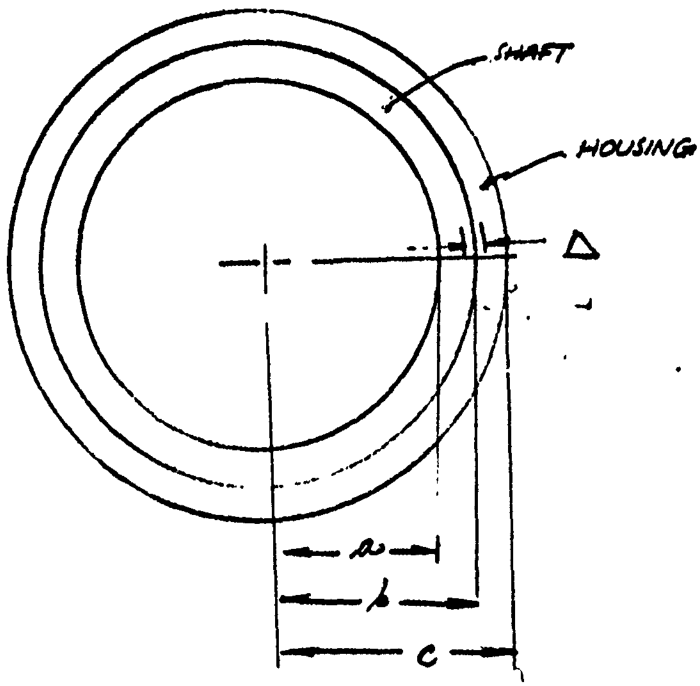

FIGURE 5. Shaft and Inner Race Interference

the total radial deflection Δ at the inner race radius b is

$$\Delta = p\frac{b}{E_s}\left[\frac{a^2+b^2}{b^2-a^2} - \xi_s\right] + p\frac{b}{E_B}\left[\frac{b^2+c^2}{(C^2-b^2)} + \xi_B\right] \qquad \text{EQ 40}$$

Δ = total interference, (radial)

E_s = Young's modulus of shaft = 44×10^6 lb/in^2
E_B = Young's modulus of bearing = 29×10^6 lb/in^2
ξ_s = Poisson's ratio of shaft = .025
ξ_B = Poisson's ratio of bearing = .25

and the shaft pressure is:

$$p_s = \frac{\Delta}{b[\frac{1}{E_S}(\frac{a^2+b^2}{(b^2-a^2)} - \xi_S) + \frac{1}{E_B}(\frac{b^2+c^2}{c^2-b^2} + \xi_B)]} \qquad \text{EQ 41}$$

From EQ 37 the radial increase of the inner race's outside radius ξ becomes

$$\Delta_c = \frac{2b^2cp}{E_b[c^2-b^2]} \qquad \text{EQ 42}$$

Substitution of EQ 41 yields the radial increase of the inner race outside diameter d_i due to shaft interference

$$\Delta C_{D,S} = \frac{2\Delta_{i,s}(\frac{c}{b})}{[(\frac{c}{b})^2-1]\{\frac{E_B}{E_S}[\frac{(\frac{b}{a})^2+1}{(\frac{b}{a})^2-1} - \xi_S] + [\frac{(\frac{c}{b})^2+1}{(\frac{c}{b})^2-1} + \xi_B]} \qquad \text{EQ 43}$$

where: $\Delta_{i,s}$ = value of interference between the shaft and the inner race. In terms of the bearing parameters and in accordance with the following definitions

$$\frac{c}{b} = \frac{\text{outside diameter of the inner race (di)}}{\text{inside diameter of the inner race (Bore)}} = R_{1,s}$$

$$\frac{b}{a} = \frac{\text{inside diameter of the inner race (Bore)}}{\text{inside diameter of the shaft}} = R_{2,s}$$

$\Delta C_{D,S}$ = decrease in diametral clearance of the bearing due to shaft interference

EQ 43 becomes

$$\Delta C_{D,S} = \frac{2\Delta_{i,s}\ R_{1,s}}{(R^2_{1,s}-1)\{(\frac{E_B}{E_S})[\frac{R^2_{2,s}+1}{R^2_{2,s}-1} - \xi_S] + [\frac{R^2_{1,s}+1}{R^2_{1,s}-1} + \xi_B]} \qquad \text{EQ 44}$$

For the condition of interference fit between the housing and the outside diameter of the outer race from EQ 38 and 39, the total radial interference at ρ = b becomes

$$\Delta = pb\{\frac{1}{E_H}(\frac{c^2+b^2}{c^2-b^2} + \xi_H) + \frac{1}{E_B}(\frac{b^2+a^2}{b^2-a^2}) - \xi_B)\} \qquad \text{EQ 45}$$

Hence, the pressure between the interfacing surfaces is

$$p_H = \frac{\Delta}{b\{\frac{1}{E_H}(\frac{c^2+b^2}{c^2-b^2}+\xi_H) + \frac{1}{E_B}(\frac{b^2+a^2}{b^2-a^2}-\xi_B)\}} \qquad \text{EQ 46}$$

From EQ 37 for the condition of $p = p_o$, $\rho = a$ the radial decrease of the inner radius of the outer race (ρ_o) is

$$\Delta_a = \frac{2b^2ap}{E_B[b^2-a^2]} \qquad \text{EQ 47}$$

and that leads to the radial decrease of the bearing fit up

$$\Delta C_{D,H} = \frac{2\Delta_{i,H}\frac{b}{a}}{(\frac{b^2}{a^2}-1)\{\frac{E_B}{E_H}[\frac{(\frac{c}{b})^2+1}{(\frac{c}{b})^2-1}+\xi_H] + [\frac{(\frac{b}{a})^2+1}{(\frac{b}{a})^2-1}-\xi_B]\}} \qquad \text{EQ 48}$$

Denoting:

$\Delta C_{D,H}$ = Diameteral clearance change due to housing interference

$\Delta_{i,H}$ = total diameteral interference

$\frac{b}{a} = \frac{\text{outside diameter of outer race (OD)}}{\text{inside diameter of outer race}} = R_{1,H}$

$\frac{c}{b} = \frac{\text{outside diameter of housing}}{\text{outside diameter of outer race}} = R_{2,H}$

ξ_H, ξ_B = Poisson's ratios for housing and bearing

Substitution of the above parameters into EQ 49 yields

$$\Delta C_{D,H} = \frac{2\Delta_{i,H}R_{1,H}}{(R^2_{1,H}-1)\{\frac{E_B}{E_H}[\frac{(R^2_{2,H}+1)}{(R^2_{2,H}-1)}+\xi_H] + \frac{R^2_{1,H}+1}{R^2_{1,H}-1}-\xi_B]\}} \qquad \text{EQ 49}$$

3.4.3 Calculation of Diametral Clearance Changes (Data)

Table III. Critical Tolerance Data

	DMA Main Bearings	
	110 MM	90 MM
• Bearings:		
OD_B (inch) - max	5.9055	4.9213
- min	5.9051	4.9209
ID_B (inch) - max	4.33070	3.54330
- min	4.33045	3.54305
• Shaft:		
OD_S (inch) - max	4.3304	3.5426
- min	4.3301	3.5423
• Housing:		
ID_H (inch) - max	5.9051	4.9209
- min	5.9047	4.9205
• Clearances - Shaft & Inner Race		
ID_B (max)	4.33070	3.54330
OD_S (min)	4.33010	3.54230
	+ .00060	+ .00100
ID_B (min)	4.33045	3.54305
OD_S (max)	4.33040	3.54260
	+ .00005	+ .00045
• Clearances - Housing and Outer Race		
$(ID)_H$ max	5.9051	4.9209
$(OD)_B$ min	5.9051	4.9209
	0.0000	0.0000
$(ID)_H$ min	5.9047	4.9205
$(OD)_B$ max	5.9055	4.9213
	(-)0.0008	(-)0.0008

Note: Positive sign denotes looseness and negative sign denotes interference fit.

Table IV. Calculation of Diametral Changes

Parameters	Bearings	
	110 MM	90 MM
Outside diameter of inner race (d_i), inch		
$d_{i,j} = d_{m,j} - (D + \frac{C_D}{2})$, inch	5.1400	4.2400
Pitch diameter (dm), inch	5.1400	4.2400
D = Ball diameter, inch	0.5000	0.4687
C_D = Diametral clearance of bearings, inch. . . .	1.3×10^{-3}	1.3×10^{-3}
$d_{i,1}$ = 5.1400-(.5000+.00065), inch	4.639350	
$d_{i,2}$ = 4.2400-(.4687÷.00065), inch		3.73935
Inside diameter of the inner race = ID_B, inch . . .	4.330575	3.543175
Inside diameter of the shaft = ID_S, inch . . .	3.740000	3.20000
Outside diameter of the outer race = OD_B, inch . .	5.9053	4.9211
Inside diameter of the outer race (do)		
$d_{o,j} = d_{m,j} + (D + \frac{C_D}{2})$, inch		
$d_{o,1}$ = 5.1400+(.5000+.00065), inch	5.64065	
$d_{o,2}$ = 4.2400+(.4687+.00065), inch		4.740650
$R_{1,S} = \frac{d_{i,1}}{ID_{B,1}} = \frac{4.639350}{4.330575}$ = ...	1.07130	
$R_{1,S} = \frac{d_{i,2}}{ID_{B,2}} = \frac{3.73935}{3.543175}$ = ...		1.05537
$R_{2,S} = \frac{ID_B}{ID_S} = \frac{4.330575}{3.74000}$ = ...	1.15791	
$R_{2,S} = \frac{ID_B}{ID_S} = \frac{3.543175}{3.20000}$ = ...		1.10724

TABLE IV. CONTINUED

Parameters	Bearings 110 MM	Bearings 90 MM
$R_{1,H} + \frac{OD_B}{do} = \frac{5.9053}{5.64065} = \ldots\ldots\ldots\ldots$	1.0469	
$R_{1,H} = \frac{OD_B}{do} = \frac{4.9211}{4.74065} = \ldots\ldots\ldots\ldots$		1.0381
$R_{2,H} = \frac{OD_H}{OD_B} = \frac{6.3000}{5.9053} = \ldots\ldots\ldots\ldots$	1.066983	
$R_{2,H} = \frac{OD_H}{OD_B} = \frac{5.1700}{4.9211} = \ldots\ldots\ldots\ldots$		1.05058
Young's modulus ratios, $E_B/E_H = E_B/E_S$	0.6591	
Poisson's Ratio, bearing ξ_B	.250	
Note: Housing and shaft Poisson's ratios $\xi_H = \xi_S = .025$		
Interference fit at housing interface = $\Delta_{i,H}$(inch) (Table III)	(-)0.0008	
Decrease of diametral clearance at housing interface (EQ 49) = $\Delta C_{D,H}$ = ...	$.682\ \Delta_{i,H}$	$.667\Delta_{i,H}$
Decrease of diametral clearance at shaft interface (EQ 45) = $\Delta C_{D,S}$ = ...	$.759\ \Delta_{i,S}$	$.734\Delta_{i,S}$
Note: $\Delta C_{D,j}$ to be used whenever applicable in consideration of thermal effects.		

3.4.4 Calculation of Installation Contact Angles

The no load value of the contact angles for the DMA bearings that include the effect of the interference fits are given in Table V. Normally, the interference fits are 80% efficient. The reduction of the interference is due to surface condition, and in our case, it approaches the value of 0.00016 inch. Table V does not include this effect in order to compensate for the bearing runouts.

TABLE V
INSTALLATION (NO LOAD) DMA BEARINGS' CONTACT ANGLES

Remarks	Parameters	Bearings	
		110 MM	90 MM
	Diametral Clearance, inch C_D	0.0013	
See Table III	Interference housing, inch $\Delta_{i,H}$	-0.0008	
See Table III	Distance between centers of curvatures, inch A	0.02000	0.018748
	Decrease in diametral clearance, inch		
See Table IV	• $\Delta C_{D,H} = .682\ \Delta_{i,H}$	-5.456×10^{-4}	
See Table IV	• $\Delta C_{D,H} = .667\ \Delta_{i,H}$		-5.336×10^{-4}
	Contact Angle, degree $\alpha'_o = \cos^{-1}\left[1-\frac{C_D + C_{D,H}}{2A}\right]$, degree	11.15	11.62

3.5 Bearing Friction Torques

3.5.1 Qualitative Aspect of the Bearing Friction Torque

The bearings' Coulomb friction is dominantly a function of the co-tangent of the load contact angle and the magnitude of the axial or thrust load. (Radial loads were not considered inasmuch as their amplitudes are small for the case of the spacecraft's platform despun condition.) The load contact angle itself varies directly at the bearing's elastic deflection and inversely as the algebraic sum of the bearings' initial diametral clearance and the shaft's and the housing's diametral changes. The latter are induced by initial bearing fits onto the housing and the shaft and the temperature variations of these elements. The functional relationships of the bearing friction torque imply that its increase is affected by either (1) diametral changes of the housing and the bearings in a direction that reduces the contact angle; or (2) an increase of the thrust load; or (3) simultaneous occurrences of both factors. In paragraphs that follow, first the necessary analytical expressions are formulated from which the bearing friction values are calculated for several hypothesized suspension system's malfunctions and the DMA's temperature gradients.

3.5.2 Analytical Formulations

3.5.2.1 Orbital Temperature

- Remarks

The following temperature expressions represent diurnal orbital temperatures of the DMA. For the purpose of the analyses, the temperature equations represent the temperature differences with respect to 72°F level. (The latter was the assembly temperature level of the DMA.) The function values at time t = 0 are these occuring at 24:00 hours 'zulu' time on 8 September 1975.

- Housing Temperature

$$T_H = A_1 + B_1 \sin(\omega t - \delta_1), \text{ °F}$$

$$T_H = 4 + 6 \sin(15t - 135°), \text{ °F} \qquad \text{EQ 50}$$

where

T_H = housing temperature difference from 72°F reference

t = time, hours

- Top Bearing Temperature (TBT)

NOTE: TBT is the shaft temperature measured in the neighborhood of the inner race of the 90 MM bearing.

$$T_{s2} = A_{2,2} + B_{2,2} \sin(\omega t - \delta_{2,2}), \text{ °F}$$

$$T_{s2} = 1 + 4 \sin(15t - 180°), \text{ °F} \qquad \text{EQ 51}$$

- Bottom Bearing Temperature (BBT)

NOTE: TBT is the shaft temperature taken in the neighborhood of the inner race of the 110 MM bearing.

$$T_{s1} = A_{2,1} + B_{2,1} \sin(\omega t - \delta_{2,1}), \text{ °F}$$

$$T_{s1} = -4.5 + 3.5 \sin(15t - 158°), \text{ °F} \qquad \text{EQ 52}$$

3.5.2.2 Radial Expansion of Elements due to Temperature

- **Basic Equation**

$$\Delta C_D = K_{1,j}[-\Delta i_{H,j}+(\beta_H-\beta_B)(T_H)OD_{B,j}] +$$

$$K_{2,j}\{\Delta i_{s,j}+ID_{B,j}[\beta_B(T_{B,j})-\beta_s(T_{s,j})]+ \qquad \text{EQ 53}$$

$$\beta_B[d_{o,j}T_H-d_{i,j}(T_{B,j})]$$

$$= \Delta_{1,j} + \Delta_{2,j} + \Delta_{3,j}$$

where

$\Delta_{1,j}$ = change in diametral clearance due to press fit of the outer race and the bearing and the housing temperature variations; outer race and the housing temperature are assumed to be equal in amplitude and time phase.

$\Delta_{2,j}$ = change in the diameteral clearance due to temperature; because both bearings are loose fitted onto the shaft, Δ_2 will be effective in changing the diametral clearances only when

$$\Delta_2 < 0$$

$\Delta_{3,j}$ = change in diameteral clearance due to temperature difference between the outer race and the inner race; both elements are subject to uniform circumferential temperatures

j = 1 refers to 110 MM bearing

j = 2 refers to 90 MM bearing

$\Delta i_{H,j}$ = value of interference at housing interface

$\Delta i_{s,j}$ = value of interference at shaft interface

(+) = the interference values associated with (+) are loose fits

(-) = the interference values associated with (-) are tight fits

$\beta_H = \beta_S$ = coefficient of expansion, (housing = shaft) = $6.4 \times 10^{-6} \frac{in}{in°F}$

β_B = coefficient of expansion, bearing elements = 5.6×10^{-6}

$T_{B,j}$ = inner race temperature less 72°F = $T_{s,j} + \Delta T_{B,j}$

$\Delta T_{B,j}$ = temperature gradient between shaft and inner race

$T_{s,j}$ = shaft temperature (°F) less 72°F

$T_{H,j}$ = housing temperature less 72°F

OD_B = outside diameter of bearing, inch

ID_B = inside diameter of bearing, inch

d_o = inside diameter of outer race, inch

d_i = inside diameter of inner race, inch

$K_{1,j}$ = compression coefficient, refer to $\Delta C_{D,H}$ in Table IV

$K_{2,j}$ = compression coefficient, refer to $\Delta C_{D,s}$ in Table IV

o <u>Specific Development of Expansion Equation Components</u>

In terms of specific values:

(1) <u>Consider $\Delta_{1,j}$:</u>

$$\Delta_{1,1} = .682\{-800+(.8)(5.905)[T_H(t)]\}\times 10^{-6}$$
$$\Delta_{1,2} = .667\{-800+(.8)(4.921)[T_H(t)]\}\times 10^{-6}$$ EQ 54

(2) <u>Consider $\Delta_{2,j}$</u>

$$\Delta_{2,1} = .76\{50+4.33[-.8(T_{s1})+5.6\Delta T_{B1}]\}10^{-6}$$
$$\Delta_{2,2} = .74\{450+3.54[-.8(T_{s2})+5.6\Delta T_{B2}]\}10^{-6}$$ EQ 55

(3) <u>Consider $\Delta_{3,j}$</u>

$$\Delta_{3,1} = 5.6\times 10^{-6}[5.64T_H-4.64(T_s+\Delta T_{B1})]$$
$$\Delta_{3,2} = 5.6\times 10^{-6}[4.74T_H-3.74(T_s+\Delta T_{B2})]$$ EQ 56

- <u>Specific Development of the Diametral Clearance Reduction Equation</u>

EQ 53 can be rearranged to the form

$$\Delta C_D = A^{*}+C_{1,j} \sin (\omega t-\delta_{1,j})+C_{2,j} \sin (\omega t-\delta_{2,j}) \qquad \text{EQ 57}$$

where

$$A^{*} = K_{1,j}[-\Delta i_{H,j}+(\beta_H-\beta_B)OD_{B,j}A_{1,j}]+\beta_B(d_{o,j}A_{1,j}-d_{i,j}A_{2,j})$$

$$C_{1,j} = B_{1,j}[K_{1,j}(\beta_H-\beta_B)OD_{B,j}+d_{o,j}\beta_B]$$

$$C_{2,j} = -\beta_B B_{2j} di,j$$

$$A'_{2,j} = A_{2,j}+\Delta T_{B,j}$$

EQ 57 is further reduced to

$$\Delta C_D = A_j^{*}+B_j^{*} \sin (\omega t-\delta^{*}) \qquad \text{EQ 58}$$

where

$$\delta^{*} = \tan^{-1}\left[\frac{-C_{1,j} \sin \delta_{1,j}+C_{2,j} \sin \delta_{2,j}}{C_{1,j} \cos \delta_{1,j}-C_{2,j} \sin \delta_{2,j}}\right] = \tan^{-1}\left(\frac{K_{3,j}}{K_{4,j}}\right)$$

$$B^{*} = [K_{3,j}^2+K_{4,j}^2]^{1/2}$$

<u>Note</u>: The specific considerations of the components of the radial expansion equation leads to the conclusion that the closure of the gap between the bore of the 90 MM bearing and the shaft due to temperature gradient is remote. Hence, the component $\Delta_{2,2}$ will not be considered in the subsequent evaluations. The component $\Delta_{2,1}$ will also be neglected in as much as its contribution is not significant. Also, in further considerations of the 110 MM bearing, the bore to the shaft fit up will be taken as line to line (zero clearance).

The specific computation constants for EQ 58 are given in Table VI.

TABLE VI. COMPUTATION CONSTANTS

<table>
<tr><th rowspan="2">Parameter</th><th colspan="2">Value</th></tr>
<tr><th>110 MM Brg</th><th>90 MM Brg</th></tr>
<tr><td>$K_{1,j}$ . . . .</td><td>.6824</td><td>.6672</td></tr>
<tr><td>$\Delta_{i,H}$, inch . . . .</td><td colspan="2">0.0008</td></tr>
<tr><td>$(\beta - \beta_B)$, $°F^{-1}$ in/in . . . .</td><td colspan="2">0.8×10^{-6}</td></tr>
<tr><td>OD_B, inch . . . .</td><td>5.9053</td><td>4.9211</td></tr>
<tr><td>$A_{1,j}$, °F . . . .</td><td colspan="2">4.0</td></tr>
<tr><td>β_B . . . .</td><td colspan="2">5.6×10^{-6}</td></tr>
<tr><td>$d_{o,j}$, inch . . . .</td><td>5.64065</td><td>4.740650</td></tr>
<tr><td>$d_{i,j}$, inch . . . .</td><td>4.63935</td><td>3.73935</td></tr>
<tr><td>$A_{2,j}$, °F . . . .</td><td>-4.5</td><td>+1.0</td></tr>
<tr><td>$\Delta T_{B,j}$, °F . . . .</td><td colspan="2">4.0</td></tr>
<tr><td>$A'_{2,j}$, °F . . . .</td><td>-0.5</td><td>5.0</td></tr>
<tr><td>$B_{1,j}$, °F . . . .</td><td colspan="2">6.0</td></tr>
<tr><td>A_j^* . . . .</td><td>-417×10^{-6}</td><td>-518×10^{-6}</td></tr>
<tr><td>$C_{1,j}$ . . . .</td><td>209×10^{-6}</td><td>175×10^{-6}</td></tr>
<tr><td>$C_{2,j}$ . . . .</td><td>91×10^{-6}</td><td>84×10^{-6}</td></tr>
<tr><td>$\alpha_{1,j}$, degree of arc . . . .</td><td colspan="2">135.0</td></tr>
<tr><td>$\alpha_{2,j}$, degree of arc . . . .</td><td>158</td><td>180</td></tr>
<tr><td>ω, degree/hour . . . .</td><td colspan="2">15.0</td></tr>
<tr><td>$B_{2,j}$, (°F) . . . .</td><td>3.5</td><td>4.0</td></tr>
</table>

TABLE VI. CONTINUED

Parameter	Value	
	110 MM Brg	90 MM Brg
$K_{3,j}$, °F	-113×10^{-6}	-123×10^{-6}
$K_{4,j}$, °F	-64×10^{-6}	-40×10^{-6}
δ_j^*, degree of arc	60	72
B_j^*, °F	130×10^{-6}	130×10^{-6}

Substitution of the particular parameters into EQ 58 yields

$$
\begin{aligned}
\Delta C_{D1} &= [-417+130\sin(15t+60°)]\times10^{-6}, \text{ for 110 MM bearing} \\
\Delta C_{D2}' &= [-518+130\sin(15t+72°)]\times10^{-6}, \text{ for 90 MM bearing}
\end{aligned}
\qquad \text{EQ 59}
$$

- <u>Qualitative Discussion of Radial Motion of Bearing Suspension Elements</u>

  Radial temperature variation of the suspension components was taken as the dominant forcing function that causes diametral changes of the housing, the shaft, and the bearing races. As indicated, three diametral variation components were considered:

  (1) Changes of the housing's inside diameter and the bearing's outside diameter with respect to the initial interference or clearance values between them, existing at a reference installation temperature of 72°F

  (2) Changes of the bearing's inside diameter and the shaft's outside diameter with respect to their initial interference or clearance values, existing at a reference installation temperature of 72°F

  (3) Changes of the bearing outer race inside diameter and the bearing inner race outside diameter as a function of their temperature variations.

  The major omissions and assumptions were:

  (1) The bearing balls were not considered by virtue of the small diameter that renders insignificant diametral changes when compared with the effects of the DMA's structural elements and the bearing races

  (2) Unless otherwise specified, the steady-state temperature of the housing was assumed to approach the temperature of the outer race outside diameter.

  To develop an understanding of the sensitivities involving the geometric changes in the bearing suspension system, the upper and the lower temperature bounds for a specific mechanical event associated with the bearing friction variations were determined. These are presented in Table VII together with remarks of plausibility. Unless otherwise noted, the calculated temperatures of elements were constrained by the assumption that except for the bearing suspension element considered, all others were retained at the reference temperature of 72°F.

The immediate effect of the mechanism of the thermal diametral component expansion is to increase the bearing friction by a reduction of the load contact angle value in the presence of a constant bearing preload. Large bearing friction increases can be only induced by closing the existing clearances between the OD of the shaft and the ID of the bearings and by forcing the bearings internal clearance to approach zero value. As indicated in Table VII, the bearing suspension components temperature conditions required to create the geometrics condusive for large friction development are not plausible in view of the orbital and the thermal simulation data.

TABLE VII
Diametric Dimensional Variation of
Bearing Suspension Components - a Function of Temperature

Mechanical Event	Temperature @ Bottom Brg.	Temperature @ Top Brg.	Remarks
• The temperature of the housing at which loose fit will occur between ID of housing and OD of bearing	(1) 241°F	(1) 275°F	(1) Temperature not plausible in view of the orbital and thermal simulation data.
• The temperature of the housing at which diametral clearance will no longer exist	(1) -162°F	(1) -220°F	(2) Possible event.
• Inner race temperature at which tight fit will occur between inside diameter of bearing and the outside diameter of shaft	(2) 70°F	(1) 49°F	(3) Introducing lubrication depletion factor external to the bearing elements will cause an increase of both the outer race and the inner race temperature levels. Lubrication depletion, both external and internal to the bearings, will cause larger gradients.
• Shaft temperature at which tight fit will occur	(2) 86°F	(1) 168°F	
• Shaft temperature at which the bearings' diametral clearance no longer exists [for assumed inner race to shaft temperature difference of 4°F]	(1) 118°F	(1) 130°F	
• Outer race temperature at which the bearings' diametral clearance does no longer exist [for assumed inner race to shaft temperature difference of 4°F]	(1) 340°F	(1) 260°F	
• Inner race temperature gradient (inner race less shaft temperature at which the bearing's diametral clearance no longer exists	(3) 50°F	(3) 62°F	

3.5.2.3 Axial Expansion of the Shaft and Housing Elements

- Basic Equation

$$\delta_{AT} = \rho\beta_H[T_{HAVG} - T_{SAVG}] \qquad \text{EQ 60}$$

where:

δ_{AT} = net increase or decrease of the bearings center-to-center distance

ℓ = center-to-center distance = 7 inches

NOTES:

1. For definition of other parameters, refer to previous paragraph
2. when: $\delta_{AT}>0 \rightarrow \ell$ increase
   $\delta_{AT}<0 \rightarrow \ell$ decrease

Of interest is to note that for $\delta_{AT}>0$ and in particular if $\delta_{AT} \geq 3\times10^{-3}$ inch, the bearing's suspension (Figure 6) preload mechanism will be saturated. The necessary axial temperature gradient to cause this condition is

$$\Delta T = [T_{HAVG} - T_{SAVG}] = \frac{3\times10^{-3}}{(7)(6.4\times10^{-6})} = 67°F$$

Magnitude of such a gradient is not consistent with either the orbital data or test and thermal simulation data. Hence, it must be concluded that the preload mechanisms saturation can not occur.

- Particular Case

Substitution of EQ 50, EQ 51 and EQ 52 into EQ 60 results in

$$\delta_{AT} = \ell\beta_H[A_1^* + B_1^* \sin(\omega t - \delta_1^*)], \text{ inch}$$

$$\delta_{AT} = \ell\beta_H[2.25 + 3.64\sin\omega t + 81] = [100 + 163\sin(\omega t + 81)]\times10^{-6}, \text{ inch} \qquad \text{EQ 61}$$

where:

$$A_1^* = A_1 - 1/2(A_{2,1} + A_{2,2}) = 2.25 \text{ °F}$$

$$\delta_1^* = \tan^{-1}\left[\frac{C_4}{C_3}\right] = 81.3 \text{ (degrees arc)}$$

$$C_3 = B_1\cos\delta_1 - 1/2(B_{2,1}\cos\delta_{2,1} + B_{2,2}\cos\delta_{2,2}) = -.62°F$$

$$C_4 = [-B_1\sin\delta_1 + 1/2(B_{2,1}\sin\delta_{2,1} + B_{2,2}\cos\delta_{2,2}) = -3.59°f$$

$$B_1^* = [C_4^{\,2} + C_3^{\,2}]^{1/2} = 3.64°F$$

$$\ell = 7 \text{ (inch)}$$

$$\beta_H = 6.4\times10^{-6}\left(\frac{\text{in}}{\text{in}°F}\right)$$

$$\delta_{AT} = l\beta_H[2.25+3.64\sin\omega t+81] = [100+163\sin(\omega t+81)]\times10^{-6}, °F$$

- <u>Qualitative Discussion of Axial Motion of Bearing Suspension Elements</u>

  The operational success of the bearing suspension design depends on the maintenance of the free floating inner race of the "top" bearing (90 MM) in both radial and axial directions in order to retain the unsaturated condition of the bearing preload mechanism (refer to Figure 6). The latter introduces a weak spring in series with the shaft's, the bearing's and the housing's axial stiffnesses. This affords axial thermal expansion of the housing with respect to the shaft without inducing large thrust loads. This thermally-induced relative displacement is a function of the product of the bearing center-to-center distance, the coefficient of thermal expansion of the materials envolved, and the difference of the average temperatures of the housing and the shaft. This displacement is dominant in considering the suspension performance. Others, i.e., displacements which are a function of the axial temperature gradients along the housing and the shaft, appear to be insignificant in comparison.

  Of interest is to note that a relative displacement of 0.003 inch will saturate the preload mechanism (Figure 6). This means that any further axial displacements will produce increases of bearing thrust load and thus the bearing friction.

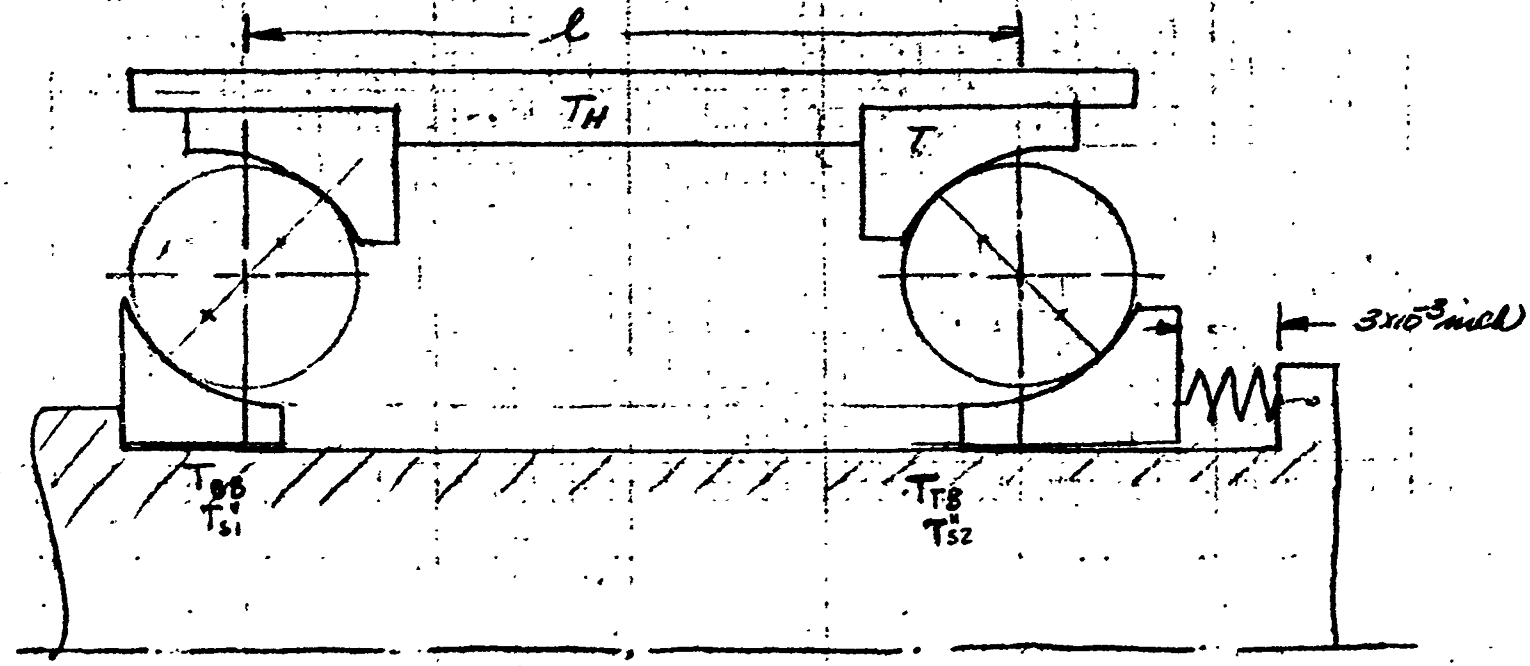

FIG 6. BEARING SUSPENSION

The temperature gradient (average temperature of the housing less the average temperature of the shaft) necessary to achieve such a condition approaches 67°F. The magnitude of such a gradient is not consistent with either the orbital data or test and thermal simulation data. Note also, that to develop the saturation of the preload mechanism, the average housing temperature must be greater than the average shaft temperature. This, of course, leads to the conclusion that the higher the shaft temperature with respect to the housing, the smaller is the possibility of saturating the preload mechanism. The last statement is somewhat mitigated by the discussions of the diametral motions from which it may be deduced that the axial motion of the inner races of the bearings can be produced in a direction that also cause the saturation of the preload mechanism. The latter occurs as a direct consequence of accommodating the changes of the contact angle caused by the thermally-induced diametral variations of the pertinent suspension components. Exemplifying, small bearing contact angles require the inner race of the DMA's top bearing to be displaced towards the preload mechanism (refer to Figure 6). These two aspects, as well as the increases of the thrust load, is further discussed in the subsequent paragraphs.

3.5.2.4 Bearing Friction Equation

- Basic Equations

The bearing friction torque developed by Palmgren (reference 1, page 446) was used in this analysis. The basic expression is given here as

$$T_{fB} = [16d_m u(F_A)^{1+n}](\frac{\beta}{C_s})^n(.9\cot\alpha), \text{ in oz} \qquad \text{EQ 62}$$

where

d_m = pitch diameter, inch

u = coefficient of friction = .001

β = static equivalent load factor = Y_s = .44

C_s = static capacity of bearing

= $400ZD^2\cos\alpha[(1-.5/f_o)^{-1}(1-\lambda)]^{.5}$

f_o = ρ_i/D = .525

$\lambda = \frac{D}{dm}\cos\alpha = C_2\cos\alpha$

D = ball diameter, inch

n = exponent = .4

Combining the terms yields

$$T_{fB} = C_1(F_A)^{1+n}\{[(1-C_2\cos\alpha)^{.5}\cos\alpha]^n\tan\alpha\}^{-1} \text{ (in oz)} \qquad \text{EQ 63}$$

where

$$C_1 = \{(16)(.9)\beta^n dmu[1-.5/f_o]^{.5+n}\}[400ZD^2]^{-n}$$

$$C_2 = D/d_m$$

- Methodology

The particular friction torque expression for the subject bearings was developed by determining the axial force for equal increments of the load angle α. The force to angle relationship used was,

$$F_A = ZD^2K\sin\alpha\left(\frac{\cos\alpha_o'}{\cos\alpha} - 1\right)^{3/2} \qquad \text{EQ 64}$$

where:

F_A = axial force (lbs)

Z = number of balls

$K \cong 4.85\times10^{+6}(\frac{A}{D})1.172(\frac{lb}{in^2})$

D = ball diameter (inch)

A = distance between centers of curvature (refer to Table II)

α_o' = contact angle as a function of installation fit-up and the radial uniform temperature gradient between the outer and the inner races

α = contact angle due to axial, radial and moment loads

Needed for the purpose of the bearing's characterizations, the elastic bearing deflection δ_{AB} was also determined at the same time by the expression

$$\delta_{AB} = A\sin(\alpha-\alpha_o')[\cos\alpha]^{-1} \qquad \text{EQ 65}$$

The latter was obtained from EQ 34 and EQ 35 by setting $\bar{\phi} = \delta_R = 0$.

Notice that for the case of heavy press fits or adverse temperature environment the bearing becomes diametrally tight and the value of

$$\cos\alpha_o' = (1 - \frac{C_D + \Delta C_D}{2A}) > 1, \text{ (refer to EQ 23)}$$

In these cases, the angle $\alpha_o' = 0$, but for the deflection calculation, the term $(1 - \frac{C_D + \Delta C_D}{2A})$ is still applicable (reference 2, page 51). Hence for $\cos\alpha_o' > 1$ EQ 65 will take the form of

$$\delta_{AB} = A(1 - \frac{C_D + \Delta C_D}{2A})\tan\alpha \qquad \text{EQ 66}$$

Since the axial stiffness of the subject bearings is not the same, incremental changes (refer to Tables VIII and IX) of ΔF_A produce different torque values. Hence, to conveniently sum the friction torques produced by each bearing, power expressions were developed. These are:

$$T_{fB} = A_1 F_{A1}^{\ b1} + A_2 F_{A2}^{\ b2} = 3.614\times10^{-3} F_A^{\ 1.277} + 3.386\times10^{-3} F_A^{\ 1.280} \qquad \text{EQ 67}$$

$$T_{fB} \cong 7\times10^{-3} F_A^{\ 1.2785} \qquad \text{EQ 68}$$

Adding the retainer friction of 4 in-oz results in the total Coulomb friction for the DMA bearing suspension system

$$T_{fc} = (7\times10^{-3} F_A^{\ 1.2785} + 4), \text{ in-oz} \qquad \text{EQ 69}$$

Again adding the viscous effect of 17 (in-oz) at 60 RPM yields

$$T_{fT} = [7\times10^{-3} F_A^{\ 1.2785} + 4] + 17, \text{ in-oz} \qquad \text{EQ 70}$$

The Coulomb friction and the total friction values for the DMA bearing assembly were plotted on Figure 7. Notice that the calculated torque correspondance with the experimental data (obtained from Aerospace corporation) is relatively good. The lower values of friction in the low axial thrust region and high in the high thrust region is characteristic of the Palmgren's expression.

TABLE VIII

Bearing Axial Force as a Function of Axial Deflection, Contact Angle, Bearing Friction, 777 DMA, 100 MM Bearing

deg	INCH	LB	INCH-OZ
α	δ_{AB}	F_A	T_{AB}
12.0	1.27×10^{-4}	5.53	.03
12.5	2.95	20.99	.16
13.0	4.63	44.28	.43
13.5	6.32	75.50	.86
14.0	8.02	115.10	1.50
14.5	9.73	163.70	2.37
15.0	11.44	222.	3.51
15.5	13.17	291.	4.96
16.0	14.[illegible]	370.	6.74
16.5	16.64	463.	8.92
17.0	18.38	568.	11.53
17.5	20.14	688.	14.61
18.0	21.91	823.	18.23
18.5	23.68	973.	22.44
19.0	25.47	1142.	27.28
19.5	27.27	1328.	32.83
20.0	23.08×10^{-4}	1535.	39.15

TABLE IX

Bearing Axial Force as a Function of Axial Deflection, Contact Angle, Bearing Friction, 777 DMA, 90 MM Bearing

deg	INCH	LBS	IN-OZ
α	δ_{AB}	F_A	T_f
12	3.03×10^{-4}	22.38	.18
12.5	4.82×10^{-4}	48.27	.50
13.0	6.62	83.25	1.03
13.5	8.40	128.	1.81
14.0	10.20	183.	2.88
14.5	12.01	249.	4.28
15.0	13.90	328.	6.07
15.5	15.74	419.	8.29
16.0	17.59	525.	11.00
16.5	19.44	646.	14.25
17.0	21.32	784.	18.11
17.5	23.19	939.	22.65
18.0	25.08	1114.	28.04
18.5	26.98	1309.	34.0[illegible]
19.0	28.88	1527.	41.03
19.5	30.81	1766	49.01
20.	32.74	2030	58.06

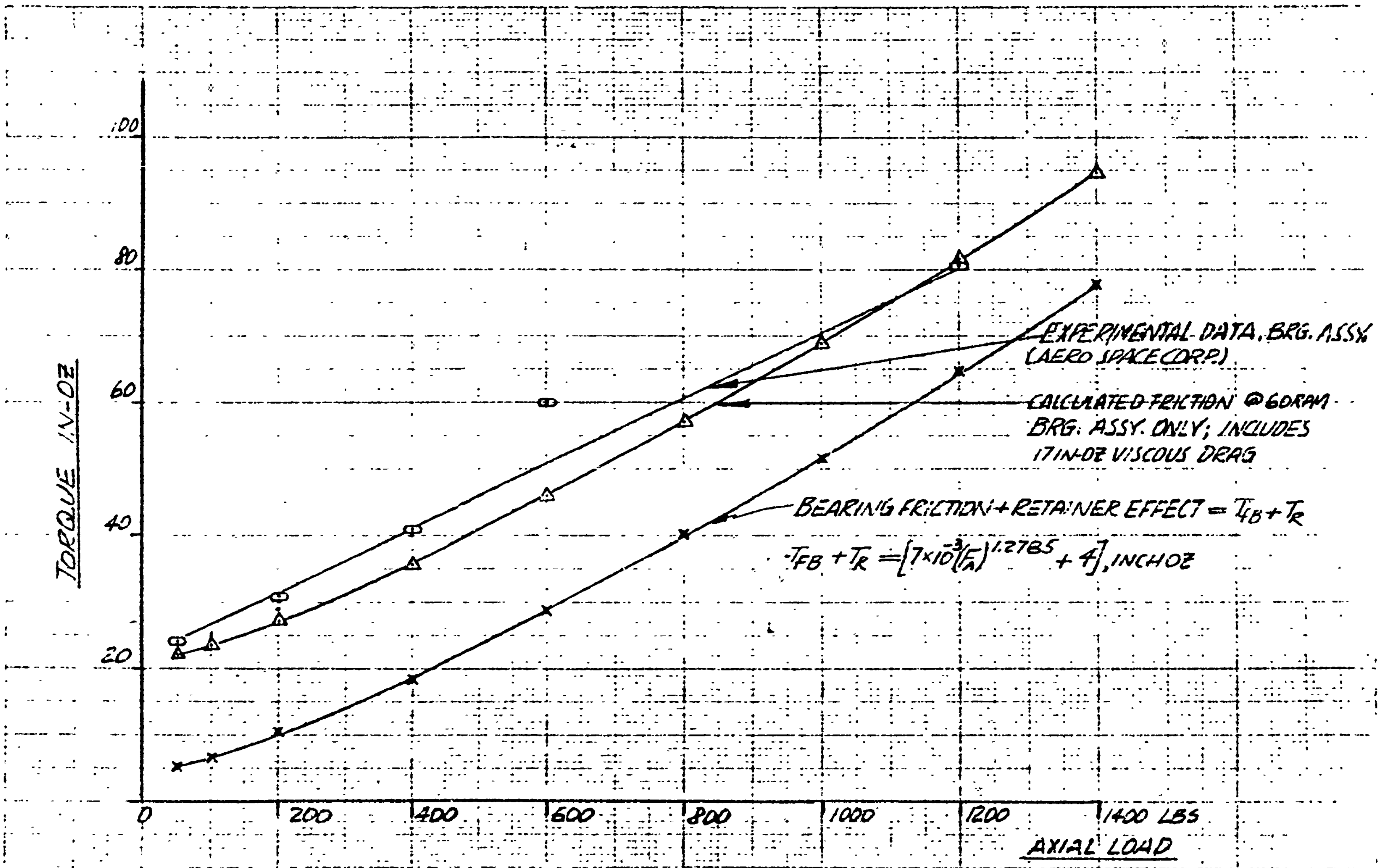

FIG 7 BRG. ASSY FRICTION TORQUE VS AXIAL LOAD

3.5.2.5 Quantitative Considerations of the Bearing's Friction Torque

- Orbital Performance

  To determine the DMA's temperature variation on the amplitude of the bearing Coulomb friction, pertinent diurnal orbital temperatures occurring on 8 September 1975 were selected. These, together with the calculated friction for both bearings, are shown on Figure 8. The plots reflect the effects of the normal preload of 64 pounds and the geometric variations of the bearing suspension components by the temperature environment. Notice the insignificant torque variation of about 0.6 inch-oz during one diurnal period.

- Performance as a Function of Stipulated Temperature Gradients

  Since the telemetered thermal data for the DMA obviously did not provide the mechanism explaining the observed anomaly, various temperature gradients between the pertinent bearing suspension components were considered and their effect on the bearing friction was estimated.

  (1) Aspect of Lubrication Depletion - It appeared reasonable to assume that depletion of lubricant in the neighborhood of the top (90 MM) bearing will cause an increase of its inner race temperature. To determine this effect on performance, a 37°F temperature gradient between the shaft and the inside diameter of the bearing was stipulated. The latter was based on an order of magnitude increase of the existing heat flow coefficient of conduction. The temperature environment of the other DMA elements was retained at levels shown on Figure 8. The imposed conditions resulted in a maximum friction torque increase of 1.5 in-oz.

  (2) Friction Torque as a Function of Inner Race to Shaft Gradient - The analysis of the hypothesized temperature gradient of item (1) was extended to the variations of the friction torque as a function of the discussed gradient with all other temperatures retained at levels defined by the thirteenth hour of the diurnal DMA's temperature profile shown on Figure 8. The results of this work

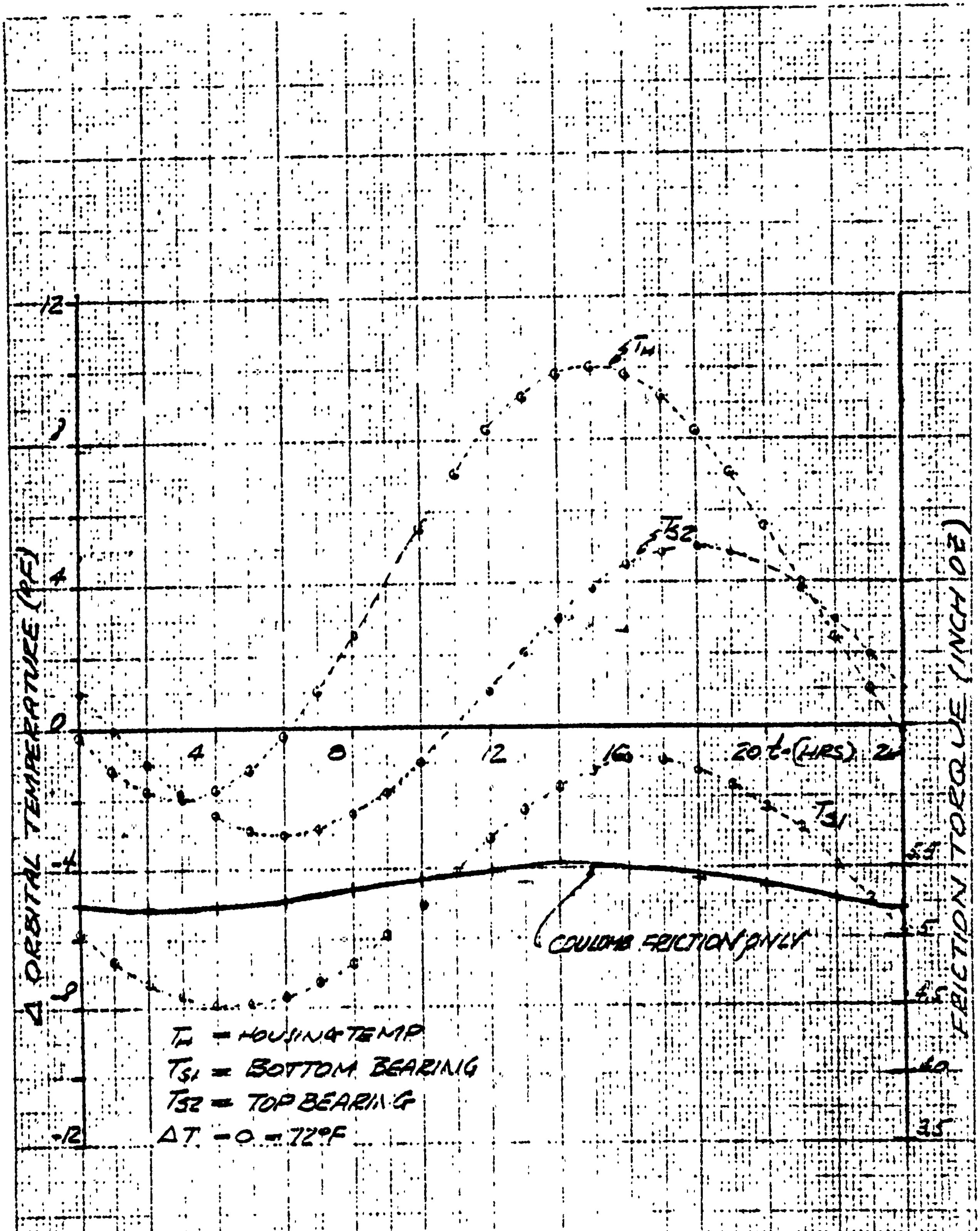

FIG. 8 NORMAL BEARING FRICTION FOR ORBITAL ENVIRONMENT

(Figure 9 and Table X) indicate that to obtain the anomaly's nominal torque increase of 60 in-oz the temperature gradient must approach 270°F. Of interest is to note that the necessity of such a large gradient is caused by a relatively low rate of change of the load contact in the region of the bearing's zero diametral clearance. It follows that the sensitivity of the friction torque to the subject temperature gradient would be much higher should the bearing's preload be reduced.

- Friction Torque as a Function of Preload Mechanism Saturation

The saturation or closure of the preload mechanism was in part discussed in paragraph 3.5.2.3. Here the subject is extended to the quantitative summary of the preload saturation effect on the bearing friction torque. There are at least three factors that influence the closure of the preload mechanism:

(a) the radial temperature gradients between the bearing suspension components

(b) the angular misalignment of the inner race of the 90 MM bearing

(c) jamming of the clearance between the inner race of the 90 MM bearing and the shaft

(1) Temperature Gradients Effect - The axial closure motion is a function of the bearing's reduction of its diametral clearance by the thermal gradients and the relative displacement of the housing with respect to the shaft due to the difference between the average temperatures of the housing and the shaft. This motion is in part mitigated by the elastic displacement of the bearings produced by the bearing's thrust load. In terms of analytical parameters, the total axial motion of the bearing's inner race is a function of the initial contact angle α_0, its changed value (α_0') due to the interference and the reduction of the diametral clearance by thermal environment, the elastic displacement (δ_{AB}) produced by the preload and the net thermal displacement (δ_{AT}) of the housing with respect to the shaft. For a given initial clearance (C_i), the closure of the preload mechanism (ΔC) is described.

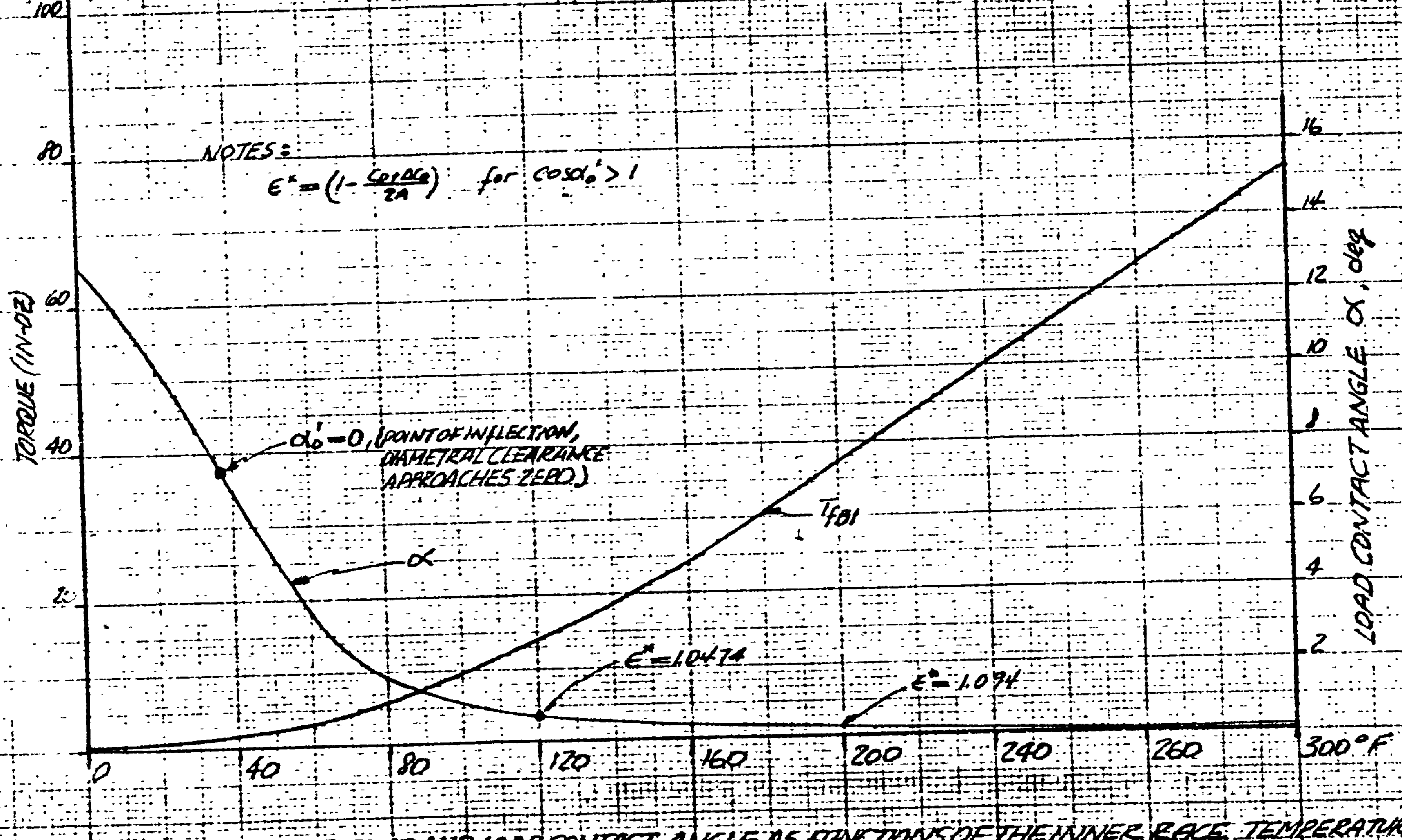

FIG 9. FRICTION TORQUE AND LOAD CONTACT ANGLE AS FUNCTIONS OF THE INNER RACE TEMPERATURE GRADIENT, 90 MM BRG.

TABLE X. Data, ΔT_{B2} = 37°F Case

HRS	INCH	INCH	INCH	DEGREE	NUMBER	DEG.	INCH-OZ
t	ΔC	δ_{AT}	δ_{AB}	α_0'	$1+\epsilon$ (1)	α	T_{FC}
0	127×10^{-6}	-61×10^{-6}	1.17×10^{-3}	5.94		9.46	2.92
2	124	-26.	1.16	5.99		9.48	2.98
4	110	42.	1.23	5.52		9.24	3.00
6	100	125	1.41	4.54		8.80	3.06
8	82	203	1.74	2.97		8.25	3.13
9	73	232	2.04	1.80		7.99	3.17
10	40	252	2.54		1.0002	7.77	3.20
11	33	262	2.48		1.0008	7.58	3.23
12	29	261	2.44		1.0012	7.46	3.25
13	28	249	2.42		1.0014	7.39	3.26
14	31.	227	2.43		1.0013	7.43	3.25
15	37	196	2.46		1.0014	7.52	3.24
16	46	158	2.52		1.0005	7.68	3.21
17	51	117	2.48	1.09		8.00	3.16
18	56	74	2.43	2.56		8.15	3.14
20	97	-3	1.77	4.28		8.7	3.07
22	117	-52	1.26	5.37		9.2	3.01
24	127	-61×10^{-6}	1.18×10^{-3}	5.94		9.5	2.98

Note: $1 < \cos\alpha_0' = 1+\epsilon$

$$C_i - A(\sin\alpha_o - \sin\alpha_o') + (\delta_{AB} - \delta_{\Delta T}) = \Delta C \qquad \text{EQ 71}$$

where:

A = distance between the curvature centers

Notice that:

$$\text{when: } \begin{cases} \Delta C > 0 \rightarrow \text{clearance exists} \\ \Delta C < \quad \rightarrow \text{clearance does not exist} \\ \cos\alpha_o' > 1,\ \sin\alpha_o' = 0 \end{cases}$$

Using the DMA's thermal conditions of Figure 8 and stipulating a 37°F temperature gradient between the inner race of the 90 MM bearing and the shaft, developed was a closure situation depicted on Figure 10. Should the temperature gradient (average temperature of housing less average temperature of shaft) reach a value of 149°F, the anomaly's Δ torque results. Notice that for a nominal temperature gradient between the inner race and the shaft of the 90 MM bearing of 3.7°F, the necessary total gradient ΔT, (average temperature of housing less shaft), to result in 60 in-oz bearing friction torque is 216°F.

Review of Table X indicates that ΔC is a strong function of the preload value. The higher the preload value, the slower is the rate of closure. Of interest, also, is to note that the decrease in the bearing stiffness as α_o' approaches zero, is approximately 40% of the initial value of 200,000 lb/in. Hence, it follows that for a given preload, relatively large bearing displacements (δ_{AB}) will occur.

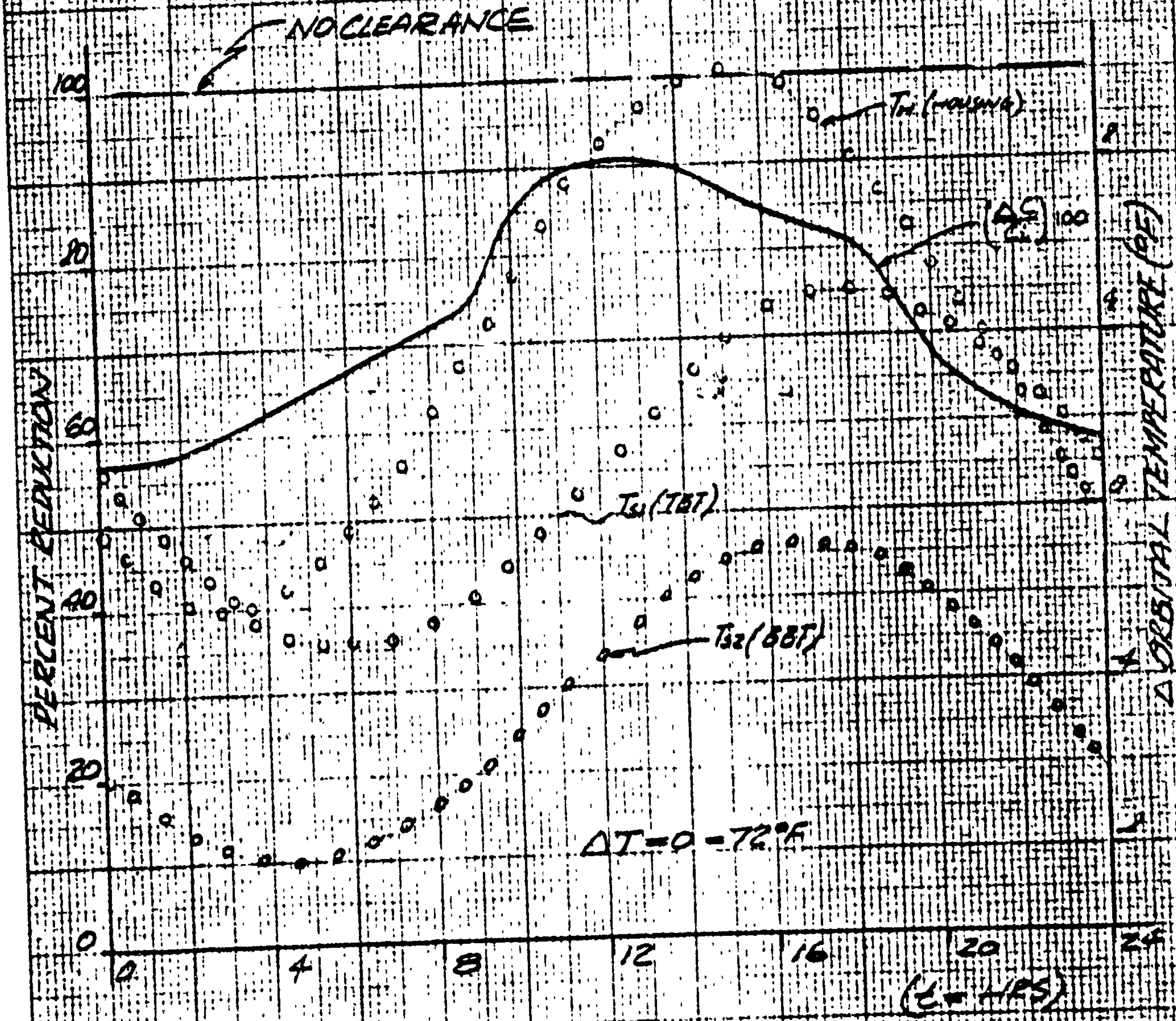

FIG 10. PERCENT REDUCTION OF CLEARANCE (BETWEEN PAYLOAD MECH. & SHAFT)

NO. 340-20 DIETZGEN GRAPH PAPER 20 X 20 PER INCH
EUGENE DIETZGEN CO. MADE IN U.S.A.

The bearing friction torque values due to the gradient (ΔT) are shown on Figure 11. In order to recognize the magnitude of the thrust load, associated with the gradient ΔT, the relationship of these two quantities is also given on Figure 11.

(2) Angular Misalingment of Bearing - Geometrically, by virtue of the pertinent radial and axial clearances (associated with the top bearing and the preload mechanism respectively), it is possible to produce an angular misalignment that saturates the preload mechanism. The maximum angular quantity about an axis perpendicular to the rotational axis of the DMA associated with the misalignment, approaches 0.0485 degree of arc. This angle produces (refer to Figure 12) an increase of the bearing friction by 16 in-oz. Hence, to achieve the anomaly-associated torque increase in accordance to Figure 11, the required temperature gradient is 128°F.

(3) Jammed Top Bearing's Inner Race - Hypothesis of the following conditions:

(a) the radial clearance of the top bearing, between the inside diameter of its inner race and the outside diameter of the shaft, is jammed by debris,

(b) the intensity of jamming is sufficient to retain the nominal (0.003 inch) relative position of the bearing with respect to the preload mechanism under load,

(c) the axial load is produced by a thermal gradient which is defined as the difference between the average housing and shaft temperatures,

produces a thermal gradient (Figure 11) of 169°F necessary to satisfy the anomaly's observed torque increase of 60 in-oz.

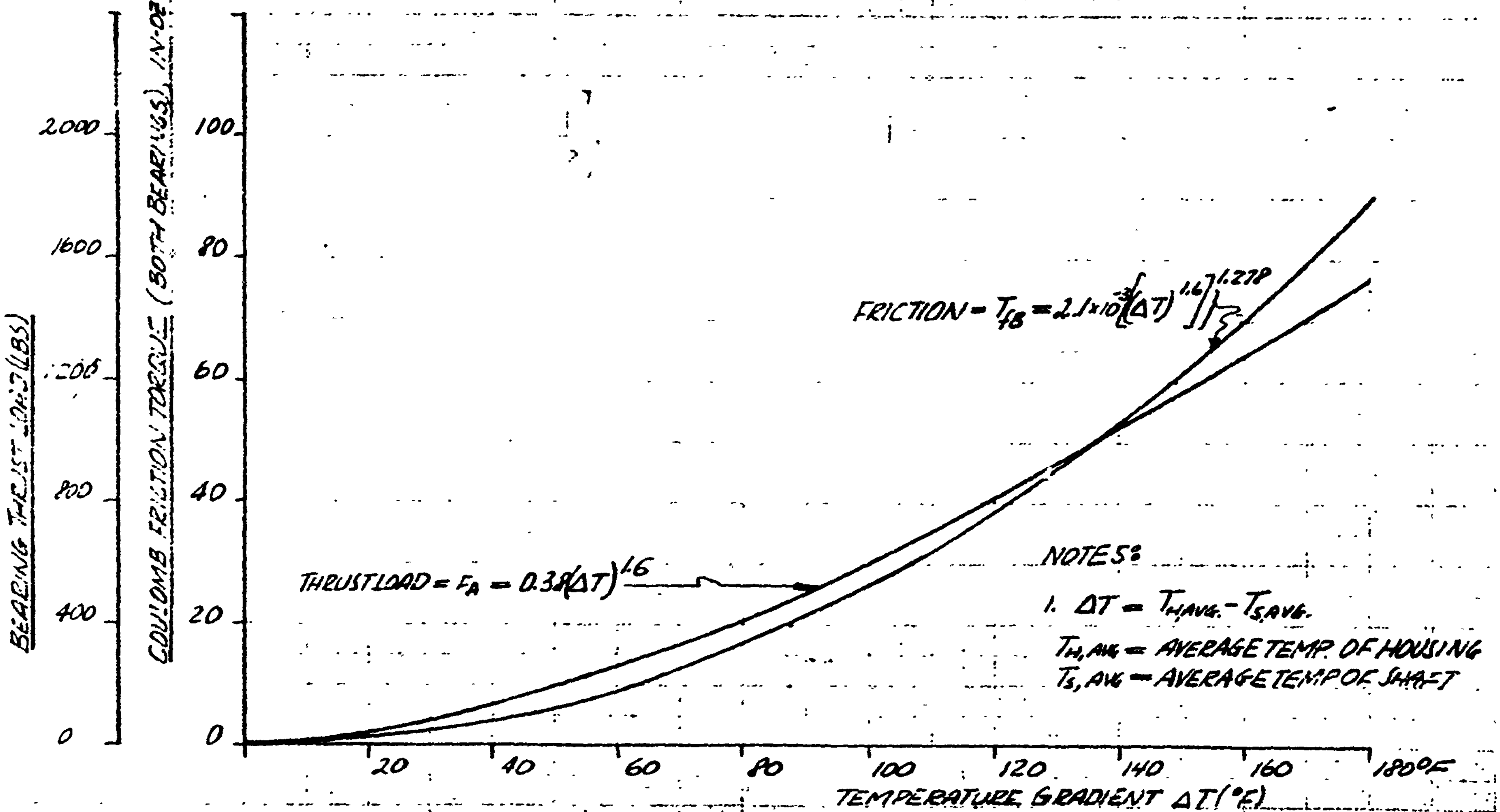

FIG. 11 BEARING Δ-FRICTION TORQUE AND THRUST LOAD VS TEMPERATURE GRAD.
(FOR SATURATED COND. OF PRELOAD MECH.)

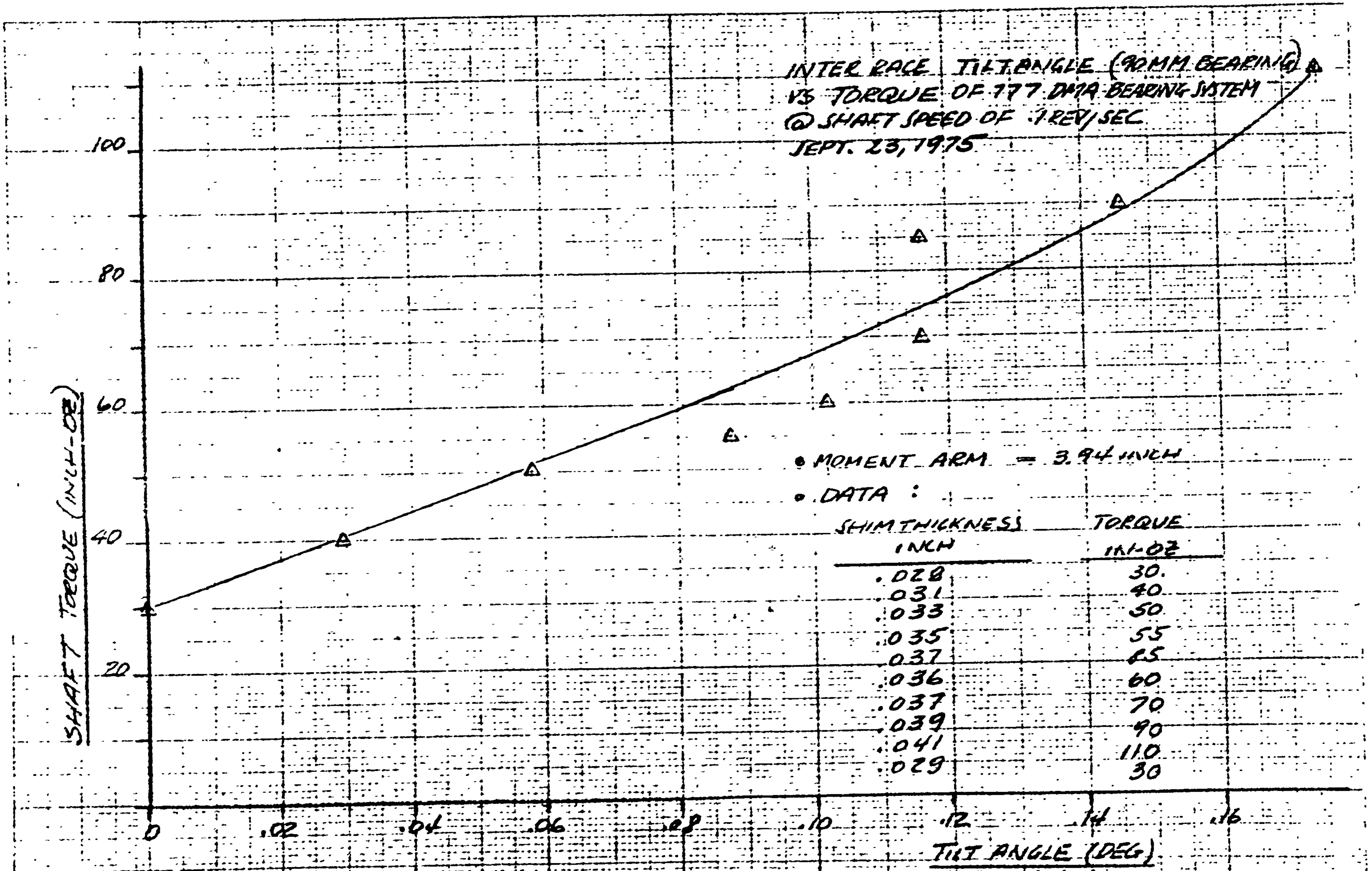

FIG 12. TORQUE VS MISALIGNMENT

- <u>Feability of Anomaly DMA Torques as a Function of Thermal Environment</u>

  Reference to Table XI, which summarizes the aspects of the bearing friction torque, induced completely or partially by the thermal gradients, indicates that the pertinent temperature gradients required to produce the steady-state friction characteristics of the DMA's orbital anomaly are inconsistent with either the orbital or the thermal simulation data.

TABLE XI
Temperature Required for Anomaly's
Δ Friction Torque Increase

Hypothesized Conditions	Gradient Required to Produce 60 in-oz Friction (°F)
• Temperature effects of local lubrication depletion in the neighborhood of the top bearing are superimposed over the typical orbital temperature environment of the DMA. The gradient between the inner race and the shaft caused by depletion is	. . . . 270°F
• Preload mechanism is saturated by a 40°F gradient between the inner race (top bearing) and shaft; superimposed over the DMA's orbital environment a gradient, ΔT, (average housing less average shaft temperatures) is	. . . . 147°F
• Nominal orbit, DMA's temperature conditions exist. Gradient ΔT is necessary to saturate the preload mechanism and produce anomaly friction is.	. . . . 216°F
• Nominal orbit, DMA's temperature conditions exist. Top bearing is misaligned; the gradient ΔT is	. . . . 128°F
• Nominal orbit, DMA's temperature conditions exist. Preload mechanism's axial clearance of 0.003 inch exists. 90 MM bearing race is jammed on the shaft by debries; the gradient ΔT is	. . . . 149°F

Note: Nominal bearing friction variation for normal orbital operation is 0.4 in-oz. If bearing misalignment is assumed to cause saturation of the preload mechanism, 17.5 in-oz torque increase would be expected.

TRW
SYSTEMS GROUP

INTEROFFICE CORRESPONDENCE

76-7345.4-043

TO: A. H. Rosenberg

CC: P. C. Wheeler

DATE: 20 January 1976

SUBJECT: 777 DMA - Dimensional Analysis of Bearing Balls Separators

FROM: J. G. Zaremba J.G.Z.

BLDG	MAIL STA.	EXT.
82	1367	50993

1.0 INTRODUCTION AND SCOPE

The documented worst case analyses envolve a review of dimensional sufficiency of the subject bearing ball retainers (separators). Considered were the separators associated with the structural assembly's bottom bearing (110 MM), the top bearing (90 MM) and the 30 MM slip ring's assembly bearing. The summary of the analyses is presented in paragraph 2.0 and the details are given in paragraph 3.0. Of interest is to note that certain manufacturing control changes are being suggested as a direct consequence of the analyses. These are presented in paragraph 2.2 with further details given in paragraph 3.5.

2.0 SUMMARY

2.1 Geometric Sufficiency Criterion and Presentation of Results

The separator's geometric sufficiency criterion used in the presented analyses were the requirements defined as:

- The (ε) between a point (P_2) at the outboard edge of the separator's thickness dimension and belonging to the locus of points defining the outside diameter of the separator, and the point of tangency (P_1), associated with the separator's pocket and its companion ball, must have a positive value. In other words, $\varepsilon \geq 0$.

- There must exist a clearance (c) between the 90 MM bearing separator's width dimension and the washer component of the preload mechanism, for the worst case dimensional considerations.

The magnitude and the direction of the defined edge distance (ε) is of interest because increases of bearing friction can occur should (ε) become less than zero.

All the computed edge distance values, as shown below, were positive

Bearing	Edge Distance (ε)
110 MM	0.026 inch
90 MM	0.017 inch
30 MM	0.011 inch

quantities and appeared to be large enough for satisfactory bearing performance, provided the edges of the separator have either sharp corners or their chamfer's dimension is limited to small values, say 0.005 inch. However, since the deburring radius or chamfer is not controlled by the fabrication drawing, possibility exists that "ε" can become less than zero. Examplifying the case by assuming an easily realizable chamfer of 0.015 inch, the separator's edge distances (ε) for the bearings of interest become:

Bearing	Edge Distance (ε)
110 MM	0.011 inch
90 MM	0.002 inch
30 MM	-0.004 inch

Although not within the scope of these analyses, an attempt was made to estimate the friction increase as a function of the negative edge distance "ε". For the retainers' steady-state condition, a coarse approximation of the increase is the product of the nominal friction torque and the ratio of the negative edge distance to the bearing ball radius. The latter indicates that small negative values of "ε" insignificantly affect the bearing performance.

The worst case value estimate of the clearance (c) resulted in a value of -0.003 inch. The latter is an insufficient dimension, especially since there exists no dimensional control of the separator's w[illegible]n-bisecting-diameter that also contains the center of the ball pockets.

The consequence is an occasional contact of the retainer with the preload washer or the bearing's inner race land or both.

Concluding, it is well to indicate that the existing separators' and the associated bearing dimension's fabrication tolerances insignificantly affect the calculated edge distance values.

2.2 Recommendations

The performed analysis indicates that the edge distance (ε) is small enough (for all bearings considered) to cause concern. The latter is further emphasized by the dimensionally uncontrolled fabrication deburring process which further reduces the distance (ε). Since the control of the deburring radii or chamfers is reasonably difficult, when relatively tight tolerances are required, increases of the outer diameter of the ball retainers are recommended. These are:

Bearing	Diametral Increase
110 MM	0.046 inch
90 MM	0.061 inch
30 MM	0.070 inch

The selection of the diametral increases was based on the desire to geometrically prevent contacts of the separator's outer diameter surfaces with that of the bearing outer ring land diameter. The suggested Δ values are also a function of the thermal deflections, the processing-caused geometric distortions and a reasonable clearance value.

Suggested is also dimensional control of two fabrication parameters. These are: (1) the maximum deburring radius or chamfer; and, (2) control dimension of a center line passing through the center of the ball pocket holes and referenced to a plane containing the edge diameter of the separators' width dimension. For further details, refer to paragraph 3.5.

To correct the separator width clearance aspect, reduction of the retainer width is being suggested.

3. ANALYSIS

3.1 Introduction and Scope

The geometry of a given bearing ball and the associated separator ball pocket is shown on Figure 1. Notice that the point of tangency of

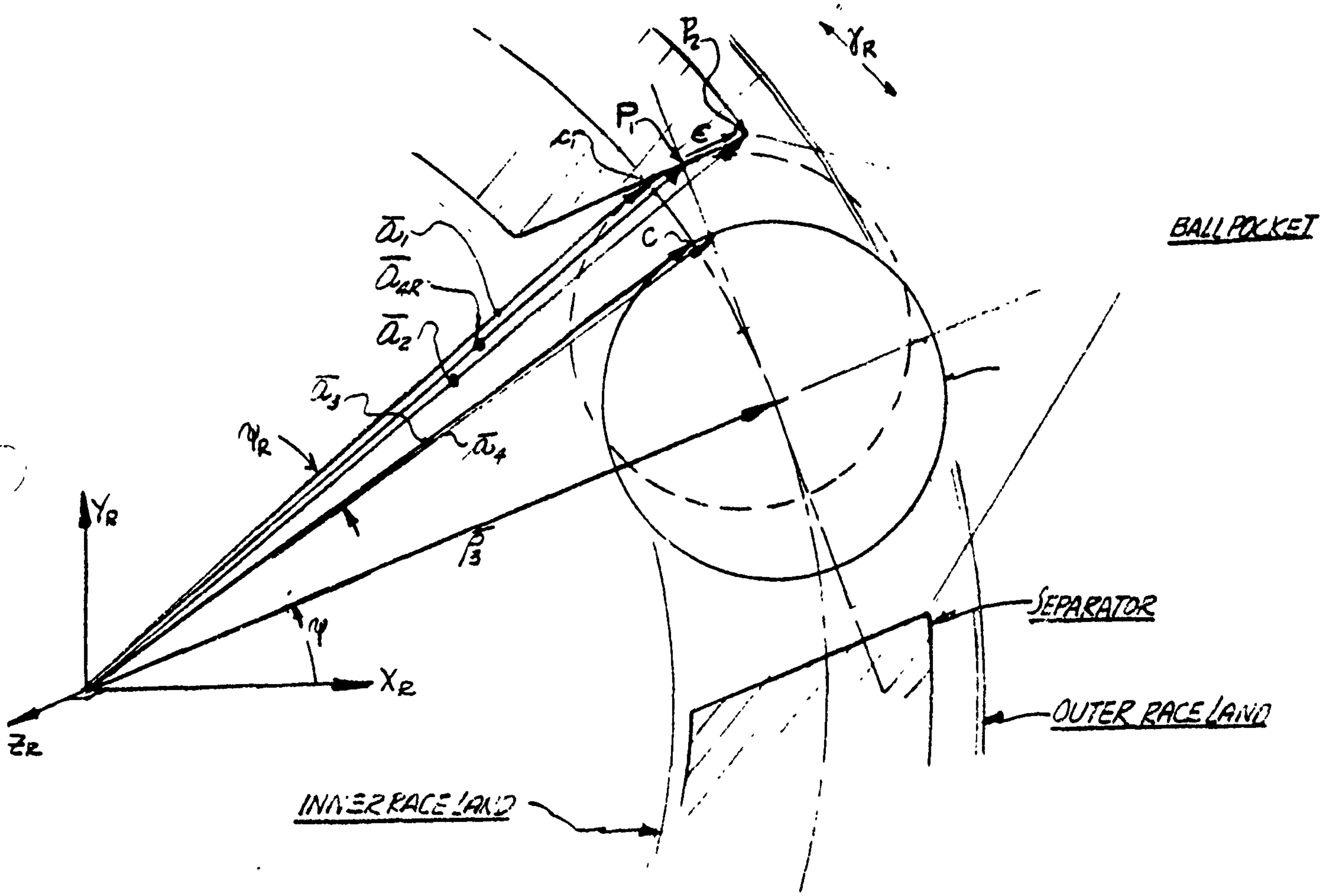

FIGURE 1. Bearing Ball and the Separator Geometry

the separator and th ball surfaces is denoted by "P_1" and point P_2 is the outboard limit of the effective separator thickness dimension.

The magnitude of the line segment $\overrightarrow{P_1P_2}$ is of interest because it is indicative of the geometric suitability of the separator with the dimensional parameters of the bearing balls and races. In particular, if the magnitude of the line segment P_1P_2, defined as

$$|\overrightarrow{P_1P_2}| = \varepsilon = |\bar{\varepsilon}| = |\bar{a}_2 - \bar{a}_{4R}| \qquad \text{EQ 1}$$

is smaller than zero, increased motor demand to rotate the bearing may be expected. A coarse estimate of the bearing torque increase can be

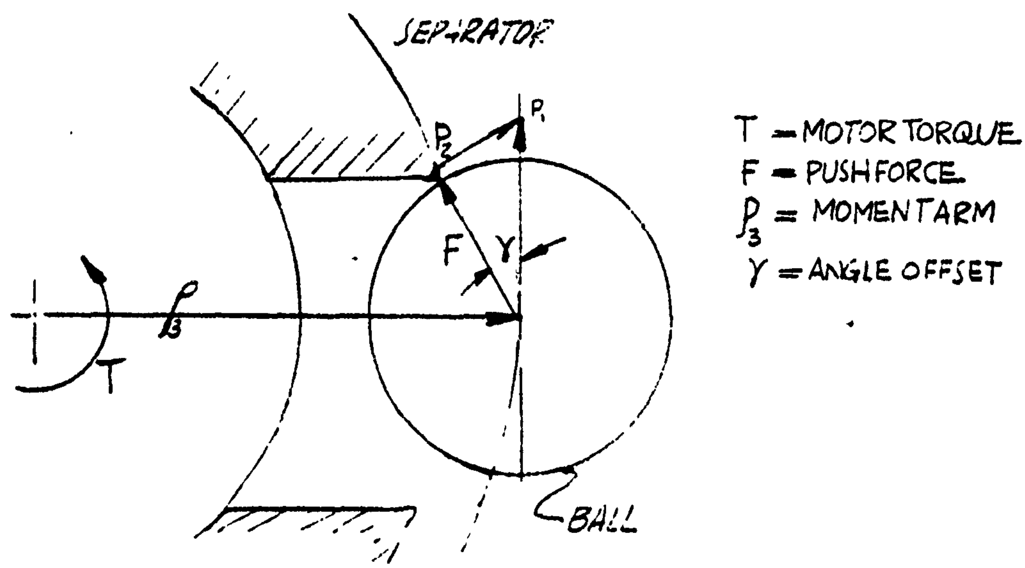

FIGURE 2. Separator and Bearing Ball Forces (for $\varepsilon<0$)

obtained from Figure 2. The shown load model yields the desired estimate of the motor torque increase as a function of the offset angle γ as,

$$\Delta T = \rho_3 F \frac{\sin\gamma}{(\cos\gamma)^2} = \tan\gamma\sec\gamma \qquad \text{EQ 2}$$

where:

ΔT = motor torque increase

T = motor torque necessary to move the separator

Notice that for a 50 percent motor demand increase the angle γ approaches 24.5 degrees. This implies that the separator's outboard edge is offset to the left from a nominal tangency point P_1 (Figure 1) by approximately 0.10 inches. The latter leads to the apparent conclusion that small ε, where $\varepsilon<0$, does not have a significant influence on the bearing performance.

Since the subject bearings exhibit a partial inner race and the ball riding separator system, increases of the bearing friction torque will occur randomly. To avoid these perturbations, and thus the spacecraft's pointing angle changes, it is desired to limit ε to values greater than zero with a reasonable margin of safety.

From Figure 1, the critical edge distance ε can be expressed as

$$\varepsilon = \bar{a}_2 - \bar{a}_{4R}$$

where the components of the vector $\bar{a}_{4R}$ are the components of the vector $\bar{a}_4$ rotated an angle ψ_R. The latter is the angular span contained by the arc segment CC_1 and can be computed by considering the angle between vectors $\bar{a}_3$ and $\bar{a}_1$.

In the analyses that follow, derived are the vector components (paragraph 3.2 and paragraph 3.3) needed for evaluation of the edge distance ε. In paragraph 3.4 derived is the quantity ε; also the worst case clearance (c) value is computed. The computations include the DMA's bottom bearing (110 MM), top bearing (90 MM) and the 30 MM slip ring assembly bearing. The separator design changes and the manufacturing control changes are given in paragraph 3.5.

3.2 Component of Vectors $\bar{a}_3$ and $\bar{a}_4$

The components of the vectors $\bar{a}_3$ and $\bar{a}_4$ are associated with the bearing's ball pitch radius (ρ_3), the bearing ball radius (ρ_B), the bearing's total runout error (ε_B) and the angular orientation (ψ) of the ball center with respect to a fixed coordinate set X_R, Y_R, Z_R.

In the bearing body coordinate set X_B, Y_B, Z_B (Figure 3), the vector $\bar{a}_3$ is defined by

$$\bar{a}_3 = \rho_3[\hat{i}_B\cos\gamma_3 + \hat{j}_B\sin\gamma_3]$$

where:

$$\gamma_3 = 2\sin^{-1}[\rho_3|2\rho_3]$$

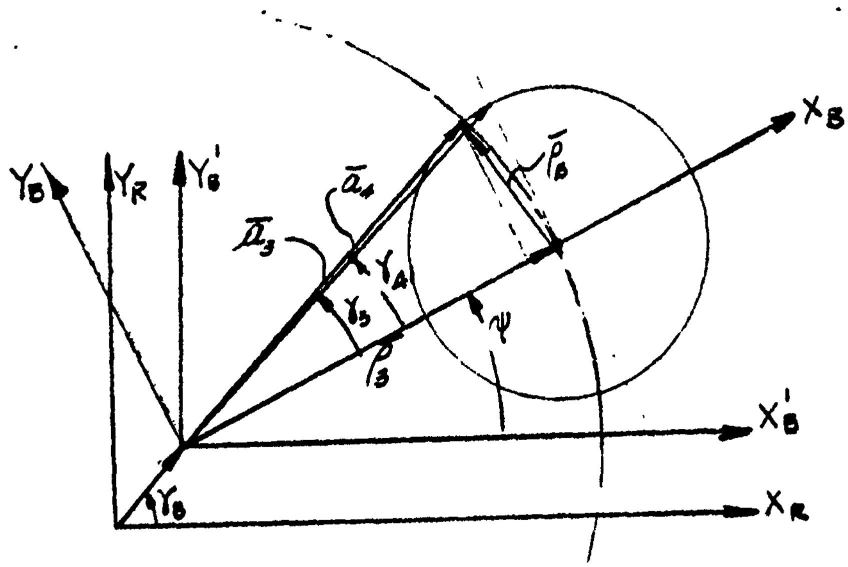

FIGURE 3. Bearing Coordinate Set

The radius ρ_3 is the bearing's ball pitch radius given by

$$\rho_3 = 1/2[\rho_i - A\cos\alpha_0] = 1/2[\rho_i-(f_i+f_o-1)D + \frac{C_D}{2}]$$

$$= 1/2[\rho_i-(f_i+f_o-1)D+\frac{C_D}{2}] \qquad \text{EQ 4}$$

where:

ρ_i = inner radius of inner race

$A = (f_i+f_o-1)D$

$f_i = r_i/D$ = inner race curvature ratio

$f_o = r_o/D$ = outer race curvature ratio

D = bearing ball diameter

α_o = free contact angle = $\cos^{-1}[1-\frac{C_D}{2A}]$

C_D = diametral clearance

The pertinent bearing specifications define the nominal value of ρ_3 but not its variation. To determine the latter total differential of ρ_3 is considered in terms of the quantities f_i, f_o, D and C_D as shown.

$$d\rho_3 = 1/2\{[(1-f_o)df_i+(1-f_i)df_o]D+[1-(f_i+f_o)]dD+\frac{dC_D}{2}\} \qquad \text{EQ 5}$$

Table I lists the differentials and the pertinent quantities leading to their evaluations.

TABLE I. Variation of Bearing Ball Pitch Radius

Quantities	Symbol	Units	Bearings		
			110 MM	90 MM	30 MM
Mean outer race curvature ratio	f_o	inch	0.52750	0.52750	0.52000
Variation (±)	df_o	inch	0.00250	0.00250	0.00500
Mean inner race curvature ratio	f_i	inch	0.51750	0.51750	0.52000
Variation (±)	df_i	inch	0.00250	0.00250	0.00500
Mean ball diameter	D	inch	0.50000	0.46870	0.31250
Variation (±)	dD	inch	←	10^{-5}	→
Mean diametral clearance	C_D	inch	0.00150	0.00150	0.00235
Variation (±)	d,C_D	inch	0.00020	0.00020	0.00035
Mean ball pitch radius	ρ_3	inch	2.57000	2.12000	0.83650
Variation (±)	$d\rho_3$	inch	0.00065	0.00061	0.00084

The vector $\bar{a}_4$ (Figure 3) in the X_B, Y_B, Z_B coordinate set is given in terms of its components by

$$\bar{a}_4 = \rho_4[\hat{i}_B \cos\gamma_4 + \hat{j}_B \sin\gamma_4]$$

where:

$$\rho_4 = [\rho_3^2 + \rho_B^2]^{1/2}$$

$$\gamma_4 = \tan^{-1}[\rho_B | \rho_3]$$

Both vectors $\bar{a}_K$ are related to the X_B', Y_B', Z_B' coordinate by

$$\begin{bmatrix} X_B' \\ Y_B' \\ Z_B' \end{bmatrix} = \begin{bmatrix} \cos\psi & -\sin\psi & 0 \\ \sin\psi & \cos\psi & 0 \\ 0 & 0 & 1 \end{bmatrix} \begin{bmatrix} X_B \\ Y_B \\ Z_B \end{bmatrix} \qquad \text{EQ 7}$$

Hence, in the X_B', Y_B', Z_B' the vectors $\bar{a}_3$ and $\bar{a}_4$ are given as

$$\bar{a}_3 = \rho_3[\hat{i}_{B'}\cos(\psi+\gamma_3)+\hat{j}_{B'}\sin(\psi+\gamma_3)]$$
$$\bar{a}_4 = \rho_4[\hat{i}_{B'}\cos(\psi+\gamma_4)+\hat{j}_{B'}\sin(\psi+\gamma_4)] \qquad \text{EQ 9}$$

By linear transformation

$$X_R = X_B'+\varepsilon_B\cos\gamma_B$$
$$Y_R = Y_B'+\varepsilon_B\sin\gamma_B \qquad \text{EQ 10}$$

where:

ε_B = bearing runout $\approx 64\times10^{-6}$ inch (RMS) for all bearings considered

γ_B = runout phase angle

the vectors $\bar{a}_3$ and $\bar{a}_4$ in the reference coordinate set (Figure 1 and Figure 3) take on the form

$$\bar{a}_3 = \hat{i}_R[\rho_3\cos(\psi+\gamma_3)+\varepsilon_B\cos\gamma_B]+\hat{j}_R[\rho_3\sin(\psi+\gamma_3)+\varepsilon_B\sin\gamma_B]$$
$$\bar{a}_4 = \hat{i}_R[\rho_4\cos(\psi+\gamma_4)+\varepsilon_B\cos\gamma_B]+\hat{j}_R[\rho_4\sin(\psi+\gamma_4)+\varepsilon_B\sin\gamma_B] \qquad \text{EQ 11}$$

3.3 Components of Vectors $\bar{a}_1$ and $\bar{a}_2$

In the separator coordinate set X_s, Y_s, Z_s, the vector $\bar{a}_1$ (Figure 4) is described in terms of its components as

$$\bar{a}_1 = \rho_3[\hat{i}_s\cos\gamma_1+\hat{j}_s\sin\gamma_1] \qquad \text{EQ 12}$$

where:

$\gamma_1 = 2\sin^{-1}[\rho_p/2\rho_3]$

ρ_p = radius of the ball pocket

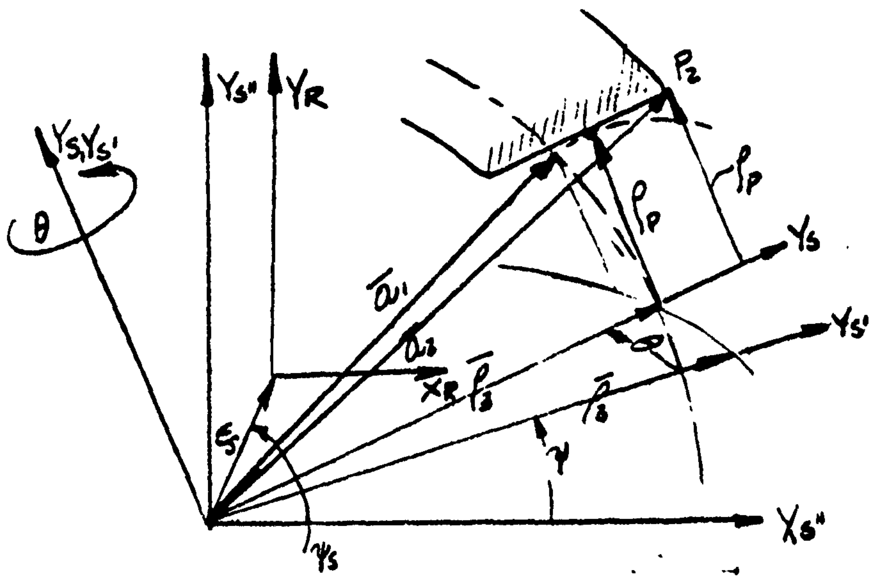

FIGURE 4. <u>Separator Ball Pocket</u>

Also, in the X_s, Y_s, Z_s coordinate set the vector $\bar{a}_2$ is given as

$$\bar{a}_2 = \rho_2[\hat{i}_s\cos\gamma_2+\hat{j}_s\sin\gamma_2] \qquad \text{EQ 13}$$

where:

ρ_2 = outside radius of separator

$\gamma_2 = \sin^{-1}\rho_p/\rho_2$

The components of both vectors in the X_s', Y_s', Z'_s coordinate sets are related by

$$\begin{bmatrix} X_s' \\ Y_s' \\ Z_s' \end{bmatrix} = \begin{bmatrix} \cos\theta & 0 & \sin\theta \\ 0 & 1 & 0 \\ -\sin\theta & 0 & \cos\theta \end{bmatrix} \begin{bmatrix} X_s \\ Y_s \\ Z_s \end{bmatrix} \qquad \text{EQ 14}$$

yielding:

$$\bar{a}_1 = \rho_3[\hat{i}_{s'}\cos\gamma_1\cos\theta + \hat{j}_{s'}\sin\gamma_1 - \hat{k}_{s'}\cos\gamma_1\sin\theta]$$

$$\bar{a}_2 = \rho_2[\hat{i}_{s'}\cos\gamma_2\cos\theta + \hat{j}_{s'}\sin\gamma_2 - \hat{k}_{s'}\cos\gamma_2\sin\theta] \qquad \text{EQ 15}$$

Notice that the angle θ arises from the specified tolerance of the ball pockets true position to within $\Delta\epsilon_\theta$ (refer to BBRC drawing No. 47446). The value of θ assumed in this analysis is

$$\theta = \tan^{-1}\left(\frac{\Delta\epsilon\theta}{\rho_{sAVG}}\right) \qquad \text{EQ 16}$$

where:

$\Delta\epsilon\theta$ = 0.005 inch for all bearings considered

ρ_{sAVG} = mean radius of separator

= 2.5400 inch for the 110 MM bearing

= 2.0900 inch for the 90 MM bearing

= 0.8117 inch for the 30 MM bearing

In the $X_{s''}$, $Y_{s''}$, $Z_{s''}$ the components of vectors $\bar{a}_1$ and $\bar{a}_2$ are obtained by the coordinate transformation matrix

$$\begin{bmatrix} X_{s''} \\ Y_{s''} \\ Z_{s''} \end{bmatrix} = \begin{bmatrix} \cos\psi & -\sin\psi & 0 \\ \sin\psi & \cos\psi & 0 \\ 0 & 0 & 1 \end{bmatrix} \begin{bmatrix} X_{s'} \\ Y_{s'} \\ X_{s'} \end{bmatrix} \qquad \text{EQ 17}$$

yielding:

$$\begin{aligned} \bar{a}_1 = \rho_3[&\hat{i}_{s''}(\cos\gamma_1\cos\psi\cos\theta - \sin\gamma_1\sin\psi) + \\ &\hat{j}_{s''}(\cos\gamma_1\sin\psi\cos\theta + \sin\gamma_1\cos\psi) + \\ &-\hat{k}_{s''}(\cos\gamma_1\sin\theta)] \end{aligned}$$

$$\text{EQ 18}$$

$$\begin{aligned} \bar{a}_2 = \rho_2[&\hat{i}_{s''}(\cos\gamma_2\cos\psi\cos\theta - \sin\gamma_2\sin\psi) + \\ &\hat{j}_{s''}(\cos\gamma_2\sin\psi\cos\theta + \sin\gamma_1\cos\psi) + \\ &-\hat{k}_{s''}(\cos\gamma_2\sin\theta)] \end{aligned}$$

Linear transformation

$$X_R = X_{s''} - \epsilon_s \cos\gamma_s$$

$$Y_R = Y_{s''} - \epsilon_s \sin\gamma \qquad \text{EQ 19}$$

$$Z_R = Z_{s''}$$

where:

ϵ_s = amplitude of radial motion of the separator

ϵ_s = inside diameter of separator - bearing inner ring radius

$\epsilon_s = \rho_{si} - \rho_{Li}$

γ_s = associated angle

and assuming θ to be small, the vectors $\bar{a}_1$ and $\bar{a}_2$ in the reference coordinate set become

$$\bar{a}_1 = \{\hat{i}_R[\rho_3\cos(\psi+\gamma_1) - \epsilon_s\cos\gamma_s] + \hat{j}_R[\rho_3\sin(\psi+\gamma_1) - \epsilon_s\sin\gamma_s] - \hat{k}\theta\cos\gamma_2\}$$
$$\bar{a}_2 = \{\hat{i}_R[\rho_2\cos(\psi+\gamma_2) - \epsilon_s\cos\gamma_s] + \hat{j}_R[\rho_2\sin(\psi+\gamma_2) - \epsilon_s\sin\gamma_s] - \hat{k}\theta\cos\gamma_2\} \qquad \text{EQ 20}$$

3.4 <u>The Edge Distance ϵ</u>

To satisfy the condition of tangency, the vector $\bar{\rho}_3$ is rotated an angle ψ_R, thus causing the terminal point of the vector $\bar{a}_4$ to be at point ρ_1. The rotation ψ_R is given by

$$\psi_R = \cos^{-1}\frac{\bar{a}_3\cdot\bar{a}_1}{|a_3||a_1|} \qquad \text{EQ 21}$$

and neglecting small terms, the value estimate for ψ_R becomes

$$\psi_R \cong (\gamma_1 - \gamma_3) \qquad \text{EQ 22}$$

Since the vector $\bar{\rho}_3$ and $\bar{a}_4$ terminate on the same body, the vector $\bar{a}_4$ is modified to

$$\bar{a}_{4R} = \hat{i}_R[\rho_4\cos(\psi+\gamma_4+\gamma_R)+\epsilon_B\cos(\gamma_B+\gamma_R)]+$$
$$\hat{j}_R[\rho_4\sin(\psi+\gamma_4+\gamma_R)+\epsilon_B\sin(\gamma_B+\gamma_R)] \qquad \text{EQ 23}$$

The above yields the desired edge distance

$$\bar{\epsilon} = \bar{a}_2-\bar{a}_{4R}$$
$$= \hat{i}_R\{[\rho_2\cos(\psi+\gamma_2)-\rho_4\cos(\psi+\gamma_4+\psi_R)]-[\epsilon_S\cos\gamma_S+\epsilon_B\cos(\gamma_B+\psi_R)]\}+$$
$$\hat{j}_R\{[\rho_2\sin(\psi+\gamma_2)-\rho_4\sin(\psi+\gamma_4+\psi_R)]-[\epsilon_S\sin\gamma_S+\epsilon_B\sin(\gamma_B+\psi_R)]\}+$$
$$-\hat{k}_R\theta\cos\gamma_2$$

Minimum edge distance is obtained by setting $\gamma_2 = \gamma_B = \psi = 0$. The latter yields

$$\epsilon_{MIN} = [A_{XR}^2+A_{YR}^2+A_{ZR}^2]^2$$
$$\bar{\epsilon}_{MIN} = \{\hat{i}_R[\rho_{2MIN}\cos(\gamma_2)_{MIN}-\rho_{4MIN}\cos(\gamma_4+\psi_R)_{MIN}-(\epsilon_S+\epsilon_B)_{MAX}]+$$
$$\hat{j}_R[\rho_{2MIN}\sin(\gamma_2)_{MIN}-\rho_{4MAX}\sin(\gamma_4+\psi_R)_{MIN}]+$$
$$-\hat{k}_R\theta_{MIN}\cos(\gamma_2)_{MIN}\}$$

The solution for the edge distance and pertinent quantities leading to this evaluation are given in Table II.

3.5 Recommended Separator Design Changes

The conducted analysis indicates that the distance (ϵ) is small enough (for all bearings considered) to cause concern. The latter is somewhat more emphasized by the dimensionally uncontrolled fabrication deburring process which further reduces the distance ϵ. Since the control of the deburring radii or chamfers is reasonably difficult, when relatively small tolerances are required, increase of the outer diameter of the ball separator is recommended.

The criterion for the recommended increases was the desire to geometrically prevent contacts of the separator's outer diameter surfaces

TABLE II. EDGE DISTANCE OF THE BEARING RETAINERS

Quantities	Formulation or Symbol	Units	Bearings 110 MM	90 MM	30 MM
Radius of separator pocket	ρ_{PMIN}	inch	0.25700	0.2410	0.1620
Radius of bearing ball	ρ_{BNOM}	inch	0.25000	0.22935	0.15625
Inner radius of separator	ρ_{siMAX}	inch	2.44550	2.00500	0.75300
Outer radius of separator	ρ_{2MIN}	inch	2.63400	2.17450	0.8700
Outer radius of separator	ρ_{2MAX}	inch	2.63900	2.1795	0.8730
Ball pitch radius	ρ_{3MAX}	inch	2.57070	2.12060	0.83730
Radius of inner ring land	ρ_{LMIN}	inch	2.42050	1.98000	0.74400
Auxiliary Radius	$\rho_4 = [\rho^2_{3MAX}+\rho^2_{BNOM}]^{1/2}$	inch	2.58283	2.13297	0.85175
Bearing runout	ε_B	inch	⟵ 64×10^{-6} ⟶		
Maximum excursion of separator	$\varepsilon_{sMAX} = \rho_{siMAX}-\rho_{LMIN}$	inch	0.02500	0.02500	0.00900
angle	$\gamma_1 = 2\sin^{-1}\left(\frac{\rho_{PMIN}}{2\rho_{3MAX}}\right)$	deg	5.738	6.526	10.965
angle	$\gamma_2 = \sin^{-1}\frac{\rho_{PMIN}}{\rho_{2MIN}}$	deg	5.599	6.451	10.731
angle	$\gamma_3 = 2\sin^{-1}\left(\frac{\rho_{BNOM}}{2\rho_{3MAX}}\right)$	deg	5.574	6.199	10.708
angle	$\gamma_R = (\gamma_1-\gamma_3)$	deg	0.164	0.327	0.257
angle	$\gamma_4 = \tan\frac{\rho_{BNOM}}{\rho_{3MAX}}$	deg	5.580	6.099	10.755
(refer to para 3.3)	$\theta = \frac{.005}{\rho_{sAVG}}$	rad	0.0020	0.0024	0.006
Edge distance	ε_{MIN}	inch	0.0265	0.170	0.011

with that of the bearing outer ring land diameter. These diametral increases, together with the parameters yielding to the recommended diameteral increases, are given in Table III. Notice from Table III that the Δ increases considered: (1) the existing minimum diametral clearance between the separator and the bearing's outer ring land; (2) the possibility of thermal and separator processing distortions; and, (3) a reasonable clearance.

TABLE III. RECOMMENDED DIAMETRAL INCREASES FOR THE DMA'S BEARING BALL SEPARATOR

Quantity Definition	Symbols	Units	Bearings		
			110 MM	90 MM	30 MM
Bearing outer ring land diameter, minimum	D_{Lo}	inch	5.436	4.518	1.856
Bearing inner ring land diameter, minimum	D_{Li}	inch	4.841	3.960	1.488
Separator outside diameter, maximum	D_{so}	inch	5.278	4.359	1.746
Separator inside diameter, maximum	D_{si}	inch	4.883	4.002	1.502
Minimum diametral clearance between outer ring land and the outside diameter of the separator of present system:					
$(D_{Lo}+D_{Li})_{MIN}-(D_{so}+D_{si})_{MAX}$ =	δ_{MIN}	inch	0.116	0.117	0.096
• Radial distortion due to processing of separator	δ_D	inch	0.015	0.012	0.006
• Radial clearance between separator and outer ring land	δ_C	inch	0.020	0.016	0.0007
MAXIMUM RECOMMENDED DIAMETRAL INCREASE OF SEPARATOR'S OUTSIDED DIAMETER					
$\delta_{MIN}-2(\delta_D+\delta_C)$ =	Δ	inch	0.046	0.061	0.070

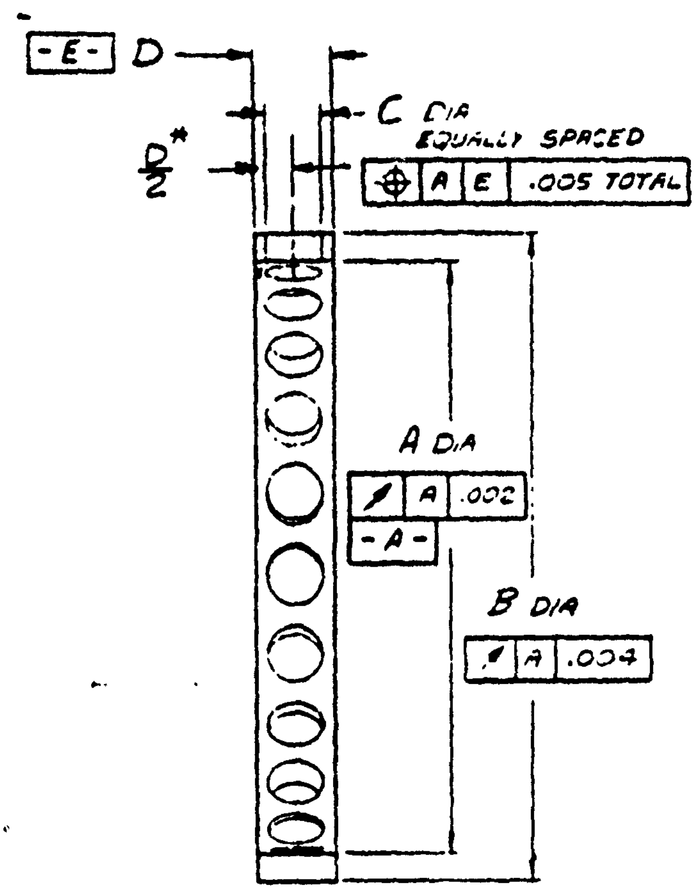

1. * RECOMMENDED DIM. CHANGE
2. MAX DEBURRING RADIUS OR CHAMFER 0.015 INCH

FIG 5. RECOMMENDED DIMENSIONAL CHANGES

Also recommeded is dimensional control of two fabrication parameters. These are:

- Maximum deburring radius or chamfer 0.015
- Control of the center line of the ball pockets with respect to a reference plane as shown on Figure 5. . . . . $\frac{D}{2}$

The minimum clearance dimension (c) (Figure 6) between the retainer's width surface and the shoulder of the bearing's inner race is given by

$$C_{MIN} = 1/2(W_{RMIN}-W_{SMAX})-D\{[(\rho_i/D)_{MAX}-.5]\sin\alpha_o+.5(\frac{D_{\rho}MAX}{D}-1)\}$$

$$= .5(.7037-.685)-.4687[(.520-.5)\sin 15.1°+.5(\frac{.488}{.4687}-1)]$$

$$= .003 \text{ inch}$$

Since no control exists for the dimension $W_s/2$ (Figure 6), the clearance (c) is insufficient and contacts between the separator and the preload mechanism's washer surface (located at the shoulder of the retainer) will occur. Decrease of the retainer width dimension is being recommended. Specifically, the maximum width dimension of the 90 MM bearing retainer should be 0.671" and its minimum width 0.666".

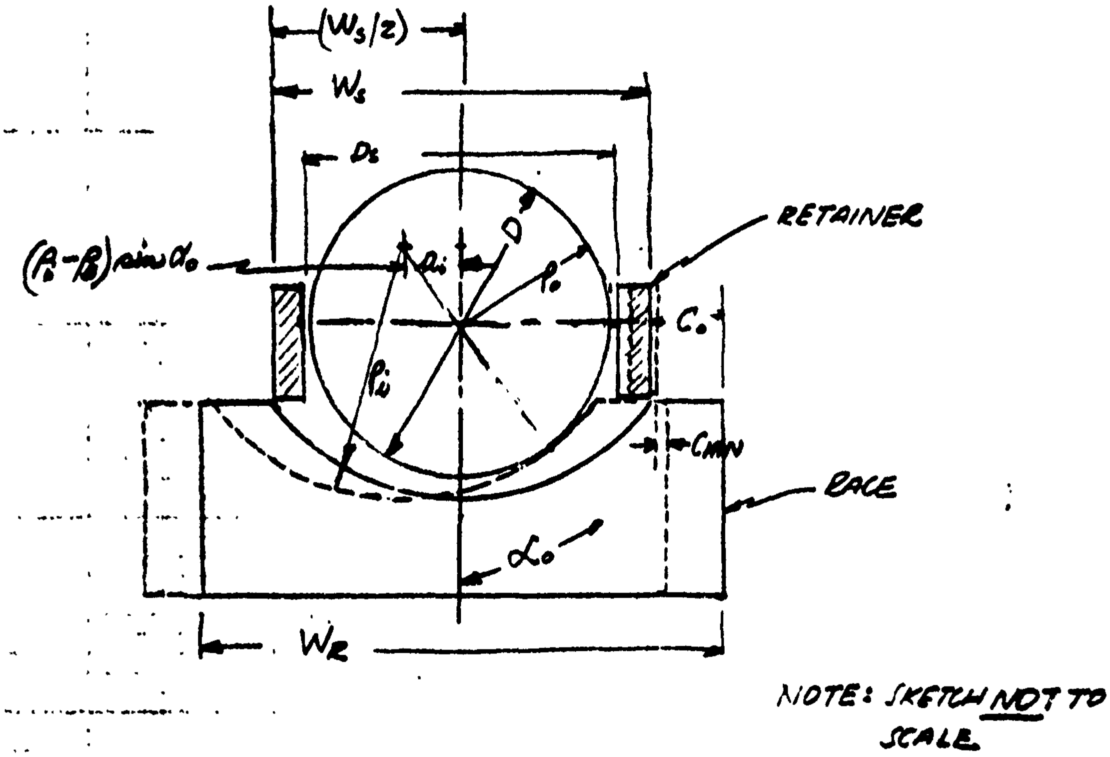

FIG6. GEOMETRIC RELATIONSHIPS OF RETAINER AND BEARING COMPONENTS

TRW
SYSTEMS GROUP

INTEROFFICE CORRESPONDENCE 76.7345-044

TO: P. C. Wheeler CC: A. H. Rosenberg DATE: 23 January 1976

SUBJECT: 777 DMA Anomaly - Miscellaneous Dimensional Analyses

FROM: J. G. Zaremba
BLDG. 82 MAIL STA. 1367 EXT. 50993

1.0 INTRODUCTION AND SCOPE

This memorandum documents miscellaneous analyses related to the 777 DMA Anomaly. The analyses are presented in the form of calculation notes assembled in Paragraph 3.0. Paragraph 2.0 summarizes the significant results.

Of particular interest is the consideration of the resolver snubber gap closure aspect for the spin down platform condition. The snubber consists of two components, the spacer and the bracket (refer to Figures 1, 2 and 3). Its function is to protect the resolver components from damage due to the launch environment. The nominal radial gap at the snubber is 0.008", a specified minimum is 0.002" and the actually measured gap is 0.006" minimum.

Other aspects of the analyses are (1) the dimensional considerations of the bearing fits, (2) the orbital temperature effects on their values, (3) the motor shaft/main shaft interface, (4) the DMA's shaft-cross beam mount interface with the spacecrafts and (5) the bearing misalignment.

The analyses were performed by W. B. Palmer, member of the SVD's Mechanical Design Department.

2.0 SUMMARY OF RESULTS

2.1 Bearing Fits (refer to calculation notes pp 1-5)

Table I, Bearing Fits

Item	Dimensions and Tolerances: 110 MM BRG	Dimensions and Tolerances: 90 MM BRG
Bearing OD/Housing, fit, inch	0.00000-0.00080, tight	0.00000-0.00080, tight
Bearing ID/Shaft, fit, inch	0.00005-0.00060, loose	0.00045-0.00010, loose
Roundness of housing, inch	0.00020	
Roundness of shaft, inch	Within the tolerance of OD dimension	
Diametral reduction of outer race due to press fit, inch	0.00644	0.000558
Bearings diamteral clearance after press fit, inch	0.00656	0.000742
Minimum installation contact angles, degree of arc	9.2913	10.2075
Axial shift of bearings per radial bearing clearance reduction, inch/inch	3.18	2.88

2.2 Orbital Temperature Effects (refer to calculation notes pp. 6-10)

Table II. Dimensional Reductions Due to Orbit Thermal Environment

Item	Dimensions (Inch)
110 MM brg. diametral clearance reuction, max.	0.000212
90 MM brg shaft to bearing diametral slip fit reduction, max.	0.000295
Interference increase between housing and OD of 90 MM brg, mzx.	0.000058
Bearings center to center change, max	0.000441

2.3 Main Shaft/Motor Shaft Interface Events (Refer to calculation notes pp. 11-12)

- 0.001 press fit expends the end of the main shaft at four mount points by — 0.000212 inch
- The motor shaft increases in dia. at a rate of 12×10^{-6} inch/^{o}F hence the diametral increase at 160^{o} is — 0.00108 inch

2.4 Main Shaft and Mounting Cross Beam Interface Events (Refer to calculation notes pp. 13-14)

NOTE: Two 0.250 inch screws connect shaft to beam at four (4) places.

- Max load to cause lateral slippage is (This twice the value possible) — 1848 lbs
- At temperature of 59^{o}F cross beam shrinks more than the shaft by (Reduction of bearing clearances results) — 0.00679 inch

2.5 Resolver Snubber Gap Closure
(Refer to calculation notes pp. 15-19)

Factors Causing Gap Closure	Worst Case Reduction
• Motor loads on shaft take up any radial clearances between shaft and inner races of bearings.	.0016"
• Spacer grows in diameter due to dimensional instability of material, accelerated by elevated temperature from motor heating.	.0023"
• Bracket grows in diameter due to dimensional instability but not as much as spacer because at lower temperature. Bracket may go out of round because of unsymmetrical grain orientation since it is fabricated from plate.	.0010"
• Spacer grows in diameter more than the bracket, due to coefficient of thermal expansion, as motor temperature rises. (Spacer 178°, brkt. 111° motor dissipation - 20 watts.)	.0016"
• The ΔT across the diameter of the motor shaft, due to location of the windings on one side, causes bending (for 12.6 watt power dissipation).	.00023"
• Loss of preload in bearings permits radial play. This could occur if the preload mechanism became jammed in a retracted position because of fretting between shaft and inner race of upper bearing.	.0019"
RSS	0.0034

2.6 Bearing Misalignment (Refer to Calculation notes p. 20)

- The misalignment of the 90 MM bearings can lock the preload mechanism.
- Maximum misalignment of the bearing alone due to inner race slip fit clearance is 0.099 degree of arc.
- The maximum misalignment possible due to DMA's geometric constraint is 0.0485 degree of arc.

JGZ/gw

J. G. Zaremba

J. G. Zaremba

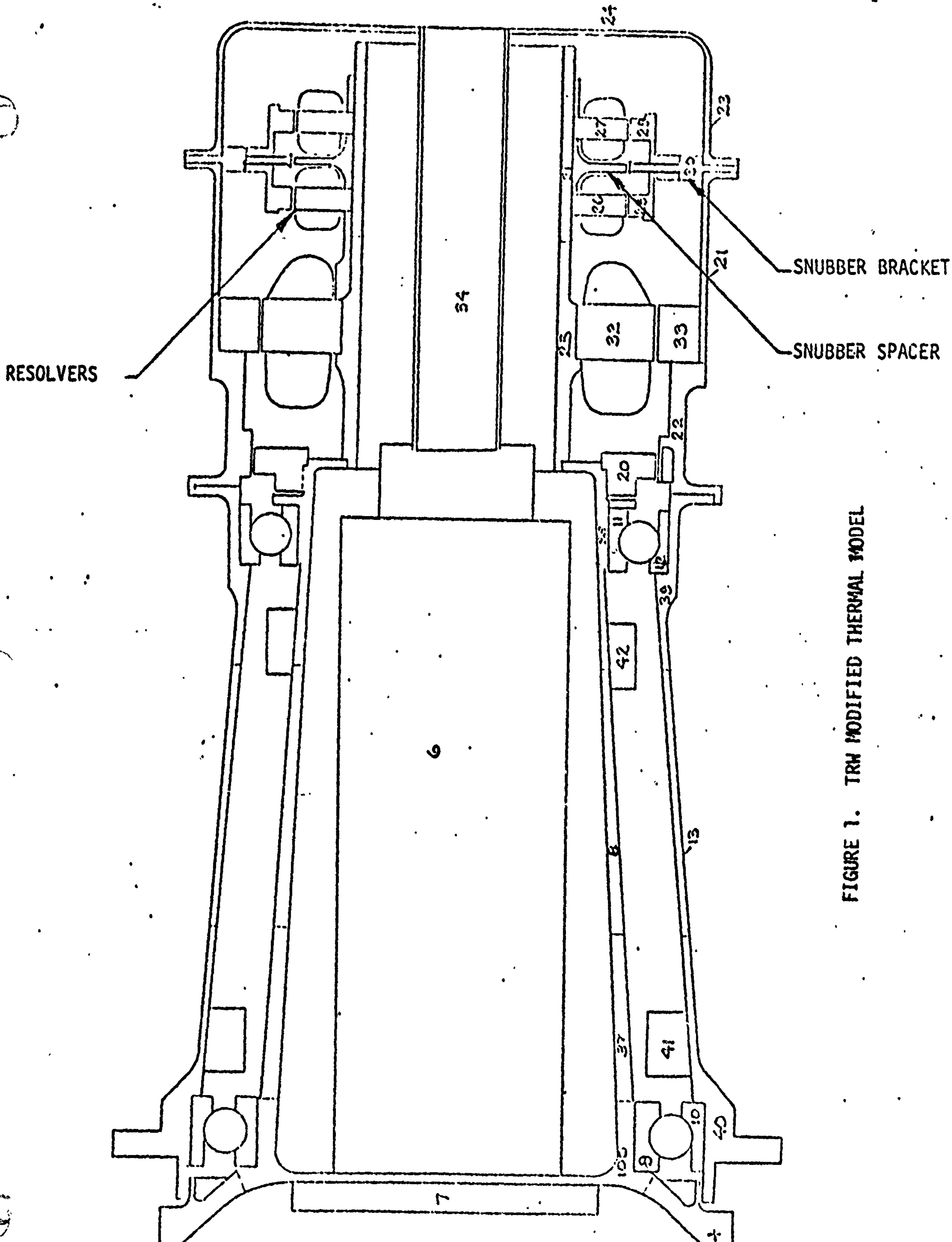

FIGURE 1. TRW MODIFIED THERMAL MODEL

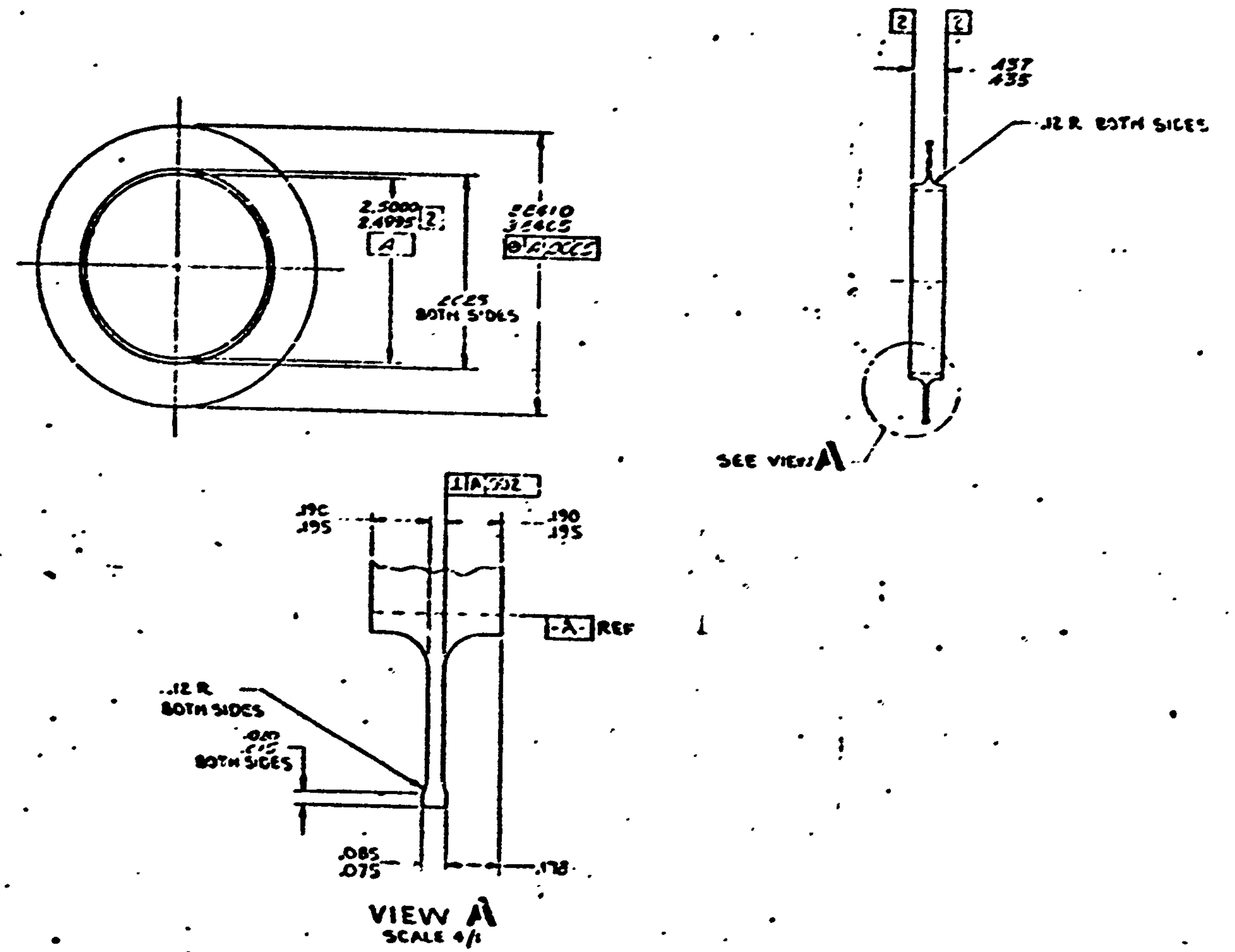

FIGURE 2. SPACER

THIS PAGE IS BEST QUALITY PRACTICABLE
FROM COPY FURNISHED TO DDC

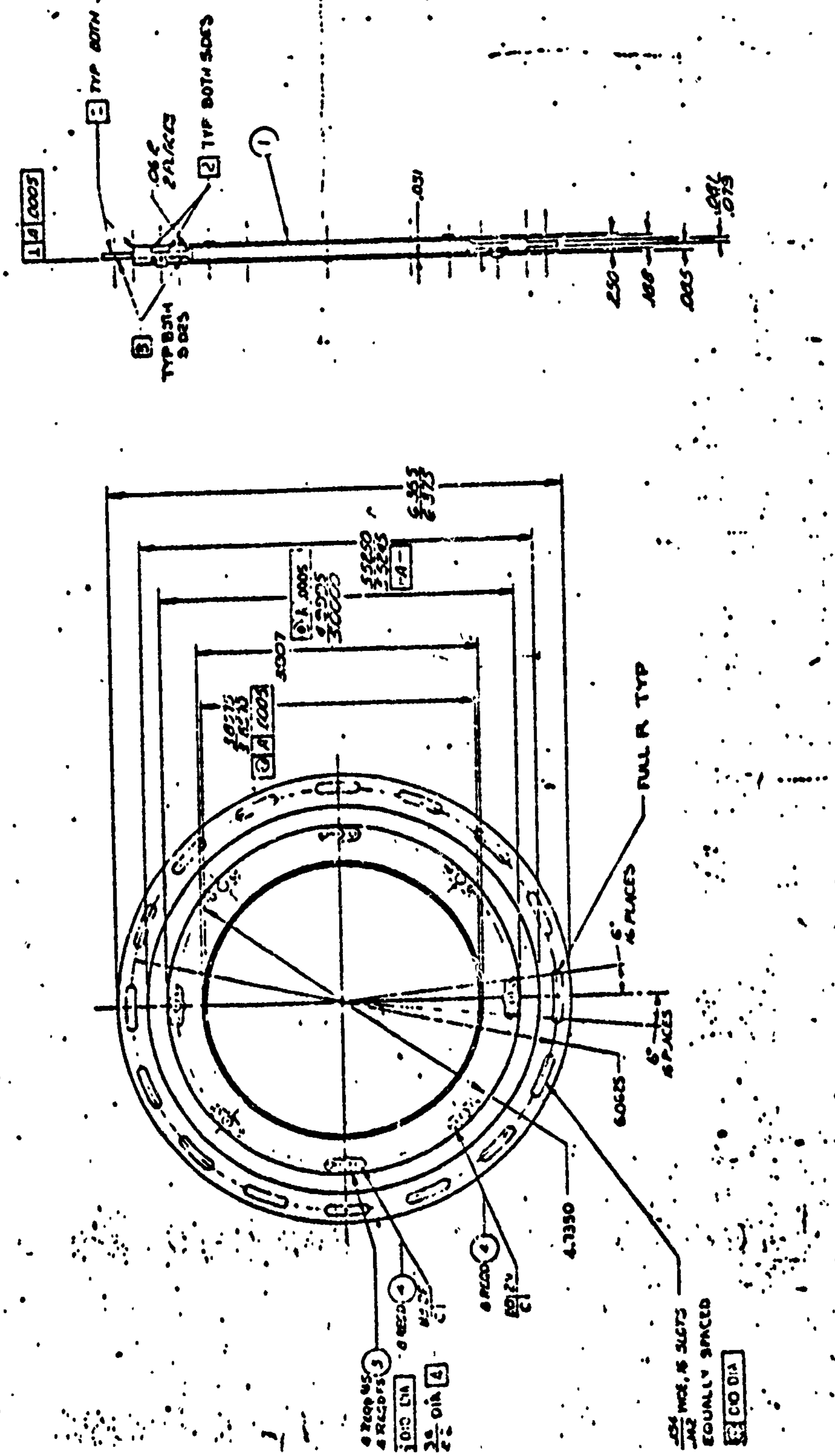

FIGURE 3. BRACKET

ANALYSES

CALCULATION NOTES

PREPARED W. PALMER 10-1-75 REPORT NO. PAGE 1

CHECKED

MODEL

HOUSING / BEARING FITS
777 DMA

LOWER BEARING

HOUSING BORE	5.9047	5.9051	-A-
BEARING OD	5.9055	5.9051	
INTERFERENCE	-.0008	0	

BORE - ALUM. OXIDE PLASMA DEPOSITED .002" - 005" THICK

8/√ LAPPED OR GROUND AFTER CHEMICAL ETCH

○ .0002 ON DIA

SHOULDER ⊥ A .001

HOUSING RADIUS .020 .030
MAX. ALLOWABLE RADIUS BEARING WILL CLEAR .039

UPPER BEARING

HOUSING BORE	4.9205	4.9209
BEARING OD	4.9213	4.9209
INTERFERENCE	-.0008	0

BORE - ALUM OXIDE PLASMA DEPOSITED

8/√ ○ .0002 ON DIA.
⊙ A .0005 TIR

SHOULDER ⊥ A .001

THIS PAGE IS BEST QUALITY PRACTICABLE
FROM COPY FURNISHED TO DDC

SHAFT / BEARING FITS
777 DMA

LOWER BEARING

BEARING BORE	4.33045	4.33070
SHAFT	4.3304	4.3301
CLEARANCE	+.00005	+.0006

ALUM. OXIDE COATED .002 -.003 THICK

LAPPED OR GROUND ✓

FILLET RAD .050 - .060

DIA. AT FILLET RAD. TANGENT MAX. = 4.3304 + .120 = 4.4504 OK

UPPER BEARING

BEARING BORE	3.54305	3.54330
SHAFT	3.54260	3.54230
CLEARANCE	+.00045	+.0010

ALUM OXIDE COATED

✓

THIS PAGE IS BEST QUALITY PRACTICABLE
FROM COPY FURNISHED TO DDC

INTERFERENCE FIT OF HOUSING
2 OUTER BEARING RACE

LOWER BEARING (-1)

OUTER RACE OD $D_h = 5.9055$ $D_h/D_2 = 1.0356$ $\left(\frac{D_h}{D_2}\right)^2 = 1.179$
OUTER RACE ID $D_2 = 5.440$
HOUSING FLANGE OD $D_1 = 7.638$ $D_1/D_h = 1.3018$ $\left(\frac{D_1}{D_h}\right)^2 = 1.695$

$E_b = 29 \times 10^6$ $E_h = 42.5 \times 10^6$

MAX INTERFERENCE $= .0008$
REDUCTION OF INTERFERENCE DUE TO GROUND SURFACES $=$
$.00008 - .00020$

LET $I = .0008 - .00008 = .00072$

REDUCTION IN OUTER RACE ID

$$\Delta_h = \frac{2I\left(\frac{D_h}{D_2}\right)}{\left[\left(\frac{D_h}{D_2}\right)^2-1\right]\left\{\frac{\left(\frac{D_h}{D_2}\right)^2+1}{\left(\frac{D_h}{D_2}\right)^2-1} - \xi_b + \frac{E_b}{E_h}\left[\frac{\left(\frac{D_1}{D_h}\right)^2+1}{\left(\frac{D_1}{D_h}\right)^2-1} + \xi_h\right]\right\}}$$

$$\Delta_h = \frac{2(.00072)1.179}{(.179)\left\{\underbrace{\frac{2.179}{.179}}_{11.873} - .3 + \frac{29}{42.5}\left(\underbrace{\frac{2.695}{.695}}_{2.85} + .3\right)\right\}} = \frac{.001697}{2.6354} = \underline{.000644''}$$

UPPER BEARING (-3)

OUTER RACE OD $D_h = 4.9205$ $\frac{D_h}{D_2} = 1.088$ $\left(\frac{D_h}{D_2}\right)^2 = 1.184$
OUTER RACE ID $D_2 = 4.522$
HOUSING FLANGE OD $D_1 = 6.000$ $\frac{D_1}{D_h} = 1.219$ $\left(\frac{D_1}{D_h}\right)^2 = 1.487$
LET $I = .0008 - .00008 = .00072$

$$\Delta_h = \frac{2(.00072)1.088}{(.184)\left\{\underbrace{\frac{2.184}{.184}}_{11.87} - .3 + \frac{29}{42.5}\left(\underbrace{\frac{2.487}{.487}}_{5.69} + .3\right)\right\}} = \frac{.001566}{2.8077} = \underline{.000558''}$$

THIS PAGE IS BEST QUALITY PRACTICABLE
FROM COPY FURNISHED TO DDC

PREPARED W. PALMER 10-6-75 REPORT NO. PAGE

CHECKED

MODEL

MINIMUM CONTACT ANGLES INSTALLED & UNLOADED

LOWER BEARING 46265-1

MIN. DIAMETRAL CLEARANCE .001300 − .000644 = .000656"

$$\alpha_{MIN} = \cos^{-1}\left(1 - \frac{P_d}{2A}\right) = \cos^{-1}\left(1 - \frac{.000656}{2(.025)}\right) = \underline{9.2913^\circ}$$

UNLOADED & NO TEMP. EFFECTS

IF P_d IS REDUCED .0001" DUE TO TEMP. CHANGES

$$\alpha = \cos^{-1}\left[1 - \frac{.000556}{2(.025)}\right] = 8.5525^\circ$$

END PLAY $P_E = 2A \sin\alpha$

$$\frac{\Delta P_E}{2} = (.025)\sin 9.2913 - (.025)\sin 8.5525 = .000318''$$

AXIAL SHIFT FOR .0001" RAD

UPPER BEARING 46265-3

MIN. DIAMETRAL CLEARANCE .001300 − .000558 = .000742"

$$\alpha_{MIN} = \cos^{-1}\left(1 - \frac{P_d}{2A}\right) = \cos^{-1}\left(1 - \frac{.000742}{2(.02344)}\right) = \underline{10.2075^\circ}$$

UNLOADED

IF P_d IS REDUCED .0001"

$$\alpha = \cos^{-1}\left(1 - \frac{.000642}{2(.02344)}\right) = 9.4931^\circ$$

AXIAL SHIFT FOR .0001" REDUCTION IN P_d

$$\frac{\Delta P_E}{2} = (.02344)\sin 10.2075^\circ - (.02344)\sin 9.4931^\circ = .000288''$$

.0041539 .0038659

LOWER BRG. -1 CONTACT ANGLE 14° TO 18°
AT GAUGING LOAD OF 58 - 68 LBS

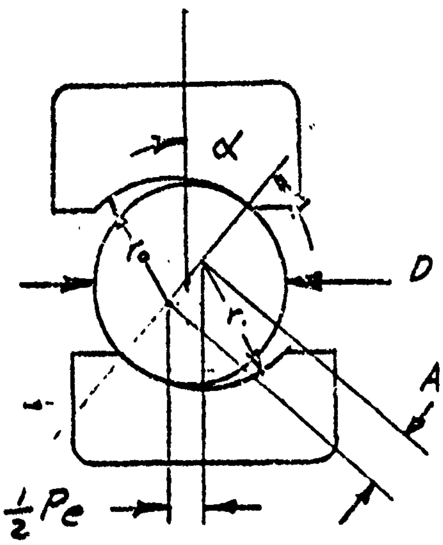

FREE CONTACT ANGLE -1 BRG.

$$\alpha^\circ = \cos^{-1}\left(1 - \frac{P_d}{2A}\right)$$

P_d = Diametral Clearance $d_o - d_i - D$
FROM BALL BROTHERS DOC. NO. 46265

$P_d = .0013$ to $.0017$

$r_o = .525D$ to $.530D$

$r_i = .515D$ to $.520D$ $\qquad D = .500$ NOM.

$A_{MAX} = .530D + .520D - D = .025$

$A_{MIN} = .525D + .515D - D = .020$

$$\left.\begin{aligned} \alpha_{MIN} &= \cos^{-1}\left(1 - \frac{.0013}{2(.025)}\right) = 13.094^\circ \\ \alpha_{MAX} &= \cos^{-1}\left(1 - \frac{.0017}{2(.020)}\right) = 16.764^\circ \end{aligned}\right\} \text{FREE CONTACT ANGLE}$$

FREE END PLAY $\frac{1}{2}P_e = A \sin\alpha = .025 \sin 13.094^\circ = .00566''$ MIN.

PREPARED W. PALMER 9-15-75 REPORT NO. PAGE

CHECKED

MODEL

TEMPERATURE HISTORY
JULY 12 TO SEPT. 12

HOUSING

HOUSING MIN. AVE TEMP PRIOR TO INCREASE IN V 61° SEVERAL DAYS PRIOR TO 8/21

HOUSING MIN AVE TEMP SINCE 8/29 69°

HOUSING MAX AVE TEMP PRIOR TO INCREASE IN V 81°

AVE. TEMP DECREASED TO 79° MAX UNTIL 9/2 THEN WENT TO 81° MAX

HEATERS ON 9/9 90° MAX

MAX TEMP W/O HTRS 85°

SHAFT AT BTM. BRG

MIN. TEMP 58°
MAX TEMP W/O HTRS 72°
MAX TEMP WITH HTRS 83°
TEMP. INCREASED FROM 8/30 TO 9/2 66° TO 71° ON 9/2
MAX TEMP 9/12 73°F

SHAFT AT TOP BRG.

MIN. TEMP 62°
MAX. T W/O HTRS UNTIL 9/2 73°
MAX T " " 9/4 80°
MAX T WITH HTRS 9/9 88°
MAX T W/O HTRS 9/12 83°

BILL PALMER

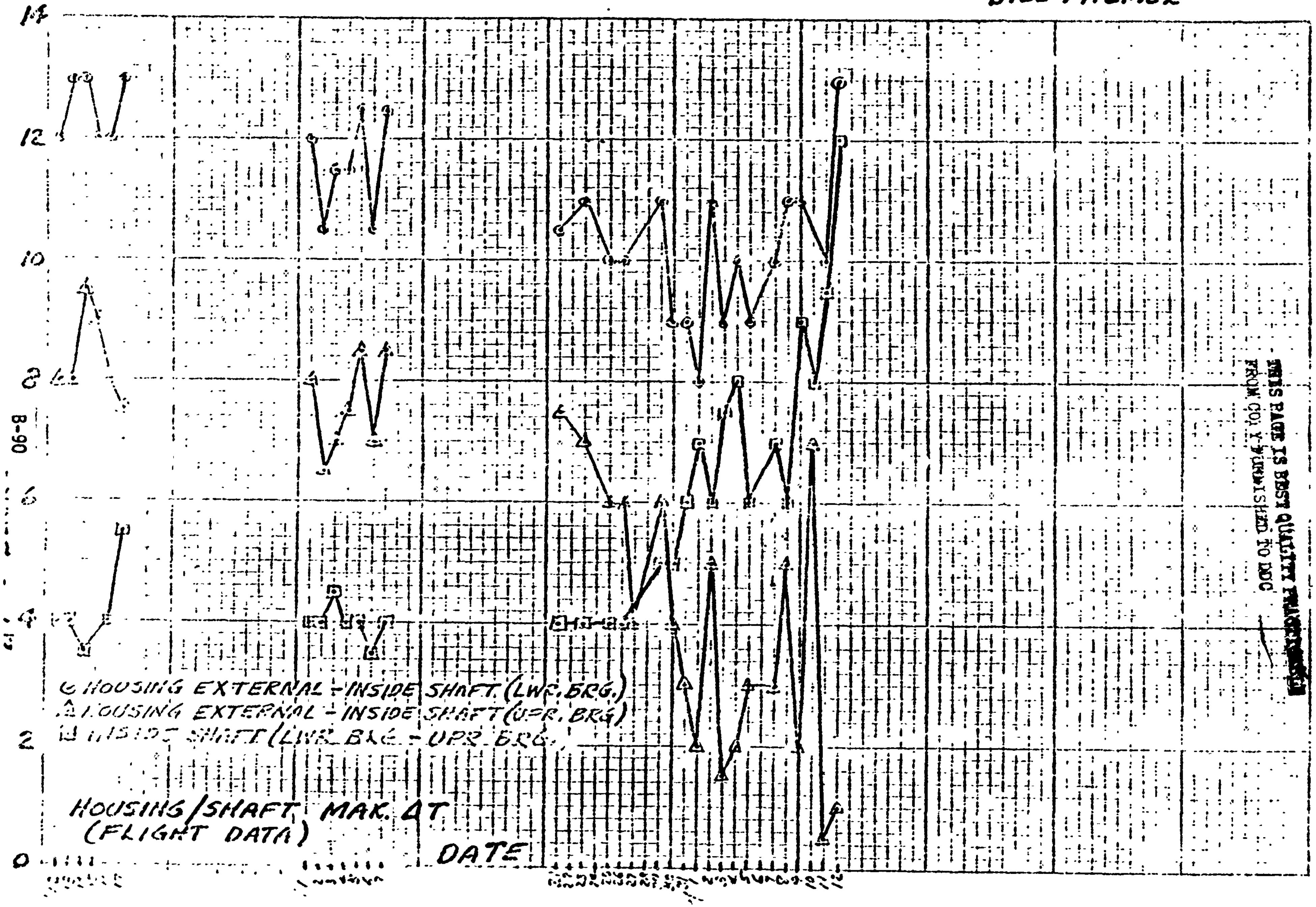

THIS PAGE IS BEST QUALITY PRACTICABLE
FROM COPY FURNISHED TO DDC

TRW
SYSTEMS GROUP
ONE SPACE PARK • REDONDO BEACH CALIFORNIA

PREPARED V. PALMER 9-17-75 REPORT NO. PAGE 8

CHECKED

MODEL

UPPER BEARING - EFFECT OF FLIGHT TEMP. OF SHAFT & HOUSING

W/O HEATERS

MAX. SHAFT TEMP = $\underline{83°}$

ASSUME BRG. ASSY. AT 70° AT INSTALLATION

AT INNER RACE/SHAFT; SHAFT INCREASE IN DIA

$\Delta D = 6.4 \times 10^{-6} \times 3.543 \times (83-70) = \underline{.000295}$" REDUCTION IN SLIP FIT

WITH HEATERS T = 88°F MAX.

MAX. ΔT ACROSS BRG. 9.5°F 7/14/75

$\Delta D = 6.3 \times 10^{-6} \times 3.543 \times 9.5 = \underline{.000212}$"

REDUCED TO ΔT = .5°F SEPT. 11 -

LOWER BEARING – EFFECT OF TEMP CHANGES

THE SHAFT TEMP. IS NEVER HIGHER THAN THE HOUSING TEMP.
FLIGHT DATA INDICATES MAX TEMP. OF 72° W/O HEATERS PRACTICALLY NO CHG. FROM INSTALLATION TEMP.

MIN. HOUSING TEMP. = 61°
TEMP. OF SHAFT AT BRG = 59°

INCREASE IN INTERFERENCE BETWEEN HOUSING & OUTER RACE

$$\Delta I = (\alpha_{Be} - \alpha_{440})D_o(T_H - T_{ASSY})$$

$$\Delta I = (6.3-5.6)\times10^{-6}\times 5.905\,(61 - 75) = -.00005 7869''$$

THE Be SHAFT WILL SHRINK AWAY FROM INNER RACE INCREASING CLEARANCE

$$\Delta C = (6.3-5.6)\times10^{-6}\times 4.330\,(59-75) = -.0000 48496''$$

THIS PAGE IS BEST QUALITY PRACTICABLE
FROM COPY FURNISHED TO DDC

PREPARED W. PALMER 9-17-75 REPORT NO. PAGE 10

CHECKED

MODEL

AXIAL GROWTH OF HOUSING - BRG SEAT TO BRG SEAT

MAX TEMP. WITH HEATERS ON +90°F 9/9/75

AVE TEMP. OF SHAFT AT SAME TIME 83°F

$\Delta T = 7°F$

HOUSING TEMP 85° 9/12/75
SHAFT AVE 77.5
7.5°F

MAX. ΔT = 10°F SEE 7/12 + OTHERS

DISTANCE BETWEEN BEARING ℄

$L = 7.125 - .875 + \frac{W_1}{2} + \frac{W_2}{2} = 6.9945$ USE 7.0

$\Delta L = 6.3 \times 10^{-6} \times 7.0 \times 10 = \underline{.000441}$" MAX. RELATIVE MOTION BETWEEN BEARINGS OR AMOUNT OF SLIP AT INNER RACE OF TOP BRG.

TRW
SYSTEMS GROUP
ONE SPACE PARK • REDONDO BEACH CALIFORNIA

PREPARED W. Palmer 10-3-75 | REPORT NO. |

CHECKED

MODEL

MOTOR SHAFT / MAIN SHAFT INTERFACE

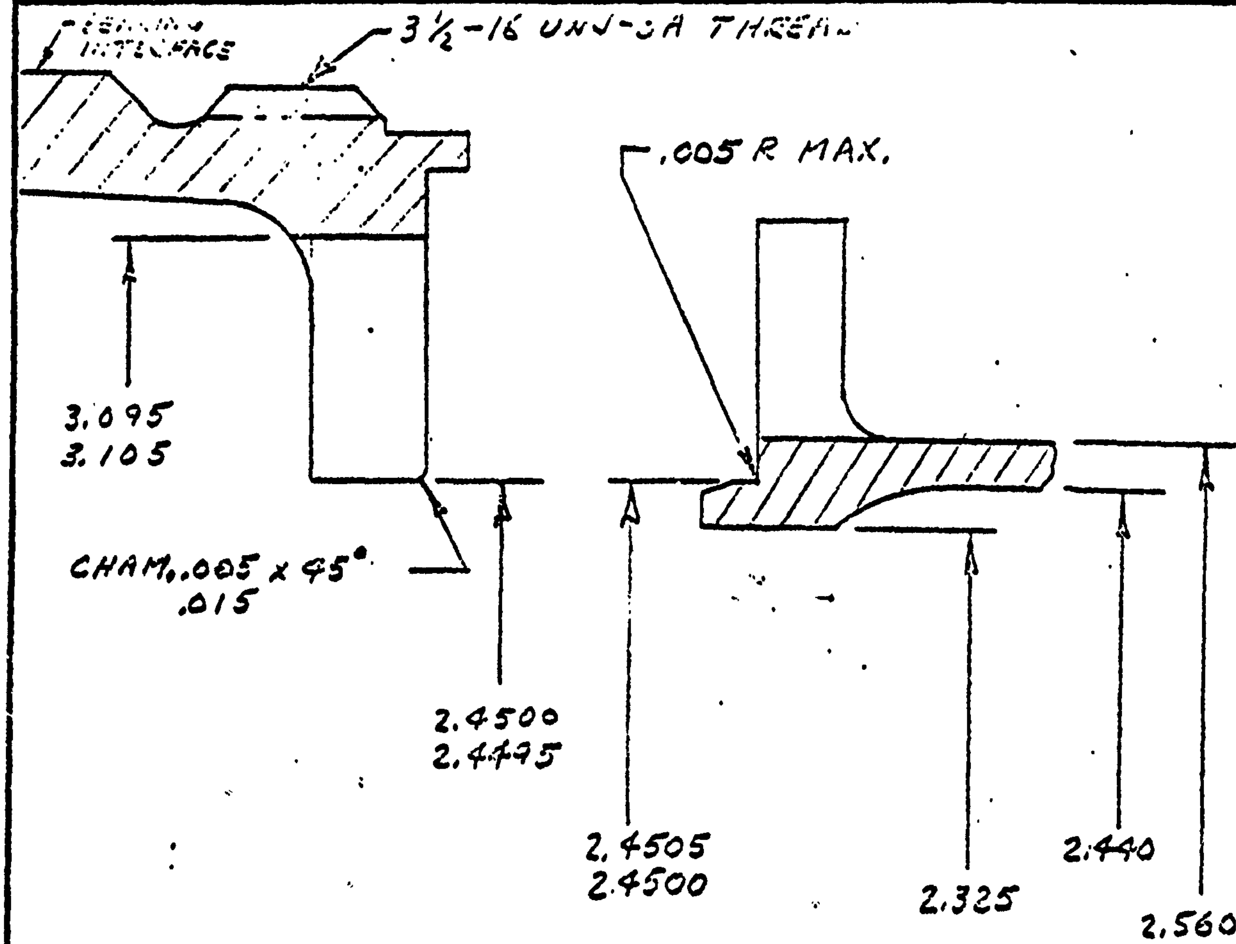

4 TIMES SIZE

FIT AT 4 LUGS

2.4500	2.4495
2.4500	2.4505
0	-.0010

SINCE THE INTERFACE HAS 4 LUGS EACH RING WILL BE LOADED AS SHOWN

	OUTER	INNER
MEAN RAD.	1.64	1.22
t	.18	.12
E	42.5×10^{6}	16×10^{6}
α	6.4×10^{-6}	4.9×10^{-6}

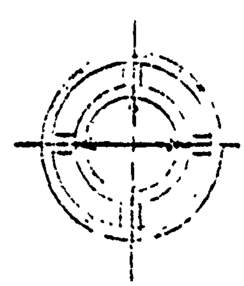

THIS PAGE IS BEST QUALITY PRACTICABLE
FROM COPY FURNISHED TO DDC

PREPARED W. PALMER 10-3-75 REPORT NO.

CHECKED

MODEL

MOTOR SHAFT/MAIN SHAFT INTERFACE - TEMP. EFFECTS

DEFLECTION AT LOAD $\theta = 0$

$$U_0 = \frac{P r_0^3}{E_0 I} \overset{.0061}{(.6427 - .6366)} \quad \text{MAIN SHAFT}$$

$$U_i = \frac{P r_i^3}{E_i I_i} .0061 \quad \text{MOTOR SHAFT}$$

$$I_{DIA.} = 2(U_0 + U_i) = .001 \text{ MAX. INTERFERENCE}$$

$$\frac{U_0}{U_i} = \frac{E_i I_i r_0^3}{E_0 I_0 r_i^3} = \frac{16}{42.5} \frac{(.12)^3}{(.18)^3} \frac{(1.54)^3}{(1.22)^3} = .270$$

$$I = \frac{b t^3}{12} \qquad t_0 = .18 \quad t_i = .12$$

LET $b_0 = b_i$

$$\frac{I_I}{I_0} = \frac{(.12)^3}{(.18)^3}$$

$$I = 2(.270\,U_1 + U_1) = .001''$$

$$2.54\,U_1 = .001$$

DIAMETRAL

DEFL. OF MOTOR SHAFT U_1 = .000393" RADIAL .000786"

DEFL. OF MAIN SHAFT U_0 = .000106" RADIAL .000212"

ON DIA. AT 4 POINTS

TEMPERATURE EFFECTS

MOTOR SHAFT

$\Delta D/_{°F} = 4.9 \times 10^{-6} \times 2.45 \times 1 = .0000120''/°F$

ASSUME 160°F TEMP $\Delta T = 160 - 70 = 90°$ $\underline{\Delta D = .00108''}$

ASSUME A WORST CASE INTERFERENCE FIT BETWEEN SHAFTS INITIALLY = .001" THEN THE MAIN SHAFT TEMP. WOULD INCREASE IN TEMP. AS WELL; HOWEVER THE THERMISTOR DATA DOES NOT REFLECT THIS. BECAUSE OF THE MASS OF THE SHAFT & BACKUP STRUCTURE THE TEMP. RISE AT THE UPPER BEARING IS NOT SIGNIFICANT.

TRW
SYSTEMS GROUP
ONE SPACE PARK • REDONDO BEACH CALIFORNIA

PREPARED	W. PALMER	9-20-75	REPORT NO. PAGE 13
CHECKED			TEMP. EFFECTS AT CROSS-BEAM / SHAFT INTERFACE
MODEL			

ELEVATED TEMP. EXTREMES

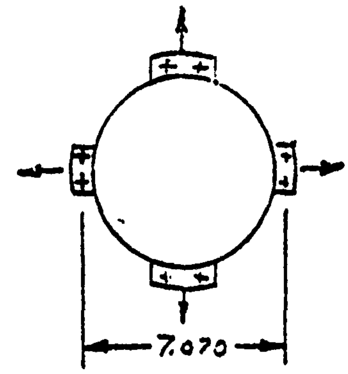

BEAM TO SHAFT (SAME TEMP) 83° WITH HEATERS ON
$\Delta T = 13°F$ FROM INSTALL.

$\Delta L_s = (12.5-6.5)10^{-6}\ 7.070 \times 13 =$ .00055" INCREASE IN SHAFT

THE BEAM IS PROBABLY EVEN HIGHER, SHAFT AT 83°F

HOUSING TEMP AT SAME TIME = 90°

$\Delta L_H = 6.5\times10^{-6} \times 5.9055 \times 20 =$ .000768" INCREASE IN HOUSING

LOWER TEMP. EXTREMES — SHAFT 59° HOUSING 61°
ASSUME BEAM & SHAFT AT 59°

$\Delta L_{S\text{-}B} = (12.5-6.5)10^{-6} \times 7.070 \times \overset{16}{(75-59)} = .000679''$ COMPRESSION OF SHAFT FROM BEAM (.000154" WILL CAUSE JOINT TO SLIP, SEE P.

$\Delta L_H = 6.5\times10^{-6} \times 5.9055 \times 75-61$

$=$ .0005374 REDUCTION IN HOUSING / OUTER RACE OF BEARING

INNER RACE SHRINKAGE

$\Delta D_i = 5.6\times10^{-6} \times 4.64 \times 16 = .000415''$

REDUCTION IN CLEARANCE $.0005374 - .000415'' = .000121''$

THIS PAGE IS BEST QUALITY PRACTICABLE
FROM COPY FURNISHED TO DDC

SP0121-4824 SCREWS   80-90 IN/LB SCREW TORQUE

142-154 IN/LB NUT TORQUE

MAX PRELOAD AT EACH SCREW

$$P = \frac{T}{0.2\,D_N} = \frac{154}{0.2(.250)} = 3080 \text{ LB.}$$

MAX. LOAD TO SLIP JOINT

$Q = 2 \times 3080 \times .3 = 1848$ LB

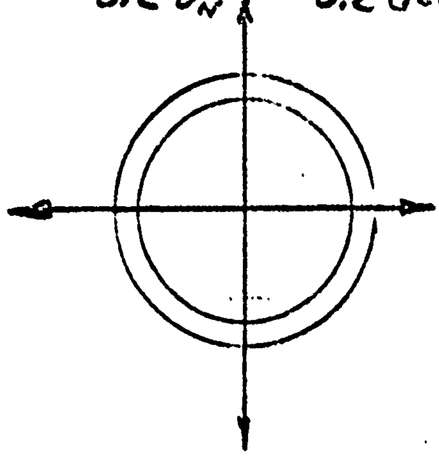

6.625
3.250
2|3.375
$h = 1.687$

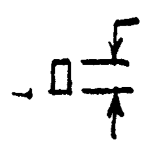

OD = 6.625
ID = 3.250
2|9.875   4.9375 = r

RADIAL DEFLECTION

$$u = \frac{Pr^3}{EI}\left[.2500(1+\theta)\sin\theta + (.6427 - .2500\theta)\cos\theta - .6366\right]$$

FOR $\theta = 0$

$$u = \frac{1848\,\overset{120.37}{(4.9375)^3}}{44\times10^6 \times .200}\left[0 + \overset{.0061}{.6427 - .6366}\right] = .000157'' \text{ DEFL.}$$

OF SHAFT AT LOAD OF 1848 LB. - SLIP LOAD

$$I = \frac{bh^3}{12} = \frac{.5(1.687)^3}{12} = .200$$

TRW
SYSTEMS GROUP
ONE SPACE PARK • REDONDO BEACH CALIFORNIA

PREPARED W. PALMER 10-5-75 REPORT NO. PAGE 5

CHECKED

MODEL

RESOLVER BUMPER CLEARANCE

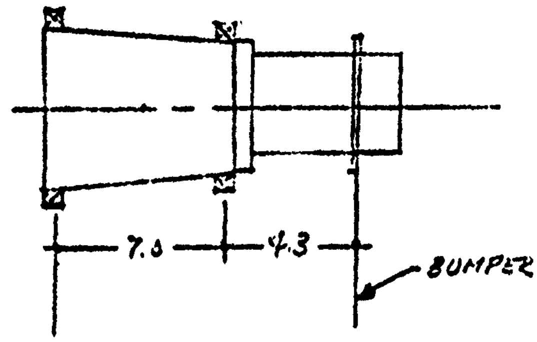

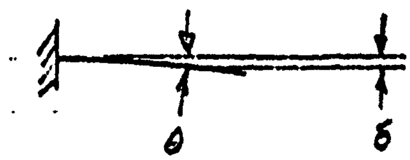

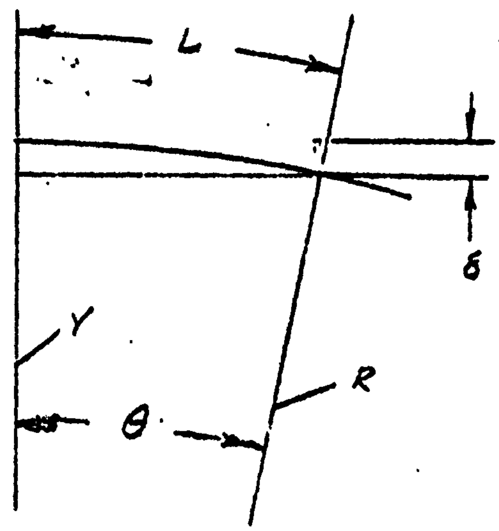

$\theta = \frac{L}{R} = \frac{L\,\Delta T\,\alpha}{D}$

$R = \frac{D}{\Delta T\,\alpha}$

$L = 4.3''$
$D = 2.5''$

$Y = R\cos\theta$

$\delta = R - Y = R - R\cos\theta$

ASSUME $\Delta T = 30°$ AVE FOR LENGTH OF SHAFT

$\theta = \frac{4.3 \times 30 \times 4.9 \times 10^{-6}}{2.5} = .00025284$

$\cos\theta = .9768$

$R = \frac{D}{\Delta T\,\alpha} = \frac{2.5}{30 \times 4.9 \times 10^{-6}} = 17006.80272$

$\delta_{\Delta T} = 17006.80272 - 17006.80218 = \underline{.00054''}$ FOR $\Delta T = 30°$

- ASSUME THE INNER RACE OF THE UPPER BEARING DOES NOT SLIP UNDER THE PRELOAD AND THAT A TEMP RISE IN THE SHAFT ELIMINATES PRELOAD & ALLOWS RADIAL PLAY IN BEARINGS.
- ASSUME NO PRESS FIT IN HOUSING, MAX. BRG. CLEARANCE BUT 0 CLEARANCE BETWEEN SHAFT & INNER RACE OF -1 BRG.

$\delta_c = \theta L = \frac{.00085}{3.5}(3.5 + 4.3) = .001894$

THIS PAGE IS BEST QUALITY PRACTICABLE FROM COPY FURNISHED TO DDC

PREPARED W. SCALMER 10-6-75 REPORT NO. PAGE 16

CHECKED

MODEL

RESOLVER BUMPER CLEARANCE

- ASSUME SHAFT HAS MOVED TO ONE SIDE AT -3 BRG. PRIOR TO LOCKING TO INNER RACE

DEFLECTION AT BRG. (MAX.) .001"

AT BUMPER

$$\delta_s = \frac{11.3}{7.0} \times .001 = .001614''$$

TOTAL RADIAL DEFLECTION AT BUMPER ASSUMING NO DISTORTION IN HOUSINGS OR MAIN SHAFT DUE TO ΔT

$$\delta_T = \delta_{\Delta T} + \delta_c + \delta_s = \underset{\Delta T = 30°}{.000544} + .001890 + .001614 = .004048''$$

RSS $\delta_T = \underline{.002546}$"

THIS INDICATES AN INTERFERENCE COULD EXIST IF THE INITIAL RADIAL CLEARANCE WAS .002" PER ASSEMBLY DRAWING

THE BUMPER SPACER FITS TIGHTLY ON MOTOR SHAFT

SPACER	2.5000	2.4995
SHAFT	2.4990	2.4995
LOOSE	.001	0

ASSUME TEMP. IN SPACER RISES TO 127° (1.8V TO MOTOR) SHAFT AT RESOLVER

BRACKET TEMP. 95° " MOTOR TEMP 164°

$\Delta T = 32°$ SHAFT AT MOTOR 150°

$\Delta R = 13 \times 10^{-6} \times 1.92 \times 32 = \underline{.000798}$" AT 1.8V

ON SERTIZ MOTOR VOLTAGE INCREASED TO 2.2V

ESTIMATED TEMPS.

SHAFT AT MOTOR 184° MOTOR 200°

SHAFT AT RESOLVER 196° HOUSING AT RESOLVER 99°

SPACER 146° BRACKET 99° → $\Delta T = 47°$

$\Delta R = 13 \times 10^{-6} \times 1.92 \times 47 = \underline{.001173}$" AT 2.2V

WORSE CASE INTERFERENCE

AT 1.8V $I = (.004048 + .000798) - .002 = \underline{.002846}$

AT 2.2V $I = (.004048 + .001173) - .002 = \underline{.003221}$

TRW SYSTEMS GROUP

ONE SPACE PARK • REDONDO BEACH, CALIFORNIA

PREPARED W. PALMER 10-10-75 REPORT NO. PAGE 17

CHECKED

MODEL

DIMENSIONAL CHANGES OF 2024-T351 PARTS

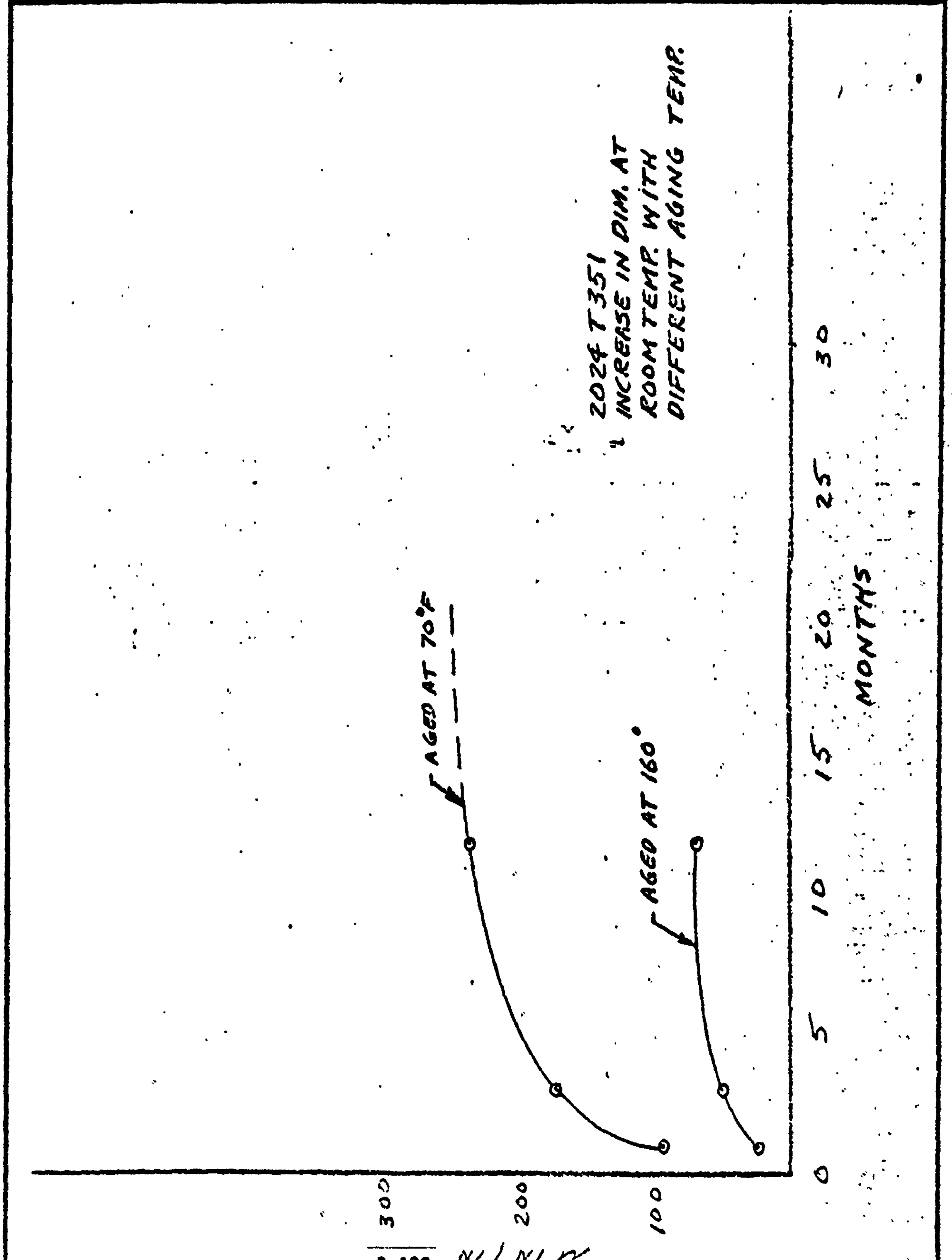

PREPARED W. PALMER 10-8-75 REPORT NO.

CHECKED

MODEL

DIMENSIONAL CHANGES DUE TO INSTABILITY OF MATERIAL

FROM DEFENSE METAL INFO CENTER
BATTELLE MEMORIAL INSTITUTE

DMIC MEMORANDUM 189 MAR 19, 1964

2024-T351
- SOLUTION HEAT TREATED AT 920°F FOR A TIME WHICH IS DEPENDENT ON SHAPE & SIZE
- COLD WORKED BY STRETCHING TO 1-3% PERMANENT SET
- AGED AT ROOM TEMP.

MEM. 189 INDICATES THIS MATERIAL WILL GROW IN SIZE AS FOLLOWS: (ROOM TEMP. EXPOSURE)

	95 μ IN/IN	IN	1 MO
	175 μ IN/IN	IN	3 MO
	240 μ IN/IN	IN	12 MO
EST.	260 μ IN/IN	IN	24 MO

THE MAX. CHANGE THAT COULD OCCUR AT HIGHER TEMP. EXPOSURE IS 1200 μ IN/IN WHICH OCCURS AT THE PRECIPITATION HEAT TREAT TEMP. 375°F (2024-T851)

CONSIDERING THE RESOLVER BUMPER CLEARANCE, A WORSE CASE CONDITION WOULD BE A 1200 μ IN/IN CHANGE IN THE SPACER SINCE IT HAS A HIGHER TEMP. AND A 260 μ IN/IN CHANGE IN THE BRACKET ALTHOUGH AN OUT OF ROUND CONDITION COULD EXIST ESPECIALLY IN THE BRACKET SINCE IT IS MADE OF PLATE.

REDUCTION IN RADIAL CLEARANCE $= \Delta D_S - \Delta D_B = (1200-260) \times 10^{-6} \times 1.92 = .00180''$

THIS PAGE IS BEST QUALITY PRACTICABLE
FROM COPY FURNISHED TO DDC

PRELOAD PLUNGER POSITION

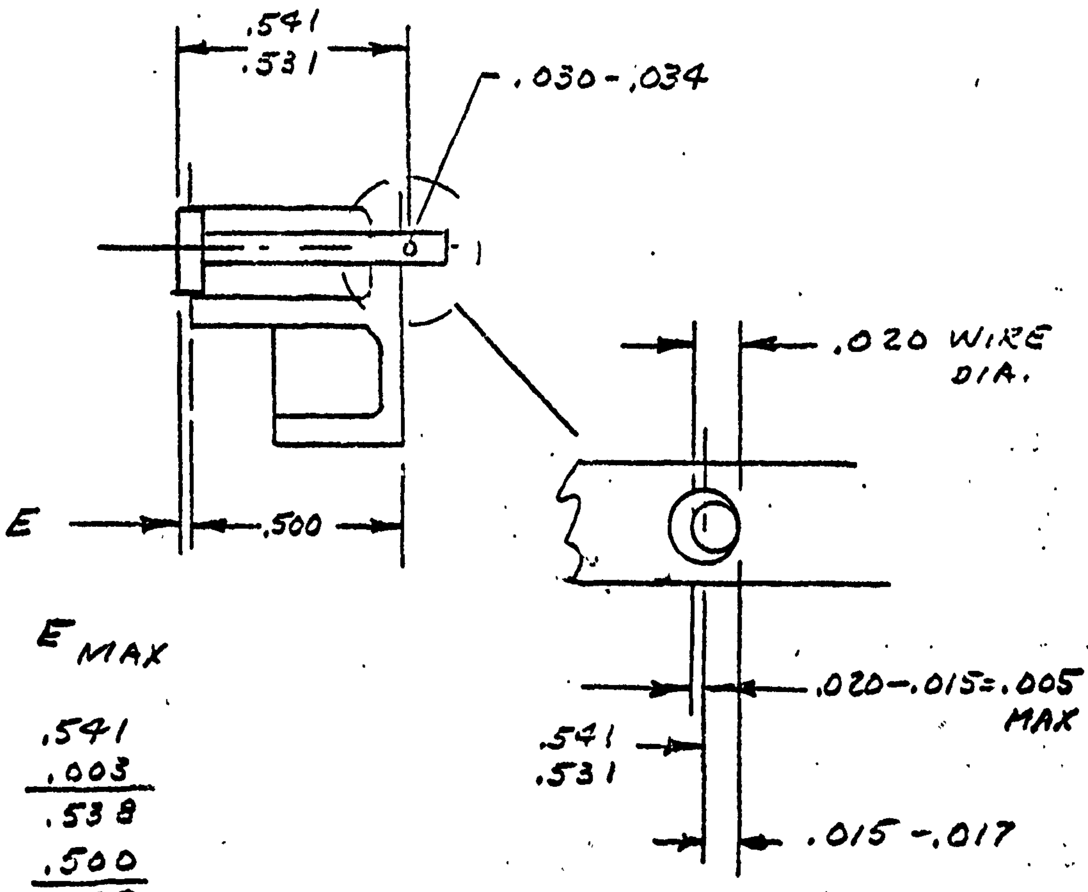

E_{MIN}	E_{MAX}
.531	.541
-.005	.003
.526	.538
.510	.500
.016	.038

MISALIGNMENT OF UPPER BEARING ON SHAFT (MAX.)

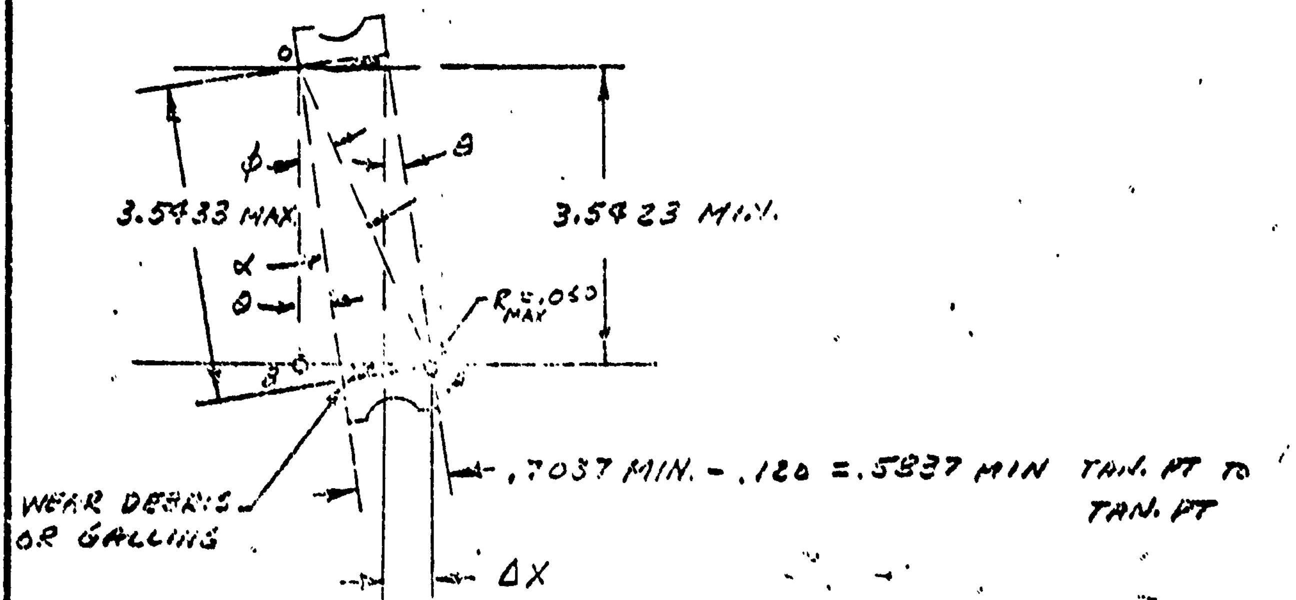

$$OA = \sqrt{(3.5433)^2 + (.5837)^2} = 3.59137$$

$$AB = \sqrt{OA^2 - (3.5423)^2} = .58982$$

$$\tan^{-1}\phi = \frac{.58982}{3.5423} = 9.45354^\circ$$

$$\tan^{-1}\alpha = \frac{.5837}{3.5433} = 9.35452$$

$$\theta = \phi - \alpha = .0990^\circ$$

$$\Delta X = 3.5433 \tan\theta = .00612''$$

SINCE THIS IS GREATER THAN STROKE OF PRELOAD MECH. OF .003" MAX,

$$\tan^{-1}\theta_{MAX} = \frac{.003}{3.5433} = \underline{.0455^\circ}$$

TRW
SYSTEMS GROUP

INTEROFFICE CORRESPONDENCE 75.7340.3-24

TO: P. C. Wheeler CC: J.G. Zaremba DATE: 02 December 1975

SUBJECT: 777 DMA Analysis FROM: R. L. Farrenkopf

BLDG. 82 MAIL STA. 2076 EXT. 63590

SUMMARY

An analysis of the preload mechanism of the 777 DMA was conducted to ascertain the likelihood of relative motion between this mechanism and the inner bearing race. The following conclusions became evident.

(i) No source of torque amplification was found due to potential "creep" of the race about the shaft. A wabble gear type operation requires extremely high radial loading, far in excess of what appears possible in any DMA meeting its specs.

(ii) An analysis was conducted (see Appendix for details) under the following conservative assumptions.

a) Elements of the DMA are treated as rigid. Thus there is no mechanical filtering of motor applied torques. This approach is conservative unless the motor torques are applied at the shaft natural frequency, an impossible condition since the motor bandwidth falls far below this value.

b) The spacecraft rotor is treated as being decoupled from the motor due to high motor-to-rotor shaft compliance. This is conservative as finite coupling would only tend to reduce the preload necessary to "lock" the inner race to the shaft.

(c) The shaft is not in contact with the inner race, and the bearing located near the platform flange experiences no frictional/mechanical hysteresis type losses. These conditions again require the most of the preload mechanism.

Under these assumptions, the preload mechanism provides the following stiction torque, T_w, when there is no relative motion between shaft and inner race.

SYSTEMS 0180 REV 3-67

$$T_w = \left[\frac{I_2 + I_b}{I_s + I_2 + 2\,I_b}\right] T_M + \left[\frac{I_s + I_b}{I_s + I_2 + 2\,I_b}\right] T_L \qquad (1)$$

where

T_M = motor torque

T_L = preload bearing friction/mechanical hysteresis torque

I_s = shaft moment of inertia

I_2 = inner race moment of inertia

and

$$I_b = \frac{I_B + m\,r^2}{4\,r^2}\,R^2\,N \qquad (2)$$

where

r = ball bearing radius

N = number of ball bearings

I_B = ball bearing moment of inertia

R = inner race outside diameter

m = ball mass + $\frac{1}{N}$ (retainer mass)

Using design values, it turns out that

$$T_w = 0.21\,T_M + 0.78\,T_L \qquad (3)$$

Considering the motor torque to be 100 in-oz, the necessary pre-load stiction to prevent relative motion is

$$T_w = 23 + 0.77\,T_L \quad \text{in - oz} \qquad (4)$$

which for reasonable values of T_L is far below the limiting value of 400 in-oz that is predicted possible. Even if no regard to numerical moment of inertia values is made in Equation (1), then

$$T_w < T_M + T_L = 100 + T_L \qquad (5)$$

which again falls well inside the available 400 in-oz unless T_L is unexpectedly large. These results essentially confirm the numerical predictions of George Zaremba in TRW report 75-7345.4-039.

R. L. Farrenkopf

R. L. Farrenkopf

RLF/gw

(1)

RLF
11-25-75

Appendix Bearing Analysis

ω_2 = ring rotation angular rate

I_2 = ring moment of inertia

ω_1 = shaft rotation angular rate

1. Basic Equation of Ring Motion

$$I_2 \dot{\omega}_2 = T_W + T_S + T_B - T_L \quad (1)$$

where

T_W = washer torque

T_S = shaft torque due to possible side load of shaft on ring

T_B = bearing inertial torques

T_L = bearing friction/hysteresis torque (lower bearing)

2. Bearing Torque (Inertial)

Each bearing must be accelerated in both rotation and translation

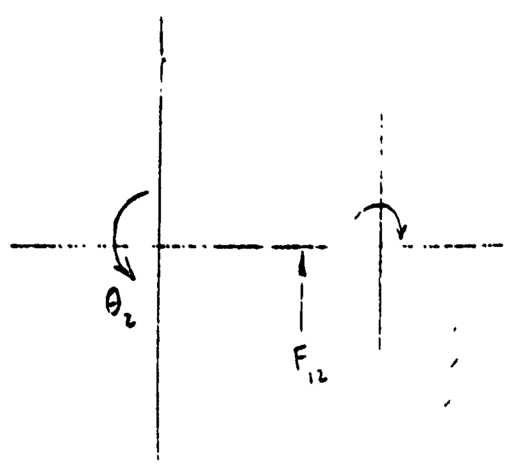

F_{12} = bearing force on ring

Then $T_B = R F_{12}$

F_{21} = ring force on bearing $= -F_{12}$

THIS PAGE IS BEST QUALITY PRACTICABLE
FROM COPY FURNISHED TO DDC

Bearing

v_c = velocity of pt. A.

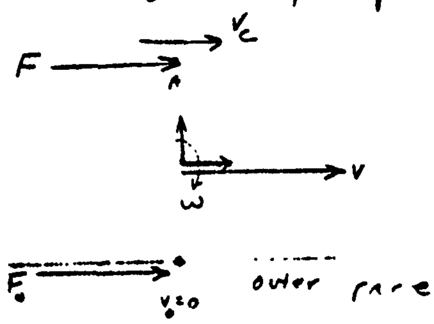

$$V_c = \omega_2 R = v + \omega r$$

$$V_0 = v - \omega r = 0 \qquad \therefore v = \omega r$$

$$\therefore \omega_2 R = 2\omega r$$

$$\omega = \frac{\omega_2 R}{2r}$$

$$v = \frac{\omega_2 R}{2}$$

$$F + F_0 = m\frac{dv}{dt} = \frac{mR}{2}\dot{\omega}_2$$

m = bearing + partial retainer mass

$$r(F - F_0) = I_B \dot{\omega} \qquad \text{or} \qquad F - F_0 = \frac{I_B R}{2r^2}\dot{\omega}_2$$

$$\therefore \; 2F = \left(\frac{mR}{2} + \frac{I_B R}{2r^2}\right)\dot{\omega}_2 \qquad F = \left[\frac{(I_B + mr^2)R}{4r^2}\right]\dot{\omega}_2$$

If there are N bearings, then finally

$$T_B = -I_b\,\dot{\omega}_2 \qquad (2)$$

where

$$I_b = \frac{(I_B + mr^2)R^2}{4r^2}N \qquad (3)$$

Substituting Eq. (3) into (1)

THIS PAGE IS BEST QUALITY PRACTICABLE
FROM COPY FURNISHED TO DDC

$$\boxed{(I_2 + I_b)\,\dot{\omega}_2 = T_w + T_s - T_L} \qquad (4)$$

Suppose that, in general, the shaft is in contact with the ring with radial force F_R $(F_R \geq 0)$. Appropriate levels of F_R permit rolling of the ring on the shaft, i.e., $\omega_2 = \frac{\rho_1}{\rho_2}\omega_1$

Define $\omega_c = \omega_1 \rho_1/\rho_2$ (5)

There are then 3 significant types of motion:

		Shaft Torque, T_s	Washer Torque, T_W
A.	$\omega_2 \neq \omega_1$ $\omega_2 \neq \omega_c$	Coulomb Friction	Columb Friction
B.	$\omega_2 \neq \omega_1$ $\omega_2 = \omega_c$	Stiction	Coulomb Friction
C.	$\omega_2 = \omega_1$	Stiction	Stiction

A.

$$T_W = r_W F_W \mu_W \operatorname{sgn}(\omega_1 - \omega_2) \quad (6)$$; F_W = washer force

$$T_s = \rho_1 F_R \mu_s \operatorname{sgn}(\omega_1 - \omega_2) \quad (7)$$ μ_W, μ_s = coefficients of Coulomb friction

B.

$$T_W = r_W F_W \mu_W \operatorname{sgn}(\omega_1 - \omega_2) \quad (8)$$

$$T_s = (I_2 + I_b)\dot{\omega}_c - T_W + T_L = \frac{\rho_1}{\rho_2}(I_2 + I_b)\dot{\omega}_1 - T_W + T_L \quad (9)$$

and also

$$|T_s| < \rho_1 F_R \eta_s \quad (10)$$ η_s - stiction limit coefficient

C.

$$T_W + T_S = (I_2 + I_b)\,\dot{\omega}_1 + T_L \qquad (11)$$

and also

$$|T_W + T_S| < \rho_1 F_R \eta_s + r_W F_W \eta_W \qquad (12)$$

η_W = washer stiction coefficient limi[t]

Shaft Equation of Motion

Assume light coupling of motor to spacecraft rotor due to high compliance of the shaft

Then

I_s = shaft moment of inertia

$$I_s \dot{\omega}_1 = T_M - T_W - I_b \dot{\omega}_1 - T_\ell$$

T_M = motor torque

or

T_ℓ = upper bearing friction / hysteresis torque

$$(I_s + I_b)\,\dot{\omega}_1 = T_M - T_W - T_\ell \qquad (13)$$

Case C - no washer slip, $\omega_2 = \omega_1$

By Eq. (11)

$$(I_s + I_b)\dot{\omega}_1 = T_M - T_\ell - (I_2 + I_b)\,\dot{\omega}_1 - T_L + T_S$$

$$\therefore \quad \dot{\omega}_1 = \frac{T_M - T_\ell - T_L + T_S}{I_s + I_2 + 2 I_b} \qquad (14)$$

Substituting Eq. (14) into Eq. (11)

THIS PAGE IS BEST QUALITY PRACTICABLE
FROM COPY FURNISHED TO DDC

$$T_W = T_L - T_s + \frac{I_2 + I_b}{I_s + I_2 + 2I_b}\left[T_M - T_\ell - T_L + T_s\right]$$

$$T_W = \left[\frac{I_2 + I_b}{I_s + I_2 + 2I_b}\right](T_M - T_\ell) + \left[\frac{I_s + I_b}{I_s + I_2 + 2I_b}\right](T_L - T_s) \qquad (15)$$

and to maintain such motion, it is necessary that

$$|T_W| < r_W F_W \eta_W \qquad (16)$$

Case B - rolling motion $\omega_2 = \frac{\rho_1}{\rho_2}\omega_1$

By Eq. (7) and (13), (5)

$$T_s \approx (I_2 + I_b)\dot{\omega}_1 + T_L - r_W F_W \mu_W \qquad (17)$$

and $|T_s| < \rho_1 F_K \eta_s$

Now $\dot{\omega}_1$ cannot remain of the same sign, i.e, $\dot{\omega}_1(t) = 0$ for some t. Thus to maintain this type of motion at $\dot{\omega}_1 = 0$,

$$T_s = T_L - r F_W \mu_W \qquad (18)$$

$$|T_s| < \rho_1 F_K \eta_s \qquad (19)$$

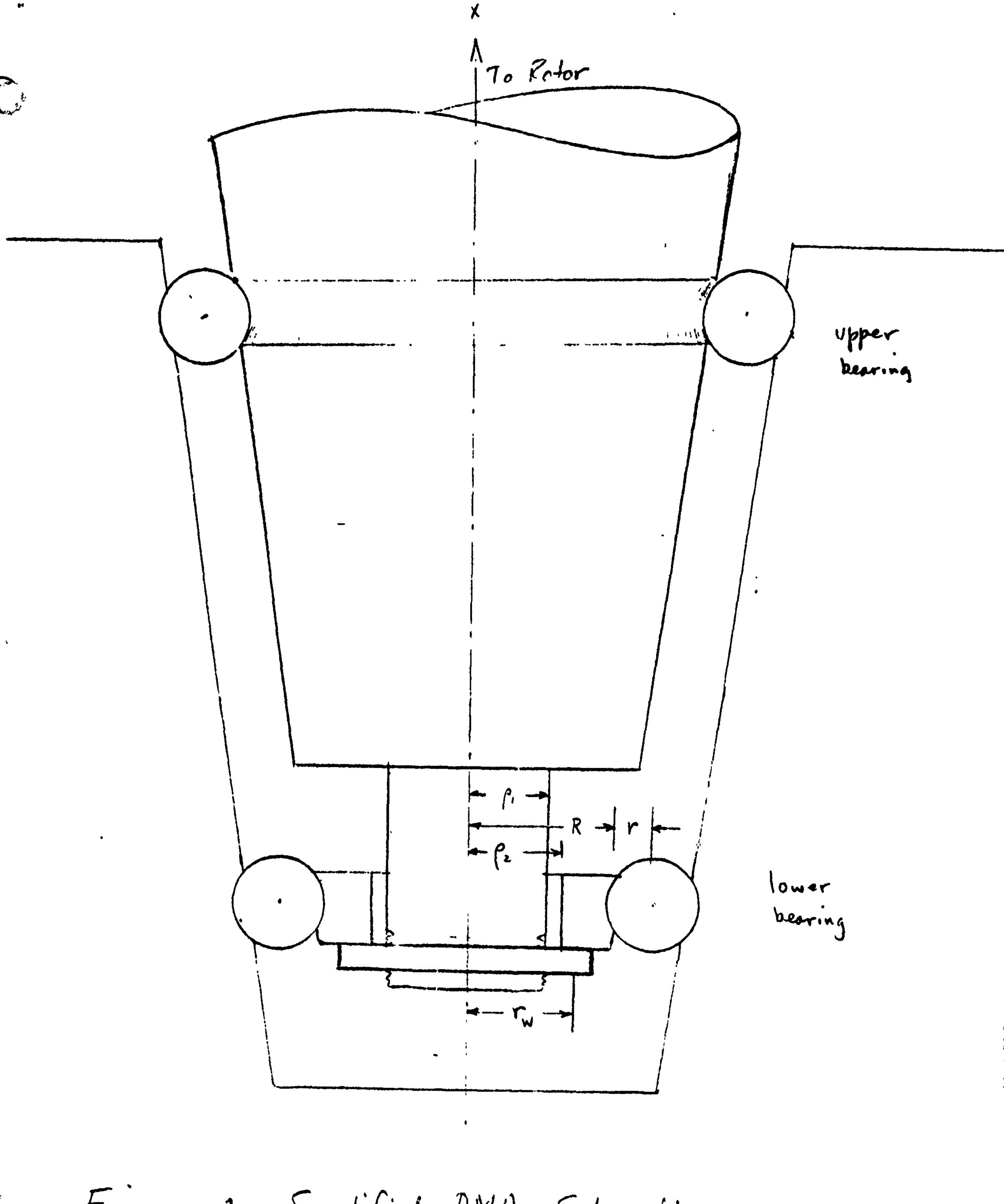

Figure 1 - Simplified DMA Schematic

TRW
SYSTEMS GROUP

INTEROFFICE CORRESPONDENCE 75-7345.4-041

TO P. C. Wheeler CC: A. H. Rosenberg DATE: 15 December 1975
Revised 1/20/76

SUBJECT: 777 Anomaly - Analyses of DMA's Dimensional Changes - As a Function of Platform Spin-Up

FROM: J. G. Zaremba
BLDG 82 MAIL STA. 1367 EXT. 50993

References: (1) New Departure Analysis of Stress and Deflections, developed by A. B. Jones

(2) 777 DMA Anomaly - Structural Bearing Assembly Analysis, IOC 75-7345.4-038

A. INTRODUCTION AND SCOPE

The DMA's flange loads, caused by the platform spun-up condition, will induce relative dimensional changes between the housing-mounted and the shaft-mounted elements. The magnitude of the elemental approachment (closure) as a function of the platform's spun-up state is of particular interest because it establishes design insufficiency should complete closure exist. The most critically influenced by the platform spin-up speeds is the resolver snubber radial gap. Hence, the estimate of its dimensional closure became the principal objective of this analyses. Also considered were the motor and the labyrinth seal (neighborhood of top bearing) gap closures, to afford the evaluation of their geometrical sufficiency for this and the subsequent DMA designs.

The details of this work are given in Section C. Section B contains a summary of results and conclusions.

B. SUMMARY AND CONCLUSIONS

1. Background. Spin-up of the "777" platform introduces the product of inertia and the center of mass offsets not present in the despun state. These, together with the vehicle spin velocity, produce moments and lateral forces (primarily centrifugal) that act on the DMA's platform flange. The consequence of the flange loads is the dimensional approachment (closure) between the housing and the shaft elements of the platform's

SYSTEMS 0180 REV 3-67

despun mechanism. The determination of the magnitude of these closures as a function of the platform's spin speed was the dominant purpose of an analysis.

The analysis considered two loading conditions; i.e., (1) the antenna's inboard; and, (2) the antenna's outboard. The "antenna's outboard" condition was taken to be the nominal state for the standby mode of operation. In this mode, the spun-up forces will cause the antennas to move outward and away from the mass center of the spacecraft. The "antenna's outboard" condition nominally exists up to speeds of 20 RPM or when it is established by command. The analysis was constrained to the following assumptions and omissions:

- Only centrifugal forces were considered
- The resulting structural forces were taken to be point loads
- The shaft was considered to have continuous securement along its interface periphery with the spacecraft. The latter is contrary to the actual four-point flexible mount situation
- The bottom bearing (110 MM) by itself is not capable of sustaining any moments applied to the housing
- Line-to-line bottom bearings fit up with shaft, and maximum clearance (0.001 inch) between the inner race of the top bearing (90 MM) and the shaft were adopted for the analyses
- It was also assumed that misalignment due to the bearings' clearance geometry will take place at the application of small magnitude loads
- The magnetic unbalance forces of the motor were neglected
- Thermal effects were not considered.

The total radial approachment between the housing-mounted and the shaft-mounted elements was modeled by considering three effects (refer to Figure B-1).

- The bearing looseness (clearance between inside diameter of bearing (90 MM) and the shaft) causes relative rotation of the housing with respect to the shaft. The direct consequence is the misalignment of the bearings' outer race with respect to the inner races. For the bearing looseness effect, the housing and the shafts of the structural and the power modules are considered to be of infinite stiffness (in bending). The housing rotates with respect to the shaft about an apparent pivot point, a function of the radial stiffness of the structural module's housing, shaft, and the bearings
- The second effect is attributed to the radial deflections of the bearings. This tends to increase the angular rotation of the housings with respect to the shafts
- The third effect considers the pertinent structural deflections. Notice from Figure 1-B that the slopes of the structural curvatures of the structural module's shaft and housing are opposite in sense and, therefore, tend to mitigate the summed effect of the first two aspects.

2. Data Presentation. The results of this analyses for the two loading cases; i.e., the antenna's "inboard" and "outboard", are presented in Table 1-B and Figures 2-B and 3-B.

Inspection of the table and the snubber closure plots reveal the following:

- The reaction forces are larger for the bottom bearing than for the top bearing in the "antenna's inboard" case and conversely in the "antenna's outboard" case. The reason for this phenomena is the polarity reversal of the despun lateral force acting on the DMA flange.

TABLE I-B

CRITICAL GAPS CLOSURE AS A FUNCTION OF PLATFORM SPIN-UP SPEEDS

Quantities	Units	Symbols	SPIN SPEED (RPM) 20		40		60		80	
			110MM Brg	90MM Brg	110MM Brg	90MM Brg	110MM Brg	90MM Brg	110MM Brg	90MM Brg
• Antennas Inboard Case										
Bearing Reactions	lbs	R_j	19.	15.	78.	62.	176.	140.	311.	247.
Resolver Snubber Gap Closure	inch	C_R	1.55×10^{-3}		-1.44×10^{-3}		1.26×10^{-3}		1.40×10^{-3}	
Motor Gap Closure	inch	C_M	1.35×10^{-3}		1.28×10^{-3}		1.17×10^{-3}		1.32×10^{-3}	
Labyrinth Gap Closure	inch	C_L	1.11×10^{-3}		1.09×10^{-3}		1.06×10^{-3}		1.22×10^{-3}	
• Antennas Outboard Case										
Bearing Reactions	lbs	R_j	53	56	212	250	477	518	848	922
Resolver Snubber Gap Closure	inch	C_R	1.44×10^{-3}		1.39×10^{-3}		0.99×10^{-3}		0.31×10^{-3}	
Motor Gap Closure	inch	C_M	1.28×10^{-3}		1.28×10^{-3}		1.07×10^{-3}		0.67×10^{-3}	
Labyrinth Gap Closure	inch	C_L	1.09×10^{-3}		1.16×10^{-3}		1.16×10^{-3}		1.10×10^{-3}	

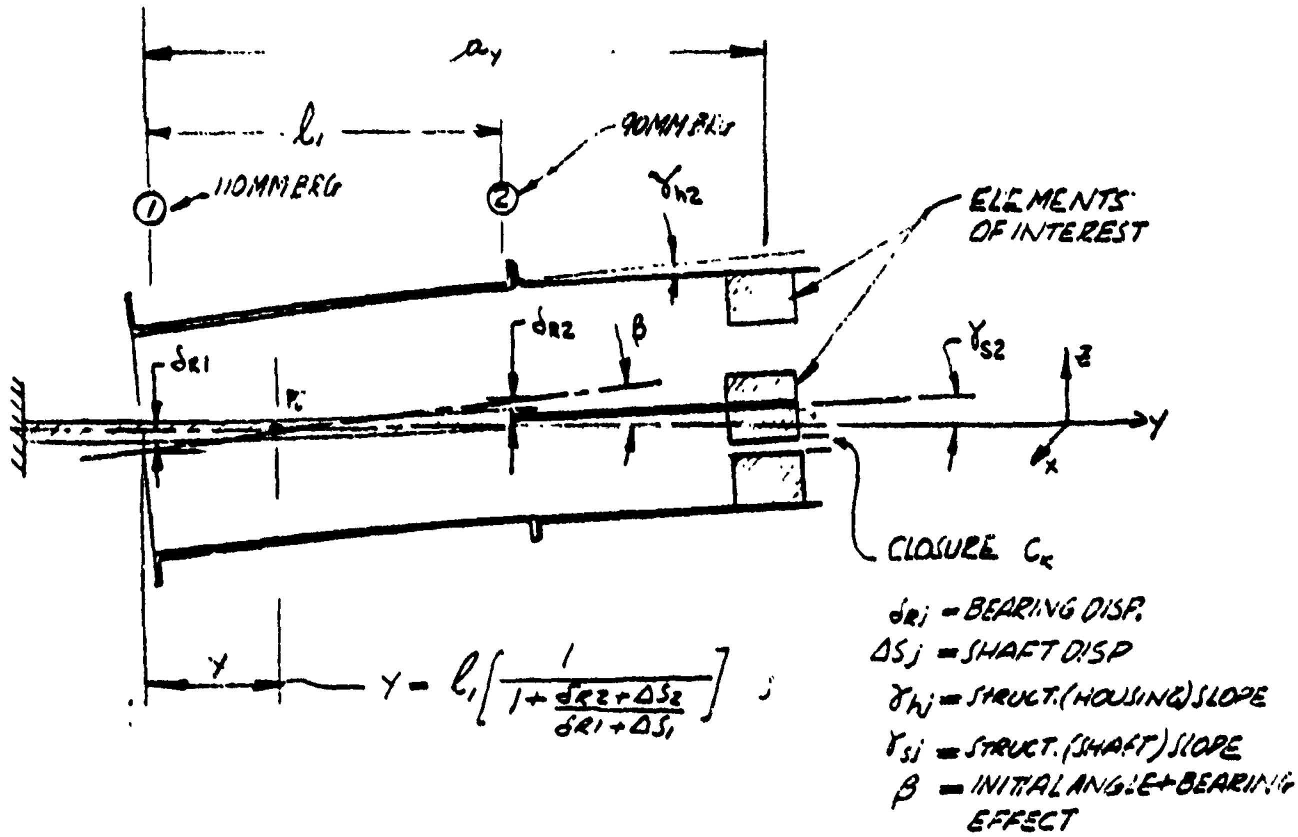

FIG. 1-B RELATIVE MOTION BETWEEN HOUSING AND SHAFT

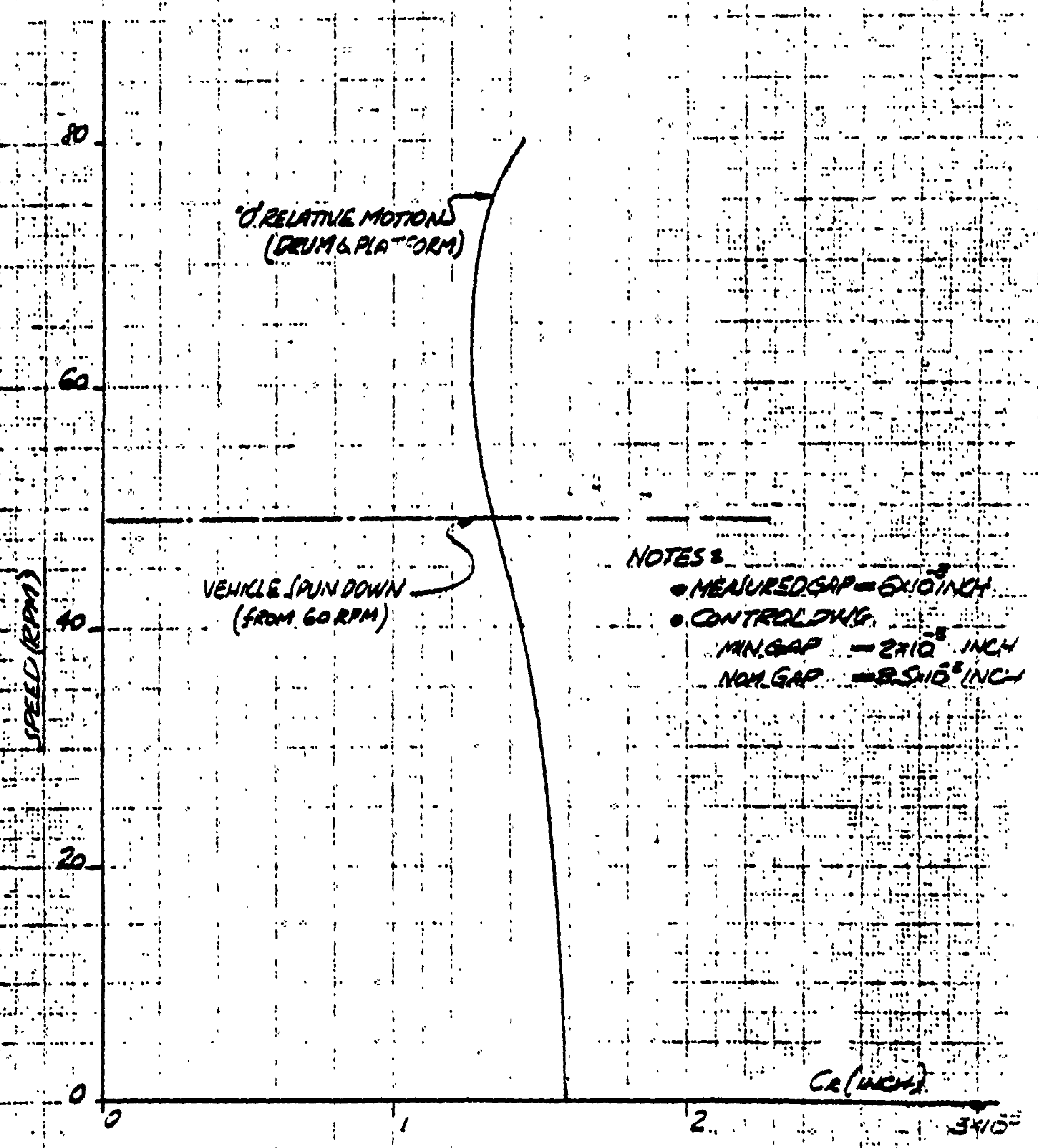

FIG 2-B RESOLVER SNUBBER ELEMENTAL APPROACHMENT (Cr)
VS
PLATFORM SPIN UP SPEED
(ANTENNAS INBOARD CASE)

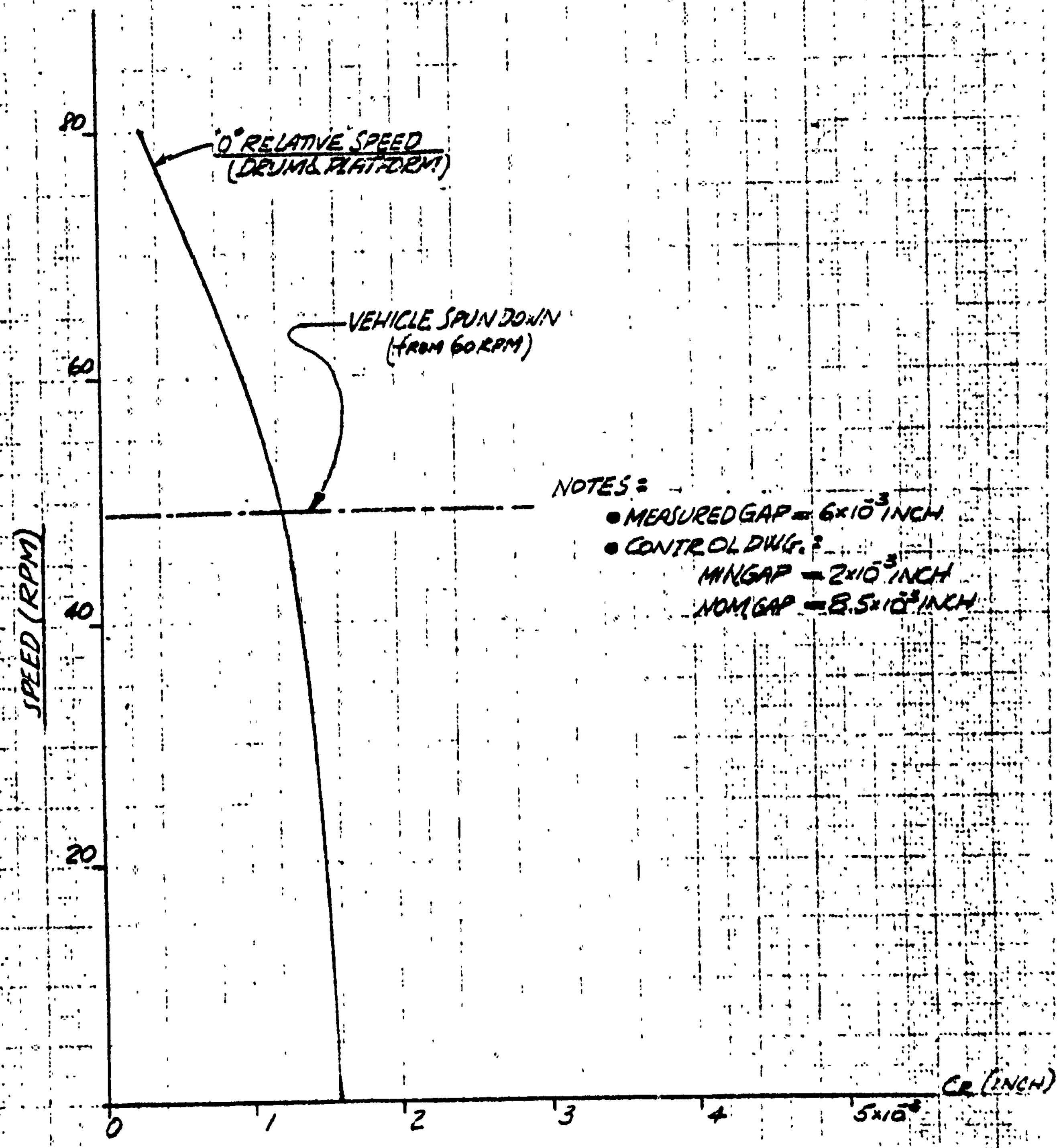

FIG 3-B RESOLVER SNUBBER ELEMENTAL APPROACHMENT (CR) VS PLATFORM SPINUP SPEED (ANTENNAS OUTBOARD CASE)

- The resolver snubber closure development versus speed does not appear to be a function of the square of the spin-up velocity. There are several effects that force this lack of correspondence. These are:

  (1) The geometric looseness of the top bearing causes almost instantaneous misalignment of the housing with respect to the shaft, upon application of small radial forces to the bearings

  (2) The bearings' elastic axial deflections, due to preload, tend to stiffen the bearings with respect to radial forces until the latter are sufficiently high in magnitude. This occurs at bearing reactions approaching 250 pounds

  (3) The initial geometric looseness noted in item (1) also influences the bearing's races misalignment angle. Analysis indicates that the rate of change of the bearings' radial deflection is lower for relatively high values of misalignment. In general, the DMA's bearing misalignment angle decreases with the application of radial load.

  (4) The bearing's radial deflection effect, excluding items (1), (2) and (3), is not dominant in establishing the value of the snubber closure. Analyses indicate that the structural curvatures of the shaft and the housing (due to external loads) are opposite in sense. Therefore, the initial value of closure will tend to decrease with increasing spin-up speed, hence load. Notice that eventually when the shaft's curvature slope becomes completely dominant, the value of the snubber closure will start to increase. The latter will occur at loads greater than these considered.

  (5) Of some interest is the snubber closure characteristic versus spin-up speed for the "antenna's inboard" case. Here, at approximately 60 RPM, the value of C_R begins to

increase, whereas for lower speeds, it was a decreasing function. The reason for this occurrence is the fast rate of decrease of the bearings' axial deflection which renders more compliant bearing to radial load.

(6) Notice from Table 1-B that the bearing radial deflection effect is more dominant for relatively short distances, a_y's to the elements of interest (refer to Figure 1-B). This is exemplified by the labyrinth seal closure (C_L), in which case, the closure values appear to very slowly decrease with with the spin-up speed and thus the bearing loads. The influence of the structural curvatures are not as significant.

3. Conclusions. The analyses indicate that for both the spun-down and the spun-up platform conditions, the probability of closure of the resolver snubber gap does not exist.

For the spun-up case, the external forces acting on the housing are fixed to the platform coordinate set. Hence, a relative rotation of the housing with respect to shaft produces no changes in the relative positions of the elements of interest, unless the aspect of permanent deformation on the system's hysteresis effect are introduced. The latter aspects appear unlikely.

C. ANALYSES

1. General Aspects

1.1 Introduction and Scope

Spin-up of the "777" platform introduces product of inertia and the center of mass offsets not present in the despun state. These, together with the vehicle spin velocity, produce moments and lateral forces (primarily centrifugal) that act on the DMA's platform flange. The consequence of the flange loads is the dimensional approachment (closure) between the housing and the shaft elements of the platform's despun mechanism. The magnitude of this approachment,as a function of the platform's spin up speed,is of particular interest because it establishes the DMA's performance success or defficiency should partial or complete elemental closure exist, respectively.

The DMA design geometry structures the resolver snubber radial gap closure to be most critically influenced by the platform's spun-up state. Hence, the determination of this particular dimensional change became the principal objective of the ensuing analyses. The latter also considered the motor and the labyrinth seal (near the "top", 90 MM bearing) gap closures to afford the evaluation of their geometric sufficiency for this and the subsequent DMA designs.

1.2 Solution Approach

The desired dimensional gap changes were established by considering the pertinent structural and bearing's deflections at two planes, nominally perpendicular to the DMA's rotational velocity vector. Plane No. 1 contained the ball centers of the 110 MM bearing, (at times referred to as the Bottom Bearing (BB)) and plane No. 2 contained the ball centers of the 90 MM bearing, (also referred to as the Top Bearing,(TB)). Two kinds of deflections were considered: the rotational and the lateral.

The rotational displacements examined defined the local angular deviations of the housing and the shaft center lines from the nominal DMA velocity vector. The relative values of housing angular displacements with respect to the shaft, at the two reference planes, constituted the bearing's misalignment angle. The latter parameter, together with the elastic-axial bearing displacements (due to preload), was used to calculate the bearings' radial deflections caused by external forces applied.

The determined lateral (radial) deflections of the structure and the bearings at each plane supplemented by the bearings' separation distance yield a relative (shaft with respect to housing) shaft angle which, together with the knowledge of the appropriate moment arm geometry, afforded the desired elemental approachment calculations.

1.3 Assumptions and Flag Notes

1.3.1 Assumptions

- Structural

  (1) All forces were considered to be point loads

  (2) The shaft was considered to have continuous securement along its interface periphery with the spacecraft. The latter is contrary to the actual four-point flexible mount situation.

  Notice that the first assumption produces a larger gap closure estimate and the second neglects the flexibilities of the four-point mount.

- Bearing Suspension

  The following were assumed:

  (1) The BB by itself is not capable of sustaining any moments applied to the housing

  (2) Line-to-line BB fit-up with shaft and maximum clearance (0.001 inch) between the inner race of the TB and the shaft were adopted for the analyses. It was also assumed that misalignment due to the bearings' clearance geometry will take place at the application of small magnitude loads.

Notice that both assumptions tend to produce conservative results and that at least 55 inch-lb moment sustaining capability of the BB can be expected for a 64 pound bearing preload.

1.3.2 Flag Notes

- Coordinate System

The coordinate system used in the analyses is a right hand XYZ set with the Y axis (positive sense) pointing outboard and along the DMA's velocity vector. The conversion to the spacecraft structural coordinates is given by

$$\begin{bmatrix} X \\ Y \\ Z \end{bmatrix} = \begin{bmatrix} 1 \\ 1 \\ -1 \end{bmatrix} \begin{bmatrix} Y_s \\ X_s \\ Z_s \end{bmatrix} \qquad \text{EQ 1}$$

where: subscript "s" denotes association with the spacecraft structural coordinates

The particular coordinate set was chosen for compatibility with the various derivations of reference (2).

- Key Usage of Subscripts

Unless obviously not applicable, the last subscript "1" and "2" appearing with a letter symbol denotes association with the bottom and the top bearings, respectively.

2. Detail Analyses

2.1 External Loads

The geometric relationship of the load application and the load reaction elements of the DMA is shown on Figure 1. The applied moment M_a and the radial force F are acting on the DMA flange, and their sense is defined by the right hand coordinate set X_R, Y_R, Z_R.

There are two loading cases, namely:

- Case I - Considers the antennas to be inboard (towards the CG of the spacecraft)
- Case II - Considers the antenna to be outboard.

The magnitude and sense of these loads for the spun-up platform state is given in Table I.

TABLE I

MAGNITUDE OF EXTERNAL LOADS AS A FUNCTION OF SPUN-UP SPEEDS

Parameter	Symbol	Antennas Inboard				Antennas Outboard			
Spin Speed (RPM)	ω	20	40	60	80	20	40	60	80
Radial Force (lbs)	F	-4.	-16.	-34.	-64.	5.	18.	42.	74.
Applied Moment (inch-lbs)	M_a	108.	432.	978	1728.	403.	1613.	3630.	6450.

Note: The load profile and the load sense were provided by John Conway of the SVD Dynamics Department.

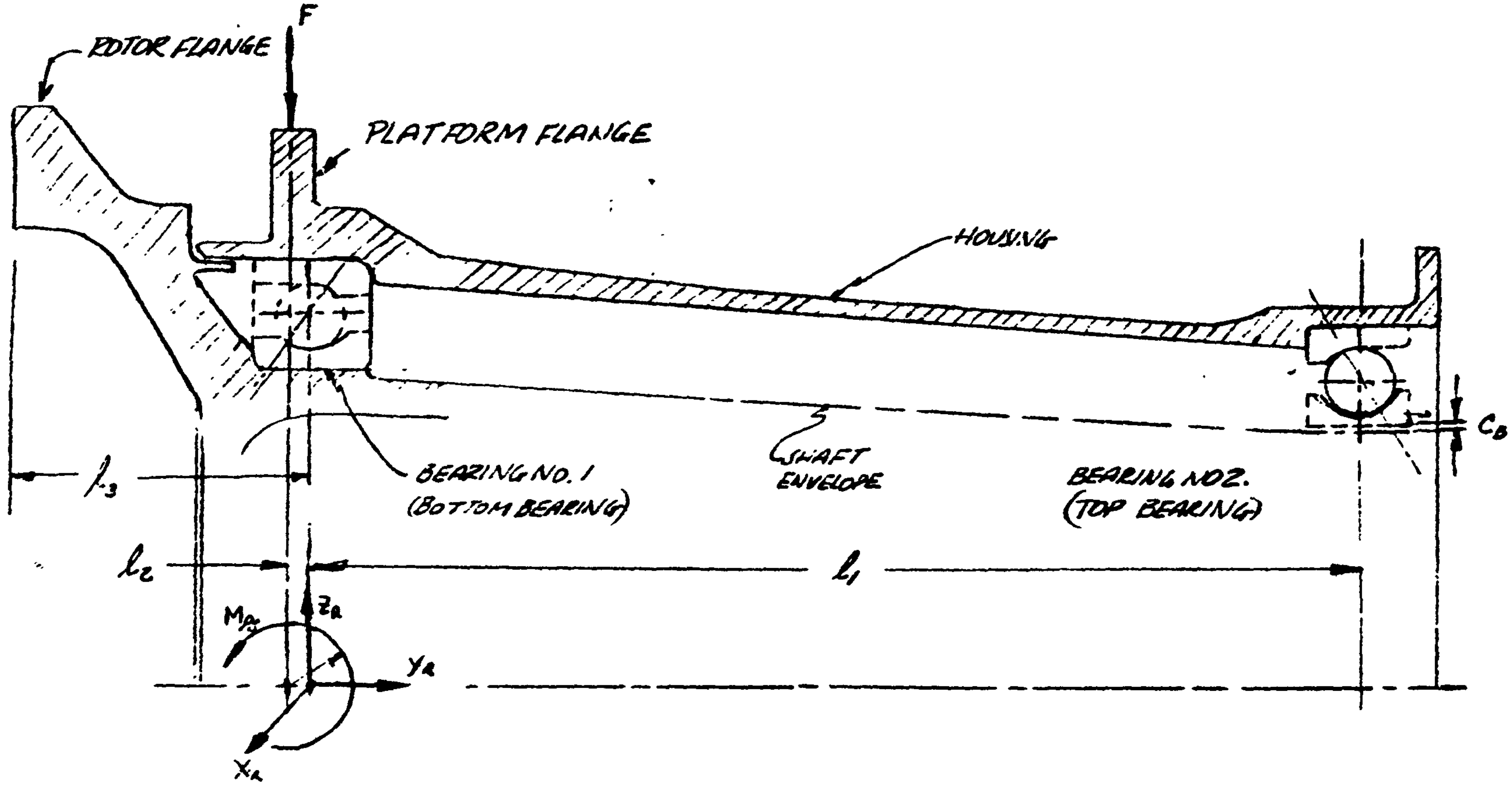

FIGURE 1. EXTERNAL LOADS ACTING ON THE DMA HOUSING

2.2 Structural Reactions and Models

- Models

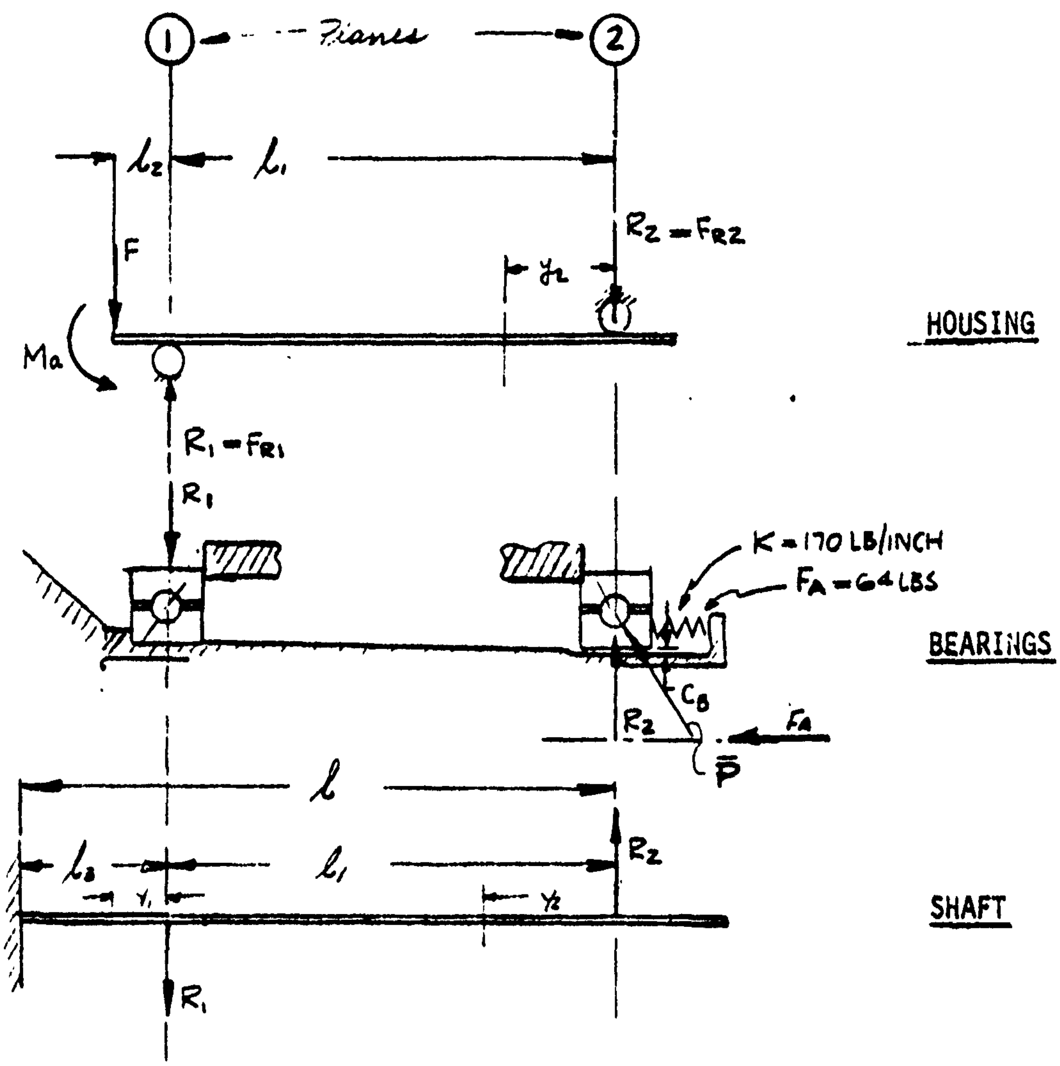

FIGURE 2. STRUCTURAL MODELS

- Reactions

From conditions of static equilibrium moment equations:

$$\sum M_{@,1} = 0 \qquad \text{EQ 2}$$

$$\sum M_{@,2} = 0 \qquad \text{EQ 3}$$

The reaction forces R_1 and R_2 become

$$\left.\begin{aligned} R_1 &= [M_a+F(\ell_1+\ell_2)](\ell_1)^{-1} \\ R_1 &\cong M_a/\ell_1+F \qquad \text{for} \left\{\begin{aligned} &\ell_1 >> \ell_2 \\ &\ell_1 = 7.0 \text{ inch} \end{aligned}\right. \end{aligned}\right\} \text{EQ 4}$$

$$\left.\begin{aligned} R_2 &= (M_a+F\ell_2)(\ell_1)^{-1} \\ R_2 &\cong M_a/\ell_1 \qquad \text{for} \left\{\begin{aligned} &\ell_1 >> \ell_2 \\ &\ell_1/\ell_2 = 47:1 \end{aligned}\right. \end{aligned}\right\} \text{EQ 5}$$

The specific values of the bearing reactions R_j are given in Table II as a function of the platform's spun-up speeds.

TABLE II

BEARINGS' LOAD REACTIONS AS FUNCTION OF SPUN-UP SPEED

Parameters	Spin Speed (RPM)							
	20		40		60		80	
Bearing Type	110MM	90MM	110MM	90MM	110MM	90MM	110MM	90MM
Load Condition, I	Antennas Inboard							
Reaction (lbs), R_j	19.	75.	78.	62.	176.	140.	311.	242.
Load Condition, II	Antennas Outboard							
Reaction (lbs), R_j	58.	58.	212.	230.	477.	518.	848.	422.

2.3 Structural Deflection (Refer to Figure 2)

2.3.1 Housing

The derivation of the housing displacements is based on the solid-foundation-simply-supported-beam model, given in paragraph 2.2. As such, and for the assumption that the external radial load acts directly on the bottom bearing, the housing deflections are reduced to the angular displacement associated with Plane 2. This deflection is derived from the beam's strain energy

$$U_h = \frac{1}{2EI_h}\int_0^{\ell_1}(M_{02}-R_2Y_2)^2 dy_2 \qquad \text{EQ 6}$$

where:

EI_h = housing rigidity = 1.77×10^8 lb-in^2

ℓ_1 = separation between bearings = 7.0 inch

R_2 = bearing reaction (lbs) in plane 2

M_{02} = auxiliary moment parameter in plane 2

M_{02} = 0

The desired angular deflection is obtained from

$$\left.\frac{\partial U}{\partial M_{02}}\right|_{M_{02}=0} = \gamma_{h2} = -\frac{R_2\ell_1^2}{2EI_h} \qquad \text{EQ 7}$$

2.3.3 Shaft (Refer to Figure 2)

The angular deflections at planes 1 and 2 are derived from the strain energy equation containing two auxiliary moments $M_{01} = M_{02} = 0$. The strain energy equation takes the form

$$U_s = 2EI_s\left\{\int_0^{\ell_1}[M_{01}+M_{02}-y_2R_2]^2dy_2+\int_0^{\ell_3}[M_{01}+M_{02}+y_1R_1-(y_1+\ell_1)R_2]^2dy_1\right\} \qquad \text{EQ 8}$$

where:

EI_s = shaft rigidity = 8×10^7 lb-in^2

ℓ_1 = separation between the bearings = 7.0 inch

ℓ_3 = distance between base of shaft and BB
= 2.0 inch

$M_{01} = M_{02} = 0$ = auxiliary moments

R_j = bearing reactions in lbs

The angular deflections at the pertinent planes were derived from EQ 8 by Castigliano theorm and are given as:

- Angular Displacement of Shaft in the Neighborhood of the 110 MM Bearing

$$\gamma_{s1} = \left.\frac{\partial U_s}{\partial M_{01}}\right|_{M_{01}=M_{02}=0} = \frac{1}{2EI_s}[\ell_3^2R_1-(\ell_3^2+2\ell_1\ell_3)R_2], \text{ radian} \qquad \text{EQ 9}$$

- Angular Displacement of Shaft in the Neighborhood of the 90 MM Bearing

$$\gamma_{s2} = \left.\frac{\partial U_s}{\partial M_{02}}\right|_{M_{01}=M_{02}=0} = -\frac{1}{2EI_s}[\ell_3^2R_1-(\ell_1+\ell_3)^2R_2], \text{ radian} \qquad \text{EQ 10}$$

The lateral radial displacements associated with the bearing planes ① and ② were derived directly from the strain energy EQ 8 and are given as

- Radial Displacements of Shaft in the Neighborhood of the 110 MM Bearing

$$\Delta_{s1} = \frac{\partial U_s}{\partial R_1} = \frac{1}{6EI_s}[2\ell_3^3R_1-(2\ell_3^3+\ell_1\ell_3^2)R_2], \text{ inch} \qquad \text{EQ 11}$$

- Radial Displacement of Shaft in the Neighborhood of the 90 MM Bearing

$$\Delta_{s2} = \frac{\partial U_s}{\partial R_2} = \frac{1}{6EI_s}[2(\ell_1+\ell_3)^3 R_2 - \ell_3^2(2\ell_3+3\ell_1)R_1], \text{ inch} \qquad \text{EQ 12}$$

2.3.4 Summary of the Structural Deflection Parameters

The summary of the deflection parameters is given in Table III.

TABLE III

Quantities	SPIN SPEED (RPM)							
	20		40		60		80	
Bearing Type	110 MM	90 MM	110 MM	90 MM	110 MM	90 MM	110 MM	90 MM
• Antenna Inboard Case								
γ_{hj}, rad	---	-2.1×10^{-6}	---	-8.6×10^{-6}	---	-19×10^{-6}	---	-34×10^{-6}
γ_{sj}, rad	2.4×10^{-6}	$.7\times10^{-6}$	10×10^{-6}	29×10^{-6}	23×10^{-6}	66×10^{-6}	40×10^{-6}	120×10^{-6}
Δ_{sj}, inch	-12.0×10^{-6}	40×10^{-6}	-50×10^{-6}	167×10^{-6}	-113×10^{-6}	379×10^{-6}	-200×10^{-6}	665×10^{-6}
• Antenna Outboard Case								
γ_{hj}, rad	---	-8×10^{-6}	---	-32×10^{-6}	---	-72×10^{-6}	---	130×10^{-6}
γ_{sj}, rad	9.9×10^{-6}	28×10^{-6}	39×10^{-6}	110×10^{-6}	88×10^{-6}	250×10^{-6}	160×10^{-6}	440×10^{-6}
Δ_{sj}, inch	-59×10^{-6}	306×10^{-6}	-228×10^{-6}	1200×10^{-6}	-514×10^{-6}	2700×10^{-6}	-915×10^{-6}	4820×10^{-6}

Notes: (1) For parameter definition refer to text
(2) For polarity or sense definition refer to referenced coordinate set

2.4 Bearing Deflections

2.4.1 General Remarks

The radial bearing deflections were derived within the following assumptions and constraints:

- The bearing preload of 64 lbs, although present for the entire radial load range considered, is effective only when the axial parameter $\overline{\delta}_A$ exists. The latter is defined as

  $$\overline{\delta}_A = \delta_A/A$$

  where:

  δ_A = Elastic axial bearing displacement, inch

  A = $[f_i+f_o-1]D$ = length between centers of radii of curvature

  f_j = ρ_j/D_j

  ρ_j = Radii of curvatures, inch

  D_j = Ball diameter, inch

- As a consequence of very low preload spring stiffness (170 lb/in), the preload force, F_A, in presence of radial load, acts as if it were a horizontal component of an off-axis force applied to the bearing (refer to Figure 2).
- Individual bearings are not capable of sustaining moment loads (refer to paragraph 1.3).
- The outer races of both bearings will incur an initial misalignment angle upon application of any radial load. This angle is defined as:

$$\gamma_{ohj} = \frac{C_B}{\ell_1} = 143 \times 10^{-6} \text{ radians} \qquad \text{EQ 13}$$

where

C_B = Maximum clearance between the 90 MM bearing's inside diameter and the shaft diameter
= 0.001 inch

ℓ_1 = Distance between bearings
= 7.0 inch

- The total bearing misalignment is defined by the relative deflections of the housing and the shaft in accordance with

$$\phi_j = -\gamma_{sj} - (\gamma_{hj} - \gamma_{ohj}) \text{ radians (refer to Table III)} \qquad \text{EQ 14}$$

The misalignment angles as function of the spin speed is given in Table IV.

TABLE IV

BEARING MISALIGNMENT ANGLE AS FUNCTION OF SPIN SPEED

Quantities	SPIN SPEED (RPM)							
	20		40		60		80	
Bearing Type	110 MM	90 MM	110 MM	90 MM	110 MM	90 MM	110 MM	90 MM
(a)	Antennas Inboard Case							
Radians, ϕ_j	141×10^{-6}	144×10^{-6}	133×10^{-6}	123×10^{-6}	118×10^{-6}	96×10^{-6}	103×10^{-6}	57×10^{-6}
(b)	Antennas Outboard Case							
Radians, ϕ_j	133×10^{-6}	123×10^{-6}	104×10^{-6}	65×10^{-6}	55×10^{-6}	-35×10^{-6}	-170×10^{-6}	-167×10^{-6}

NOTE: (1) In general, the misalignment angle will decreased with load since ϕ_j is a relative quantity of the angular displacement of housing with respect to the shaft, and the housing incurs initial angle γ_{ohj}.

(2) Notice that for the "antennas outboard case," the sense of ϕ_j reverses at 60 RPM.

(3) For polarity or sense definition, refer to reference coordinates set.

2.4.2 Basic Equations and Bearing Parameters

- Basic Equations

The principal constraint in the calculations of the bearing deflections δ_{Aj} and δ_{Rj} for given ϕ_j, was that the parameters $\bar{\delta}_{Aj}$, $\bar{\delta}_{Rj}$, and $\bar{\phi}_j$ must simultaneously satisfy the following expressions (reference 1):

$$\frac{F_{Aj}}{Z_j D_j^2 K_j} = \frac{1}{\pi}\int_{\Theta}^{0}\left[\frac{\cos\alpha'_{oj}+\bar{\delta}_{Rj}\cos\theta}{\cos\alpha_j}-1\right]^{3/2}\sin\alpha_j d\theta \qquad \text{EQ 15}$$

$$\frac{F_{Rj}}{Z_j D_j^2 K_j} = \frac{1}{\pi}\int_{\Theta}^{0}\left[\frac{\cos\alpha'_{oj}+\bar{\delta}_{Rj}\cos\theta}{\cos\alpha_j}-1\right]^{3/2}\cos\alpha_j\cos\theta d\theta \qquad \text{EQ 16}$$

where:

δ_{Aj} = Elastic displacement of bearing due to axial load, inch

δ_{Rj} = Elastic displacement of bearing due to radial load, inch

ϕ_j = Misalignment angle, radian

$\bar{\delta}_{Aj}$ = δ_{Aj}/A

$\bar{\delta}_{Rj}$ = δ_{Rj}/A

$\bar{\Phi}_j$ = ϕ_j/A

A = Distance between radii of curvature, inch

F_{Aj} = Axial load, lb

F_{Rj} = Radial load, lb

Z_j = No. of balls

D_j = Diameter of balls, inch

K_j = Stiffness = $\frac{lb}{in^2}$ = $4.85\times10^6(\frac{A_j}{D_j})^{1.172}$

α_j = Load contact angle

$$\alpha_j = \tan^{-1}\frac{\sin\alpha_j+\bar{\delta}_{Aj}+\rho_{ij}\bar{\phi}_j\cos\theta}{\cos\alpha'_{aj}+\delta_{Rj}\cos\theta} \qquad \text{EQ 17}$$

θ = Rotational angle about Y axis (rad)

α'_{oj} = Installation contact angle of bearing (reference 2)

ρ_{ij} = Outside radius of inner race (reference 2)

Θ = Limit of integration constrained to the following conditions:

- $$\left\{[\sin\alpha'_{oj}+\bar{\delta}_{Aj}+\phi_j\cos\Theta]^2+[\cos\alpha'_o+\bar{\delta}_R\cos\Theta]^2-1\right\} = 0 \qquad \text{EQ 18}$$

- when, $\cos\Theta \leq -1$

  $\Theta = \pi$

  $\phi^*_j = \rho_{ij}\bar{\phi}$

- Bearing Parameters Defined

  Notice that the numerical values for the defined parameters are delineated in Table V.

TABLE V. BEARING PARAMETERS

PARAMETERS	BEARINGS	
	110 MM BEARING	90 MM BEARING
D, inch	0.500	0.4687
A, inch	0.200	0.01875
ZD^2K, lb	641.2×10^3	514.5×10^3
ρ_{ij}, inch	2.577	2.127

2.4.3 Method of Derivation of $\bar{\delta}_A$ and $\bar{\delta}_R$ for given $\bar{\phi}_R$

- <u>Principal Approach</u>

(a) From EQ 15, a number of curves, $F_A = f\left\{\bar{\delta}_A[g(\bar{\delta}_R)]\right\}$ for given $\bar{\phi}$, were developed for both bearings. These are given on Figure 3 to Figure 12, inclusively.

(b) From EQ16 , a number of curves, $F_R = f\left\{\bar{\delta}_R[g(\bar{\delta}_a)]\right\}$ for given $\bar{\phi}$, were developed for both bearings. These are given on Figure 12 to Figure 24.

(c) Using plots of item (a) for F_A = 64 lbs, the intersecting values of $\bar{\delta}_A$ and $\bar{\delta}_R$ for given $\bar{\phi}$ were selected. These were plotted on Figure 25 and Figure 26 for the bottom bearing and the top bearing, respectively.

(d) Using plots of item (b) for $F_R = F_{RK}$, the intersecting values of $\bar{\delta}_A$ and $\bar{\delta}_R$ for various values of $\bar{\phi}$ were selected and cross-plotted on Figure 25 and Figure 26. The intersection of the curves for given $\bar{\phi}$ allowed determination of a particular $\bar{\delta}_A$, $\bar{\delta}_R$, and $\bar{\phi}$ that simultaneously satisfied EQ 15 and EQ 16. Thus, solution for the desired bearing deflections was obtained.

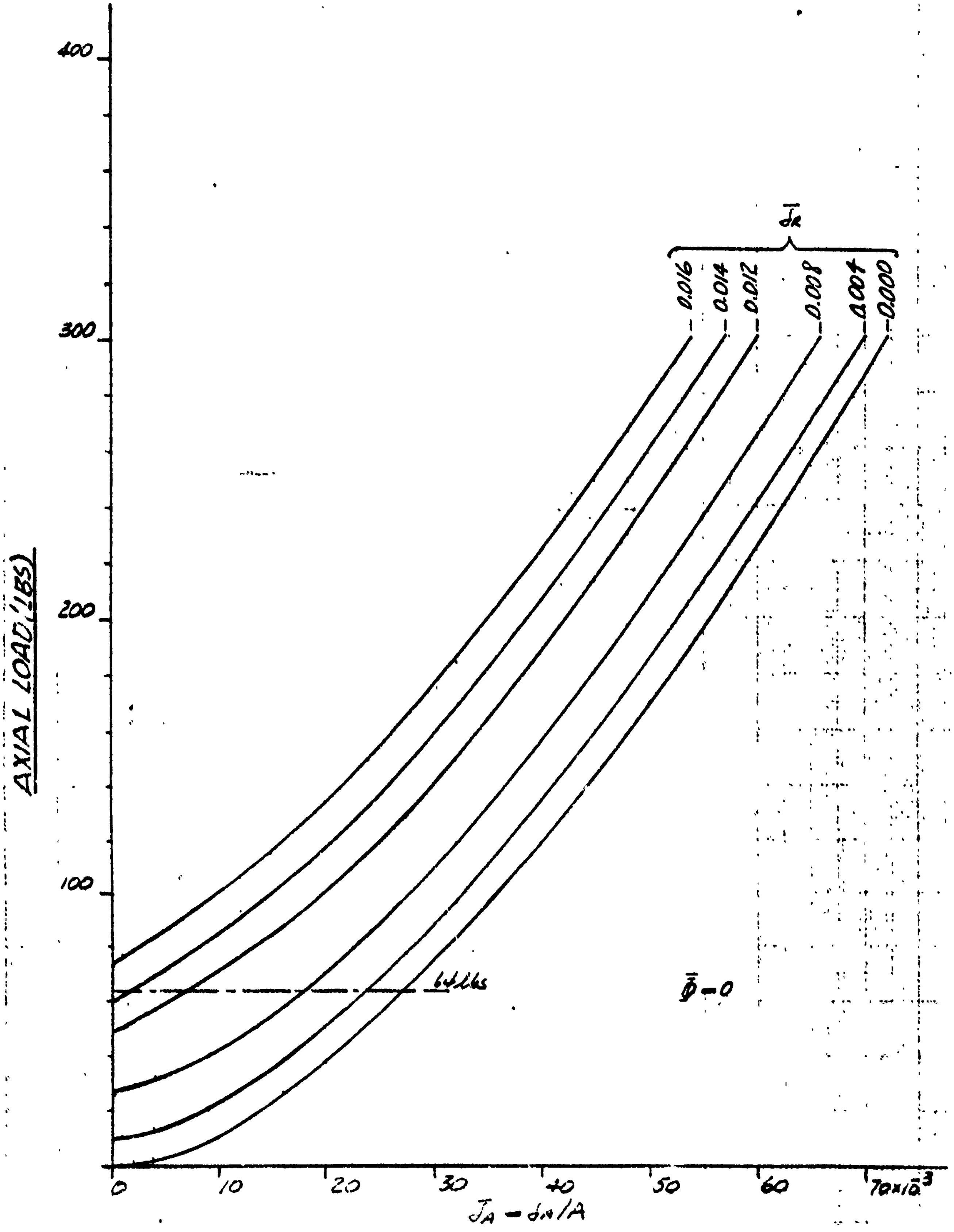

FIG 3 $F_A = f\{\bar{\delta}_A[\S\bar{\delta}_R]\}$ for $\bar{\Phi} = 0$, 110MM BRG

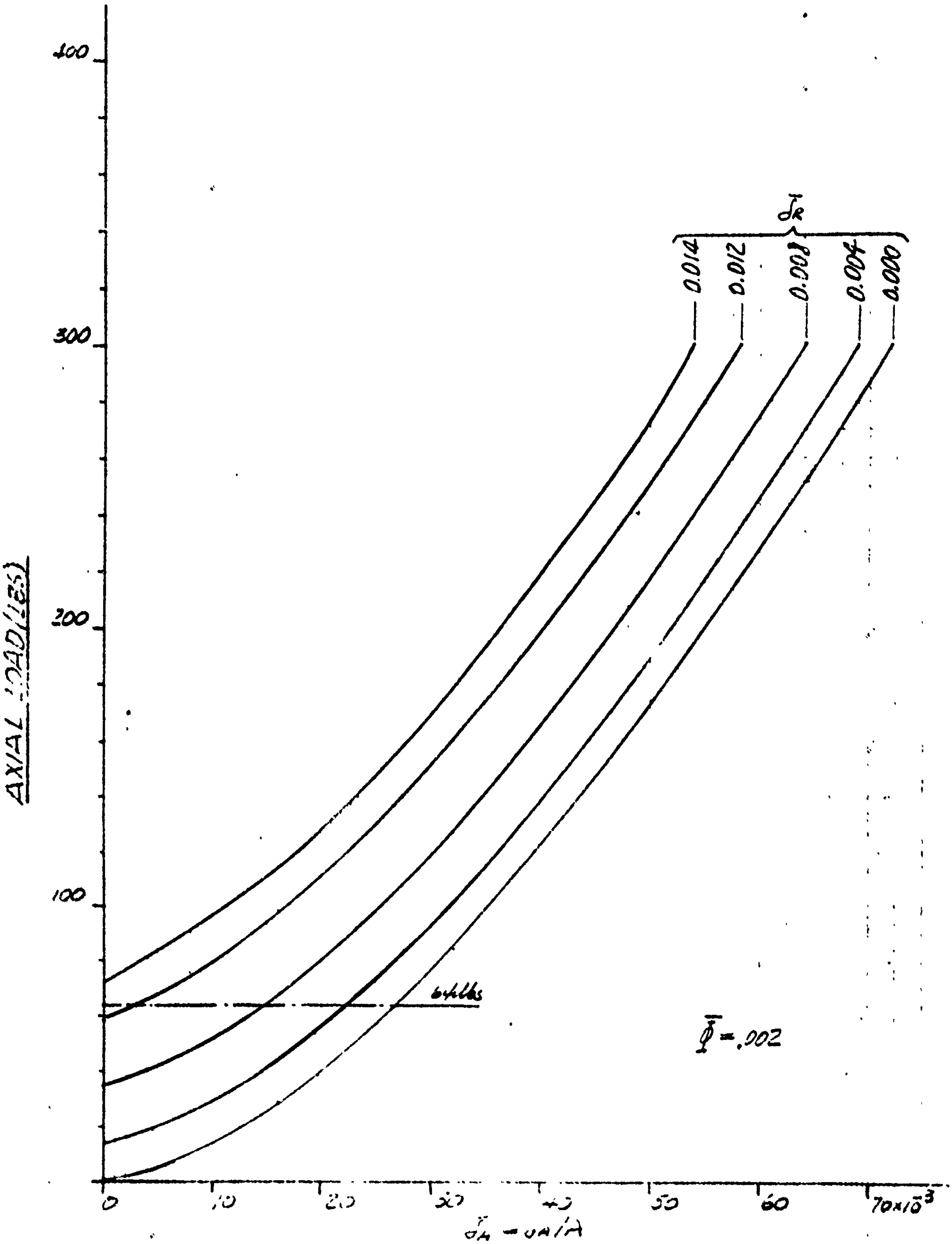

FIG 4. $F_A = f\{\delta_A[g(\delta_R)]\}$ for $\bar{\Phi} = 0.002$, 110 MMERG

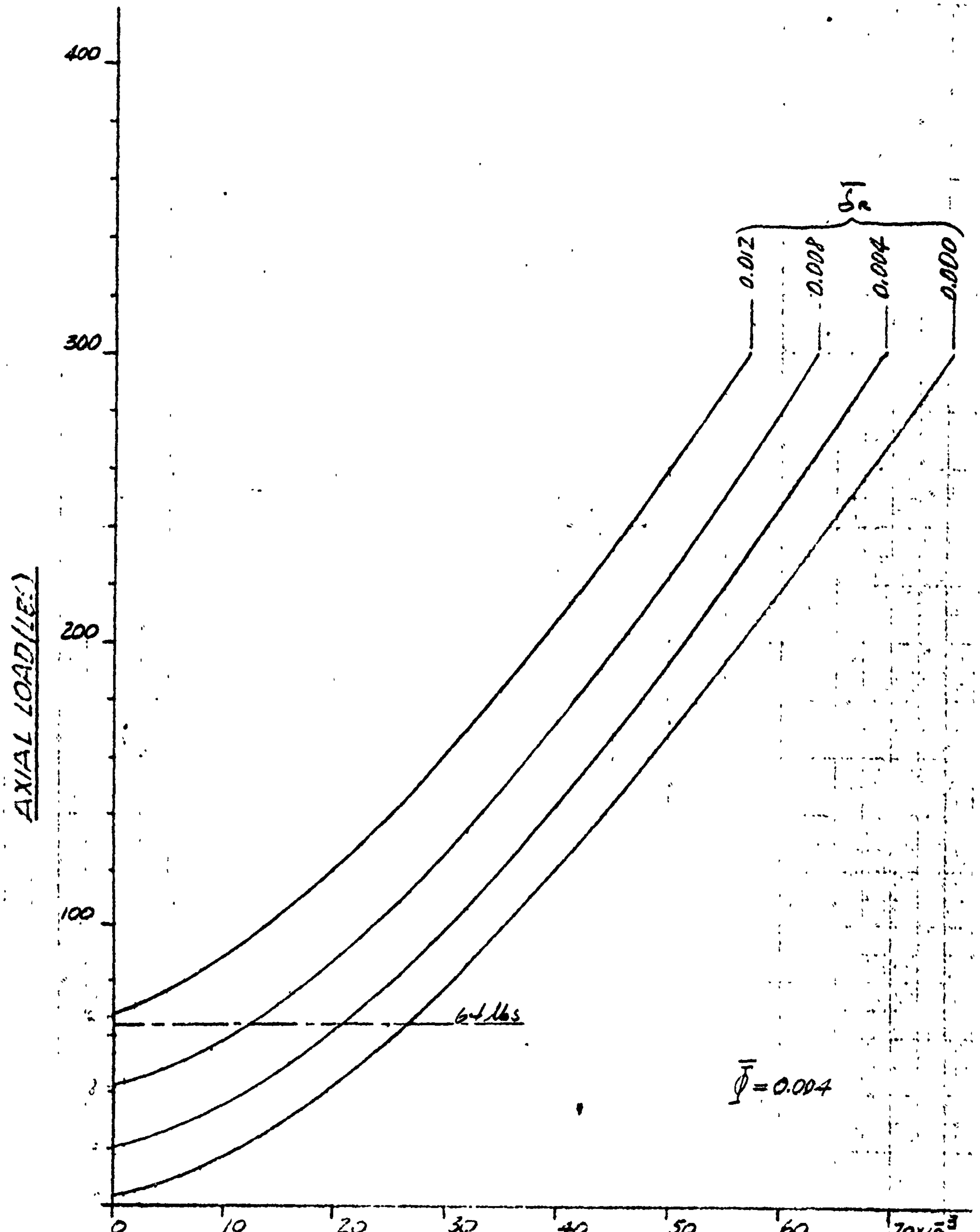

FIG 5. $F_A = f\{\bar{\delta}_A [g(\bar{\delta}_R)]\}$ for $\bar{\Phi} = 0.004$, 110 MMBRG

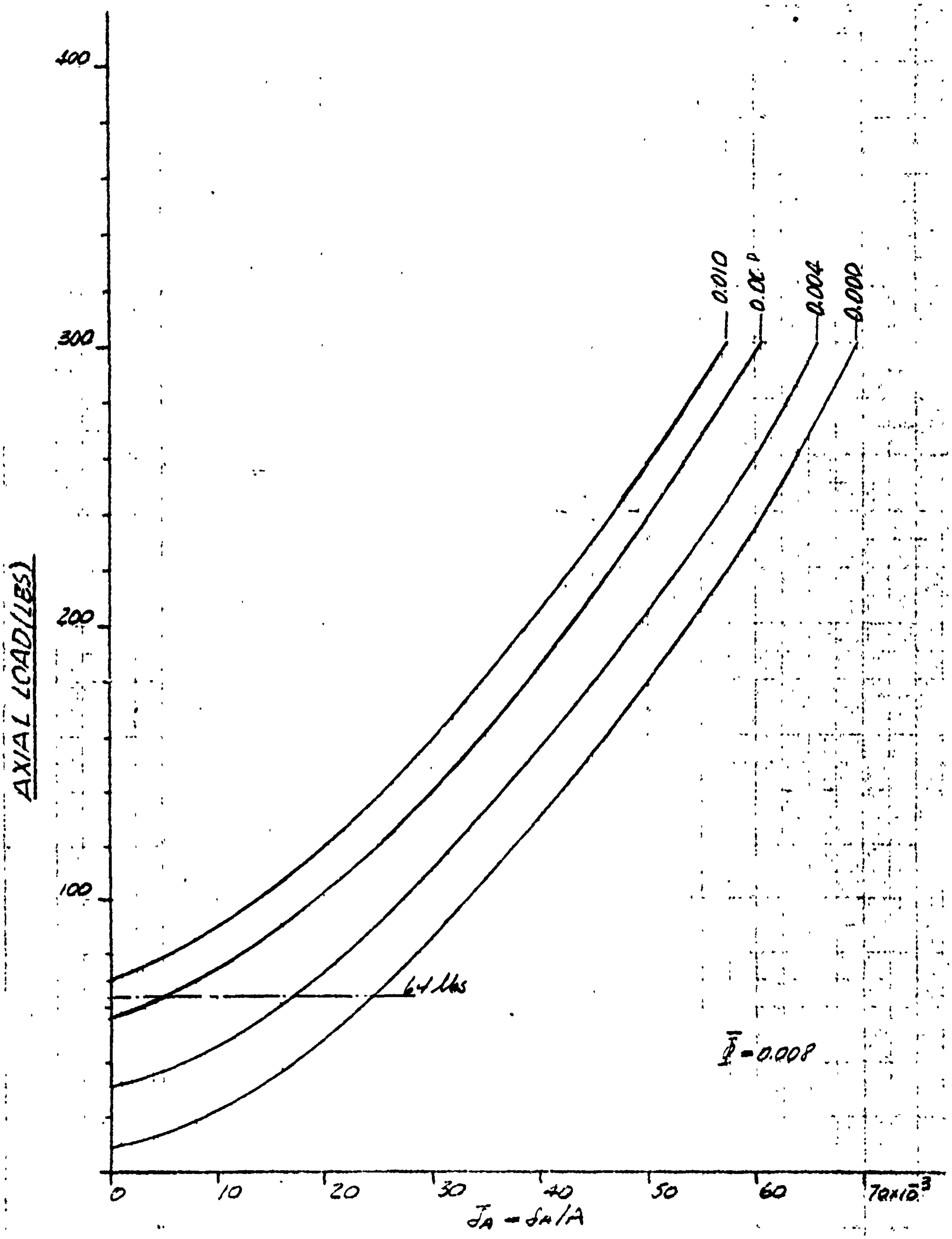

FIG 6 $F_A = f\{\bar{\delta}_A[g(\bar{\delta}_R)]\}$ for $\bar{\Phi} = 0.008$, 110 MM BRG.

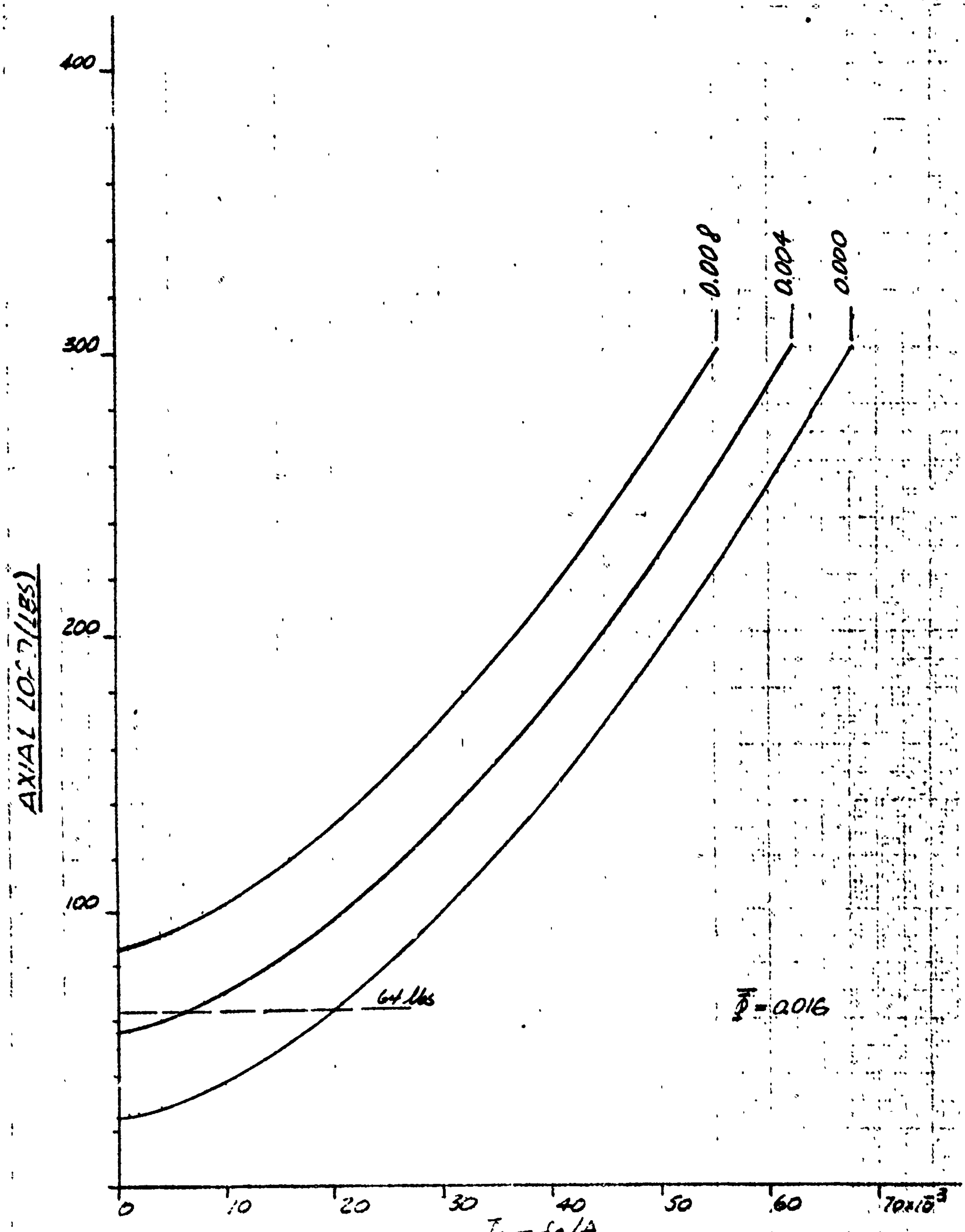

FIG 7 $F_A - f\{\bar{\delta}_A[g(\bar{\delta}_R)]\}$ for $\bar{\Phi} - 0.016$

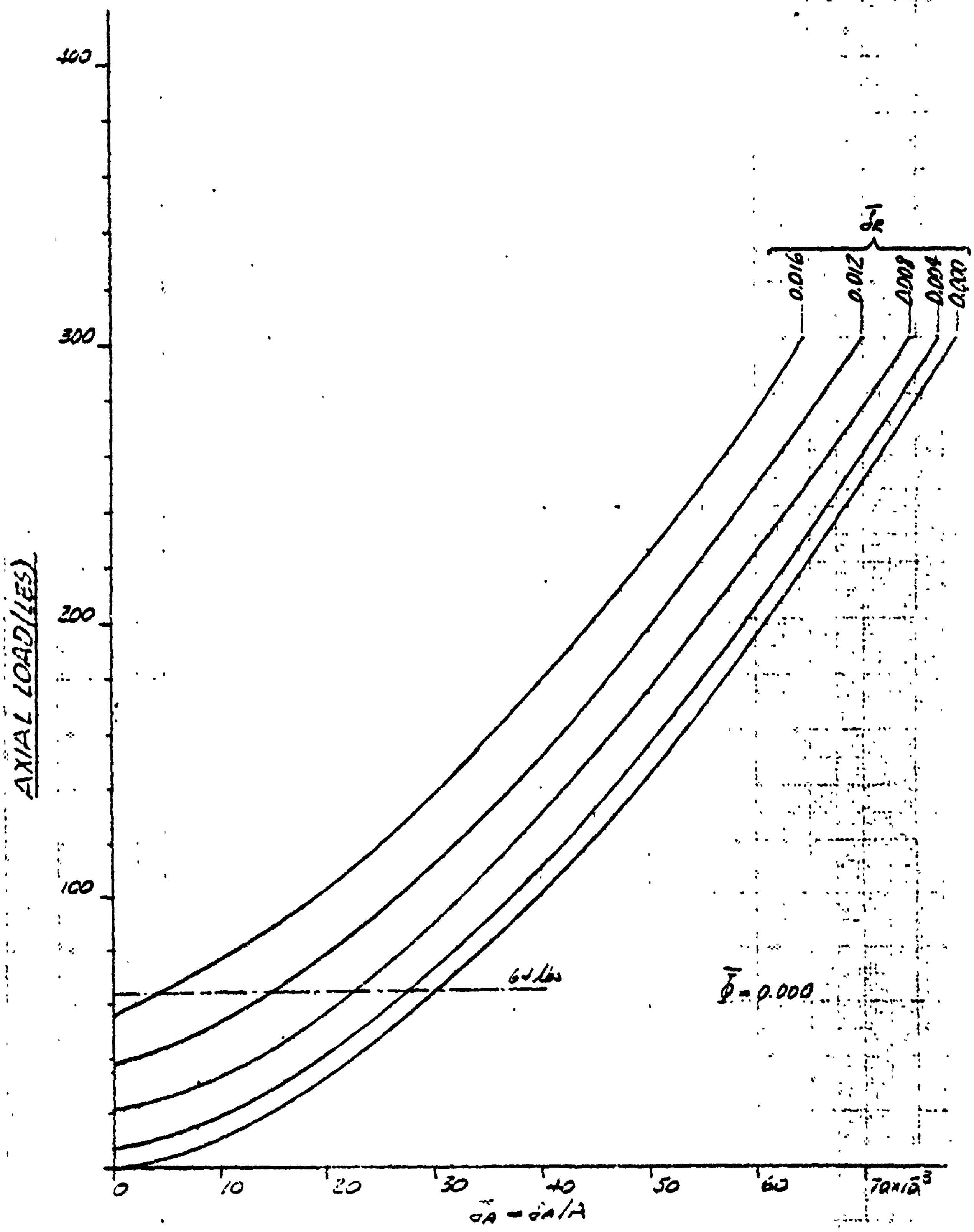

FIG 8 $F_A = f\{\bar{\delta}_A[g(\bar{\delta}_R)]\}$ for $\bar{\Phi} = 0.000$, 90 MM BRG

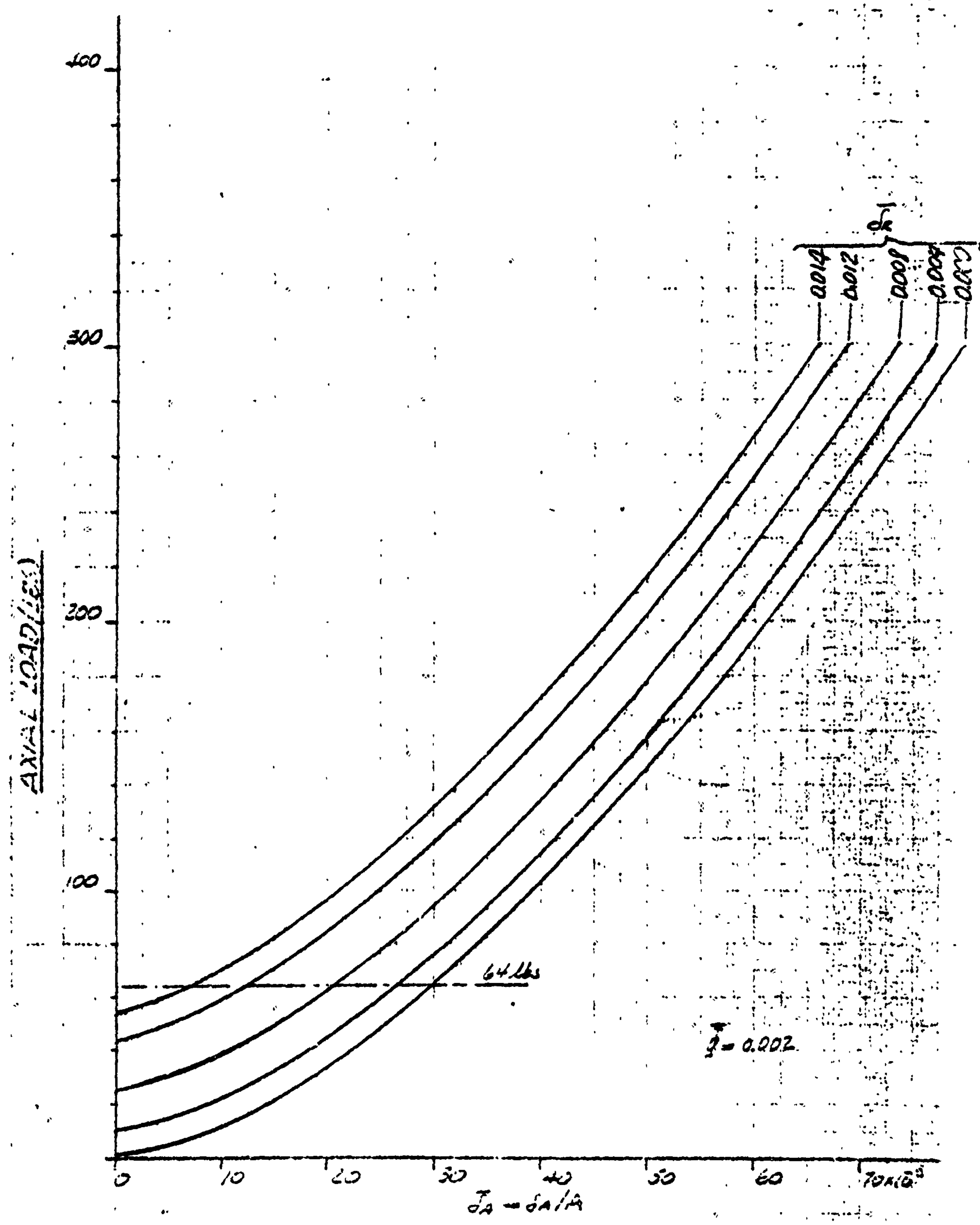

FIG 7. FA = $f\{\bar{\delta}_A[g(\bar{\delta}_R)]\}$ for $\bar{\xi}$ = 0.002, 90MM BRG

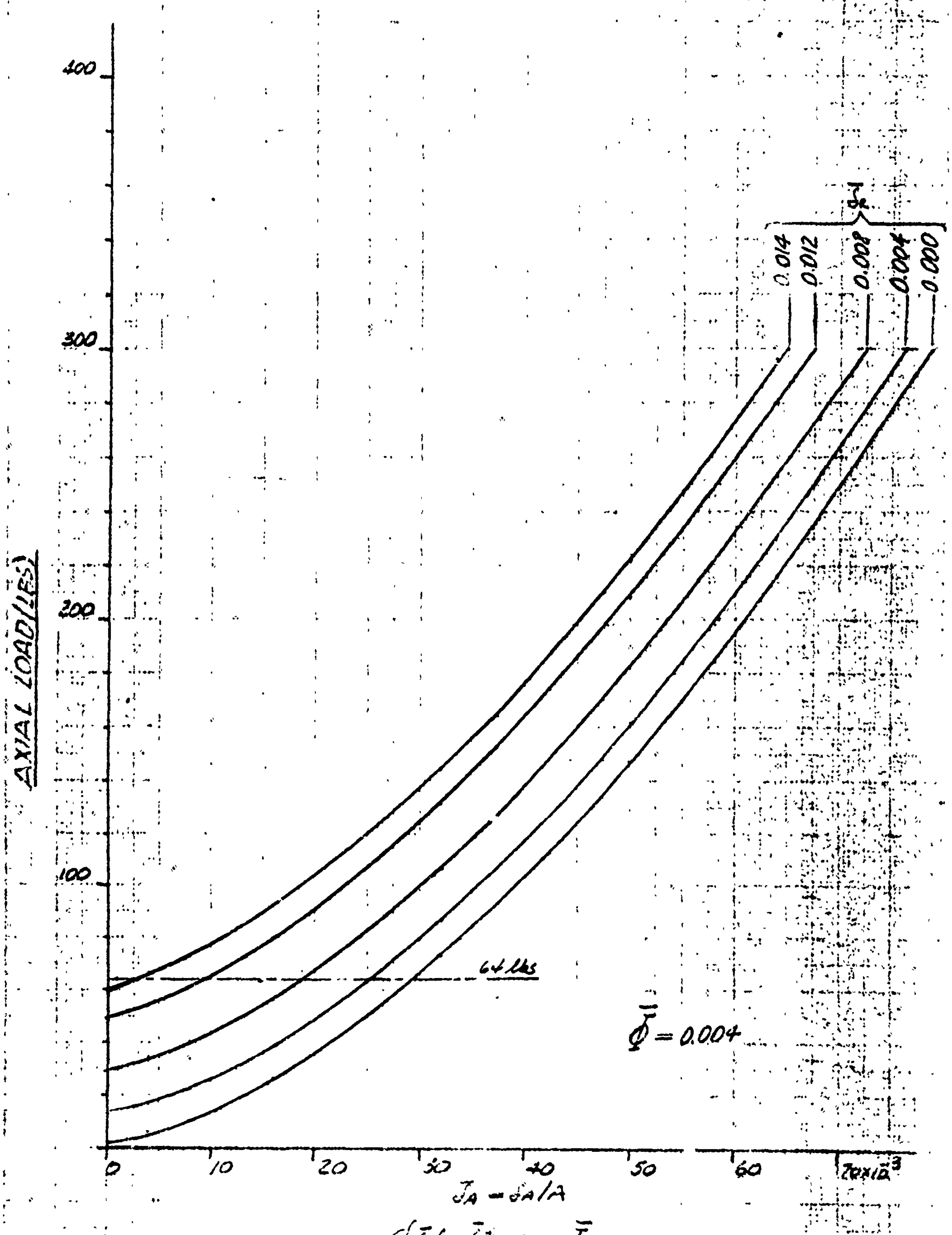

FIG 10 FA = f{ω[g(δ)]} for $\bar{\Phi}$ = 0.004, 90 MM BRG.

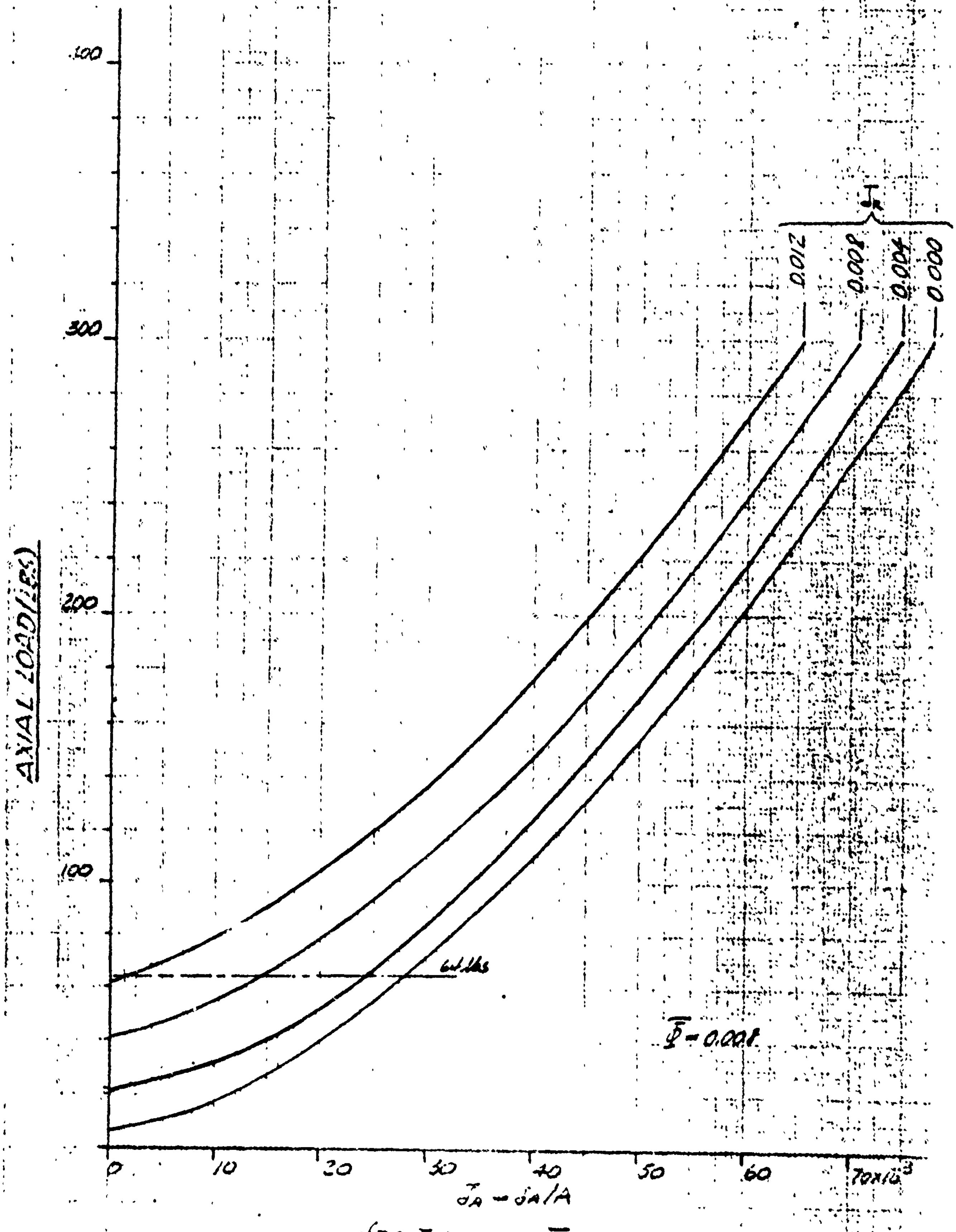

FIG 11. $F_A = f\{\bar{\delta}_A[\bar{\delta}_R(\bar{\delta}_A)]\}$ for $\bar{\Phi} = 0.008$, 40MM BRG

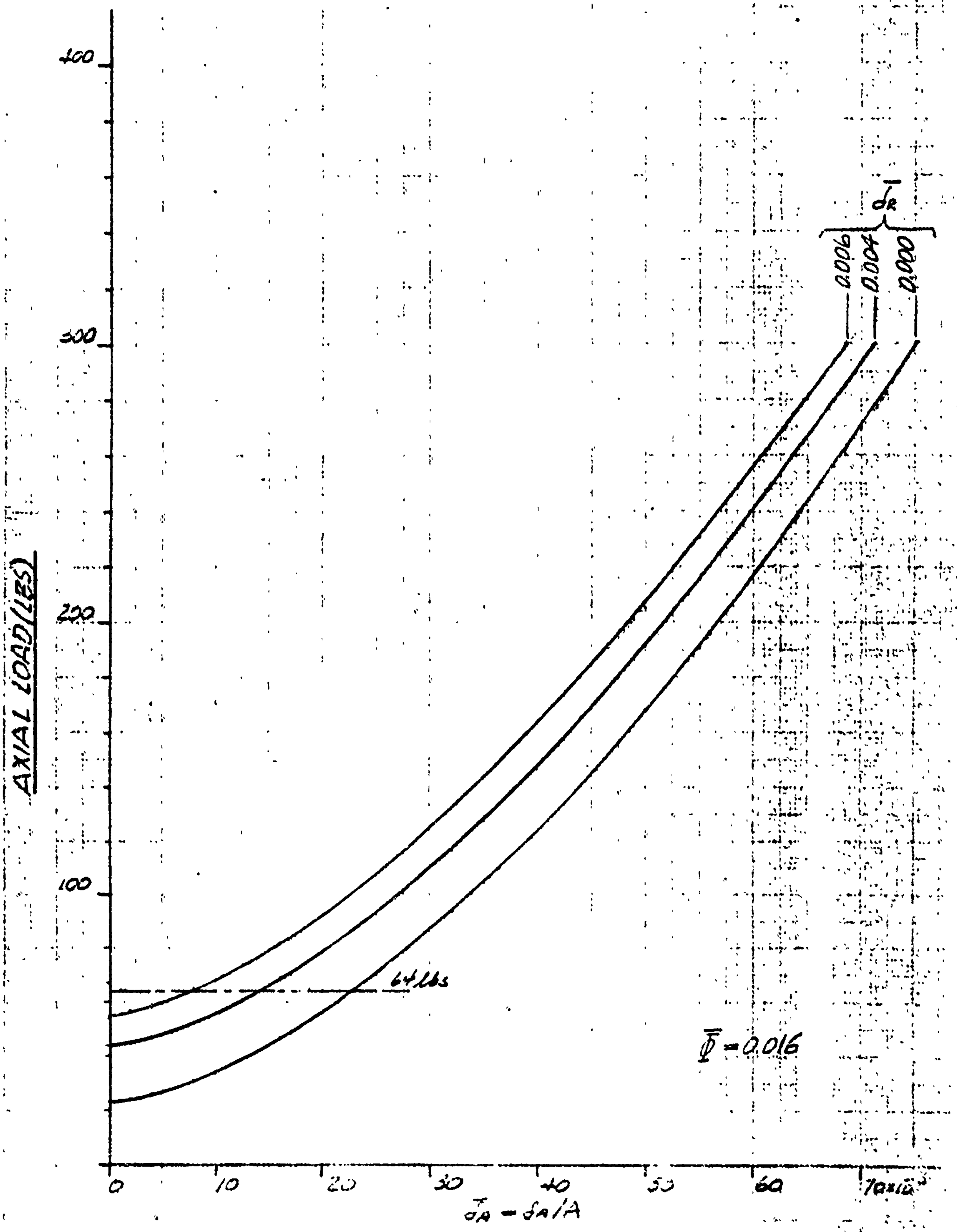

FIG 12. $F_A = f\{\bar{\delta}_A[g\bar{\delta}_R]\}$ for $\bar{\Phi} = 0.016$

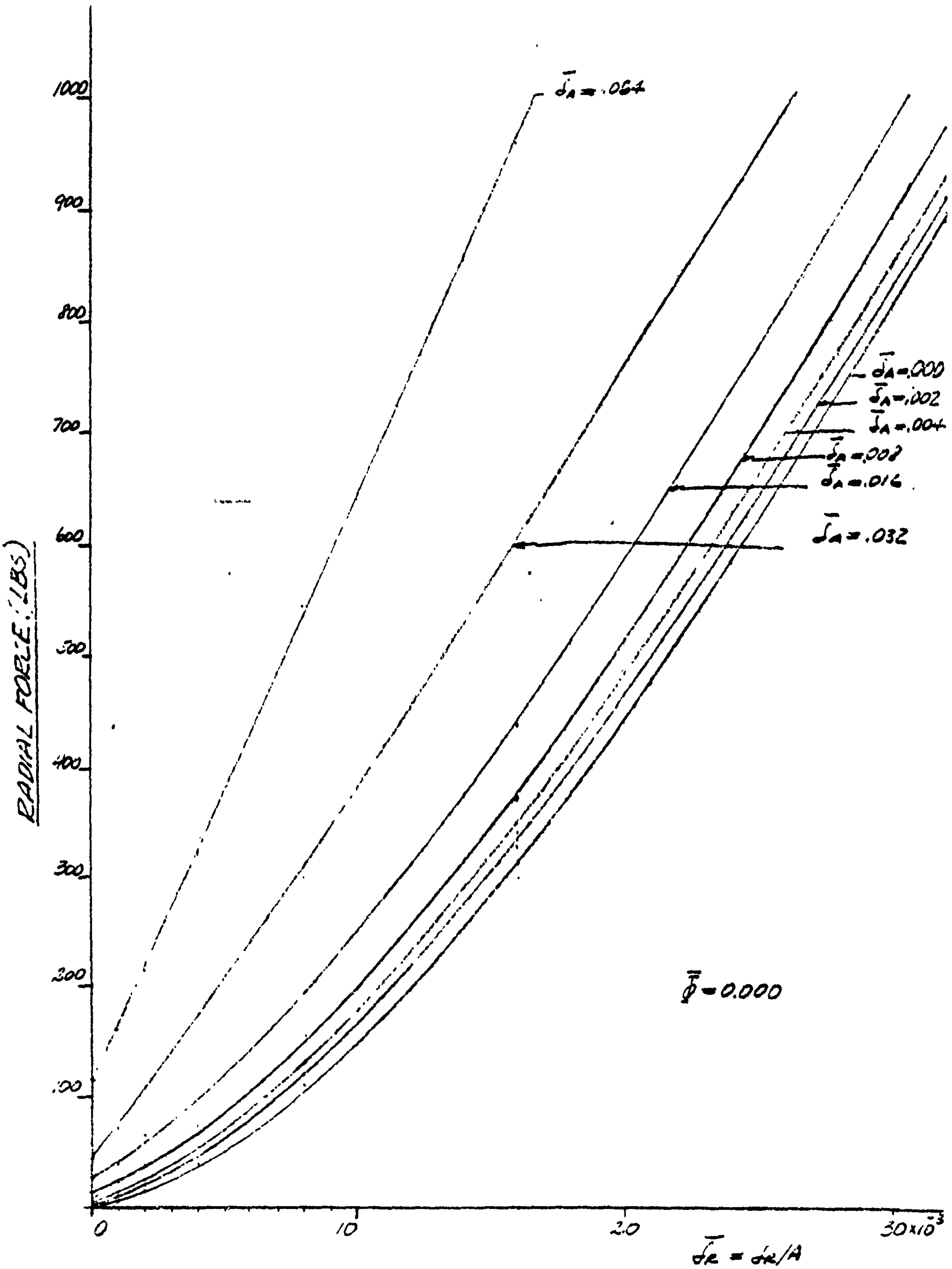

FIG 13 $F_R = f\{\bar{\delta}_R[g(\bar{\delta}_A)]\}$, FOR $\bar{\Phi} = 0.00$, 110MM BRG

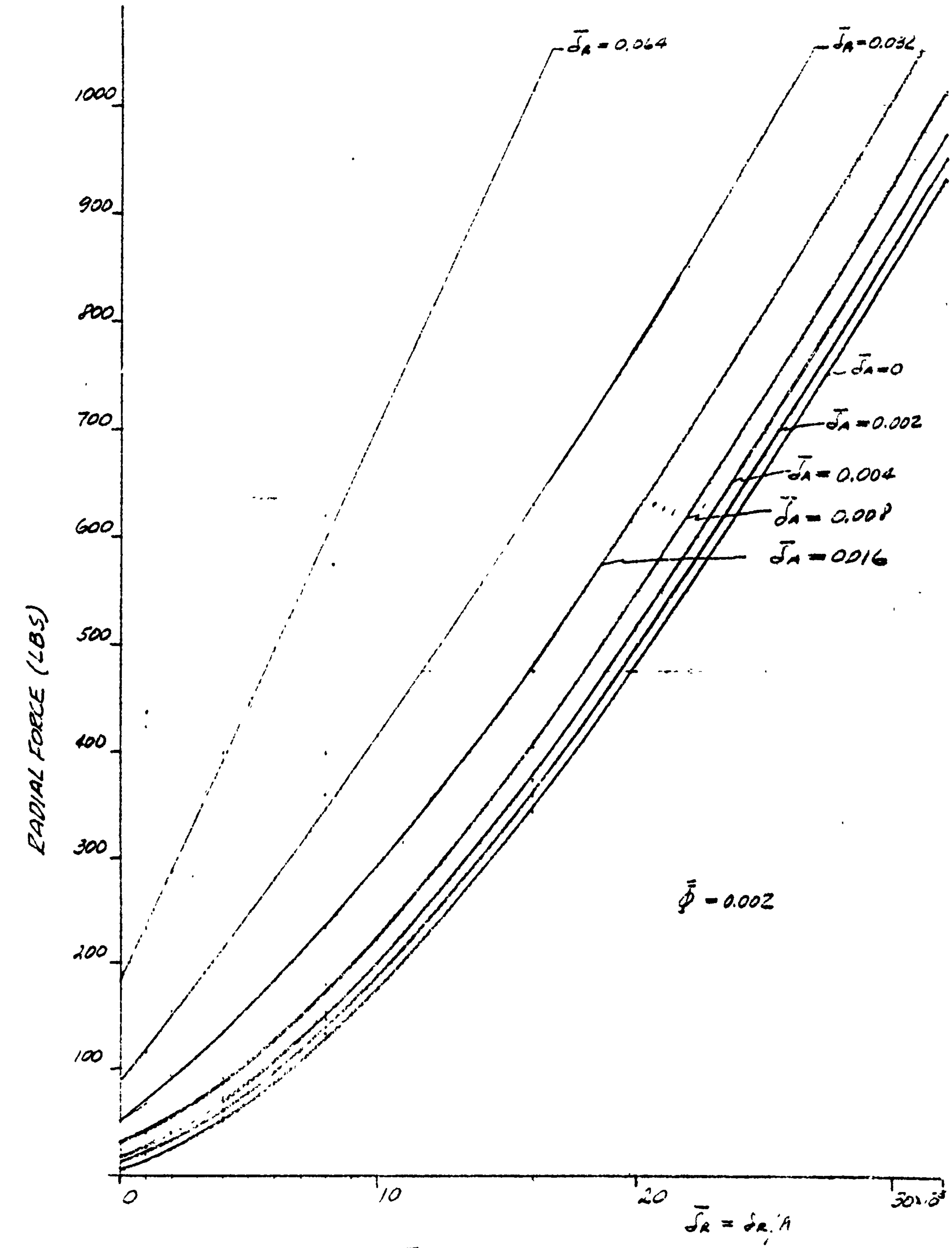

FIG 14 $F_R = f\{\bar{\delta}_R[\bar{\delta}_A]\}$, for $\bar{\Phi} = 0.002$, 110 MM BRG

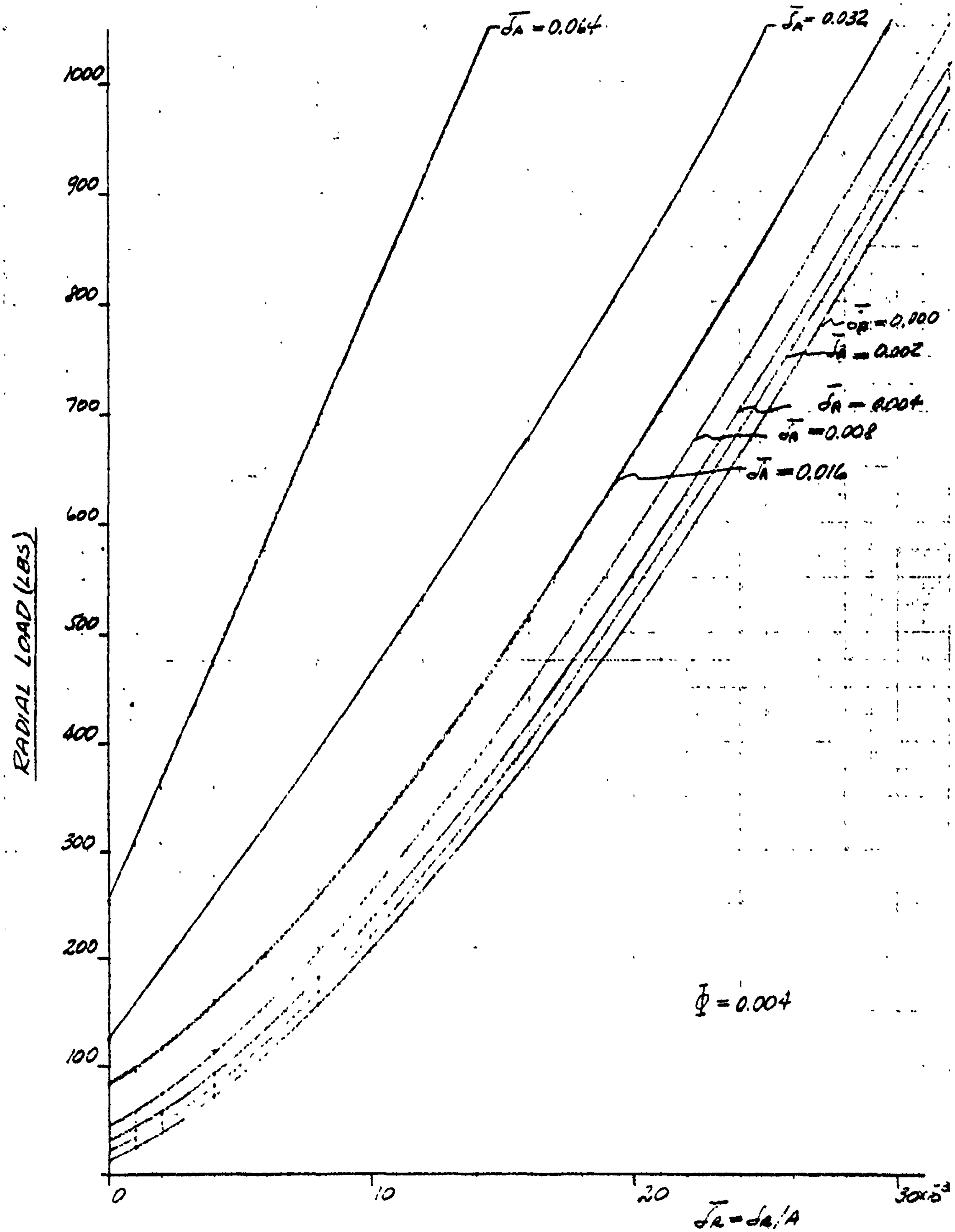

FIG 15 $F_R = f\{\bar{\delta}_R[g(\bar{\delta}_A)]\}$, $\bar{\Phi} = 0.004$, 110 MM BRG

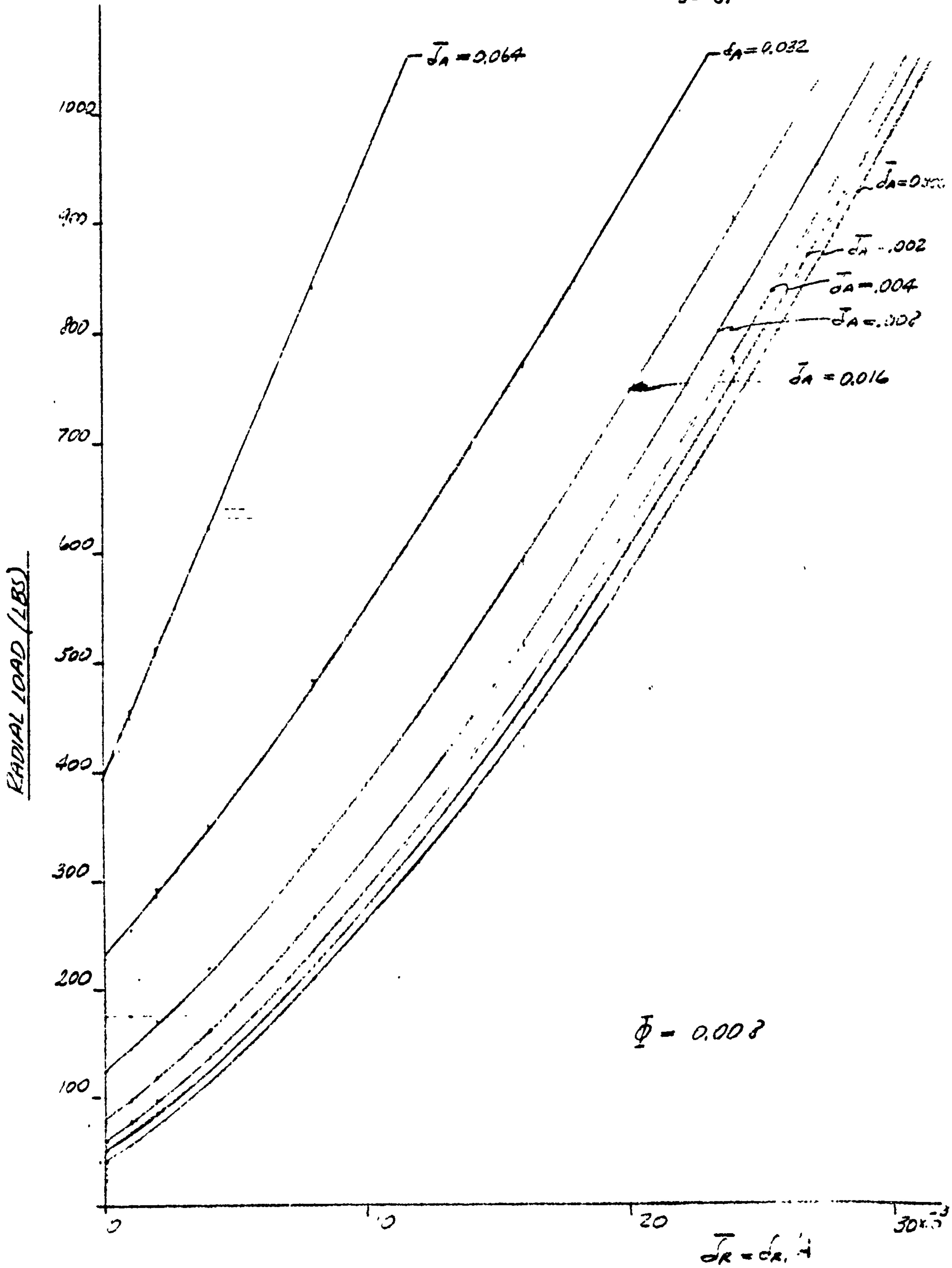

FIG 16 $F_R = f\{\bar{\delta}_R [g(\bar{\delta}_A)]\}$, $\bar{\Phi} = 0.008$, 110 MM BRG

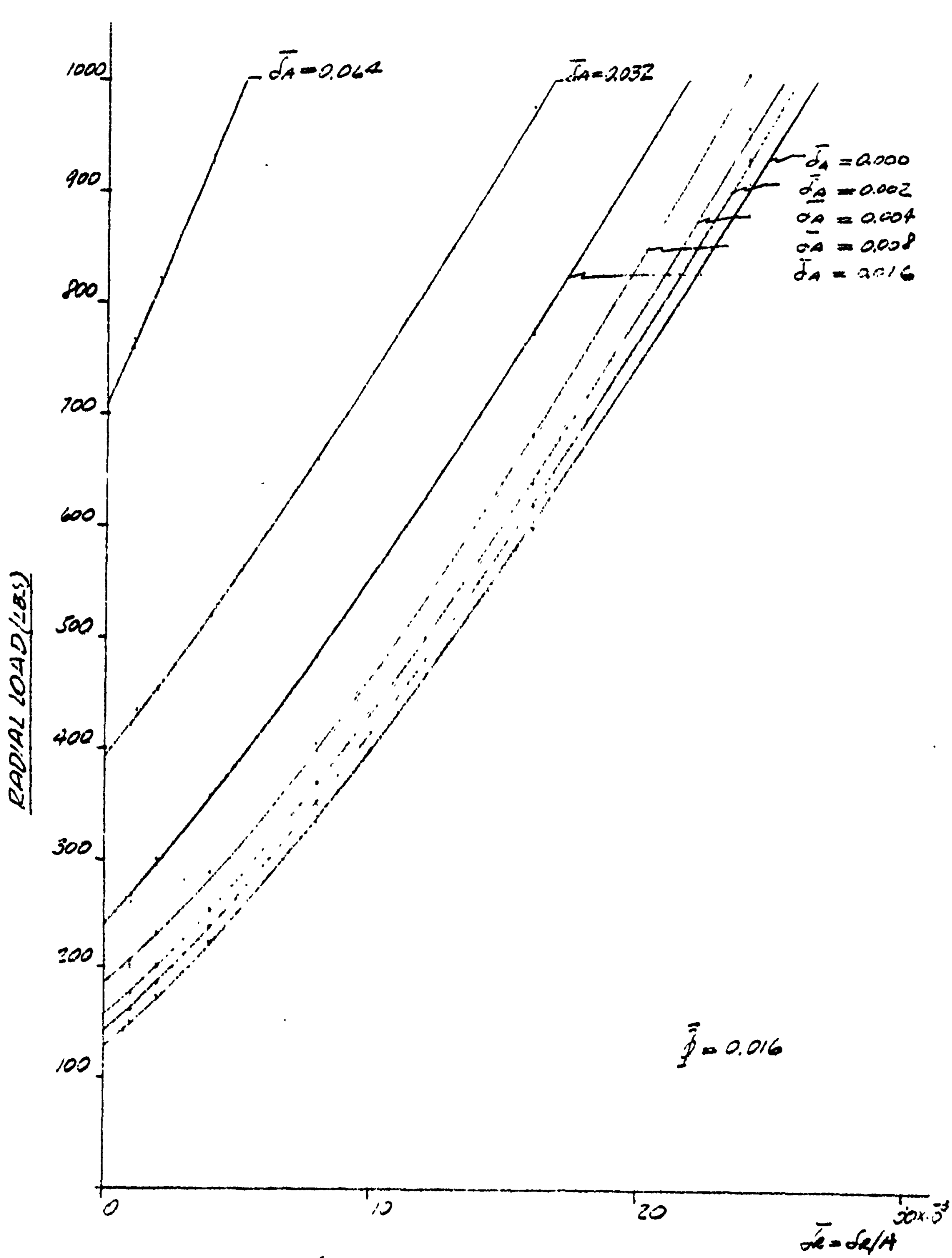

Fig 17 $F_R = f\{\bar{\delta}_R[g(\bar{\delta}_A)]\}$, $\bar{\phi} = 0.016$, 110MM BRG

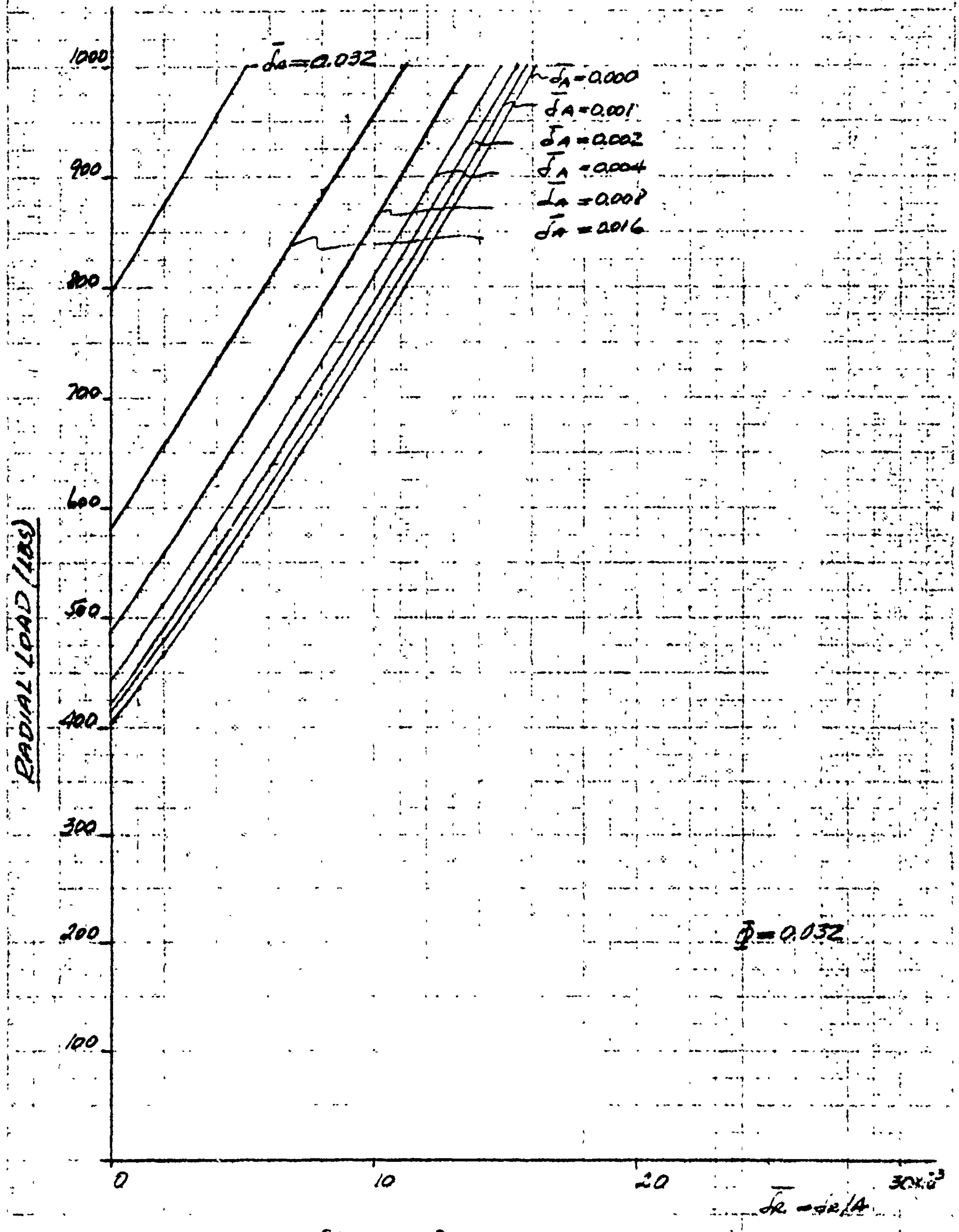

FIG 18 $F_R = f\{\bar{\delta}_R[g(\bar{\delta}_A)]\}$, $\bar{\Phi} = 0.032$, 110 MM BRG

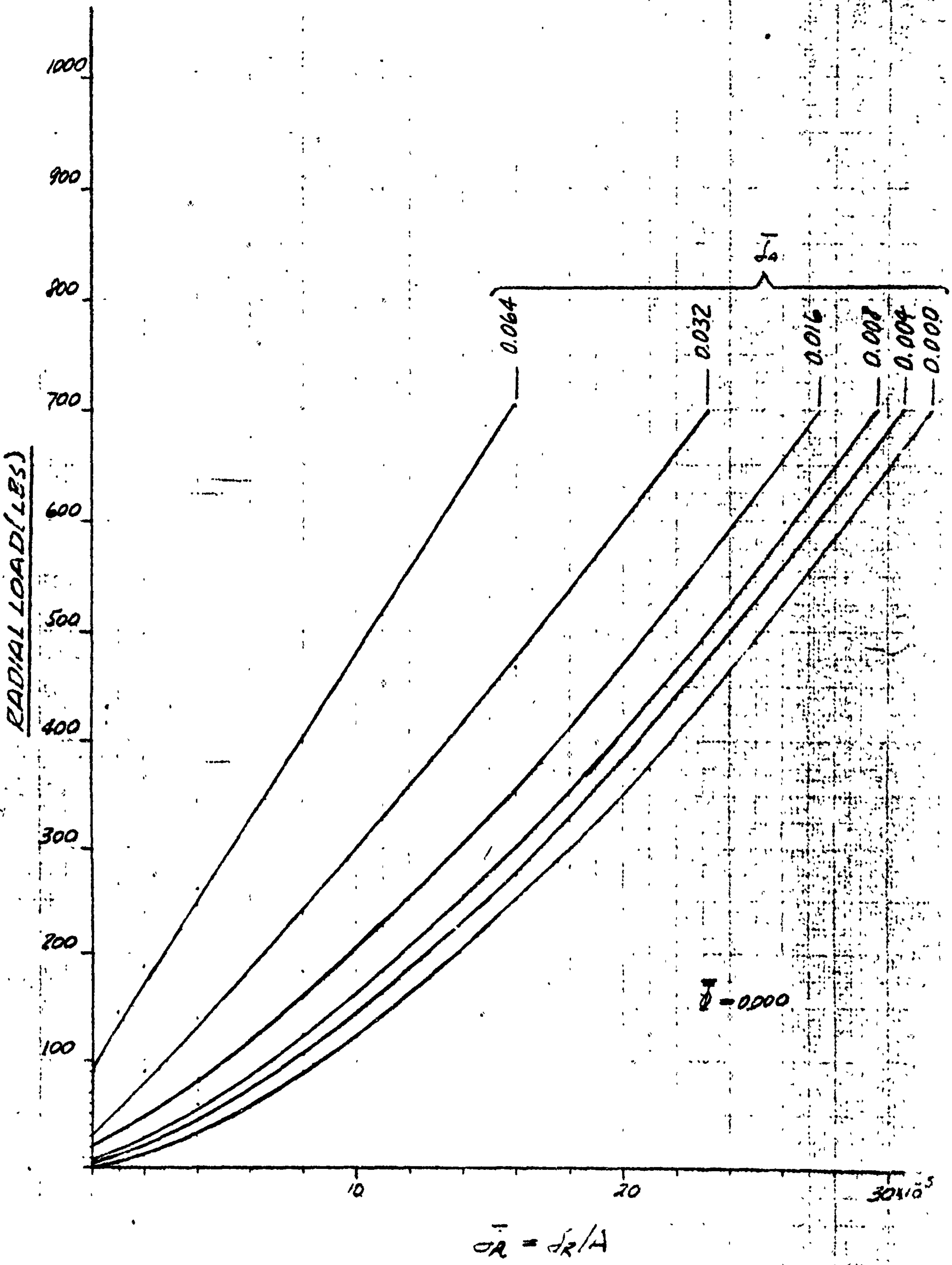

FIG 19. FR = f{σ̄R[g(σ̄A)]} for Φ̄ = 0.000, 90MM BRG

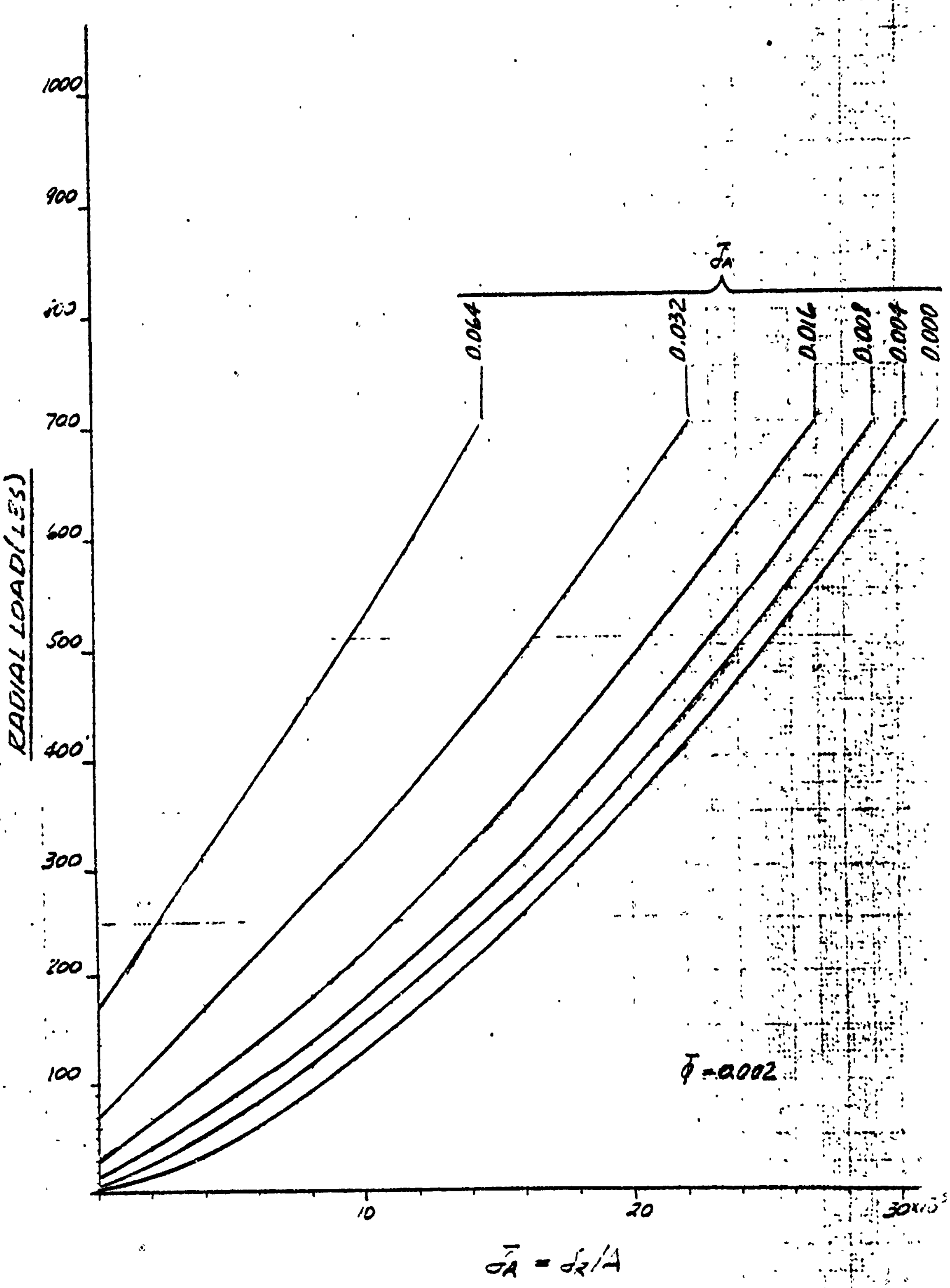

FIG 20 $F_R = f\{\bar{\delta}_R[z(\bar{\delta}_A)]\}$, for $\Phi = 0.002$, 90 MM BRG

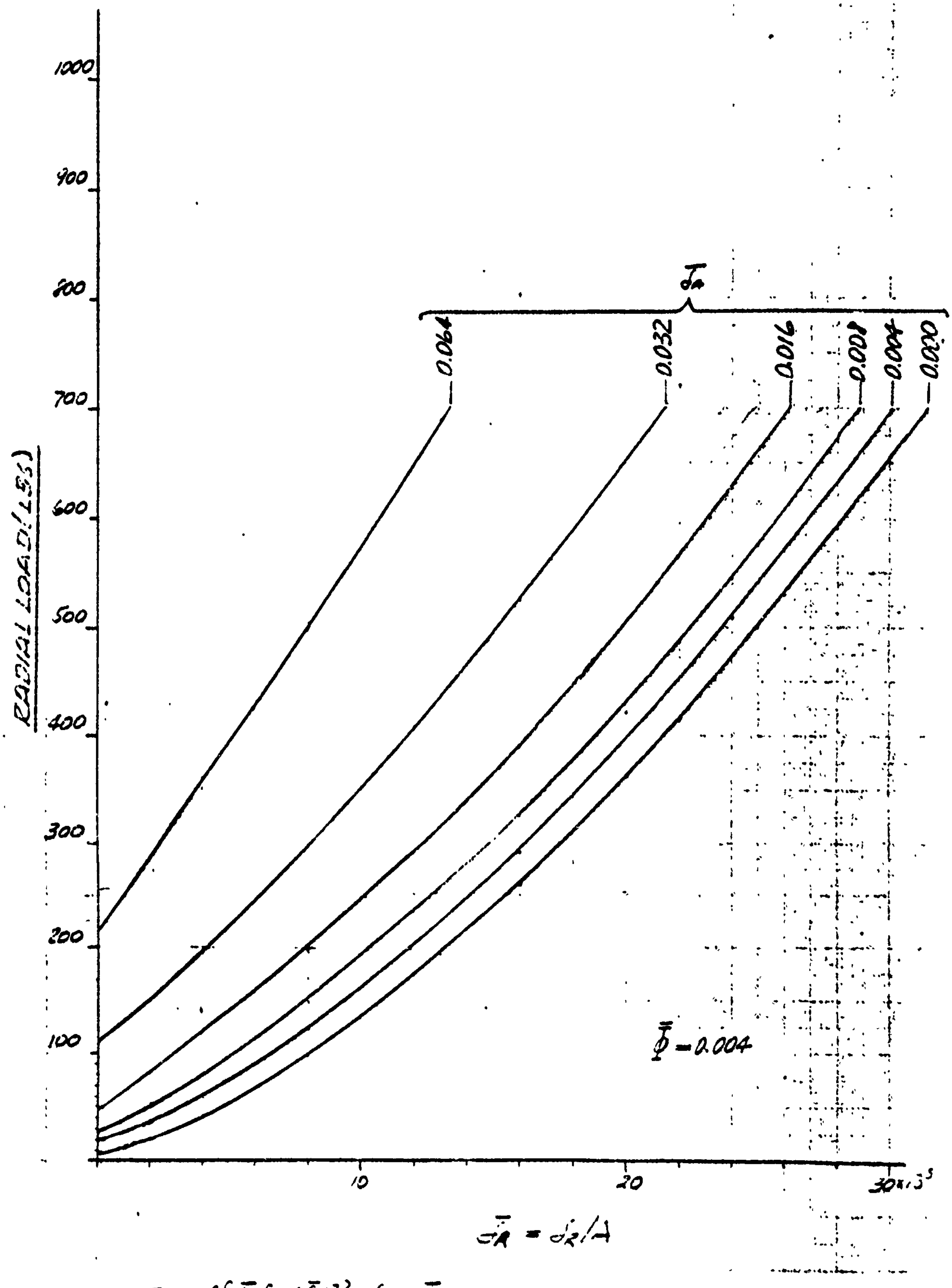

FIG 21. $F_R = f\{\bar{\delta}_R[g(\bar{\delta}_A)]\}$, for $\bar{\Phi} = 0.004$, 40MMBRG

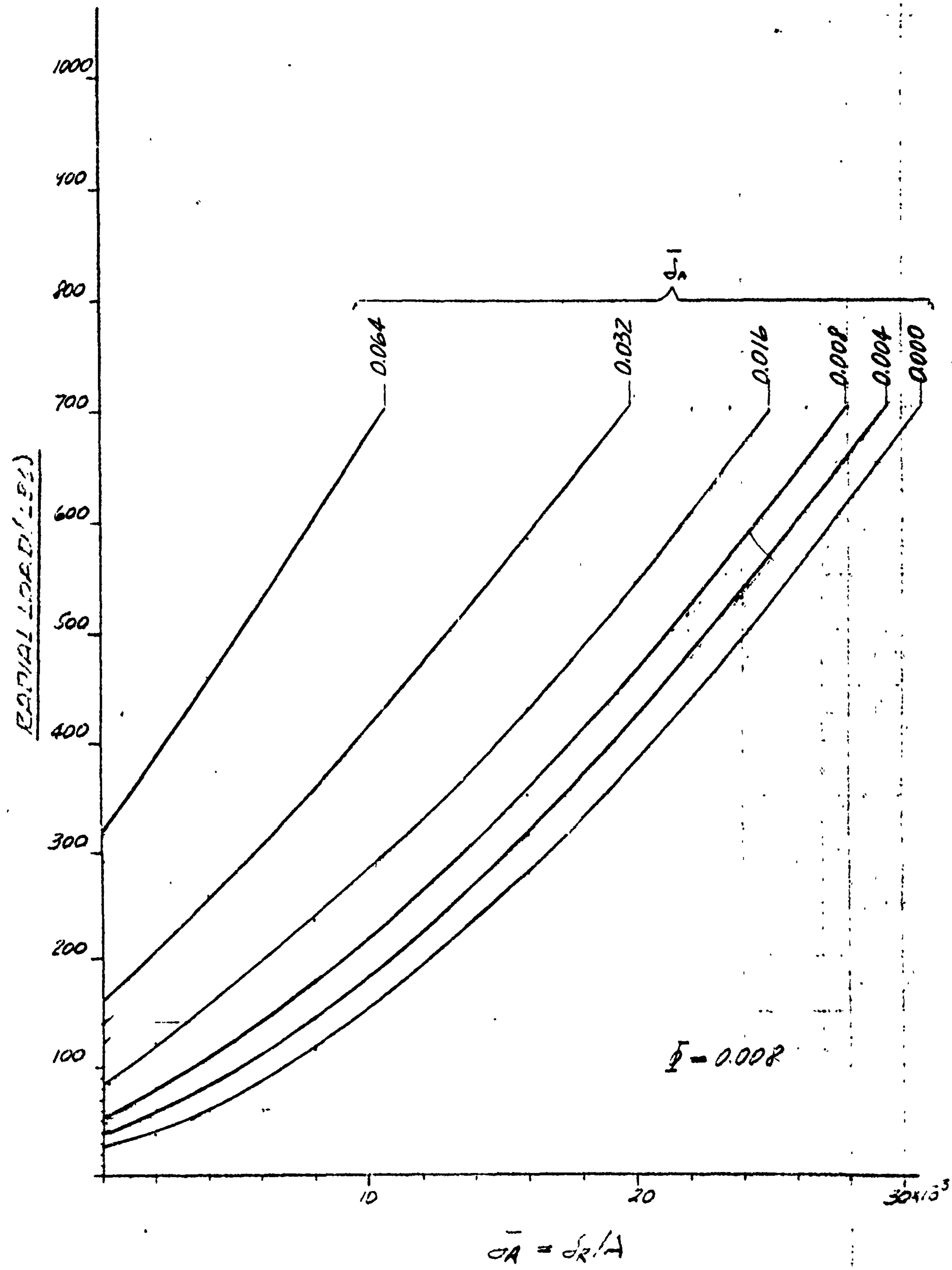

FIG 22 . $F_R = f\{\bar{\delta}_R[g(\bar{\delta}_A)]\}$, for $\Phi = 0.008$, 90 MM BRG

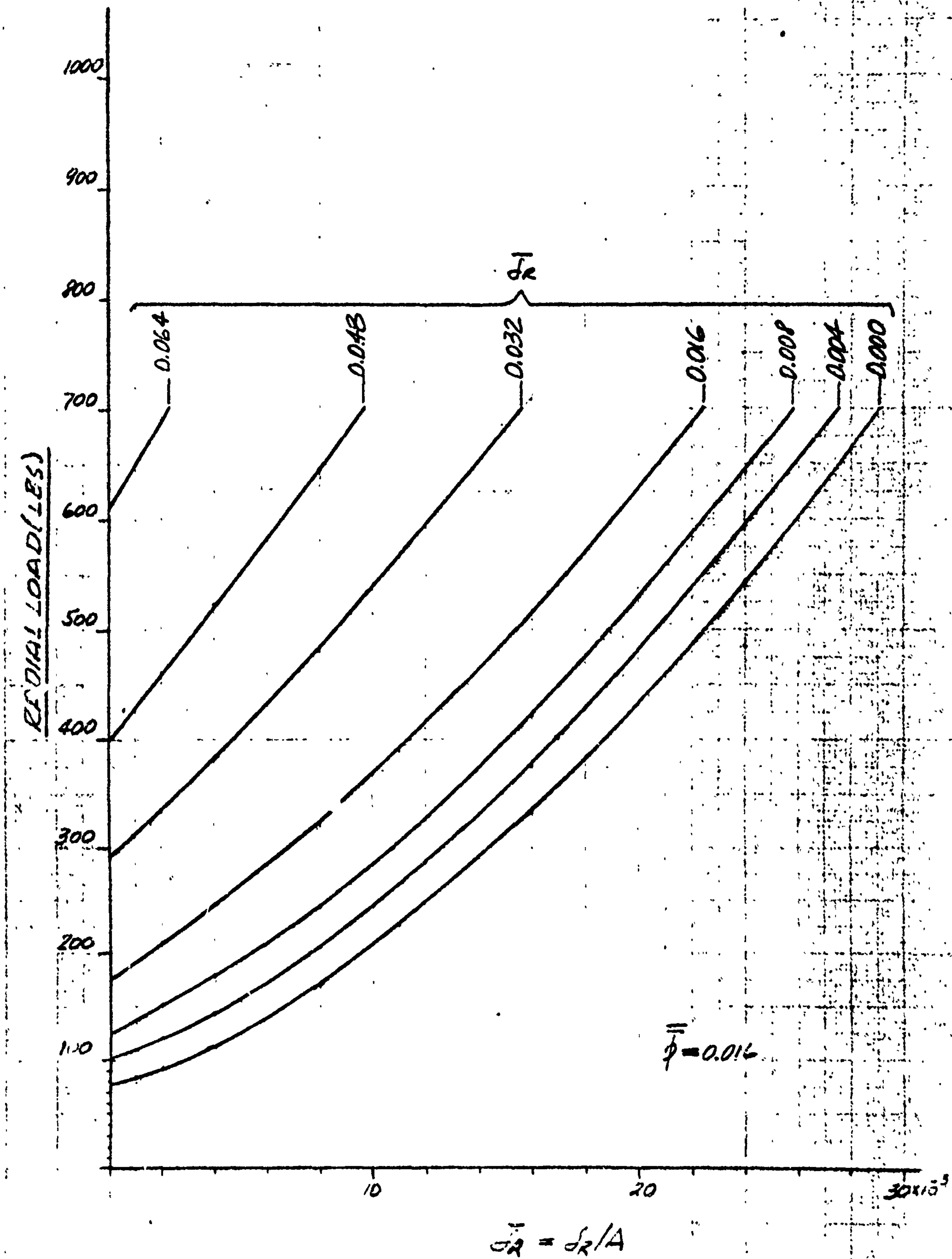

FIG 23 $F_R = f\{\bar{\delta}_R[g(\bar{\delta}_A)]\}$, for $\phi = 0.016$, 90MM BRG

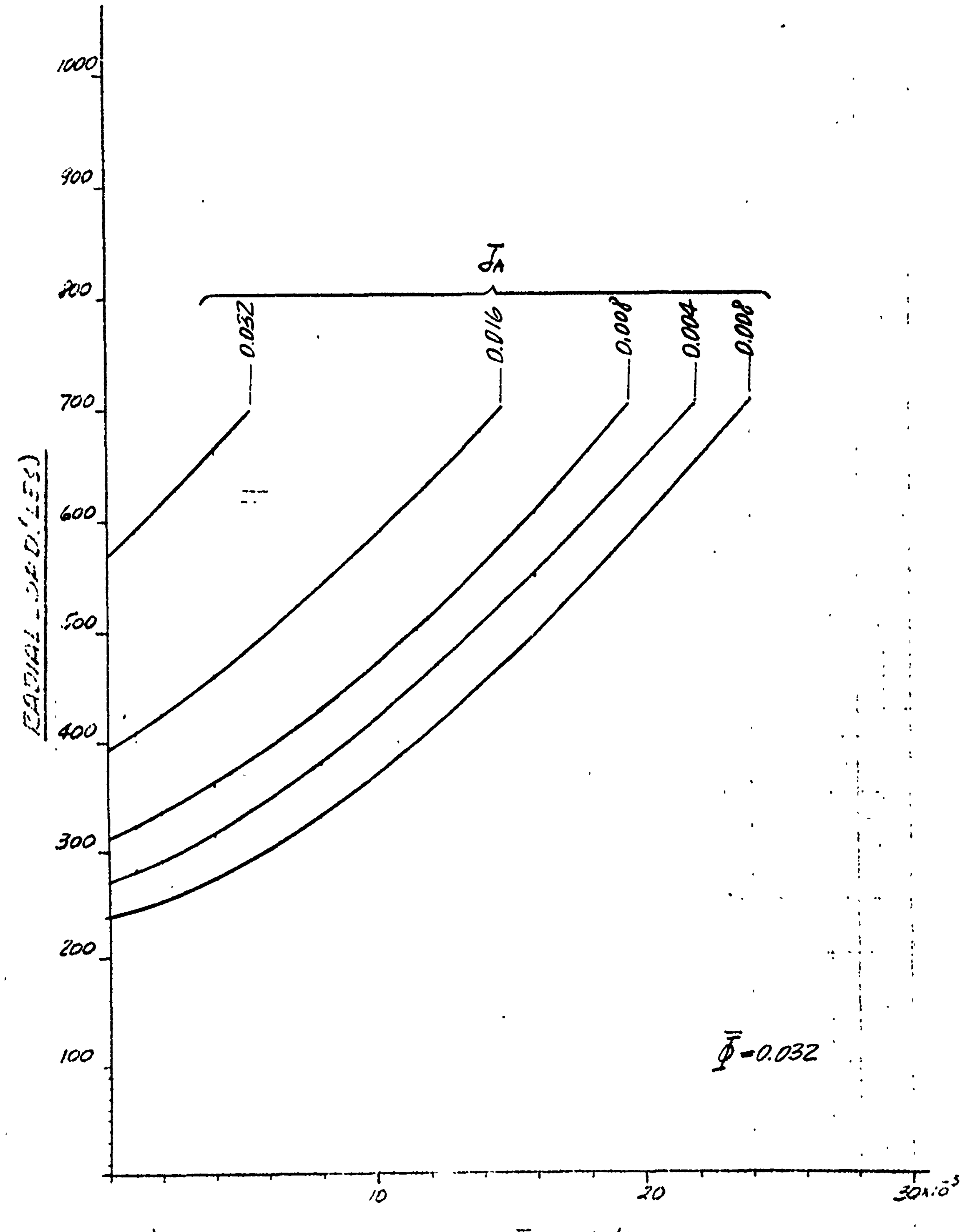

FIG 24 $F_R = f\{\bar{\delta}_R[g(\bar{\delta}_A)]\}$, for $\bar{\Phi} = 0.032$, 90MM BRG

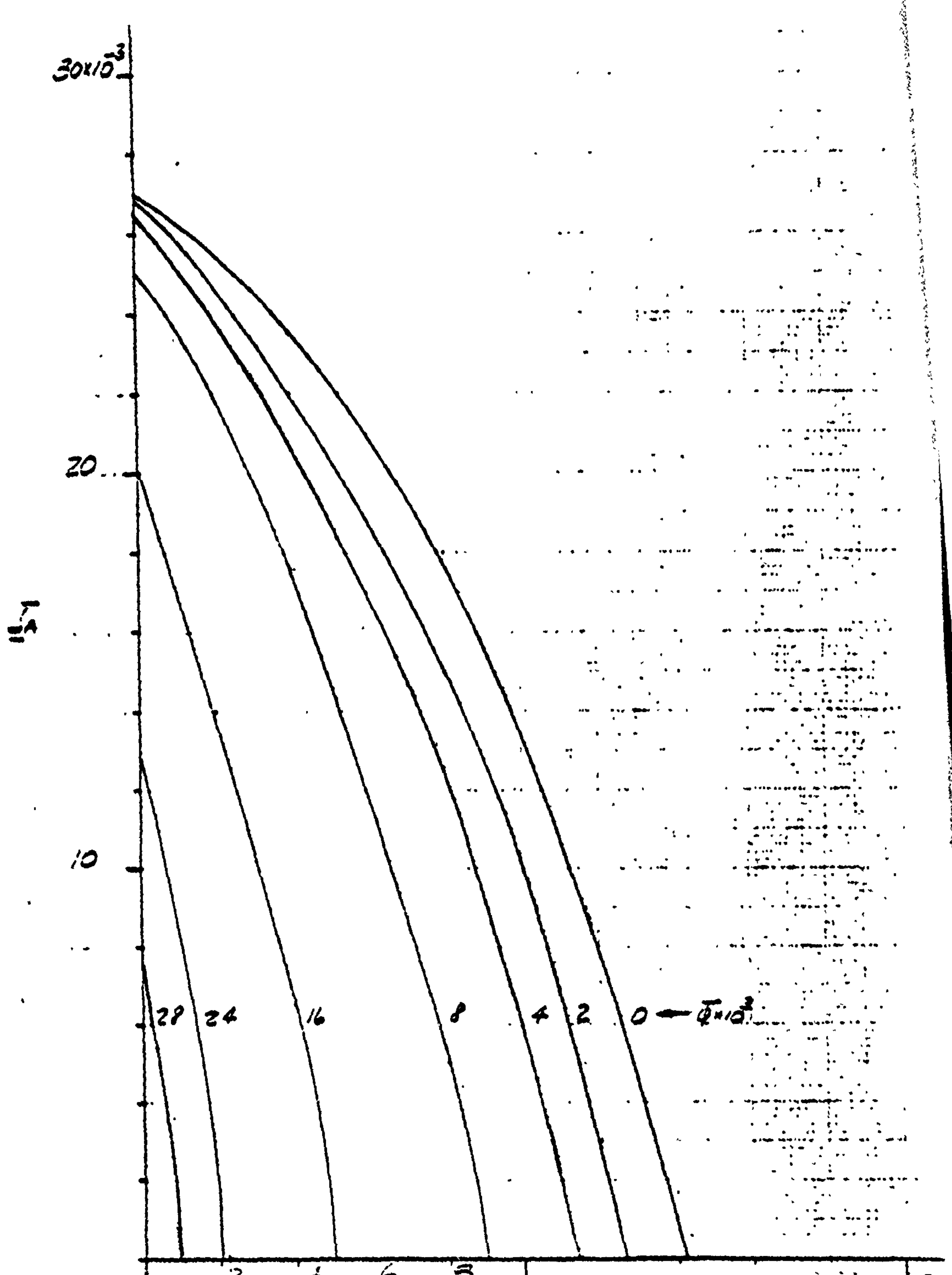

FIG 25. $\bar{T}_A = f\bar{T}_R$ for $\bar{\Phi}_x$, 110MM BRG

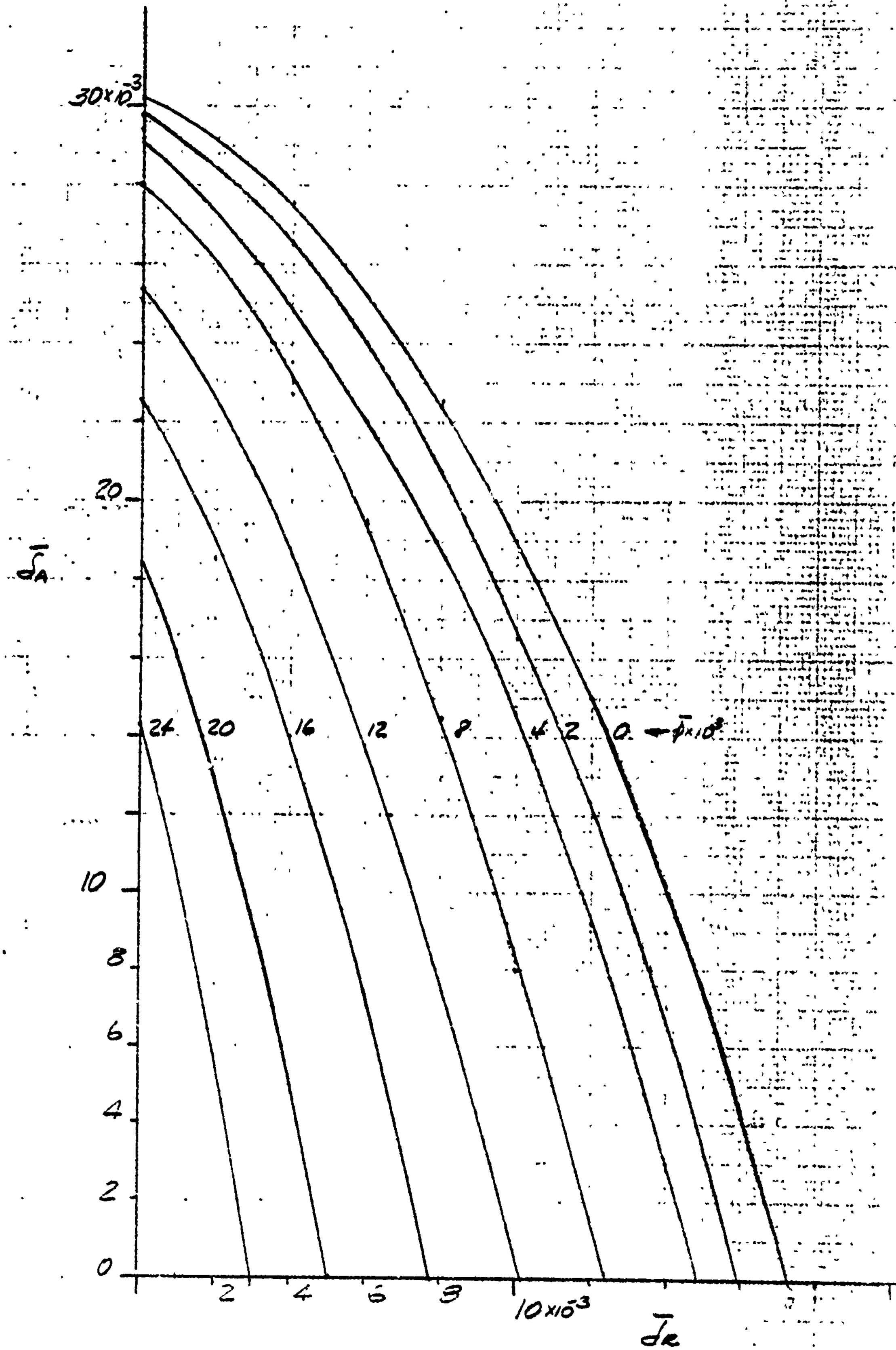

FIG 26 $\bar{\delta}_A = f(\bar{\delta}_R)$ for $\bar{\Phi}_K$, 90MM BRG

- Supplementary Equations

Since the granularity of the plots given on Figure 25 and Figure 26 is too coarse, for values of $\bar{\delta}_R$ approaching zero, a set of auxiliary equations based on the data points, obtained via EQ 15 and EQ 16, was developed for both bearings. The general expressions for the developed equations are:

$$F_{Aj} = a_1(\bar{\delta}_A)^{b1}+a_2(\bar{\delta}_R)^{b2}(\bar{\delta}_A)^{a_3}(\bar{\delta}_R)^{b3}+a_4(\bar{\delta}_R)^{b4}+a_5(\bar{\phi})^{b5}+a_6(\bar{\phi})^{b6}(\bar{\delta}_R)^{a_7}(\bar{\phi})^{b7} \quad \text{EQ 19}$$

$$F_{Rj} = a_1(\bar{\delta}_R)^{b1}+a_2(\bar{\delta}_A)^{b2}(\bar{\delta}_R)^{a3}(\bar{\delta}_A)^{b3}+a_4(\bar{\delta}_A)^{b4}+a_5(\bar{\phi})^{b5}+a_6(\bar{\phi})^{b6}(\bar{\delta}_A)^{a7}(\bar{\phi})^{b7} \quad \text{EQ 20}$$

and the pertinent constants are given in Table VI. These equations are sufficiently accurate to be used instead of EQ 15 and EQ 16.

TABLE VI

BEARING EQUATIONS CONSTANTS

		a1	b1	a2	b2	a3	b3	a4	b4	a5	b5	a6	b6	a7	a8
[illegible] Bearing	F_A	20,367	1.61	1,508,000	2.12	1.96	.254	29,600	1.45	8,330	1.36	25,000	.77	700	-0.003
	F_R	156,000	1.5	265,900	1.10	.78	.0013	2,980	1.16	85,900	1.58	453,000	1.05	1.77	.12
90 [illegible] Bearing	F_A	17,500	1.6	618,500	1.96	1.97	.274	28,600	1.50	17,500	1.60	182,000	1.18	1.14	.07
	F_R	125,000	1.5	212,700	1.28	.94	.122	6,120	1.55	60,000	1.59	740,200	1.17	1.65	.11

2.4.4 Bearing Deflection Data

The pertinent bearing deflections are delineated in Table VII as a function of the spin speed.

TABLE VII

Bearings' Deflections as a Function of Spun-Up Speed

PARAMETERS	SPIN SPEED (RPM)							
	20		40		60		80	
BEARING TYPE	110 MM	90 MM	110 MM	90 MM	110 MM	90 MM	110 MM	90 MM
o ANTENNAS INBOARD CASE								
$\bar{\delta}_R$	$<-1\times10^{-9}$	$<-1\times10^{-9}$	$.05\times10^{-3}$	0.5×10^{-3}	$.24\times10^{-3}$	1.3×10^{-3}	15×10^{-3}	9×10^{-3}
$\bar{\delta}_A$	25.1×10^{-3}	27.8×10^{-3}	25.3×10^{-3}	28.3×10^{-3}	25.1×10^{-3}	26.9×10^{-3}	0	13×10^{-3}
$\bar{\gamma}_R$	7×10^{-3}	7.7×10^{-3}	6.7×10^{-3}	6.6×10^{-3}	5.9×10^{-3}	5.1×10^{-3}	5.1×10^{-3}	3.04×10^{-3}
Inch, δ_R	$<-1\times10^{-6}$	$<-1\times10^{-6}$	$<-1\times10^{-6}$	$<-1\times10^{-6}$	-4.8×10^{-6}	25×10^{-6}	-300×10^{-6}	-168×10^{-6}
• ANTENNAS OUTBOARD CASE								
$\bar{\delta}_R$	$<-1\times10^{-9}$	$<-1\times10^{-9}$	4.0×10^{-3}	14.6×10^{-3}	21×10^{-3}	25.8×10^{-3}	31×10^{-3}	37.8×10^{-3}
$\bar{\delta}_A$	27×10^{-8}	28.2×10^{-3}	18×10^{-3}	2×10^{-3}	0	0	0	0
$\bar{\gamma}$	6.65×10^{-3}	6×10^{-3}	5.2×10^{-3}	3.5×10^{-3}	2.7×10^{-2}	2.0×10^{-3}	0	8.9×10^{-3}
Inch, δ_R	$<-1\times10^{-6}$	$<1\times10^{-6}$	-98×10^{-6}	$+274\times10^{-6}$	-420×10^{-6}	$+484\times10^{-6}$	-620×10^{-6}	709×10^{-6}

2.5 Elemental Approachment Calculations

2.5.1 Derivation of Approachment Equation

The dimensional approachment (closure) between the shaft and the elements of the DMA was derived by first considering the radial displacements of the bearings and the shaft. Subsequently, the influences of the shaft and the housing curvatures were superimposed.

Since the bearings and the shaft are in mechanical series, it is apparent (from Figure 27) that the angular deflection of the housing, (with respect

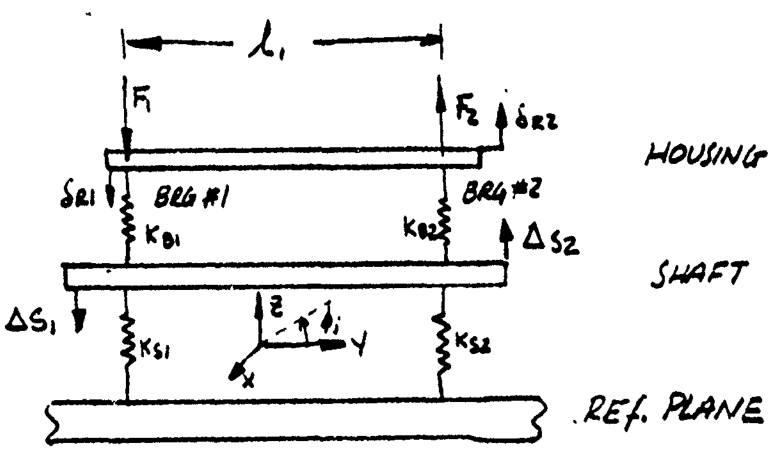

FIG 27 STRUCTURAL SCHEMATIC

to a reference plane) due to forces F_1 and F_2 is a function of the stiffness K_{ij}. For the small angle assumption it can be expressed as

$$\phi_h = [(\delta_{R1}+\Delta S_1)+(\delta_{R2}+\Delta S_2)]\frac{1}{\ell_1} \qquad \text{EQ 21}$$

where, δ_{ij} and Δ_{kj} are the radial displacements of the bearings and the shaft.

Similarily, the angular displacement of the shaft with respect to the reference plane

$$\phi_s = (\Delta_{s1}+\Delta_{s2})\frac{1}{\ell_1} \qquad \text{EQ 22}$$

Hence, the relative displacement of the housing with respect to the shaft becomes

$$\Delta\gamma_h = (\delta_{R1}+\delta_{R2})\frac{1}{\ell_1} \qquad \text{EQ 23}$$

and the housing will rotate about the X axis at a pivot point P_o defined as

$$y = \ell_1[1+\frac{\delta_{R2}+\Delta_{S2}}{\delta_{R1}+\Delta_{S1}}]^{-1} \qquad \text{EQ 24}$$

where:

y = horizontal distance of P_o from the plane of BRG No. 1

Now, let us examine elements mounted to the housing and the shaft (Figure 28). The ordinate R defining the location of a housing-mounted element can be

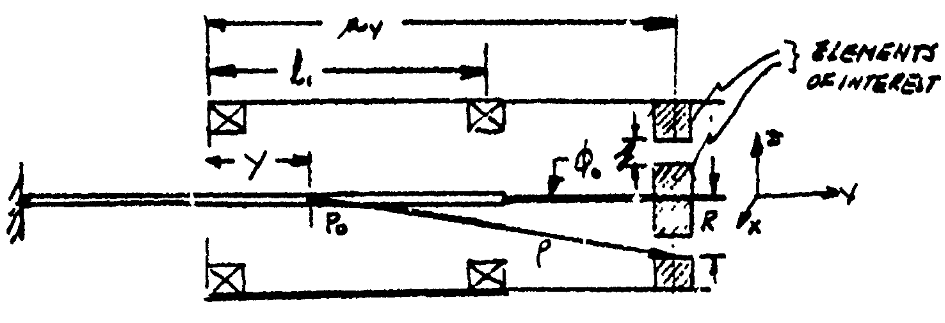

FIG 28 SHAFT & HOUSING MOUNTED ELEMENTS

expressed as

$$R = \rho \sin\phi_0 \qquad \text{EQ 25}$$

and its variation with respect to ϕ_0

$$dR = \rho \cos\phi_0 d\phi_0 \qquad \text{EQ 26}$$

can be taken as an estimate of the approachment of the housing mounted to the shaft-mounted elements. Hence, the approachment (closure of gap "g") can be given by

$$C_k^1 = \rho \cos\phi_0 \Delta\gamma_h = (a_y - y)\Delta\gamma_h \qquad \text{EQ 27}$$

Introducing EQ 23 and EQ 24 yields

$$C_k^1 = \{\frac{a_y}{\ell_1} - [1+\frac{\delta_{R1}+\Delta_{S1}}{\delta_{R2}+\Delta_{S2}}]^{-1}\}(\delta_{R1}+\delta_{R2}) \qquad \text{EQ 28}$$

C_k^1 must be supplemented by the effects of the top bearing loosness and the structural bending of the shaft and the housing. The latter is illustrated on Figure 29. The composite approachment (closure) is given by

$$C_k = \frac{a_y}{\ell_1} C_B + [\frac{a_y}{\ell_1} - (1+\frac{\delta_{R1}+\Delta_{S1}}{\delta_{R2}+\Delta_{S2}})^{-1}](\delta_{R1}+\delta_{R2}) - \ell_1(\gamma_{S2}+\gamma_{h2})(\frac{a_y}{\ell_1} - 1) \qquad \text{EQ 29}$$

Note: EQ 29 requires the use of obsolute values of the variables.

2.5.2 Data and Conclusions

The closures "C_k" of the elements of interest were calculated for various spin-up speeds and are given in Table VIII. Review of the calculated data indicates the following:

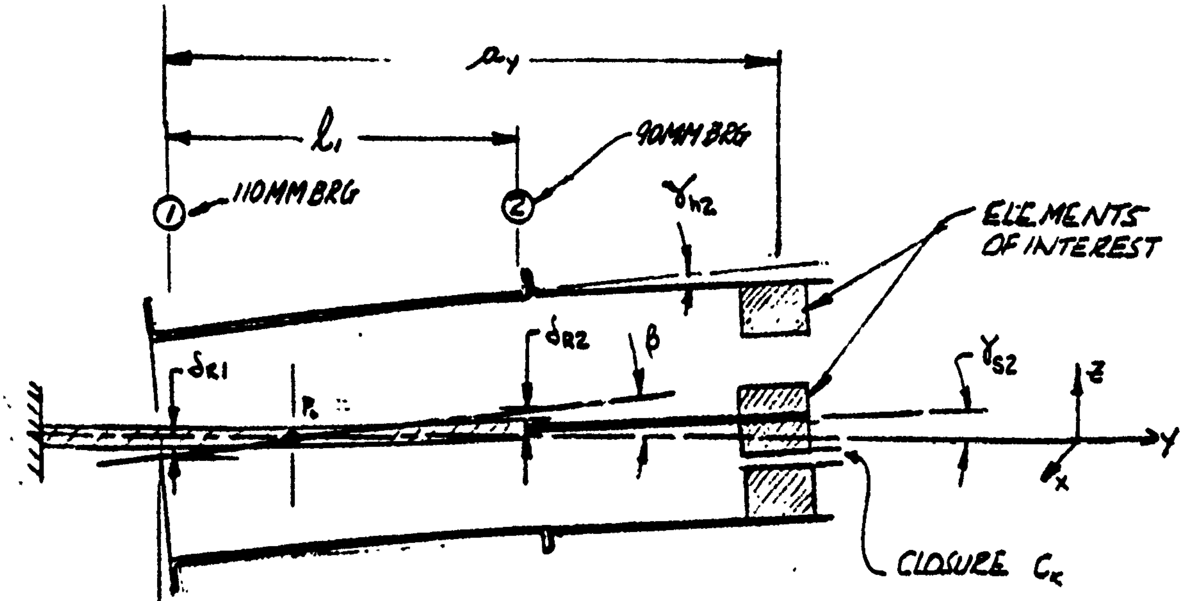

$$Y = \ell_1\left[\frac{1}{1+\frac{\delta_{R2}+\Delta S_2}{\delta_{R1}+\Delta S_1}}\right];$$

δ_{Rj} = BEARING DISP.
ΔS_j = SHAFT DISP
γ_{hj} = STRUCT. (HOUSING) SLOPE
γ_{sj} = STRUCT. (SHAFT) SLOPE
β = INITIAL ANGLE + BEARING EFFECT

FIG. 29 RELATIVE MOTION BETWEEN HOUSING AND SHAFT

TABLE VIII

CLOSURE VALUES FOR VARIOUS DMA ELEMENTS AS A FUNCTION OF SPIN SPEED

Quantity	SPIN SPEED							
	20		40		60		80	
Bearing Type	110 MM	90 MM	110 MM	90 MM	110 MM	90 MM	110 MM	90 MM
• Antenna Inboard Case								
Bearing deflection (inch), δ_{Bj}	0	0	0	0	5×10^{-6}	25×10^{-6}	300×10^{-6}	168×10^{-6}
Shaft deflection (inch), Δ_{Sj}	12×10^{-6}	40×10^{-6}	50×10^{-6}	167×10^{-6}	113×10^{-6}	379×10^{-6}	200×10^{-6}	665×10^{-6}
Housing struct. def. (rad), γ_{hj}	NA	2×10^{-6}	NA	7×10^{-6}	NA	19×10^{-6}	NA	34×10^{-6}
Shaft struct. def. (rad), γ_{Sj}	NA	7×10^{-6}	NA	29×10^{-6}	NA	66×10^{-6}	NA	120×10^{-6}
Center-to-center dis. (inch), a_j	7.0							
Snubber moment arm (inch), A_R	11.1							
Motor moment arm (inch), A_M	9.6							
Labyrinth moment arm (inch), A_L	7.8							
Snubber closure, C_R	1.55×10^{-3} inch		1.44×10^{-3} inch		1.26×10^{-3} inch		1.40×10^{-3} inch	
Motor closure, C_M	1.35×10^{-3} inch		1.28×10^{-3} inch		1.17×10^{-3} inch		1.32×10^{-3} inch	
Labyrinth closure, C_L	1.11×10^{-3} inch		1.09×10^{-3} inch		1.06×10^{-3} inch		1.22×10^{-3} inch	
• Antennas Outboard Case								
Bearing def. (inch), δ_{Bj}	0	0	198×10^{-6}	274×10^{-6}	420×10^{-6}	484×10^{-6}	620×10^{-6}	705×10^{-6}
Shaft def. (inch), Δ_{Sj}	65×10^{-6}	395×10^{-6}	225×10^{-6}	1200×10^{-6}	614×10^{-6}	2700×10^{-6}	915×10^{-6}	4820×10^{-6}
Housing struct. def. (rad), γ_{hj}	NA	8×10^{-6}	NA	32×10^{-6}	NA	75×10^{-6}	NA	130×10^{-6}
Shaft struct. def. (rad), γ_{Sj}	NA	28×10^{-6}	NA	110×10^{-6}	NA	250×10^{-6}	NA	440×10^{-6}
Snubber closure, C_R	1.44×10^{-3} inch		1.39×10^{-3} inch		$.99\times10^{-3}$ inch		$.31\times10^{-3}$ inch	
Motor closure, C_M	1.28×10^{-3} inch		1.28×10^{-3} inch		1.07×10^{-3} inch		$.67\times10^{-3}$ inch	
Labyrinth closure, C_L	1.07×10^{-3} inch		1.16×10^{-3} inch		1.16×10^{-3} inch		1.20×10^{-3} inch	

- The bearing radial deflection effect is more dominant than the structural bending for relatively short distances a_y's to the elements of interest (refer to Figure 29). This is examplified by the labyrinth seal closure C_L. In which case, the closure values appear to increase with the spin up speed and thus the bearing loads. The influence of the structural curvatures are exhibited at higher speeds.

- For larger "a_y" values (examplified by the resolver snubber closure), the effects of the structural curvature slopes appear to dominate the value of the closure "C_R". Notice from Figure 29 that the shaft structural curvature slope is positive and that of the housing is negative. When these are superimposed onto the positive angle "β", [a function of both (1) the elastic bearing deflections δ_{Rj}; and, (2) the rotation of housing due to fit up looseness of the 90 MM bearing], the value of the closure C_R decreases until the shaft's curvature slope (γ_{S2}) becomes greater than β. The latter will occur at loads greater than these considered. Hence, in general the closure C_R will decrease with the increase of the spin speed. Of some interest is the snubber closure characteristic versus spin up speed for the "antenna's inboard" case. Here, at approximately 60 RPM the value of C_R begins to increase whereas for lower speeds it was a decreasing function. The reason for this occurrance is the fast rate of decrease of the bearing's axial deflection which renders more compliant bearing to radial load.

From Figure 29 it appears that relative rotation (about the spin axis) of the housing, with respect to the shaft, will produce no changes in relative positions of the elements of interest in as much as the external forces are fixed to the housing. Hence, unless the shaft's structural hysteresis is assumed, the snubber closure cannot cause any interference when attempting to spin down the housing with respect to the shaft.

TRW
SYSTEMS GROUP

INTEROFFICE CORRESPONDENCE

75-7345.4-040

TO: Y. Wakamiwa

CC: A. H. Rosenberg
P. C. Wheeler

DATE: 31 October 1975

SUBJECT: Angular Velocities of 777 DMA Bearing Suspension Elements

FROM: J. G. Zaremba

BLDG	MAIL STA.	EXT.
82	1367	50993

1. PURPOSE

To provide an aid in correlation of the mean square torque noise versus frequency plots to the particular performance characteristic of the 777 DMA bearing suspension elements, a tabulation of the rotational velocities and frequencies of the pertinent bearing elements was constructed. The latter is attached and is part of this memorandum.

J. G. Zaremba

J. G. Zaremba

SYSTEMS 0180 REV 3-67

TABLE 1

Angular Velocities and/or Frequencies of Bearing Elements Along Rotational Axis of the DMA

PARAMETERS		Bearings 110 MM	Bearings 90 MM
• Inner Races of Shaft			
(1) Angular Velocity, rad/sec	$= \omega_S$	2π	
(2) Frequency (Hz)		1.0	
• Ball			
(1) Velocity (rad/sec)			
$\dfrac{\omega_S[(\cos\alpha+\tan\beta\sin\alpha)\gamma'\cos\beta]^{-1}}{[1+\gamma'\cos\alpha]^{-1}+[1-\gamma'\cos\alpha]^{-1}}$	$= \omega_B$	32.006	28.113
where:			
(a) contact angle (degree)	$= \alpha$	12.740	13.330
(b) ball aspect angle (degree) $\tan^{-1}[\frac{\sin\alpha}{\cos\alpha-\gamma'}]$	$= \beta$	14.098	14.965
(c) $\dfrac{\text{Ball diameter}}{\text{Pitch diameter}}$	$= \gamma'$	.0973	.110
(2) Frequency (Hz)	$= f_B$	5.0939	4.474
(3) Frequency difference (Hz)	$= \Delta f_B$	.619	
• Retainer			
(1) Velocity (rad/sec)			
$\dfrac{\omega_S[1-\gamma'\cos\alpha}{2}$	$= \omega_R$	2.843	2.803
(2) Frequency (Hz)	$= f_R$	.4525	.4462
(3) Frequency difference (Hz)	$= \Delta f_R$	.006	

APPENDIX C

DMA DISASSEMBLY PROCEDURE

TRW
SYSTEMS GROUP

75-DSCS-C5-015
75-7345.11-009

INTEROFFICE CORRESPONDENCE

TO: P. C. Wheeler

CC: L. C. Anderson
J. A. Durschinger
D. E. Kendall
J. G. Zaremba

DATE: 30 October 1975

SUBJECT: Disassembly and Inspection Procedure 777 DMA Life Test Unit.

FROM: A. H. Rosenberg

BLDG	MAIL STA.	EXT.
82	1355	51651

A disassembly and inspection procedure for the 777 DMA life test unit is attached and includes the major step-by-step operations to assure proper control. Deviation from this procedure may occur if unusual observations are made and will be documented.

The documents used for this task are:

1. BBRC P-110,330 - Assembly Procedure for Despin Mechanical Assembly
2. BBRC Drawing 32701 - DMA Assembly
3. TRW DA-032 - Life Test Procedure for 777 DMA

Items 1 and 3 are attached to this IOC.

AHR:bb

A H Rosenberg
A. H. Rosenberg

attachments

DISASSEMBLY & INSPECTION PROCEDURE - 777 DMA LIFE TEST UNIT S/N 3-5

ITEM NUMBER	DESCRIPTION OF OPERATION	APPLICABLE DOCUMENT	REMARKS
1	PERFORM FUNCTIONAL TESTS WITH UNIT IN VACUUM TEST CHAMBER AS FOLLOWS:	TRW DA-032 Para 5.4.9 & 5.4.10	Document Results on Data Sheets
	(a) Measure resistance of all motor windings at ambient temperature.		
	(b) Measure DMA running torque at 20, 40, 60, 80, and 100 RPM using method specified in life test procedure, DA-032, Para.5.4.9 & 5.4.10, using motor/resolver set #1. (NOTE: Calculate torques after Kv measurement.)		
	(c) Measure Kv (BEMF Constant) of Motor #2. Use to calculate K_T (motor torque constant). Measure during 1b at 60 RPM only.		
	(d) Repeat (1a) using motor-resolver set #2		
	(e) Repeat (1b) using motor #1		
	(f) Measure all MPU signals at 40 and 80 RPM	TRW DA-032 Para 5.4.12 & 5.4.13	
2	SLOWLY BACK FLUSH VACUUM CHAMBER WITH DRY NITROGEN. REMOVE BELL JAR. REPEAT FUNCTIONAL TEST OF 1b, 1c, 1d, 1e, and 1f.		Document Results on Data Sheets

ITEM NUMBER	DESCRIPTION OF OPERATION	APPLICABLE DOCUMENT	REMARKS
3	MEASURE RADIAL AND AXIAL DISPLACEMENTS OF HOUSING FLANGE WITH DIAL INDICATOR. REFERENCE TO ALIGNMENT MARK ON FLANGE.		Document Results on Data Sheets
4	MEASURE MPU GAPS FOR MPU'S 1 & 2	BBRC 32701	Document Results on Data Sheets
5	DMA SHALL BE REMOVED FROM VACUUM CHAMBER AND DELIVERED TO M2/1313 FOR DISASSEMBLY. CAUTION: DMA SHALL BE COVERED WITH CLEAN NYLON BAG, FOR TRANSPORTING. DMA MUST BE HANDLED WITH CLEAN, LINT-FREE GLOVES.		
6	DMA DISASSEMBLY SHALL BE CONDUCTED IN A CLASS 100,000 CLEAN AREA PER FED-STD-209. DISASSEMBLED PARTS SHALL BE VISUALLY INSPECTED AND MAINTAINED IN A CLASS 100 BENCH AREA. CLEAN GLOVES SHALL ALWAYS BE USED WHEN HANDLING DMA AND ITS PARTS. ALL PARTS REMOVED SHALL BE STORED IN CLEAN NYLON BAGS AND SEALED WHERE POSSIBLE, AND IDENTIFIED.		

ITEM NUMBER	DESCRIPTION OF OPERATION	APPLICABLE DOCUMENT	REMARKS
6 (cont'd)	ALL LOOSE CONTAMINENTS OBSERVED SHALL BE STORED ON CLEAN FILTER PAPER IN HOLDERS AND IDENTIFIED THE FOLLOWING OPERATIONS ARE THE DISASSEMBLY AND INSPECTION SEQUENCE: NOTE: PHOTOGRAPHS SHALL BE TAKEN AT EACH INSPECTION POINT AND OF ALL QUESTIONABLE OBSERVATIONS		
7	REMOVE BELL PLATE (34451), END BELL (32719), AND CABLE CLAMP (84971).	BBRC 32701 ITEMS 8,12,64, P 110330, Para 5.14	
8	VISUALLY INSPECT BELL END FOR EVIDENCE OF CONTAMINANTS. MEASURE RESOLVER SNUBBER CLEARANCE AND REFERENCE TO ALIGMENT MARK ON SHAFT.	BBRC 32701	Remove sample of any observed contaminant.
9	DISASSEMBLE AND REMOVE SLIP RING ASSEMBLY. NOTE: CABLE BUNDLES J1, J2, AND J3 MUST BE UNLACED AND LOOSENED AT BOTTOM OF SHAFT. UNLACE J7 AND REMOVE MPU'S.	BBRC 32701 P 110330 Para 5.13	Store slip ring for further disassembly

ITEM NUMBER	DESCRIPTION OF OPERATION	APPLICABLE DOCUMENT	REMARKS
10	REMOVE RESOLVER STATORS EXAMINE FOR EVIDENCE OF DEBRIS AND/OR RUBBING. PAY SPECIAL ATTENTION TO SNUBBER PARTS	BERC 32701 P 110330 Para 5.10a & 5.11 a	Document Observations
11	MEASURE MOTOR GAP CLEARANCE. REFERENCE TO ALIGNMENT MARK ON SHAFTS	BBRC 32701	Documents Observations
12	DISASSEMBLE MOTOR HOUSING FROM BERYLLIUM HOUSING INSPECT MOTOR ROTOR FOR DEBRIS AND /OR RUBBING. INSPECT OUTER RING FOR EVIDENCE OF CRACKS OR DEFORMATION. INSPECT RESERVOIR IN HOUSING - DO NOT REMOVE.	BBRC 32701 P 110330 Para 5.9 & 5.7	Document Observations- Store with reservoir up for later inspection.
13	CUT THERMISTOR #1 AND #2 LEADS NEAR J7, REMOVE MOTOR SHAFT HARDWARE. NOTE: WIRE RETAINER (33279) ITEM 31 ON 32701 MUST BE BROKEN TO ALLOW MOTOR CABLE TO BE DRAWN THRU SHAFT. REMOVE MOTOR/ RESOLVER SHAFT.	BBRC 32701	Exercize caution so not to disturb bearings.
14	VISUALLY INSPECT PRELOAD MECHANISM AND TOP BEARING FOR EVIDENCE OF DEBRIS, CONTAMINANTS & LUBRICATION		Document Observations

ITEM NUMBER	DESCRITPION OF OPERATION	APPLICABLE DOCUMENT	REMARKS
15	MEASURE PRELOAD GAP CLEARANCE	P 110330 Para 5.3	Document Results
16	REMOVE PRELOAD MECHANISM. EXAMINE ALL PARTS FOR DEBRIS, CONTAMINANTS AND LUBRICATION. INSPECT FOR VISUAL EVIDENCE OF WASHER ROTATION. INSPECT INNER RACE JOURNAL FOR ROTATION AND AXIAL MOTION.	P 110330 Para 5.3	Document Results
17	SEPARATE SHAFT FROM BEARINGS EXERCIZING CARE NOT TO DISTURB LUBRICATION AND DEBRIS	BBRC 32701 P 110330 para 5.2	
18	INSPECT SHAFT FOR EVIDENCE OF LUBRICATION ON SURFACE AND CONDITION OF BOTH BEARING JOURNALS		Document Results. Store for further inspection and analysis
19	INSPECT HOUSING FOR EVIDENCE OF LUBRICATION. INSPECT BEARINGS FOR EVIDENCE OF DEBRIS, CONTAMINANTS AND LUBRICATION. NOTE: AT THIS POINT THE DECISION WILL BE MADE TO MAKE BEARING MEASUREMENTS PRIOR TO REMOVAL FROM HOUSING.		Document Results. Store for further inspection and analysis

ITEM NUMBER	DESCRIPTION OF OPERATION	APPLICABLE DOCUMENT	REMARKS
20	REMOVE RESERVOIRS FROM BOTH HOUSING AND SHAFTS AND INSPECT.		Document Results. Store for further inspection and analysis.
21	REMOVE BEARINGS FROM HOUSING AND PERFORM A DETAILED INSPECTION AS REQUIRED BY LIFE TEST PLAN. A DETAILED PLAN WILL BE ISSUED PRIOR TO INSPECTION		Document results.
22	SLIP RING ASSEMBLY SHALL BE DISASSEMBLED, EXAMINED AND ANALYSES PERFORMED AS REQUIRED BY LIFE TEST PLAN. THIS WILL FIRST INCLUDE SLIP RING AND BRUSHES, FOLLOWED BY SLIP RING BEARING INSPECTION. A DETAILED PLAN WILL BE ISSUED PRIOR TO INSPECTION.		Document results.

DA-032

REVISIONS

SYM.	AUTHORITY	DESCRIPTION	DATE	APPROVAL

DA-032
777-GX-173
71-7533.1-08

RELEASE DATE		
PREP. BY R. S. Davidson	DATE 5-11-71	
APPROVED		
APPROVED		
APPROVED		
APPROVED		
APPROVED		

Life Test Procedure
for
777 DMA

TRW SYSTEMS
ONE SPACE PARK, REDONDO BEACH, CALIFORNIA

DA-032

SHEETS

TABLE OF CONTENTS

LIFE TEST PROCEDURE FOR
777 DMA

1.0 SCOPE

This procedure establishes the conditions and the minimum test requirements for life testing the Despin Mechanical Assembly (DMA) for the 777 Project.

2.0 APPLICABLE DOCUMENTS

9670 TES006-02 Special Life and Survivability Test Plan

3.0 PERSONNEL

(a) Test Operator

(b) Test Engineer (Optional)

4.0 PREPARATION

4.1 Utilities. No special utilities required.

4.2 Reference Documents. The following documents will be useful as references during the performance of this test:

TRW

EQ2-186	Equipment Specification for Despin Mechanical Assembly, Project 777
EV2-23	Environmental Specification for Electrical and Mechanical Equipment for Program 777
C310380	Despin Mechanical Assembly

BBRC

32701	Despin Assembly, Mechanical

TRW Sketches

DE-015	DMA Slip Ring Test Set Layout
DE-023	Slip Ring Test Set Schematic
DE-031	Complete DMA Test Set Schematic
---(No number)	DEA Portable Interface Test Set

TRW Sketches, continued

SK-HD-501	Despin Drive Subassembly - DDS Power Control
SK-HD-502	Drive Subassembly - Power Amp. Bd. Schematic
SK-HD-503	Drive Subassembly - Mod/Demod Bd. Schematic
SK-HD-504	Current Limiter Board, Despin Drive Subassembly

4.3 Test Equipment

4.3.1 Vacuum Pumping Gear. This equipment is used to establish, maintain, and monitor the vacuum which simulates the space environment. Calibration is not required except by request of responsible test engineer.

Equipment	Manufacturer	
Roughing System	Ultek	CFR
Cold Cathode Discharge Gauge	Hughes	PG-7E (tube) PGC-301 (control)
Vacuum Pumping System	Ultek	CN-985
Ion Pump Control	Ultek	222-0600
Boostivac Control	Ultek	224-0540

4.3.2 Special Test Circuitry. This equipment is special, having been developed as part of the overall test setup. Calibration is not required and no substitutes are allowed.

a) DMA Life Test Console

b) Temperature Sensor Bridge

c) Slip Ring Switching Panel

Note: Schematics for all these circuits are given on the the drawings listed in paragraph 4.2.

4.3.3 Measuring Equipment. This equipment, or equivalent as determined by test engineer, will be used to measure test parameters. All units should carry a current calibration sticker.

Equipment	Manufacturer	Model
Digital Integrating Voltmeter	Hewlett Packard	2401C
Digital Voltmeter	Hewlett Packard	3440A
Digital Voltmeter DC Multifunction Plug-in	Hewlett Packard	3444A
Digital Voltmeter Hi Gain Autorange Plug-in	Hewlett Packard	3443A
Electronic Counter	Hewlett Packard	5245L
Oscilloscope	Tektronix	RM 503
Resistance Meter	Hathaway	C6B
Current Probe	Tektronix	P6042
Differential Plug-in	Tektronix	2A63

4.3.4 Power Supplies. These supplies, or equivalent as determined by the responsible test engineer, provide power for the test circuitry. They are not used for measuring parameters and calibration is not required.

Equipment	Manufacturer	Model
Dual DC Power Supply	Hewlett Packard	6255A
DC Power Supply	Hewlett Packard	6284A
DC Power Supply	Harrison Labs	6271A
DC Power Supply	Harrison Labs	8103

4.4 Communications. None required.

4.5 Special Hazards.

4.5.1 Glass Vacuum Chambers. When evacuated, these glass chambers are subject to implosion, especially if they should sustain any sort of impact. The chambers should always be covered with a metal cage to protect them from impacts and to protect personnel in the area from flying glass should an implosion occur.

4.5.2 High Voltage. The ion pump control delivers more than 4000 volts DC at one amp to the pump. This cable should never be handled with the power on and should be routed through a protected area when in use.

4.6 Test Conditions

4.6.1 Mechanical. The DMA will be tested as a complete, unmodified unit. The only operations performed on the unit for the test are the attachment of two temperature sensors external to the case and the removal of some electrical cable clamps to allow routing of the cables through the heat exchanger.

4.6.2 Electrical. All electrical connections are made in special adapters and separate jumpered connectors. No modifications are made to the DMA wiring itself.

4.6.3 Installation Setup. The DMA is mounted with its spin axis vertical. The four mounting feet are down and attached to the heat exchanger.

4.6.4 Environmental. The unit shall be tested in a vacuum chamber at 10^{-6} Torr or lower. The heat exchanger plate shall be maintained at 50°F during the cold cycle and 110°F during the hot cycle.

4.7 Data Sheets. Review section 6.0, pull all data sheets needing reproduction, and print up all extra copies necessary before starting tests.

5.0 PROCEDURE

5.1 Procedure Performance

5.1.1 Test Sequence. The DMA shall be operated continuously for 36 months at a speed of 60 ±10 rpm.

During the first three months, the heat exchanger plate shall be maintained at the cold temperature (50°F); then it shall be raised to the high temperature (110°F) for three months. This three months cold and three months hot cycle shall continue throughout the test.

At the end of the first, second, and third year, the power shall be temporarily switched to the secondary motor and resolver to determine if they are still operational. Record their voltage and current on the appropriate data sheets with some identifying notation.

5.1.2 Test Parameters. The following measurements shall be taken once a month for the first year and once every three months during the remaining two years.

1) Vacuum Chamber Pressure
2) Rotational Speed
3) Resolver Voltage
4) Resolver Current
5) Temperature (5 places)
6) Slip Ring Noise
7) Slip Ring Contact Resistance
8) Motor Voltage
9) Motor Current
10) Motor Torque
11) Magnetic Pick-up Amplitude (6 pick-ups)
12) Magnetic Pick-up Slope (6 pick-ups)

The following tests, in addition to those listed above, shall be conducted at the termination of the life cycle test:

a) Functional test
b) Overall visual examination
c) Microscopic and metallographic examination for brush and slip ring wear. Determine the individual wear rates of the rings - metallographic sectioning of the rings. will be performed at the end of the life test. Brushes will also be inspected for significant wear and examined under magnifications of at least 50 times.
d) Lubricant reservoir weight
e) Analyses of slip ring and bearing wear debris (amount, type, size, and placement)
f) Determine individual wear rates of the rings and brushes.
g) Brush contact pressure.
h) Radiometric analysis of bearing wear debris.
i) Detailed microscopic examination of the bearing assemblies including balls, retainers, and raceways.
j) Profilometer trace of the rings and brushes.

k). Rundown time at a minimum frequency of one each data gathering period.

l) Hardness test of 4 slip rings.

5.1.3 Data Recording. All data shall be recorded in Section 6. Results of the special tests conducted at the termination of the life cycle will be covered in the final test report. No data sheets for these tests are included in this procedure.

5.2 Special Precaution. Test operators shall be alert to data trends indicating degradation which could lead to imminent failure. In such cases, the responsible Subproject Manager or Program Office representative shall be notified and consideration shall be given to interrupting the test in order to evaluate this condition.

5.3 Criteria for Failure. Failure is defined as inability of the motor to drive the DMA at rated speed with nominal voltage (28 volts DC on the bus) applied. Other than this, the unit is to be opened and inspected prior to the end of the specified life cycle only in the event of some other significant anomoly in this test, or in the event of need for analysis resulting from failure of a DMA on-orbit.

5.4 Test Data Acquisition.

5.4.1 Vacuum Chamber Pressure. The test chamber pressure is determined by reading the ion pump current at the pump controller and converting to pressure by using curves supplied by the ion pump manufacturers. This pressure can also be measured directly using the cold cathode discharge gauge.

5.4.2 Rotational Speed. Use any one of the six (6) MPU's. The MPU puts out one pulse per revolution. Determine the period per revolution by measuring the time in milliseconds between successive pulses with an electronic counter. Calculate the speed in rpm as follows:

$$\text{rpm} = \frac{60{,}000}{\text{milliseconds}}$$

5.4.3 Resolver Voltage. Using an oscilloscope with a differential plugin, measure the peak-to-peak voltage across the terminal labeled "Resolver Excitation" on the DEA Portable Test Set Panel. Connect both the high and low test points to an amplifier input. Do not ground either one.

5.4.4 Resolver Current. Using the oscilloscope with the auxiliary current probe, clamp the probe around one of the resolver excitation wires in the wire bundle connected from the test kit to the vacuum chamber, and measure peak-to-peak amperes.

5.4.5 Temperature at the DMA Internal Thermistors. Using a digital voltmeter, measure the voltage at the test points on the "DMA Life Test Panel" labeled "DMA Temperature #1 and #2." Convert the voltage to temperature through use of Figure 1.

5.4.6 DMA Temperature at External Sensors. Using the DE-014 Test Set and the accessory cable, measure the bridge output voltage. Convert to degrees F. by using Figure 2.

5.4.7 Slip Ring Noise. Using the DE-023 Slip Ring Test Set and an oscilloscope, measure the peak-to-peak noise per series pair of slip rings in millivolts. Apply 10 milliamps to the signal rings and 2.0 amperes to the power rings to make these measurements.

5.4.8 Slip Ring Contact Resistance. For this test, apply 10 ma to the signal rings and 2.0A to the power rings and use an oscilloscope and the DE-023 test set as in the Noise Test. Before making the measurement, ground the scope input and zero the trace. Apply the scope to each two slip ring series circuit under test and measure the voltage from zero to the center of the noise band. Convert this voltage to ohms using the appropriate current as specified above.

5.4.9 Motor Voltage. Using an oscilloscope with a differential plugin, measure the peak-to-peak voltage across the terminals labeled "Motor ϕA" and "Motor ϕB" on the DEA Portable Test Set panel. Connect both the high and low test points to an amplifier input. Do not ground either one.

5.4.10 Motor Current. Using the oscilloscope with the auxiliary current probe, clamp the probe around the ϕA Current Probe Loop on the face of the DMA Life Test Panel and measure peak-to-peak amperes. Repeat for ϕB.

5.4.11 Motor Torque. Motor torque is computed from motor current in the following manner:

$$I_{pk} = \frac{I_{p-p}}{2}$$

$$\text{Torque} = I_{pk} \times K_t$$

For both motor #1 and #2,

$$K_t = 112.6 \text{ oz-in/amp}$$

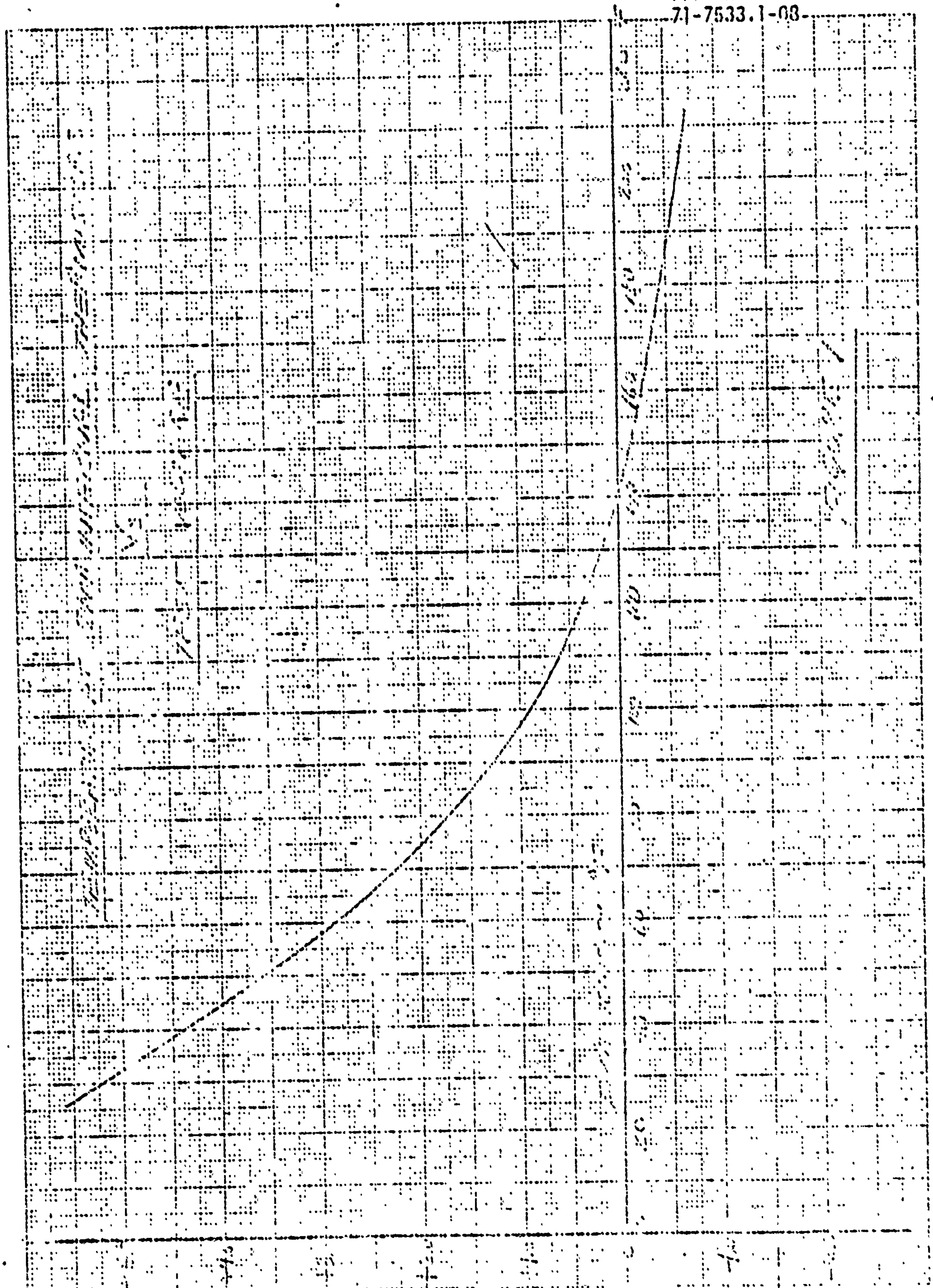

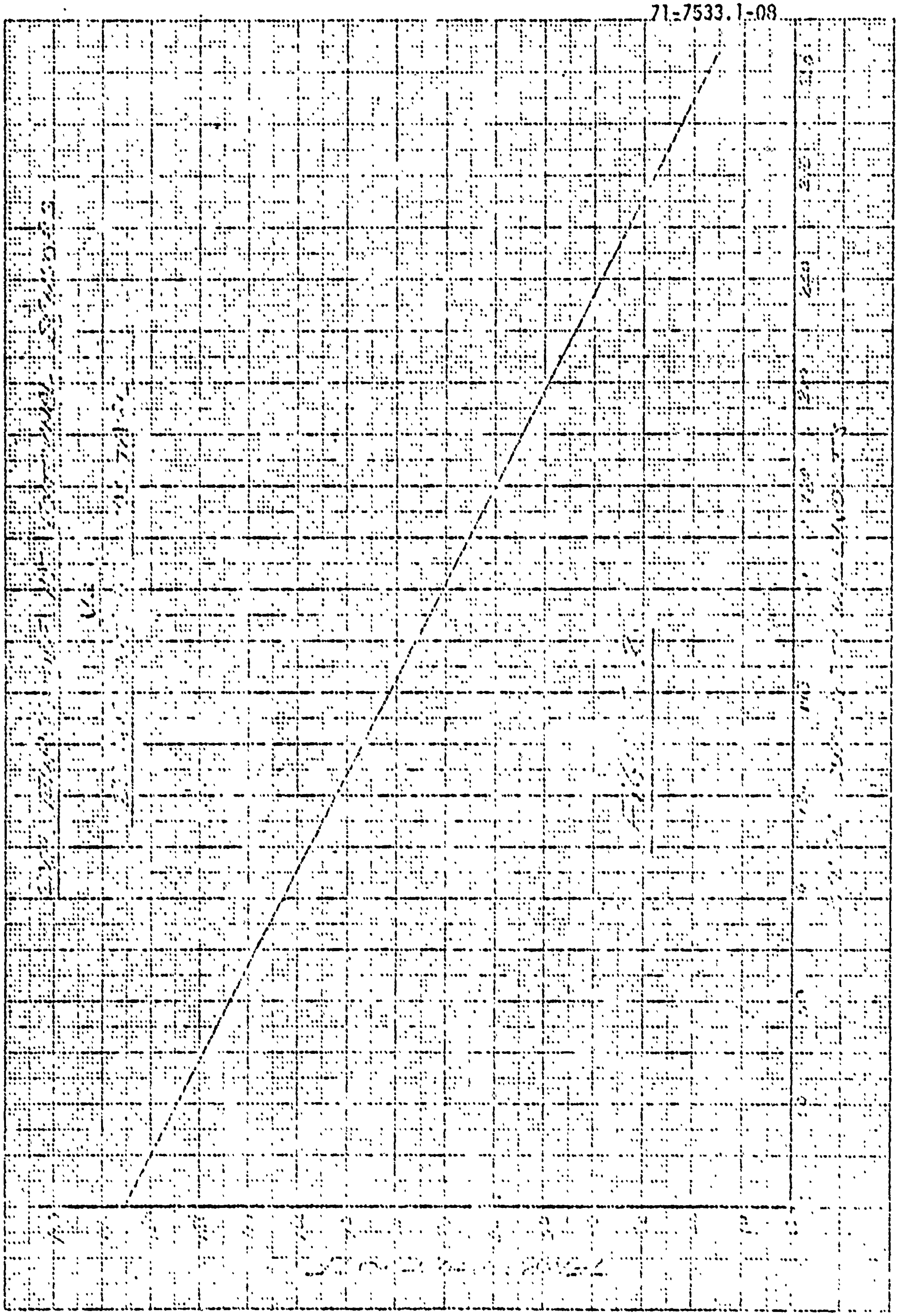

5.4.12 MPU Amplitude. Using an oscilloscope, display the output of the "Magnetic Pickoff Test Points" on the DMA Life Test Panel. Measure the amplitude "A" (see Figure 3) in volts for all six MPU's.

5.4.13 MPU Slope. Using the same oscilloscope display as in 5.4.12, measure the average slope of the trace section between +A/2 and -A/2 (see Figure 3) in volts per millisecond.

$$\text{Slope} = \frac{A}{X}$$

5.5 Breakdown Procedure. If, for any reason, it is necessary to interrupt the test and break the vacuum, the following procedure shall be used.

1) Shut off the ion pump and backfill the chamber with dry nitrogen gas.

2) Keep a positive pressure in the chamber by maintaining a continuous flow of nitrogen throughout the rework activity.

3) If the specimen must be removed, it shall be bagged or otherwise maintained in an atmosphere of dry nitrogen gas until being re-evacuated.

4) If the vacuum system itself requires rework, it shall be pumped down and re-backfilled with dry nitrogen before reinstalling the specimen. A positive pressure of dry gas shall be maintained by continuous flow during re-insertion of the test module.

MIPU OUTPUT TRACE

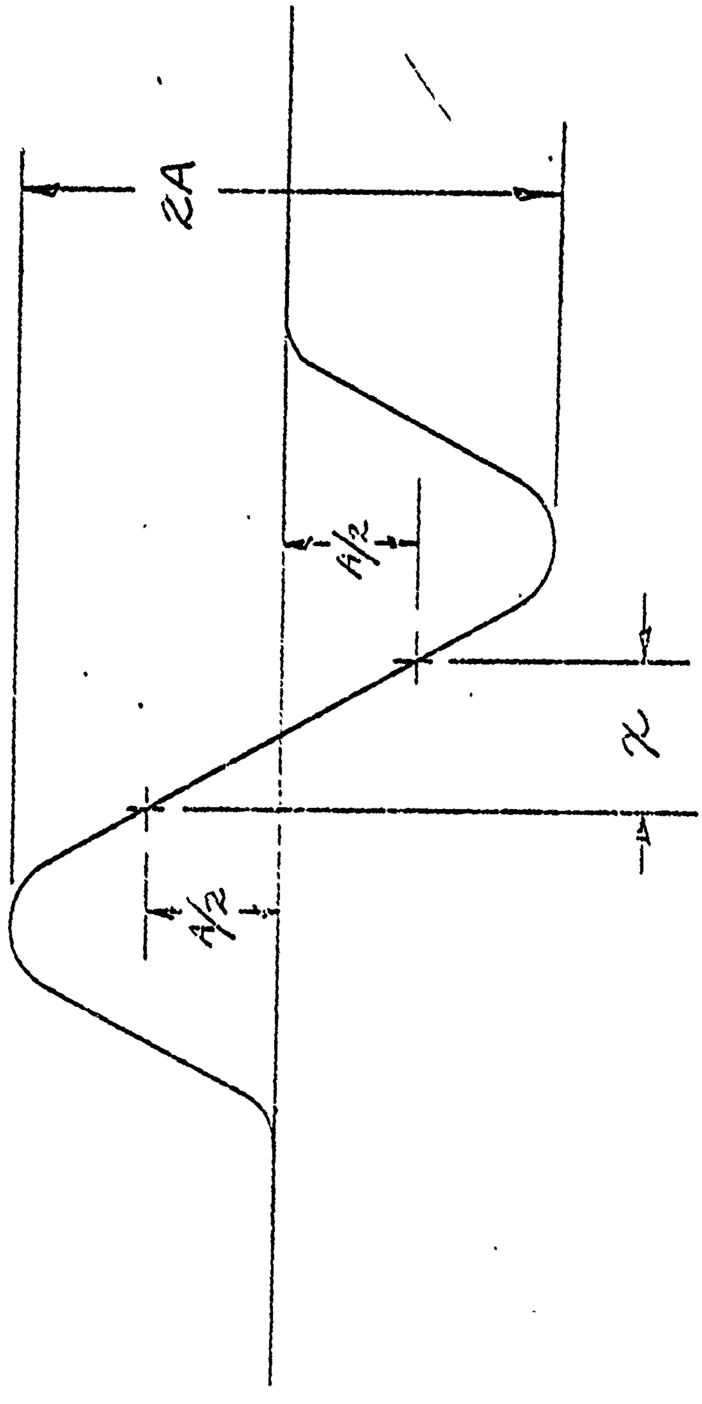

FIGURE 3

RELEASES	DATE
DEVELOPMENT	3-24-70
BASIC	3-24-70
REVISIONS	DATE

A	6-9-70	Para. 5.11 (b) (1), (2) $ (3) Motor Resolver Alignment were clarified.	M.R. Maxwell
B	7-9-70	All Connector operations were modified, and Production Document P-110348 added to page (2) to implement TRW Potting Process.	M.R. Maxwell
C	8-20-70	Changed Para. 5.12 (a) (b), Para. 5.13 (h) (k), and Para. 5.18 to reflect Revision J of 32701.	M.R. Maxwell

AUG 13 1975

PREPARED BY M. Maxwell 3-24-70	PRODUCTION PROCESS TITLE ASSEMBLY PROCEDURE FOR DESPIN MECHANICAL ASSEMBLY 32701-1 DS12A	BALL BROTHERS RESEARCH CORPORATION BBRC BOULDER, COLORADO
PRODUCTION SHOP - CHECKED		CONTRACT NUMBER 3092
PRODUCTION - APPROVED 3-24-70	CODE IDENT. NUMBER 13993 C-24	PROCESS NUMBER P- 110,330
	DWG. SIZE A	SHEET 1 OF 23

1.0 SCOPE

This procedure defines the sequence of operations and the methods required for Mechanical Assembly of the basic TRW Despin Drive Mechanism 32701-1. The sequence of operations as noted is suggested and may be altered as conditions dictate. The applicable engineering drawings take preference in event of conflict.

2.0 DRAWINGS AND DOCUMENTS

2.1 Applicable Engineering Drawings and Documents

Document	Title
22772	Handling Procedure for Vac Kote Parts
25030	Shop Standards
32701	Despin Assembly Mechanical
32717	Slip Ring and Tube Assembly
32725	Wiring Diagram
35326	Qual. Test Specification and Procedure
36469	Acceptance Test Procedure, Despin Mechanical Assembly - TRW
P110348	Wire Preparation and Potting of Connectors TRW DMA

2.2 Standard Documents

Document	Title
BPS 1.01	Installation Torque for Threaded Fasteners
BPS 1.07	Crimping Connector Contacts
BPS 2.31	Shielded Wire Connections, Soldered Assembly of
BPS 2.45	Electrical Connections, Soldered Assembly of
BPS 4.01	Cable Straps and Cable Clamps, Installation of

2.2 Continued

Document	Title
BPS 9.26	Bonding Wire Bundles and Electrical Components
BPS 9.31	Bonding Procedure - Epoxy Low Thermal Expansion
BPS 9.55	Potting Encapsulating, or Sealing Silicone, Space Grade
BPS 13.12	Lubrication Treatment (Proprietary)
BPS 16.15	Stainless Steel Passivation
BPS 16.32	Primer Zinc Chromate
BPS 19.01	Packaging and Sealing
BPS 21.00	Cleaning Tools for Use on Clean Parts
MS 33540	Safety Wire, General Practices for

3.0 MATERIAL

Alcohol

Xylene

Freon

Pylox Gloves

Assembly (BMS 15.10 Proprietary)

4.0 REQUIREMENTS

4.1 CAUTION: Extreme care should be exercised when handling beryllium shaft and housing. Because of brittleness associated with beryllium, sudden shocks and bumps, as well as dings, nicks, and scratches, should be avoided. Protective flange rings called out in preceeding assembly paragraphs should be used at all times.

(d) With Bearing 32708-3 in position, reverse Housing 32713-1 end and install Bearing 32708-1 by the same procedure, using tool T100547-3C.

CAUTION: Do not gall sides of Housing.

(e) Install Reservoir, Lubricated 33281-1 to Housing 32713-1 and secure in place with (8) NAS 1352C04-LL10 screws and NAS 620C4 washers; torque per Note 2.

5.1 Shaft Subassembly

(a) Install protective Flange Ring T100547-5C to the base of Shaft 32713-1 with 1/4 inch diameter screws and bolts.

NOTE* check continuity of each Thermistor Assembly before and after potting.

(b) Install (2) Thermistors 32721-1 in Shaft 32712-1 per Section J-J and N-N per Despin Drive Assembly 32701-1, Sh. #2.

(1) Prepare surfaces to be bonded per BPS 9.26, Para. 3.2.1.

(2) Referring to Figure 3, spread a thin layer of epoxy BPS 9.26 over inside surface of Shaft, aft end, 45° radially located per Section J-J of 32701-1 Sh. #2.

(3) Carefully position Thermistor 32721-1 on epoxy area and press into bond.

(4) Encapsulate Thermistor with epoxy resin, using teflon mold keeping Thermistor and cable approximately parallel to angle of Shaft.

(5) Support 37.0 inch long cable so it will not dead weight Thermistor in epoxy and route through Retainer Wire 33279-1 per Despin Drive Assembly 32701-1. Cure epoxy overnight.

(6) Referring to Figure 4, spread a layer of BPS 9.26 epoxy over the forward or bell-shaped end of Shaft.

(7) Carefully position Thermistor 32731-1 on epoxy area and press into bond per Figure 4.

(8) Encapsulate Thermistor with epoxy resin, using teflon mold and support 37.0 inch long cable during overnight cure.

(c) Wipe internal surfaces of Shaft 32712-1 with Solution No. 4 per BPS 13.12. Install Retainer 33279-1 to Shaft 32713-1 and secure in place with (4) NAS 1081C04D6L screws. Set screws shall be flush with exterior surface of Shaft; torque per Note 2. Bond per BPS 9.26.

(d) Install Reservoir, Lubricated 33280-1 to Shaft 32712-1 and secure in place with (8) NAS 1352C04LL6 screws and NAS 620C4 washers; torque per Note 2.

(e) Install Reservoir, Lubricated 32707-1 to Shaft 32712-1 and secure in place with (8) SP0060-04-6 screws; torque per Note 2.

5.2 Assembly of Shaft 32712-1 and Housing 32713-1

(a) Remove tool T100547-2C, tool T100547-1C, and position Housing 32713-1 in a vertical position on tool T100547-6C (large diameter facing up).

NOTE: Housing may be heated to 60°C + 10° to facilitate installation.

(b) Carefully position Shaft into Housing and lower until 4.3301-4.3304 diameter of shaft contacts surface of Bearings 32708-1 and 32708-3. Align position of Shaft with Bearings. Place tool T100547-7C on large diameter of Shaft and with uniform pressure position Bearings to shoulder stop.

CAUTION: Do not gall Shaft.

(c) After assembly of Shaft 32712-1 and Housing 32713-1, re-install T100547-5C to the base of Shaft 32712-1 with 1/4 inch diameter screws and nuts, and T100547-2C to small flange of Housing 32713-1 with 1/8 inch diameter screws and nuts.

5.3 Assembly of Retainer, Assembly Spring 32705-1 to Shaft 32712-1, Reference Figure 1.

(a) Mask aft flange of 7.688 inch diameter of Housing 32713-1 with amber teflon tape to prevent marking surface when installing 1/4 inch diameter bolts. Bolt Shaft 32712-1 to Base plate of Housing Assembly D.M.A. Vibration Fixture 33990, using the (8) 1/4-20 by 3/4 inch long bolts and nuts through the .252-.255 inch diameter holes of Shaft; torque per Note 2.

(b) Lube threads on Shaft with #23560 grease prior to assembly. Assemble .1147 inch thick test washer T100583 and Retainer Assembly Spring 32705-1 carefully to threaded end of Shaft 32712-1 and hand tighten in place. Torque with spanner wrench tool T100539 to 28-33 ft.-lbs.

(c) Measure gap between test washer T100583 and Retainer Assembly Spring 32705-1. Add this amount to.1147 thick test washer and subtract .0025. This is the dimension that Washer 32711-1 must be finished to. Washer must be flat and parallel within .0002, and it is to be passivated after machining per BPS 16.15.

(d) Remove Retainer Assembly 32705-1 from Shaft 32712-1, remove test washer T100583, and carefully slip machined Washer 32711-1 over threaded Shaft. Re-install Retainer Assembly 32705-1 and torque to 28-33 ft.-lbs. with tool T100539. Check gap for .002-.003 inches loose. Safety Wire per MS 33540.

(e) Remove unit from base of Housing Assembly D. M. A. Vibration Fixture 33990 and remove amber teflon tape from Flange.

(f) Replace T100547-5C with 1/4 inch diameter screws and nuts, and T100547-2C with 1/8 inch diameter screws and nuts to protect Flanges.

5.4 Measure the insulation resistance between the unit Housing and Shaft at 5 volts D. C. The resistance must be greater than 10K ohms.

5.5 Installation of Actuators 32733-1, Magnetic Pickups 32731-1, and 35574-1.

(a) Install (2) Actuator Brackets 32734-1 to flange of Housing 32713-1 with (2) NAS 1352C04LL4 screws and AN960C4 washers (2 Places). Hand tighten screws.

(b) Install (2) Actuators 32733-1 to Brackets 32734-1 with (2) NAS 1291C04 nuts, An 960C4 washers, and NAS 1352C04-6 screws (2 places). Hand tighten only as Actuators have to be shimmed .004-.006 inches clearance with 35927-1 shim at alignment with Magnetic Pickups.

(c) Lube 32731-1 Magnetic Pickups with #23560 grease and install in (4) .402-.404 inch diameter holes provided in flange of Shaft 32712-1 and install (4) 35668-1 nuts and S712-102-16 washers. Shim as required using 36166-1, -3 and -5, to achieve .004-.006 clearance with actuator. Use assembly aid 3092-1 to hold the Magnetic Pickups during this operation. Torque nuts 45-50 in-lbs maximum.

(d) Lube 35574-1 Magnetic Pickups with #23560 grease and install in (2) .505-.510 inch diameter holes provided in flange of Shaft 32712-1 and install (2) 35667-1 nuts and 35641-1 washers. Shim as required using B3-14, B3-12, and B3-11 shims, to achieve .004-.006 clearance with actuator, Use assembly aid 3092-2 to hold the Magnetic Pickups during this operation. Torque nuts 45-50 in-lbs maximum.

(e) Rotate Shaft 32712-1 360° and adjust Actuators 32733-1 per item (b) above. After final alignment per TP-36469, epoxy Actuators to Actuator Bracket and Actuator Bracket to (be) Shaft per BPS 9.31.

5.6 Referring to Despin Assembly Mechanical 32701-1, prepare Shaft Motor Resolver Assembly

WARNING: Do not under any circumstances remove Motor from Stator without keeper in place during assembly.

(a) Prior to installation, Motor 32720-1 shall be cleaned to remove any trace of mold, release agents, finger prints, and other soluable residues with the following solvents in the following order. Either a rinse as from a pressure can, or a dip will be satisfactory. If a rinse is used, the solvents must run copiously from the motor to remove any particulate solids.

(1) Chlorothene Nu

(p) Install Retainer, Resolver 32727-1 into slot of Shaft 32726-1 and against Key, Resolver 32724-1.

(q) Lube Motor Shaft threads with no. (23560) grease. Install nut, Resolver 32730-1 to threaded end of Shaft and hold Retainer 32727-1 in place while torque is applied to Resolver Nut with 3092-4 assembly aid and torque 18 to 23 ft-lbs, using tool T100561. Safety wire nut to Motor Shaft 32726-1 per MS 33540.

CAUTION: Keep Resolver Guard, assembly aid 3092-4, over Resolvers at all times to protect Resolver wiring from damage.

(r) Install (2) SP0009-5-4 plus (1) SP0009-5-5 clamps with (3) NAS 1352C04LL4 screws and AN960C4 washers. Use (1) 1021CC lug under each clamp at horizontal position and (2) 1021CC lugs under clamp at vertical position. Gap between motor and screw shall be .031 min, use washers as required. Ref. view E-E of 32701-1 Sh. # 1.

(s) Route (2) 20 AWG bundles through oblong window cutout of shaft through SP009-5-4 clamp and out top oblong window. One group of motor bundles goes inside and out the top and the other goes inside the top and out the bottom. Ref. Section L-L of 32701-1 Sh. # 2.

(t) Route (3) 28 AWG bundles from resolver 32735-1 through each 5609-21 washer at vertical location per section L-L of 32701-1 Sh. #2. Flare each cable shield approximately as shown over washer. Ref. view H or 32701-1, Sh. #2.

(u) Deglaze outer surface of 5609-21 washers (2 places) and pot flared cable, and cables per BPS 9.26. Ref. view H of 32701-1 Sh. # 2.

(v) Ground resolver bundles (6) places between resolver and 1021 CC lug, per Section L-L and view H or 32701-1 Sh. # 2. Install SP0057-14 tubing over ground and resolver bundles. Lace bundles per BPS 4.01.

(w) Route bundles through SP0009-5-4 clamp per Section L-L of 32701-1 Sh. # 2.

(x) Ground motor cables (4) plases between motors and 1021 CC lugs per Section L-L and view G of 32701-1 Sh. #2. Install SP0057-8,-14, -20 tubing over ground and motor cables.

(y) Lace motor and resolver cables per BPS 4.01 and install SP0057-8 tubing 1.43 inches from 32726-1 shaft. Ref. main view and view P of 32701-1 Sh. # 2. Pay particular attention to dress wires for minimum height to clear bellows of torque tube.

5.7 Refer to Despin Assembly Mechanical 32701-1, Sh. # 1 for Assembly of Housing 32728-1. Remove T100547-2C.

(a) Install Reservoir, Lubricated 32716-1 into groove of Housing 32728-1.

(b) Install (4) Guide Pins T100584 into (4) tapped holes of Housing 32728-1.

NOTE; Housing 32728-1 may be heated to +60°C maximum and Stator cooled to -20°C minimum to facilitate installation.

(c) Carefully remove (4) outer screws through Stator. Place Stator over already installed Guide Pins, and carefully lower into position.

CAUTION: Do not let keeper move from Stator.

(d) Place tool T100547-8C over Stator and Mounting Ring and slowly press into position with arbor press.

(e) After Stator 32720-1 is seated into position with 5.4965-5.4980 diameter, remove (4) Guide Pins and install (4) NAS 1352C04-12 screws and NAS 620C4 washers; torque per Note 2.

5.8 Assembly of Shaft Assembly Section C-C of 32701-1, Sh. #1 to Shaft 32712-1

(a) Route thermistor, resolver, and motor wires along I.D. of 32712-1 Shaft per main view of 32701-1 Sh. #2. Clamp cables from motor # 2 and resolver # 2 and cables from motor #1, resolver # 1, and thermistor # 2 with (2) SP0009-5-5 clamps, NAS 1352C04LL4 screws, and AN 960C4 washers per BPS 4.01. Ref. Section A-A of 32701-1, Sh. #1 and Sections M-M and K-K of 32701-1 Sh. # 2.

(b) Attach Shaft Assembly Section C-C to Shaft 32712-1 using (3) NAS 1352C04-10 screws, NAS 620C4 washers, and NAS 1291C04 nuts. Attach (1) 1021 CC lug opposite thermistor location as a ground for thermistor. Using (1) NAS 1352C04-10 screw, NAS 1291C04 nut, and NAS 620C4 washer; torque per Note 2.

5.9 Assembly of Housing, Motor Resolver 32728-1 to Housing 32713-1

(a) Attach T100817 over windings of 32735-1 resolver and hold in place with clamp. This will prevent keeper from touching windings of resolver. Remove T100817 and hose clamp after keeper has been removed.

(b) Carefully remove (4) inner screws that hold keeper mounting ring. Do not touch windings of resolver during removal of keeper mounting ring.

CAUTION: Keeper must not be removed from Stator, until Stator is in place. The Resolver Guard 3092-5 should be installed over the resolvers for protection during assembly.

(c) Gently align Housing, Motor Resolver 32728-1 over Motor Rotor 32720-1 and push in place, removing keeper from field by pushing out as Stator and Housing, Motor Resolver are installed.

CAUTION: Length of Stator exposed outside of keeper to be .040 maximum when inserting Rotor into Stator. Keeper to be flush with face of Motor within .010. Failure to comply will result in permanent damage to Stator Magnets.

(d) Attach Housing, Motor Resolver 3272801 to Housing 32713-1 with (16) NAS 1352C04-8 screws and NAS 620C4 washers, and NAS 1291C04 nuts; torque per Note 2.

5.10 Assembly of Resolver Stator 32735-1 to Bracket Assembly 33277-1.

(a) Attach (2) Resolver Stators to Bracket Assembly 33277-1 using (4) NAS 1352C04-6 screws and NAS 620C4 washers, each plate.

5.11 Attachment of Resolver Stators 32735-1 and Bracket Assembly 33277-1 to Housing, Motor Resolver, including Motor Resolver Alignment and D.M.A. Preliminary Test

(a) Install Resolver Stators 32735-1 and Bracket Assembly 33277-1 to Housing, Motor Resolver 32728-1 with (2) NAS 1352C04-8 screws, NAS 620C4 washers, and NAS 1921C04 nuts, 180° apart. This is a temporary attachment until Motor Resolver Alignment is complete. After alignment test, install (16) NAS 1352C04-8 screws, NAS 620C4 washers, and NAS 1291C04 nuts; torque per BPS 1.01.

(b) Motor Resolver Alignment

(1) Set up the circuit as shown in Figure 5. The D.M.A. shall be mounted on the 33990 base using (4) 1/4 in. bolts, one through each shaft foot. Attach leads to the applicable binding post of the D.M.A. Breakout Box T100607. Refer to Drawing 32725 for proper D.M.A. lead identification.

(2) Position the select switches on the test console to Motor and Resolver # 1 and turn the Motor Drive switch to ON. Slowly turn the speed control CW and observe the D.M.A. for movement. Rotation in the CW direction (viewed from above) is required. Rotate the Stator of Resolver #1 until smooth operating in a CW direction is obtained. Observe the D.M.A. motor current and set the Resolver position for a minimum reading. Switch the D.M.A. test console to run Motor and Resolver # 2 and position the Stator of that Resolver to obtain smooth CW rotation of the D.M.A. with a minimum motor current. The position of Resolver # 1 Stator must not be changed while aligning # 2 so it may be necessary to work back and forth between resolvers to achieve alignment of both.

(3) Set the console to Drive Motor and Resolver # 1, then attach the dual channel scope per Figure 5. Open the Sin windings of Motor # 1 by positioning the switch on the Breakout Box to the open position. Adjust the motor for approximately 60 r.p.m. using the speed control and adjust the gain of that scope channel to get a full sin wave. Check the signal on the other scope channel as the D.M.A. is rotating less than 60 rpm. An aligned condition of the Motor-Resolver is indicated by an in-phase condition of the signals on both channels. The Resolver Stator may need to be rotated slightly to obtain good alignment.

(4) Set up to drive MTR/RES #2 and repeat the previous step to align the Resolver to the Motor. When both Resolvers are aligned, mark the rotational position of the Bracket Assembly and the Housing using mylar tape over the edges. Remove the Bracket Assembly and torque eight (8) NAS 1352C04LL6 screws per Note 2. Mark the position of each Resolver Stator with Warnowink per Note 33 of 32701. Reassemble the Bracket Assembly in the proper position using the tape to locate the parts.

(5) Recheck alignment of both resolver stators using the Sanborn recorder as in steps 3 and 4 and secure with 2 screws and nuts. Mark the Bracket Assembly and Housing with Warnowink per Note 33 of 32701

(c) D.M.A. Preliminary Tests

(1) Motor Checks

-a Leads must be temporarily connected to the Breakout Box per 32725.

-b Continuity check Motor, Resolver, MPU and Thermistor Circuits using para. 4.2.2.1 of 35326 as a guide.

-c Check Motor-resolver phasing per para. 4.2.2.6 of 35326. Label all leads with pin numbers after satisfactorily completing these two checks.

-d Measure the resistance of both windings of MTR #1 using a bridge.

-e Measure the Vrms outpost of both windings of MTR #1 while driving the DMA with MTR/RES #2 at speeds of 60 and 80 rpm.

-f Measure the friction level at 40 and 80 rpm using para. 4.2.4.2 of 35326 as a guide.

(2) MPU Checks

-a The D.M.A shall be set up as in Figure 5. Using the D.M.A. test console or drive circuit, apply power to either motor to cause the D.M.A. to rotate at 40 rpm.

-b Using an oscilloscope, observe the output of each MPU and note the P-P amplitude and slope (V/sec) of the signal through crossover. Record the indications.

-c Reduce the speed to zero and disconnect all leads. Submit all data to B4213 test engineer for review prior to continuing build.

5.12 Assemble Slip-Ring and Tube Connector Subassembly

(a) Place the Slip-Ring and Tube Assembly in T100828. Process J1, J2, and J3 per P110348 Para. 4.2. Wire length will be determined by routing cables through the hooks provided on the tool and cutting at the bracket. Lace per BPS 4.01. Slide item 98 over bundles per view G of 32701. Do not shrink at this time. Install pins, items 93, 94 and 95. Observe note 11 (pull test) insert pins into their connectors, items 59, 61 and 62. Install protective brackets 3092-7.

(b) Lay out wires for J4, J5 and J6. Lace per BPS 4.01 and P110348 Para. 4.2. Cut wires to length. Slide item 98 over bundles per view G of 32701. Do not shrink at this time.

5.13 Assembly of Slip-Ring and Tube Assembly 32717-1 to Shaft 32712-1 and Drive Assembly Mechanical 32701-1

(a) Install Retainer 35553-1 to Slip-Ring Tube Assembly 32717-1 using NAS 1291C06 nuts N.S., NAS 1352C06-10 screws F.S., and AN 960C6 washers (4 places). Shim as required between Slip-Ring Tube Assembly 32717-1 and Retainer 35553-1 using Shims B3-34, B3-32, and B3-31 to maintain .001-.005 clearance between Retainer 35553-1 and Shaft 32712-1.

BS-73
2-66

(b) Carefully place Slip-Ring Tube Assembly 32717-1 with Retainer 35553-1 through Shaft 32712-1, Retainer 33279-1, and Shaft, Motor Resolver 32726-1.

NOTE: Be sure thermistor, motor, and resolver wires are positioned between I.D. of Shaft 32712-1 and O.D. of Slip Ring and Tube Assembly 32717-1.

(c) Attach Slip Ring Tube Assembly 32717-1 and Retainer 35553-1 to (Be) Shaft 32712-1 with (4) NAS 1352C04LL6 screws and NAS 620C4 washers. Torque per Note 2.

(d) Route motor, resolver, and thermistor cables through slotted cutout in 32717-1 Slip Ring. Attach SP0057-8 tubing (2inch long typ.) where cables run between slipring and retainer.

(1) Tube required for each motor cable 4 places
(1) Tube required for (2) resolver cables 2 places.
(1) Tube required for (2) resolver cables and (1) thermistor cable. Ref. left end view of 32701-1, Sh. # 2.

(e) Carefully place the D.M.A. in T100828. Process J4, J5 and J6 per P110348 Para. 4.2. Lace per BPS 4.01. Install pins, items 93, 94 and 95. Observe note 11 (pull test). Insert pins into their connectors, items 59, 61 and 62. Install Protective Brackets.

(f) Ground magnetic pickup and thermistor wires (7 places using ST 22623-4 wire and SP0057-20 tubing. Tubing is not to exceed 3.0 inches in length. Lace cables per BPS 4.01. Ref. left end view of 32701-1, Sh. # 2. Ground per view "G" of 32701-1, Sh. # 2.

(g) Attach power cable from Slip Ring Tube Assembly 32717-1 to (Be) Shaft 32712-1 with SP009-5-7 clamp, NAS 1352C04LL4 screw, and AN 960C4 washer (1 place); torque per Note 2. Ref 32701-1, Sh. #1 and 2 left end view.

(h) Attach signal cables from Slip Ring Tube Assembly 32717-1 to (Be) Shaft 32712-1 with SP0009-5-6 clamp, NAS 1352C04LL4 screw, AN 960C4 washer, and 1021 CC lug under clamp (2 places); torque per Note 2. Ref. 32701-1, Sh. #1 and #2 left end view. J3 bundle must be kept to minimum height. Care must be taken in wire dress and lacing the bundles to item 97, retainer. See view G, page 2 of 2, 32701.

(j) Attach motor, resolver, and thermistor cables to (Be) Shaft 32712-1 with SP0009-5-7 clamp, NAS 1352C04LL4 Screw, and AN 960C4 washer (2 places); torque per BPS 1.01. Ref. 32701-1, Sh. #1 and #2 left end view.

(k) Cut J7 wires to print length. Process per P110348 Para. 4.2. Lace per BPS 4.01. Slip item 98 over bundles per view G of 32701. Do not shrink at this time. Pin wires with items 92 and 94 observing note 11 (pull test). Insert pins into item 60. Install protective bracket 3092-7.

5.14 Attachment of Bell 32719-1 to Housing Motor Resolver 32728-1 and Plate 34451-1.

(a) Remove (2) NAS 1291C04 nuts used during motor, resolver alignment. Keep alignment marks of Housing, Motor Resolver 32728-1 and Resolver Stator Bracket in line.

(b) Pot Resolver Stator to Resolver Bracket, and Resolver Bracket to Motor Housing per section D-D of print and note 26.

(c) Install items 64, 43, 79 and 50 to Bell 32719-1. Install Bell 32719-1 to Housing, Motor Resolver 32728-1 and Resolver Stator Bracket 33277-1 with (16) NAS 1352C04-8 screws, NAS 620C4 washers, and NAS 1291C04 nuts. Torque per Note 2.

(d) Clamp wire bundle with clamp installed in step (c) with items 43 and 47.

(e) Attach the torque tube to Bell 32719-1 using items 96, 41 and 49 and assembly aid 3092-6. Attach item 8 with item 40 and 45. Torque per Note 2.

5.15 Conduct insulation resistance and dialectric strength and continuity test per 36469 test procedure prior to potting.

5.16 Connector Potting

Pot Connectors per P110348 Para. 4.3.

5.17 Installation of Mirrors 34453-1 and 35574-1

(a) Attach Mount, Mirror Assembly 34456-3 to .171-.179 diameter hole and .550-.560 diameter spotface of Shaft 32712-1 with AN 960C8 washer and MS 20364D832A nut, using assembly aid 3092-7 and 3092-8. Torque per note 2. After Alignment per Test Procedure 36469, epoxy Mount, Mirror Assembly 34456-3 to Shaft 32712-1 per BPS 9.31.

(b) Attach Bracket 34453-1 to Housing 32713-1 with (2) NAS 1352C04LL4 screws and AN 960C4 washers; torque per Note 2. Attach Mount, Mirror Assembly 34456-1 to Bracket 34453-1 with AN 960C8 washer and MS 20364D832A nut. Torque per Note 2. Afer Alignment per Test Procedure 36469, epoxy Mount, Mirror Assembly to Bracket 34453-1 and Bracket 34453-1 to Housing 32713-1 per BPS 9.31.

5.18 Using Despin Assembly Mechanical 32701-1 as a Reference, Locate and Affix Identification Plate, item 91 per Noted Dimensions. Mark connectors per note 43 of 32701.

5.19 Test per 35326 or 36469 as applicable.

5.20 Package Unit for Shipment

(a) Cap connectors for protection using Cannon P/N DC-59-20, DC-60-20, DD-59-20, DD-60-20. Double-bag and seal in a polyethylene bag per BPS 19.01. Bags shall be at least .003 inches thick. Place an AEC 826004 indicator between inner and outer bag. Draw 30 gallon steel drum from Project Store 30. Remove polystyrene insert from drum and carefully place DMA between both halves, tape insert all the way around and lower into drum. Lock wire, lock ring in place.

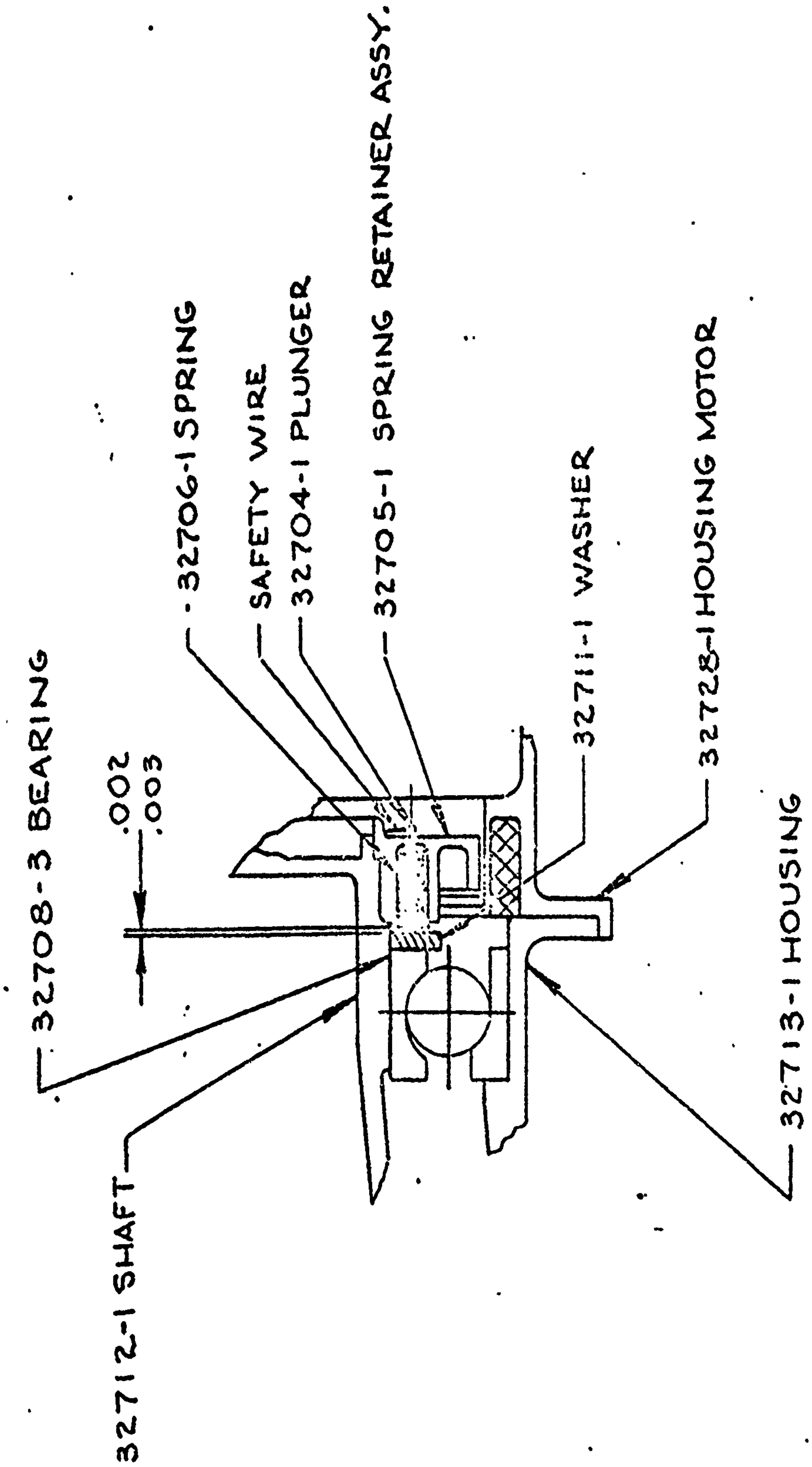
32708-3 BEARING
.002
.003
32706-1 SPRING
SAFETY WIRE
32704-1 PLUNGER
32705-1 SPRING RETAINER ASSY.
32711-1 WASHER
32728-1 HOUSING MOTOR
32713-1 HOUSING
32712-1 SHAFT

FIG. 1

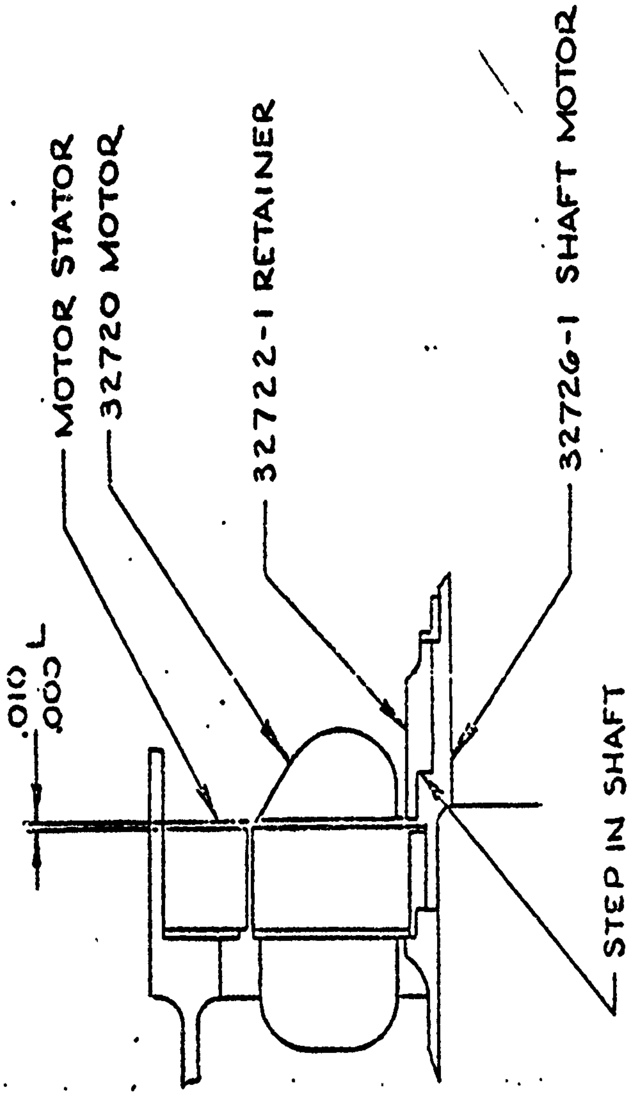
MOTOR STATOR
32720 MOTOR
32722-1 RETAINER
32726-1 SHAFT MOTOR
.010
.000 L
STEP IN SHAFT

FIG. 2

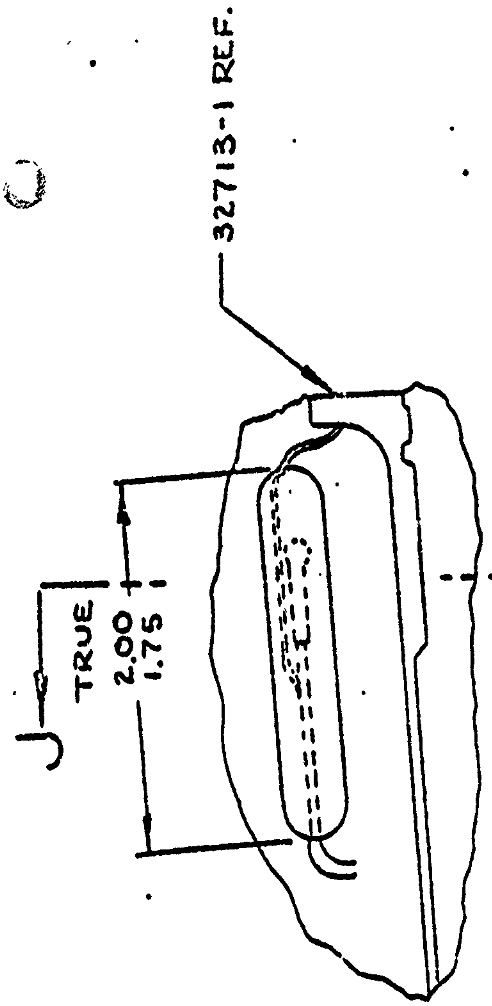

FIG. 3

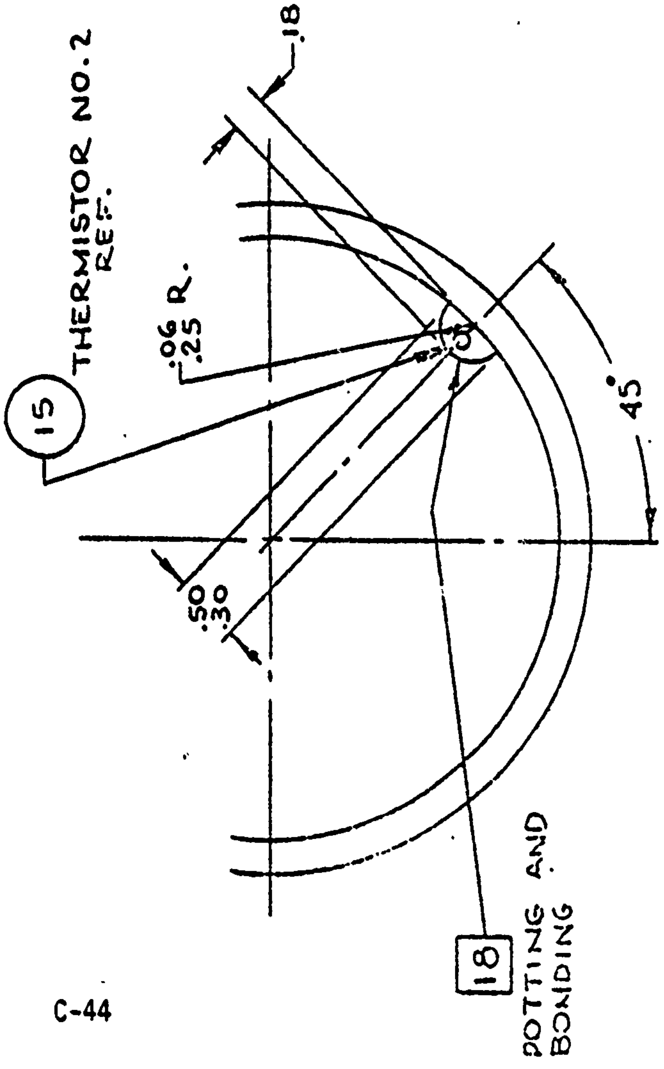

SECTION J-J

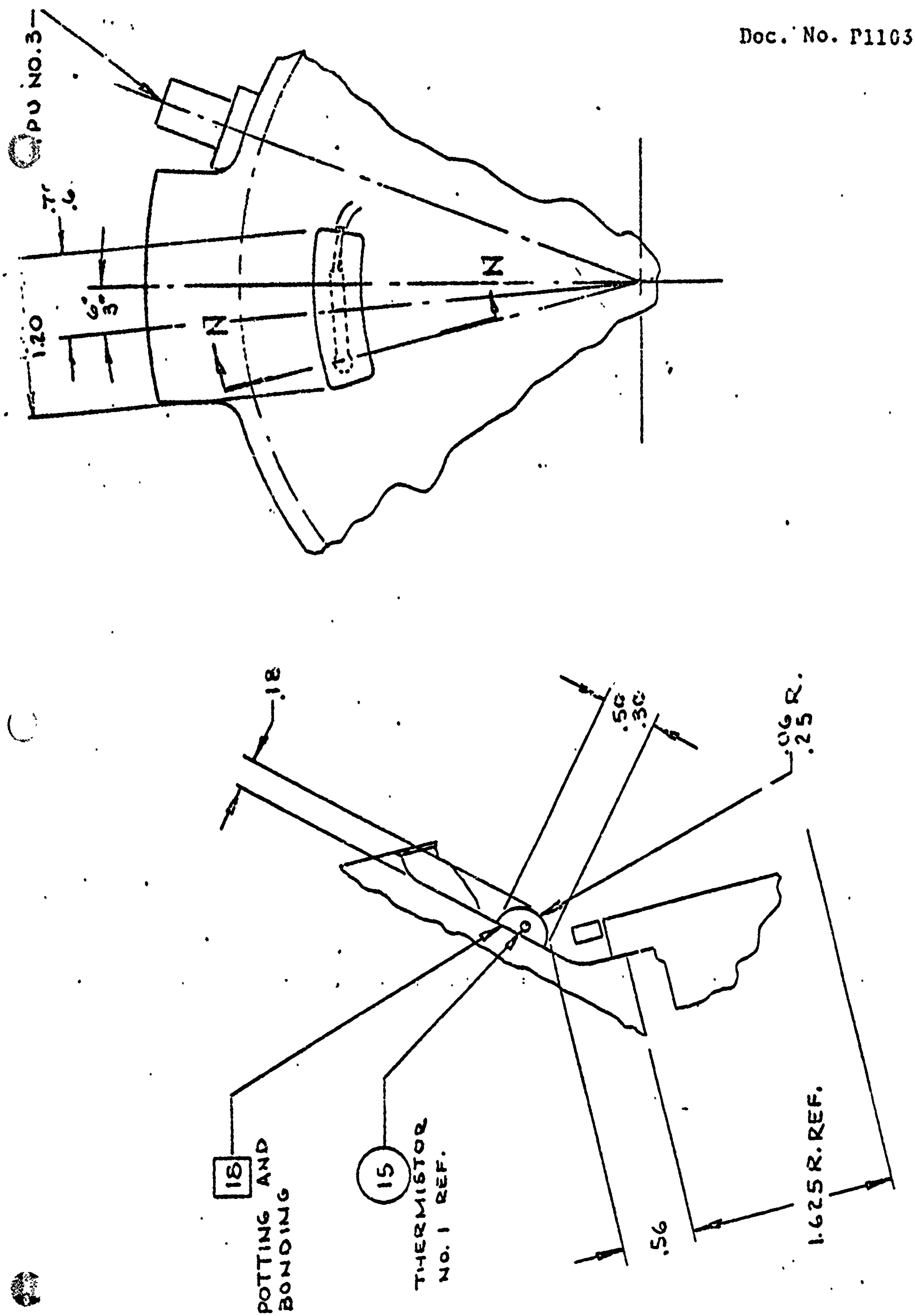

SECTION N-N

FIG. 4

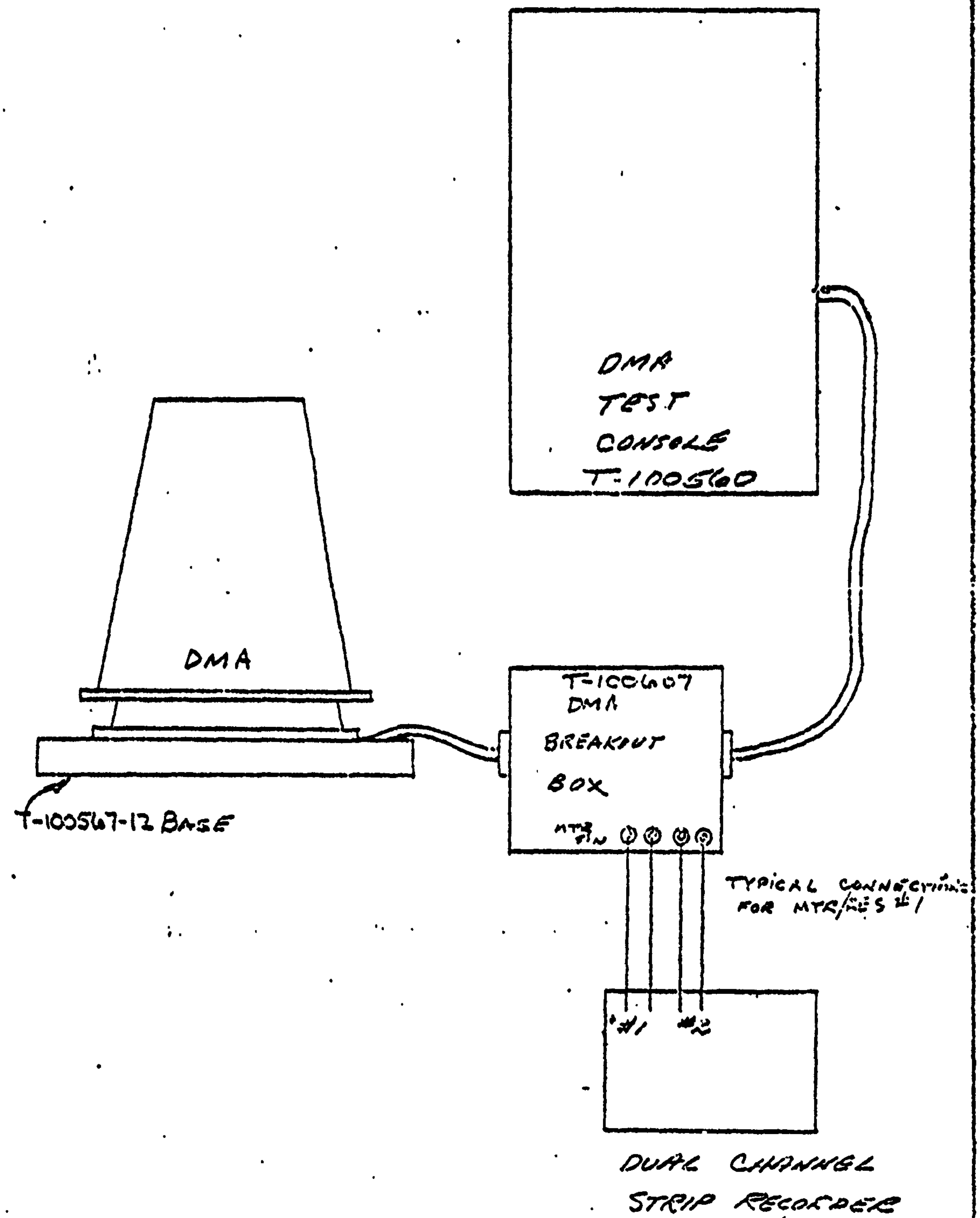

MOTOR - RESOLVER ALIGNMENT

FIGURE 5

APPENDIX D

DMA HISTORICAL DISCREPANCY DATA

Included in this appendix are tables of unit discrepancies that occurred during assembly and acceptance tests along with copies of the NMR's.

DMA S/N 3-2

(FLOWN ON 9433)

DMA S/N 3-2 (3C3-3)

UNIT DISCREPANCY HISTORY AT BBRC

DATE	DISCREPANCY	DISPOSITION
5-21-70	Slip ring assy	
	Leads from rings 4, 42, 64, 68, 83, and 85 had nicked insulation.	All leads covered with shrink tubing.
	Lead from ring 45 damaged insulation and shield.	Cut off ring and brushblock leads to ring 45. Used leads from spare Ring 57.
D-3 7-13-70	Dent in band around torque motor 4.490 DIA.	Use as is
	Small metal slivers along edge torque motor.	Removed during pre-assy cleaning.
7-29-70	Slip ring assy	
	Wire #9 shaft end abraded	Repaired per TRW SRP 7-1
	Wire #85 shaft end insulation cut 16" from end of bellows housing.	" " " " "

DATE	DISCREPANCY	DISPOSITION
8-14-70	**SLIP RING ASSY**	
	Following wires abraded: 50, 75, 77, 84, 86; cut & abraded: 72, 74, 80, 82	Reworked to drawing spec.
8-17-70	**Magnetic pickup**	
	Dim. on S/N B09 is 0.421, S/B .400/.398	Returned to vendor
	Strain relief extended 1 1/4", S/B 0.125	Use as is
	S/N B02 & B09 had cracked insulation at shrink tube & pickup potting. S/N B12 had potting void at tube & pickup	Rework at BBRC
8-24-70	During Y axis vibration no current on motor #1 due to operator error (failed to place switch on test equip. to correct position)	Use as is (SIR #11721)

NOTE: DMA WAS INSTALLED ON S/C 3-2 ON 9-18-70

DMA WAS REMOVED FROM S/C 3-2 ON 11-3-70 TO RETURN TO BBRC FOR SUSPECT BEARINGS

NO TRW REJECTION DOCUMENT INITIATED AT THIS TIME.

DMA RETURNED TO BBRC FOR SUSPECT BEARINGS

DATE	DISCREPANCY	DISPOSITION
12 -70	P/N 32708-1 S/N 017 retainer unacceptable.	Scrapped & replaced with S/N 020.
	P/N 32708-1 S/N 017 races & balls were acceptable however, due to reprocess time span to restore lubrication to flight status, these parts were not reinstalled in DMA 3-2.	Replaced with S/N 026.
	P/N 32708-3 S/N 017 races, balls, and retainer were also acceptable however due to reprocess time span to restore lubrication to flight status these parts were not reinstalled in DMA 3-2.	Replaced with S/N 026.

NOTE: Reassembly of DMA 3-2 was per procedure except the thermistor in-line connections were made per special rework procedure.

Acceptance test per modified ATP 36469 (exceptions per TWX 777-SI-3081, 3064, & 3090)

NOTE: DMA 3-2 WHEN RETURNED TO TRW WAS INSTALLED ON S/c 3-3 (12-21-70)

(3-2) 1

BALL BROTHERS RESEARCH CORPORATION
POST OFFICE BOX 1062 · BOULDER INDUSTRIAL PARK
BOULDER, COLORADO 80302

NONCONFORMING MATERIALS REPORT

NMR - 25905
PAGE 1 OF 2

PART NUMBER 32701-1 REV. J.	VENDOR BBRC.
PART NAME DESPIN ASSY., MECH.	MANUFACTURER BBRC
SERIAL/LOT NO. S/N 3-2 (FLT #2)	PROJECT 3092 · LOG TIME AT FAILURE — N/A —
LOT QTY 1 · QTY INSP. 1 · QTY REJECTED 1	ORDER NO. 5692 · ITEM/REQ

DEFECTS

SPECIFICATION:

Bearing Surface Finish to be 4 micro inches max.

ACTUAL:

Brgs in this unit are suspect as a result of inspections of similar bearing which have evidence of separator defects and raceway finish problems

INSP. TYPE	INSP. PROCEDURE	INSP. STAMP	DATE	QA SUPERVISOR	DATE	CUSTOMER REQUIRED?
Assy	DWG	25	12-2-70		12-2-70	YES NO

DISPOSITION OF DEFECTIVES

NMR - 25905

DISPOSITION #1:

1. Disassemble unit as required to remove main shaft bearings (P/N 32703-1,-3). Disassembly to be recorded in unit CERT LOG and all parts are to be identified for future traceability. QA Monitor required.

Continued on Page 2

- USE AS IS
- COMPLETE TO DWG
- REWORK
- SCRAP
- REJECT REFER TO PURCHASING
- REJECT REFER TO MATERIAL CONTROL
- ←OTHER

REWORK PER AFQAR

3 Dec 70

OKAY 12/3/70

CUSTOMER REP. SIGN & DATE	DESIGN SIGN & DATE	QUALITY ASSURANCE SIGN & DATE
17 Dec 70	12/3/70	12/17/70

CORRECTIVE ACTION FOLLOW UP

Retainer defects have been attributed to machining practices. Replacement retainers are being machined by a different vendor. ABC

FAILURE REPORT NUMBER · DEPT. RESPONSIBLE

MATERIAL CONTROL ACTION SIGN & DATE · PURCHASING ACTION SIGN & DATE · RETURN SHIPPING REQUISITION NO.

VENDOR SHIPPING DATE

RETAIN ORIGINAL - RECORD COPY

QUALITY

3R 97

RED. ... ROOM

(3-2) 2

NONCONFORMING MATERIALS REPORT

CONTINUATION SHEET

PART NUMBER 32701-1 Rev. 5	NMR - 25905
PART NAME DESPIN ASSY, MECHANICAL	
SERIAL/LOT NO. S/N 3-2 (FLT #2)	

~~DEFECTS~~

DISPOSITION #1 CONTINUED:

2. Disassemble the bearings (P/N 32708-1 and -3) using appropriate fixtures by cooling inner race to -100 ± 10°F while heating the outer race to +250 ± 10°F. Q.A. Monitor required.

3. Inspect bearing raceways with 10X magnification and use stylus-feel method for surface finish measurement. Record surface finish and any defects found. Report results to MRB for further disposition. (MRB to adjust BBRC readings to correlate with surface finish measurements made by SUNDSTRAND CORP. using a Bendix Profilometer.)

4. Inspect each bearing retainer per Quality Assurance Directive (QAD) #57A. Report results to MRB for further disposition.

H E Christensen 12/3/70
R G Galin 12/3/70

INSPECTION RESULTS per DISP. #1:

P/N 32708	S/N	Bearing Surface Finish Inner	Bearing Surface Finish Outer	Adjusted Bearing Surface Finish Inner	Adjusted Bearing Surface Finish Outer	Retainer (Visual per QAD #57A)
-1 (Large)	017	4/6	4/6	2/4	2/4	Unacceptable 12/4/70
-3 (Small)	017	4/8	4	3/5 12/7/70	2/4 12/7/70	Acceptable 12/7/70

* BBRC readings adjusted to correlate with measurements obtained by SUNDSTRAND CORP. using a Bendix Profilometer.

~~INSPECTOR~~ ~~DATE~~ INSP

BA 67-2 7-63

(3-2) 3

NONCONFORMING MATERIALS REPORT

CONTINUATION SHEET

PART NUMBER 32701-1 Rev. J

PART NAME DESPIN, ASSY, MECHANICAL

SERIAL/LOT NO. S/N 3-2 (Flight)

NMR - 25905

DISPOSITION #2

P/N 32708-1 (Large) S/N 017 RETAINER ONLY
Retainer is Unacceptable. SCRAP

NOTE: Retainer from S/N 020 will be used ~~as~~ as a replacement.

	USE AS IS
	COMPLETE TO DWG
	REWORK
X	SCRAP
	REJECT REFER TO PURCHASING
	REJECT REFER TO MATERIAL CONTROL
	← OTHER

REWORK PER AFQAR

CUSTOMER REP. SIGN & DATE	DESIGN SIGN & DATE	QUALITY ASSURANCE SIGN & DATE
N/A HEC 12/7/70	N/A HEC 12/7/70	H. E. Christensen 12/7/70

DISPOSITION #3

P/N 32708-1 (Large) S/N 017 RACES & BALLS
Races & balls are acceptable. Reprocess Races, balls and Retainer from S/N 020 per the attached rework treatment instructions to restore lubrication to flight status.

NOTE: Due to reprocess time span, these parts will not be used in DMA S/N 3-2.

	USE AS IS
	COMPLETE TO DWG
X	REWORK
	SCRAP
	REJECT REFER TO PURCHASING
	REJECT REFER TO MATERIAL CONTROL
	← OTHER

REWORK PER AFQAR

CUSTOMER REP. SIGN & DATE	DESIGN SIGN & DATE	QUALITY ASSURANCE SIGN & DATE
[illegible] 12-7-70	R.C. Culver by HEC 12/7/70	H. E. Christensen 12/7/70

DISPOSITION #4

P/N 32708-3 (Small Bearing) S/N 017
Races, balls & retainer are acceptable. Reprocess components per the attached rework treatment instructions to restore lubrication to flight status.

NOTE: Due to time required to reprocess, this bearing will not be used in DMA S/N 3-2.

	USE AS IS
	COMPLETE TO DWG
X	REWORK
	SCRAP
	REJECT REFER TO PURCHASING
	REJECT REFER TO MATERIAL CONTROL
	← OTHER

REWORK PER AFQAR

CUSTOMER REP. SIGN & DATE	DESIGN SIGN & DATE	QUALITY ASSURANCE SIGN & DATE
[illegible] 12-7-70	R.C. Culver by HEC 12/7/70	H. E. Christensen 12/7/70

CORRECTIVE ACTION NAME & DATE	FAILURE REPORT NUMBER	DEPT. RESPONSIBLE
SEE PAGE 1. HEC		

PURCHASING OR MATERIAL CONTROL ACTION	SIGN & DATE	RETURN SHIPPING REQUISITION NO.
		VENDOR SHIPPING DATE

(3-2) 4

NONCONFORMING MATERIALS REPORT

CONTINUATION SHEET

PART NUMBER 32701-1 Rev. J.	NMR - 25905
PART NAME DESPIN ASSY, MECHANICAL	
SERIAL/LOT NO. S/N 3-2 (FLIGHT)	

~~[illegible]~~

DISPOSITION # 5 :

1. After reprocessing of Bearings, P/N 32708-1, S/N 026 and P/N 32708-3, S/N 026 per NMR's 25821 (Disp. #7) and 25832 (Disp. #6) respectively, reassemble the DMA per the applicable paragraphs of P-110330 (DMA ASS'Y PROCEDURE) and 32701, Rev. L with the following exception: The Thermistor in-line connections are to be made per the attached rework procedure.

Thermistor #1 & #2 Reworked with TRW Furnished Pins & Sockets per Procedure #2. 12/16/70

2. Perform the "~~[illegible]~~ MODIFIED" ACCEPTANCE TEST per ATP 36469 which includes exceptions mutually agreed upon with TRW. Reference the attached TRW TWX's 777-S1-3081 and 777-S1-3064 and 777-S1-3090.

12/16/70

R.C. Culver by HEC 12/7/70

H.E. Christensen 12/7/70

[illegible] 12/7/70

INSPECTOR DATE

REWORK TREATMENT

TRW BEARINGS P/N 32708-1 & -3

1. Rinse all bearing components by agitating in a solution consisting of 1% of solution 1, BPS 14.01 and 99% Freon (PCA) for 10-15 seconds.

2. Assemble each bearing per 35323 Para. 3.11.3, steps 2 thru 4.

3. Immerse bearing assembly in solution 1 of BPS 14.01 for 12 hours minimum at 50 ± 10 degrees C.

4. Proceed with Paragraphs 5.9 and 5.10 of BPS 14.01.

5. Final lubrication and test shall be done per 34083, Para. 3.11.

B-26

attached

Procedure #1 (Preferred)

1. Tin conductor wires.
2. Twist conductor wires together a minimum of three wraps.
3. Solder and inspect the twisted wire.
4. Sleeve each soldered wire to overlap the primary insulation at least 1/8 inch, each side.
5. Solder the shielded ends to prevent loose ends from piercing the insulation.
6. Sleeve the entire area to cover the original sleevings and the exposed shields to overlap the cable jacket.

Procedure #2 (To be used in lieu of procedure #1 when length of thermistor leads is too short to make a reliable connection)

1. Use TRW furnished pins and sockets P/N PT2-95-3 and P/N PT2-95-4. Use SP0057 heat shrinkable tubing (applicable size and amount).

2. Terminate the thermistor leads using the method shown in TRW Document EQ3-235, Figure 4, page I-26.

3. The shielding of Thermistor #2 shall be turned back over the outer insulation approximately 1/8" and soldered around shielding to capture loose strands.

4. The entire termination shall be enclosed in SP0057.

Notes Applicable to Both Procedures:

1. Heat shrink tubing to be applied per TRW's SRP7-1.

2. Care to be taken not to reflow solder when shrinking the tubing.

3. Above rework to be inspected by DCAS and TRW's QA Representative.

H. E. Christensen
QA Engineer
12/10/70

MESSAGE REC.

TWX ☒
WESTERN UNION
TIME 7:30
DATE 12-3-70

SYS 8400

CT-48

4:44 PM

910-940-2241 U 910-325-6614 12-2-70 MSG12211 CC2376 31
FROM/J R GROSS TRW SYSTEMS REDONDO BEACH CALIFORNIA
TO/BOULDER COLORADO BALL BROTHERS RESEARCH CORPORATION
ATTENTION R PATTON

777-51-2064 70-2376-RX-931

SUBJECT: RE 501-SC, S/N NOS. 3-2 AND 3-4 MODIFIED ACCEPTANCE
TEST PROCEDURE

REFERENCES: (1) TRW TWX 777-51-2017 DTD 11/20/70
(2) TRW TWX 777-51-2053 DTD 11/30/70
(3) BBRC TWX 2092-0213-12-1-70

PER REFERENCES 1, 2 AND 3, THE FOLLOWING CONSOLIDATES AND FINALIZES TRW'S AUTHORIZATION TO PERFORM A MODIFIED ACCEPTANCE TEST ON SUBJECT REWORKED UNITS IN ACCORDANCE WITH BBRC'S ACCEPTANCE TEST PROCEDURE NO. 36449:

A. 3.7 TESTING SEQUENCE - IT IS PERMISSIBLE TO DEFER THE RUN-IN OF 4.2 IN THE SEQUENCE, BUT IT MUST BE COMPLETED PRIOR TO THE TESTS OF 4.3.3, 4.3.4 AND 4.3.7.
B. DELETE 4.3.1.3 DIELECTRIC STRENGTH
C. DELETE 4.3.1.4 INSULATION RESISTANCE
D. DELETE 4.3.1.6 PHASING
E. DELETE 4.3.4.5 POWER AT 90 RPM AND 40 IN/OZ
F. MODIFY 4.3.5 TO MEASURE TRANSFORMATION RATIO AND NULLS AT ONLY FOUR (4) POINTS ON EACH WINDING.
G. DELETE 4.3.7.1 CURRENT CARRYING CAPACITY.
H. MODIFY 4.3.7.2 TO RUN NOISE TEST AT 90 RPM ONLY.
I. DELETE 4.3.7.3 CONTACT RESISTANCE
J. MODIFY 4.4 TO RUN AT ACCEPTANCE LEVEL RANDOM VIBRATION FOR X AXIS ONLY. MONITORING PER 4.4.2 IS NOT REQUIRED.
K. MODIFY 4.6 THERMAL VACUUM TO SUBJECT UNIT TO FOLLOWING ENVIRONMENT ONLY:

1. STABILIZE TEMPERATURE WITH BASEPLATE AT PLUS 35 DEGREES F. DWELL FOUR (4) HOURS MINIMUM.
2. TEST PER 4.6.3 DURING THE DWELL PERIOD.

THIS TWX HAS BEEN COORDINATED WITH J. VAN DORN OF TRW'S QUALITY ASSURANCE, AND A COPY HAS BEEN FORWARDED TO M. MAY OF DCAS.
TWX/JG
TRANS/4:47 PM SJ

RPC BLDR

SYS 8400

(3-39)

Page 5 of 5

[illegible] BLDR

TRW SYS RNDO
[illegible]
[illegible]-2041 U [illegible]-6411 12-9-70 [illegible]2317 CC0274 14
MICHAEL S DROSS TRW SYSTEMS REDONDO BEACH CALIF
BX/BOULDER COLO BALL BROTHERS RESEARCH CORP ATTN R PATTON

[illegible]-3380. 70-6274-[illegible]-041. SUBJECT: RF 501-80, DIPPER AND [illegible]. REF: (A) TRW TWX 777-81-[illegible]70 DTD 11/19/70. (B) BBRC TWX [illegible]-11-24-70.

PURSUANT TO REFERENCES (A) AND (B), TRW WILL ISSUE A SPECIFICATION CHANGE NOTICE TO CHANGE [illegible]-184 REVISION A, PART I AND SCN NO. 1 AS FOLLOWS:

1. PAGE I-24 (SCN NO. 1) CHANGE "A = 1.5 TO 6.0 VOLTS AT 40 THROUGH 80 RPM FOR 0 DEGREE DIPPER" TO "A = 1.5 TO 6.0 VOLTS AT 60 THROUGH 80 RPM FOR 0 DEGREE DIPPERS."

2. PAGE I-24 ITEM 2 CHANGE ". . . 40 THROUGH 80 RPM" TO ". . . 60 THROUGH 80 RPM".

TRW IS CONSIDERING OTHER REQUESTED CHANGES TO THE DIPPER SLOPE AND AMPLITUDE REQUIREMENTS; HOWEVER, IT IS MY UNDERSTANDING NO FURTHER CHANGES ARE REQUIRED TO S/N 2-4.

THIS TWX HAS BEEN COORDINATED WITH J. VAN [illegible] OF TRW'S QUALITY ASSURANCE, AND A COPY HAS BEEN FORWARDED TO M. [illegible] OF DCAS.
END/CT
[illegible] YS
BBRC BLDR

TRW SYS RNDO

(9-2)10

BALL BROTHERS RESEARCH CORPORATION
POST OFFICE BOX 1062 · BOULDER INDUSTRIAL PARK
BOULDER, COLORADO

NONCONFORMING MATERIALS REPORT

NMR-24063
PAGE 1 OF 1

PART NUMBER 32720-1 REV E		VENDOR 8878	
PART NAME TORQUE MOTOR		MANUFACTURER WESTINGHOUSE	
SERIAL/LOT NO. 004		PROJECT 3092-007	LOG TIME AT FAILURE NA
LOT QTY 1	QTY INSP. 1 QTY REJECTED 1	ORDER NO. C1023	ITEM/REQ 10

DEFECTS

SPECIFICATION:	ACTUAL:
1. QUAD II CERT'S	1. VENDOR DID NOT FURNSH CERTIFICATION OF MATERIAL.
2. ~~[illegible]~~ USUAL	2a) ONE DENT IN BAND AROUND MOTOR REF. 4.489/4.490 DIA. b) SMALL METAL SLIVERS ALONG EDGE.

INSP. TYPE | INSP. PROCEDURE | INSP. STAMP | DATE | QA SUPERVISION | DATE | CUSTOMER REQUIRED?

DISPOSITION OF DEFECTIVES

NMR-24063

1) BUYER TO OBTAIN CERT. OF COMPLIANCE
UAI CERT. OF COMPLIANCE REC'D 7/10/70 HEC.
2) ~~[illegible]~~ METAL SLIVERS ~~[illegible]~~
b) WILL BE REMOVED DURING PRE-ASSEMBLY CLEANING
a) UAI - DENT IS NEAR CENTER OF HYPER-NICK BAND - APPROX .010 DIA & .005 DEEP MECHANICAL INTEGRITY IS NOT COMPROMISED)

X	USE AS IS
	COMPLETE TO DWG
	REWORK
	SCRAP
	REJECT REFER TO PURCHASING
	REJECT REFER TO MATERIAL CONTROL
HEC	← OTHER

REWORK PER AFQAR

CUSTOMER REP. SIGN & DATE	DESIGN SIGN & DATE	QUALITY ASSURANCE SIGN & DATE
[signature] 7-13-70	K. [signature] 6/23/70	H.E. Christensen 7/13/70

CORRECTIVE ACTION FOLLOW UP

Vendor was contacted via telephone by Subcontract Administrator (J. Meeks). HEC.

FAILURE REPORT NUMBER | DEPT. RESPONSIBLE

MATERIAL CONTROL ACTION SIGN & DATE | PURCHASING ACTION SIGN & DATE | RETURN SHIPPING REQUISITION NO.

VENDOR SHIPPING DATE

RETAIN ORIGINAL - RECORD COPY

QUALITY ASSURANCE COPY

BR 47

(3-3) 11

BALL BROTHERS RESEARCH CORPORATION
POST OFFICE BOX 1062 • BOULDER INDUSTRIAL PARK
BOULDER, COLORADO 80302

NONCONFORMING MATERIALS REPORT

NMR-24306
PAGE 1 OF 1

PART NUMBER 32685-1 N/R		VENDOR 4935	
NAME SLIP RING ASSY		MANUFACTURER ~~GE~~ Electric-Tech	
SERIAL/LOT NO. 005		PROJECT 3092-006-00	LOG TIME AT FAILURE N/A
LOT QTY 1	QTY INSP. 1 / QTY REJECTED 1	ORDER NO. C11024-B	ITEM/REQ 6

DEFECTS

SPECIFICATION:	ACTUAL:
① Visual Wires for Damage	① Wire #9, shaft end Abraded – 11" from end of bellows housing Wire #85, shaft end Cut, 16" from end of bellows housing Note – Bellows housing was not removed, no insp. on that portion of harness. ASSY located in MEP CLN RM.

INSP. TYPE Rec. | INSP. PROCEDURE Insp Comp | INSP. STAMP | DATE | QA SUPERVISOR | DATE | CUSTOMER REQUIRED NO

DISPOSITION OF DEFECTIVES

NMR-24306

① Repair damaged insulation by applying heat shrinkable tubing (SP0057) per TRW spec SRP 7-1, "Repair of Damaged Wire Insulation."

7/26 7/23 OK TO Rework HE Christensen 7/20/70

	USE AS IS
	COMPLETE TO DWG
X	REWORK
	SCRAP
	REJECT REFER TO PURCHASING
	REJECT REFER TO MATERIAL CONTROL
	← OTHER

Concurrence to rework does not imply DCAS acceptance of item or the tubing.

REWORK PER AFQAR [signature] 20 July 70

CUSTOMER REP. SIGN & DATE [signature] 27 Jul 70 | DESIGN K. Ziegler SIGN & DATE 7/17/70 | QUALITY ASSURANCE HE Christensen SIGN & DATE 7/24/70

FAILURE REPORT NUMBER | DEPT. RESPONSIBLE

CORRECTIVE ACTION FOLLOW UP
32701 REV "G" WILL REQUIRE APPLICATION OF SP0057 TUBING TO ALL UNSHIELDED LEADS. HEC

MATERIAL CONTROL ACTION SIGN & DATE | PURCHASING ACTION SIGN & DATE | RETURN SHIPPING REQUISITION NO. | VENDOR SHIPPING DATE

RETAIN ORIGINAL - RECORD COPY
QUALITY ASSURANCE COPY
32685-1 3092-006-00

S3-212

BALL BROTHERS RESEARCH CORPORATION
POST OFFICE BOX 1062 · BOULDER INDUSTRIAL PARK
BOULDER, COLORADO 80302

NONCONFORMING MATERIALS REPORT

NMR - 24425
PAGE 1 OF 1

PART NUMBER 32717-1 Rev D		VENDOR Electro-Tec Corp.	
PART NAME Slip Ring & Tube Assy		MANUFACTURER 4935A	
SERIAL/LOT NO. S/N 5 FLT		PROJECT 3092.007-00	LOG TIME AT FAILURE N/A
LOT QTY 1	QTY INSP. 1 / QTY REJECTED 1	ORDER NO. 5-517	ITEM/REQ 6

DEFECTS — **SPECIFICATION:**

① VISUAL 10X

INSP Comp.

ACTUAL:

① WIRE #
72 } cut &
74 } Abraded ½" from End of Shaft
75 } abraded " " " "
77 }
80 } cut &
82 } abraded " " " "
86 } abraded " " " "
84 }
50 abraded " " " "

XX }
XX } = twisted pairs

INSP. TYPE	INSP. PROCEDURE	INSP. STAMP	DATE	QA SUPERVISOR	DATE	CUSTOMER REQUIRED?
Recv			7-27-70			NO

DISPOSITION OF DEFECTIVES

① COMPLETE TO DWG PER 32701 REV. "H", NOTES 51 & 52.

OKAY
HEChristiansen
8/4/70

SK/70 8/1/70
BBRC 5 QA

NMR - 24425

	USE AS IS
X	COMPLETE TO DWG
	REWORK
	SCRAP
	REJECT REFER TO PURCHASING
	REJECT REFER TO MATERIAL CONTROL
	← OTHER

REWORK PER AFOAR

CUSTOMER REP. SIGN & DATE	DESIGN SIGN & DATE	QUALITY ASSURANCE SIGN & DATE
N/A HEC	K. Ziegler by HEC 8/4/70	[illegible] 8/1/70

FAILURE REPORT NUMBER | DEPT. RESPONSIBLE

CORRECTIVE ACTION FOLLOW UP

C.A.R. # 331 to be sent to Vendor. HEC

MATERIAL CONTROL ACTION SIGN & DATE	PURCHASING ACTION SIGN & DATE	RETURN SHIPPING REQUISITION NO.
		VENDOR SHIPPING DATE

RETAIN ORIGINAL · RECORD COPY

QUALITY ASSURANCE COPY

BR 67 9-69

(7-2-13)

BALL BROTHERS RESEARCH CORPORATION
POST OFFICE BOX 1062 • BOULDER INDUSTRIAL PARK
BOULDER, COLORADO

NONCONFORMING MATERIALS REPORT

NMR-24573
PAGE 1 OF 1

PART NUMBER 32731-1 REV. H
NAME MAGNETIC PICKUP
SERIAL/LOT NO. S/N B02, B09, B30, B12, B16, B34 (FLIGHT)
LOT QTY. 6 | QTY INSP. 6 | QTY REJECTED 6

VENDOR 1627
MANUFACTURER ELECTRO PRODUCTS INC.
PROJECT 3002-007
LOG TIME AT FAILURE ~4
ORDER NO. 65515
ITEM/REQ 1

DEFECTS / SPECIFICATION:	ACTUAL:
① 400/308	① IS 421 ON B09
② .125 STRAIN RELIEF (VISUAL)	② STRAIN RELIEF EXTENDED BEYOND DWG. CALLOUT 1¼"
③ WORKMANSHIP	③ S/N B02, B09 HAS CRACKED INSULATION AT SHRINK TUBE & PICK-UP POTTING S/N B12 HAS POTTING VOID AT TUBE & PICKUP INTERSECTION

INSP. COMPLETE
INSP. TYPE | INSP. PROCEDURE | INSP. STAMP | DATE | QA SUPERVISOR | DATE | CUSTOMER REQUIRED?

DISPOSITION OF DEFECTIVES

NMR-24573

① RETURN TO VENDOR, S/N B09
② USE AS IS - EXTRA ~~SEEEA~~ STRAIN RELIEF PROVIDES PROTECTION AGAINST HANDLING DAMAGE AND WILL BE REMOVED DURING ASSEMBLY TO DRAWING CALLOUT DIMENSION.
③ REWORK AT BBRC - S/N'S B02 & B12 AS FOLLOWS:
B-02 - REMOVE VENDOR'S STRAIN RELIEF TUBING, REPLACE WITH SPC0ST AND POT STRAIN RELIEF TO POTTING INTERFACE USING BPS 9.31.
B-12 - APPLY BPS 9.31 TO VOID.

X USE AS IS ITEM ②
COMPLETE TO DWG
X REWORK ITEM ③
SCRAP
X REJECT REFER TO PURCHASING ITEM ①
REJECT REFER TO MATERIAL CONTROL
← OTHER

REWORK PER AFQAR
10 Aug-70

CUSTOMER REP. SIGN & DATE: J. A. Bibber 18 Aug. 70
DESIGN 767 SIGN & DATE: 8/7/70
QUALITY ASSURANCE SIGN & DATE: H.E.C.
DEPT. RESPONSIBLE

CORRECTIVE ACTION FOLLOW UP
BBRC HAS MADE SEVERAL SOURCE TRIPS TO ELECTRO-TEC TO DISCUSS & RESOLVE QUALITY PROBLEMS. 8/11/70

FAILURE REPORT NUMBER

MATERIAL CONTROL ACTION SIGN & DATE
PURCHASING ACTION SIGN & DATE
RETURN SHIPPING REQUISITION NO.
VENDOR SHIPPING DATE

RETAIN ORIGINAL - RECORD COPY
QUALITY ASSURANCE COPY

CLOSED

BALL BROTHERS RESEARCH CORPORATION
POST OFFICE BOX 1062 • BOULDER INDUSTRIAL PARK
BOULDER, COLORADO 80302

NONCONFORMING MATERIALS REPORT

NMR - 24716
PAGE 1 OF ____

PART NUMBER: 32701-1 Rev. J	VENDOR: N0070 (VIB LAB)
PART NAME: Despin Assy, Mechanical	MANUFACTURER: BBRC
SERIAL/LOT NO.: 04	PROJECT: 3092-007 / LOG TIME AT FAILURE:
LOT QTY: 1 / QTY INSP.: 1 / QTY REJECTED: 1	ORDER NO.: 3522 / ITEM/REQ:

DEFECTS

SPECIFICATION:
TS 36469 Rev. A para 4.4.2 c.
Monitor motor current & voltage ..... during vibration run. (Random)

ACTUAL:
During Y axis voltage was applied to Motor #2. No current was monitored on Motor #1 during the vibration exposure.

Note: this was due to operator error; operator failed to place switch on test console to correct position to record the current.

INSP TYPE	INSP. PROCEDURE	INSP STAMP	DATE	QA SUPERVISOR	DATE	CUSTOMER REQUIRED?
VIBRATION	36469 A	60	[illegible]	[illegible]	[illegible]	YES / NO

DISPOSITION OF DEFECTIVES.

NMR - 24716

INTERIM DISPOSITION:
CONTINUE ACCEPTANCE TESTING PENDING DISPOSITION OF SIR 11721.
NOTE: TRW HAS BEEN NOTIFIED BY TELECON. THIS DISCREPANCY IS CONSIDERED AN OPERATOR ERROR AND NOT A FAILURE.
H E Christensen 3/24/70

FINAL DISPOSITION:
USE AS IS. SIR 11721 HAS BEEN APPROVED BY TRW. KAJ 9/2/70

X	USE AS IS 9/2/70
	COMPLETE TO DWG
	REWORK
	SCRAP
	REJECT REFER TO PURCHASING
	REJECT REFER TO MATERIAL CONTROL
X	OTHER 3/24/70

REWORK PER AFQAR: [illegible] 24 May 70

CUSTOMER REP SIGN & DATE	DESIGN SIGN & DATE	QUALITY ASSURANCE SIGN & DATE
[illegible] 9-2-70	K. Ziegler 9/2/70	[illegible] 9/2/70

CORRECTIVE ACTION FOLLOW UP
Operator and QA inspector have been instructed to double check test set-up prior to start of actual vibration run. [illegible] for H. Christensen 9/2/70

FAILURE REPORT NUMBER: | DEPT. RESPONSIBLE:

MATERIAL CONTROL ACTION SIGN & DATE	PURCHASING ACTION SIGN & DATE	RETURN SHIPPING REQUISITION NO.
		VENDOR SHIPPING DATE

RETAIN ORIGINAL - RECORD COPY

QUALITY

BR-67

SPACE PARK • REDONDO BEACH, CALIFORNIA

0-216

SUPPLIER INFORMATION REQUEST (SIR)

INSTRUCTIONS TO SUPPLIER:

1. Use this form to request preliminary evaluation only of defective material.
2. Contact Buyer, prior to initiating this request, for his direction.
3. Processing of this SIR and resultant comments by TRW SYSTEMS GROUP should not be regarded as relieving the Supplier in any way of his contractual obligations, but as only a preliminary recommendation.
4. Combination of SIR's on the same lot of parts, or latent defects not detectable at the time of preliminary evaluation, may show the items to be unacceptable.
5. Do not ship material, or submit to TRW SYSTEMS GROUP Source Inspection, until this form has been processed by TRW SYSTEMS GROUP and returned to you.
6. Include in all shipments of finished parts: (1) original SIR, (2) Certificate of Conformance referencing SIR serial number, (3) Shipper referencing SIR serial number.

SUPPLIER'S NAME AND ADDRESS	INITIATED BY	TITLE	PHONE	DATE INITIATED
Ball Brothers Research Corp. Boulder, Colorado 80302	H.E. Christensen	QA Engineer	444-5300	5/21/70
	PURCHASE ORDER NO.	BUYER		MJO NUMBER
	BF 501-SC	J. R. Cross		1957-44

PART NUMBER	REV.	PART NAME/DESCRIPTION	QUANTITY AFFECTED	SERIAL NUMBER(S)
32685	E	Slip Ring (DMA Flt # 2)	1	05

Description of defect and probable cause (showing zone location of drawing). Provide sketch, as required, in sufficient detail and clarity for full understanding of defect and proposed corrective action:

The rotor leads in this assembly have the following defects (reference BBRC drawing 32725):

1. Leads from rings 4, 42, 64, 68, 83 and 85 have slight nicks in teflon insulation, but no conductor or shield damage.

2. Lead from ring 45 has damaged insulation and shield.

PROPOSED DISPOSITION:

1. Apply short pieces of heat shrinkable tubing to cover damaged insulation. All places except lead to ring 4 will be inside the DMA torque tube. Lead bundle is laced and clamped at end of torque tube.

2. Cut off ring and brushblock leads to ring 45 and use leads from spare ring 57.

3. *Continue with assembly. Submit end item to TRW/MRB. 5-25-70

Description of Supplier's proposed corrective action: Include effectivity point by: Serial numbers, lot, date, etc.)	List all SIR's previously submitted against this part number: SIR SERIAL NUMBERS	DATE ISSUED
BBRC technical personnel are continuing their effort to help Electro-Tec improve the manufacturing processes	11827	3/23/70
	11828	3/25/70
	11088	5/21/70

WILL YOUR SCHEDULE BE AFFECTED? Yes IF YES, IN WHAT WAY? Delayed, if unit is unacceptable

RECOMMENDATIONS TO SUPPLIER	TRW SYSTEMS GROUP QUALITY ASSURANCE CONCURS IN THE RECOMMENDATIONS TO THE SUPPLIER, AS APPLICABLE. THIS IS NOT TO BE CONSTRUED AS TRW SYSTEMS GROUP QA ACCEPTANCE OF MATERIAL.
REPAIR PER PROPOSED DISPOSITION NOTED ABOVE. INSULATION REPAIR SHALL FORM WITH TRW REPAIR SPEC PR1-1 USING SHR TUBING SPEC 57	TRW SYSTEMS GROUP QA [illegible] DATE 5-25-70
	CONCURRED: AFQA [illegible] DATE [illegible]
ENGINEERING SIGNATURE [illegible] DATE [illegible]	MATERIEL SIGNATURE [illegible] DATE [illegible]

NO. 11[illegible]

[illegible] SPACE PARK [illegible] BEACH CALIFORNIA

0-412

SUPPLIER INFORMATION REQUEST (SIR)

INSTRUCTIONS TO SUPPLIER:

1. Use this form to request preliminary evaluation only of defective material.
2. Contact Buyer, prior to initiating this request, for his direction.
3. Processing of this SIR and resultant comments by TRW SYSTEMS GROUP should not be regarded as relieving the Supplier in any way of his contractual obligations, but as only a preliminary recommendation.
4. Combination of SIR's on the same lot of parts, or latent defects not detectable at the time of preliminary evaluation, may show the items to be unacceptable.
5. Do not ship material, or submit to TRW SYSTEMS GROUP Source Inspection, until this form has been processed by TRW SYSTEMS GROUP and returned to you.
6. Include in all shipments of finished parts: (1) original SIR, (2) Certificate of Conformance referencing SIR serial number, (3) Shipper referencing SIR serial number.

SUPPLIER'S NAME AND ADDRESS: Ball Brothers Research Corp. Boulder, Colorado 80302

INITIATED BY: H.E. Christensen | TITLE: QA Engr. | PHONE: 444-5300 | DATE INITIATED: 25 August 197

PURCHASE ORDER NO.: BF 501-SC | BUYER: F.R. GROSS | MJC NUMBER: 1757-44

PART NUMBER: 32701-1 | REV.: J | PART NAME/DESCRIPTION: Despin Mechanical Assy. | QUANTITY AFFECTED: 1 | SERIAL NUMBER(S): 3-2

Description of defect and probable cause (showing zone location of drawing). Provide sketch, as required, in sufficient detail and clarity for full understanding of defect and proposed corrective action:

DISCREPANCY: TS 36469 "A", para. 4.4.2 requires that the motor voltage and current be monitored during random vibration. During the vibration run of the Y-axis, the test operator failed to place a test console switch in the correct position. Result was that the voltage and current on motor #1 was not recorded on a strip chart (monitored).

NOTE: Voltage and current prior to and after vibration run of Y-axis was checked and found to be acceptable. Also, voltage and current was monitored during vibration of X and Z axes and was acceptable. This discrepancy is not considered to be a failure and no failure report will be issued.

RECOMMENDED DISPOSITION: Use as is. S/N 3-2 only (conc.)

C. K. Carlinecht

Description of Supplier's proposed corrective action: (Include effectivity point by: Serial numbers, lot, date, etc.)

Operator and QA inspector have been instructed to double check test set-up prior to start of actual vibration run Deviations on S/N 3-2

List all SIR's previously submitted against this part number:

SIR SERIAL NUMBERS		'70 DATE ISSUED	
11833	11087	4/27	5/08
11834	11724	4/30	7/27
11086		5/08	

WILL YOUR SCHEDULE BE AFFECTED? Yes IF YES, IN WHAT WAY? Delayed if disposition is unacceptable.

RECOMMENDATIONS TO SUPPLIER: SUBMIT TO TRW FOR MRB ACTION

TRW SYSTEMS GROUP QUALITY ASSURANCE [illegible] TIONS TO THE SUPPLIER, AS [illegible] AS TRW SYSTEMS GROUP [illegible] OF MATERIAL.

TRW SYSTEMS GROUP QA [signature] DATE 9-1-70

CONCURRED AFQR [signature] DATE [illegible]

ENGINEERING SIGNATURE [signature] DATE 9-1-70

MATERIEL SIGNATURE [signature] DATE 8-28-70

SIR RECEIVED BY (SUPPLIER) DATE

MATERIAL SHIPPED TO TRW SYSTEMS GROUP [illegible]

SYSTEMS [illegible]

DMA S/N 3-1

(FLIGHT SPARE)

DMA S/N 3-1

UNIT DISCREPANCY HISTORY AT BBRC

DATE	DISCREPANCY	DISPOSITION
5-25-70	MOTOR — STATOR KEEPER IS RUSTY	REWORK, RETEST
6-11-70	MAGNETIC PICKUP .005 MIN. DIM. IS FLUSH	USE AS IS
	.044/.040 DIM. IS .046 - .048	USE AS IS
	WIRE CRIMPED AT BASE OF STRAIN RELIEF	RETURN TO VENDOR
	SHIELD DAMAGED WHERE STRAIN RELIEF IS CUT	RETURN TO VENDOR
	POTTING IS CRYSTALIZING ALL 3 PICS	REWORK AT BBRC
	TIP IS DAMAGED	REWORK AT BBRC
6-10-70	.400 - .398 DIA IS .3969, .3951	USE AS IS
	.336 - .334 DIA IS .3332	USE AS IS
	STAPLE THROUGH WIRE B-21	REWORK
7-1-70	INNER SHIELDINGS ARE FRAYED	REWORK AT BBRC (22) RETURN TO VENDOR (6)
3-5-70	BRACKET MOUNTING MIRROR .570 ± .010 DIM. IS .596	USE AS IS

DATE	DISCREPANCY	DISPOSITION
5-21-70	SLIP RINGS — RINGS 69 & 70 (SPARE RINGS) ARE SHORTED TOGETHER INTERNALLY (CAUSED BY KNOWN VOID IN PLASTIC PRIOR TO PLATING) POWER RING 71 (OR LEAD) SHORTED TO GROUND	SIR # 11088 REPAIR, CUT OFF LEADS TO SLIPRING & BRUSH BLOCK RINGS 70 & 71. TWIST 69 & 73 TO REPLACE PAIR FROM 71 & 73
	DEBRIS BARRIER BETWEEN POWER RINGS 88 & 89 HAS A CHIP OUT OF IT APPROX .050 X .010 DEEP	REPAIR SEE SIR # 11088
	DEBRIS BARRIER BETWEEN SIGNAL RINGS 51 & 52 HAS A CHIP OUT OF IT APPROX .100 LONG & DOWN TO THE GOLD	CUT OFF RING & BRUSH BLOCK LEADS TO RING 52, USE SPARE LEADS FROM SPARE RING 57
	BROKEN SPOT IN OUTER TEFLON JACKET OF SHIELDED LEAD TO POWER RING 67	REPAIR WITH SHRINKABLE TUBING
4-22-70	TORQUE MOTOR — MIN TORQUE AT 80 RPM SHOULD BE 120 OZ-IN., MOTOR #1 WAS 116 OZ-IN. MOTOR #2 WAS 116 OZ-IN.	USE AS IS SEE SIR # 11831

DATE	DISCREPANCY	DISPOSITION
7-27-70	DESPIN ASSY — SIGNAL RINGS: P-P NOISE LIMIT 100 MV CIRCUIT PAIRS 17 & 18, 53 & 54 ARE 300 MV P-P	SEE SIR # 11724
7-16-70	DESPIN ASSY — WIRES 5 & 22 TO J4 HAVE PIN HOLES EXPOSING SHIELDING	REPAIR TRW SRP 7-1
	POTTING S/B APPROX .75, IS .27, .70, 1.90	USE AS IS
7-10-70	DESPIN ASSY — WIRE 3 & 4 INSULATION CUT	REPAIR TRW SRP 7-1
	5 & 6 INSULATION CUT	" " "
	WIRE 3 & 4 TO RESOLVER INSULATION CUT	" " "
7-31-70	DESPIN ASSY — J2 CABLE LENGTH 10.5" ± .5 J2 IS 30" J5 " " 30.0" ± .5 J5 IS 10.5	CORRECTED DATA SHEET
	MARKING .19 HIGH, IS .250 HIGH	USE AS IS
7-1-70	DESPIN ASSY — PUNCTURE IN JACKET OF SHIELDED WIRE TO J3	REPAIR
7-10-70	SLIP RING ASSY — INSULATION DAMAGE AT WIRES: 88 & 90, 87 & 89, 83 & 85, 72 & 74, 77 & 75, 73	REWORK AT BBRC SIR # 11734

DATE	DISCREPANCY	DISPOSITION
12-14-70	DESPIN ASSY - ABRADED OUTER JACKET J5 ALSO PIN HOLE	REPAIR
11-9-70	BEARING, BALL RADIAL, SUSPECT RETAINER DELAMINATION 32708-3 SUSPECT RACE SURFACE > 4 μ inch	
	S/N 004 RETAINER ONLY	FOR ENGR TEST ONLY
	S/N 006 RETAINER ONLY	SCRAP
	S/N 038 RACES & BALLS ONLY	RETURN TO VENDOR
11-6-70	32708-1 BALL BEARING, SUSPECT RETAINER DELAMINATION & RACE SURFACE > 4 μ inch	
	S/N [illegible] & 012 RACES & BALLS ONLY	RETURN TO VENDOR
	S/N 005, 006, 011, [illegible], 038 RETAINERS ONLY	SCRAP
	32701-1 S/N 008 RETAINER ONLY	SCRAP
	32708-1 32708-3 S/N 005 RACES & BALLS & RETAINER ACCEPTABLE, BUT DUE TO TIME TO REPROCESS WILL NOT REINSTALL IN DMA 3-1	REPLACE

NOTE: AFTER REWORK FOR SUSPECT BEARINGS, RETAINERS, ETC, UNIT WAS ACCEPTANCE TESTED PER ATP 36469 AS MODIFIED BY TWX 777-SI-3081, 777-SI-3064, AND 777-SI-3090

DATE	DISCREPANCY	DISPOSITION
12-22-70	SPEED CONSTANT SHOULD BE .76 MIN VOLTS/RAD/SEC FOR BOT MOTORS; IS .74 VOLTS/RAD SEC	USE AS IS NCR 4+852
	NO LOAD SPEED SHOULD BE 220 RPM MAX; IS 231 AND 236 RPM FOR MOTORS 1 AND 2 RESPECTIVELY	USE AS IS NCR 4+858

NOTE: VENDOR TDR's: #V57209
V57225
V58617

DMA S/N 3-3

(FLOWN ON 9431)

DRA S/N 3 S/N 3-3 (S/C 3-1)

UNIT DISCREPANCY HISTORY AT BPRC

DATE	DISCREPANCY	DISPOSITION
8-12-70	Unsupported AWG bundles could rub against resolver stator	Loops laced to rotor
	Harness cable to J2 riding on nut	Covered with shrink tubing
	Two spot ties loose, 1 ea J7, 1 ea J5	Replaced laces
	Magnetic pickup has small dings on each side	Performed bench test
	Magnetic pickup has .004 over pipper but .001 over one edge, S/B .004/.006 dim. pipper to actuator.	Reworked & retested
	Minor scratches on housing finish	Use as is

DMA S/N 3-3 DISASSEMBLED FOR INSPECTION OF SUSPECT BEARINGS ... BBRC

DATE	DISCREPANCY	DISPOSITION
11-29-70	Case ground wire spec is .10 Ω max. Housing to J4 shell is .13 Ω " " J5 " " .14 Ω " " J6 " " .14 Ω	Clean slipring surface free of epoxy and retest

NOTE! • ALL BEARINGS & SEPARATORS WERE ACCEPTABLE

• THERMISTOR CONNECTIONS WERE REWORKED PER SPECIAL REWORK INSTRUCTIONS (SIR 12851)

• ACCEPTANCE TEST MODIFIED PER TWX 777-51-3017, 777-51-3053, 777-51-3064

~~DMA S/N 3-4~~

~~UNIT FLOWN ON FLIGHT 2 (9432)~~

DMA S/N 3-4

(FLOWN ON 9432)

70

DMA S/N 3-L' (S/C 3-2)
S/N 3-4

UNIT DISCREPANCY HISTORY AT BBRC

DATE	DISCREPANCY	DISPOSITION
8-3-70	MOTOR #2 WIRE 7-8 ABRADED INSULATION NEXT TO MOTOR	USE AS IS
7-23-70	SLIPRING ASSY — WIRE # 70 — SPLIT INSULATION 37 — CUT " 71 & 73 ABRADED INSULATION 77 & 75 CUT INSULATION 68, 79 & 81 SPLIT INSULATION	RWK TO DWG
8-10-70	UNSUPPORTED HARNESS COULD RUB AGAINST RESOLVER STATOR	REWORKED LOOPS
8-25-70	BROKEN BARRIER BETWEEN CKTS 87, 86, 85, AND 84	REWORKED— CONNECTED LEAD #84 TO PIN 45 (J2 & J5) INSTEAD OF PIN 28. CONNECTED LEAD #86 TO PIN 28 (J2 & J5) INSTEAD OF PIN 45.
9-10-70	SHIELDING ON 6 MOTOR WIRES WILL NOT ACCEPT SOLDER. SHIELDS TURN BLACK WHEN HEAT IS APPLIED.	REWORK PER P-110359

DMA · 4
3-4

2

DATE	DISCREPANCY	DISPOSITION
9-25-70	SLEEVING INSULATION DAMAGED (2 PLCS) J5	REPAIR
11-6-70	P/N 32708-3 S/N 037 RACES & BALLS ONLY SURFACE FINISH 4 TO 8 MICROINCHES,	RETURN TO VENDOR
12-1-70	P/N 32708-1 S/N 037 RETAINER ONLY, UNACCEPTABLE TO QAD #57A	SCRAP
12-1-70	P/N 32708-3 S/N 039 RACES & BALLS ONLY, TOOL MARKS OR SCRATCHES IN BALL TRACK	USE FOR ENGR TEST
12-1-70	P/N 32708-3 S/N 004 RETAINER ONLY	USE FOR ENGR TEST
	S/N 006 " "	SCRAP
	S/N 038 RACES & BALLS ONLY	RETURN TO VENDOR
	S/N 028 RACES, BALLS, & RETAINERS	REWORK
	S/N 016 " " "	REWORK
12-3-70	WIRE BROKEN OFF NEXT TO POTTING ON THERMISTOR #1	REWORK
12-5-70	ACTUATOR HIT A NUT HOLDING AN ACCEL. (ACCEPTANCE TEST)	–
	ACTUATOR P/N 32733-1	SCRAP
	BRACKET P/N 32734-1	RWK TO DWG

DMA S/N 3-6

(FLOWN ON 9434)

DMA S/N 3-6 ([illegible])

UNIT DISCREPANCY HISTORY AT BBRC

DATE	DISCREPANCY	DISPOSITION
3-10-70	Mirror mounting bracket dim. is 0.596, S/B 0.570 ± 0.010	Use as is
4-23-70	Bell end assy – 1.360 dia., minor oversize, 1.364 MAX	Use as is
	0.062 +/- .010 dim undersize, 0.043 MIN	Use as is
1-1?-70	Resolver assy – 2.5000/2.5001 DIA, out of round (4 PARTS)	Use as is
12-3-70	Slip ring assy – 3 wires with damaged insulation	Repaired per TRW SRP 7-1
	Reservoir cup length S/B 7.815 inch ref, is 7.817	Use as is
	Signal circuit number 8 has high meg reading and high pot short.	Repaired – cut leads to circuit 8. Connected slip ring spare circuit #57 to pin 37 of connectors J4 & J1. Left pin 26 of J3 & J6 blank

DATE	DISCREPANCY	DISPOSITION
NOTE:	DMA 3-6 DISASSEMBLED FOR INSPECTION OF SUSPECT BEARINGS AT BBRC	
11-30-70	P/N 32708-1 Bearing retainers – following S/N unacceptable: 003, 005, 006, 018, 026, 038	Scrap
11-30-70	P/N 32708-1 Races & balls only — S/N [illegible] had scratches in ball track. S/N 012 had surface finish of 4 TO 8 microinches	Return to vendor
12-1-70	P/N 32708-3 Bearing retainer S/N 006 unacceptable	Scrap
	Races & balls only S/N 038, surface finish unacceptable is 4 to 8 microinches	Return to vendor
12-[illegible]-70	magnetic pickup — wire #3 broken during potting of J1	Repair, install new pin

NOTE: • AFTER REPROCESSING OF BEARINGS, UNIT REASSEMBLED PER P-110330 AND 32701

• PERFORMED ACCEPTANCE TEST PER ATP 36469

APPENDIX E SYSTEM SIMULATION

The simulation used to study the 777 anomalies is the digital simulation SIM777 which is documented in References 2 and 3. Description of the system will not be repeated in this appendix, but the simulation block diagram is shown in Figure E-1 for easy reference. For this study, two modeling changes were made -- in the motor and in the rate mode integrator.

E1 Motor Model

A block diagram of the motor is shown in Figure E-2.* The input voltage to the motor is the signal voltage from the control system, e_m. In the model, e_m is limited (e_{VL}), combined with the back emf (e_{emf}) and then multiplied by the motor torque constant, $K_m = K_I/R$ to yield the motor control torque, T_m^L. As can be seen from the diagram, T_m^L is indirectly a function of the relative spin speed Ω because the back emf varies as $e_{emf} = K_V \Omega$ where K_V is the motor speed constant. Table E-1 lists the nominal parameter values for this motor model.

In the original simulation, the relative spin speed Ω was nearly constant because only small platform rate variations were considered. Thus the back emf was modeled as a constant. However, in this study Ω could no longer be considered a constant.

The motor as it appears in the simulation program is shown in Figure E-3. Note that the first voltage limiter is neglected on the assumption that the current limit takes effect before the voltage limit is reached. With this assumption, the two motor models in Figures E-2 and E-3 are equivalent. In Figure E-3 the current limit is represented by an effective torque limit and the back emf is expressed as equivalent torque.

---

* This model was incorporated into the simulation prior to development of the motor model of Appendix F and the motor tests repeated there. A new simulation model reflecting these later analyses and test results is under development.

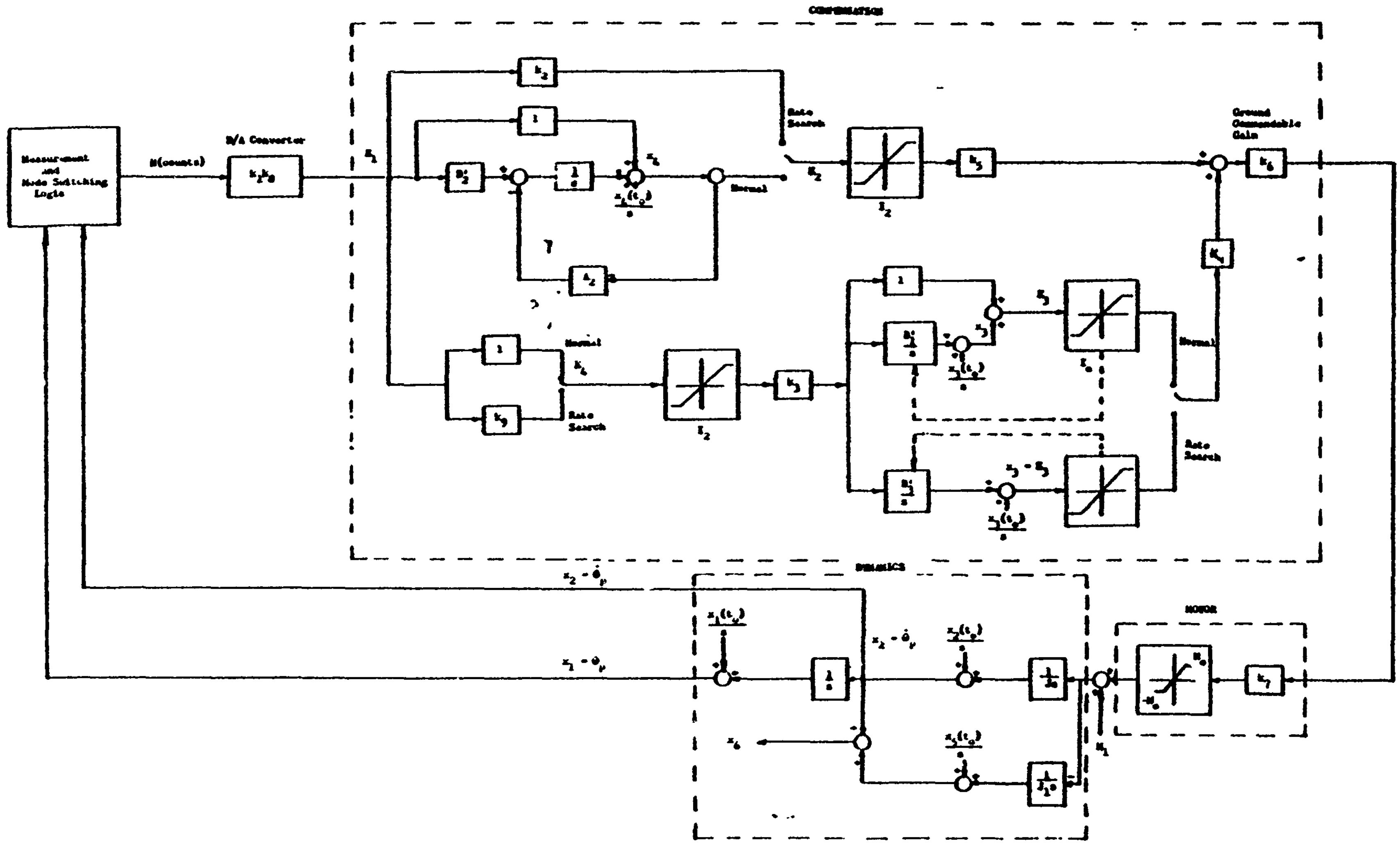

Figure E-1 Program 777 Despin Controller Simulation Model

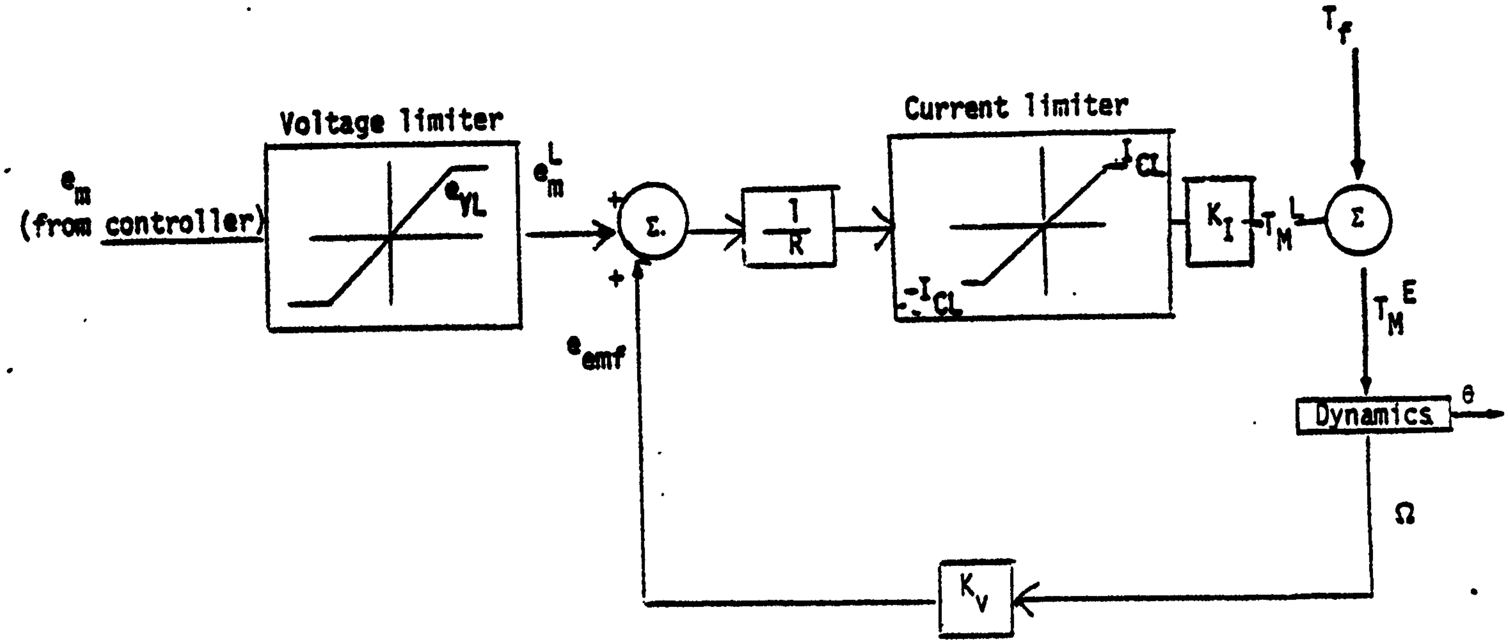

Figure E-2 Motor Model

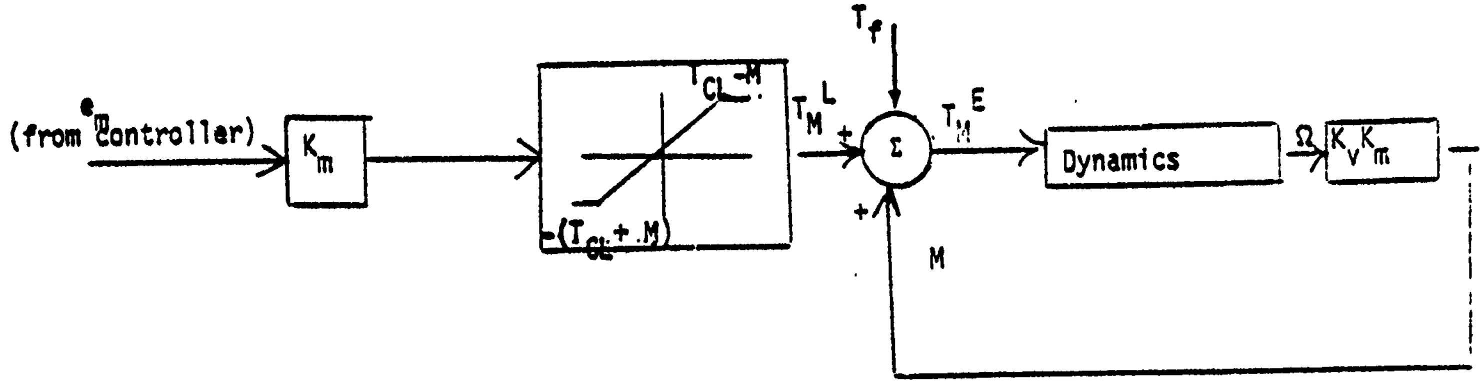

$K_m = K_I/R$

$M = K_m \, e_{emf}$

Figure E-3 Motor as Simulated in SIM 777

TABLE E-1. MOTOR MODEL PARAMETERS

VARIABLE	VALUE	DESCRIPTION
K_m	0.0516 ft-lb/volt	Motor Torque Constant
K_v	0.81 volts/rad/sec	Motor Speed Constant
Ω	rad/sec	Relative Spin Speed
K_I	.542 ft-lb/volt	Motor Torque Constant
R	10.5 ohms	Motor Winding Resistance

One other change to the motor model was in the torque limits of the motor, T_{CL}. In the past, values of T_{CL} ranging from 140 in-oz to 200 in-oz were used. However, on further investigation, it was discovered that the maximum output of the motor (assuming square wave current waveforms) is in the form of a fully rectified sine wave, which varies between 140 in-oz and 200 in-oz as shown in Figure E-4.

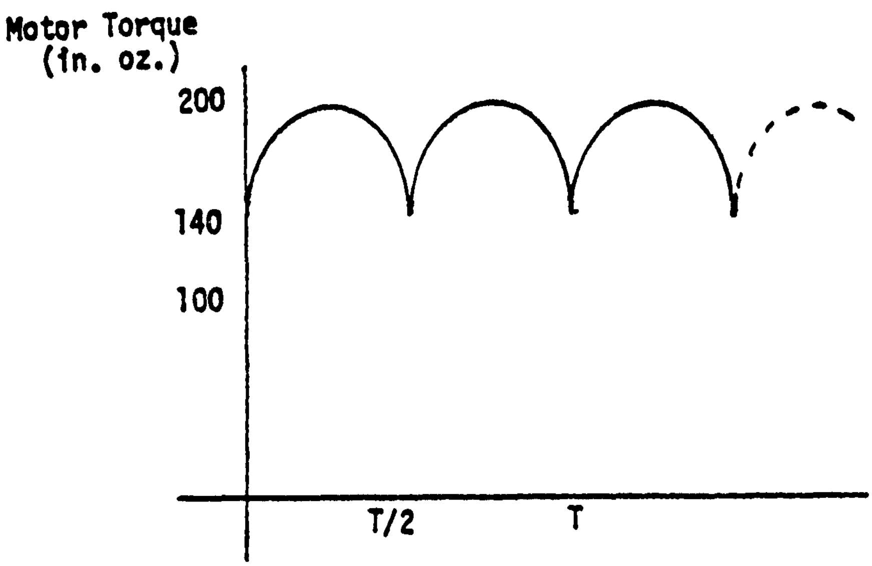

Figure E-4 Motor Torque output

The average value of this waveform is 178 in-oz. This is an extreme upper bound, assuming a nominal value for the motor torque constant. For this study, a value of 170 in-oz was used for simulation.

E.2 Integrator and Amplifier Saturation Models

The electronics of the 777 spacecraft uses operational amplifiers in the realization of some of the filters. Because of the required range of operation, some of these amplifiers are driven into saturation. If an amplifier becomes saturated it will not respond to changes in the input signal until the signal has changed by such an amount so as to allow the amplifier to operate in the linear region again. In the original 777 simulation (Reference 3) one of these saturation effects was not properly modeled.

More specifically, this modeling deficiency affects the operation of the integrator circuit in the rate mode since this amplifier is the one most likely to go into saturation. In addition, the previous simulation limits on the voltage output of this integrator have not taken into account a Zener diode which makes the limits unsymmetric. This section present a model for the integrator in the rate mode, taking into account the effects of saturation and the unsymmetric limits.

A simplified diagram of the integrator circuit is shown in Figure E-5. If the amplifier is in the linear range, the equivalent circuit is Figure E-6, and the transfer function is:

$$\frac{V_{out}}{V_{in}} = \frac{-Z_2(s)}{Z_1(s)} = \frac{-1}{RC\ s}$$

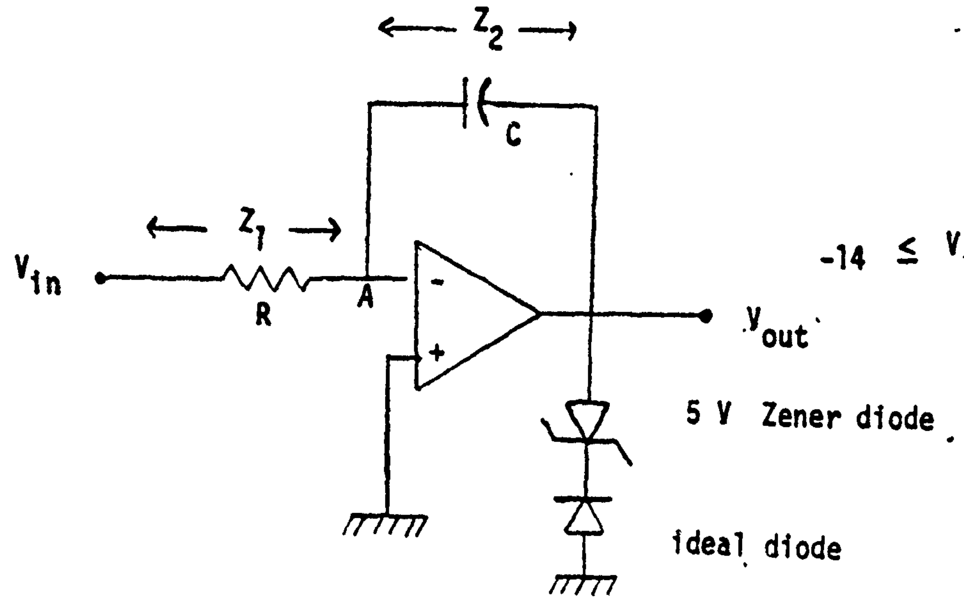

R = 12.7 Meg

C = 9 µf

$-14 \leq V_{in} \leq 14$ v

Figure E-5 Simplified Integrator Circuit

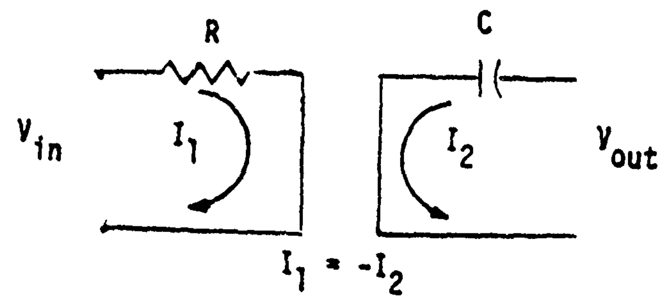

$$V_{out} = -\frac{1}{RC}\int V_{in}\,dt$$

Figure E-6 Equivalent Circuit in Linear Region

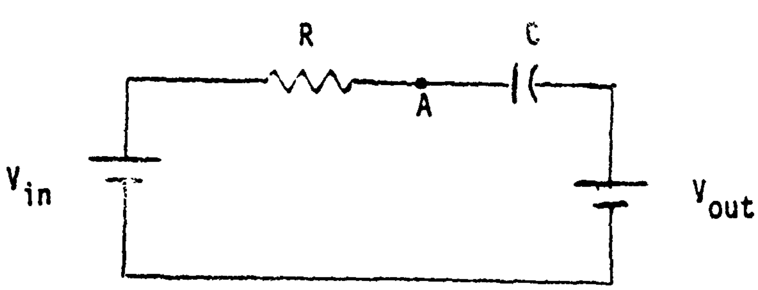

$$V_{out} = \begin{cases} -5 \text{ v} \\ \text{or} \\ +14 \text{ v} \end{cases}$$

$$V_c = V_{in} - V_{out} + (V_{c\,\text{initial}} - V_{in} + V_{out})\, e^{-t/RC}$$

Figure E-7 Equivalent Circuit in Saturated Region or

$$V_{out} = \frac{-1}{RC} \int V_{in}\, dt$$

The saturation limits for V_{out} are :

$$V_{+sat} = 14 \text{ volts}$$

$$V_{-sat} = -5 \text{ volts (limited by Zener diode)}$$

(The limits on V_{in} are $\pm$ 14 v)

Figure E-6 is a correct model for the amplifier as long as the voltage V_A at the summing junction is ≈ 0 volts.

Once in saturation, however, the voltage at the summing junction is no longer zero. The equivalent circuit becomes that of Figure 2-7, which shows that the capacitor can charge up to $V_{in} - V_{out}$. If V_{in} is at its maximum level this means that the capacitor can charge up to -28 volts ($V_{in} = -14$, $V_{out} = +14$) or +19 volts ($V_{in} = 14$, $V_{out} = -5$) with a time constant of RC = 114 sec. Once the input voltage starts to change, the capacitor will start to discharge with the same time constant, until the voltage at the summing junction, V_A is 0 volts. During this time, the output voltage remains in saturation. The equivalent circuit for both charging and discharging of the capacitor in the non-linear region of the amplifier is shown in Figure E-7

Since the differential equation for the voltage V_c across the capacitor in this region is

$$-V_{in} + [V_{out}\,(sat)] + RC\,\frac{dV_c}{dt} + V_c = 0$$

then

$$V_c = V_{in} - V_{out}(sat) + [V_{c_{initial}} - V_{in} + V_{out}]e^{-t/RC}$$

The transfer function is

$$\frac{V_c}{-V_{in} + [V_{out}(sat)]} = \frac{1}{RC\ s + 1}$$

The above equations are valid until V_c has discharged to $-V_{sat}$, at which time $V_\beta = 0$ (the voltage at the summing junction) and the amplifier is in the linear region again.

The block diagram of the system is shown in Figure E-8. As long as the amplifier is in the linear range of operation, the output V_{out} (or E_3) is the same as the capacitor voltage V_c (or X_3). Once the amplifier saturates the output E_3 is the saturation voltage, and remains there until the input voltage V_{in} (or E_4) switches direction sufficiently allowing the capacitor voltage X_3 to discharge. When X_3 has discharged to the point where $E_4 + E_3 = 0$, the circuit is again in the linear mode of operation, and E_3 comes out of saturation.

Old Model - Rate Mode

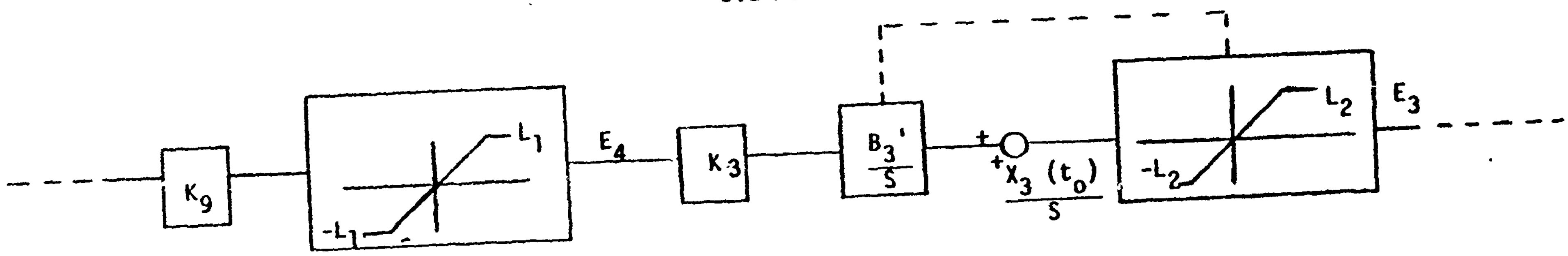

New Model - Rate Mode

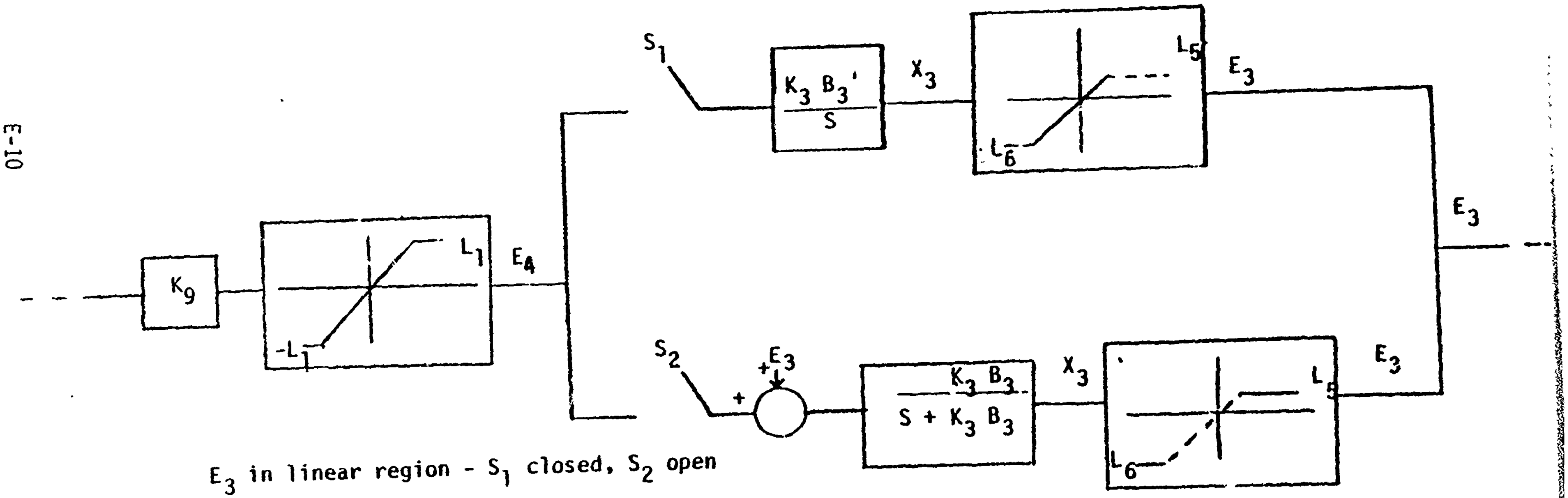

E_3 in linear region - S_1 closed, S_2 open

E_3 in non-linear region - S_1 open, S_2 closed

Figure E-8. Block Program of Rate Mode Integrator

TABLE E-2 VALUES FOR FIGURE E-7

Symbol	Value	Description
B_3	0.0667 sec^{-1}	Integrator gain (rate/search mode)
K_3	0.131	Integrator Gain
K_9	183.9	Integrator Input Path Gain
L_1	14 volts	Saturation level
L_2	14 volts	Saturation level
L_5	5 volts	Saturation level
L_6	-14 volts	Saturation level

APPENDIX F. MOTOR ANALYSES

1. Motor Model with Saturation

For analytical purposes, the motor and its drive circuitry (including the DEA current limit) have been modelled as shown in Figure F-1. Key parameters are I_m (current limit level) and I_c (commanded current level) where

$$I_c = \frac{K_V V_c - K_B \omega}{R} \quad \text{or} \quad I_c = \frac{V_B - K_B \omega}{R} \tag{1}$$

whichever is less, where: V_c is the compensated error signal; K_V is the voltage gain (7.85 volts/volt); ω is the rotor-platform relative rate; K_B is the back-emf constant (0.765 volts per rad/sec); R is the effective motor resistance (including DEA effects); and, V_B is the effective bus voltage (with fixed DEA voltage drops considered). Note that two types of saturation can occur:

(i) limiting due to I_c exceeding I_m

(ii) limiting due to $K_V V_c$ exceeding V_B

This analysis formulates torque, power, and total current as a function of $k = I_m/I_c$.

With the assumption of no phase shift between the magnetic field and the drive waveforms:

- Torque: $T_m = K_m(f_1 \sin 8\Theta + f_2 \cos 8\Theta)$
- Power: $P = R(f_1^2 + f_2^2)$ (2)
- Current: $|I| = |f_1| + |f_2|$

where the drive current waveforms are given by:

$$f_1 = \underset{I_m}{\mathrm{sat}}\{I_c \sin 8\Theta\} \quad f_2 = \underset{I_m}{\mathrm{sat}}\{I_c \cos 8\Theta\} \tag{3}$$

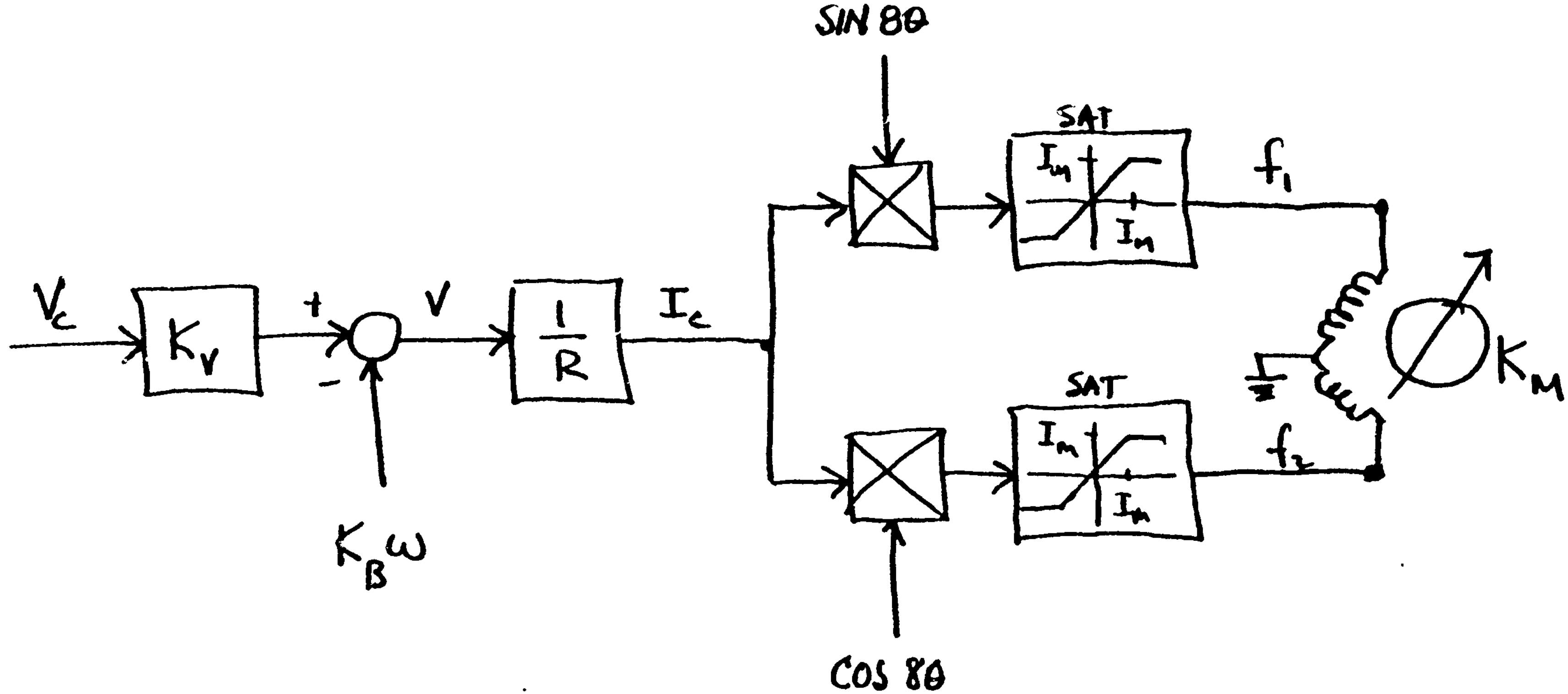

$$T_M = K_M(f_1 \sin 8\theta + f_2 \cos 8\theta)$$

FIGURE F-1. MOTOR MODEL FOR ANALYSIS

For rotational convenience, define $\psi = 8\theta$.

In the unsaturated case ($I_c \leq I_m$), the average torque, power, and current are given by:

$$\begin{aligned} T_{mAV} &= K_m I_c \\ P_{AV} &= R I_c^2 \\ |I|_{AV} &= \frac{4}{\pi} I_c \end{aligned} \tag{4}$$

The expressions for average torque, power, and current are considerably more complex with $I_c > I_m$. In this case, f_1 and f_2 become clipped sinusoids, approaching quadrature square waves in the limit. Employing the fundamental equations above:

$$\begin{aligned} T_{mAV} &= K_m I_m \left\{ \frac{2}{k\pi} \left(\sin^{-1} k + k\sqrt{1-k^2} \right) \right\} \\ P_{AV} &= I_m^2 R \left\{ \frac{4}{\pi} \left[\frac{1}{2k^2} \left(\sin^{-1} k - k\sqrt{1-k^2} \right) + \frac{\pi}{2} - \sin^{-1} k \right] \right\} \\ I_{AV} &= I_m \left\{ \frac{4}{\pi} \left[\frac{1}{k} \left(1 - \sqrt{1-k^2} \right) + \frac{\pi}{2} - \sin^{-1} k \right] \right\} \end{aligned} \tag{5}$$

where $k = I_m/I_c$ is less than or equal to unity.

Figure F-2 shows the preceding results graphically, in normalized form. Note that I_c depends upon resistance (hence, winding temperature), spin rate, compensated error signal, and bus voltage, as in equation (1).

2. Effect of DEA Phase Shift

Motor-DEA tests have shown an effective phase shift between the motor excitation and the resolver signals, resulting in a decrease in torque. This torque decrease is a function of I_c (or V_c) and spin rate.

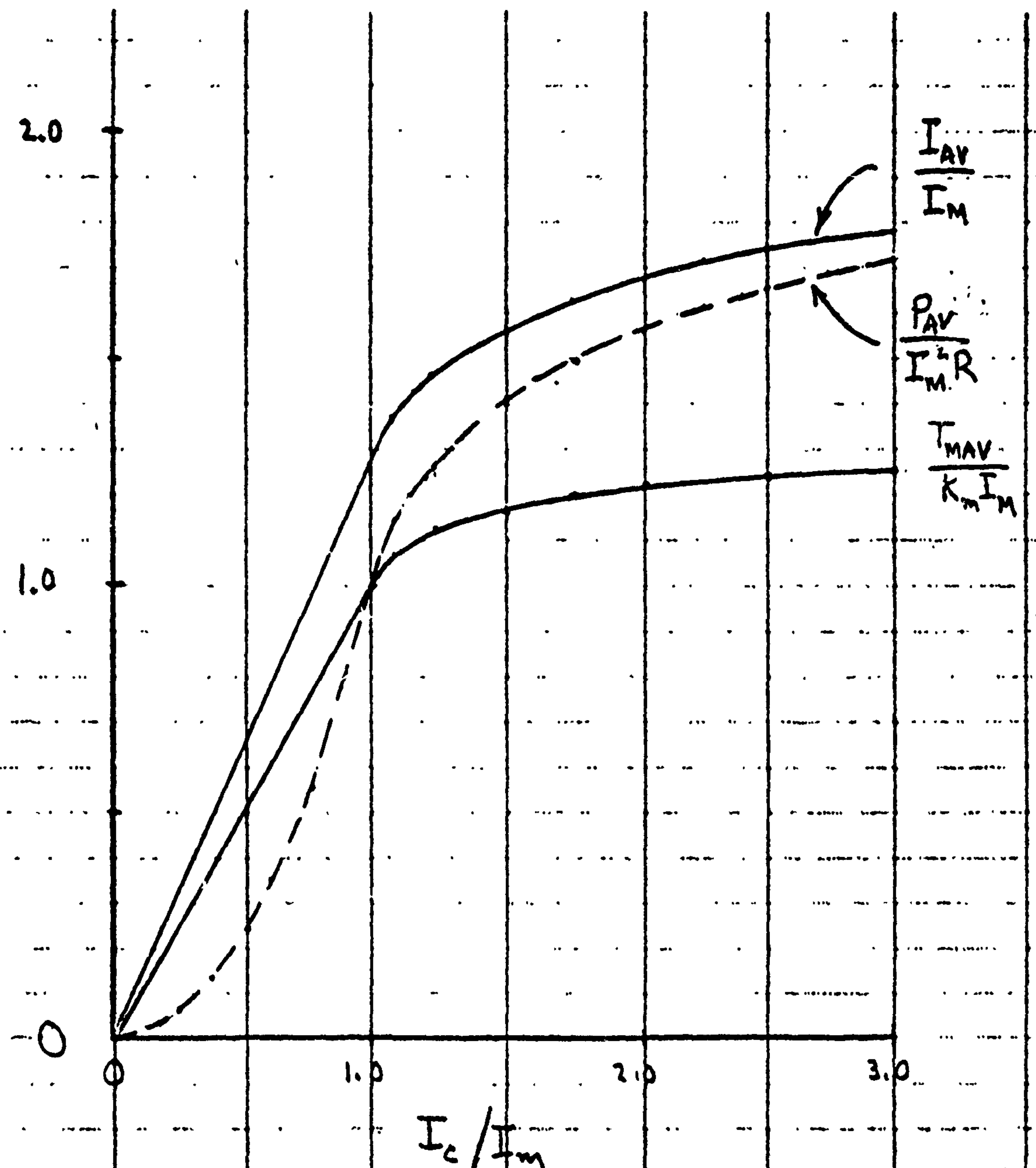

FIGURE F-2. MOTOR TORQUE, POWER, AND CURRENT

The torque equation of (2) can be modified to include an electrical phase shift ϕ:

$$T_m = K_m[f_1 \sin(\psi+\phi)+f_2 \cos(\psi+\phi)] \tag{6}$$

The expression for average torque in the saturated regime becomes:

$$T_{mAV} = K_m I_m \left\{\frac{2}{k\pi}(\sin^{-1} k+k\sqrt{1-k^2}\right) (\cos\phi) \tag{7}$$

where the effect of phase shift is a torque attenuation, as seen in the last term.

The phase shift, ϕ, can be modelled as arising from a time delay, τ, in the electronics. For a spin rate ω:

$$\phi = \omega\tau \tag{8}$$

It has been theorized that the effective increase in phase lag with increased saturation (higher I_c) is due to the decrease in the effective gain of the servo loop around the switching regulator - which causes a reduction in the bandwidth of this loop and, therefore, an increase in its time constant. Using a simple first-order model

$$\tau = \frac{C}{K} = \frac{CI_c}{I_m} \tag{9}$$

showing an increase in τ in proportion to the increase in I_c, with C a proportionality constant which must be analytically or empirically derived.*

Combining (7), (8), and (9):

$$T_{mAV} = K_m I_m \frac{2}{k\pi}\left\{(\sin^{-1} k+k\sqrt{1-k^2})\right\}.\cos\left(\frac{C\omega}{K}\right) \tag{10}$$

Until confirmed by analysis or correlation with test data, the phase shift term should be regarded as speculative.

---

* This model for τ is the simplest available. Detailed analysis of the DEA would yield one more complex and realistic.

3. Interpretation of Torque Voltage Telemetry

The torque voltage telemetry readings are, during normal operation, the only measure of running friction available. With V_c denoting the "torque voltage" (compensated error signal):

$$N = 108\ I \text{ in-oz}$$

$$I = V/R \text{ amps}$$

$$V = 7.85\ V_c - 0.765\omega \text{ volts}$$

yields the nominal torque, N, in inch-ounces (where ω is the platform-rotor relative rate in rad/sec). Note, however, that R (the motor resistance) depends upon the winding temperature, T:

$$R = R_o[1+\alpha(T-77)]$$

with T in °F, $\alpha = 0.00237$, and $R_o = 10.5\Omega$. Note that the effective DEA resistance is neglected in this analysis. In addition, the motor power consumption is given by: $P = V^2/R$.

During the anomaly investigations, winding temperature has been derived as a function of motor power, under steady-state conditions, by thermal simulation of the DMA.* Using this data and the above equations, plots of torque versus torque-voltage can be derived which apply to steady-state operation (see Figure F-3). These results yield somewhat lower levels of running friction than have been estimated earlier without considering motor winding temperature variations.

It should be noted that the equations presented above and used in this analysis are based on unsaturated operation of the drive electronics (current below 1.4 amps).

---

* Motor winding temperature is influenced primarily by motor power dissipation, and can be considered to be independent of diurnal and yearly variations in ambient spacecraft temperatures.

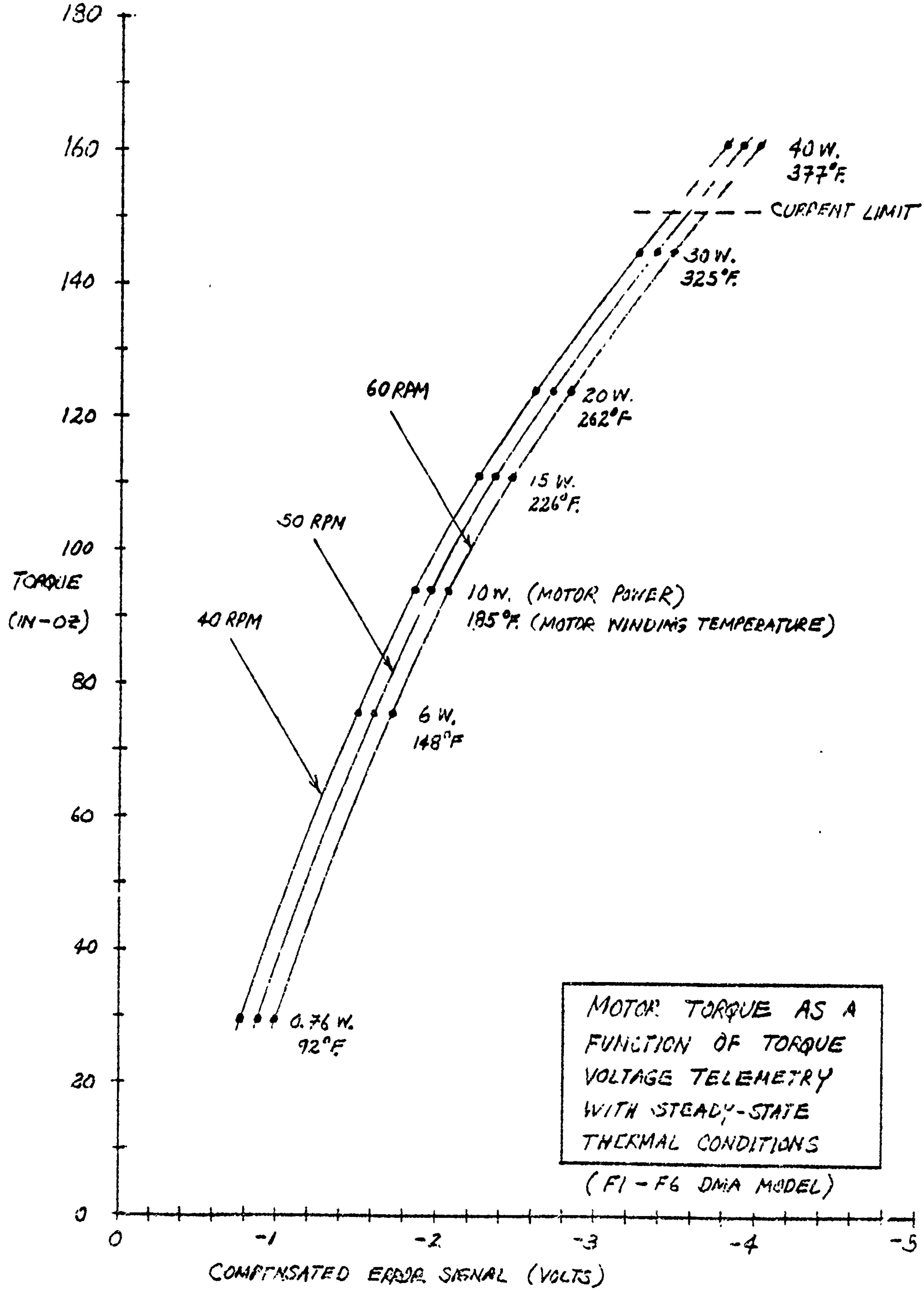

FIGURE F-3. STEADY-STATE RUNNING TORQUE AS A FUNCTION OF TELEMETERED TORQUE VOLTAGE AND SPIN RATE

APPENDIX G

CONSULTANT EVALUATION REPORTS

Presented in this appendix are the evaluation reports received from consultants engaged during the 9433 anomaly investigation.

G.1 REPORT OF D.H. BUCKLEY

NATIONAL AERONAUTICS AND SPACE ADMINISTRATION
LEWIS RESEARCH CENTER
CLEVELAND, OHIO 44135

AMERICAN REVOLUTION BICENTENNIAL 1776-1976

REPLY TO
ATTN OF: 2615

November 14, 1975

Dr. Philip C. Wheeler
TRW, Inc.
Electromechanical Equipment Dept.
One Space Park
Redondo Beach, CA 90278

Dear Phil:

Enclosed herewith are my proposals to your questions relative to DSCS-II.

Sincerely,

Donald H. Buckley

Donald H. Buckley
Head, Lubrication Fundamentals Section

Enclosure

PROPOSALS

1. Assessment of Current Status

From an examination of the data presented, it would appear that failure was a result of inadequate bearing lubrication (lubricant starvation).

2. Hypothetical Scenario

The data presented are typical of those indicating lubricant starvation. This starts with either insufficient initial lubricant supply or loss of lubricant due to evaporation or polymerization. The latter appears to be the case in the present situation. As long as a continuous lubricant film can be maintained in the bearing contact zone and the lubricant does not "dewet" the surface, the bearing torque will remain low and relatively constant (first part of the operational life of these bearings).

With continued operation, if the continuous lubricant film is not maintained, metal-to-metal contact will occur. This will give rise to random spikes in the bearing torque. It can even result in a periodic sustained high bearing torque followed by a sharp decrease when random-chance pickup of some lubricant occurs. These random excursions in bearing torque can continue for some time until sufficient continuous metal-to-metal contact occurs and residual surface oxides are penetrated. At this point in time, the bearing torque will remain high until failure of the bearing ultimately occurs.

3. Related Experience

See NASA TN D-2908, July 1965, by Nemeth and Anderson on the effects of lubricant starvation.

In the various components of Sphynx, QCSEE, Apollo, MJS-77 and Viking, solid film lubricants were used because of the difficulties presented by lubrication with liquids.

4. Recommended Design Improvements

Short-term "fixes" could include means for retaining more liquid lubricant in the bearing and substitution of the lubricant with a liquid that has lower volatility and less tendency to dewet in vacuums. These are means for prolonging life and providing more effective lubrication.

Long-term improvements should include the use of solid film lubricants in place of the liquids. Use of solids eliminates the need for concern over volatility, tendency to polymerize and the dewetting problem. There is already considerable history in the use of these materials in Sphynx, QCSEE, Apollo, MJS-77 and Viking systems.

5. Recommended Process Improvements

Close control of bearing quality and checking very carefully the condition of the lubricant just prior to use and after storage. Changes in liquid lubricant viscosity should be checked just prior to use and IR examinations done.

G.2 REPORT OF DELCO ELECTRONICS

Delco Electronics

General Motors Corporation
Santa Barbara Operations
6767 Hollister Avenue
Goleta, California 93017
(805) 968-1011

November 24, 1975

Dr. P. C. Wheeler
Manager, Electro-Mechanical Dept.
TRW Systems Group
One Space Park
Redondo Beach, Ca. 90278

Subject: DSCS II Anomaly Diagnosis

Dear Dr. Wheeler:

The orbital data presented in our series of meetings suggests a bearing "failure" has occurred in the flight system.

The time-wise generally increasing nature of the following symptoms suggests this failure mode:

1. Increasing average DMA drive torque demand

2. Increasing pointing error excursions. The random nature of these "short term" (.5 ⟶ 5 minute) demand torque "impulses" is typical of performance perturbations observed in smaller high performance bearing assemblies.

The "hang-up" and successful breakaway from the locked condition suggests a dry bearing with a locked retainer during the hang-up interval. The bearing failure is most likely the result of inadequate lubrication for the specific bearing in the flight system.

Factors which probably led to the resultant failure are:

1. Inadequate oil supply in the critical raceway and retainer areas with respect to the demand of the bearing. A hydrodynamic oil film is required to minimize the wear and resulting breakdown of the bearing surface. The bearing raceway and ball surface characteristics greatly influence the oil supply demand for hydrodynamic film lubrication.

2. The oil supply in the raceway and useable retainer areas is marginal at best in the basic design and production process employed for the flight system. This oil supply is being depleted "naturally" during use due to the vapor pressure replenishment demand. The fact that the "bearing-retainer" are operating at an elevated temperature with respect to the "reservoir" provides confidence that the absolute rate of oil loss from the retainer-bearing combination is faster than that of the reservoir per unit surface area. If the temperature were the same, the rate of oil loss from the bearing and the reservoir would be comparable per unit area. The fact that the bearing oil film is thin, and the exposed total bearing retainer surface area large and warmer leads one to question the actual value of the "reservoir" in preventing the bearing oil from depleting its supply while the reservoir is still full. Clearly, better approaches are available in any new design.

3. The bearing surface imperfections must be less than the hydrodynamic film developed due to parts geometry, speeds, loads, and oil supply. The bearing surface finish problems encountered in the build of the flight assemblies suggests this may be a factor.

4. Contamination introduced during the build test-storage cycle may also have affected the life expectancy of the unit by either creating unwettable surface areas or debris, both of which would cause premature wear. A possible source of debris is wear particles from a rotating unlocked inner race rubbing on its adjacent surfaces.

Delco Electronics has been building ball bearing gyros and inertial platform assemblies for more than twenty years. Many forms of premature failure have been observed by the Delco DSCS II anomaly team members during this period of time. Perhaps more directly related to this "failure" are the mutual observations which we made from observing some of your bearing assemblies that were in various TRW DSCS II life test programs. The DMA bearings displayed prominent race and ball wear signs in addition to dark deposits of lube and wear debris on the races and in the retainer ball pockets. Although these bearing assemblies were not judged failures during your tests, they displayed all the visual symptoms of bearings that are in the process of failing. A critical assessment of these bearings clearly supports the position that the observed bearing condition would not have been tolerated on an assembly to be flown.

The aforementioned failure mode possibilities suggest the following design improvements:

1. More lubricant is needed. Many possibilities exist in this area, some of which are (a) increase the amount of lubricant initially introduced in the assembly on all cavity surfaces, (b) increase and elevate the temperature of the reservoirs specifically installed to provide vapor pressure, (c) increase retainer oil capacity, (d) consider periodic automated "oiling" approaches, (e) design a "real reservoir" for the bearings.

2. Reduce bearing oil film demand for long life by (a) reducing the bearing race and ball finish and geometry imperfections allowed, (b) introduce 100% bearing low speed and high speed qualification tests and related pre-post visual inspections to insure no indications of growing torque disturbances, wear and/or wear products are detected during this "burn-in cycle".

3. Review cleaning and DMA processing to insure that all practical steps have been taken to reduce the potential for contamination. Special checks should be made to provide this assurance, both from a surface contamination and debris point of view. Non-rotatable inner races would reduce the possibility of self-generated debris.

These comments reflect the Delco team members general recommendations.

We offer our services in the review of the specific approaches and documented procedures you select to solve this problem. It has been our pleasure to support you in the evaluation of this anomaly. Please feel free to call upon us again.

Sincerely,

Robert Breneman

George Campbell

Ed Loper

Cc: D. Kendall

Attachment to G.2: Gyro Bearings Life Test Data

The data which follows are the results of gyro bearing tests conducted by Delco Electronics. The main parameters for these milliwattmeter-Dynamometer tests are summarized below.* This data is representative of the build-up of torque transients in a bearing with progressive deterioration due to inadequate lubrication. Note that even after the onset of large torque transients (data of 3/11/71), periods of relatively low torque occurred (data of 3/25/71).

Wattmeter Test Parameters

- Lubricant : V-78 with TCP
- Speed : 24,000 rpm
- Bearing Size : R-4

*This method of testing is described in "Gyro Ball Bearings - Technology Today," by A.P. Freeman, February 1968 (presented at the Sixth AGARD Guidance and Control Meeting); see G.3.

BEARING LIFE DATA

SN # 2 Unit # 18005 Brg. Upper ______
Brg. Lower ______

START 12-28-70

Passed ______ Failed ______ Date 12-29-70

Milliwatt Hrs 24 PLD. ______ lbs. Power Level 1.8 watts

19.3 START 313 sec

Total Brg. Hrs 29 Rundown Time 298 sec

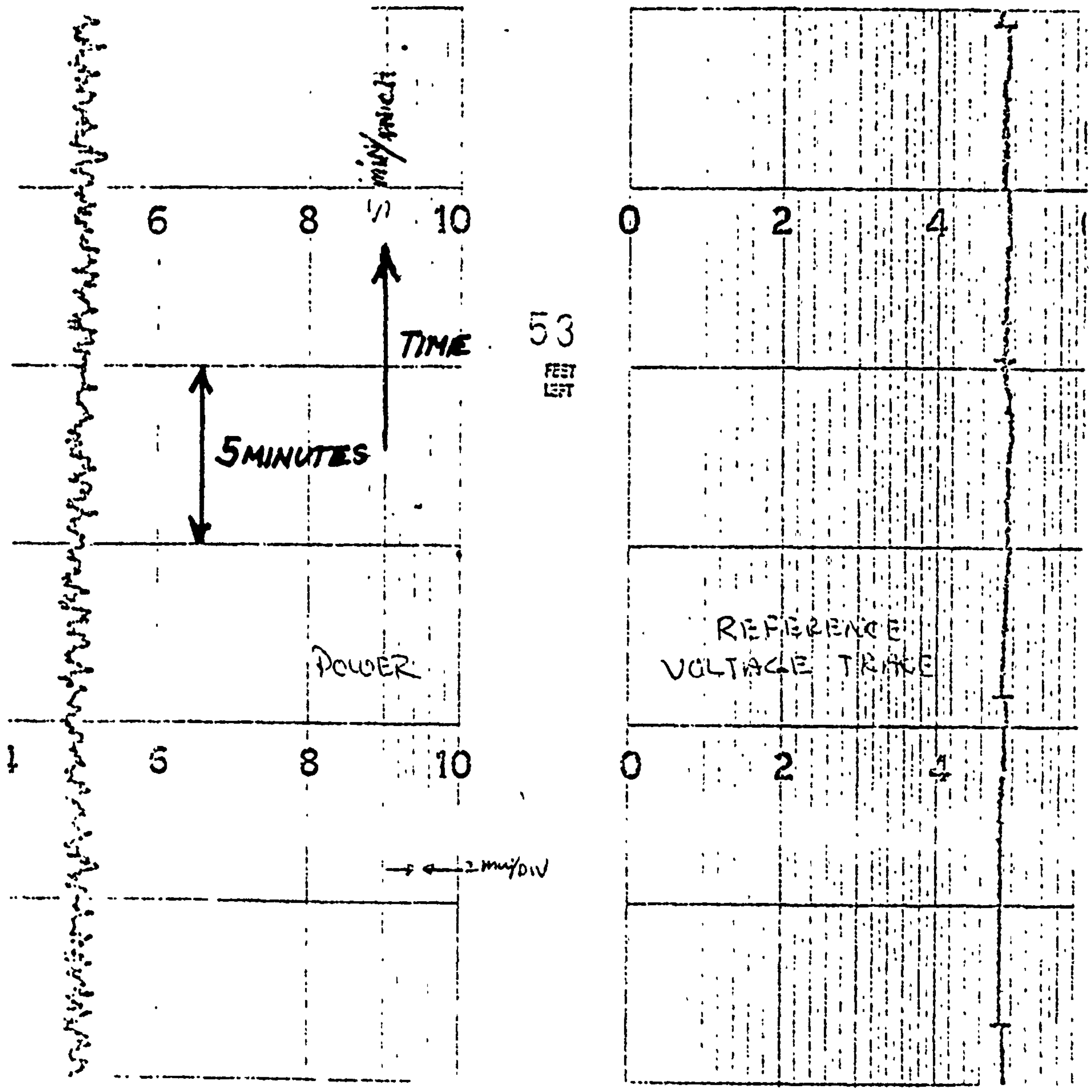

Remarks:

NO JOG

5 to 6 MW HASH SAMPLE FROM 2ND HR ON MW.

BEARING LIFE DATA

MW # 9 Unit # 18005 Brg. Upper ______ Brg. Lower ______

Passed ______ Failed ______ Date 1-7-71

Milliwatt Hrs 24 PLD. 18.6 lbs. Power Level 1.9 watts

Total Brg. Hrs 245 Rundown Time 305 sec

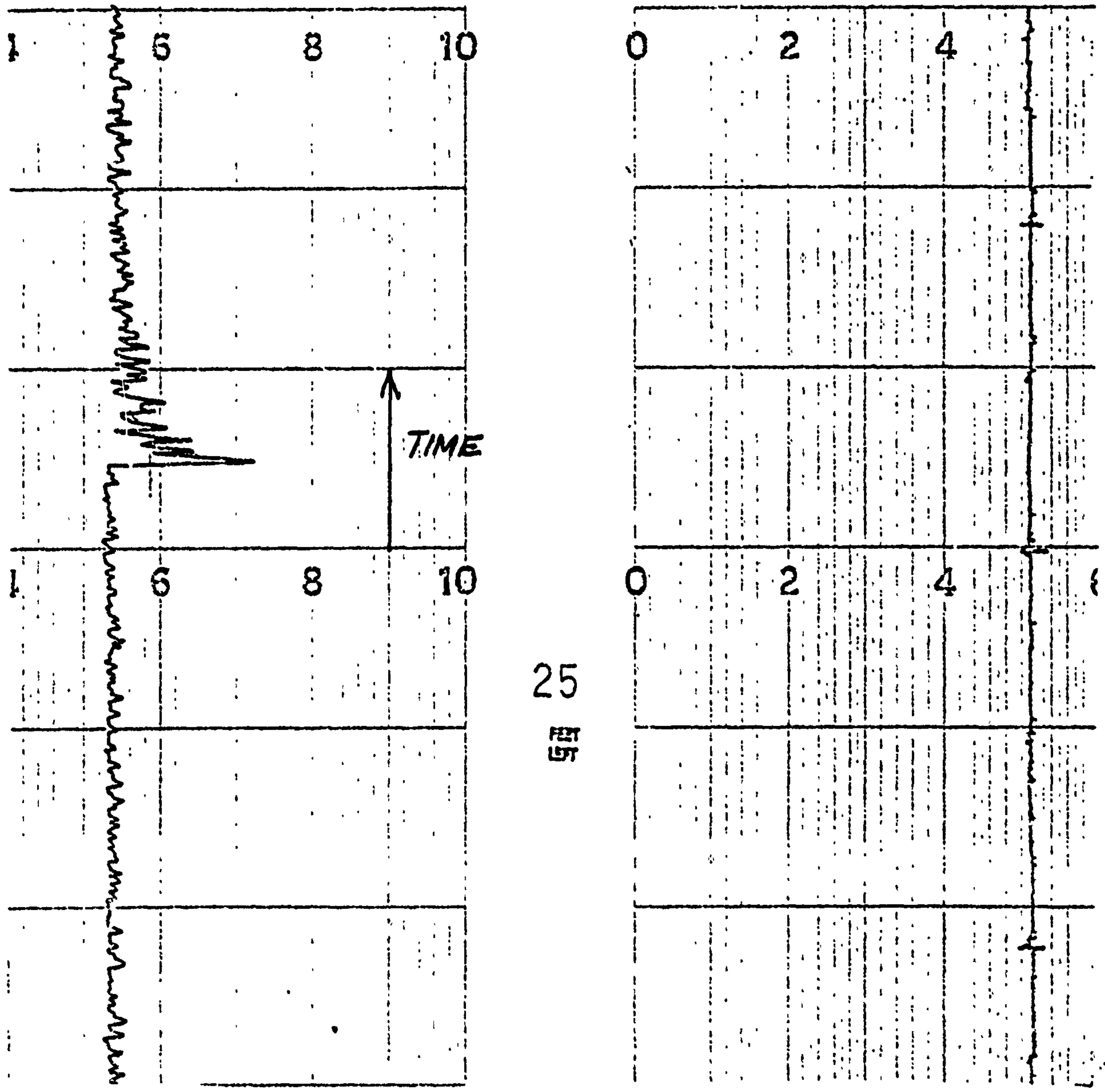

Remarks:

(1) 11 MW CLASSICAL JOG AS SHOWN

(1) 8 MW IRREGULAR JOG

SEVERAL 4 TO 10 MW NEG. & POS. PWR SHIFT

AND SOME 3 TO 4 MW PWR DRIFTS

1 TO 4 MW HASH

BEARING LIFE DATA

W # 6 Unit # 18005 Brg. Upper ______ Brg. Lower ______

Passed ______ Failed ______ Date 1-15-71

Milliwatt Hrs 24 PLD. 20.1 lbs. Power Level 1.8 watts

Total Brg. Hrs 432 Rundown Time 308 sec

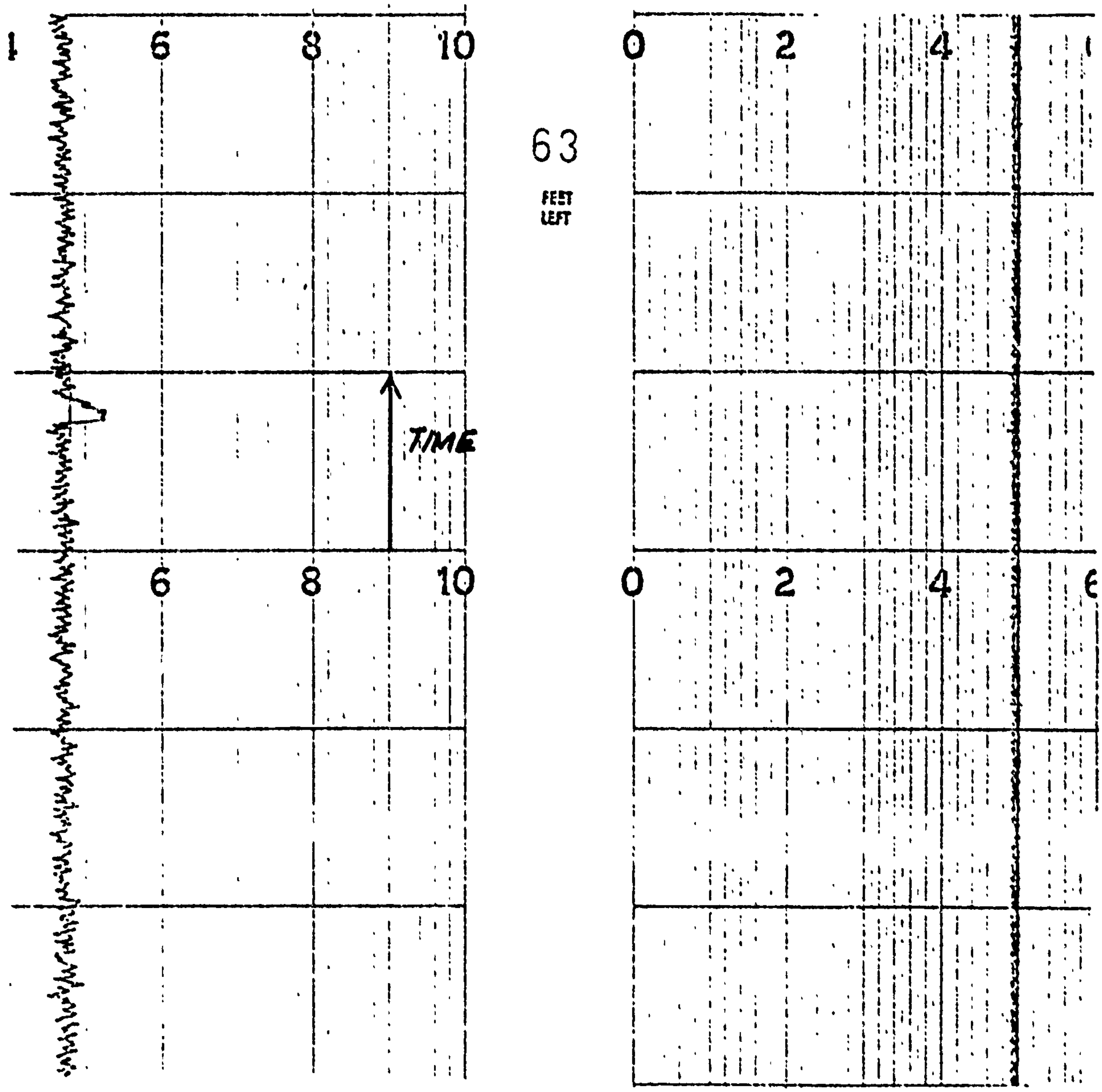

Remarks:

(1) 3 MW JOG SHOWN

LOST 9 HRS OF TRACE — OUT OF STAB LOOP

5 M HASH

BEARING LIFE DATA

5   Unit # 18005   Brg. Upper ________ Brg. Lower ________

Passed ________ Failed ________ Date 1-21-71

Milliwatt Hrs 24   PLD. ________ lbs.   Power Level 1.85 watts

18.8

Total Brg. Hrs 576   Rundown Time 281 sec

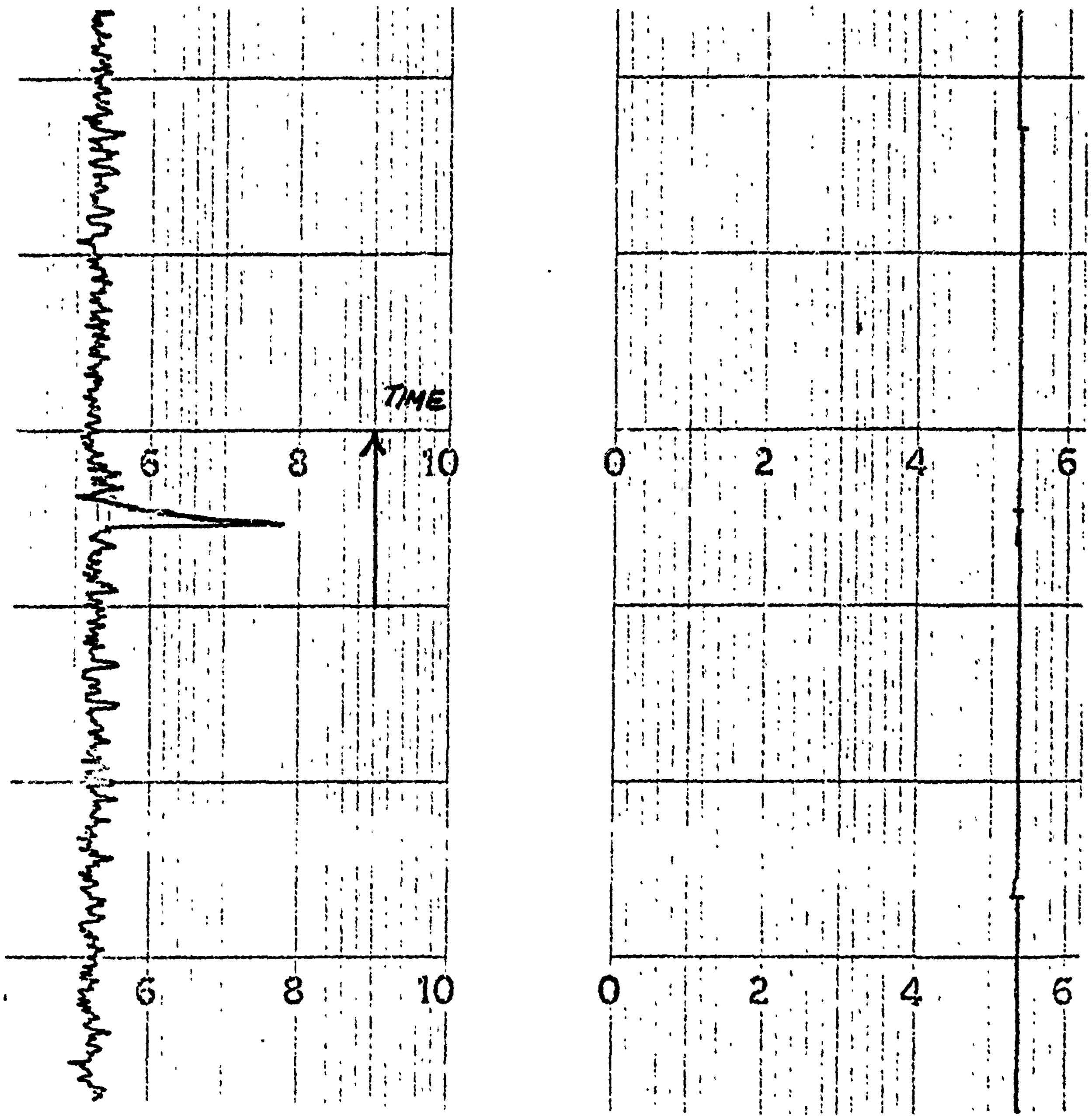

Remarks:

HAD (1) 1 HR PERIOD OF 3 TO 5 MW CYCLING PATTERN

(2) CLASSICAL, SPIKED JOGS AS SHOWN

5 TO 6 MW HASH

BEARING LIFE DATA

Brg. Upper ________
Brg. Lower ________

1   Unit # 18005

Passed ________   Failed ________   Date 1-29-71

Milliwatt Hrs 24   PLD. 15.9 lbs.   Power Level 1.9 watts

Total Brg. Hrs 768   Rundown Time 266 sec

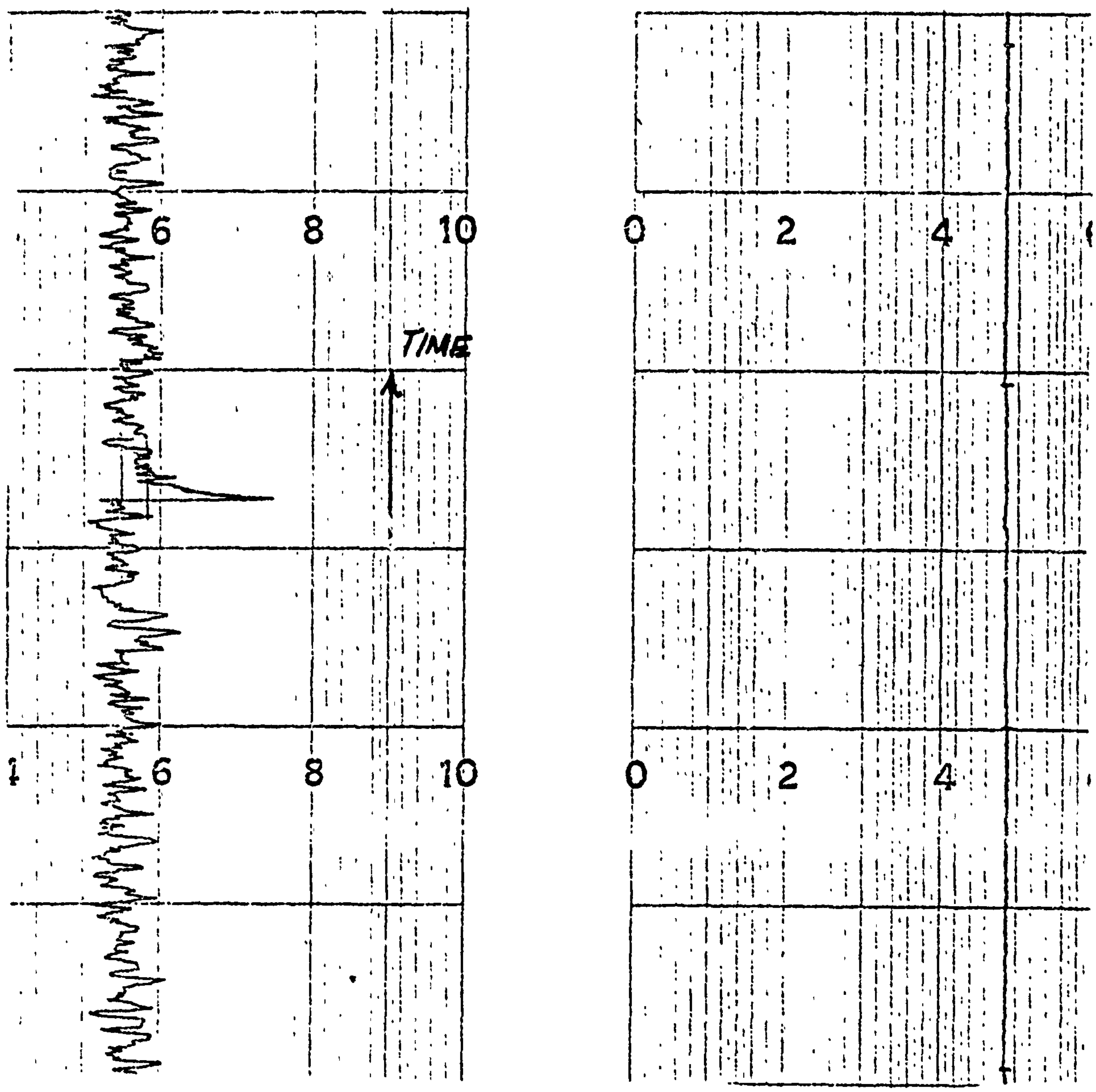

Remarks:
(1) 7MW CLASSICAL JOG SHOWN
8 TO 12 MW HASH

BEARING LIFE DATA

Brg. Upper ______
Brg. Lower ______

\# 4 Unit # 18005

Passed ______ Failed ______ Date 2-5-71

Milliwatt Hrs 24 PLD. 15.6 lbs. Power Level 1.7 watts

Total Brg. Hrs 936 Rundown Time 286 sec

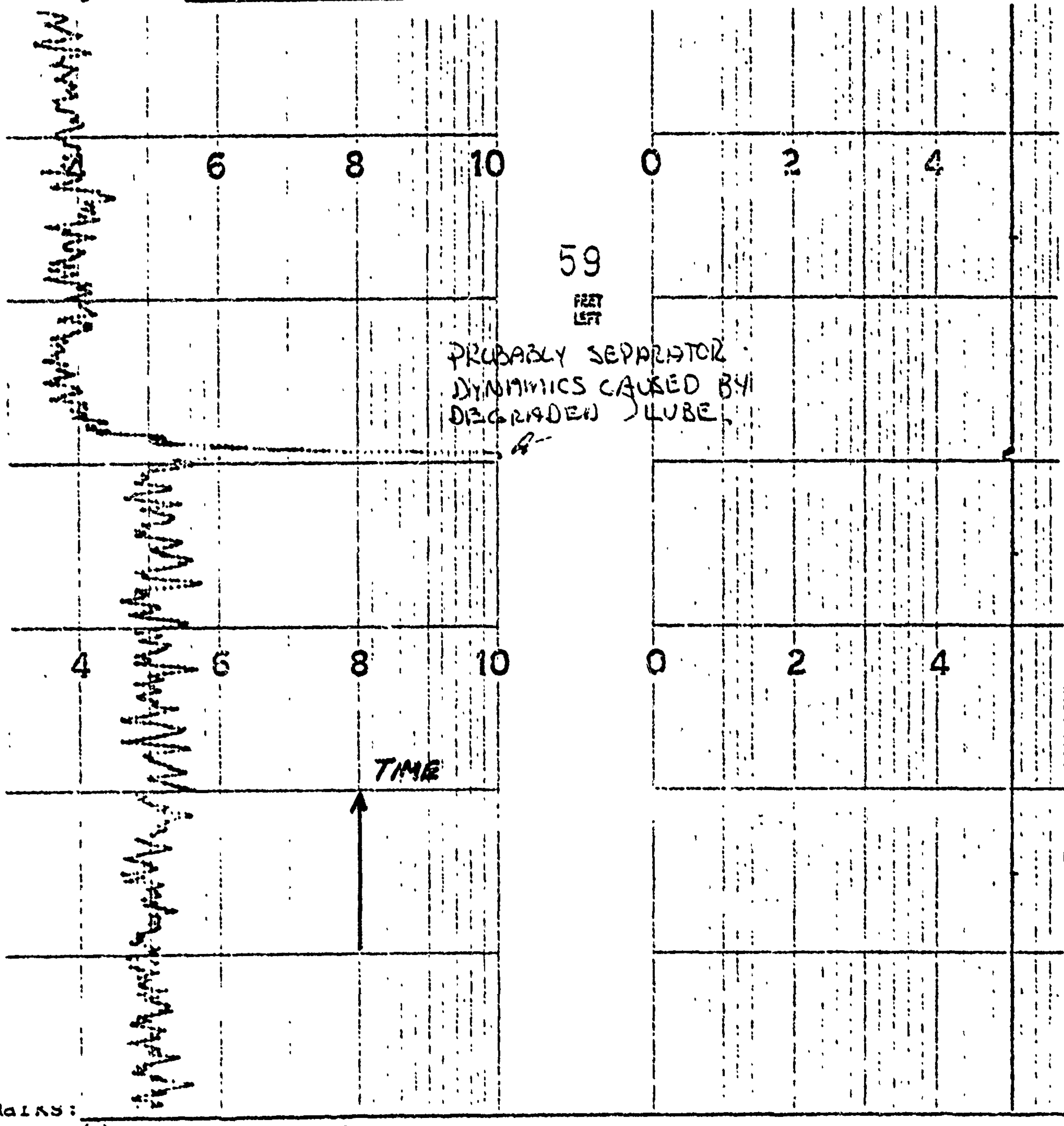

Remarks:
(1) SPIKE JUG SHOWN

WANDER TRACE

6 TO 12 MW HASH

BEARING LIFE DATA

Run # 2 Unit # 18005 Brg. Upper ________ Brg. Lower ________

Passed ________ Failed ________ Date 2-11-71

Milliwatt Hrs 24 PLD. 14.5 lbs. Power Level 1.8 watts

Total Brg. Hrs 1080 Rundown Time 275 sec

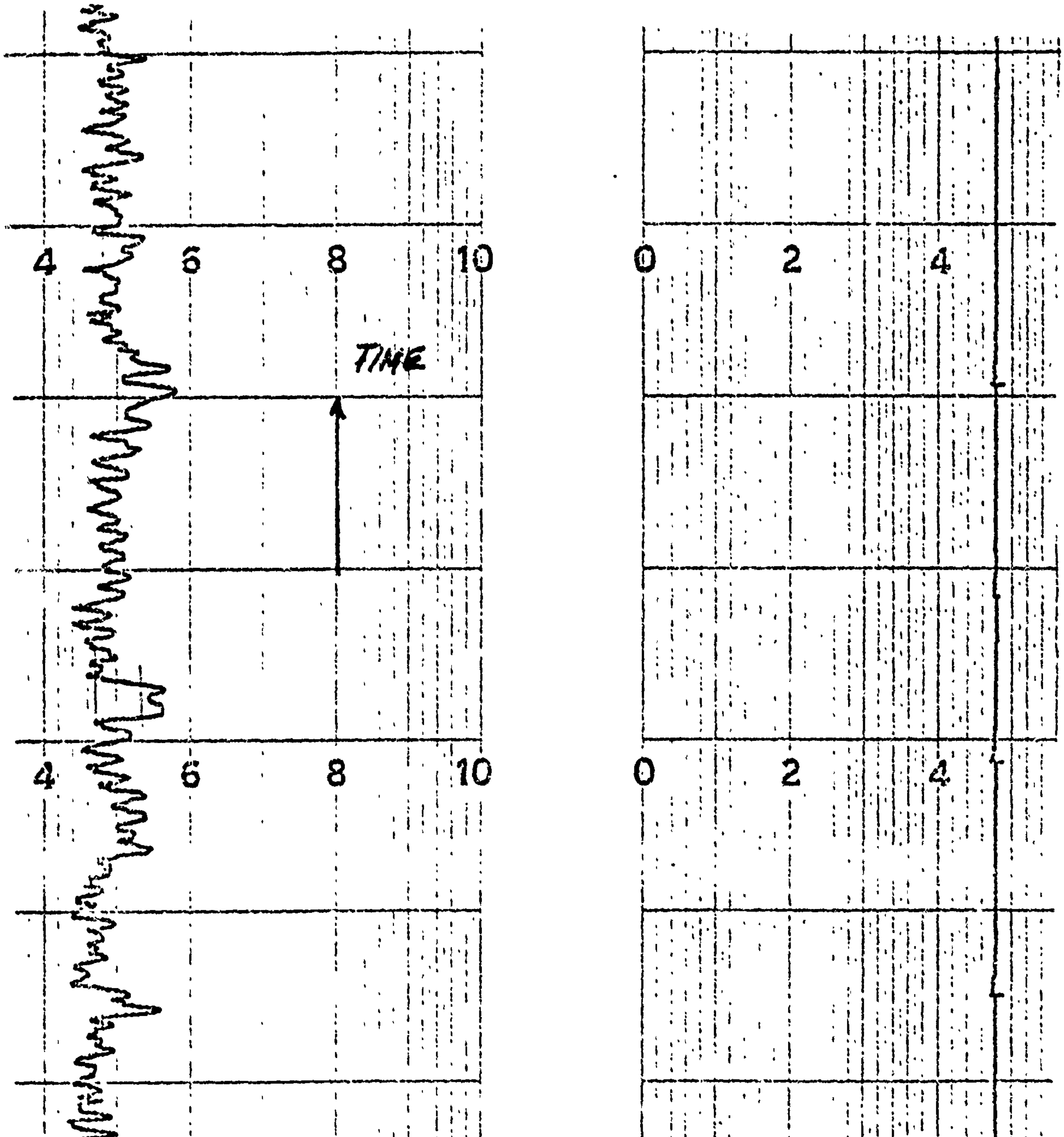

Remarks:

1 IRREGULAR JAG SHOWN 13MW

SEVERAL OTHER, SMALLER IRREGULAR JAGS

WANDERING TRACE

GT 12 MW HASH

BEARING LIFE DATA

MW # 7 Unit # 18005 Brg. Upper ______ Brg. Lower ______

Passed ______ Failed ______ Date 2-18-71

Milliwatt Hrs 24 PLD. 15.0 lbs. Power Level 1.8 watts

Total Brg. Hrs 1248 Rundown Time 287 sec

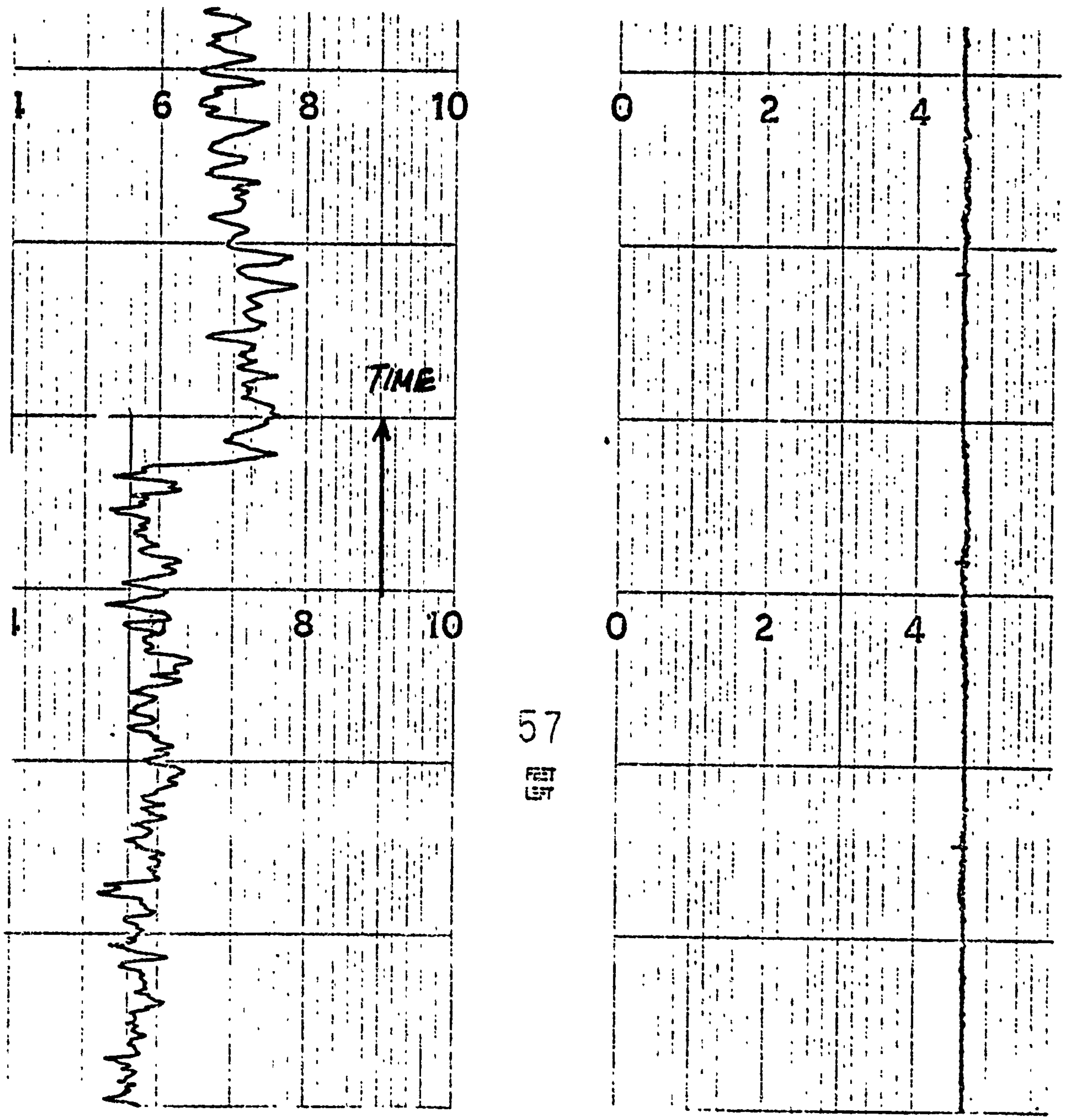

Remarks: .1 33MW PWR. SHIFT

WANDERING TRACE

.1 TO 12 MW HASH

BEARING LIFE DATA

MW # 8　　Unit # 18005　　Brg. Upper ______　Brg. Lower ______

Passed ______　　Failed ______　　Date 2-25-71

Milliwatt Hrs 24　　PLD. 16.3 lbs.　　Power Level 1.9 watts

Total Brg. Hrs 1416　　Rundown Time 286 sec

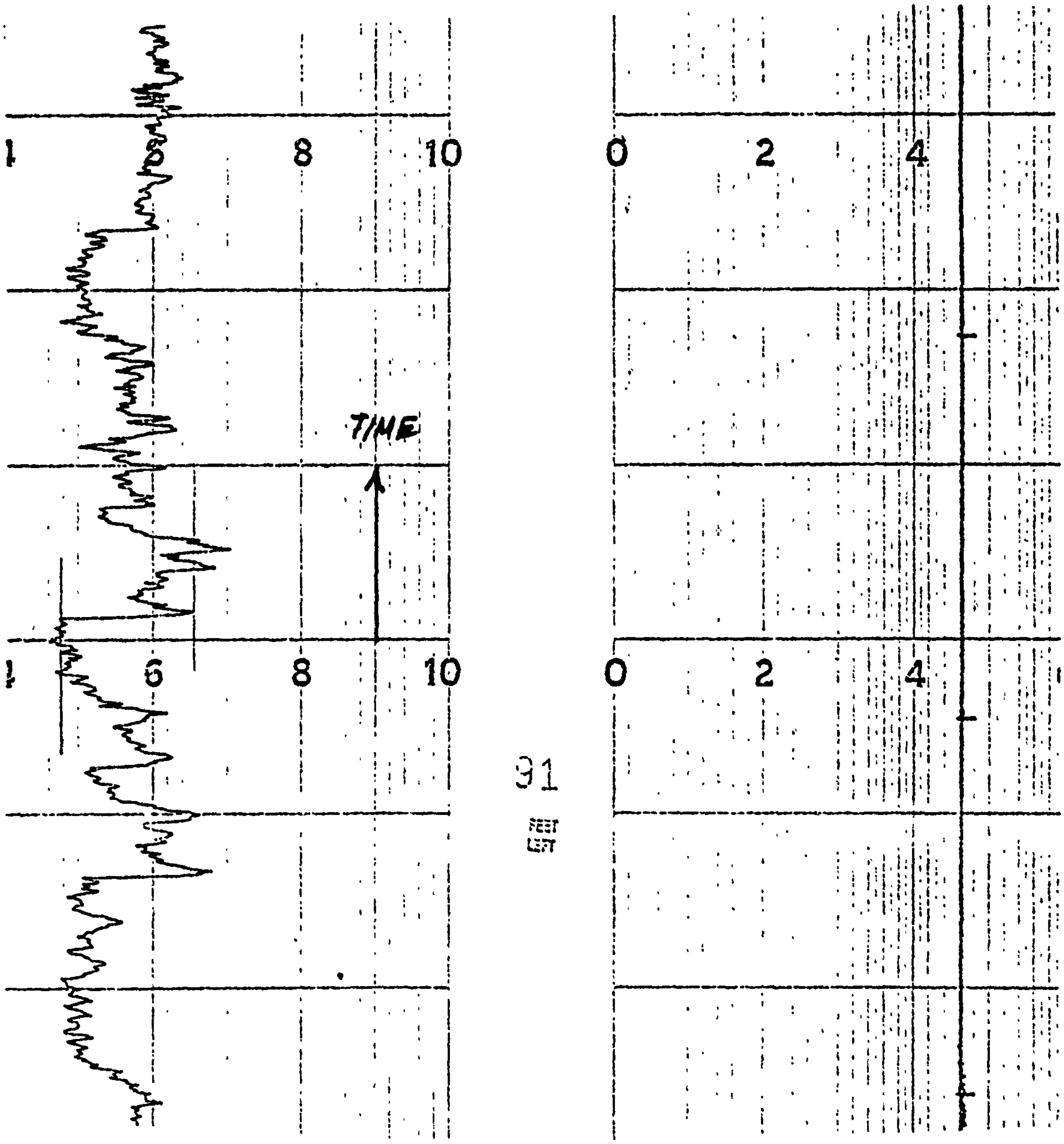

Remarks:

1. 36 MW POWER VARIATION SHOWN

SEVERAL PERIODS OF PWR VARIATIONS OF 20 TO 24 MW

WANDERING TRACE

BEARING LIFE DATA

W # 6   Unit # 18005   Brg. Upper ______ Brg. Lower ______

Passed ______ Failed ______ Date 3-11-71

Milliwatt Hrs 24   PLD. ______ lbs. 17.0   Power Level 1.9 watts

Total Brg. Hrs 1752   Rundown Time 240 sec

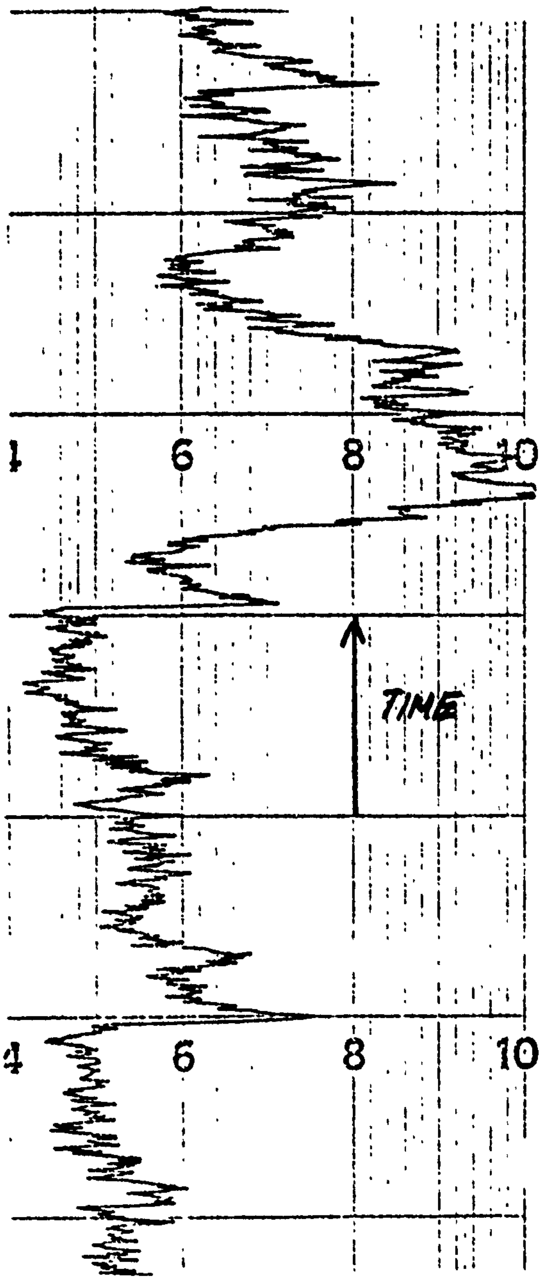

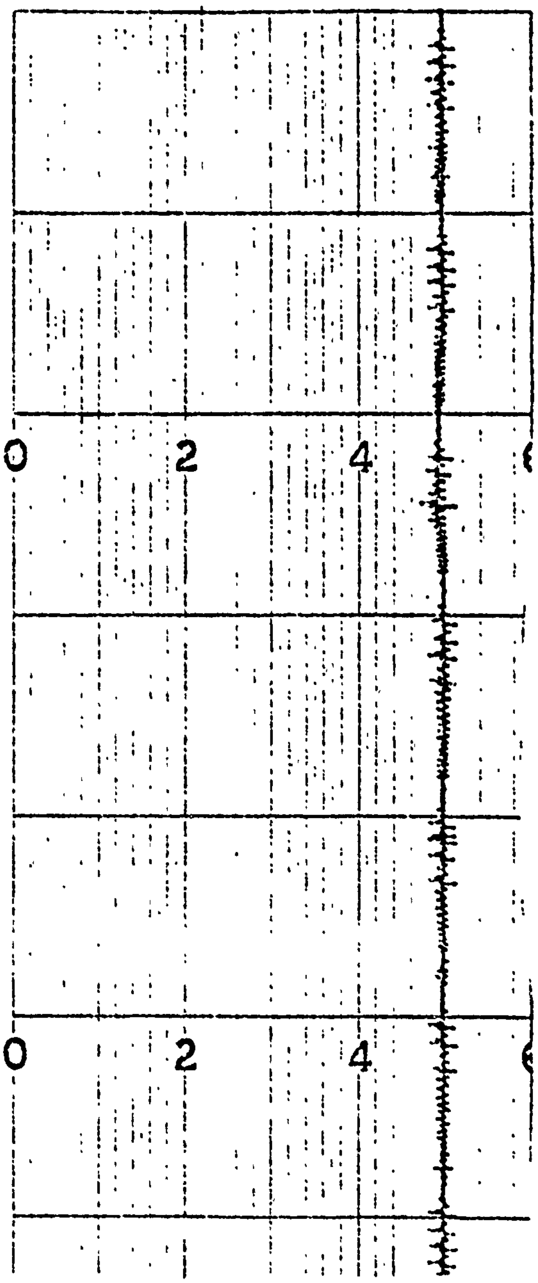

Remarks:

1 100MW JOG

20 TO 60MW JOG, THRU-OUT MOST OF TRACE

20 to 30MW HASH

BEARING LIFE DATA

Brg. Upper ______
Brg. Lower ______

Gyro # 2\ Unit # 18005

Passed ______ Failed ______ Date 3-25-71

Milliwatt Hrs 24 PLD. ______ lbs. Power Level 1.9 watts

15.1

Total Brg. Hrs 2088 Rundown Time 238 sec

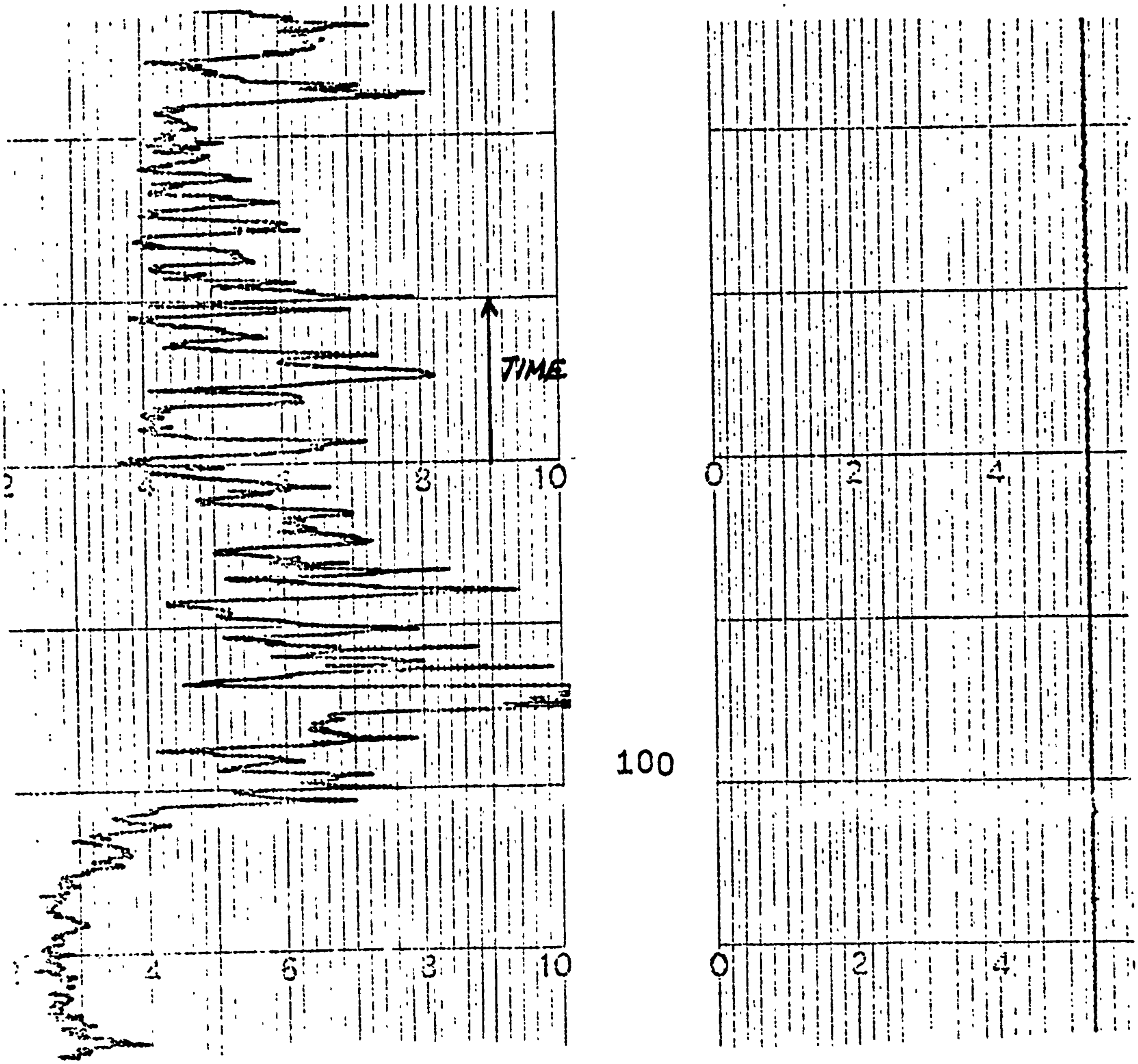

Remarks:

30 to 120MW Power Transients

20 to 60MW HASH

BEARING LIFE DATA

MW # ______ Unit # 18005 Brg. Upper ______
Brg. Lower ______

Passed ______ Failed ______ Date 3-31-71

Milliwatt Hrs 3 PLD. ______ lbs. Power Level ______ watts
17.3

Total Brg. Hrs 2232 Rundown Time 212 sec

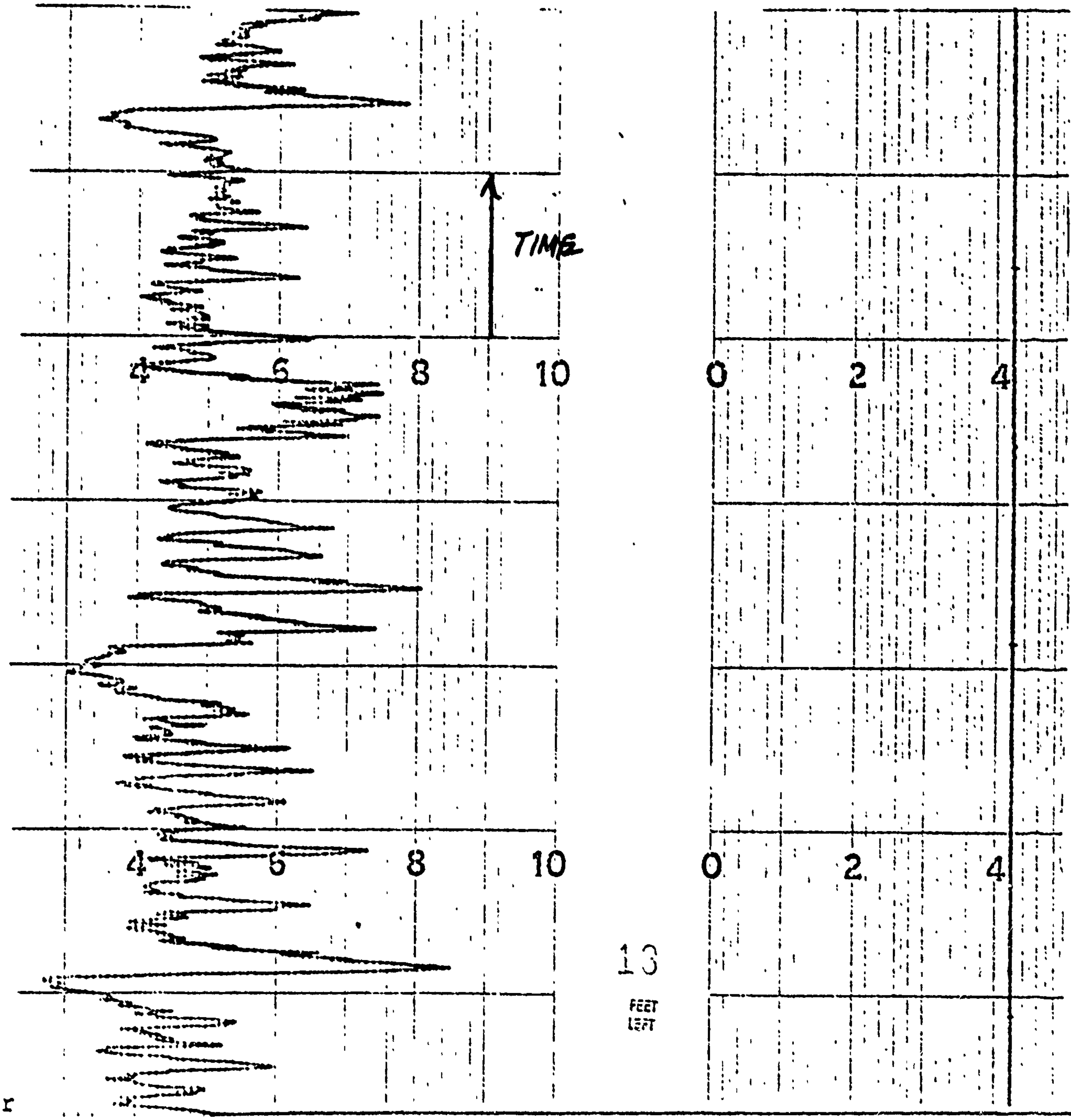

Remar

UP TO 80MW POWER TRANSIENTS

20 to 50 MW HASH

G.3 REPORT OF DRAPER LABS

The Charles Stark Draper Laboratory, Inc.

68 Albany Street, Cambridge, Massachusetts 02139 Telephone (617) 258-3429

November 17, 1975

TRW, Inc.
1 Space Park
Redondo Beach, California 90278

Attn: Dr. P.C. Wheeler, Manager
Electromechanical Equipment Department

Dear Phil:

As per your letter of November 4, 1975 to R.J. Schiesser, enclosed please find CSDL's DMA anomaly investigation report. If there are any questions please let me know.

Sincerely yours,

Herbert B. Singer
Section Chief, CSDL Bearing Center Section

HBS/ppc
Enclosure

cc: E. Kingsbury
R. Schiesser

The Charles Stark Draper Laboratory, Inc.

68 Albany Street, Cambridge, Massachusetts 02139 Telephone (617) 258-

November 17, 1975

TRW DMA ANOMALY

The numbered sections correspond to the items called out in a letter from P. Wheeler, TRW to R.J. Schiesser, CSDL.

1. The perturbations observed in the DMA driving torque demand appear to be of two kinds: a) sporadic short-duration steps probably associated with retainer instability and in themselves not terribly distructive of either bearings or performance, b) a gradual irregular increase in torque demand starting a few months ago, now approaching the limit of the motor system and causing large pointing errors. The second type is believed to be due to lubricant breakdown within at least one of the bearings in the assembly and will probably get worse with further running. The slip-ring bearings are probably operating acceptably since there is no signal problem and these bearings absorb less power.

   The exact processes which lead to lubricant breakdown are unknown, but result in a progressive thickening of the oil followed by deposition of solid degradation products in the pressure zones. As the fluid lubricant is used up, EHD operation becomes impossible, leading to wear and adhesive metal damage. The degradation products also roughen the wear track and build up in the ball pockets, causing an increase and large variability in the driving torque.

   Several factors leading to lubricant breakdown are known: a) insufficient lubricant, b) abrasives embedded in the wear track as a result of finishing operations in bearing manufacture, c) certain physical-chemical surface conditions (as yet undefined) inimical to the lubricant, d) contamination, e) improper preloading.

2. A senario resulting in the observed failure would be 1) thinning of the EHD film in the rolling contacts due to inadequate lubricant supply, (we believe that the lubricant supply system is the weakest link in the DMA design), 2) relatively rapid degradation of the fluid oil when a critical film thickness is reached, 3) build up of solid degradation products in the ball pocket clearances and also solidly attached to the rolling surfaces, 4) increased and irregular torque demand as the balls roll over this detritus.

   CSDL has seen many instances of lubricant breakdown. We are presently engaged in a joint program with NRL to characterize those surface conditions which promote this failure. Reference (1) summarizes NRL's initial work, reference (2) gives some examples of lubricant breakdown caused by insufficient lubricant.

3. Design changes are recommended as follows:
   1. Remove dams to provide a "fall apart" assembly configuration. This will prevent metal damage during assembly, but will entail fixturing for DMA assembly.
   2. Increase conformity on inner race to promote EHD film formation.
   3. Design a positive lubricant supply system.
   4. Use a full ball compliment to eliminate retainer instability problems.

4. Process changes are recommended as follows:
   1. Require all metal parts to be handled only with assembly fixtures--no finger contact, no finger cots, no gloves.
   2. Require that no detergent be used during race manufacture
   3. Require that only reagent grade benign solvents be used during cleaning of the races and balls.
   4. Soak all 440C metal parts (after solvent cleaning) in a mixture of 25 ml chromic acid (Chromerge ®) in 9lb concentrated H_2SO_4, at room temperature for 5 minutes with agitation. Follow by a thorough rinsing in copious hot distilled H_2O. Vacuum off H_2O and dry with methanol. This treatment (called acid cleaning) will result in dry metal surfaces free from most organic contaminants. Commence the lubrication process immediately after the acid clean.

4. Inspect the metal surfaces for birefringent embedded abrasive particles using polarized light.

5. Inspect the bearing assemblies for contamination and metal damage using Low Speed Dynamometer (Ref. 3), both as individual bearings and preloaded assemblies.

REFERENCES

1. Surface Chemistry of Ball Bearing Steel I, J.R. Murday and E.G. Shafrin, NRL; E.P. Kingsbury and S. Allen, CSDL

2. Lubricant Breakdown in Ball Bearings, Preliminary Unpublished Report; E. P. Kingsbury

3. Gyro Ball Bearing-Technology Today, A.P. Freeman

Attachment to G.3: "Lubricant Breakdown in Ball Bearings," by E.P. Kingsbury, October 1975.

Edward P. Kingsbury
October 1975

PRELIMINARY

LUBRICANT BREAKDOWN IN BALL BEARINGS

INTRODUCTION

Large mechanical and thermal stresses in an EHD contact may result in oxidation or polymerization of the lubricant (1, 2). If the contact is also starved, as in a slip ring assembly or an instrument ball bearing, failure quickly follows, either because of loss of fluid lubricant or by mechanical effects of the degradation product. The chemical-physical state on the rolling surface strongly influences the onset and rate of degradation (3), but no clear picture of this effect is available.

A joint program at NRL and CSDL is underway to define those measurable surface conditions which discourage lubricant breakdown in ball bearings. NRL has been studying, by means of Auger spectroscopy, those elements (and to some extent their chemical state) which are found on steel bearing surfaces as a result of manufacture and processing. A description of technique and some initial results are given in (4). CSDL's effort is to determine which surface conditions give premature lubricant breakdown, and which give satisfactory operation in a typical instrument ball bearing. Techniques and initial results are given in the present paper.

BASIC SPEED RATIO

Measurement of Basic Speed Ratio ρ allows a quick reproducible evaluation of lubricant performance in a starved EHD contact. Rho (ρ) is given by

$$\rho = \frac{\dot{\delta}}{\dot{\gamma}_o - \dot{\gamma}_i} \qquad (1)$$

where $\dot{\delta}$ is ball spin rate, and $\dot{\gamma}_{o(i)}$ is outer (inner) race rotation rate. Rho (ρ) is defined for all possible modes of bearing operation except solid body rotation ($\dot{\gamma}_o = \dot{\gamma}_i$), in particular for counter rotation when the ball group orbit rate is zero.

Rho (ρ) can be accurately measured by counter rotating the races so that the ball group remains stationary. Delta dot ($\dot{\delta}$) is obtained with a stroboscope. A small hole bored through the test ball establishes a preferred spin axis (6, 7) and facilitates stroboscopic isolation of its rotation. The Basic Speed Ratio has been measured with this techique to an uncertainty of one or two parts in 10^5 in small instrument bearings.

It is shown in (5) that ρ depends only on the geometry of the bearing and on the slips induced at the ball race contacts. In the present experiments geometry is fixed by keeping the total speed $S = \dot{\gamma}_o - \dot{\gamma}_i$ (see 5, kinematic equivalence) and the load constant. Thus, measured changes in ρ during a test are caused by changes in ball-race slip. Since the bearing is starved, any change in amount of oil available to the EHD contacts will produce a change in film thickness (8), hence shear and slip; alternatively, at constant thickness, any change in lubricant viscosity caused by degradation will alter the ball-race slip. Test conditions have been selected such that the oil available to the contacts remains nearly constant unless degradation occurs. This is done by running the bearing without a ball retainer in the full complement configuration. A controlled amount of oil is applied to the balls before assembly, and serves as the only lubricant in the test.

Both oil diminution and degradation thickening produce a decrease in ball-race slip which increases the ball spin rate. Hence failure is signalled by an increase in ρ.

TEST CONDITIONS

The bearing used in the present tests is a 2171 size 52100 instrument type.

The value of ρ calculated from its nominal geometry (zero slip) (5) is

$$\rho = \frac{E^2 - d^2 \cos^2 B}{2Ed} = 1.75 \qquad (2)$$

E = pitch diameter = 8.89 mm (0.35 inch)

d = ball diameter = 2.38 mm (3/32 inch)

B = contact angle = 20^0

The test bearing has 11 balls, is loaded to 3.18 Kg (7.01 lbf) by a weight, and is counter rotated at S = 215 Hz (12,900 r/min). Lubricant for all tests is KG80 mineral oil, applied only to the balls by evaporation from dilute solution in Freon, either one part in 500 or one in 1000 by volume. This results in a total oil supply of about 100×10^{-6} gm (2×10^{-7} lbm) as established by weighing, when the 500/1 solution is used. All tests are at room temperature in air.

RESULTS

Typical BSR data shown in Fig. 1 were taken on a new 2171 bearing whose as-received balls and races were ultrasonically cleaned in pure Freon. For test 1 the balls were dried from a 500/1 Freon KG-80 solution. The essentially constant value for ρ indicates normal running over the 30 minutes of the test. Subsequently the disassembled bearing was cleaned in Freon, and the balls dried from a 1000/1 oil solution for test 2. A higher level for ρ was found, with a sharp break after 15 running minutes. The higher initial level results from starvation: less available oil (1000/1) gives less slip, a larger ball spin rate and a larger measured ρ. The sharp break indicates lubricant degradation with loss of fluidity and consequent larger ball spin rates.

After run 2 solid lubricant breakdown products were removed from the bearing elements using a soft back lap and a slurry of 3 micron Al_2O_2 in medicinal mineral oil. It is possible to do this if the lubricant failure is not allowed to progress to the point where metal damage occurs.

The clean dry races were then again assembled with balls dried from a 1000/1 oil solution and run 3 obtained. Agreement in general features between runs 2 and 3 shows the reproducibility of the technique. The initial level of ρ gives a check on the amount of oil stored on the balls.

EVALUATION

These conclusions are supported by microscopic examination of the bearing elements as shown in Fig. 2. These are photos at about 25X of the bored test ball which is resting at the bottom of a hole in a translucent slug, illuminated from below (Fig. 2C). The black spot in the center of the ball is the image of the top of the hole. This setup allows photos of details on the highly reflective ball surface which are otherwise very difficult to see.

Figure 2A shows the ball after oil deposition from the 500/1 solution of run 1. The oil is not uniformly distributed, but fringe systems can be seen, showing the ball to be wettable. Figure 2B shows the ball after run 1 followed by a Freon wash to remove fluid oil. Recalling that the hole in the ball establishes its spin axis, so that the wear track is located on the corresponding equator, a faint darkening can be seen. This is evidently normal, being present after all non-failed tests.

Figure 3A shows a portion of the groove in the outer race after run 1. Oil originally on the balls has been transferred to the track which is wettable. The two spots are the footprints of adjacent balls when they came to rest. Figure 3B shows the same track after a Freon wash to remove fluid oil and confirms the absence of metal damage in the wear track.

Figure 4A shows the washed ball after run 2. There are short sections of Freon-insoluble degraded oil attached to its surface, but no metal damage. Figure 4B shows the washed outer race after run 2. There is extensive Freon-insoluble degradation product located symmetrically on either side of the pressure zone. Figure 4C shows the outer race after the soft back lap. The comets were produced by the lap but are usually not in the wear track and have had no measurable influence on lubricant breakdown. Run 3 was made on the track shown in Fig. 4C.

DISCUSSION

The failures experienced in runs 2 and 3 were caused by insufficient lubricant. The full complement test bearing has no lubricant reservoir and running evidently uses up the oil at a definite rate, causing its starved EHD films to thin. When they are thin enough, lubricant breakdown accelerates to failure. The experimental techniques outlined in this paper give a convenient way of following the process, which is reproducible with time. ~~This~~ These data establish~~es~~ the normal behavior of the bearing, since the rolling surfaces are in a production condition. Special surface treatments have produced both longer and shorter failure times in the BSR test. These include silicone, detergent and embedded abrasive exposure; detailed results will be given in future reports. It is hoped that a correlation between these data and specific surface characterization obtained at NRL from Auger analysis of the test bearing parts will be possible.

REFERENCES

1) Molecular Degradation of Lubricants in Sliding Elastrohydrodynamic Contacts, D.L. Walker and W.O. Winer, TRANS ASLE JOLT, 97F, No. 3, 1975.

2) Analysis of Infrared Spectra of Fluid Films in Simulated EHD Contacts, J.L. Laner and M.E. Peterkin, TRANS ASLE JOLT, 97F, No. 2, 1975.

3) Ball Bearing Surface Chemistry, A.P. Freeman, S. Allen, and H.B. Singer, CSDL Report E-2298, 1968.

4) Surface Chemistry of Ball Bearing Steels I, (J.R. Murday, et al.) NRL Memorandum Report 3047, 1975.

5) Experimental Observations on Instrument Ball Bearings, E.P. Kingsbury, CSDL Report E-2316, 1968.

6) Ball Motion in Angular Contact Bearings, E.P. Kingsbury, Wear 11, 1968.

7) The Motion of Analysis of Ball Motion in High Speed Deep Groove Ball Bearings, R.I. Boness and J.J. Chapman, TRANS ASLE JOLT, 97F, No. 3, 1975.

8) Correlation of Gyro Spin-Axis Bearing Performance with the Dynamic Lubricating Film, J.D. Horsch, ASLE TRANS 6, 1963.

FORM 3 T

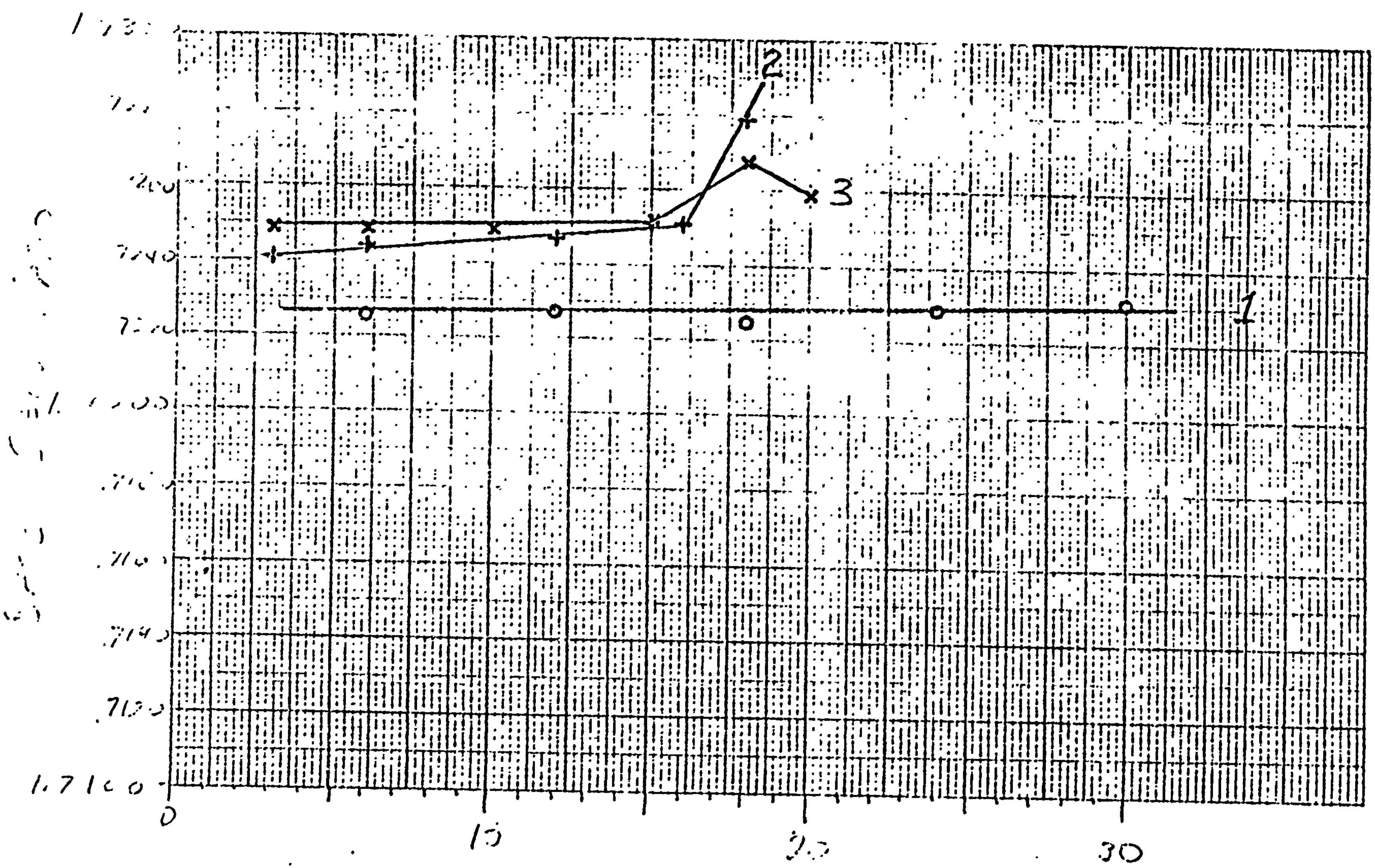

ROUNNING TIME @ 3.18 Kg LOAD
MINUTES
2.15 Hz SPEED

JUN 27 1975 1

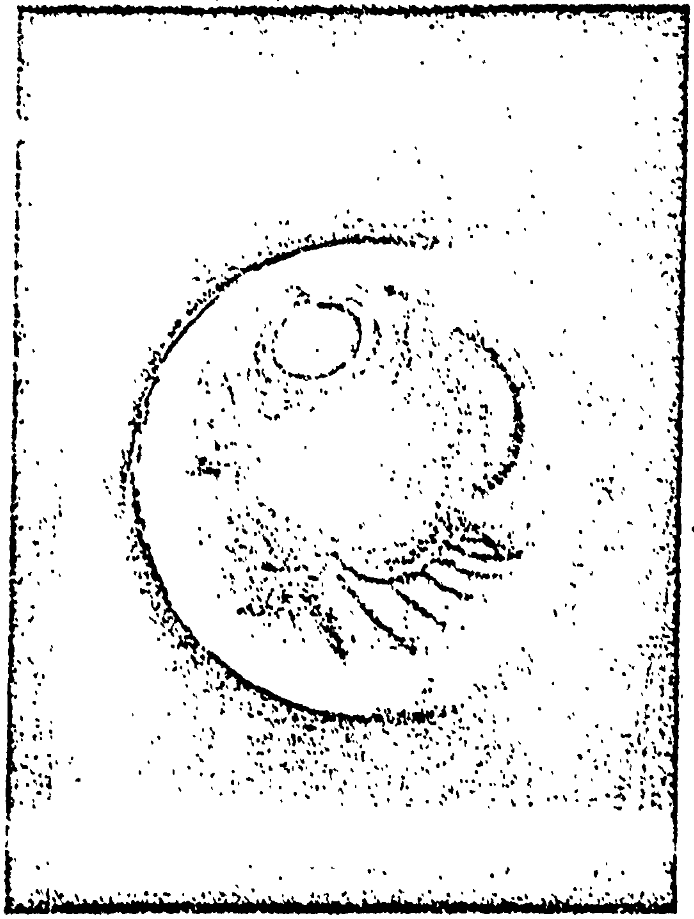

JUN 27 1975 3

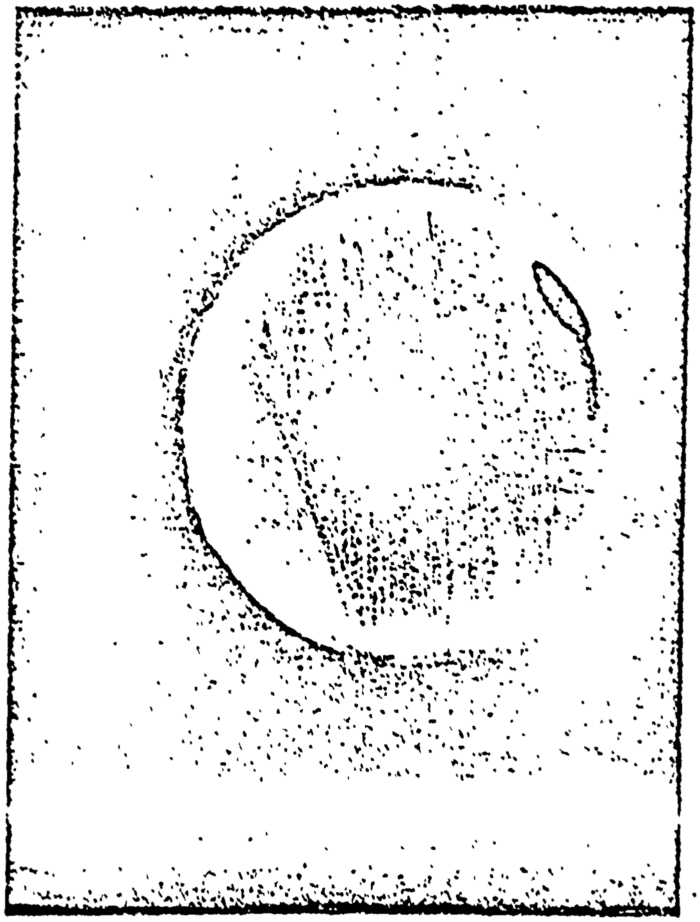

2A

2B

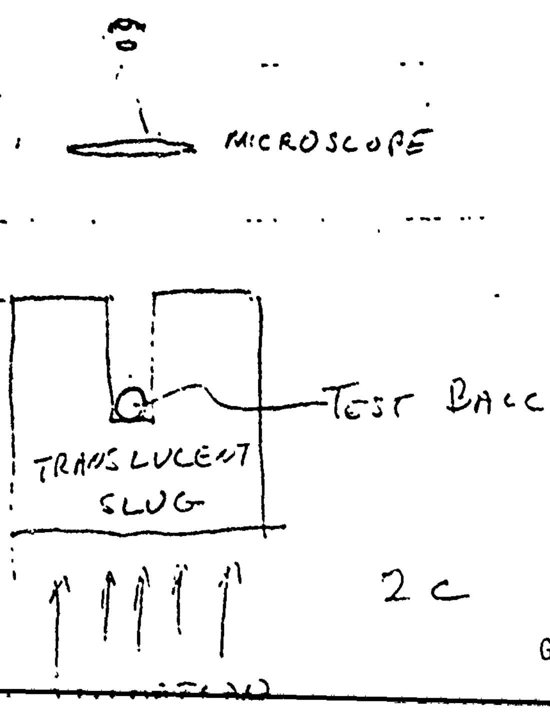

2C

JUN 27 1975 4

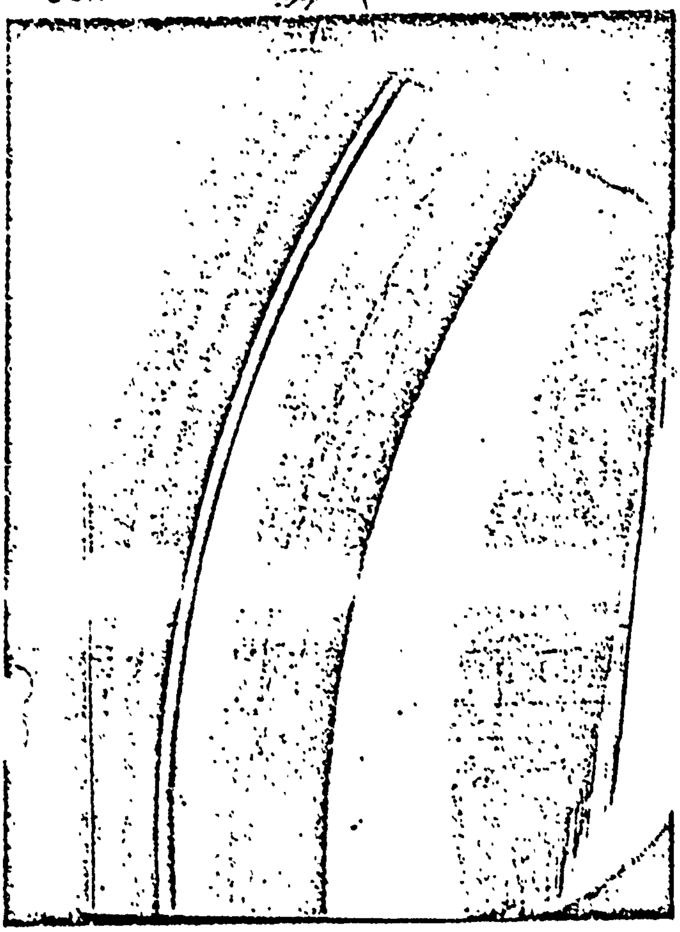

JUN 27 1975 5

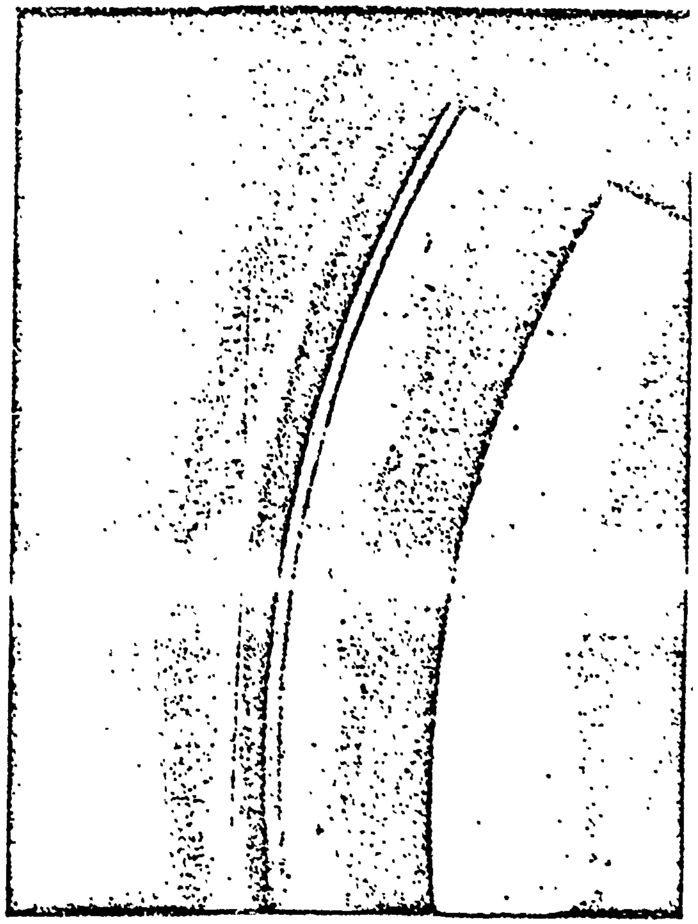

Fig 3A

3B

4A

4B

JUN 27 1975 8

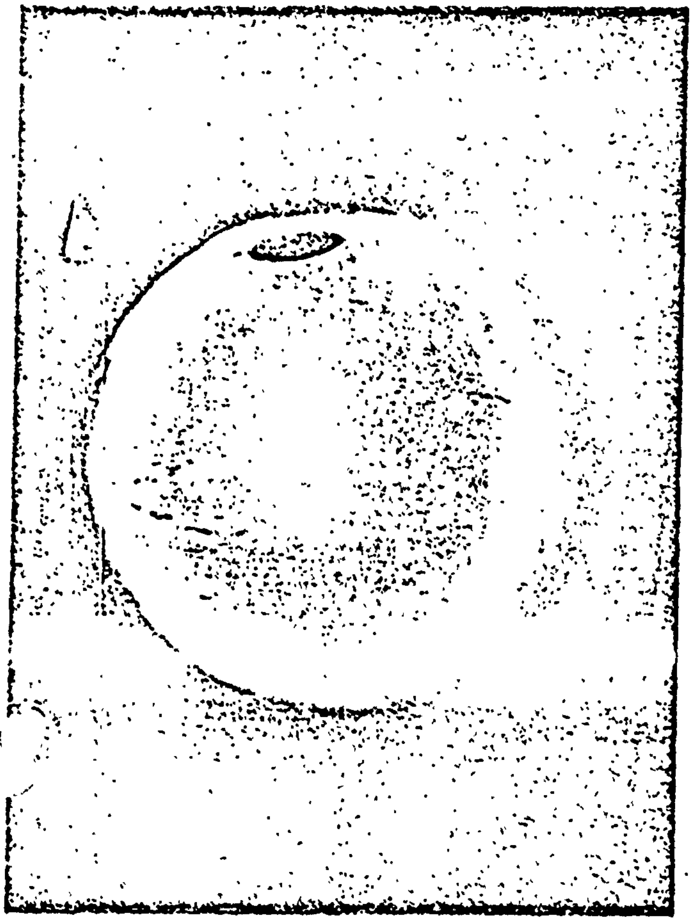

JUN 27 1975 10

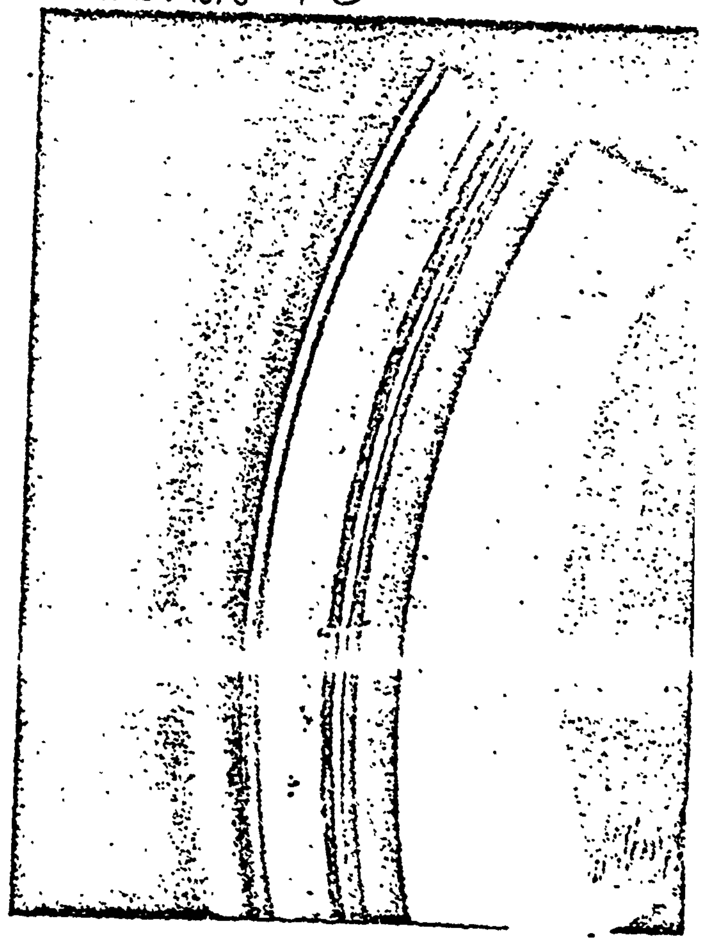

JUL 9 1975 JUL 9 1975 4

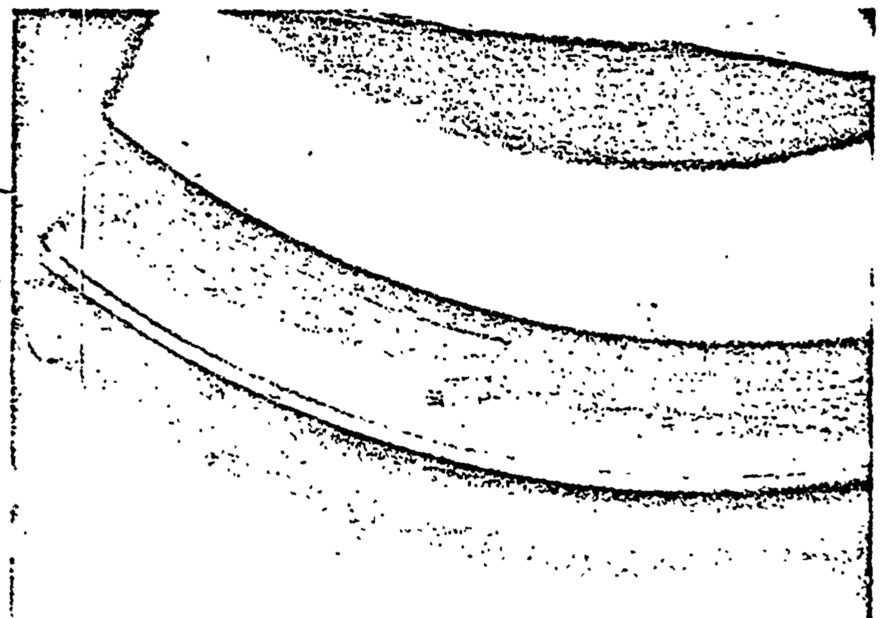

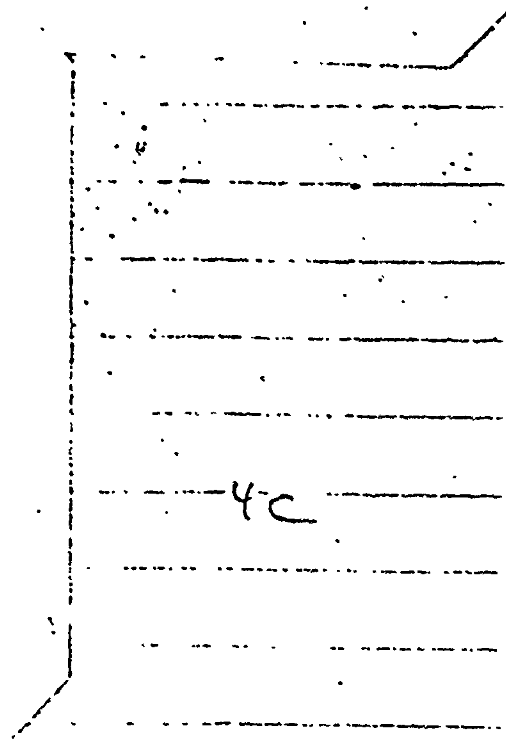

4C

Attachment to G.3: CSDL's Review of BBRC Lubrication Analysis (presented in Phase II DMA PDR Data Package)

CSDL'S REVIEW OF BBRC " BEARING LUBRICATION AND LIFE ANALYSIS DSCS II PHASE II DMA"

December 11, 1975

I. LUBRICANT LOSS CALCULATION

Figure 2 of the BBRC report is a plot of the flow rate per unit area (G, units of $gm/cm^2/year$) vs temperature for the VacKote of interest, to be expected through a circular orifice which separates a region at pressure p from space. It is not completely clear if this is meant to be a theoretical curve or of it shows experimental data, but the inference drawn by CSDL is that it is a theoretical result. If so, its basis is not specified. The equation which represents this curve is:

$$G_1 = 4.80 \times 10^{11} e^{-\frac{9146}{T_k}} \tag{1}$$

where T_k is absolute temperature, ^oK.

Other investigators (1,2) and in fact BBRC themselves in a different report (3) have consistantly used a form of the Knudsen Equation (4) based on kinetic theory of gases to predict vacuum flow rates. Using the Salmon and Apt form for comparison, we get

$$G_2 = 1.84 \times 10^5 \quad p(M/T_k)^{\frac{1}{2}} \tag{2}$$

where p is the vapor pressure in mm Hg and M the molecular weight in gm/mole of the VacKote in question. Taking a wild stab at these numbers, we could have for example $p=10^{-9}$ mm Hg and M=300 gm/mole.

Then (2) becomes

$$G_2 = 1.84 \times 10^{-3} \left(\frac{300}{T_k}\right)^{1/2} \qquad (3)$$

Table I shows the differences between G_1 and G_2 calculated at various temperatures

	BBRC	Salmon & Apt
$T_f\,^oF$	G_1 gm/cm^2/yr	G_2 gm/cm^2/yr
0	.000134	.00199
50	.00450	.00189
70	.0152	.00186
100	.0806	.00181
140	.573	.00175
150	.900	.00173

TABLE I

The two equations are evidently quite different in their predictions. The basis for Figure 2, and the BBRC conclusion that 25% (due to the difference in geometry between a circular orifice and the DMA loss aperture) of 1 gm will be lost per year thus seems open to question.

Also, the conclusion that a decrease in temperature from 150 to 100F will result in a decrease in oil losses by a factor of 10 is not supported if calculations are based on the Knudsen equation rather than on Figure 2. Gardos (1) has discussed some of the reasons for large discrepancies that have been observed between calculations based on the Knudsen equation and laboratory measurements. He finds, among other things, that a complex lubricant can not be represented by a single vapor pressure, and that frothing of the lubricant when first exposed to vacuum (outgassing) can saturate leak gaps with bulk fluid.

It does not appear that the problem of oil frothing in the DMA cavity due to outgassing on exposure to vacuum has been considered in the BBRC lubrication system.

BBRC has addressed the fractionation problem with a calculation technique discussed in (3). It provides a periodic upgrading of the constants in the Knudsen equation based on special experimental measurements. BBRC claims agreement between predictions and this calculation within 10%. CSDL was unable to use this calculation to check the DMA application in the absence of the specialized experimental data characterizing VacKote. In any case, Figure 2 does not seem to be based on this type of calculation.

CSDL is of the opinion that, irrespective of the results of specific calculations, and their underlying uncertainties, the 33 gms of lubricant originally supplied to the DMA is plenty for a seven year mission if it is guaranteed of delivery to the rolling contacts.

II LUBRICANT DISPOSITION WITHIN THE DRIVE

BBRC claims that a lubricant film 500Å thick or thicker behaves the same with regard to evaporation rates as does a pool of oil, and that the rates are given by Figure 2. It is not clear what the connection between flow through a circular orifice (Fig. 2) and evaporation from a pool of oil is.

CSDL agrees that evaporation and condensation result in net oil migration to the cooler parts of the assembly. However, any analogy with heat transfer (depending on the 4th power of the temperature difference) is not clear. Flux to a surface depends on vapor pressure, from the surface on the average residence time of a lubricant molecule, which is an exponential function of temperature (5).

Since the bearings are the hottest part of the DMA, CSDL believes that they will loose lubricant to their cooler surroundings if evaporation-condensation is the only supply mechanism at work.

III BEARING LIFE

The life analysis in the BBRC report is based on the AFBMA specific dynamic capacity concept,which assumes failure will be caused by metal fatigue. At the stress levels seen by the DMA bearings fatigue life is infinite, hence the AFBMA calculations do not apply.

Reference 6 presents a "detailed analysis of lubrication performance in despin mechanical assemblies". Its authors have identified 12 failure modes which have been experienced in ground tests or space, shown in Table IV from their report. CSDL believes, in agreement with these authors, that the present state of the art does not allow life calculations. However, a better understanding of lubricant breakdown is hopefully not far off, and the problems of lubricant dewetting, compatibility, transfer, volatility, creep and film thickness can be addressed through the rational design of a positive lubrication system. Torque variation, cage wear and instability can be attacked through the use of retainerless bearings which take advantage of sucn a positive supply system. It appears its benefits would far outweigh any added mechanical complication.

TABLE IV (From Reference 6)

FAILURE MODES IDENTIFIED

Lubricant Degradation

Lubricant Dewetting

Slip Ring and Brush Wear

Improper Lubricant Transfer

Inadequate Lubricant Quantity

Lubricant Volatility Effects

Lubricant Incompatibility

Torque Variations

Cage and Bearing Instability

Cage Wear

Lubricant Creep

Film Thickness

Miscellaneous Extraneous Effects

REFERENCES

1. "Labyrinth Sealing of Aerospace Mechanisms - Theory and Practice", M. Gardos, ASLE TRANS 17, 4, 1974.

2. "A Lubrication Systems for Space Vehicles" Salmon and Apt, Automobile Engineering Congress, Detroit, 1963

3. "Bearing Lubrication for Long-Term Space Applications", Perrin and Ahlborn, International Ball Bearing Symposium, Cambridge, 1973.

4. "Vacuum Technique", S. Dushman, J. Wiley, 1949.

5. "The Dynamical Character of Adsorption", J.H. DeBoer, Clarendon Press, 1952

6. "Failure Mode Analysis of Lubricated Satellite Components", Benzing and Strang, Technical Report AFML-TR-73-188, 1974

Attachment to G.3: "Gyro Ball Bearings - Technology Today," by A.P. Freeman, Feb 1968.

GYRO BALL BEARINGS – TECHNOLOGY TODAY

by

Albert P. Freeman
Deputy Associate Director
Instrumentation Laboratory
Massachusetts Institute of Technology
Cambridge, Massachusetts

February 1968

Prepared for presentation at the Sixth AGARD Guidance and Control Meeting, "Inertial Navigation: Components," at Braunschweig, Germany, 7-9 May, 1968.

ACKNOWLEDGMENT

This paper covers work on gyro ball-bearing technology carried out under various U.S. Air Force, U.S. Navy, and National Aeronautics and Space Administration contracts. Current work in the bearing dynamics area is being performed under the auspices of DSR Project 52-306, sponsored by the Avionics Laboratory of the Air Force Systems Command through Contract F33615-68-C-1155 with the Instrumentation Laboratory, Massachusetts Institute of Technology, Cambridge, Massachusetts. Current work in the area of surface chemistry is being carried out under the auspices of DSR Project 55-219, sponsored by the Manned Spacecraft Center of NASA through Contract NAS 9-3079 with the MIT Instrumentation Laboratory. In the lubricant replacement program, current effort is under the auspices of DSR Project 52-275, sponsored by the Space and Missile Systems Organization of the Air Force Systems Command under contract AF 04(694)-999 with the MIT Instrumentation Laboratory.

The contributions of various governmental and private agencies to the status of the bearing technology reported here are also acknowledged.

GYRO BALL BEARINGS – TECHNOLOGY TODAY

Albert P. Freeman

SUMMARY

The spin-axis bearing package is a major determinant of gyro reliability and performance. Fractional microinch position stability over extended time periods, reliably achieved for tens of thousands of running hours, is required. Whether the ball bearing thus used runs successfully on an elastohydrodynamic fluid film or succumbs to early failure may be determined by whether or not today's bearing technology is applied. This specialized technology, applicable in many aspects to other bearings, has been developed over the past twenty years and continues to advance.

Achievement of current state-of-the-art is the result of parallel development of the bearing parameters and of the means for their evaluation. Bearing metallurgy, geometry, groove-surface topography and chemistry, lubrication, ball-retainer, contamination control, dynamic behavior, testing, and processing variables have all been improved. Particularly significant have been the efforts in surface-film-piercing asperity reduction, surface-chemistry improvement, and lubrication-mechanism advancement. Also of major importance has been development or adaptation of measuring devices to join with functional tests in evaluation of bearing characteristics and of potential life and performance at various processing stages.

Continued current effort in the areas of the lubrication mechanism, bearing dynamics, and groove surface promise further gains in consistency of achievement of life and performance goals. Application of today's technology can in most cases, however, yield the required thousands of hours of reliable operation.

TABLE OF CONTENTS

LIST OF ILLUSTRATIONS

LIST OF ILLUSTRATIONS (Cont.)

LIST OF TABLES

SECTION 1

INTRODUCTION

The gyro spin-axis ball bearing is unique. At the heart of the inertial guidance system, it is a major determinant of performance and reliability. Today's bearing technology is the product of more than twenty years of development, though current practice is in many cases frozen at a point dating back many years. Use of the knowledge available now can improve bearing yield, performance, life, and reliability.

1.1 Requirements

The principal requirement of the inertial gyro spin-axis ball bearing can be stated very simply: long life at the required performance level. We can divide this requirement into two broad subcategories: freedom from physical or chemical degradation of all elements of the bearing package and maintenance of dimensional stability of the gyroscopic element. Depending upon the application, failure criteria can range from slight deterioration of gyro performance to inability of the wheel to turn because of bearing seizure.

This paper is concerned with bearing performance in precision floated inertial gyros of the type shown in Fig. 1, and with those factors that influence stability of the gyro wheel package. As indicated by Fig. 2, average wheel location must be stable to a fraction of a microinch, and mass stability of other float elements must be similarly very closely maintained.

In order to satisfy the stability requirements, the bearings must be supported on a full, stable elastohydrodynamic (ehd) lubricant film. Piercing of this film during running causes chemical and physical degradation in the lubricant and of the metal surface, which in turn influences the location of the gyro wheel. This sort of deterioration is progressive, as the debris formed by the high-speed metallic contact leads to further piercing of the film. The lubricant sludge then collects beside the pressure zones and, like a sponge, withdraws the oil from the region in which it is needed to maintain the film. As this mode of failure progresses, bearing torque becomes erratic, the lubricant varnishes, the metal wears, and ultimately the torque increases to the point at which the wheel will

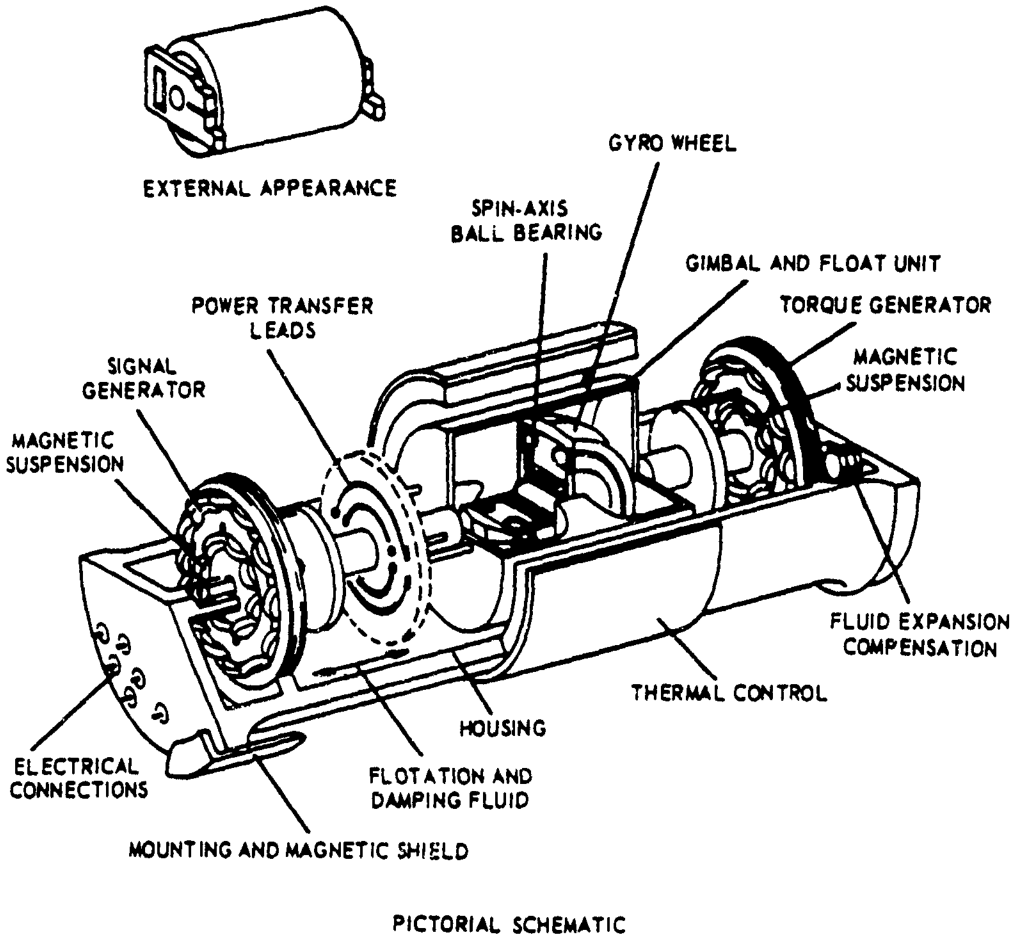

Fig. 1. Single-degree-of-freedom floated gyro.

no longer run at operating speed. The bearing running time between the onset of performance degradation and wheel failure can be several thousand hours. It is interesting to note that metal fatigue, one of the classic modes of bearing failure, plays essentially no part in gyro bearing failure.

Generation and maintenance of the ehd film demands the continued existence of many conditions. In operation, the metal components (races and balls) must have a geometric form that generates the required ehd film with acceptable stress levels over the entire pressure zone. The metal must sustain the load essentially without plastic flow or surface damage. The surfaces must be free of film-piercing asperities and must chemically support a boundary lubricating film at low speed and an elastohydrodynamic film at operating speed. The lubricant must demonstrate the chemical and physical properties needed to achieve these films with acceptable torque levels, along with chemical and thermal stability.

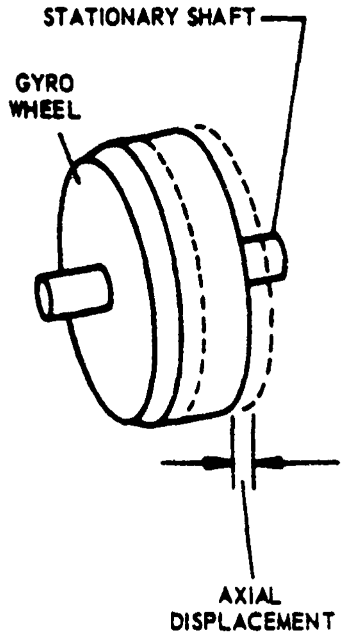

FOR ONE MILE-PER-HOUR NAVIGATIONAL ACCURACY ON EARTH'S SURFACE (A gyro drift rate of ~ 1.0 meru, or 0.015°/hour)	
THE WHEEL LOCATION STABILITY REQUIRED IS:	THE MAXIMUM OIL DROP MIGRATION PERMITTED ACROSS A SINGLE (R4) BEARING IS:
0.2×10^{-6} INCH	0.3 MILLIGRAM
OR	OR
50 ANGSTROMS	0.030-INCH DIAMETER
GYRO WHEEL: MASS – 225 GRAMS; ANGULAR MOMENTUM – 2×10^{6} GM-CM^2/SEC	

Fig. 2. Navigational accuracy vs. stability requirements at one g.

The ball retainer must maintain a controlled lubricant reservoir and circulate this lubricant as needed for a full ehd film, and run with required stability at acceptable torque levels. The environment must be chemically, physically, and thermally compatible with the bearing package. Finally, and of extreme importance, the bearing package must be free of contamination that can cause bearing degradation due to piercing of the film.

In addition to the demands just noted, which are associated primarily with retention of the lubricant film, the bearing package must also demonstrate other properties needed for mass stability. The combination of geometry, lubrication, and operating parameters must assure such factors as:

a. relative insensitivity of wheel location to acceleration field variation

b. film uniformity and stability of the bulk lubricant

c. stability of ball group and retainers

d. constancy of bearing torque

Inadequacies in the first group of parameters discussed, which are associated with rupture of the ehd film, result in bearing deterioration and gyro performance degradation. The second group, associated with mass instability, generally influence instrument quality without necessarily reducing bearing life at the degraded performance level.

Of utmost importance in any discussion of bearing requirements is processing, or handling. Achievement of the basic bearing properties is vitally dependent upon quality control during manufacture, which can be accomplished with proper engineering supervision. Retention of these properties is then a major battle. The bearing is a precise device and must be treated as such. During processing from package to completed instrument, its integrity can be compromised by particulate contamination, chemical contamination, overheating, mounting distortion, overstressing, scratching, denting, shock, overlubrication, underlubrication, exposure to corrosive environments, etc., etc. Thus, the processing variables are extremely important in both initial achievement of required bearing parameters and in their retention during instrument fabrication.

1.2 Status

The requirements noted in Section 1.1 have been achieved. They can be achieved consistently. Gyro performance of the highest quality has been demonstrated in instruments that have accumulated about 30,000 wheel running hours. However, as will be noted in subsequent sections, further advances can still be made in some areas of bearing surface, lubrication, and dynamics.

Achievement of today's status results from more than twenty years of development work, some phases of which are still in progress. Figure 3 illustrates this wo One of the first major development efforts, initiated in the late 1940's, led to improved preloading techniques. Subsequent efforts in the bearing package have encompassed metallurgy, geometry, lubrication, retainers, surface finish, surface chemistry, dynamics, contamination, manufacturing techniques, and processing variables.

Progress in the field of bearing evaluation has been following a parallel path of equal importance. For example, the early preloading improvement noted above was accompanied by development of an axial yield gauge. Other developments include improved geometric measurement devices, optical measurement techniques, the low-speed dynamometer, the milliwattmeter, the lubricant-film electrical-resistance gauge, taper sectioning, stroboscopic observation, race counter-rotation devices, high-speed torque testers, and many others.

The gyro itself is one of the most useful bearing diagnostic devices. It alone is capable of determining bearing position stability to the required performance levels. It also provides a convenient means for the application of known inputs to the bearing package, along with precise readouts of the accompanying bearing behavior.

Bearing package evaluation in early gyro construction and test stages is extremely important. The ball bearing is unfortunately quite forgiving on a

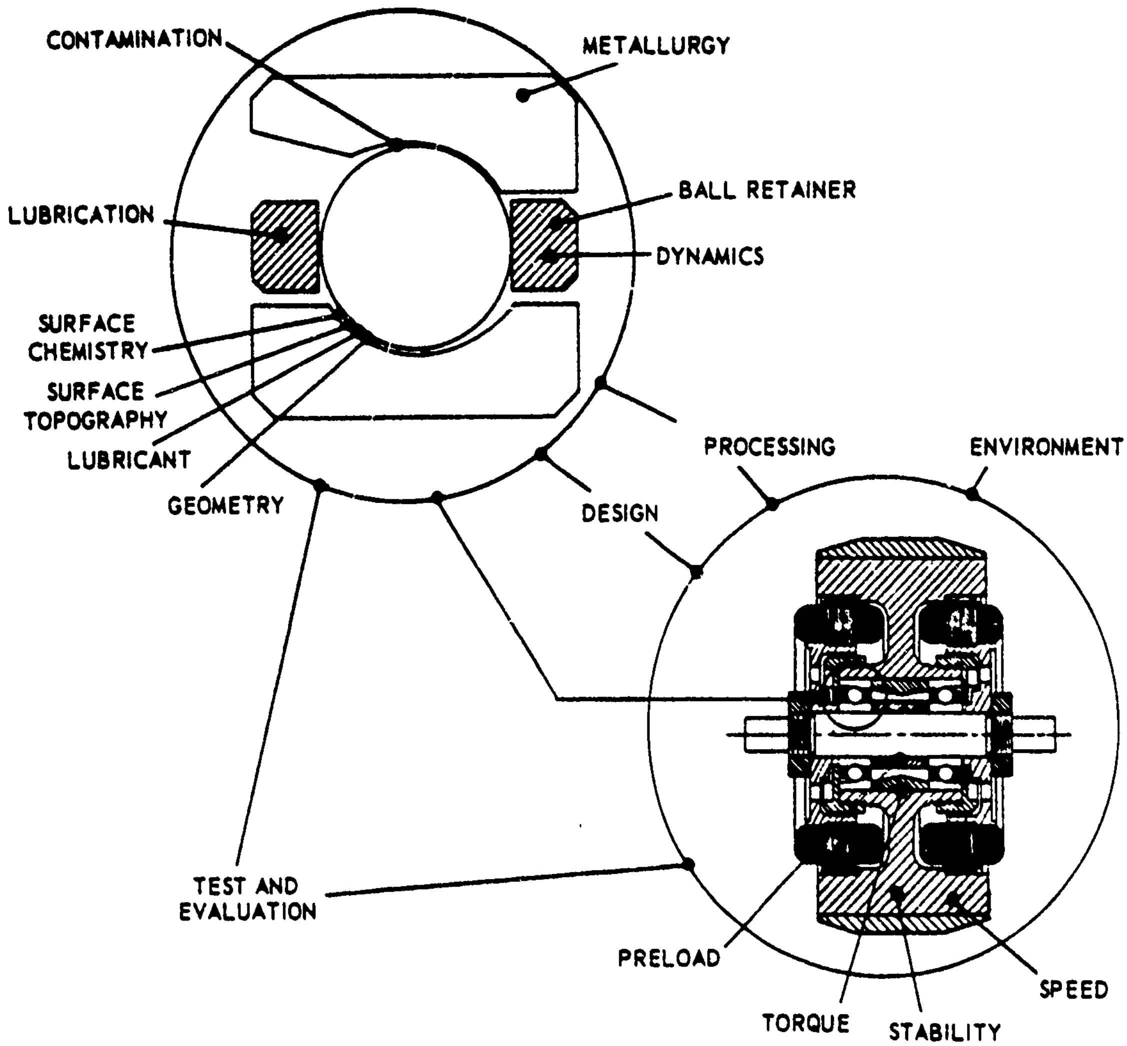

Fig. 3. Major areas of bearing progress.

short-term basis, and early degradation symptoms are frequently ignored. Progressive deterioration can lead to later severe performance degradation, perhaps when the gyro is the heart of a complex, critical, operating navigation system.

The following sections of this paper will discuss the current status of gyro ball-bearing technology, with particular emphasis on areas known to be critical. No attempt will be made to cover the history of the developments that have led to today's status, except where required for perspective. Due to the complexity of the subject, the treatment will be limited in this paper and discussion of each subject will be relatively brief. References providing further details are included in the bibliography.

SECTION 2

CONFIGURATION

Gyro bearing design must consider not only the normally accepted criteria but also those peculiar to the precision gyro, such as microstability, isoelasticity, lubrication limitations, bearing dynamics, and long-term physical and chemical stability. These factors coupled with specific instrument requirements and configurations yield the basic bearing design. Among the design features are basic size and configuration, materials, mounting method, preload, speed, lubrication, contact angle, race-groove curvature (groove-to-ball conformity), inner or outer-land relief, retainer configuration, and many others. (The bearing nomenclature used here is defined in the Appendix.) Tolerances must also be assigned to most of these parameters.

Metal and geometry are discussed in this section, with particular emphasis on adherence to nominal values, or tolerance control. Design criteria leading to the specific configuration are not discussed because of their complexity and dependence upon the details of the requirements of the gyro in question. For example, depending upon the acceleration environment to which the gyro will be exposed and the performance demanded during acceleration (vibration or steady-state), critical bearing parameters may be contact angle, number of balls, race-groove curvature, and preload. On the other hand, torque limitations may emphasize basic size, speed, preload, race-groove curvature, atmosphere, lubrication, and retainer. As these brief examples point out, bearing design is critical, but it is too complex a subject for coverage here. The influence of specific geometric variables on lubrication and on bearing dynamics will be discussed in later sections.

2.1 Metal

The demands made upon the steel of the gyro ball bearing differ somewhat from those made on other more heavily loaded bearings and are in some respects more severe. The gyro bearing typically is lightly loaded, with the maximum Hertz stress generally in the vicinity of 200,000 lb/in.^{2} or less. It operates in a moderate ambient temperature, circa 150°F in an inert atmosphere, generally helium, after having been very carefully processed from production through application. Why, then, are we concerned with the properties of the steel from which the bearing is made?

The steel must satisfy two major requirements. First, the level of gyro performance as discussed in Section 1.1 demands the ultimate in microdimensional stability both under stress and unloaded as well as over a wide temperature range, such as a -85°F to +225°F range of in-process thermal cycling and storage. Second, the microstructure must be such as to permit the ready generation and maintenance of race-groove and ball surfaces physically and chemically capable of both boundary and elastohydrodynamic (ehd) lubrication under the unique running conditions of the gyro bearing. In this regard, freedom from ehd-film-piercing asperities is extremely important.

Both 52100 and 440C, the most commonly used gyro bearing steels, have demonstrated the ability to meet these requirements. Other steels have also been used successfully in gyro bearings, such as M-2, M-50, and WB-49. The steel most commonly used in gyro bearings through the years has been, by far, 52100. It has been quite satisfactory, but recurring unpredictable instances of corrosion have presented a problem. In the past several years, 440C has been attaining greater popularity for its resistance to corrosion and because of successful application. Both steels are readily fabricated to the required geometry and surface finish, in spite of the difference in microstructure primarily caused by the relatively large carbides in 440C, as seen in Fig. 4. In controlling the steel, factors of concern include chemical composition; microstructure; carbide type, size, and distribution; and response to heat treatment. The last, in turn, encompasses microstructure, strength, hardness, retained austenite, corrosion resistance, and stability.

Specific precautions are still warranted in the selection and application of both 52100 and 440C, in spite of the demonstrated ability of both of these steels to yield successful gyro bearings. These precautions include the assurance of freedom of the steel from nonmetallic inclusion and control of processing variables concerned with heat-treatment and metal-removal operations in the hardened state.

The presence of inclusions in other types of bearings which are highly stressed is detrimental because inclusions provide initiation points for fatigue failure. In gyro bearings, inclusions are also a serious problem, but for a different reason: they limit the surface achievable for the generation of a full hydrodynamic film, are associated with film-piercing asperities, and can cause chemical and particulate contamination problems. These effects will be covered more fully in Section 3; this section is more concerned with recognition of the problem in the steel.

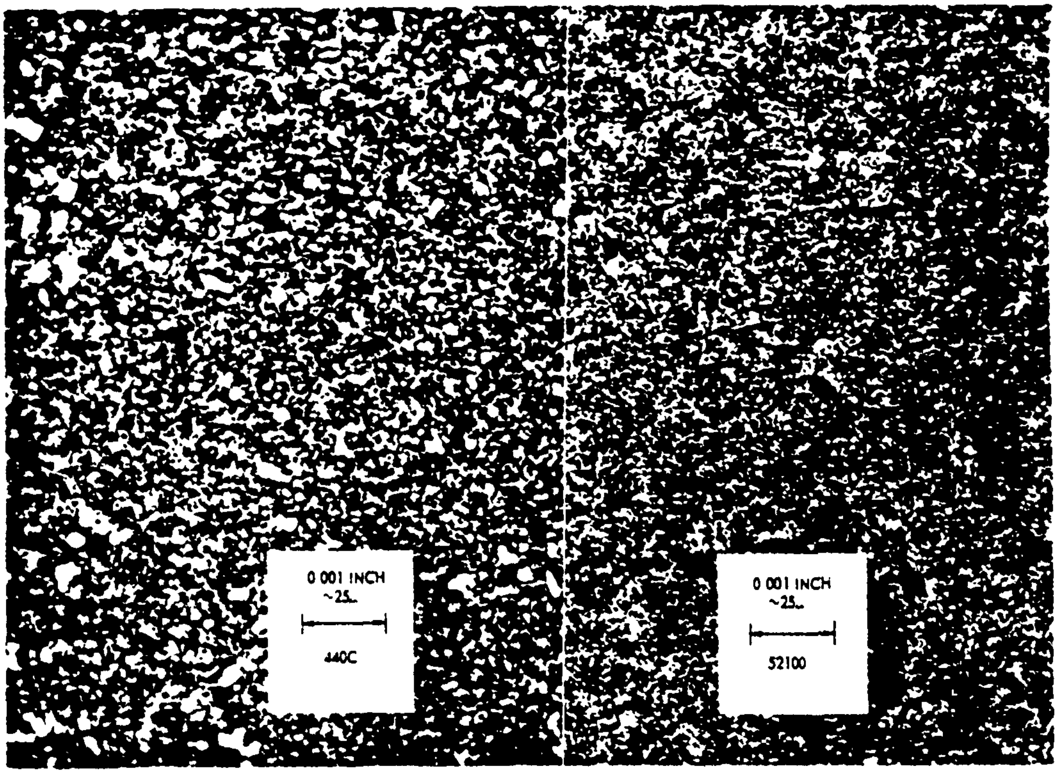

Fig. 4. Comparison of microstructure of 440C vs. 52100 steel.

Bearings with poor surfaces and low manufacturing yield, both attributable to inclusions in the steel, occur in spite of inspection of the steel for cleanliness by accepted rating methods, e.g., the JK (Jernkontoret) method. Stringers in the steel are particularly difficult to detect by conventional means. One approach to an improved steel-rating method is to examine steel surfaces in regions of the bar more representative of the bearing than the small flat sections normally examined. This is done by machining sample bars with steps at successively smaller diameters, representing diameters of the race-groove functional surfaces. These steps are then honed and examined microscopically for inclusions, as seen in Fig. 5. Steel lots evaluated by both this technique and the conventional approach have shown the honed step-down bar evaluation to correlate far better with race-groove surface topography and manufacturing yield.

Heat treatment of the bearing parts plays a major role in establishment of the previously noted properties of the finished bearing. It is important not only to determine optimum heat-treatment parameters but also to assure rigid adherence to the values selected. For this, the testing of sample pieces is needed.

HONED STEP-DOWN BAR

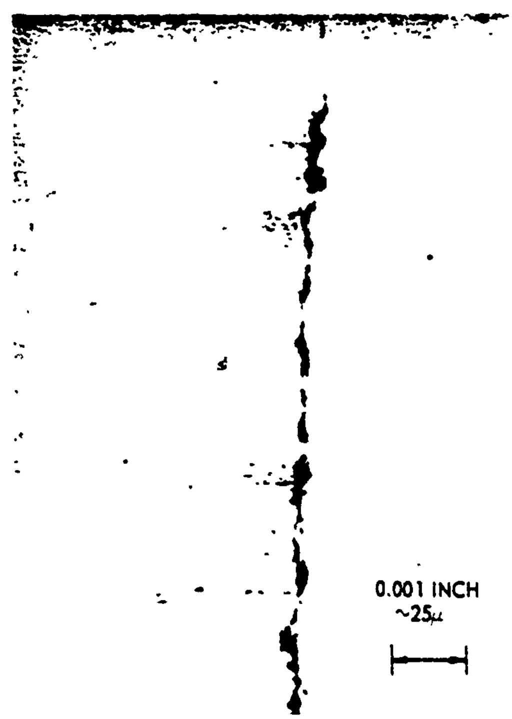

STRINGER INCLUSION IN BAR

Fig. 5. Inspection of metal for inclusions.

During austenitization, critical control often is required of the atmosphere and of the temperature level and timing cycle. Important to quenching are temperature, timing, oil-bath cleanliness, and agitation. Subcooling and tempering demand control of timing, temperature, and in some cases medium. Tests conducted to assure quality may include, as required, hardness, metallographic examination for surface modification and microstructure as shown in Fig. 6, retained austenite, and dimensional stability.

Properly selected, tested, and processed, today's steels are capable of the most rigid performance requirements demanded of current gyros.

2.2 Geometry

Nominal bearing geometry and variations therefrom play a major role in establishing gyro life and performance. With regard to life, geometry influences stress levels, thickness of the ehd film separating balls from races, and lubricant control. With respect to gyro performance, geometry influences bearing dynamics, lubrication stability, and response of the gyro to acceleration fields. In addition to the foregoing, geometric tolerance levels influence gyro producibility.

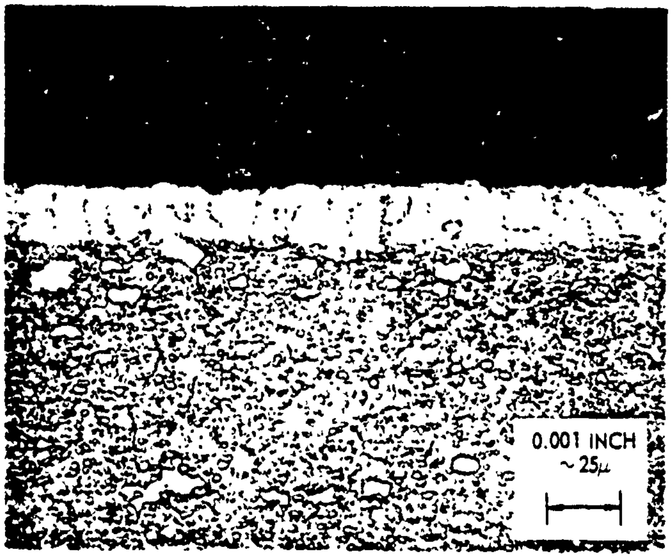

MICROSTRUCTURE OF SURFACE OF 440C BEARING
SHOWING DECARBURIZATION

Fig. 6. Heat-treatment surface modification.

One of the early major efforts leading to present gyro bearing technology was the development of measurement tools and techniques and then fabrication methods to achieve an order-of-magnitude improvement in geometric tolerances, from typical 0.0002-inch values to levels of 20 microinches. Gyro producibility immediately benefited by this improvement, as bearing-to-wheel and bearing-to-shaft fits became achievable on a tolerance rather than a selection basis. In addition, preloading certainty improved as did bearing dynamic behavior. Bearing life itself, however, was not significantly affected until race-groove geometry was further improved along with advances in groove surface characteristics, as is noted in Section 3.

It is quite apparent that the ehd film thickness is influenced by local stress levels, which in turn are affected by race-groove runout and cross curvature. Groove runout itself is the product of various geometric parameters, including roundness, lobing, groove-to-face and face-to-face parallelism, concentricities, face-to-bore and face-to-OD (outside diameter) squareness, and mounting distortions. Bearing manufacturing technology has advanced to the point that runouts can be held to the five- to fifty-microinch region. Mounting dimensions and forces must be carefully controlled, however, to prevent significantly greater runout due to distortion.

Race-groove cross curvature must also be closely controlled. Thickness of the ehd film in the pressure zone is a function of the local cross curvature. It is important to guard against excessive breaking of the corner at the conjunction of the groove and land. The resultant rounding or chamfer encroaches on the pressure zone and affects the local curvature, in some cases nonuniformly around the race. Figure 7 illustrates the results of this edge rounding.

Development of the Talyrond and a number of other roundness-measuring machines has made reliable measurement of race-groove runout and cross curvature possible. Thus, the generation and measurement of geometry to levels required today is within the capability of current bearing technology.

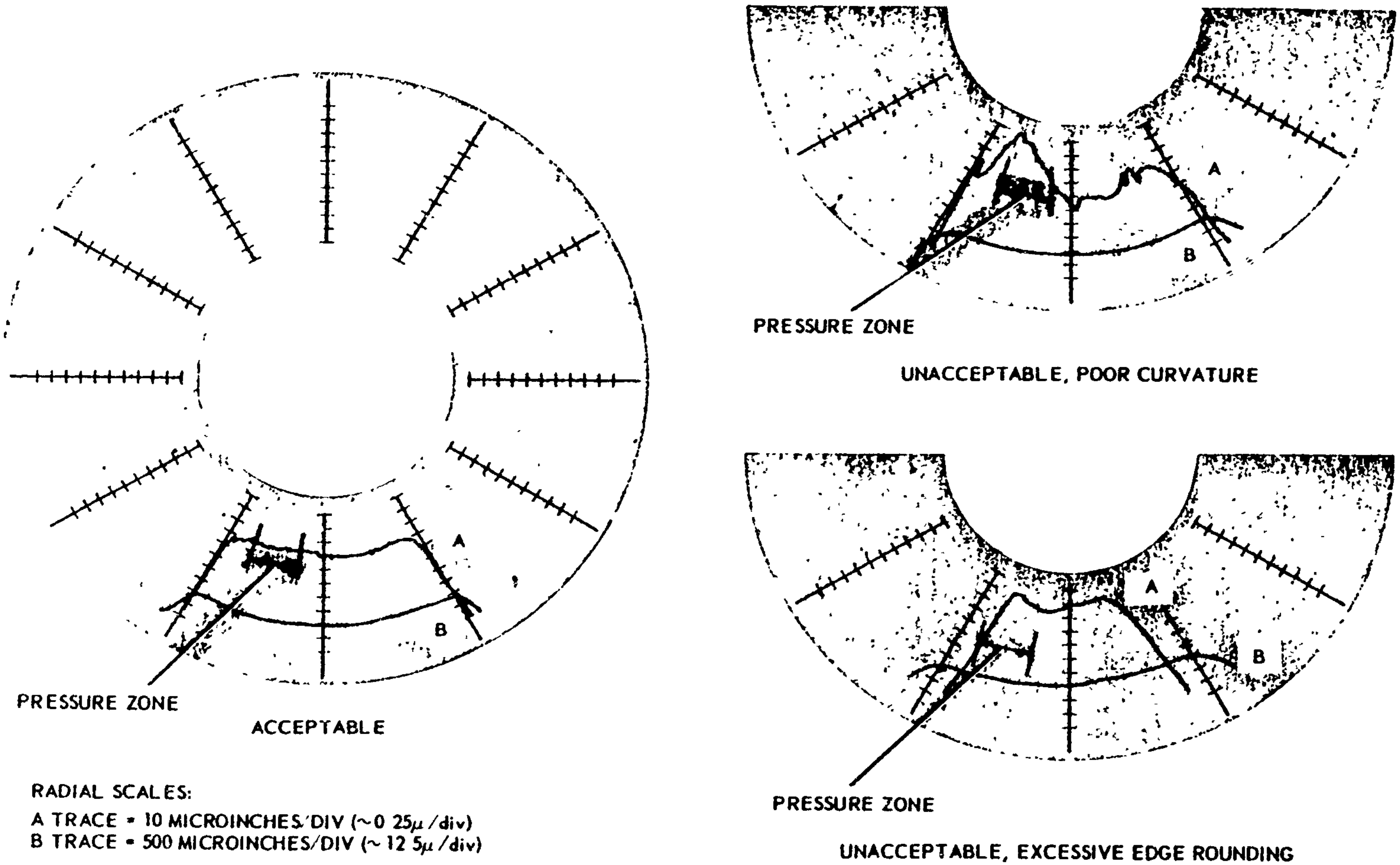

Fig. 7 Bearing race-groove cross-curvature Talyrond traces

SECTION 3

SURFACE

Generation and maintenance of the needed ehd film is a function of race-groove surface topography and chemistry. The surface must be free of film-piercing asperities and must chemically support a lubricating film. Low-speed boundary lubrication similarly depends upon these factors.

3.1 Topography

Shiny or dull, smooth or grooved? This question concerning optimum race-groove surface topography has been one of the most frequently debated for years. The smooth-surface camp wants to maintain the maximum possible ehd-film spacing between opposing surface peaks, by reducing hill-to-valley height, while the striated-surface devotees reason that the valleys between the heights provide a lubricant reservoir. Each group cites convincing data as the basis of its own cause and offers various additional reasons for the superiority of one type of finish to the other.

Actually, both types of surface have operated successfully for many thousands of hours under the most rigorous gyro-bearing running conditions. On the one side have been mirror-like race grooves generated by first running the bearings heavily loaded and submerged in ethylene glycol; surface-finish readings of these bearings were less than 0.3 microinch. Coarse-finish lapped bearings with 3-microinch surface-finish readings have also run very successfully. Smooth surfaces generated by ball lapping and by honing have also fared well. Examples of these finishes are seen in Fig. 8.

Within reason, average surface finish does not appear particularly significant. Individual asperities that project above the average surface can, however, pierce the ehd film and bring about failure. Returning to the need for a coarse finish to maintain a lubricant reservoir, any surface that will wet properly with the oil will hold a sufficient thickness of lubricant to permit generation of the required five- to fifteen-microinch ehd film.

Let us examine, then, the factors that should influence the selection of the race-groove finish. Achievement of the required geometry, circumferentially

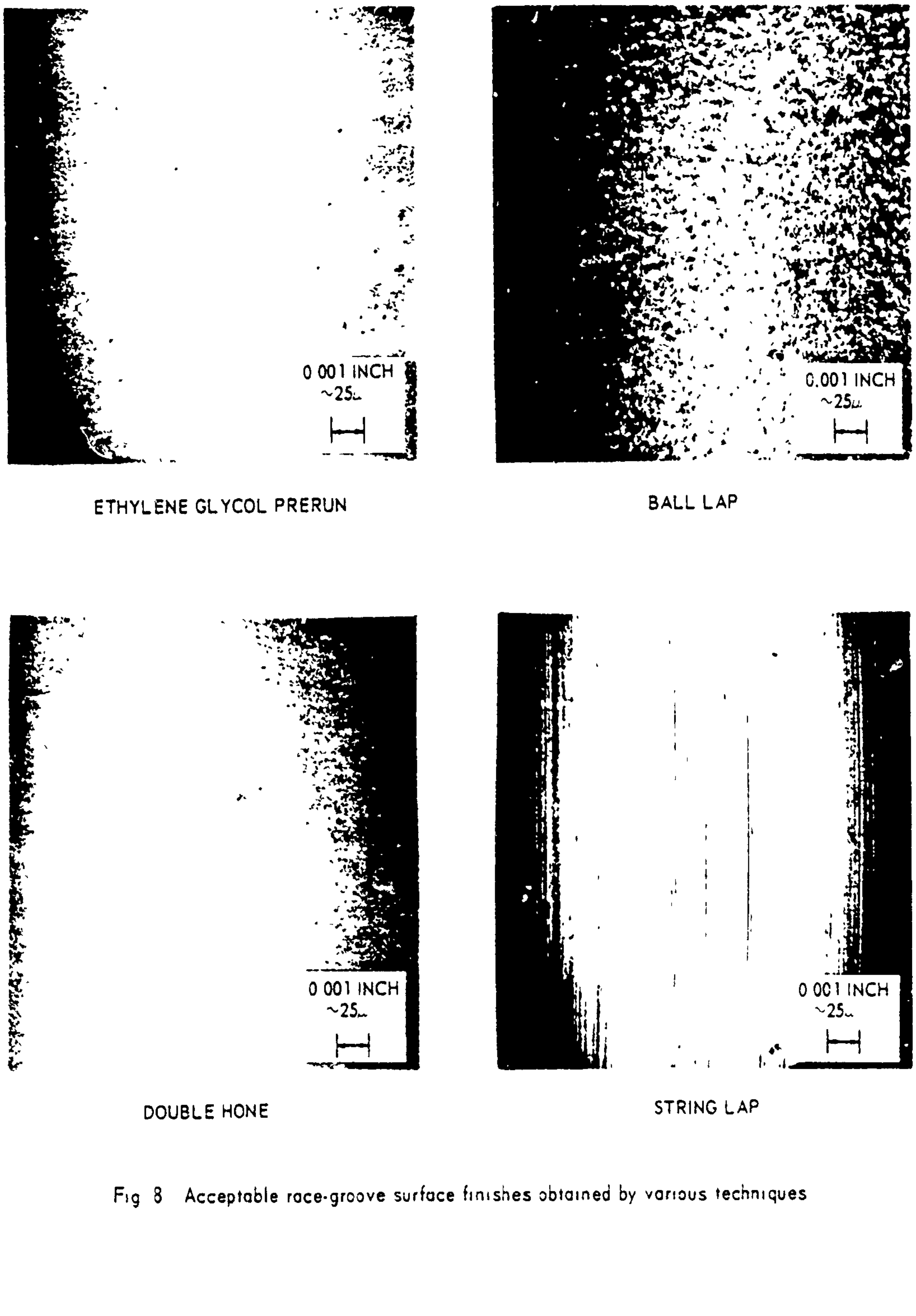

Fig 8 Acceptable race-groove surface finishes obtained by various techniques

and across the race groove, as well as generation of surfaces that are free of asperities are the two major factors. But we must also be concerned with particulate and chemical contamination, surface integrity (including freedom from "smear"), the "lay" of the finishing marks, ease of inspection and economics. Some bearing race-groove finishing techniques are illustrated in Fig. 9.

Perhaps the most commonly used finishing technique is lapping with an abrasive on a string, tape, paper, replica, or other backing. This approach generally improves as-ground roundness, but tends to degrade the cross-groove geometry. It typically produces a striated surface and reacts quite sensitively to irregularities in the metal or particulate contaminants by forming comets, as seen in Fig. 10. The grooved surface texture camouflages raised comets and other peripheral asperities, thus making inspection for these features more difficult and expensive. The striated finish, if accompanied by good geometry and freedom from asperities, contamination, and other deleterious factors, has been shown to yield very long successful life. An example is seen in Fig. 11.

Honing the groove with a reciprocating, shaped abrasive stone is another common finishing method. If the process parameters are properly controlled, honing yields excellent geometry. Finish depends upon the cycle, choice of abrasive materials, and honing fluid. This process can also generate raised asperities, and the surface finish can range from striated to nearly bland. Figure 12 shows successive improvements in finish accompanying development of improved honing techniques. This process can also yield excellent bearings.

Ball lapping is a newer process that involves lapping the race-groove by an abrasive slurry and groove-conforming balls driven by a rotating cone. This procedure does not improve on the initial race-groove roundness, but it yields excellent cross curvature characterized in some cases by an omega (ω) shape whose central rise is controlled to keep it out of the pressure zone. Ball lapping yields a uniform matte finish, as seen in Fig. 13, and does not generate raised asperities. This natural freedom from certain asperities significantly eases inspection problems. Bearings finished by this technique have demonstrated excellent yield and life.

Other finishing and run-in techniques have been used with varying degrees of success. One experimental approach, prerunning with special fluids, is worth noting for its demonstration of the ability of a bearing with mirror-like race-groove surfaces to run successfully. Running heavily loaded bearings at relatively low speed while submerged in recirculating filtered ethylene glycol will generate very highly polished race-groove surfaces. Such bearings, subsequently tested under gyro operating conditions, have demonstrated long successful life.

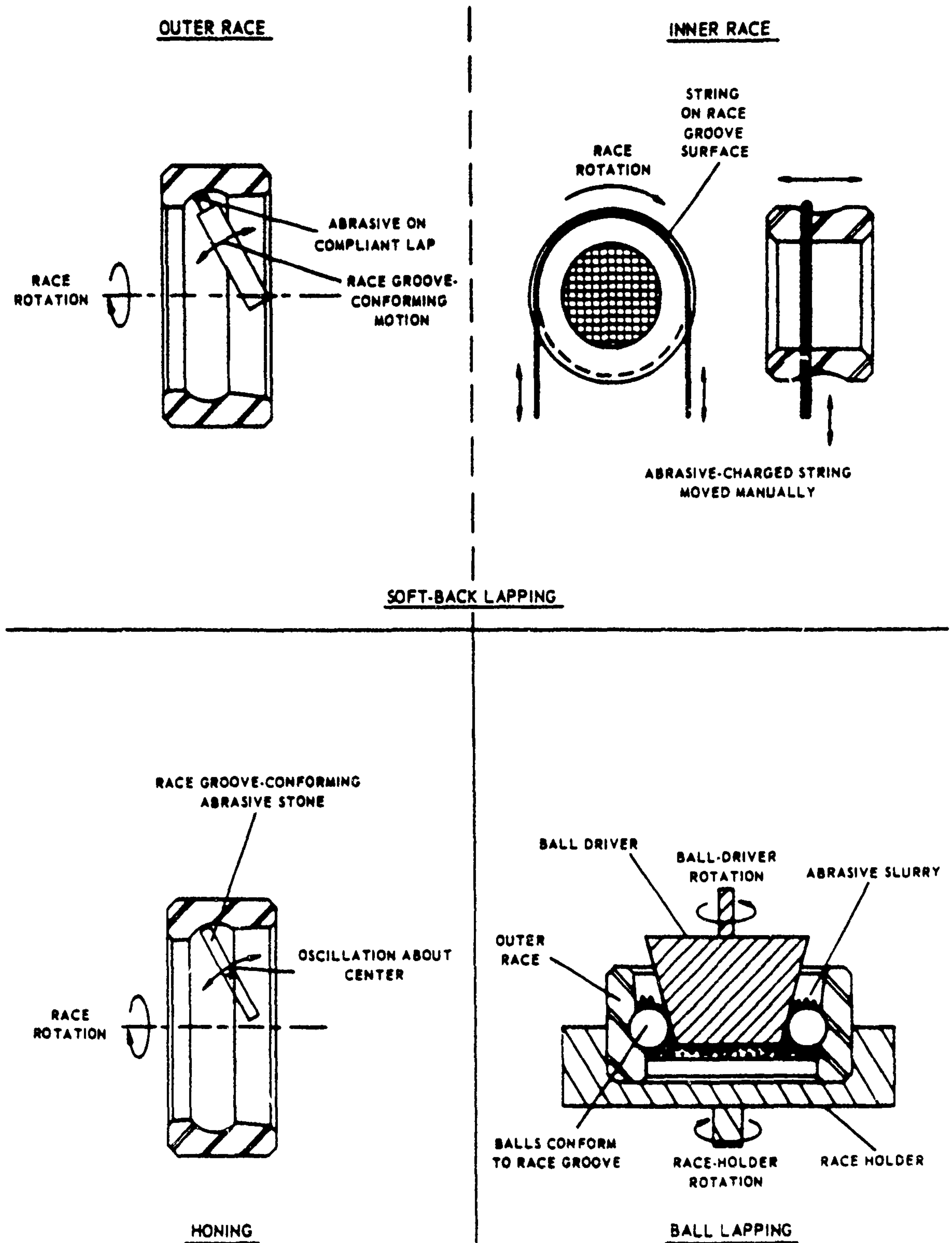

Fig. 9. Race-groove surface-finishing techniques.

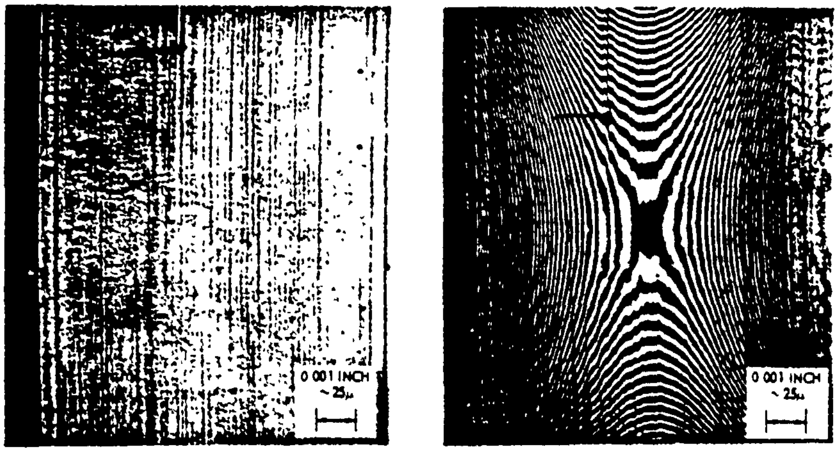

NORMAL MICROSCOPIC APPEARANCE

INTERFERENCE FRINGE PATTERN OF SAME FIELD SHOWING COMET IS RAISED. FRINGE SPACING IS 10.6 MICROINCHES (0.27μ).

Fig. 10. Comet on bearing inner race-groove surface.

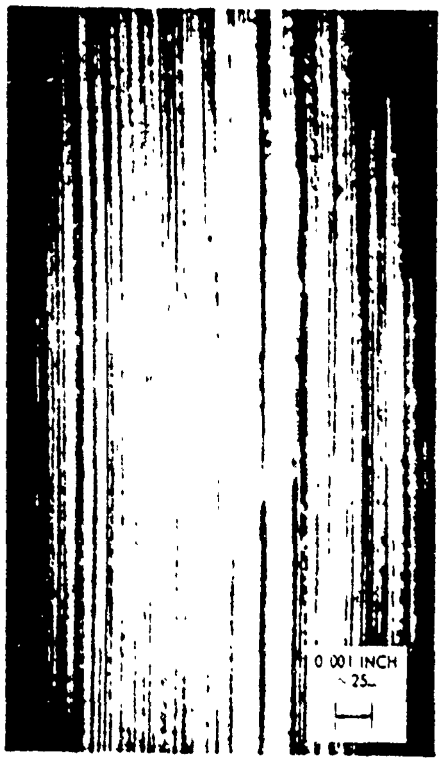

Fig. 11. R4 bearing outer-race groove after 10,000 hours of successful operation at 24,000 rpm

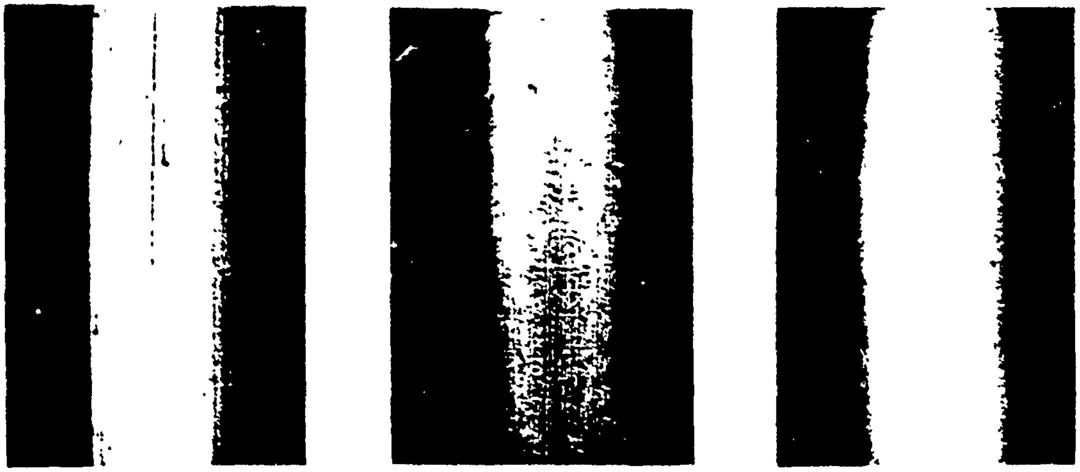

SINGLE-HONED DOUBLE-HONED DOUBLE-HONED MODIFIED

0.01 INCH
~ 250μ

Fig. 12. Progress in honed 440C outer race-groove finishes.

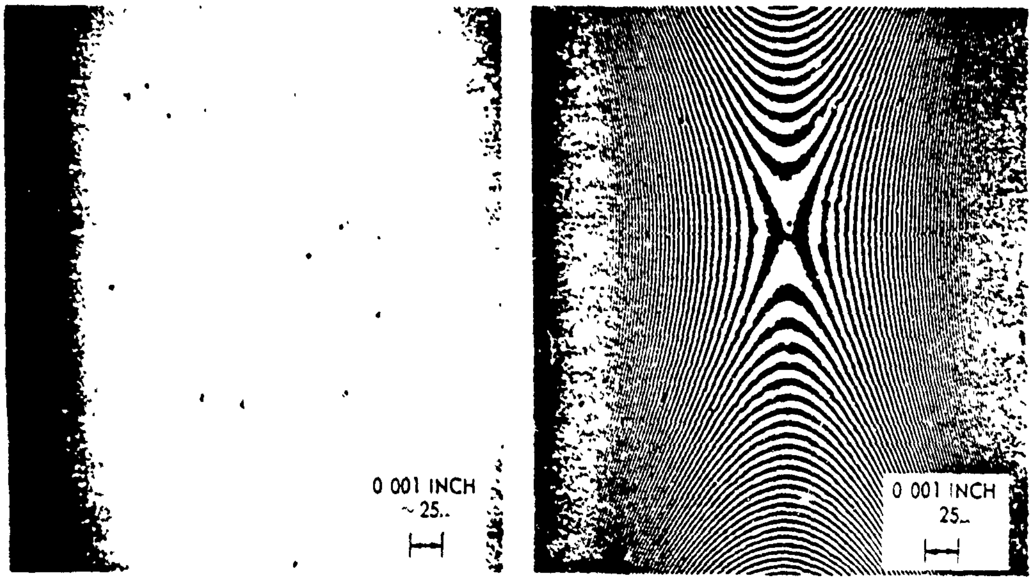

NORMAL MICROSCOPIC APPEARANCE

INTERFERENCE FRINGE PATTERN
OF SAME FIELD FRINGE SPACING
IS 10 6 MICROINCHES (0 27μ)

Fig. 13 Typical ball-lapped finish, R4 440C inner-race groove

Another interesting prerunning technique is that performed in hot TCP (tricresyl phosphate). The resultant surface appearance is only slightly changed, but the bearings demonstrate the beneficial effects of TCP coating discussed under Chemistry in Section 3.2. In addition, bearing yield and life can, under certain conditions, be dramatically improved by this method. A group of bearings made from metal with a high inclusion content and conventionally lapped showed a high incidence of comets. This group also demonstrated low yield and short life. Several pair of these bearings were TCP prerun, and their yield and life were very dramatically improved. Reduction in the frequency and severity of raised asperities is believed to be the principal reason for this remarkable improvement.

The importance of surface topography, which motivated the work on improved finishing methods, has also led to significant developments in the area of surface finish evaluation. Electromechanical surface-finish measuring devices have been improved, as have the techniques for application of light and electron microscopy. The simple interference microscope has been particularly useful, as is seen in Figs. 10, 13, 25 and 26.

One interesting technique for surface topography evaluation is the lubricant-film electrical-resistance gauge shown in Fig. 14. This device provides for loading a lubricated ball against a rotating race groove that drives the ball. A ball-to-race electrical circuit provides a measure of asperity contact or conjunction by counting the number of occurrences per revolution of drops in the electrical resistance below a pre-set level. Specific surface features can also be evaluated on a cathode-ray tube. Load, speed, and lubricant are varied. This device is limited by the electrical conductivity of the surfaces and asperities, and chemical coatings on the surfaces. Its use is generating further insight into race-groove surface topography.

Another technique useful in surface and immediate subsurface evaluation is taper sectioning of races, illustrated in Fig. 15. A race groove is electroplated for edge preservation, and a chordal sector ground off at a shallow angle. The resultant section is polished and etched to provide a mechanically magnified (by virtue of the taper) race-groove surface contour. The metal microstructure close to the surface can also be evaluated by this technique, and microhardness readings can be taken. Such readings typically show that the metal close to the surface is slightly harder than the bulk of the race.

Because of the correlation between bearing life and surface topography, this factor has been improved in many aspects. Today's bearing technology does not have to be limited by surface-topography inadequacy.

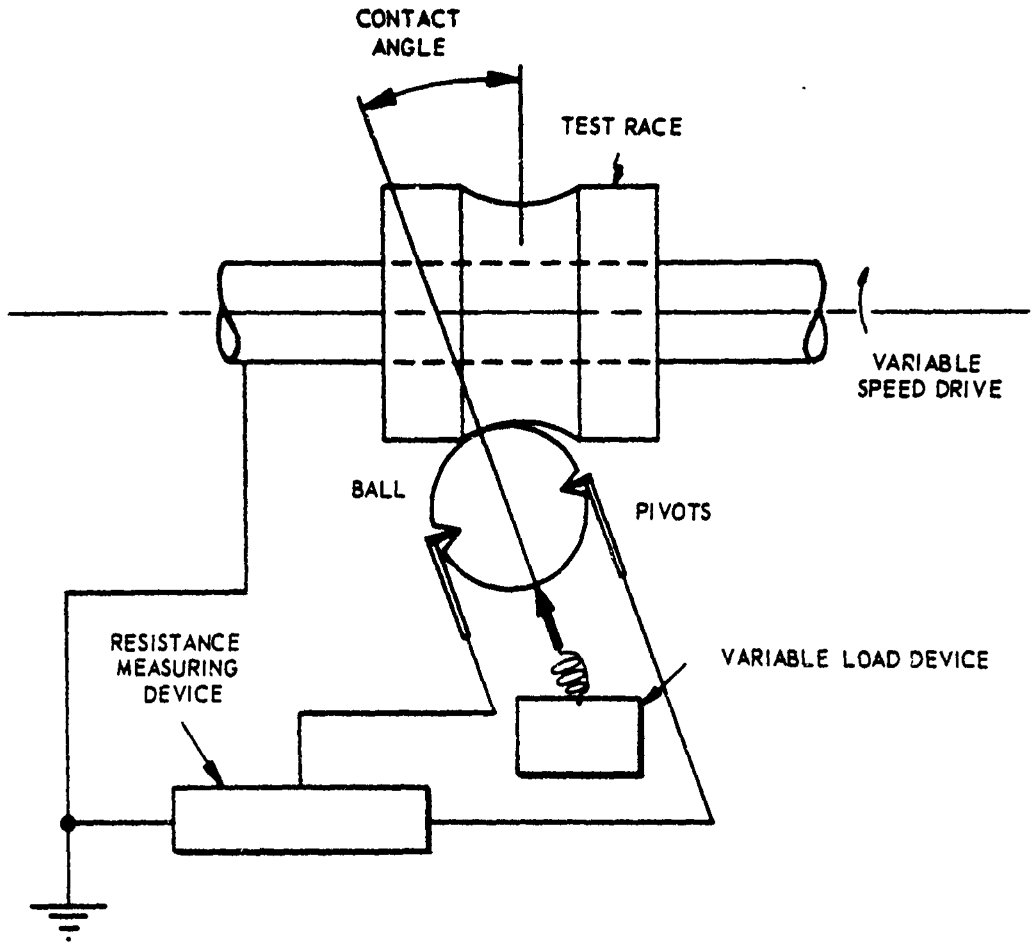

Fig. 14. Lubricant-film electrical-resistance gauge.

3.2 Chemistry

Bearing metal surface chemistry has for many years been cited as a possibly significant determinant of bearing performance. For several years, surface chemistry has been deliberately modified to improve the boundary lubrication capability of the bearing. It has been only recently determined, however, that inadvertently applied chemical surface modifications can adversely affect bearing life under both boundary and ehd conditions.

It has been shown that a lubricated untreated 52100 or 440C bearing will suffer lubricant degradation and surface distress in a running period of less than one hour to several hours at one rpm under normal load conditions. Another interesting phenomenon associated with the boundary lubrication condition experienced at very low speed is the large difference in bearing torque among apparently identical bearing batches received at various times. Bearing torque at one rpm may vary by a factor of three from batch to batch.

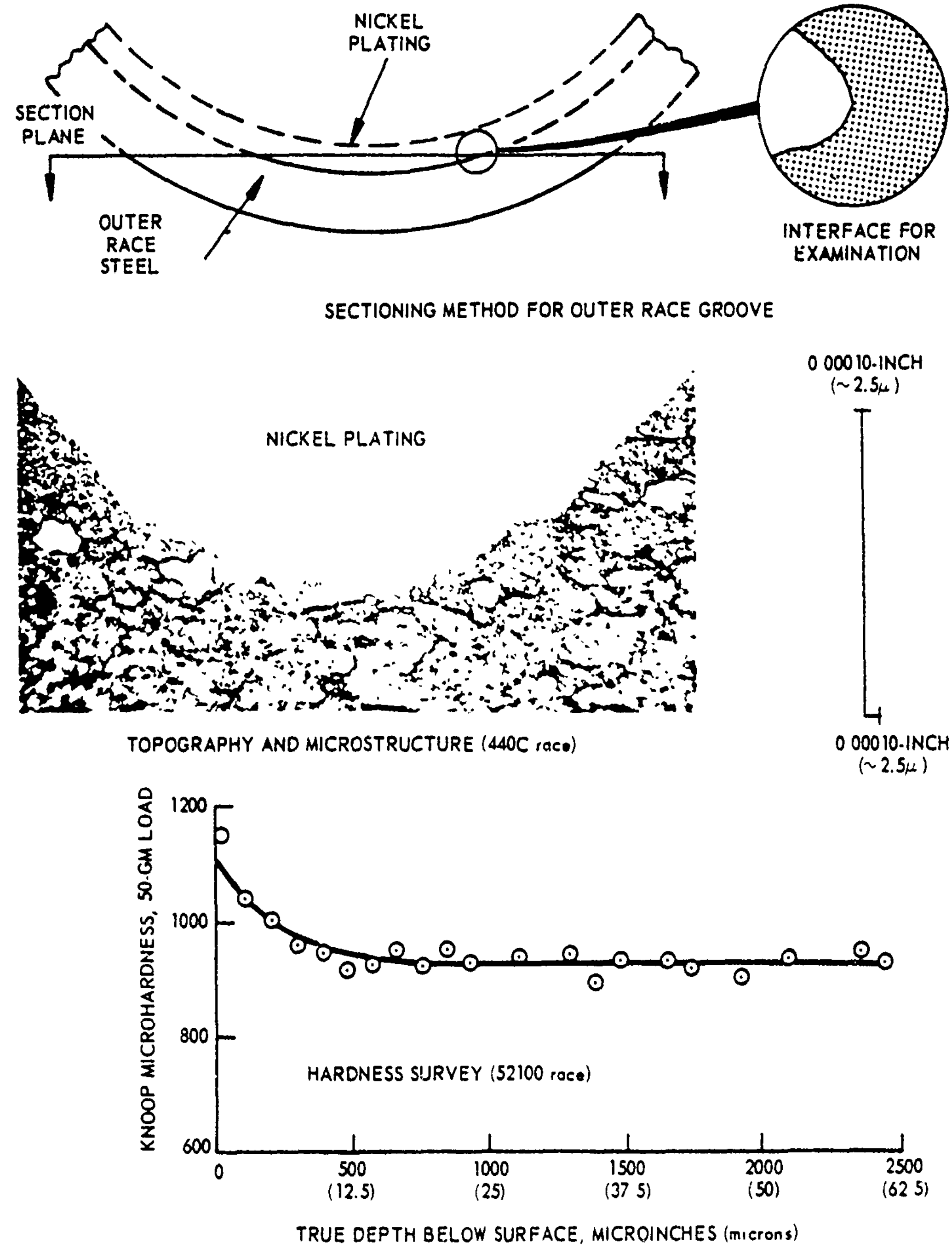

Fig. 15. Taper sections of outer-race grooves

Both of these conditions can be corrected by a very simple expedient: prolonged hot soaking of the metal components of the bearing in TCP; the effects of this can be seen in Table 1. Life at one rpm then increases from one or a few hours to several hundred or thousand hours. One-rpm friction torque of various batches of bearings then group close together at the low level. It is thought that beneficial effects result from chemical reaction of the acid phosphates present as impurities in TCP with the steel surface. Nitric-acid passivation of 440C steel surfaces has also yielded low-speed life longer than that achieved with untreated surfaces. Prerunning of bearings in TCP, as described in Section 3.1, also produces the beneficial effects described above.

Table 1. Effects of TCP coating on low-speed endurance and torque.

R4 BEARING, 1 RPM 10 POUND AXIAL LOAD (4.5 KG)	AS FINISHED	TCP COATED
Torque (gm-cm)	2 to 6	2 to 3
Time to failure (hours)	1 to 5	200 to 1000+

Evidence of detrimental surface chemical modification, or contamination or "poisoning", is more recent and of potentially very great significance. The problem was first recognized when two groups of bearings, which by all conventional evaluation techniques were considered excellent, demonstrated early atypical failure under both boundary and ehd running conditions. These bearings also showed strangely modified surfaces when prerun immersed in TCP, as discussed in Section 3.1. Figures 16, 17, 18 and 19 illustrate these phenomena.

The most effective means for recognition of this contamination was found to be the rate of oil-drop spreading on the race-groove surface; contaminated bearings showed poor oil wettability. A spreading test and typical results are shown in Fig. 20. Investigation led to discovery of the probable cause of the poisoning, and its correction led to the delivery of the remaining bearings from one of the two groups in an uncontaminated condition. These "clean" bearings have been used very successfully in a gyro build program, thus further supporting the thesis.

It is important to note that poor wetting of the surface is a symptom pointing to the presence of this contamination, not necessarily an explanation of why early failure occurs. For example, the bearing surfaces can be made to wet with the oil by any of a few techniques, such as immersion in oil or deposition from a solvent solution, and once wet the oil does not spontaneously retract from the

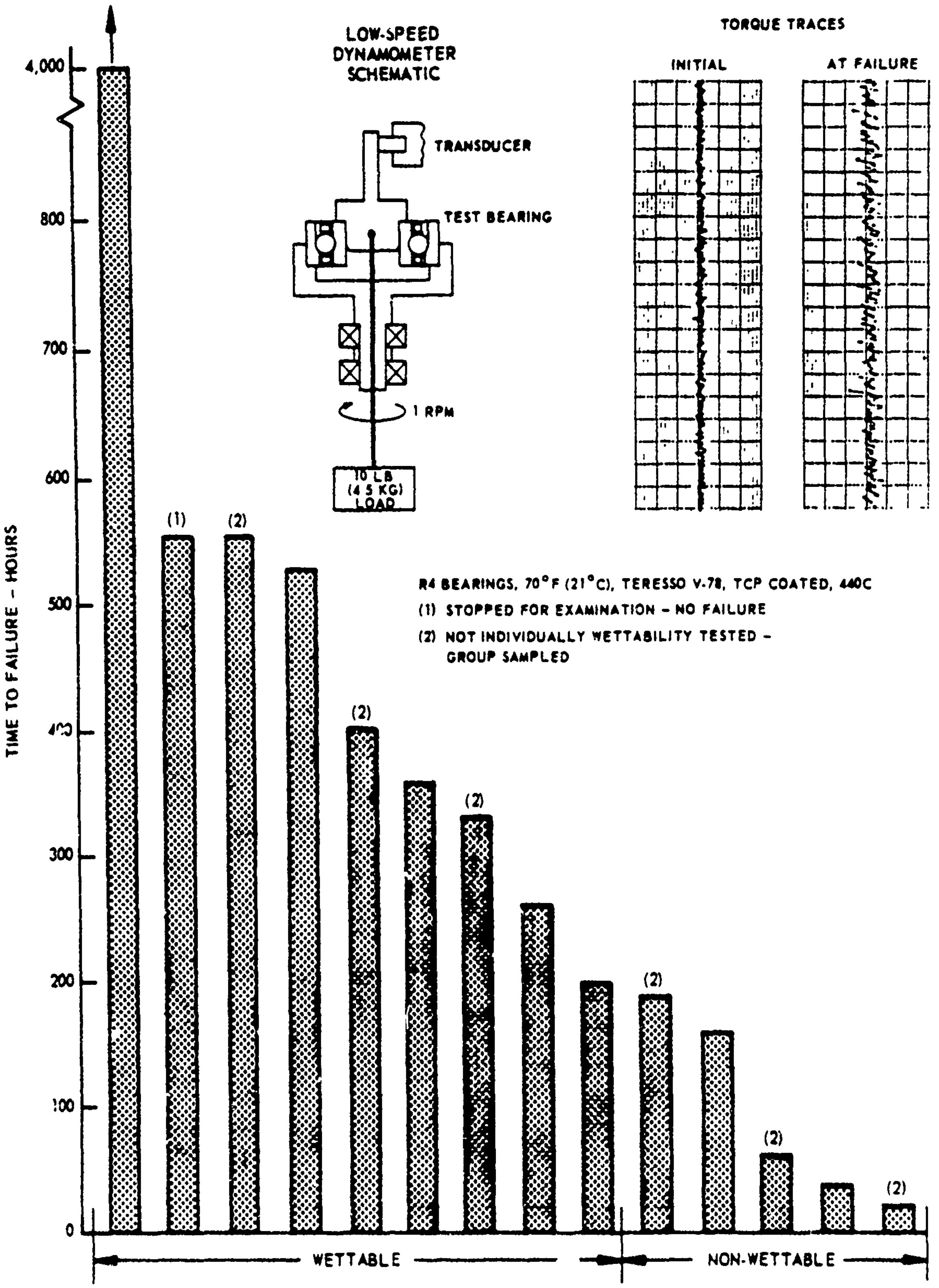

Fig. 18. Surface chemistry effect on low-speed endurance (1-rpm continuous)

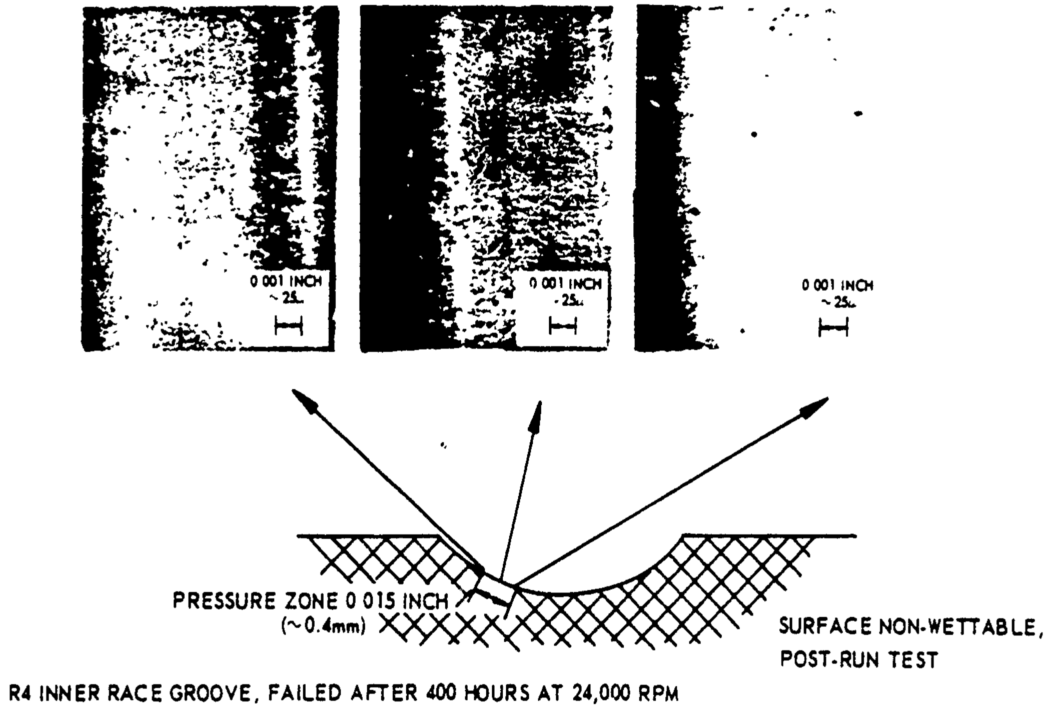

Fig. 16. Chemically contaminated bearing surface, early failure.

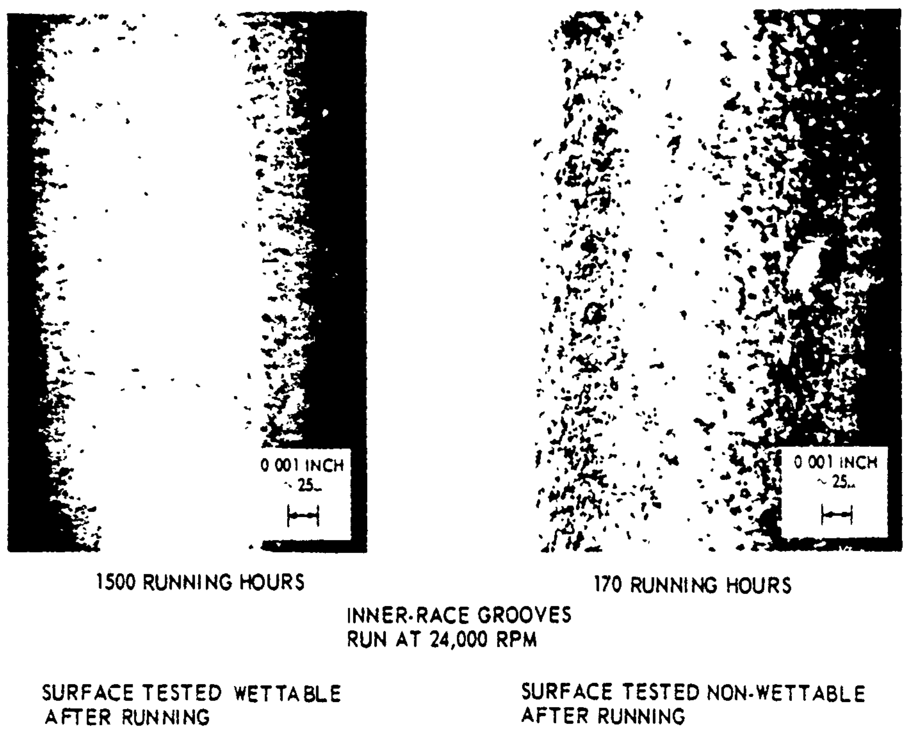

Fig 17 Surface changes, early bearing failure.

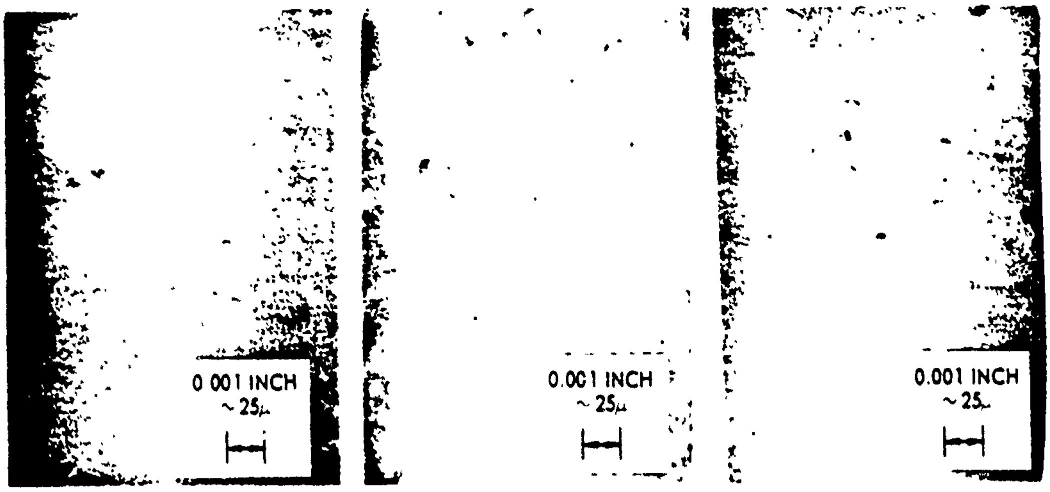

AS RECEIVED | TCP PRE-RUN SURFACE NON-WETTABLE | TCP PRE-RUN SURFACE WETTABLE

R4 BEARING PRERUNNING CONDITIONS IN FILTERED RECIRCULATING TCP
PRELOAD: 14 LBS (6.4 KG) SPEED. 30 RPM TEMP 130°F (54°C) TIME OF RUN: 100 HRS

Fig. 19. Surface changes, inner-race grooves, tricresyl phosphate (TCP) prerunning.

surface. An oil drop then applied to a wet surface will spread quite rapidly. Most bearings are used in this prewetted condition. The explanation for failure may lie in the difference in the lubricant properties in the high-pressure zone, particularly the behavior of the molecules next to the surface.

By special solvent-cleaning techniques, a number of the poisoned bearings were rendered "wettable". These bearings are demonstrating greatly improved life under both boundary and hydrodynamic running conditions. An interesting facet of this investigation is the apparent validation of an occasionally reported beneficial effect derived from aging of bearings stored in oil, and an association of this effect with surface chemistry. Briefly, some of the poisoned bearings have been made wettable by artificial aging (elevated-temperature soaking) in oil, as shown in Fig. 21.

It is interesting to speculate on the possible significance of surface chemistry in the age-old problem of unpredictability of bearing-batch behavior: early failure and low yield versus long successful life from batch to batch, with no known difference in the bearing or its application. Current efforts in this investigation are aimed at establishing the fundamentals concerned with the effects noted, improved recognition, prevention, rehabilitation, and means for specifying required surface chemistry. Rudimentary recognition techniques are known today, and means for corrective or preventive action are at hand.

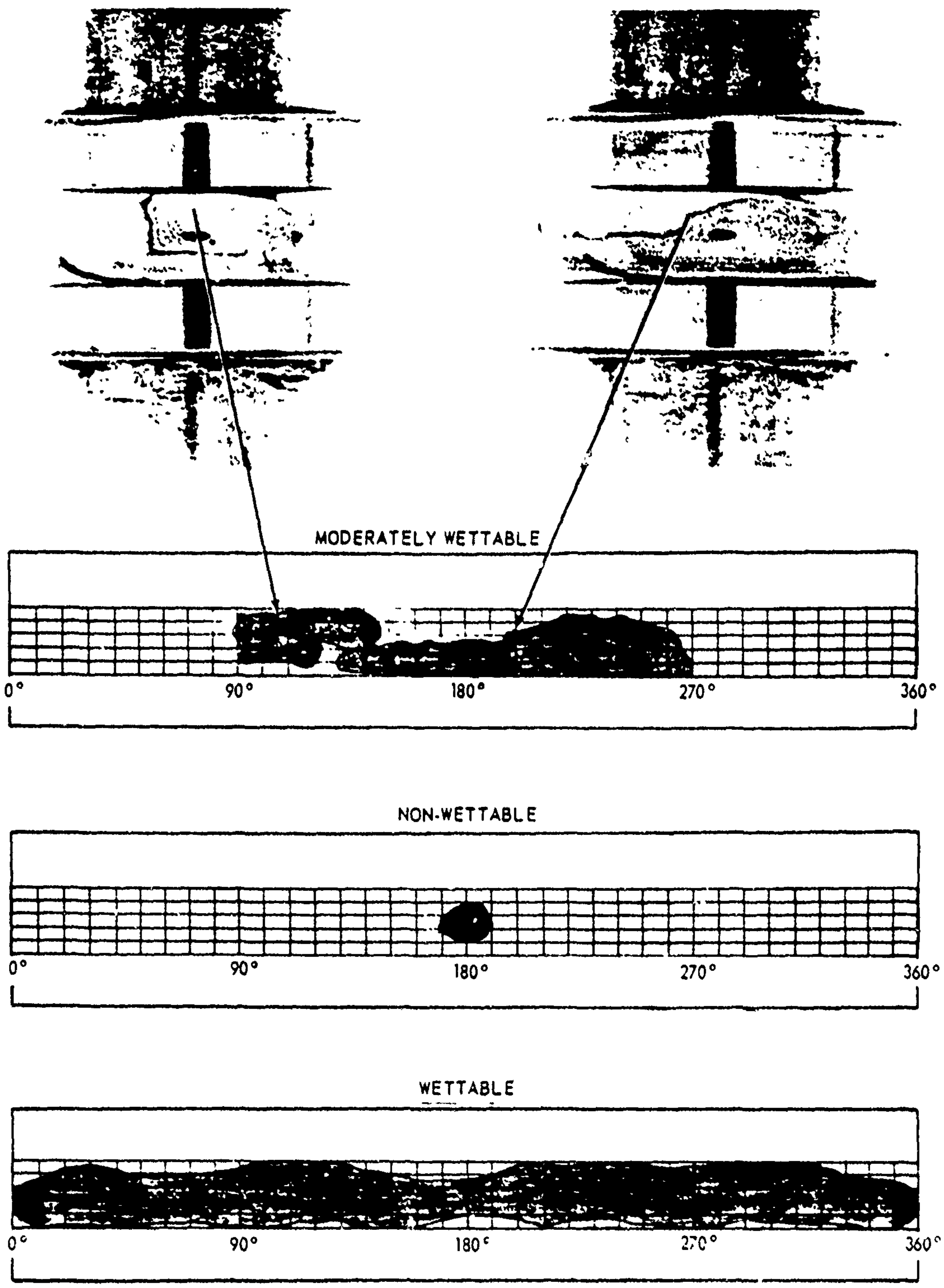

NOTE. OIL DROP SPREADING TIME 19 HOURS

Fig. 20 Oil spreading records – inner races

OIL SPREADING RECORDS

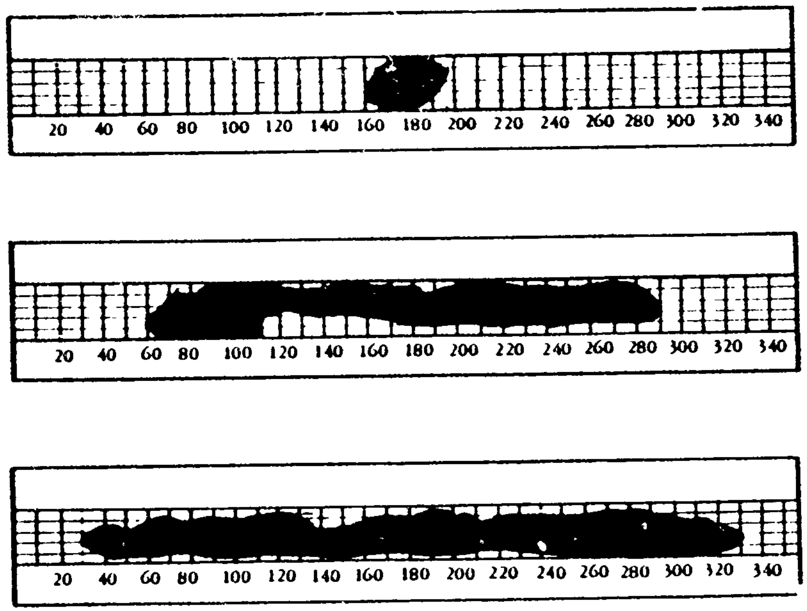

AS RECEIVED

AGING TIME AT 180°F (82°C)	EQUIVALENT TIME* AT 70°F (21°C)
1 WEEK	1¼ YEARS
2 WEEKS	2½ YEARS

SURFACES AGED BY EXPOSURE TO TERESSO V-78 OIL AT 180°F (82°C)

*EACH WEEK AT 180°F (82°C) IS EQUIVALENT TO 1¼ YEARS AT 70°F (21°C), ASSUMING REACTION RATE DOUBLING WITH EACH 10°C RISE

Fig. 21. Aging effect on wettability.

SECTION 4

LUBRICATION

The importance of geometry and surface to the generation and maintenance of a stable ehd film has been discussed in the preceding sections. Lubrication is the other significant factor. Maintenance of the film demands that the ball retainer deliver to the balls in a stable manner the required amount of a lubricant with the needed properties. Stability of the film requires that the circulation of the lubricant be controlled to prevent excessive local oil buildup that can periodically cause film-thickness changes, as discussed in Section 6.1.

The demand for stability limits the total quantity of oil that can be carried in the lubrication system, but sufficient oil must be available for long life and maintenance of a low-friction coupling between the balls and retainer. Therefore, control is needed of lubricant function, quantity, and disposition. Severe demands are thus made on both the lubricant and the retainer.

4.1 Lubricant

Most precision ball-bearing gyros use oil rather than grease as the bearing lubricant. The lubricant quantity and distribution needed to assure long life is more stable in the form of oil impregnated in a porous-plastic ball retainer than grease packed around the balls.

The oil used in most gyros for more than twenty years has been Humble's Teresso V-78, a paraffinic mineral oil formulated with an anti-oxidant, an anti-foam agent, and a lubricity additive. Its nominal viscosity is 78 SSU at 210°F, or about 15 cs at 210°F. This lubricant, formulated originally as a steam-turbine oil, has performed very well in the gyro application. At various times through the years, comparative testing has been performed in attempts to find improved oil but with no marked success.

Teresso V-78 is no longer being manufactured and a replacement must soon be specified. A program to formulate and test this replacement is currently underway. The successful candidate will be one of a family of lubricants of varying viscosities for use under different operating conditions. The first approach is to match V-78 in major properties and sensitivities, thus making the substitute useful in the wide range of applications now seen by V-78. The current principal candidate, KG-80 (Kendall Refining Co.), is also a paraffinic mineral oil of approximately the same viscosity as V-78. It is commercially superrefined and incorporates an anti-oxidant (Ethyl AO 702) and a boundary additive (TCP). Preliminary tests are encouraging but not yet conclusive.

There is some question as to the specific lubrication mechanism that maintains the ehd separation of the balls and races. One school presents a mechanical concept of lubrication, relating the configuration of the ehd film to bearing and environmental factors such as geometry, speed, temperature, elastic modulus, and load, and to lubricant physical properties such as viscosity and viscosity-temperature and viscosity-pressure relationships. To this concept, another school adds more chemical concerns such as composition of the lubricant, polar-component properties, surface chemical interactions, and effect of molecules adsorbed to surfaces on pressure-zone viscosity. The significance of the chemical interface of the lubricant to the metal is emphasized by the current work in the area of surface chemistry noted in Section 3.2.

Additional significant lubricant properties include thermal, oxidative, chemical and hydrolytic stability, volatility, chemical compatibility with bearing materials, and surface tension. The lubricant must, of course, be able to withstand fine filtration without detriment. It must also provide boundary lubrication under low-speed conditions. Teresso V-78 provides the properties for long successful operation; its potential replacement family hopefully will perform as well or better.

4.2 Retainer

Gyro performance, life, and torque requirements demand the use of an oil-impregnated porous-plastic ball retainer, or separator, to perform the dual functions of ball separation and provision of a lubricant reservoir and control mechanism. As demands for performance, life, wheel speed, and preload become more severe, the demands on the retainer also grow.

The most commonly used retainer material in the gyro bearing has traditionally been a paper or cloth phenolic laminate. It has had some measure of success under certain operating conditions, but has proven inadequate for the more difficult jobs. A major problem with the tubes or rods from which phenolic separators are manufactured has been lack of repeatability of physical and chemical properties from piece to piece and even along the length of a single rod. Because of the structure of the material, the retainer holds most of its lubricant on and close to the surface. Oil retention in normal phenolic-laminate retainers is only one to five percent by weight. Oil-feed characteristics are poor, and it is difficult to adjust the lubricant quantity to the narrow range between insufficient lubricant to maintain an ehd film and excess lubricant resulting in poor instrument performance.

Porous sintered nylon (Nylasint) has provided solutions to many of the problems inherent in the use of phenolic laminates. Nylasint is a through-porous material with more than twenty-five percent total porosity. Figure 22 compares laminated phenolic and Nylasint porosity characteristics. In use, the oil content is held to a value closer to fifteen percent in order to avoid the oil jag (Section 6.1) and migration problems associated with excess lubricant. The pore structure of Nylasint is bimodal, with the larger pores generally around 3.5 microns and the smaller ones around 0.6. Total porosity, pore-size distribution, sling-out characteristics, and strength are adjustable within fairly broad limits.

As a retainer material, Nylasint is not without problems. It is more difficult to machine and deburr than laminated phenolic. Its properties are better controlled than those of the phenolic, but not as well as desired, and it is weaker and softer than phenolic. It is more subject to whirl or squeal under the more rigorous operating conditions of performance, load, and speed to which it is subjected (as discussed in Section 6), though treatment of ball-pocket surfaces as well as other remedies alleviate this.

Bearing life tests and gyro performance attest to the marked superiority of Nylasint over laminated phenolic. Operating Nylasint-bearing gyros approaching 30,000 running hours are still showing excellent performance with no sign of degradation.

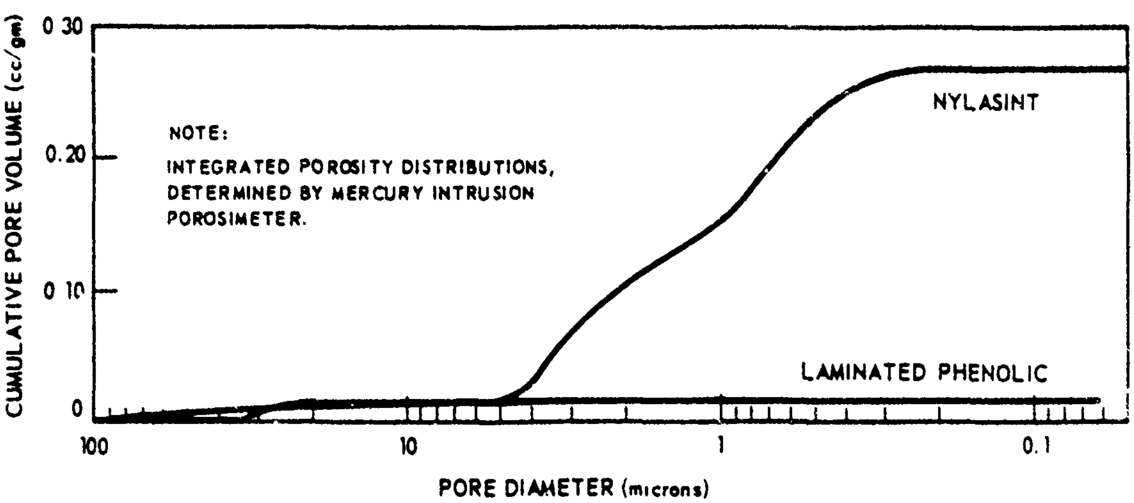

Fig. 22. Pore size distribution for porous nylon and laminated phenolic retainer materials.

Both the increased oil quantity and the through-porosity of the material contribute to its success. A series of tests was conducted to establish the validity of the theory that complete circulation of the bearing lubricant occurs with use of through-porous retainers. Retainers were cut approximately in half and re-cemented with impermeable walls separating the two halves, as shown in Fig. 23. Before rejoining, one half was impregnated with clear lubricant and the other with blue-dyed oil. Studies were made of the rate and mode of oil circulation as a function of running hours for a range of geometry, speed, lubricant, surface

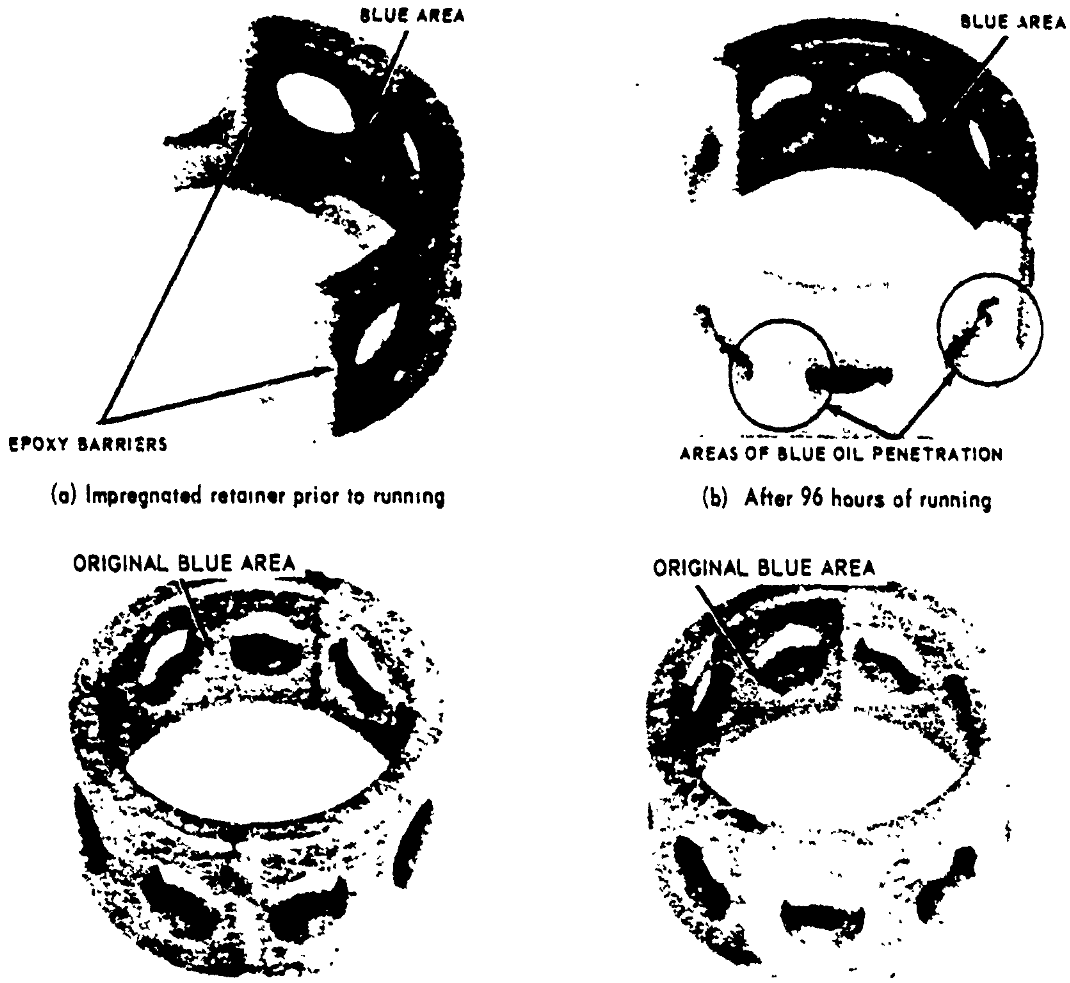

(a) Impregnated retainer prior to running

(b) After 96 hours of running

NOTE: LEFT-HAND RETAINER HAS A LARGER AREA ORIGINALLY IMPREGNATED WITH BLUE OIL, WHICH ACCOUNTS FOR THE DARKER RIGHT-HAND SIDE OF THAT RETAINER

(c) After 1786 hours of running

Fig. 23. Oil circulation, Nylasint retainer.

treatment, retainer permeability, preload, and ambient pressure. It was established that complete circulation of the lubricant does occur and that lubricant transfer takes place at the ball-to-groove and ball-to-retainer interfaces.

Dramatic evidence of the need for a through-porous retainer at higher speeds is seen in Fig. 24. Typically, for a specific set of running conditions for R4 bearings, 12, 000-rpm life with Nylasint retainers exceeds 20, 000 hours. With laminated phenolic, it ranges from 5, 000 to 15, 000 hours; and with solid nonporous nylon with oil retention nearly equal to that of the phenolic, it approximates 2, 000 hours. Doubling the speed to 24, 000 rpm leaves Nylasint life essentially unchanged, reduces phenolic life to about 500 to 2, 000 hours, and drastically cuts life of solid nylon to less than 24 hours.

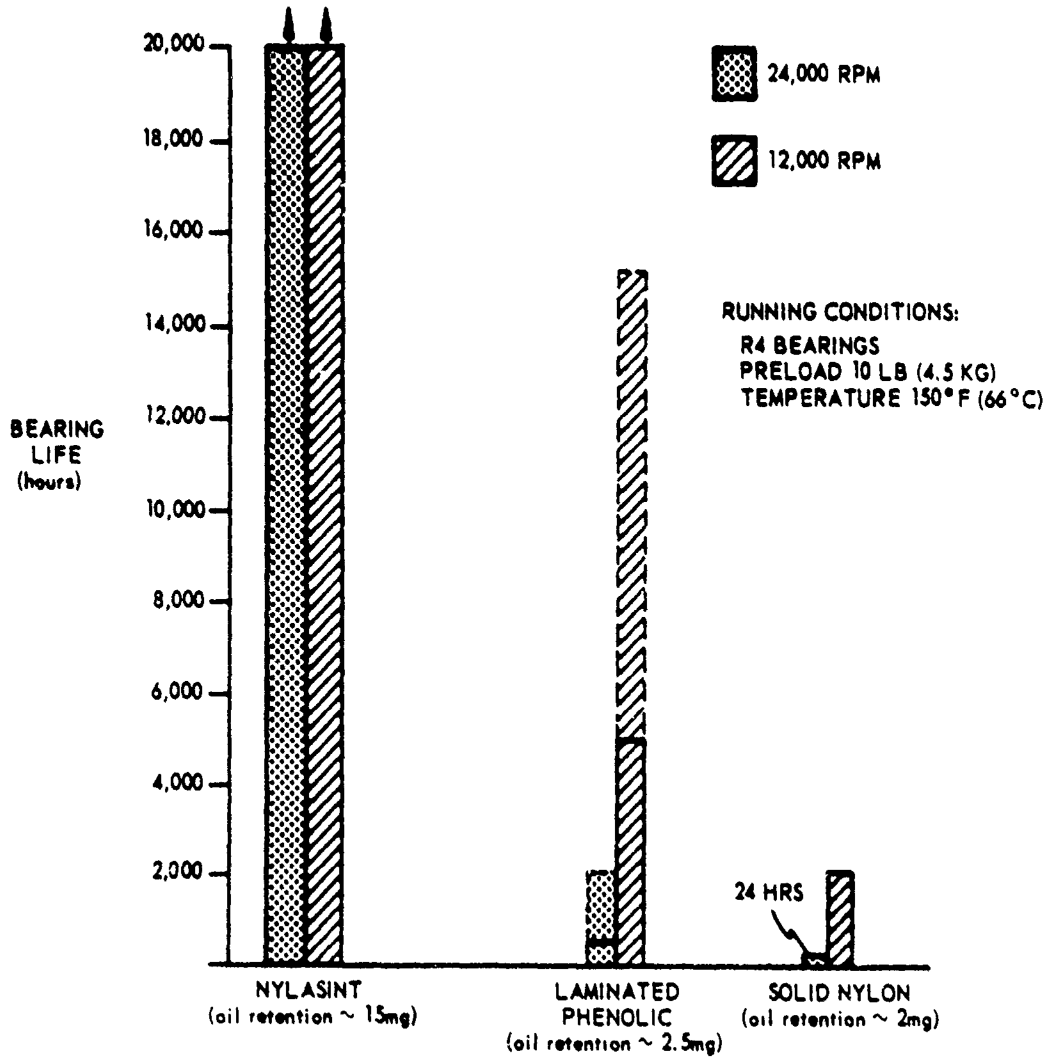

Fig. 24. Expected bearing life vs. speed for three retainer materials.

It is interesting to speculate on the possible role of a through-porous separator as an oil filter, since complete circulation of the oil occurs. Is particulate matter, initially in the bearing or generated on occasions of momentary asperity contact or lubricant degradation products, strained from the lubricant by the Nylasint? Dark deposits are frequently seen in the ball pockets after bearing operation.

Nylasint ball retainers perform well, but additional work is needed. Improvement in some properties as well as in quality control is desirable.

SECTION 5

PROCESSING

Bearing processing, from completion of manufacture through gyro construction, must preserve or improve upon bearing built-in quality. In addition, this quality as well as various performance parameters must be monitored at critical construction stages. Development of processing techniques and evaluation means has played a major role in the evolution of gyro bearing technology.

5.1 Quality Retention

Contamination control is a critical factor in bearings that must maintain a fractional microinch ehd film stability and that do not have a frequent fresh supply of lubricant to flush out debris. Chemical, particulate, and even atmosphere contamination must be avoided.

Chemical contamination of the metal surfaces, as discussed in Section 3.2, impedes the maintenance of either boundary or ehd lubrication. Its prevention is important particularly in final bearing manufacturing and early instrument-processing stages. Exposure to various cleaning agents and processing and storage fluids must be evaluated for potential deposition of unwanted films or detrimental surface chemical reactions. Housekeeping practices must be well controlled to prevent contaminated fluids, dirty glassware, improper processing, or human contamination from affecting the metal surfaces. At the moment, the only reasonably economical nondestructive test for monitoring a subtle form of chemical contamination is the spreading rate of oil on the surface.

Particulate contamination is a more commonly recognized problem, and at one point abrasive contamination during lapping was the cause for many early bearing failures. Recognition of this problem by microscopic inspection with polarized light led to improved cleaning techniques, and this issue has been largely resolved.

There are many potential sources of particulate contamination, as in bearing manufacture, packaging, instrument construction, in the solvents or the lubricant, and from the ball retainer. Soft as well as hard particles can be detrimental under the high pressures of the films between the balls and races. Ball-retainer deburring and cleaning are particularly significant in the prevention of particulate contamination, especially since the retainer remains a possible source of contamination throughout the running life of the bearing. Figures 25 and 26 are examples of brinelling by soft and hard particles.

Atmosphere contamination refers to the condition of the ambient atmosphere in which the bearings are run, both in test chambers and in the final-sealed gyro float. One concern is control of the atmosphere to prevent detrimental chemical changes in the lubricant or on the metal surface. The other is retention of the physical properties needed for acceptable windage torque, heat transfer, and float leak detection.

Another area of concern in bearing processing is retention of bearing geometry. Factors associated with bearing geometry, potentially affected by variations due to processing, include basic instrument design sensitivities as well as bearing dynamics and ehd film generation and maintenance. Of obvious concern are the changes in race-groove roundness that occur with interference fitting of out-of-round shafts or wheels to round bearing bores and OD's; a representative example is shown in Fig. 27. Less obvious, but equally significant, are out-of-square and out-of-parallel clamping distortions.

A gross geometric change within the race grooves, attributable to processing, is brinelling due to overloading, as shown in Fig. 28. This can occur during faulty preload application, inadvertent overload due to fixturing or assembly problems, or just poor handling. It presents a serious problem, and its detection is very important to prevent further processing of bearings that will fail later due to this damage.

5.2 <u>In-Process Testing</u>

The extreme importance and inaccessibility of the bearing package in the gyro make it mandatory that in-process quality-assurance tests be conducted. These tests must detect conditions that might lead to early bearing failure or poor instrument performance. Various test methods and devices have been developed for this in-process evaluation.

When the bearing is accessible in the unassembled condition, as in early processing stages or in diagnostic testing following problem detection, a wide range of test methods is available. These include microscopic inspection with normal or polarized light and with the interference microscope, which is particularly useful for recognizing and characterizing topographic aberrations. Also available are various means for measuring and tracing geometry and surface finish. In addition, a wide range of destructive tests can be performed for diagnosis or quality control.

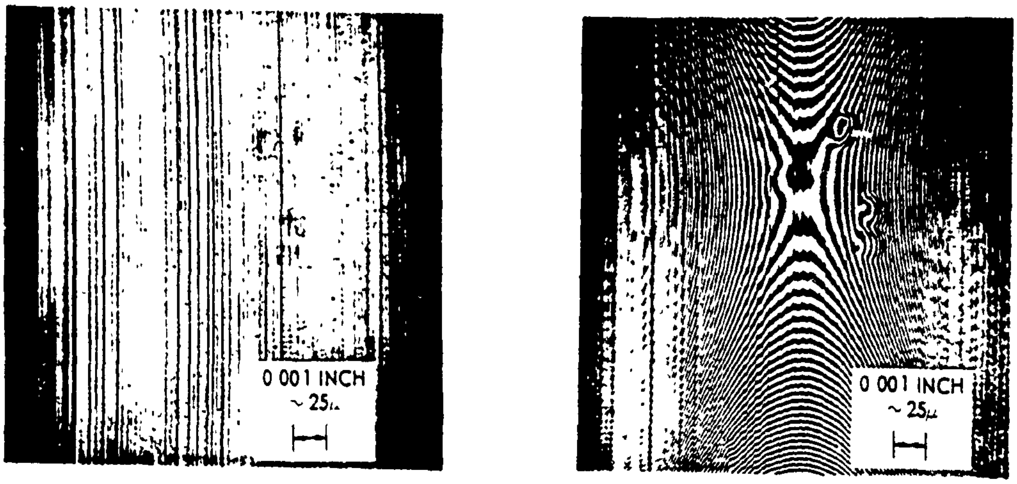

NORMAL MICROSCOPIC APPEARANCE

INTERFERENCE FRINGE PATTERN OF SAME FIELD FRINGE SPACING IS 10.6 MICROINCHES (0 27μ) NOTE SHALLOW SIDES OF INDENTATIONS.

Fig. 25. Brinells on inner race-groove surface caused by soft particles.

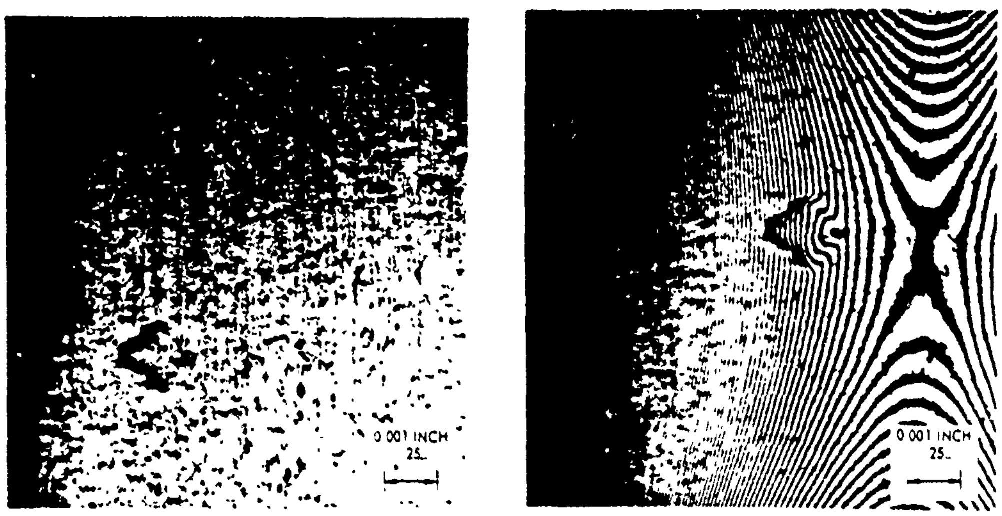

NORMAL MICROSCOPIC APPEARANCE

INTERFERENCE FRINGE PATTERN OF SAME FIELD FRINGE SPACING IS 10 6 MICROINCHES (0 27μ) NOTE STEEP SIDES OF INDENTATION

Fig. 26. Brinell on inner race-groove surface caused by hard particle.

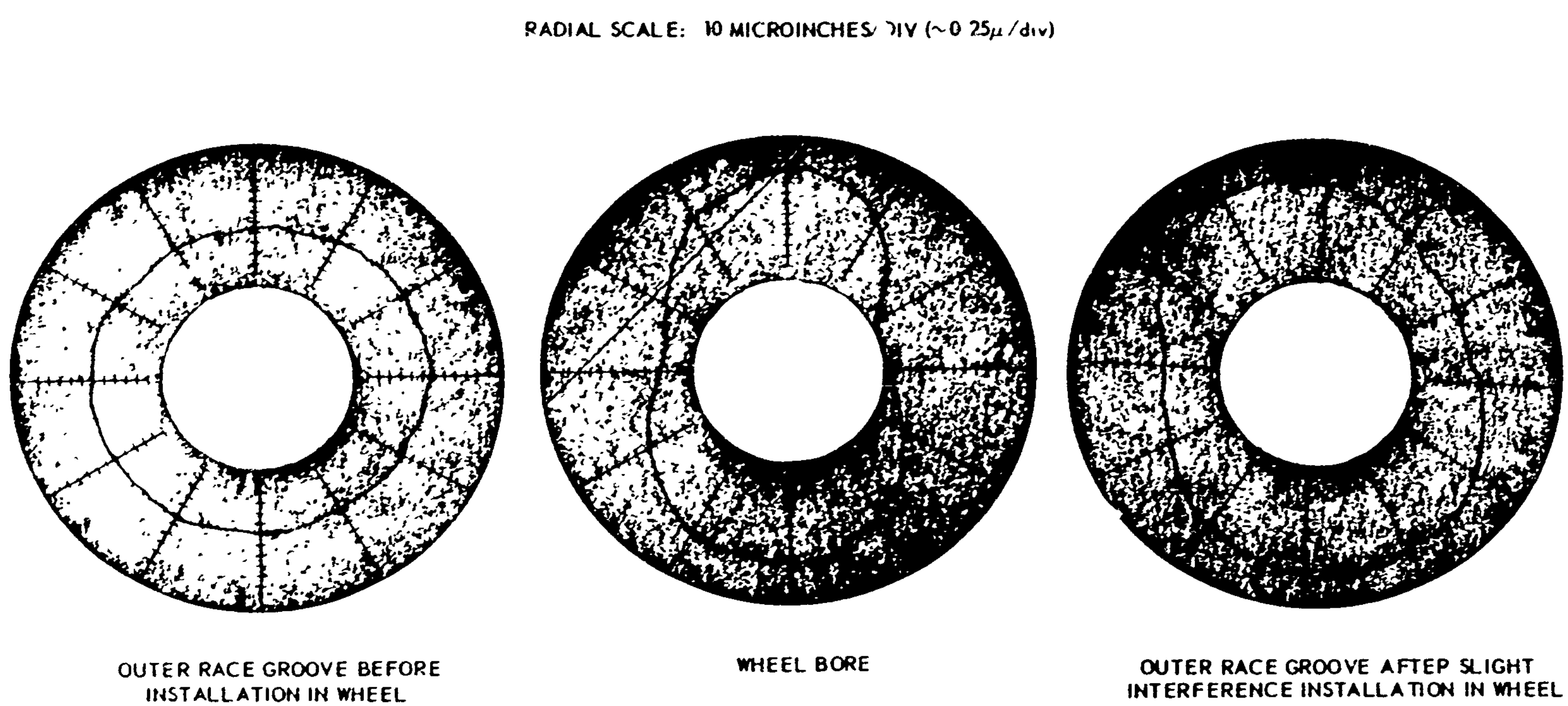

Fig. 27 Distortion of race groove by interference fit to out-of-round member.

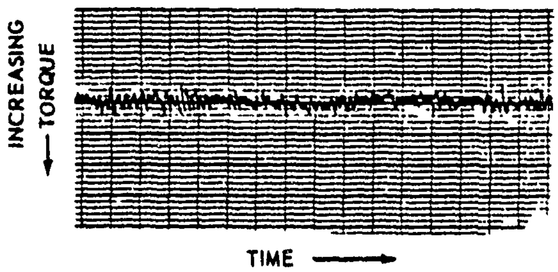

INITIAL LOW-SPEED DYNAMOMETER
TRACE – ACCEPTABLE BEARING

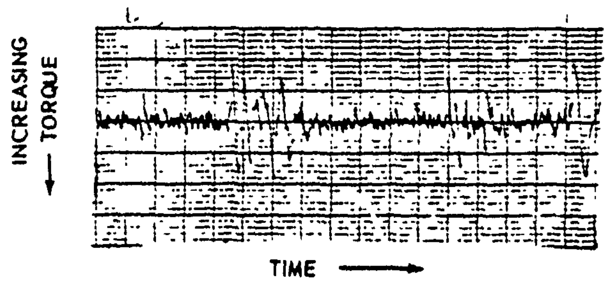

SUBSEQUENT LOW-SPEED DYNAMOMETER
TRACE – METAL DAMAGE

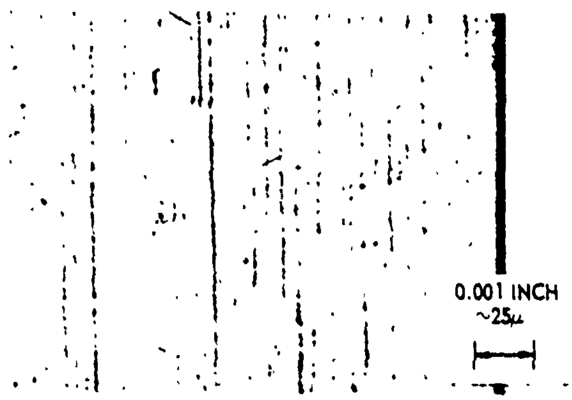

NORMAL MICROSCOPIC APPEARANCE
METAL DAMAGE DIFFICULT TO DETECT

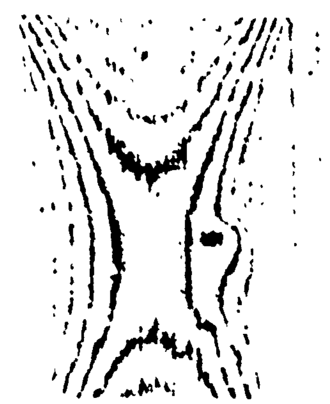

INTERFERENCE FRINGE PATTERN
BRINELLS IN INNER-RACE GROOVE
READILY APPARENT FRINGE
SPACING IS 10.6 MICROINCHES (0 27μ).

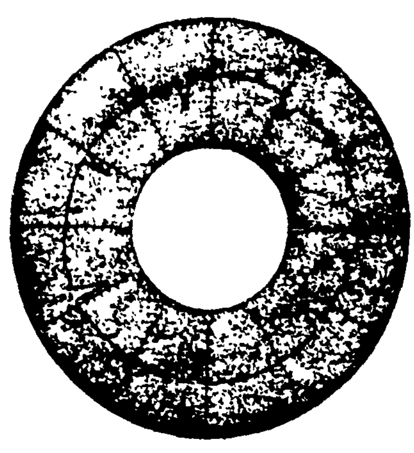

ROUNDNESS TRACE – 7 BALL
INDENTATIONS IN INNER RACE

Fig. 28. Detection of metal damage during bearing processing.

One of the most useful test devices for assembled bearing surface and lubricant characterization is the low-speed dynamometer (LSD), illustrated along with representative traces in Fig. 29. It consists of a spindle on which is mounted the bearing outer race (or races in the case of a preloaded bearing pair), a deadweight axial-loading system for a single test bearing, a means for rotating the spindle slowly (generally at 1 rpm), a beam on which a strain gauge is mounted to restrain the inner race or races from rotation, and a means for recording the strain-gauge output. Provision is also made for reversal of direction of rotation, load and speed variation, zero setting, and calibration. The resultant torque trace tells a great deal about the torque level, metal surfaces, lubricant condition, contamination, and geometry. For example, a high hash level generally characterizes a poor surface finish, contamination, or lubricant or metal degradation, the specifics of which are readily determinable by other means. Individual trace features show metal damage or dirt; the former is characterized by an initial sharp torque drop followed by a rise, whereas the dirt shows an initial increase. Spacing of torque disturbances pinpoints discontinuity location as being inner race, outer race, or ball.

The LSD can be used following various critical processing stages of the individual bearing or preloaded pair until the wheel package is sealed into the float. Changes in trace character rather than absolute levels are monitored as bearing degradation symptoms. One of the most valuable functions of the LSD is early detection of lubricant degradation. It frequently provides the first test to disclose bearing deterioration problems and is therefore very important. Perhaps just as important is the user's willingness to conduct the test and act upon the evidence.

The other of the two most important diagnostic tools is the recording milliwattmeter-dynamometer, generally called the wattmeter or milliwattmeter. The milliwattmeter is used at bearing operating speed and simply provides a sensitive (zero-suppressed) trace of motor-power input. Assuming a stable power supply, variations in the power trace reflect variations in the bearing torque demand, which in turn generally correlate with variations in factors influencing gyro wheel axial position. Thus the wattmeter provides a measure of potential gyro performance. Figure 30 shows milliwattmeter traces representing various classes of gyro performance.

A particularly valuable aspect of the wattmeter is its usefulness in a wide range of test configurations, including bearings assembled in a test fixture, final wheel and bearing assembly, sealed float, and the completed gyro. Thus it is a useful diagnostic and research tool as well as a valued in-process tester. Some of the specific behavior patterns monitored by the wattmeter are discussed in Section 6.

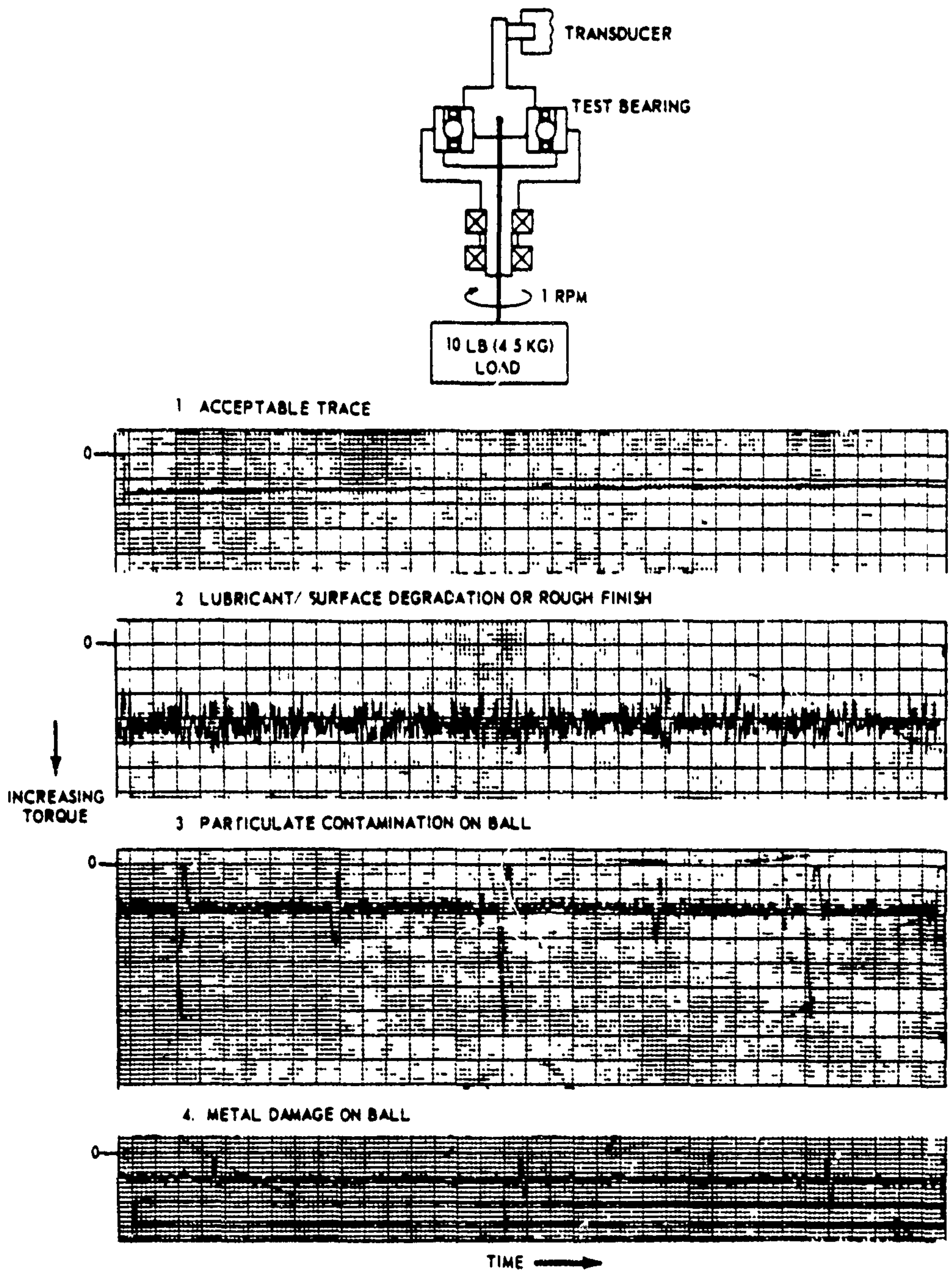

Fig 29 Low-speed dynamometer and typical traces

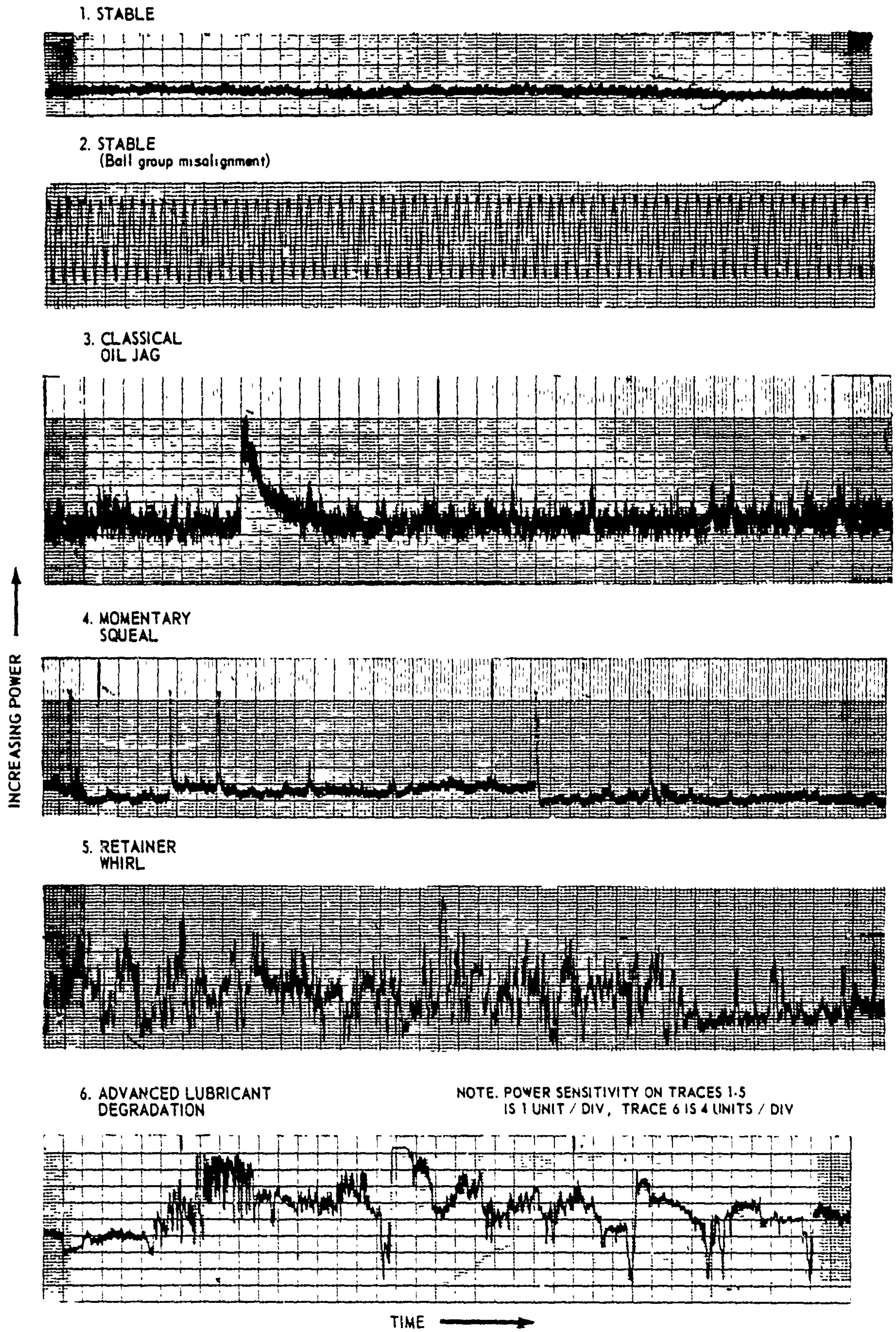

Fig. 30 Bearing behavior as seen on milliwattmeter

Other test devices fulfill some of the same functions as the milliwattmeter. One is a high-speed dynamometer which has a torque readout, and therefore does not depend upon power-supply stability. Its usefulness extends to the float assembly stage. Various other high-speed torque testers are in use both as research and production tools.

Another useful series of in-process tests is a group using wheel runup and rundown for bearing and motor torque evaluation. Deceleration at high speed yields bearing friction and windage torque data, while the low-speed end is essentially not influenced by windage torque. Total rundown time provides a rough monitor of stability of running conditions. These tests are useful over a wide range of gyro construction steps and are particularly useful in gyros subjected to prolonged or repeated testing. Bearing degradation can be detected by this test as well as by milliwattmeter evaluation, but generally not until hundreds of running hours after the inception of failure.

Various other test methods are useful either as in-process steps or as special diagnostic tests, depending upon the requirements of the particular program. One of these is the mounting of a wheel package or float on a cradle with vibration pickups and monitoring the bearing dynamics at the retainer and ball-group frequency. Some bearing configurations demonstrate performance particularly correlatable with ball-group frequency.

Another useful test device is the inner-package evaluator. This is a temperature-controlled hydrostatic-gas-bearing-supported horizontal element restrained by a torque feedback loop on which a bearing package or float can be mounted and the wheel run. Recordings are taken of torque to balance, ball-group-frequency vibration amplitude about the output axis, and motor-power input. Though this device is far less sensitive and less versatile in discerning disturbing inputs than a completed gyro, it is very useful.

Many in-process test methods are available for bearing package evaluation, as shown in Fig. 31. Their usefulness is a function of the specific instrument requirements and problems. The two most useful functional test devices through the years, though, have been the low-speed dynamometer and the recording milliwattmeter-dynamometer.

EVALUATION TECHNIQUE	SINGLE BEARING	BEARING PAIR TEST	FINAL WHEEL	SEALED FLOAT	GYRO
OPTICAL	●	●			
LOW-SPEED DYNAMOMETER	●	●	●		
MILLIWATTMETER		●	●	●	●
DECELERATION TEST		●	●	●	●
FREQUENCY ANALYSIS		●	●	●	●
WHEEL PACKAGE BALANCE STABILITY TEST			●	●	●
GYRO TEST					●

Fig. 31. Bearing evaluation at successive processing stages.

SECTION 6

PERFORMANCE

Gyro performance reflects, among other factors, spin-axis bearing package performance. Some aspects of bearing dynamic behavior affect instrument precision without influencing bearing life, but bearing degradation almost always causes gyro performance degradation.

6.1 Bearing Dynamics

Though many aspects of bearing dynamic behavior are now understood, there are still gaps in the understanding of the fundamentals. The old theories, based on a model with metallic contact between race and ball, do not adequately account for viscous effects or for ball-retainer coupling. Work is currently underway to close these gaps.

One of the earliest of the bearing dynamics phenomena to be explained was the "classical jag", or "oil jag". The jag was first seen in gyro performance as an abrupt change in float balance along the spin axis, followed by an exponential decay. Later development of the milliwattmeter disclosed the existence of a simultaneous sharp increase in motor power, also followed by an exponential return. Microscope observation of stroboscopically illuminated bearings showed the power increase to be accompanied by the centrifugal release of an oil droplet from the ball retainer OD to the outer-race groove. This is a brief version of an investigation that spanned several years in various places by various people. It is now apparent that oil is deposited by the balls in the retainer ball pockets and that it runs out and tends to collect on the retainer OD. When the centrifugal force on the oil drop exceeds that of the surface tension, the drop is thrown to the outer race. If it lands in the race groove, it presents the balls with a sharp increase in film thickness. This film thickening in one bearing increases axial load on both bearings and moves the wheel center of gravity, thus changing the gyro float balance. Bearing torque and therefore motor power also increases due to added viscous drag and increased load. Equilibrium conditions return exponentially.

As expected, improved control of lubricant quantity reduced the severity of the problem. Bearing design also influences jagging incidence and severity. For example, the problem becomes more acute with a full outer race than with one with a land ground off, and is alleviated by a more open groove-to-ball conformity.

Another aspect of bearing dynamics that has yielded to investigation is the interaction of the ball groups in a preloaded bearing pair at their beat frequency. A characteristic sinusoidal milliwattmeter trace reflects the varying bearing torque as the two misaligned ball groups beat with respect to each other, and the effective preload is increased and decreased by the varying phase relationships of the larger balls in the two ball groups. In addition, each ball varies its speed and moves across its ball pocket (at the beat frequency), and the ball retainer center of gravity is driven in a circular path around the bearing axis (also at the beat frequency) with respect to the ball group. Modification of this dynamic behavior can be achieved by varying the size match of the balls and their relative position in each bearing, and by varying basic ball-group size of one bearing with respect to the other, thus changing the contact-angle match and therefore the beat frequency.

Variation of the beat frequency occurs as the direction of an acceleration (e.g. gravity), is changed with respect to the spin axis. The wheel mass acted upon by the changing acceleration direction alters the effective load on the two bearings differentially, and therefore affects their contact angles and beat frequency.

High-speed ball-retainer whirl (eccentric motion of the retainer center of gravity around the bearing axis) and in a limiting case squeal, are serious bearing dynamics problems. Synchronous whirl, or translation of the retainer center of gravity around the bearing axis at the wheel frequency, is not generally a problem. Its severity is a function of wheel unbalance and bearing preload, generally occurring only in lightly loaded bearings. More serious is high-frequency whirl caused by ball-to-retainer frictional coupling, which, in generation mechanism, is similar to journal-bearing dry-friction whirl. Severe cases of this whirl are accompanied by very high erratic torque and in many cases by audible squealing or chirping. This condition appears on the milliwattmeter as a power disturbance with a high-erratic, hashy trace. It may be momentary or intermittent, appearing as a sharp short power spike, undetectable by other means. The squeal condition is intolerable and, depending upon its severity, it is accompanied by poor gyro performance, excessive torque, and early bearing failure.

The best method of correction is reduction of the frictional coupling of the ball to retainer, generally by improved lubrication. In the case of the Nylasint retainer, this can be accomplished by salt-blasting the ball pockets, which compacts the surfaces and provides better lubrication. Other means for compacting the ball-pocket surfaces are also effective.

Another approach is to randomize the driving mechanism of retainer squeal. This can be done by deliberately mismatching ball sizes within the bearing or by spacing the ball pockets nonuniformly in the retainer. Though effective, these methods exact a penalty in higher bearing torque.

Additional investigations into the fundamentals of bearing dynamics are in progress. One test device rotates the inner and outer races of an axially loaded bearing in opposite directions, as seen in Fig. 32, maintaining the ball group and retainer (when one is used) fixed in space. This permits microscope observation of ball motions and use of instrumentation to measure retainer forces. Some tests are conducted with balls with small diametral through-holes, providing a preferred ball-rotation axis and an observation and analysis tool for ball-motion study. Another device permits outer-race rotation of a preloaded bearing pair, with independent torque measurements of the two bearings. It is also instrumented for axial and radial retainer-motion monitoring.

Studies conducted with these test devices will disclose fundamental bearing knowledge. Factors being studied include ball precession, ball slip as shown in Fig. 33, retainer forces, ball-group speed ratio, retainer dynamics, and bearing

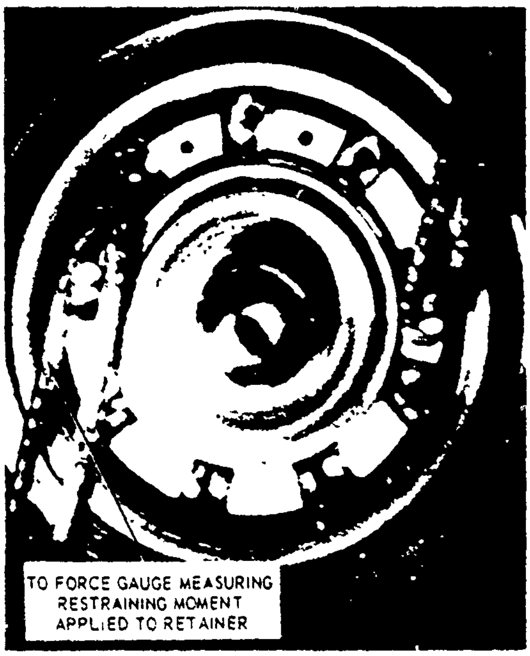

R4 BEARING, RACES COUNTER-ROTATING, BALL GROUP STATIONARY

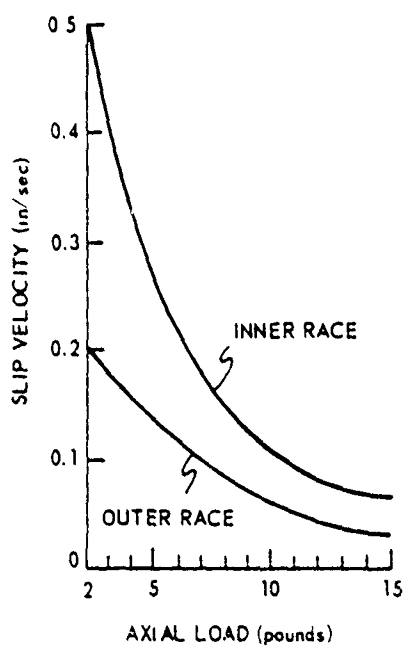

Fig 32 Slip of ball to race groove, with fixed retainer moment.

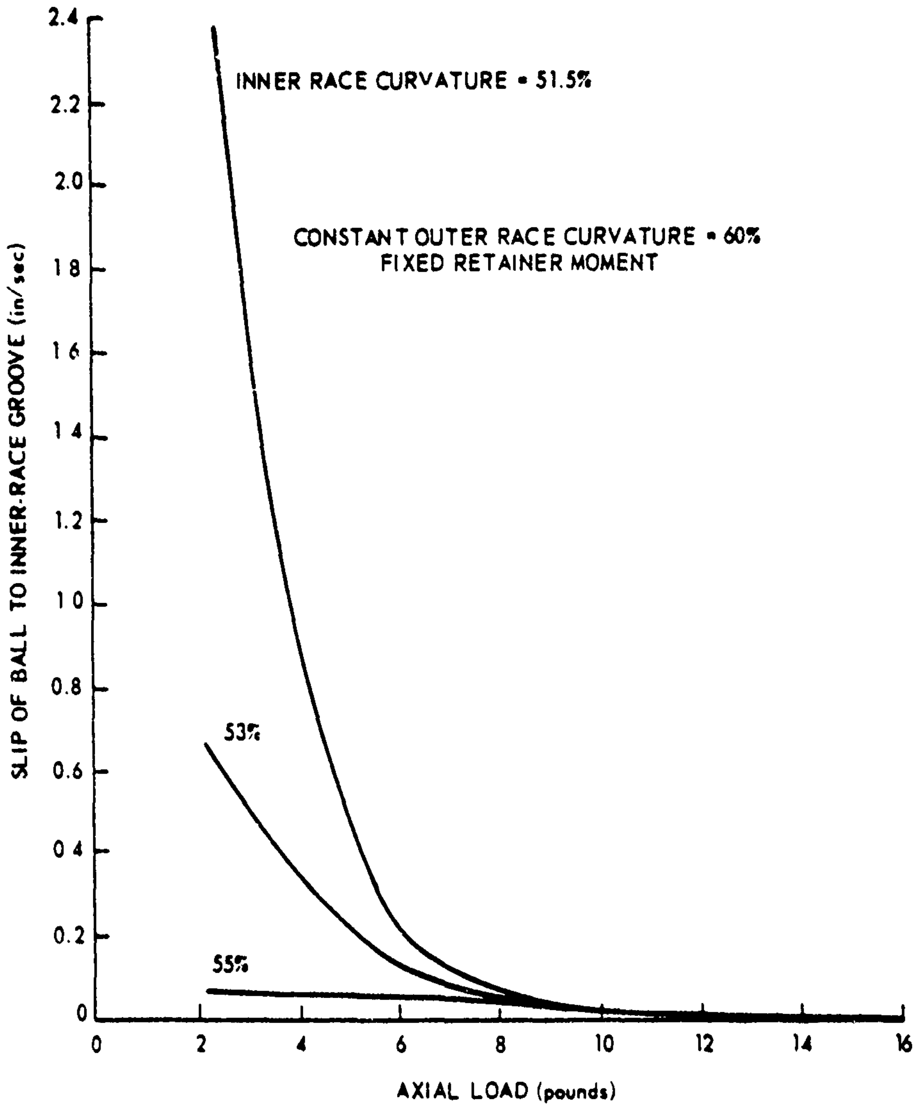

Fig. 33. Slip of ball to inner race vs. axial load for different inner race curvatures.

torque versus variables of speed, lubricant type and quantity, geometry, load, retainer configuration, metal surface characteristics, and others. These studies will lead to continued improvement in gyro life and performance.

6.2 Gyro Performance

The gyro itself is the only device sensitive enough to tell whether or not bearing performance goals are achieved. In addition, it is a very useful diagnostic tool for bearing parameter evaluation and improvement. Finally, it can be easily monitored to disclose the health of the bearing package at any time during the life of the gyro.

Gyro stability, determined by a variety of tests in both fixed and varying acceleration fields, combines factors associated with and independent of the bearing package. Various means are used to separate bearing performance from other factors. One common test, for example, uses the gyro to stabilize a servo-controlled turntable in inertial space, thus causing the gyro to tumble in the earth's gravity field. Repeatability of gyro unbalance from revolution to revolution provides a record of balance stability. Comparison of this stability for gravity positions in which random motion along the spin axis will show as torque uncertainties, with positions not affected by spin-axis instability, provides an indication of bearing performance. Coupling of this information with simultaneous recordings of motor input power and signal-generator output at the ball-group frequency provides a more complete picture, as shown in Fig. 34.

Various other tests of float balance with the gyro tumbling and in various fixed-gravity orientations and subjected to higher vibratory and steady-state acceleration levels reveal bearing package data. In each case, the power and output frequency analyses are necessary correlative tools. In fact, these tests combined with specific bearing parameter or running condition variables provide useful design information.

No ball-bearing gyro should experience severe bearing failure without warning. As bearings degrade, they show very distinctive symptoms. Perhaps the first sign of impending bearing failure is evidenced by gradually degraded performance, particularly with regard to spin-axis stability. The milliwattmeter trace develops erratic periods as degradation progresses, with both degree of power variation and ratio of rough-to-smooth trace becoming greater. Changes

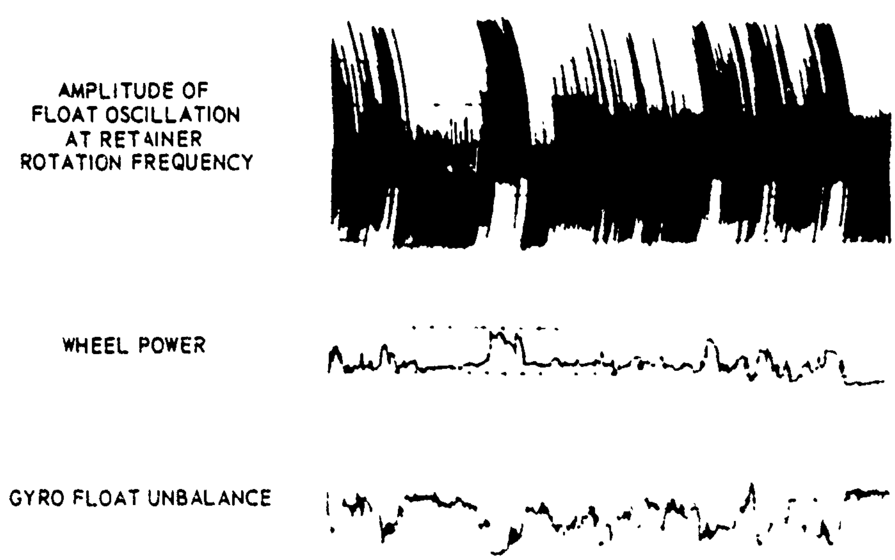

Fig 34 Correlation of gyro unbalance with wheel power and with retainer and ball group motion

may also occur in the signal at the ball-group frequency. With continuing degradation, wheel deceleration tests show changes in both character and total rundown time. The time from the first detectable failure symptoms until appreciably higher power demand occurs can amount to several hundred or thousands of running hours.

Use of current ball bearing technology has permitted the construction of gyros demonstrating performance levels unexcelled by any other spin-axis suspension. Long life has also characterized these instruments, both in terms of wheel running hours and shelf life, examples of which are cited in Table 2. Successful bearing use does demand, however, rigorous adherence to the highest quality control standards in both manufacture and processing. Some of these standards have been discussed in this paper.

It is expected that future efforts in ball-bearing technology will yield further advances in both understanding of fundamentals and development of improvements. Work is being performed, for example, in the fields of bearing dynamics, the lubrication mechanism, and the race-groove and ball surfaces. These efforts should result in more consistent achievement at lower cost of currently demonstrated excellent performance and long reliable life. They should also provide the basis for meeting even more rigid requirements in the future.

Table 2. Gyro bearing running time.*

SYSTEM	GYRO	TOTAL RUNNING TIME		GYRO AGE AT MOST RECENT BEARING OPERATION (years)
		HOURS	YEARS	
A	6-1	28,700	3.3	5.7
	6-2	28,300	3.3	5.7
	6-3	26,500	3.0	5.4
B	6-4	26,500	3.0	4.0
	6-5	25,200	2.8	3.4
	6-6	25,600	2.9	3.7
	6-7	22,500	2.6	3.9
C	9-1	13,900	1.6	2.9
	9-2	8,900	1.0	2.6
	9-3	6,400	0.8	1.4
D	2-2	5,300	0.6	7.7
	2-3	8,500	1.0	7.4
	2-4	6,700	0.8	7.3
Gyro Life	1-1	31,600**	3.6	6.0
Tests	2-1	48,300***	5.5	8.5

*Data as of 1 January 1968
**Performance failure at ~ 5000 hours (0.6 years)
***Still running

APPENDIX

BEARING NOMENCLATURE

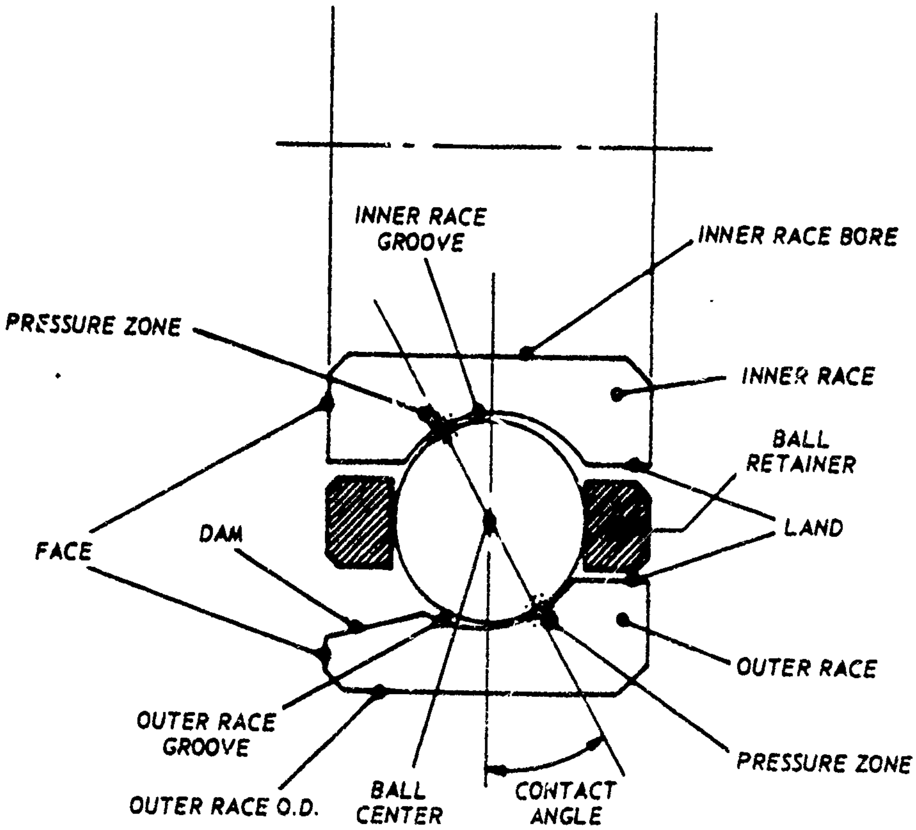

$$\text{RACE GROOVE CURVATURE} = \frac{\text{RACE GROOVE RADIUS}}{\text{BALL DIAMETER}} \times 100\%$$

BIBLIOGRAPHY

1. Gyro Spin-Axis Hydrodynamic Bearing Symposium, Instrumentation Laboratory, Massachusetts Institute of Technology, Cambridge, Mass., 12-14 Dec. 1966. References 2-15 below from the Ball Bearing Proceedings.

2. Denhard, W. G., Cost Versus Value of Ball Bearings, Report E-1990, Instrumentation Laboratory, Massachusetts Institute of Technology, Cambridge, Mass., July 1966.

3. Lement, B. S., Kreder, K., and Cairoli, A. M., Quality of Steels Used in Gyro Ball Bearings, ManLabs Inc., Cambridge, Mass., December 1966.

4. Palmieri, J. R. and Allen, S., Heat Treatment of Bearing Steels, Report E-2085, Instrumentation Laboratory, Massachusetts Institute of Technology, Cambridge, Mass., December 1966.

5. Farago, F. T., Dimensional Measurements of Gyro Bearing Components by Autocollimation and Other Advanced Methods, New Departure-Hyatt Bearings, Div. of General Motors Corp., 1966.

6. Orcutt, F. K. and Cheng, H. S., Lubrication of Rolling-Contact Instrument Bearings, Mechanical Technology, Inc., Latham, N. Y., December 1966.

7. Allen, S. and Palmieri, J. R., A Metallurgical Modification Caused by Finish Operations on Ball-Bearing Race Grooves, Report E-2084, Instrumentation Laboratory, Massachusetts Institute of Technology, Cambridge, Mass., December 1966.

8. Gereg, C. V., Lubricant Film Electrical Resistance Gage – Its Application to Ball Bearing Raceways, The Barden Corp., Danbury, Conn., 1966.

9. Hannan, C. H., Observations of Oil and Water Absorption Characteristics of Spin Axis Bearing Retainers, Miniature Precision Bearings, Inc., Keene, N.H., 1966.

10. Leveille, A. R., Properties of a Power Function Model of Ball Bearing Axial Load vs. Deflection, The Barden Corp., Danbury, Conn., 1966.

11. Roberts, M., A Study of Oil Circulation in the R4 Spin-Axis Bearing with Sintered Nylon Ball Retainer, Report E-2082, Instrumentation Laboratory, Massachusetts Institute of Technology, Cambridge, Mass., December 1966.

12. Klaus, E. E., A Study of Deposit Forming Tendencies with Gyro-Bearing Lubricants, Petroleum Refining Laboratory Div., Chem. Eng. Dept., The Pennsylvania State University, University Park, Pa., 1966.

13. Singleterry, C. R., Some Factors Affecting the Movement of Oil over Metal Surfaces, Naval Research Lab., Washington, D. C., 1966.

14. Wyatt, O. H., British Experience with Gyro Spin Axis Ball Bearings with Special Reference to Geometric Factors, Royal Aircraft Establishment, Farnborough, Hants., England, 1966.

15. Kingsbury, E. P., Torque Variations in Instrument Ball Bearings, Report E-1675, Instrumentation Laboratory, Massachusetts Institute of Technology, Cambridge, Mass., June 1964.

16. Bearings Conference at Dartmouth College, Hanover, N. H., 7-9 September 1966. References 17-28 below from Proceedings.

17. Draper, C. S., Bearings, Instrumentation Laboratory, Massachusetts Institute of Technology, Cambridge, Mass., 1966.

18. Griffths, C. A., Retainer Instability in Thin Section Instrument Bearings, Split Ball Bearing Div., Miniature Precision Bearings Inc., Lebanon, N. H., August 1966.

19. Grant, C. L., Pelton, P. A., and Downer, R. J., Measurement of Oil Movement in Ball Bearings with Porous Retainers, Univ. of New Hampshire, Durham, N. H., 1966.

20. Dane, E. B., The Manufacture of Consistently Good Ball Bearings, Instrumentation Laboratory, Massachusetts Institute of Technology, Cambridge, Mass., June 1966.

21. Devine, M. J., Stallings, L., and Cerini, J. P., Anti-Friction Bearing Concepts for Non-Conventional Lubricants, Naval Air Materials Laboratory, Philadelphia, Pa., 1966.

22. Esterly, D. D., Using Bearing Characteristic Frequency Amplitudes to Predict Bearing Performance, Ampex Corp., Redwood City, Calif., July 1966.

23. Zaretsky, E. V. and Anderson, W. J., Material Properties and Processing Variables and Their Effect on Rolling-Element Fatigue, NASA TMX-52227, Lewis Research Center, Cleveland, Ohio, 1966.

24. Ehrich, F. F., Bearing Influence on Rotor Dynamics, General Electric Co., West Lynn, Mass., August 1966.

25. Given, P. S., Lubricant Film Effects on Rolling Contact Fatigue, SKF Industries Inc., Philadelphia, Pa., September 1966.

26. Cron, R., Lubrication to Improve Reliability of Components of Servomechanisms, U.S. Naval Ammunition Depot, Crane, Indiana, 1966.

27. Jones, A. B., Jr. and Poplawski, J., A Computer Study of the Effects of the Various Design Parameters and Operating Conditions on Rolling Element Bearing Performance, Pratt & Whitney Aircraft Corp., Hartford, Conn., 1966.

28. Hannan, C. H., Chemical Treatment of Rolling Element Bearing Surfaces, Miniature Precision Bearings Inc., Keene, N.H., 1966.

29. Elastohydrodynamic Lubrication, a Symposium conducted by the Lubrication and Wear Group of the Institution of Mechanical Engineers, Leeds, Proceedings 1965-66, Vol. 180, part 3B.

30. Contact Angle, Wettability, and Adhesion, the Kendall Awards Symposium honoring W. A. Zisman, American Chem. Society, 2-3 April 1963. Advances in Chemistry Series No. 43, A.C.S., Washington, D.C., 1964.

31. Bowden, F. P., and Tabor, D., The Friction and Lubrication of Solids, Parts I and II, Oxford Univ. Press, London, 1954 and 1964 respectively.

32. Cameron, A., The Principles of Lubrication, John Wiley & Sons Inc., 1966.

33. Denhard, W. G., Freeman, A. P., and Singer, H. B., Failure Analysis of Critical Ball Bearings, Report E-1781, Instrumentation Laboratory, Massachusetts Institute of Technology, Cambridge, Mass., April 1965.

34. Dowson, D. and Higginson, G. R., A Numerical Solution to the Elastohydrodynamic Problem, Journal of Mech. Eng. Science, I, 1, 1959.

35. Essex, A. R., Measurement and Generation of Truly Circular Form, Paper No. 15 of Gyro Symposium, Institution of Mechanical Engineers, London, 1965.

36. Fein, R. S., Possible Role of Compressional Viscoelasticity in Concentrated Contact Lubrication, ASME Transactions, 89F, 1967.

37. Final Report on the Gyro Spin-Axis Bearing Program, Report R-418, Instrumentation Laboratory, Massachusetts Institute of Technology, Cambridge, Mass., September 1963.

38. Fitzsimmons, V. G., et al., A New Approach to Lubricating Ball Bearings, NRL Report 6356, U.S. Naval Research Laboratory, Washington, D.C., 28 December 1965.

39. Furey, M. J., Surface Roughness Effects on Metallic Contact and Friction, ASLE Transactions, 6, 1963.

40. Harris, T. A., Rolling Bearing Analysis, John Wiley & Sons Inc., 1966.

41. Hersey, M. D., Theory and Research in Lubrication, John Wiley & Sons Inc., 1966.

42. Horsch, J. D., Correlation of Gyro Spin-Axis Ball Bearing Performance with the Dynamic Lubricating Film, ASLE Transactions, 6, No. 2, 1963.

43. Howles, D. J. and Munson, H. E., Summary Report, Spin-Axis Bearings, N66-35016, NASA Scientific and Technical Information Facility, 27 June 1966.

44. Jones, A. B., Analysis of Stresses and Deflections, New Departure, 1946.

45. Kannel, J., Bell, J. C., Walowit, J. A., and Allen, C. M., A Study of the Influence of Lubricants on High-Speed Rolling-Contact Bearing Performance, ASD-TDR-61-643, Parts VI and VII, August 1966 and December 1967 respectively.

46. Palmer, P. J., Precision Inertial Gyro Testing at MIT, AGARD Lecture Series No. XXX on Inertial Component Testing-Philosophy and Methods, Paris, 24-29 June 1968.

47. Pressure-Viscosity Report, Vols. I and II, ASME Research Publication, 1953.

48. Tallian, T. E., et al., Lubricant Films in Rolling Contact of Rough Surfaces, ASLE Transactions, 7, No. 2, April 1964.

G.4 REPORT OF THOMAS BANISH

THOMAS BARISH
CONSULTING ENGINEER

3407 PUENTE STREET
FULLERTON, CALIF. 92635
(714) 871-7000

December 15, 1975

T.R.W. Systems Group
One Space Park
Redondo Beach, California 90278

Attn: Mr. A.H. Rosenburg, Subproject Manager DSCS II Controls

T.R.W. Systems Group

COMSAT

Despin Ball Bearings Malfunction

Subject: C.C.C. 7345: Job # 2513-28: P.O. C53677 C.A.B.K.

1. References:
   Conference at this office with A.H. Rosenburg, George Zaremba, and L. Anderson, early in October.

Data submitted at that time, and first examination of bearings that were tested. Also, multiple phone calls.

Technical References: (Copies enclosed)

(a) "Ball Bearing Troubles", "Product Engineering", March 1939 by T.B.
(b) SKF Publication, "Bearing Failures and Their Causes".
(c) "Ball Speed Variation in Ball Bearings and It's Effect on Cage Design." ASLE Preprint 68AM 6C-2 by T.B.

2. Problem: The despin assembly, (drawing on page 2) after 20 months satisfactory operation showed:

(a) A sudden jump of about 50% in friction.
(b) After 1-2 days further operation the friction jumped to 100% excess and locked up the unit.
(c) After vigorous tilting (as much as could be applied), the unit re-started with the friction again 50% over normal. And the last information was that it was still operating at this point.

3. The Procedure in arriving at a simple solution is dictated by the fact that we have very little direct information, and we cannot observe the bearings:

(a) Careful tabulation of everything we know indicating the pattern of failure.

BALL AND ROLLER BEARINGS • GEARING • FAILURE ANALYSIS

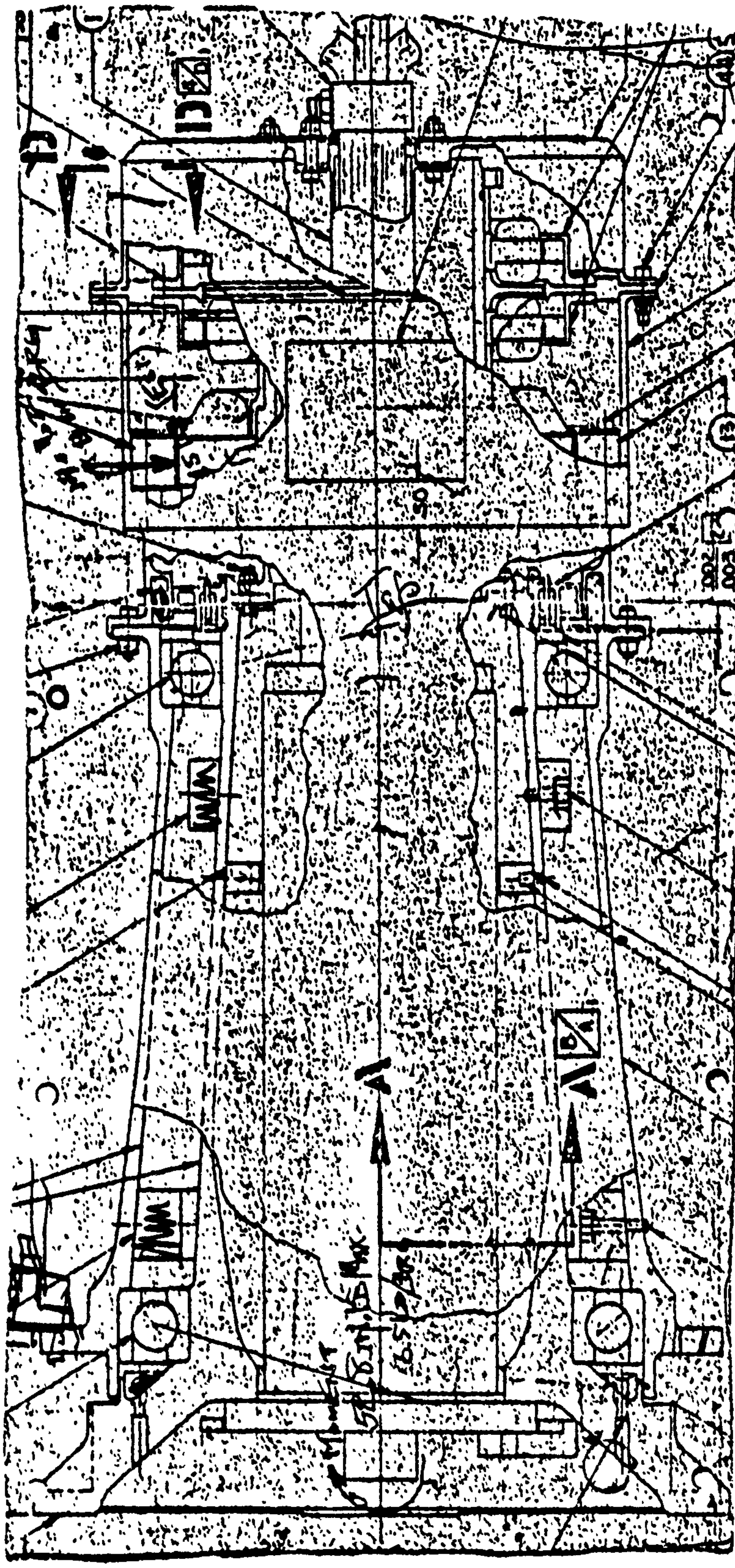

1/2 SIZE

(b) A thorough analysis of all the details of the bearings specification and other bearings in stock.
(c) A complete examination of the test bearings which operated for over two years on earth with no indication of failure.
(d) Consider all the possible modes of failure to see which of them fit the pattern indicated above.
(e) For each possible candidate mode-of-failure, we must <u>try to re-produce the symptoms</u>.

To avoid the 2-year lead time, we must introduce what each mode of failure would do to the bearing in the first two years. For example, the lack of lubrication requires that we put in the bearing where we have taken out all of the oil before we attempt to produce the symptoms. Likewise for possible cage-break, we need to break a cage the way it would normally fail and put it in the bearing to obtain symptoms.

4. <u>Candidate Failure Modes</u>:
(a) Loss of Lubricant:
(b) Cage Failure due to BSV (Ball Speed Variation)

Less Likely Causes:
(c) Broken parts momentarily lodged in the bearing: Particularly one of the oil reservoirs and the critical space being on the outside of each bearing where there is very little debris space.
(d) Failure in the Slipring Assembly.

5. <u>Failure Patterns Symptoms</u>:
(a) Over two years operation without failure in testing machine. Note this did not include the radial load generated by the half motor, and possible momentary larger loads due to gyroscopic action in space.
(b) 21 months operation with no indication of difficulty in orbit.
(c) Sudden increase of friction by 50%.
(d) Sudden jump to more than double and locking up.
(e) Shaking of the unit permitted it to re-start operation with 1.5 normal friction.

6. <u>Design Analysis</u>: indicates that; (calculations on the next page)

(a) The fits and tolerances seem to be excellent.
(b) The initial contact angle (allowing for press fits) will be:

	Bottom Bearing	Top Bearing
	32709-1	32709-3
Max Angle	16.70	17.[illegible]
Min Angle	10.39	10.74
Average	13.57	14.[illegible]

DESPIN BRGS (FROM TEST UNIT) 4

	BOTTOM		TOP	
PART NO. (SYSTEMS)	32709-1		32709-3	
BRG SIZE (EXTREMELY LIGHT SERIES)	No. 922		No. 918	
	110 × 150 × 20 MM.		90 × 125 × 18	
BALLS	23 - 1/2"		21 - 15/32	
COMPARE MRC	No. 1922 R	27-15/32	No. 1918 R	24-15/32
COMPARE SKF	No. 6922	19-15/32	No. 6918	18 - 15/32
	1922	24-9/16	1918	29-1/2"
SPECS CURVATURES	51.5-52%	52.5-53%	→ Same	
SPECS RADIAL PLAY	.0013-.0017"		.0013-.0018"	
FITS in MILS SHAFT	.35-.60 Loose		.45-1.0 Loose	
FITS in MILS HOUSING	0 -.80 Tight		.0 -.80 Tight	
CONTACT ANGLE	MAX	MIN	MAX	MIN
TOTAL EXCESS CURV.	.025"	.020"	.02344	.01875
Clearance Less 6×PRESSFIT	.0017	.00082	.0018	.00082
1 - cosine	.0425	.0164	.045	.0175
ANGLE	16.76°	10.39°	17.82°	10.74°

RING SECTIONS (Measured) 2X SIZE

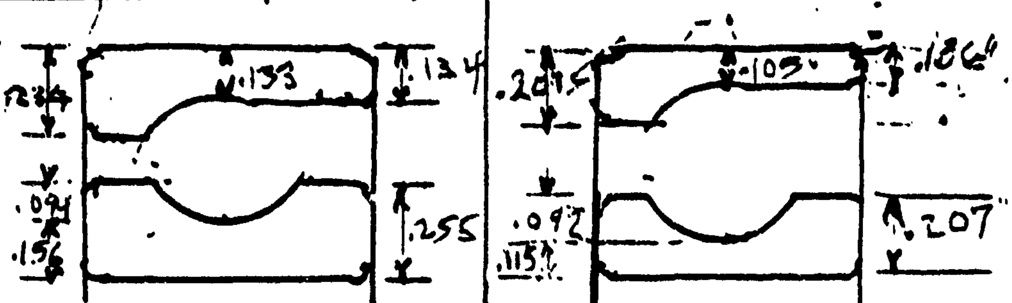

Change in angle with Load	NI^2K		ANGLE (FINAL)			ANGLE (FINAL)		
THRUST	T/ND^2K	632500		928000	T/ND^2K	50600		664500
30	.000114	16.81°	.000342	11.4°	.000311	18.4°	.00045	11.7°
64	.000612	16.85°	.000773	11.9°	.000126	18.8°	.00096	12.3°
100	.00158	17.96°	.00121	12.2°	.00197	19.1°	.00160	12.8°

RING DIAM CHANGE (Hoop Stress) at 64 LB	Outer	50 M" *	119 M"	47 M"	73 M"
	Inner	32 M"	46 M"	31 M"	45 M"

* 17" [illegible] .000 001

6. The <u>Brinelling Capacities</u> are not high enough for the loads given in the specifications.

TABLE 2

Brinelling Capacity

Specs	38,000 lb Radial	59,000 lb thrust
	Bearing-1 (bottom)	Bearing-3 (top)
Load/Ball at 38,000 Radial	7,220 lb	7,925 lb
Hertz Stress	791,000 PSI	854,000 PSI
Max Brinelling Capacity (at 690,000 PSI)	25,000 lb Radial	20,000 lb Radial

The Brinelling Stresses for the thrust load specification are slightly lower than the above. However, these loads are not expected to occur in a normal launch. In fact, the launch of this particular comsat gave less than usual.

7. The calculated <u>Fatigue Life</u> is so large as to be meaningless: Over 1,000 years B-10 life. (10% failure point).

8. The <u>expected friction</u> for these two bearings with a 64 lb thrust load (with the angle indicated) would be 24 in.oz. Hence, specifications are in order and should be obtainable, even without a complete EHD (Elasto-hydro-dynamic) film.

9. In the "<u>extremely light</u>" series of ball bearings, the races are very thin. In the top bearing, the outer ring is only .105" thick. This introduces two problems: first, the races will distort more under the load. However, the load is quite small. The maximum hoop yeild is

Outer ring of the bottom bearing, 119M".
Innor ring of the top boaring, 73M".

("M" = minch = .000 00 ")

The second problem: these races are kept round primarily by the housing and shaft. Also, they are very difficult to manufacture because of the chucking problem. One test bearing showed a 2" length of contact that was narrower than the remainder. A micrometer indicated this to be .0002", thinner wall on the original race.

These extremely light series have large variations in control of race thickness amoung the manufacturer. Recommendation: These test beearings and some from stock be measured for race thickness variation and roundness.

10. The <u>test loads</u> did not include two effects which occur in orbit: first, a radial load from the half motor. Rough estimate indicates 15 lbs maximum at the bearing. Second: a possible radial load from a gyroscopic action.
Using the prescribed maximum rate change showed about 4 lbs/bearing. Also, this load exists for a very short time.

The continuous load from the half motor would not produce appreciable BSV (ball speed variation), until the radial load approached the thrust load. This may have accounted for the original increase in pre-load from 20 to 64 lbs. Did the original development include frictional effects requiring much higher pre-load?

A calculation of the shaft deflection (misalignment) under the radial loads gives less than .000 0014":7" completely negligble.

Another possibility: that the tilt excursions of the comsat occurred at much greater rate than that used for correction. This would have to be at least 5 times to produce any appreciable BSV, but if did occur, cage failure would be rapid.

11. The most common cause of BSV is misalignment. (See figure, from reference 3)

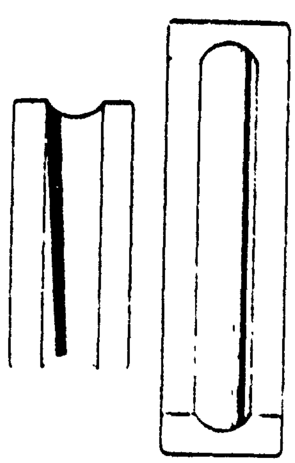

Fig. 7—Contact patterns—with off-square inner

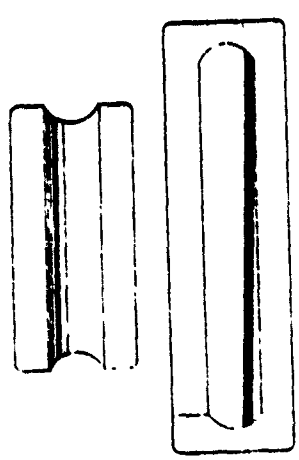

Fig. 8—Contact patterns—with off-square outer

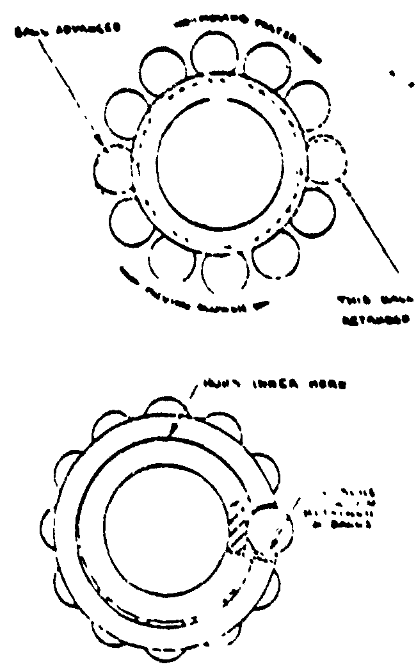

Fig. 10—BSV moves cage off-center.

The balls riding higher on the inner race travel faster. Hence, the binding in figure 10.

A similar effect occurs with radial load about the same size as thrust load. With larger radial loads, the top balls are unloaded and free. Hence, no binding.

A very loosecage will permit higher BSV without cage bind: looseness at the cage-race or the ball pockets or both. The current brgs incorporated this feature amply.

12. The probable thermal differentials seem harmless. At the top bearing it would take 25° T, from the inner ring to the shaft to absorb the minimum looseness which would prevent sliding, this is very unlikely. A thermal change at the other bearing fits exceed 20, and that would produce only .0005" change in fit and a small change in bearing contact angle.

There might be larger differences in axial length between housing and shaft because of localized heat, also because the resistance to heat transfer in stainless steel is about 3 times that of Burillium. About 25° T would produce and axial motion, of .001", at the inner race of the top bearing. There were indications of sticking or tilt at this location in one of the test bearings.

<u>Examination of Test Bearings</u>:

13. The <u>top bearing</u>, 32709-3 <u>outer race</u> contact area was well aligned, .065" wide. (calculations Page 8) The contact area was a smooth gray color, with appreciable coining of the fine asperities and the probable removal of all lubricant in this area.

The outer race did have one arc of about 20° where the contact area was appreciablly narrower, only .04. This could happen if the outer race were distorted by the housing or if the bearing race itself had a "pocket". There was no sign of difficulty on the O.D.: so this must have been an error in race thickness. There were other smaller "pockets". Recommendation: rounded check, on this race and perhaps sample new bearings. The O.D. of the bearing did show a narrow worked or scraped band about [illegible] the width nearer to the shallow shoulder. This indicated some taper distortion or a poor housing bore since contact occurred.

<u>The inner ring</u> had a wider contact (expected) but it seemed fuzzier. Most of it displayed uniformly distributed very fine pits, which showed up only with magnification. The pits were about .0001 in size. These did not resemble a rusty or lubricant deterioration condition (see figure), Page 9.

Load Calculations from measured Contact area width and location (recorded at bottom of page)

	Bottom Brg 32709-1		Top Brg 32709-3	
	Inner	Outer	Inner	Outer
BALL PATH, A	.47	.30	.43	.28
BALL PATH, B	.07	.07	.08	.065
BALL PATH, C	.13		.125	.135
GROOVE RADIUS (DRG. SPECS)	.2588"	.2638"	.2426"	.2473"
INCHES Per Degree	.00452	.00494	.00425	.00432
race depth	.099	.101	.092	.0965
degrees to edge of shlder	51.9°	49.9	51.6	52.4
arc" should equal A	.469		.439	
℄ CONTACT TO Shoulder C + .5 B	.165"	.170"	.165"	.1675"
	36.5°	34.4°	38.8°	33.8°
Contact Angle	15.4°	15.5°	12.8°	13.6°
Load/Ball from B (Nomographic Chart)	34 lb	85 Lb	51 Lb	71 Lb.
Total Thrust	208 Lb	520 LB	237 LB	350 LB
Ball Path for 64# Thrust	.050	.041	.050	.041

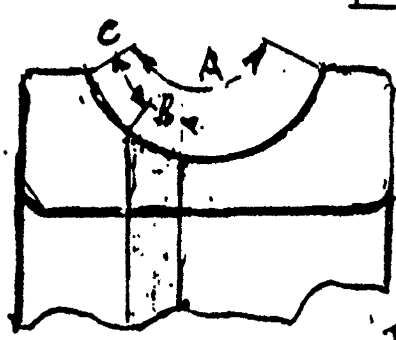

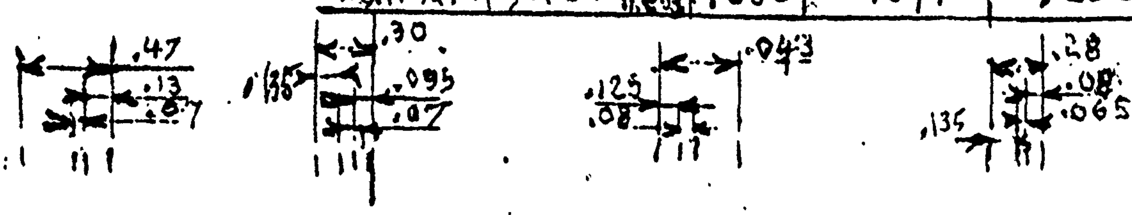

-1 Brg -2 Brg

INNER Outer INNER OUTER

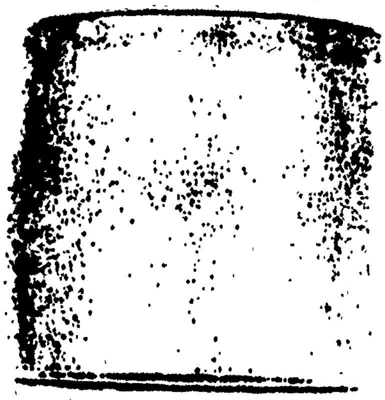

Fig. 52.—Corrosion of roller surface caused by formation of acids in lubricant with some moisture present.

Such pits have streaks in them, more color and are not so uniform. The condition on this race resembles what is called "frosted" and happens when a race has a thin layer (less than .001") of residual tensile on the surface. Usually caused by improper coolant in the grinding.

The contact angle does not vary appreciably around the circle. However, it did seem to have two separate bands (or even three) not in the same place and overlapped. This would indicate a change contact angle due to expansions or sticking of the inner race when it was supposed to slide.

14. The <u>bore of this bearing</u> was quite unusual:
It had a thin coating of a dull blue gray color which peeled off when scraped. Pieces had come off in operation for about half of the width unevenly and on the side away from the thrust. Where the coating had come off, the bore showed initial grind with no apparent contact. This was not lubricant coating, it was much thicker. It appeared more like an epoxy sometimes used as a patch for excessive looseness.

15. <u>The cage</u> showed no deterioration: no signs of rubbing on the races or on the ball pockets. There was ample clearance on the inner race about .015" per side.

The inner race did show a rub at the cage contact.

16. <u>The Balls showed</u> no problem. They were all equal and not worn and showed the initial polish. They should have shown bands if the preload had existed at all times, but there were no or at least extremely faint ones, and distributed. The implication is that there were times when the pre-load was not fully on or was changed: and that these were repeated often enough so that the rings were small and distributed.

17. The lower bearing, # 32709-1 outer race showed (an erratic) contact path, of varying width, with fuzzy edges. There were no fine pits, (as in the other bearing), just a few scattered pits. The contact was in good condition and showing only the same dull gray color. The width change indicated race "pockets".

The O.D. had the same localized scrubbing on the shallow shoulder and showing an uneven support or a tapered housing.

18. The inner ring contact was too wide, of varying width, with fuzzy edges. The same light gray color with burnishing showing up under the glass, and a few scattered pits.

There was a slight cage rub on the shoulder. The bore again showed uneven contact on the shaft, with none on the thrust side.

19. The cage again appeared untouched, like new. Again the balls were polished, and no apparent wear and round, without bands to within .0001".

Evaluation of Failure Modes

20. The lubricant would hardly give sudden jumps in friction: either up or down. Even if it deteriorated into clumps (unlikely, because there is so little), the jump would not be sudden, unless the clumps were hard. It could have caused a cage failure because of uneven drag or scraping.

In any case, a test should be run with a bone dry bearing (or a heavy residue if any were found in test bearings.

21. The failure points to some real positive scraping from some foreign body or piece. A fatigue failure in the races is very remote. Also, there would be fairly slow increase in friction some time before failure.

A cage failure from BSV would leave segments (see figure). The laminated cage is particulary susceptible to such failures, especially in thin section bearings. On the outside of the bearing, the segment could lodge against the adjacent parts.

22. A similar effect would result if the oil reservoirs on the outside of the bearings had pieces break off.

Suggestion: Examine these parts on the test outfit.

23. Other possible sources of rubbing:

(a) the slipring assembly
(b) the half motor

24. The ball bearings all showed wide ball paths. Loads calculated from these were 3x to 8x too large.

This means the path varied; especially on the sliding inner (top bearing). This inner ring is so narrow and flexible that it will surely stick and tilt. This certainly happened on the test bearing.

A similar application shown in the technical literature used ann elaborate flexure mounting to avoid this problem.

Thomas Barish

Thomas Barish

TB/ds

G.5 REPORT OF C. J. PENTLICKI

TRW/Aitken

COMMUNICATIONS SATELLITE CORPORATION

Jan. 14, 1976

B. Hendrickson
Aerospace Corporation
P.O. Box 92957
Los Angeles, Calif. 90009

Dear Bill:

I am sorry to be tardy in offering my written views on the DCSC-II anomaly, but I was involved in the INTELSAT V proposal evaluation for an extended period. Perhaps it is just as well as we have the benefit of the early December observation that the drive's high torque dropped to normal between telemetry frames, etc.

So far, I prefer the "bearing failure" theory. It best fits the experience as I understand it. The thinking goes as follows:

We know that the DMA bearings are "lightly" lubricated to keep torque modest. We also are told that retainer instability has been observed on the 9433 spacecraft and other 777s. I believe this instability to be principally symptomatic of marginal lubrication for this retainer/bearing system and only secondarily related to the particulars of the retainer design. That is, with enough lubricant the retainer can be stable, but with less than that necessary quanity, the instability is certain. This situation, I believe led to increased retainer wear and attendant debris production. The increasing frequency of torque transients in May and June of 1975 were indicative of a degrading lubricant state as the wear debris "absorbed" lubricant and retainer instability become more pronounced due to higher friction forces between the metal parts and the retainer. Bearing temperatures rose and retainer debris deposited on the balls and raceways and caused the rapidly increasing torque observed in the 7/11/75 to 9/12 period.

The high DC running torque is from the debris coating on the balls. The debris causes some balls to lag and to be forcefully driven by the cage. These resultant forces on the cage inhibit the cage instability by reducing its effective clearance. The sudden torque drop is explained by a cage driven ball(s) which is tumbling suddenly beginning to roll normally, perhaps because of the infusion of lubricant due to high retainer temperatures and/or the purge of debris.

This immediately free's the cage and torque is reduced to more normal levels. The step change to a higher, but intermediate, torque after three hours of normal torque is witness to a return of continuous retainer instability. The lubricant state continues to degrade, torque increases and once again some balls begin tumbling and a high steady state torque results. This model of the trouble can be made more credible if we add the contention that the pre-load is or was higher than the nominal levels. It is particularly attractive to assume that the pre-load mechanism is sticking or stuck leading to higher axial loads which encourages the adhesion of debris by high local temperatures as well as causing greater debris production. Maybe, it explains differences between units.

To see whether a failed bearing of this size could produce torque levels of the right order, I ran one that was failed in one of our previous test programs. The failure mode was adhesion of retainer debris to balls and races with ball tumbling reported.

The strip chart (A) is enclosed. It shows operating torque values above 8 in-lbs. with a 90 lb. pre-load. Starting torque exceeded 10 in-lbs. at some angular positions of the bearing. This bearing was essentially dry. Note that bearing performance with a 60 lb. load was markedly better than it was with 90 lbs. The test bearing parameters were:

Bore	: 90 mm + 0 - 0.00025
O.D.	: 140 mm + 0 - 0.0004
Ball Number	: 21
Ball Diameter	: 0.5625
Contact Angle	: 15° nominal, 13.4° - 18.4°
Lubricant	: Vac Kote impregnated phenolic retainers
Material	: 52100
Curvature	: 0.5850 ± 0.001
Tolerance	: ABEC 7
Retainer	: Inner race guided; diametral clearance .022"
Ball Pocket Clearance	: 0.015" diametral

The test program that produced this bearing included air and vacuum tests of Vac Kote'd bearings. Temperatures, speeds and axial loads were manipulated to seek failure modes. The tests in air with high axial loads as the acceleration factor showed retainer wear and adhesion of the debris accompanied by lubricant depletion, as a dominant failure mode. So much so that in one case, the bearing endplay grew as much as .003" and torque reached as high as 44 in-lbs. in another case. On bearings with lower axial loads this retainer debris was less pronounced. A vacuum test with a different bearing showed at normal speed and load, a similar condition described as a black tar like adherent. With this test the operating temperature was 90°C. Failure occurred after 70 days of operation of which only about 30 days were at 90°C. The test was stopped when the torques exceeded 2.4 in-lbs. because the bearings were considered to have failed.

Strip chart (B) is for a different bearing of the same size and failure mode as chart A. It also had debris on the balls and races, but never showed the high torques of the first bearing. The bearing when quite dry showed high torque noise, but when oil was added it became markedly smoother. Note that the torque scale is different than on chart A - anything over 24 in-oz. exceeds scale. The chart shows the torque history with increasing lubricant quanity. The 0.2 cc additions etc. refer to a 100:1 mix of Freon-Apiezon C applied to a single ball at each lube addition event with the bearing stopped.

As an aside, I have included a graph of a dry lubricated bearing pair tested in 1969. Notice the marked torque drop and recovery in the region of 440 hrs. into the test. At that time, I attributed it to debris purging and accumulation. The time scale is more extended than is your experience, but the marked torque/temperature change has an interesting similarity. There were several more of these cycles before I gave up on the bearing. Retainer wear was the source of the debris, some of which adhered to the balls, while some was discharged. It was about a 4" Kaydon bearing with a 10 lb. pre-load.

I would be happier with the DMA's design if it had more generous lubrication and a pre-load that could not hang up.

I hope you find these thoughts useful. I would be happy to discuss them with you or Art.

Chet Pentlicki

C. J. Pentlicki, Asst. Manager
Structural/Mech. Design Dept.

CJP:md

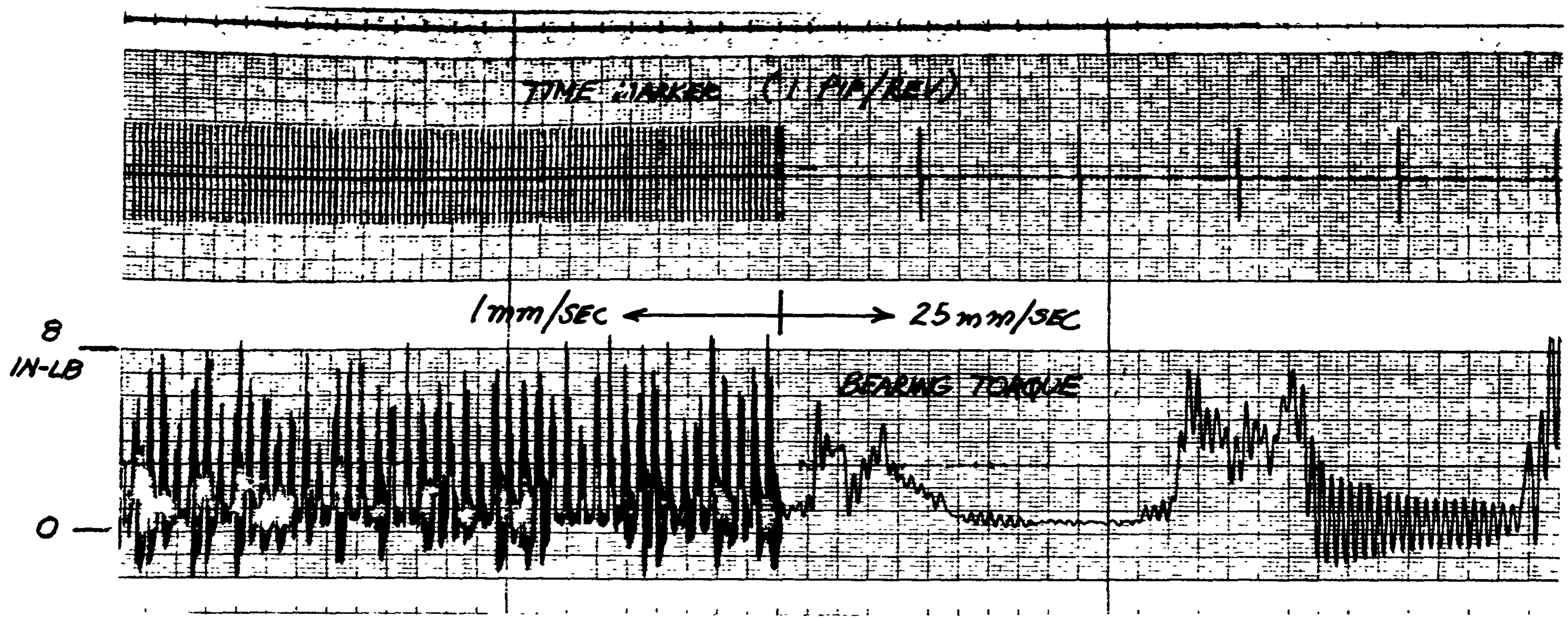

SEGMENT FROM CHART A (50 RPM; 90 LB PRELOAD)

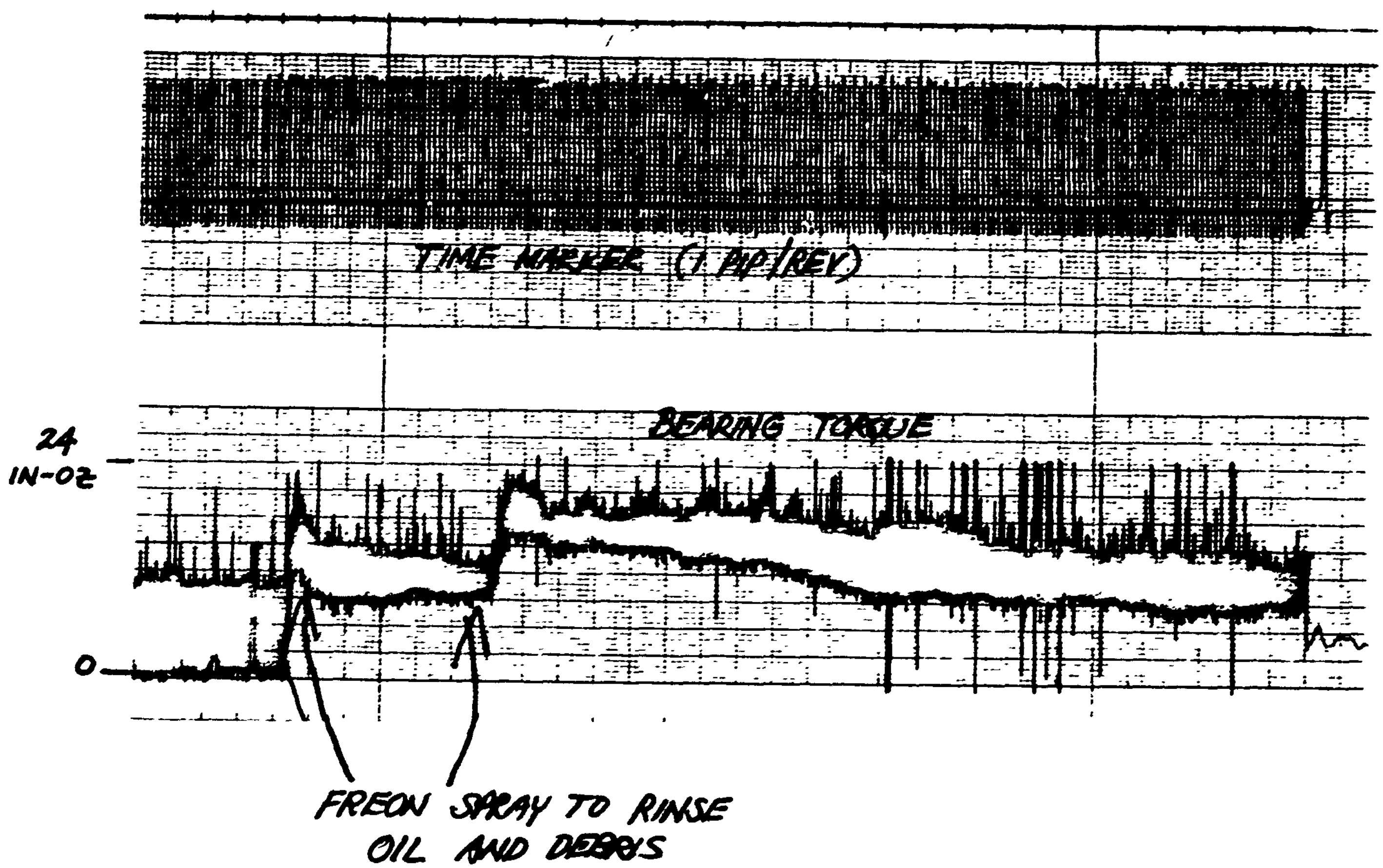

SEGMENT FROM CHART B (75 RPM, 60 LB PRELOAD)

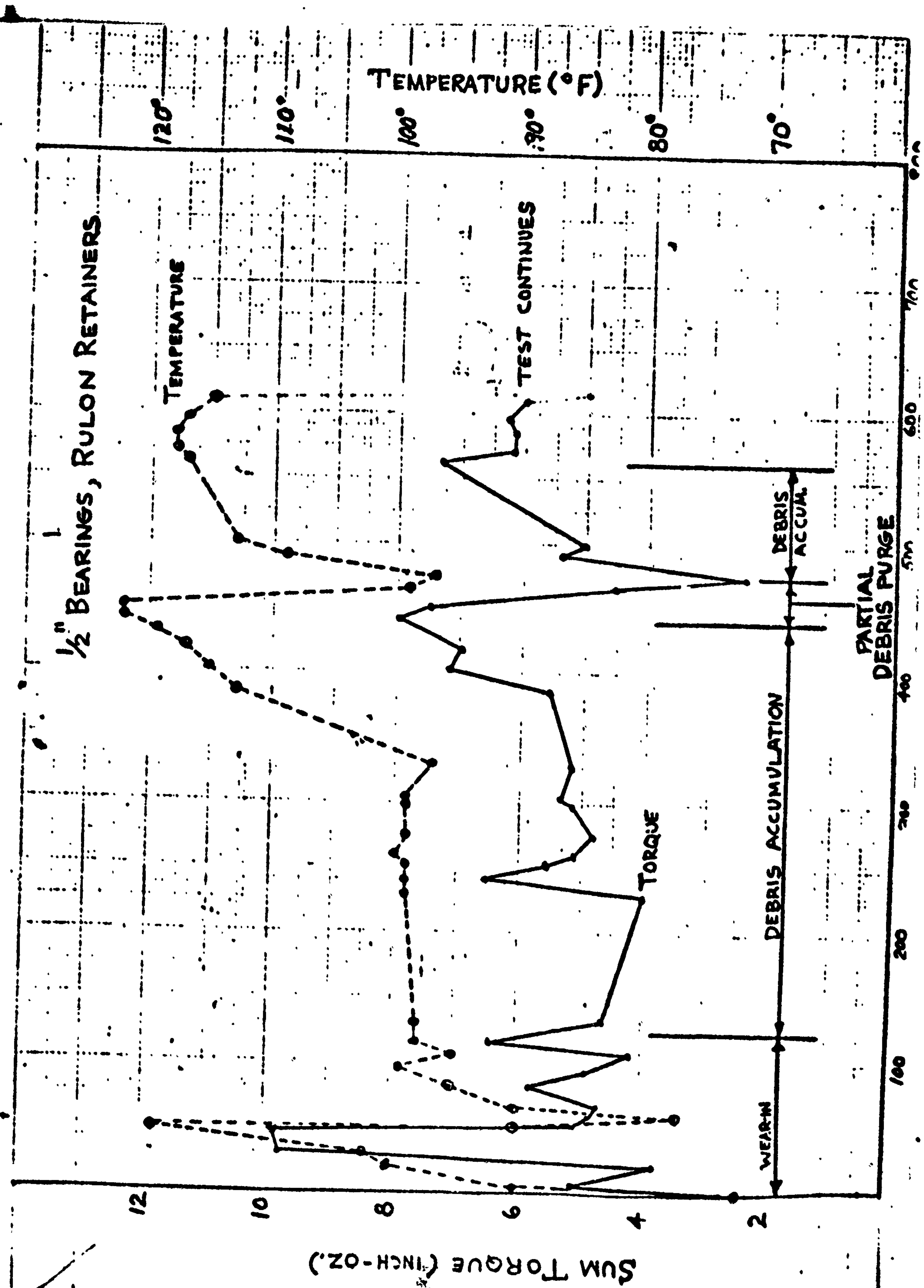

1/2" BEARINGS, RULON RETAINERS
TEMPERATURE (°F)
120°
110°
100°
90°
80°
70°
TEMPERATURE
TEST CONTINUES
TORQUE
WEAR-IN
DEBRIS ACCUMULATION
DEBRIS ACCUM.
PARTIAL DEBRIS PURGE
SUM TORQUE (INCH-OZ.)
12
10
8
6
4
2
100
200
400
600

APPENDIX H

NON-DMA INTERFERENCE MECHANISMS

TRW
SYSTEMS GROUP
ONE SPACE PARK • REDONDO BEACH • CALIFORNIA 90278

INTEROFFICE CORRESPONDENCE 8521.0.76-001

TO: Distribution CC: DATE: 15 January 1976

SUBJECT: Spacecraft #3 Anomaly FROM: W.B.J.Shakespeare

BLDG.	MAIL STA.	EXT.
M3	2264	53587

During the investigation of the "Spin Up" anomaly potential structural areas of interference were identified and analyzed.

This was accomplished by physically examining the existent qual spacecraft with a small team comprising of representatives from Integration and Test, Thermal and Mechanical/Thermal Design.

Specifically identified and analyzed were the attached "Conditions".

W.B.J. Shakespeare

W.B.J.Shakespeare

WBJS:dg

Attachment

Distribution

J. Durschinger
J. Gliksman
A. Parker
G. Perry
W. Wannlund
P. Wheeler

CONDITION 1

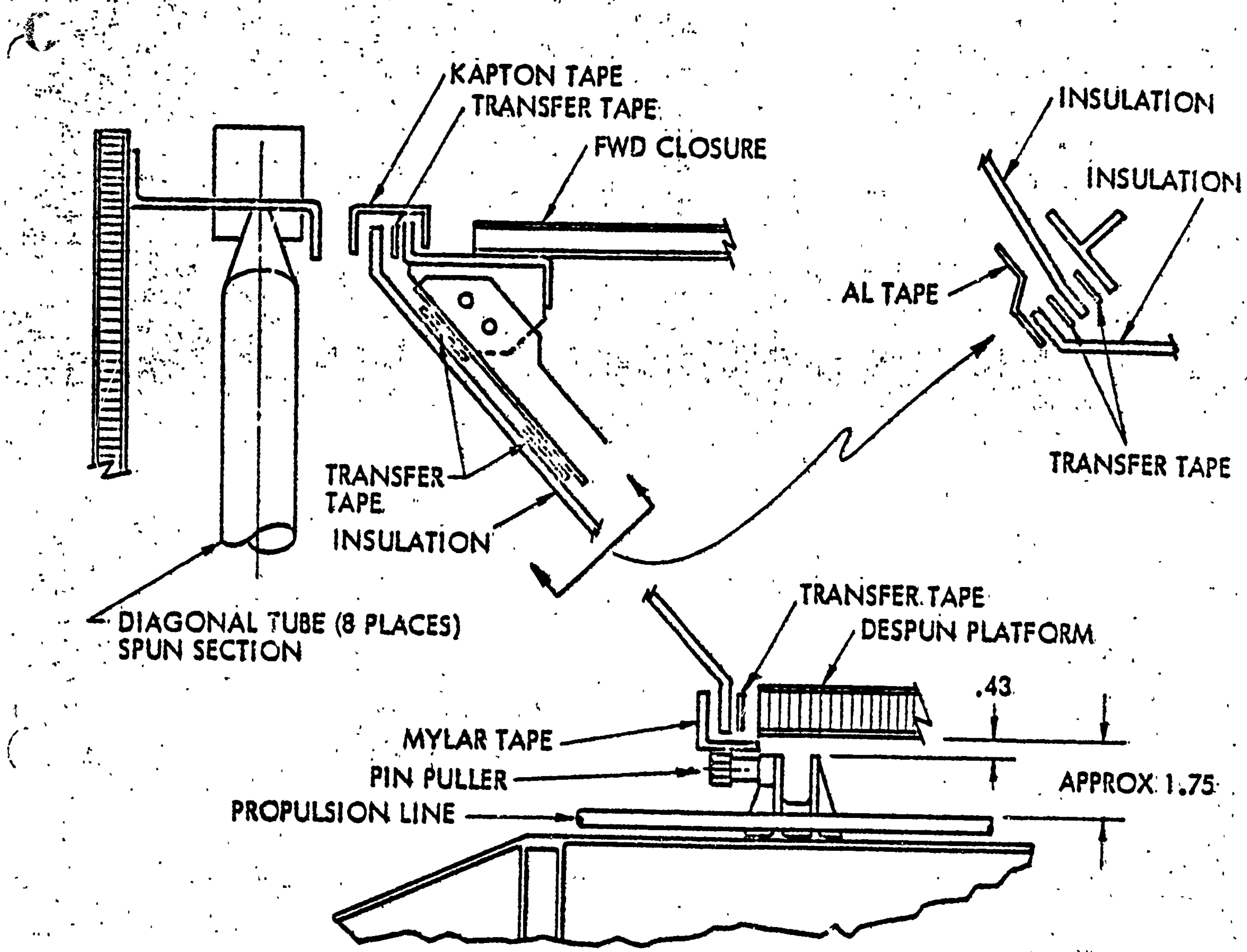

TO LOSE A SECTION OF THE CONICAL INSULATION - OR ANY OTHER BLANKET - WOULD REQUIRE THE FAILURE OF A LARGE QUANTITY OF TAPE. THERE IS NO PAST HISTORY TO SUPPORT THIS POSSIBILITY.

IF THIS FAILURE MODE OCCURRED IT WOULD BE NOTICED BY A TEMPERATURE REDUCTION OR INCREASE IN THE DESPUN AND SPUN COMPARTMENTS RESPECTIVELY ALONG WITH A MORE SENSITIVE CHANGE OF DESPUN TEMPERATURE DURING ECLIPSE. THIS PHENOMENON HAS NOT BEEN OBSERVED.

IF HYPOTHESIS IS MADE THAT RESISTENCE IS CAUSED BY IMPACT FROM A SECTION OF TAPE OR INS BLANKET BETWEEN THE SPUN AND DESPUN SECTIONS, THEN THE MAGNITUDE OF THE FORCE WOULD BE DEPENDENT ON THE RELATIVE SPIN RATE OF THE TWO ASSEMBLIES. FLIGHT DATA INDICATES THAT THE RESISTIVE FORCE IS CONSTANT FOR ALL RELATIVE SPEEDS BETWEEN 0 AND 60 RPM. THEREFORE, POTENTIAL OF THIS CAUSING THE PROBLEM IS NEGLIGIBLE.

CONDITION 2

THE PIPPERS AND ALIGNMENT MIRRORS ARE MECHANICALLY FASTENED IN PLACE. IF AN INTERFERENCE OCCURED BETWEEN PIPPER SECTIONS IT WOULD SEEM THAT THE RPM READOUT WOULD BE CONTINUALLY FALSE OR NON-EXISTENT. THE MIRRORS HAVE ADEQUATE CLEARANCE AND IN ORDER TO HAVE ANY INTERFERENCE WOULD REQUIRE THE FAILURE OF MECHANICAL FASTENERS.

CONDITION 3

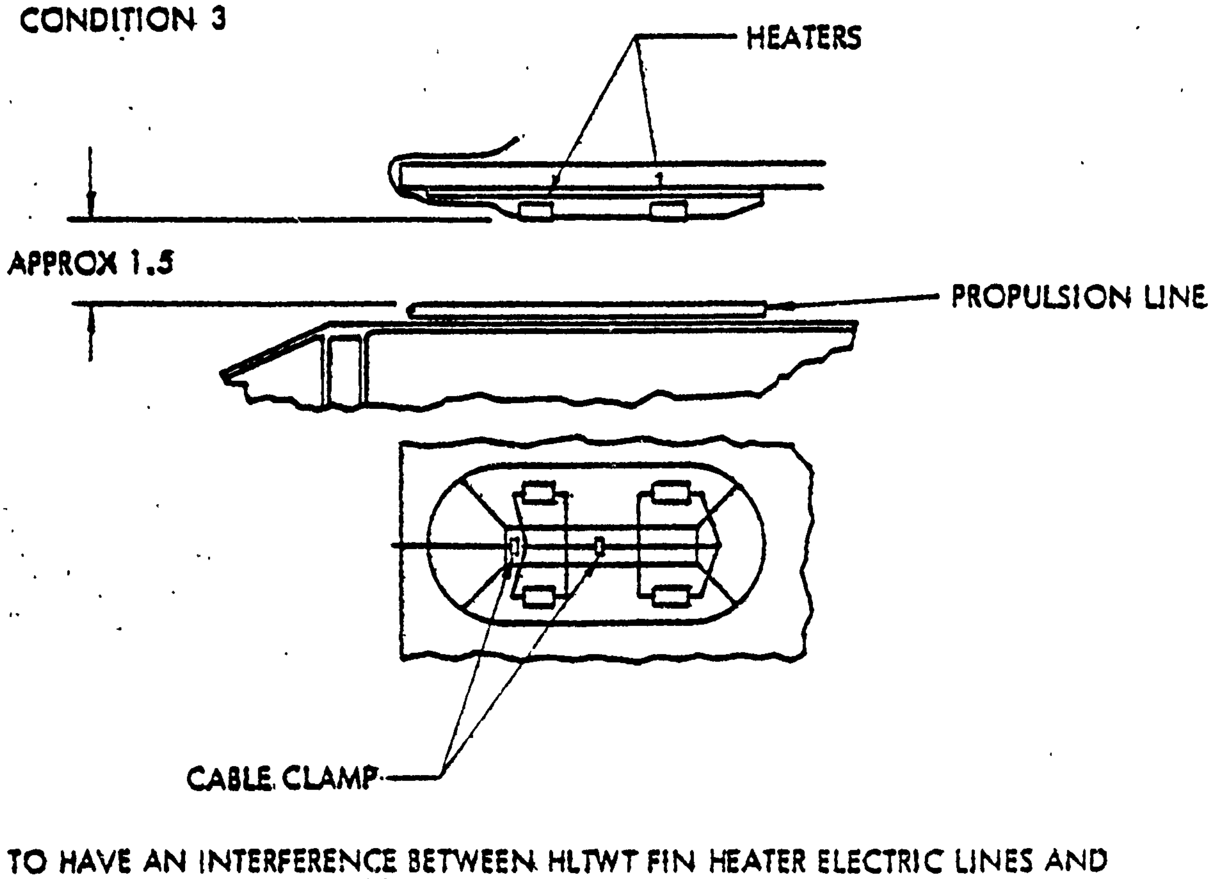

TO HAVE AN INTERFERENCE BETWEEN HLTWT FIN HEATER ELECTRIC LINES AND SPUN SECTION WOULD REQUIRE THE FAILURE OF SOLDER JOINTS AT HEATER AND FAILURE OF SPOT BONDS (WIRE TO STRUCTURE) AND/OR LOSS OF CABLE CLAMPS.

FAILURE OF SPOT BONDS ONLY, WOULD NOT ALLOW WIRES TO SAG THE REQUIRED DISTANCE TO INTERFERE WITH THE SPUN STRUCTURE. FAILURE OF SOLDER JOINTS AT HEATER WOULD BE INDICATED BY THE LOSS OF HEATER USAGE AND THIS HAS NOT HAPPENED.

CONDITION 4

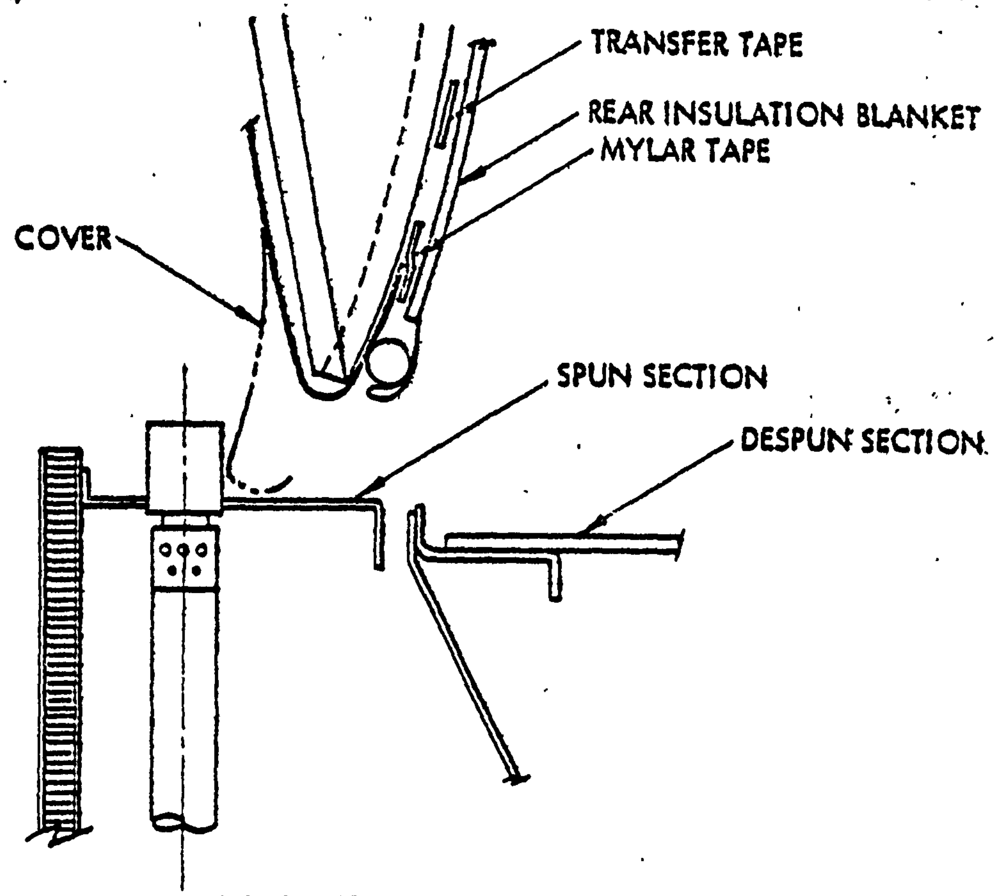

FOR N/C COVER TO COME LOOSE AND CAUSE AN INTERFERENCE WOULD REQUIRE THE SIMULTANEOUS FAILURE OF 3 OR 4 TAB TAPE SECTIONS AND SOME FORCE TO FREE THEM FROM UNDER THE BACK-UP RING AND REAR INS BLANKETS. SEE HYPOTHESIS IN FIRST CONDITION.

CONDITION 5

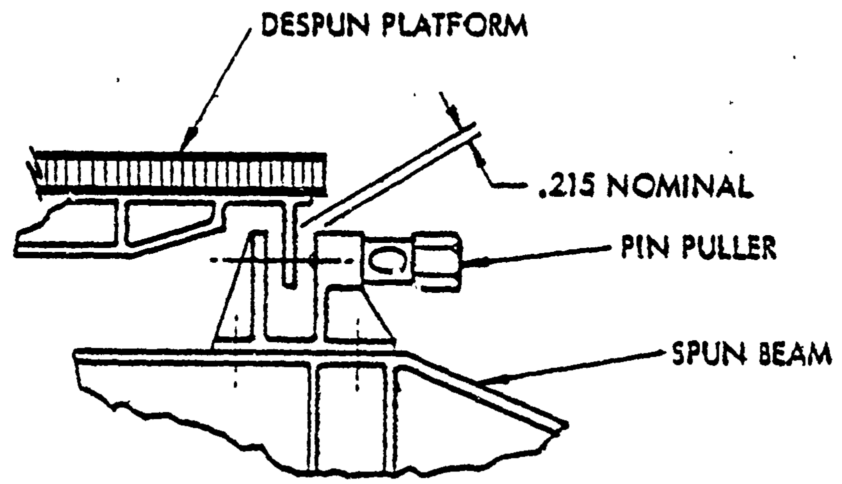

THE PIN-PULLER HAS A RELIABILITY OF .999 FOR PROPER OPERATION. FOR THE PIN TO DRIFT OR THERMAL CYCLE BACK IT WOULD HAVE TO OVERCOME INTERNAL GAS PRESSURE OF THE CHARGE AND THE INHERENT FRICTION OF UNIT-O' RING AND CARBON BUILD-UP FROM THE EXPLOSIVE CHARGE OR CHARGES. ALSO, THERE IS A CENTRIFUGAL FORCE ACTING ON PIN TO KEEP IT RETRACTED.

CONDITION 6

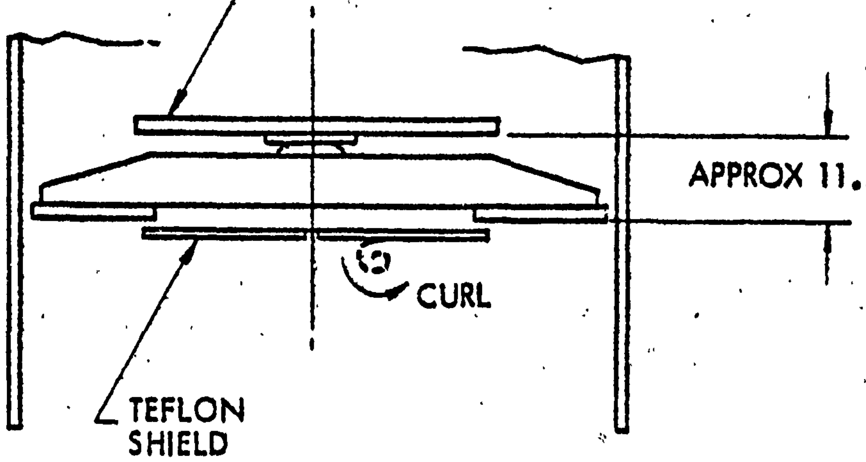

CONTRACTION - DUE TO COLD CONDITION - APPEARS TO BE ONLY MEANS THAT SHIELD WOULD COME LOOSE, AND IF THIS DID HAPPEN, THE TEFLON HAS A CHARACTERISTIC OF "CURLING-UP". THIS WOULD BE AWAY FROM THE DESPUN SECTION. AT A WARMER TEMPERATURE ALMOST 50% OF TAPE AND HOOK AND PILE TAPE WOULD HAVE TO FAIL IN ORDER FOR BLANKET TO REACH BOTTOM SURFACE OF DESPUN PLATFORM (PIN-PULLER BEAM OR HLTWT FINS). ONCE AGAIN THE HYPOTHESIS OF CONDITION ONE WOULD PREVAIL.

APPENDIX I SPECTRAL ANALYSIS

Details of the spectral analysis summarized in Section 9.2 are provided in this appendix: Assumptions regarding the data base, summary of the 777 bearing characteristics, details of sensor noise, and the various analytical models (transfer functions) relating sensor noise, torque noise, and platform pointing error power spectral densities (PSD) are discussed.

I.1 Pointing Error PSD Data Base Considerations

Figures 9.2-1A through 9.2-4A (upper left hand figures) shown in chronological order (06/27/75 to 09/12/75) are the PSD pointing error data base selected for analysis. This data was provided by Aerospace Corporation in the form of listings and plots and have the mean value and long-term low frequency trends removed. Not all PSD points were used in every case, but enough points were selected to show the general frequency dependent trends for the pointing error PSD data.

I.2 Aliasing Effects in Data Interpretation

The PSD pointing error data was computed from platform pointing error position data which was sampled at a rate of 1 Hz. Transformation of this data to PSD information therefore is band limited to one half the sampling frequency or 0.5 Hz. Frequencies larger than 0.5 Hz are folded back into the frequency spectrum and are therefore indistinguishable from the true data. How much the folding process influences the true data interpretation depends on the band pass characteristics of the pointing error data at high frequencies. In this case, the control band (about 0.038 Hz) is much lower than the sampling frequency; therefore, the pointing error PSD due to disturbance torque at frequencies higher than the control frequency is attenuated at a rate of 80 DB per decade. The effects of aliasing in the pointing error PSD can be small; however, with potential disturbances for the retainer in the 0.4 Hz to 0.06 Hz range and in the 1 Hz range for the shaft frequency, these effects can contribute aliased peaks at unexpected frequencies.

Figure I-1, for example, shows a sketch of the sampled pointing error PSD, plus the pointing error displaced and centered about the 1 Hz sampling frequency or carrier. The sketch represents one term taken from the ideal sampling formula PSD shown in Equation (I-1)

$$|\theta(j\omega)|^2 = \frac{1}{T} \sum_{n=-\infty}^{n=+\infty} |\theta(j\omega + j\, n\omega s)|^2 \qquad \text{(I-1)}$$

Figure I-2 shows two examples of pointing error PSD curves, when summed could result in the same composite curve shown in Figure I-1. Curve A, for example, shows a large energy content at low frequencies with a low frequency resonant peak occurring at f_p Hz. Curve B shows a lower energy content at low frequencies but also a rising PSD out to the sampling frequency, showing a resonant condition occurring in this neighborhood. Also shown is a peak at (1 - f) Hz. The effect of the PSD at frequencies higher than 0.5 Hz, on the PSD in the frequency range below 0.5 Hz can be obtained by folding the high frequency characteristics about one half the sampling frequency on 0.5 Hz. Curve B therefore has the high frequency peak $(1 - f_p)$ in the same position f_p as the peak shown in curve A. The true frequency source of these peaks however is indistinguishable by examining the sampled PSD data. However, for pointing error where the load inertia acts as a low-pass second-order filter to load disturbances, large-amplitude high-frequency folded effects can be small; however the resonant peaks such as f_p can show up in the data.

I.3 Sensor Noise and Quantization Effect Considerations

The sensor noise and nonlinear quantization effects in digitizing pointing error define the lower limitation for interpretating the pointing error PSD. Sensor noise was considered as Gaussian wide-band white noise with zero mean and a standard deviation of sigma. The quantization effects are nonlinear but, if small, can be neglected.

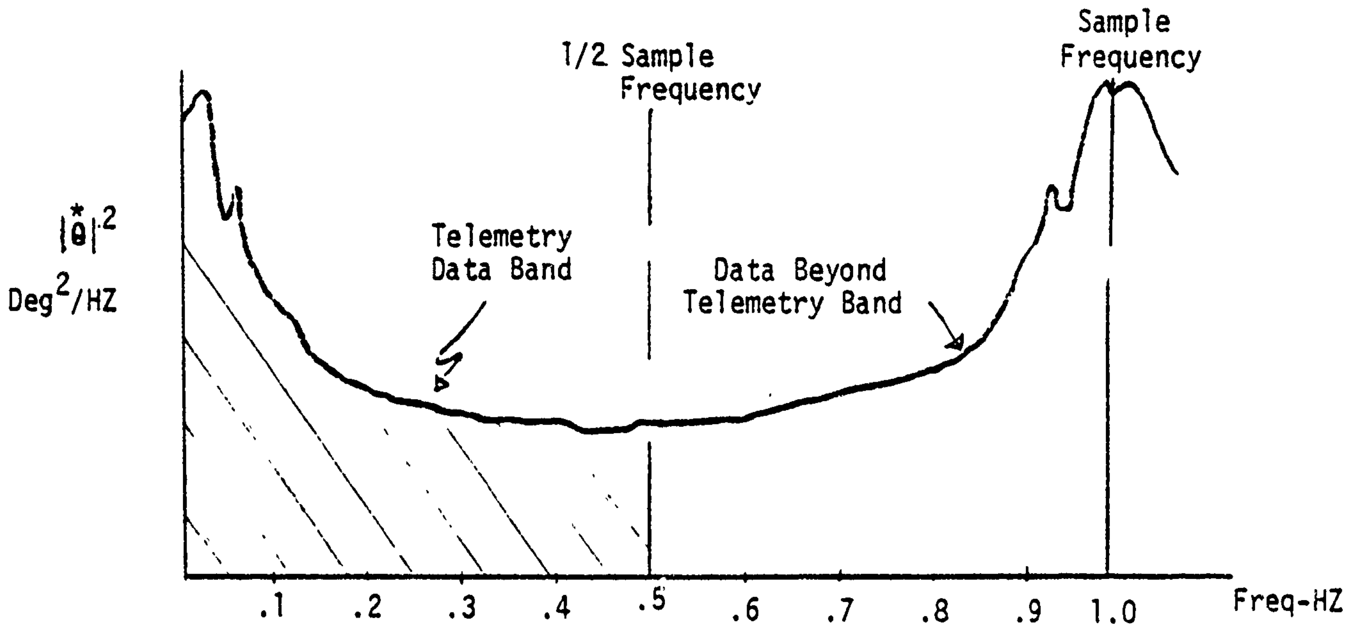

Figure I-1. PSD Pointing Error PSD VS Frequency

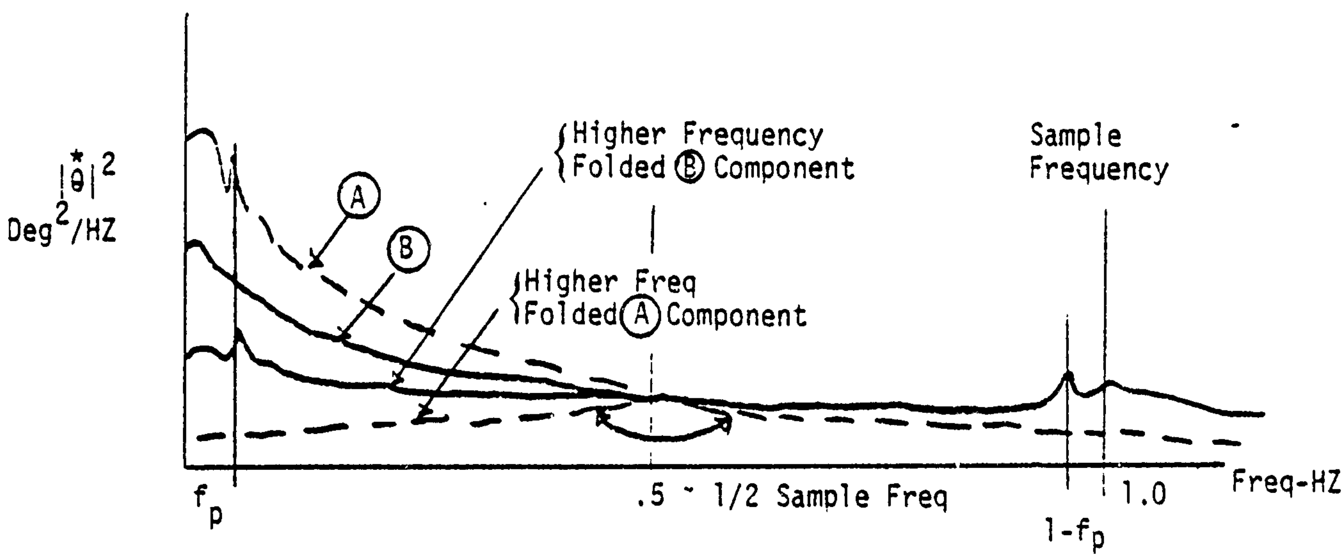

Figure I-2. Possible PSD Spectrums Resulting in Same Flight Data

For the purposes of data interpretation, the effect of quantization uncertainty (half the quantization interval) has been lumped into the noise characteristics. This effect will tend to quantize the normal probability distribution of the noise to the uncertainty interval, thereby decreasing the noise sigma by the uncertainty interval.

I.4 Frequency Characteristics of the DMA Bearing Components

Disturbance torque mechanisms can be related to the relative periodic motion of the various DMA bearing components, (e.g., the inner race, balls and retainers). The relative frequency relationships were calculated for the two DMA bearings and these calculations are summarized in Table I-1. The ball frequency range covers the interval from 4.5 to 5.0 Hz. The retainer frequencies are around 0.45 Hz and the outer race and shaft frequencies at 1.0 Hz. Table I-2 shows a frequency difference matrix for the primary component frequencies listed in Table I-1. These frequencies are also of interest in interpreting the PSD peaks observed on the data and appear to range from 0 to 4 Hz. The significant frequency difference contributors in the 0 to 1 Hz range appear to be the retainer difference frequency (0.006 Hz) and the ball difference frequency (0.62 Hz) and the shaft/retainer frequency differences (0.55 Hz).

I.5 Torque PSD Transformation

The pointing error PSD data can be transformed back to equivalent disturbance torque PSD to show the spectral content of the disturbance. Although this process is straight-forward for a linear system, the resulting torque PSD spectrum requires careful evaluation. For example, the high frequency folded effects in the data must be considered in the torque calculation even with the bandpass-limiting effect of the platform inertia at high frequencies. Then, the resolution limitation of transforming low amplitude pointing error PSD data a high frequencies must be considered. This requires estimating the effects of sensor noise, and pointing error quantization contributions on the high frequency data (i.e., a signal-to-noise ratio consideration).

Table I-1. Summary of Control Constant & Equation Definitions

Definition	Symbol	Value	Units
Control Gain	K_V	350 "G" (G57)	Ft-Lb/Rad
(Gain State Function)		498 "H" (G58)	Ft-Lb/Rad
Platform Inertia	I_P	72.0	$Ft-Lb-Sec^2$
Compensation Pole	A	10.0	Rad/Sec
Compensation Zero	B	0.6	Rad/Sec
Compensation Zero	C	0.6	Rad/Sec
Quantization	-	0.0137	Deg/Count

Equation Definitions	Units
$H_1 = K_V(S + A)(S + B)/S(S + A)$	Ft-Lb
$H_2 = 1/I_P\, S^2$	$(Ft-Lb)^{-1}$
$H_3 = Z-1/ZS$	Sec
$H_3^* = 1$	None
$\overline{H_1 H_2}^{*} = \frac{K_V}{I_P} \frac{1}{GT} [F_2 + F_3 (B + C) + F_4 (B * C)]$	None
$Z = e^{ST}$; $P = e^{-AT}$	
$G_P = 1-P/Z-P$; $G_0 = T/Z-1$; $G_1 = Z/Z-1$	
$G_2 = (Z + 1)/_2$; $G_3 = T(Z + 2)/6$; $F_1 = G_1 * GP/A$	
$E_1 = G_0 * G_1$; $E_2 = E_1 * G_0 * G_2$; $E_3 = E_2(G_0 + G_3/G_2)$	
$F_2 = (E_1 - F_1)/A$; $F_3 = (E_2 * F_2)/A$; $F_4 = (E_3 - F_3)/A$	
$\overline{H_2 H_3}^{*} = T^2 (Z + 1)/ 2*IP (Z - 1)^2$	$(Ft-Lb)^{-1}$

Table I-2 Bearing Frequency Components
(Reference 75-7345.4-040)

Symbol	Description			Units
	Bearing	A	B	
D_B	Bearing Diameter	110	90	MM
f_S	Inner Race and Shaft Frequency	1.0000	1.0000	Hz
f_B	Ball Frequency	5.0939	4.4740	Hz
f_R	Retainer Frequency	0.4525	0.4462	Hz

Table I-3 Bearing Frequency Component
Difference Matrix

*f(X)A - f(X)B	f_{SB}	f_{BB}	f_{RB}
f_{SA}	0	- 3.474	+ 0.5538
f_{BA}	-4.093	+ 0.619	+ 4.0493
f_{RA}	+ 0.5475	+ 4.0245	+ 0.0061

* Note: (X) Designates First Subscript

The transformation approach used was to first develop the linear transfer function which would relate an assumed sensor noise PSD and pointing error data PSD to a torque PSD. Examination of the resultant torque PSD spectrum showed that the results could be studied in two parts; (1) examination of the torque data in the frequency range of the control band where the control system dominated performance; (2) examination of the torque PSD in the high-frequency rangc where the load inertia dominated performance.

The calculated torque PSD characteristics generally followed the data trends observed in one piece of ground test data performed on the system in the low frequency or control band range shown in Figure I-3. In the data time interval studied, the peak torque levels in increased significantly (see Table 9.2-1), and some of this increase could have been caused at frequencies near 1 Hz, folded back to very low frequency ranges 0.001 Hz.

At the high frequency end of the spectrum, (out to 0.5 Hz), an increasing torque PSD with frequency trend was noted. This frequency range also coincided with the frequency range of the retainer disturbances so these results were examined more carefully. Since the effects of sampling or folding were not considered in the linear system, the effect of the zero order hold was included in an advanced form of the linear model. Then, using a simple model of torque driving a load inertia, a weighted correction factor was developed which corrects the torque at high frequencies.

To study the effects of sampling on the torque PSD calculation in more detail, a sampled data model was developed which included calculating the system impulse transfer functions. In this case, however, the torque PSD cannot be calculated directly, because of the location of the sampler in the feedback loop relative to the torque disturbance. However, open loop pointing error can be calculated, and this calculation then can be compared to the pointing error data curve at high frequencies with the effects of sensor noise and sampling are taken out of the open loop calculation.

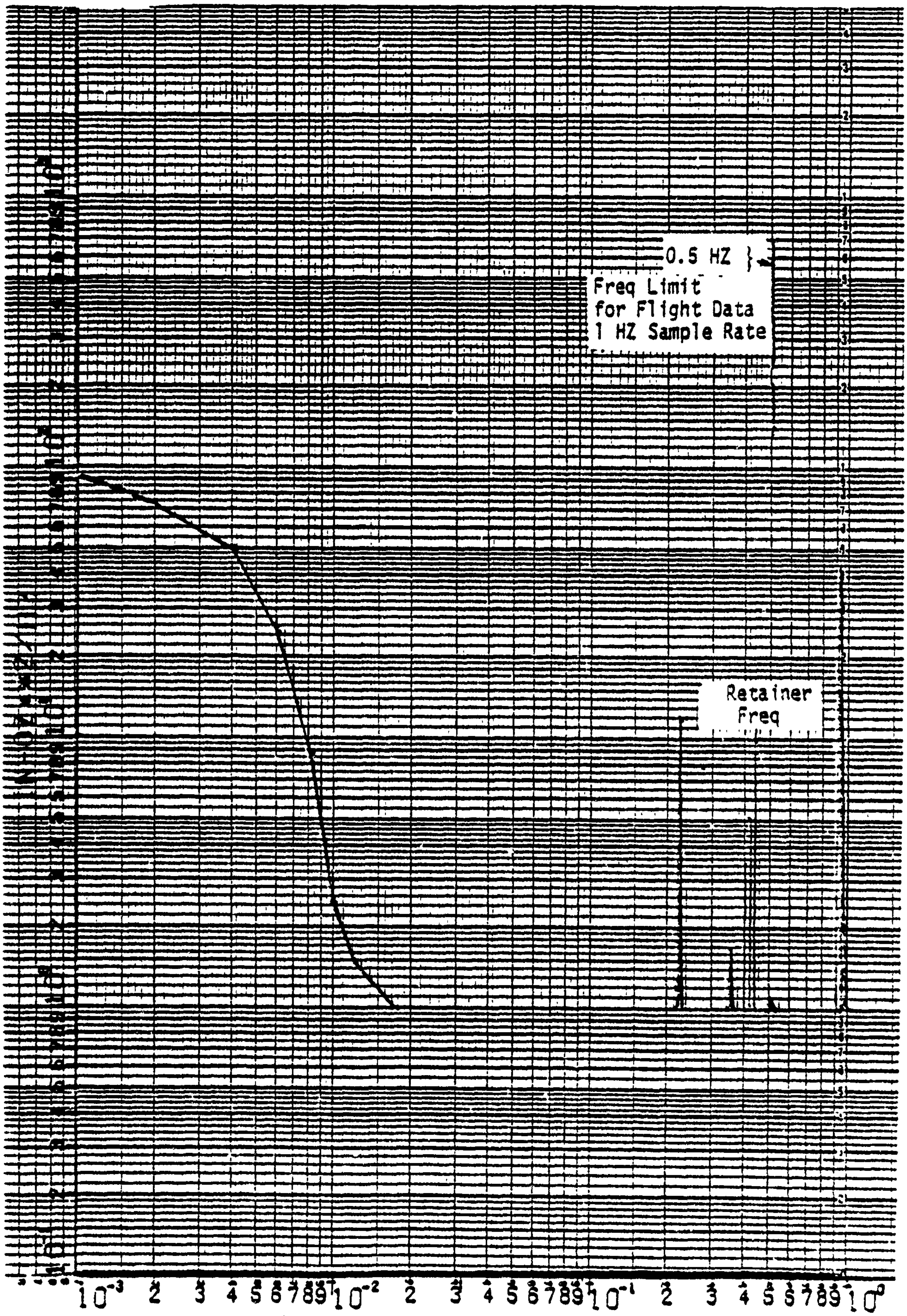

Figure I-3. Torque PSD of DMA Bearings; (From 69.7231.9-68 Figure 8.3)
Sample Rate 5 HZ, 10 min Data S/C Speed Equals 60 RPM

The results of using these models can be summarized as follows:

(1) In the low frequency band, the linear model and linear model with the zero order sample hold provide similar results. The torque profile compares well with the ground test torque PSD data, especially with the early 6/27/75 performance data.

(2) Applying the correction factor to the pointing error data appears to straighten out the data at high frequencies and this data tends to approach the inertia load time to a greater degree. When this data is transferred to torque PSD, the torque PSD still exhibits a rising amplitude trend at high frequencies. This could be due to torque disturbances provided in the retainer range of frequencies or in part due to nonlinear effects not accounted for in the low amplitude pointing error data. However, examination of the 09/12/75 torque PSD shows similar results and, in this case, the pointing error amplitudes are well outside the sensor noise PSD, indicating large amount of folding in this data.

(3) The sampled data model also shows the torque PSD broadband peaking at both high and low frequencies. At high frequencies, this peaking ranges to 30 DB above the nominal 80 DB per decade constant torque band inertia load line. The peaking also substantiates the torque PSD analysis models, and points to the strong possibility of high frequency torque disturbances occurring within the frequency disturbance range of the DMA retainer (0.44 Hz).

I.6 Linear PSD Transformation

The pointing error PSD can be transformed into an equivalent disturbance torque PSD using the square of the real parts of the transfer function of the control system which relate the disturbance power inputs to power output. This transformation assumes that the disturbance sources (torque and sensor noise) are uncorrelated so that the cross-PSD relationships are zero. The linear control system model showing the position of the torque and sensor noise inputs and pointing error output is shown in Figure I-4. Table I-3 shows a list of nominal gains for the control system. Figure I-5 shows the block diagram of the linear torque transformation relationship. The torque PSD can be defined in terms of transfer relationships as follows:

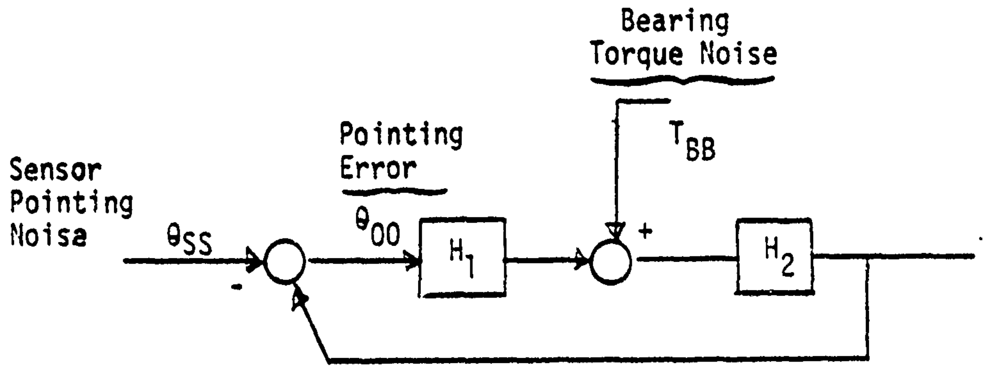

Figure I-4. Assumed Linear Control Model

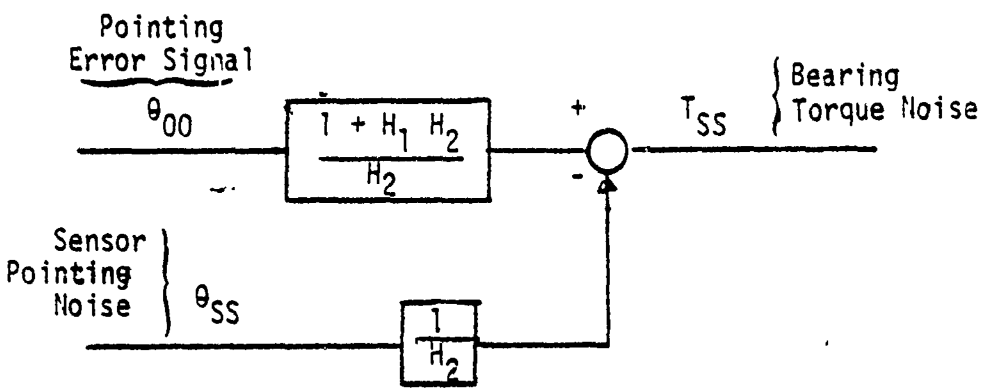

Figure I-5. Transformed Linear Model With Bearing Torque Noise as Output

$$|T_{ss}|^2 = |\theta_{oo}|^2 * \left|\frac{1 + H_1 H_2}{H_2}\right|^2 - |\theta_{ss}|^2 * \left|\frac{1}{H_2}\right|^2 \quad \text{(I-2)}$$

The linear model contains the implicit assumption that the control system components are operating in the linear non-limited ranges of operation. Figure I-6, for example, shows an expanded control system block diagram with the position of the chief limiters in the control loop. These limiters can be classified as integrator limiting, providing a limiting function only at very low frequencies (less than 0.001 Hz), and sensor pointing error limiting, providing position error limiting from 5 to 7 degrees. These limiting functions are confined to the open loop control block H_1, while the load inertia block H_2 contains no limiting function.

It should be noted that the limiting effects require extreme operation of the control system, and these nonlinearities should effect the data to any degree with the possible exception of the preanomaly 09/12/75 data.

The torque PSD was obtained by substituting "jω" for "s" with transfer functions and then calculating the square of the real part of these transformations. The pointing error PSD obtained from the telemetry data in the primary input, and the sensor pointing noise, considered wide band gaussian white noise with a standard deviation sigma (σ) as the secondary input. The sensor noise is also assumed to be adjusted for the quantization uncertainty effects. For a sampling period T (one second) the sensor noise PSD becomes

$$(\theta_{ss})^2 = \sigma^2/T \quad \text{(I-3)}$$

I.7 Sampled Data PSD Torque Transformation

Sampled data models of the control system were developed in order to obtain a better understanding of the data trends of the pointing error PSD noted from the results of the linear torque PSD transformation. Figure I-7 for example shows a model of a sampled control where a sampler with period T is included in the forward loop. The output of the sampler through the transfer function H3 (zero order hold) represents the telemetered pointing error output signal.

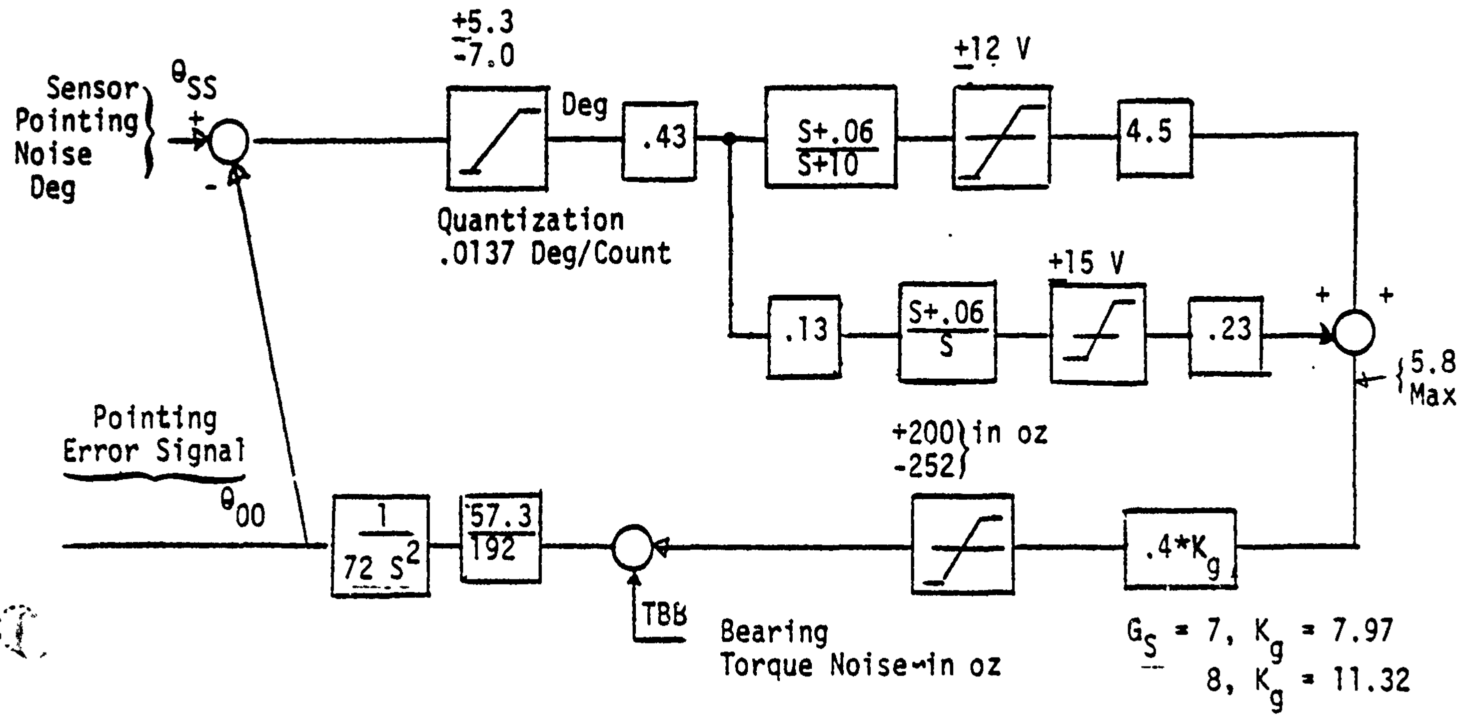

Figure I-6. Linear System Model Showing Location of Limit Blocks Reference (74.7531.9-07)

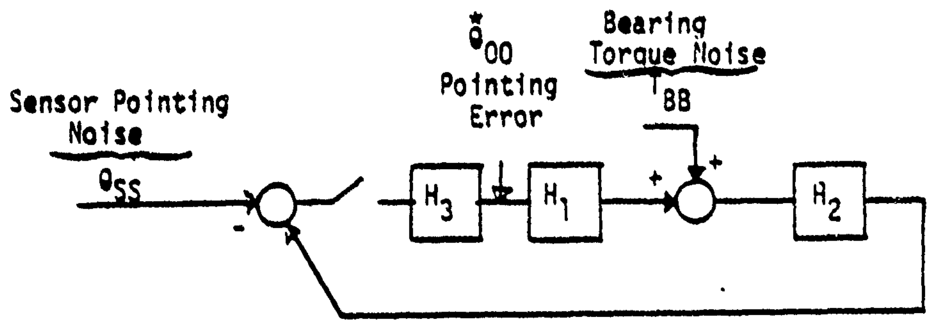

Figure I-7. Assumed Sampling Model Block Diagram

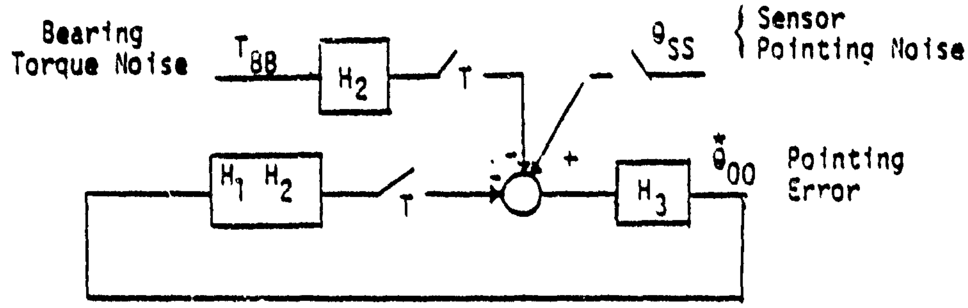

Figure I-8. Modified Sampling Block Diagram for Analysis

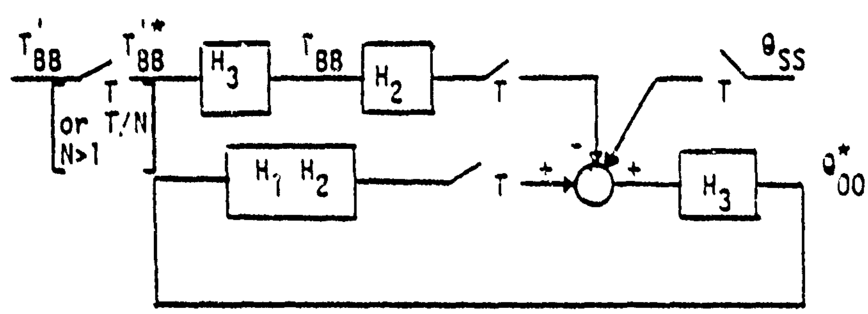

Figure I-9. Modified Sampling Block Diagram With ZOH Modified Torque Noise Input for System Transfer Function Determination

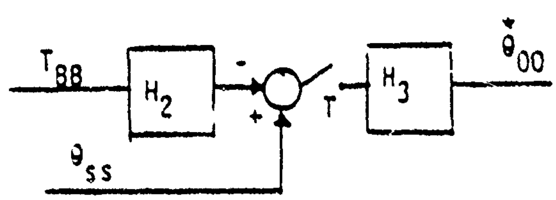

Figure I-10. High Frequency (>.05 HZ) Equivalent Block Diagram

Figure I-8 shows the movement of the sampler to equivalent positions in the diagram to clarify the analysis. In this case, the impulse transfer functions for the products $\overline{T_s H_2}^*$ and $\overline{H_1 H_2}^*$ and θ_{ss}^* must be calculated in order to obtain the sampled output error explicity. In other words, the disturbance torque cannot be directly obtained with the sampled system model by reversing the procedure described by Equation I-2 as was done in the linear case. Note that the output which is obtaining $(\overline{T_{xx}H_z})^*$ represents open loop pointing error, i.e., pointing error without the control feedback. At high frequencies, beyond the control band width, (0.05 to 0.5 Hz) the controlled pointing error is also equivalent to the open loop pointing error plus the effect of sensor noise.

As a note, Figure I-9 shows a further modification in the sampling diagram in an attempt to obtain a transfer function relationship which would permit calculating an approximate torque PSD directly. In this case, a fictitious sampler is placed ahead of the torque disturbance and a zero order hold (H3) establishes quantized torque steps (T_{ss}) over the sampling interval. This substituted torque function however, effectively filters T_{ss} to one half the sampling frequency of 0.5 Hz. This model would be useful in establishing the disturbance torque spectrum if the disturbance spectrum were bandlimited to 0.5 Hz. Higher multirate sampling (T/N where N > 1) would provide the torque input T_{ss} with a higher frequency capability. However, with this arrangement of samplers as shown in Figure I-9 (fast, first in series with slow), torque TBB cannot be solved explicitly. In other words, the transfer relationship is obtainable when all samplers have the same sample rate, and bandlimiting of the torque noise input to 1/2 the sample frequency will result.

The open loop pointing error model was therefore accepted as the sampled data model which shows the effects of sampling over the entire spectrum. The results can be interpreted by comparing the open loop pointing error trend to a superimposed 80 DB/decade asymptote. This asymptote represents a constant torque band line on the pointing error plots, where the DB values above the asymptote line represent the multiple increase over the constant nominal, and values below the asymptote represent the multiple decrease from the constant nominal.

I.8 Torque PSD Evaluation

Figures 9.2-1B through 9.2-4B show the linear torque PSD transformation for the operational time periods ranging from 06/27/75 to 09/12/75.

Figures 9.2-1C through 9.2-4C show similar curves of the linear torque transformation model with a zero order sample hold and with the torque calculation corrected for sampling effects a high frequencies. Also shown superimposed on these torque plots is the ground torque PSD test data for comparative purposes. Figures 9.2-1D through 9.2-4D (lower right hand plots) show the integral of the torque PSD, or one half the mean square torque error as a function of frequency.

At frequencies less than the control bandwidth (approximately 0.038Hz), the torque PSD tends to follow the ground test data trend, except for the 09/12/75 data. For the data in the 06/27/75 to 09/01/75 time range, the peak torque PSD tends to increase from 140 to 800 $(\text{in-oz})^2/\text{Hz}$ (See Table 9.2-1 for a complete summary). The comparable ground test torque in approximately 94 $(\text{in-oz})^2/\text{Hz}$. For the 09/12/75 data, shortly before the first anomaly, the torque PSD increases to 101,000 $(\text{in-oz})^2/\text{Hz}$. RMS of the torque within the control band frequency changes from 3.6 to 25.8 in-oz during the time period ranging from 09/01/75 to 09/12/75.

At high frequencies the torque trend shows a broadband increase to 0.5 Hz. The torque at these frequencies was calculated from low amplitude pointing error PSD data near the sensor noise level for the first 3 cases (06/27/75 to 09/01/75. (For the 09/12/75 case however, the pointing error data is over 30 DB higher than sensor noise PSD). Additionally, the pointing error PSD is further influenced by nonlinear quantization effects and sampling or folding effects.

In order to clarify the sensor noise contribution in influencing the torque PSD shape at high frequencies, a series of torque PSD transformation were made varying sensor noise sigma. Values of sensor noise between zero and .05 deg (1σ) were used in these calculations and it appeared that 0.03 deg resulted in the best compromise noise value. Larger sigma values tend to result in a large number of negative torque PSD values at high frequencies. Since this is an invalid power balance condition, the noise value was decreased to where the negative values were in the minority, and less than the positive torque values of neighboring frequencies. The absolute value of torque PSD was then plotted to establish the high frequency trend.

The effects of ideal sampling or folding were also compensated in the calculation at high frequencies. Comparisons between the "C" and "B" plots show the differences. The zero order hold linear model with torque attenuated by the following factor is shown in the "C" sensed torque PSD plots.

$$K = [\mathrm{sinc}(\pi f/f_s)]^4/f_s^{\,2} \qquad \text{I.4}$$

where f = PSD frequency ~ Hz

f_s = sampling frequency ~ Hz(=1.0 Hz)

This factor represents the ratio between the pointing error PSD resulting from a system with sampling to a system without sampling for a constant torque band input disburbance to an inertia load. This factor accounts for approximately 15.5 DB rise in pointing error amplitude ratio at 0.5 Hz. The results of a calculation showing this effect along with added increments of sensor noise sigma is shown in Figure I-11. The pointing error PSD trend shown for these combined effects of sampling with sensor noise of SIG = .03 deg, for example, compares closely with the 08/12/75 pointing error data in the high frequency range shown in Figure 9.2-2. The broadband rise in the corrected torque PSD still exists at high frequencies as shown in Figures 9.2-1C through 9.2-4C. It is therefore tempting to attribute the torque PSD rise within this frequency band to possible DMA retainer disturbance torque inputs since retainers have a frequency inputs of about 0.43 Hz. These results however, are not conclusive because the low pointing error PSD amplitudes for the 06/27/75 through 09/01/75 data are near the sensor noise levels. However, for the 09/12/75 data where amplitude levels are large, the torque PSD levels in the high frequency range should be valid. These results show extreme data folding and possible pointing error limiting effects. The inset in Figure 9.2-4A shows a plot of the compensated data where the original data break to a 25 DB/decade asymptote is straightened out to a 40 DB per decade asymptote).

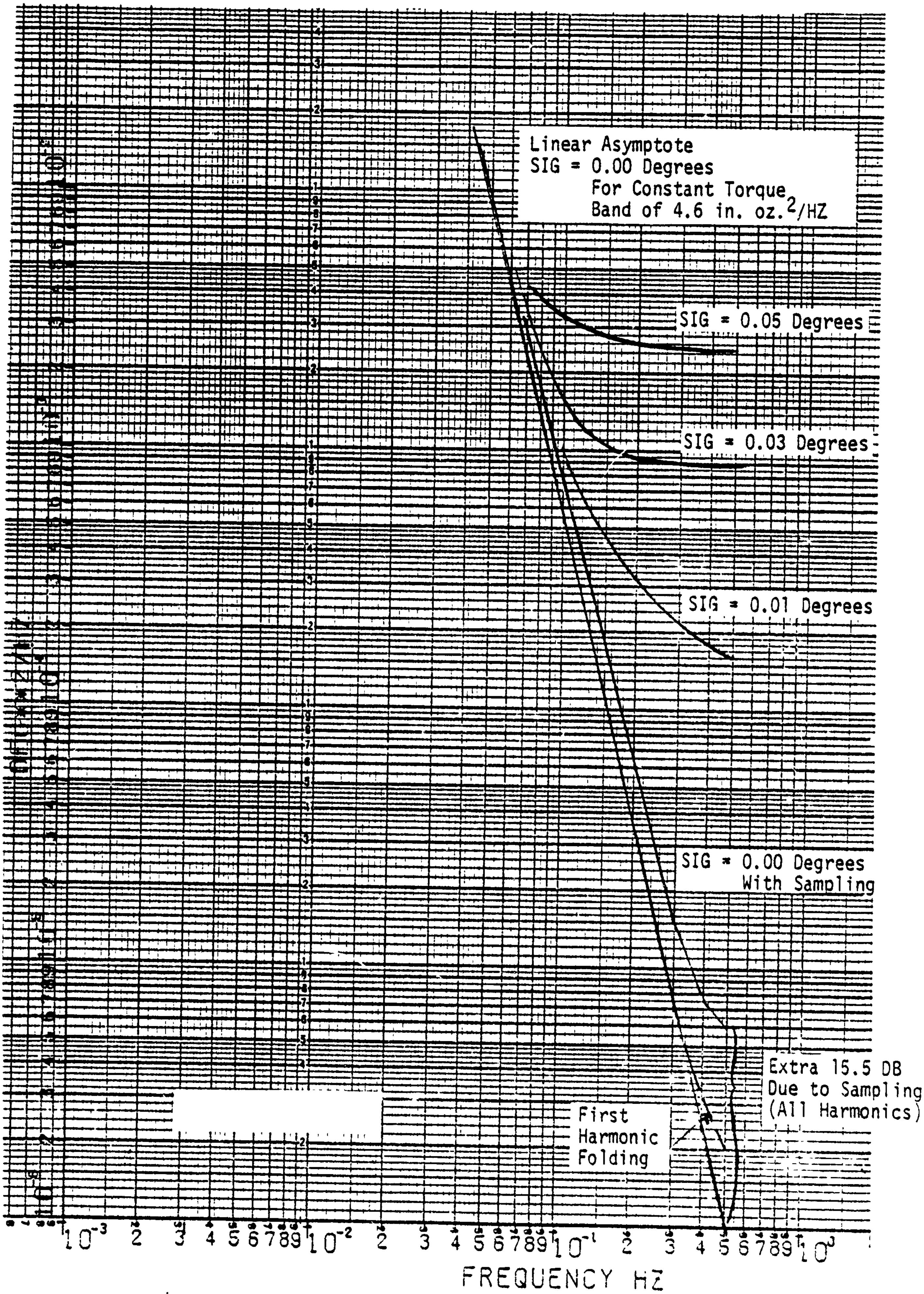

Figure I-11. Pointing Error PSD at High Frequencies for Various Sensor Noise SIG. and for Constant Input Torque PSD Band of 4.6 in. oz.^{2}/HZ

To investigate further the sampling effects at high frequencies, a sampled data model of the control system shown in Figure I-7 was used in the analysis. Figures 9.2-5B through D show respectively the open loop pointing error $\overline{T_{ss}Hz}^{*}$ for zero noise input and for 0.03 deg 1σ without and with the data sampling correction factor K. Figure 9.2-5A shows a replot of the telemetry data for comparative purposes. Superimposed on these plots is an 80 DB/decade constant torque PSD load line, which is drawn as a best fit thru the data at frequencies just above the control frequency range. As mentioned previously, the torque PSD input (T_{ss}) cannot be obtained explicitly for the sampled data system, however by comparing the open loop pointing error with the inertia load line asymptote, useful information on torque trends can be obtained in the low and high frequency ranges of operation.

Figure 9.2-5B shows the data in 9.2-5A transformed into open loop pointing error with zero noise input. The data generally follows the asymptote in the mid frequency range (0.03 to 0.1 Hz) and shows higher amplitude (torque) values in the low and high frequency ranges (the asymptote would have to shift to the left to high torque intersect the data). Near the sampling frequency, where the data in Figure 9.2-5A and 9.2-5B should match, the open loop pointing error appears about 3 DB lower.

Figure 9.2-5C shows the closed loop pointing error PSD with the sensor noise equal to 0.03 σ deg and Figure 9.2-5D with the sampling correction factor K included in the analysis. The figures show that high frequency peaks still remain above the 80 DB per decade asymptote even with the sampling correction factor K considered in Figure 9.2-5D. (Note all PSD amplitude less than 10^{-5} deg squared per Hz are plotted as 10^{-5} deg squared per Hz to keep the data on the paper). The effect of the correction factor reduces the level of the high frequency trend, however, this trend remains at least 20 DB above the asymptote indicating the possibility increased torques above the asymptotic torque value at these frequencies.